CRANIAL PLACODES AND NEURAL CREST INTERACTIONS IN CRANIOFACIAL DEVELOPMENT

EDITED BY: Jean-Pierre Saint-Jeannet, Lisa Taneyhill and Patrick Blader
PUBLISHED IN: Frontiers in Physiology

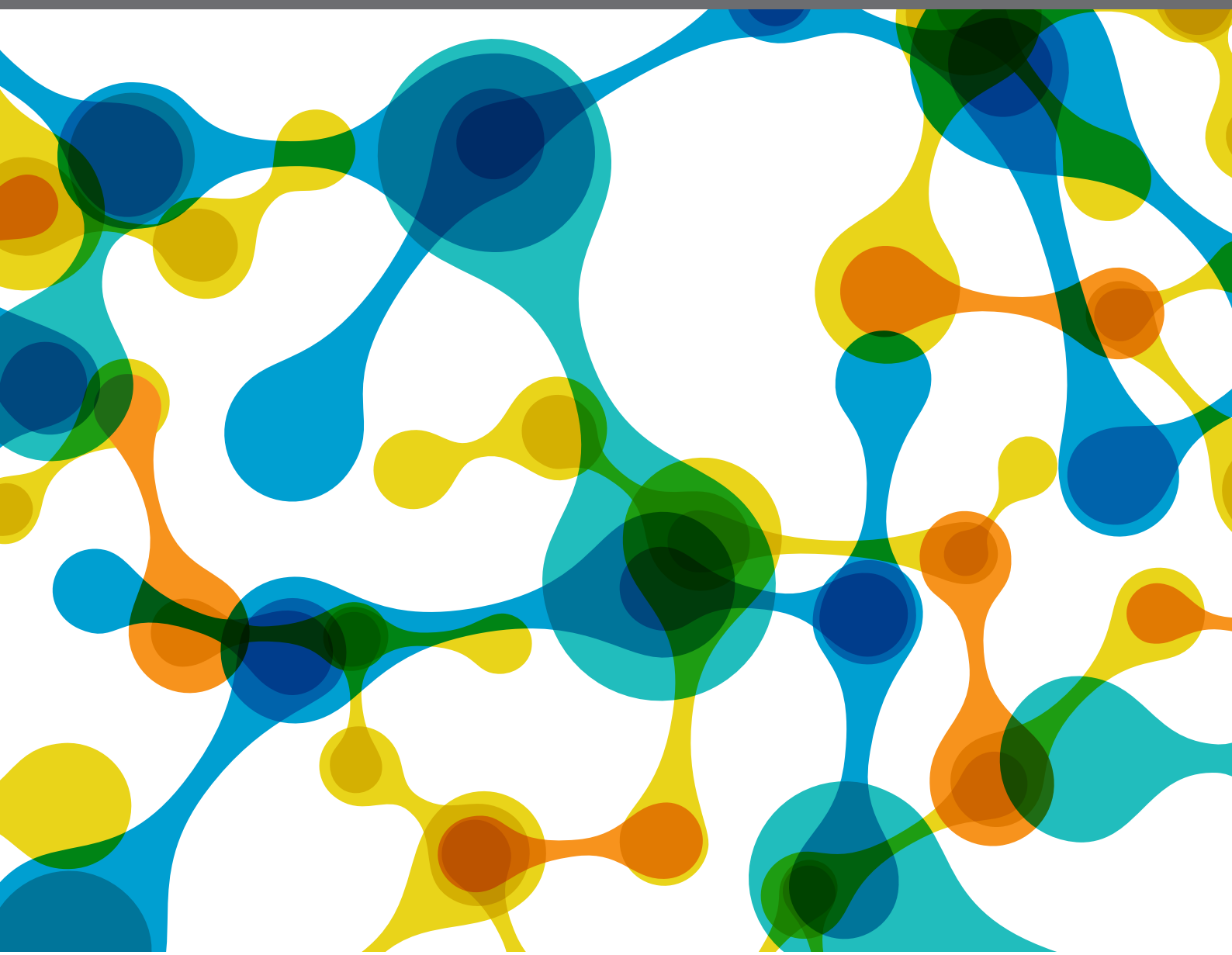

frontiers Research Topics

frontiers

ISSN 1664-8714
ISBN 978-2-88966-882-3
DOI 10.3389/978-2-88966-882-3

About Frontiers

Frontiers is more than just an open-access publisher of scholarly articles: it is a pioneering approach to the world of academia, radically improving the way scholarly research is managed. The grand vision of Frontiers is a world where all people have an equal opportunity to seek, share and generate knowledge. Frontiers provides immediate and permanent online open access to all its publications, but this alone is not enough to realize our grand goals.

Frontiers Journal Series

The Frontiers Journal Series is a multi-tier and interdisciplinary set of open-access, online journals, promising a paradigm shift from the current review, selection and dissemination processes in academic publishing. All Frontiers journals are driven by researchers for researchers; therefore, they constitute a service to the scholarly community. At the same time, the Frontiers Journal Series operates on a revolutionary invention, the tiered publishing system, initially addressing specific communities of scholars, and gradually climbing up to broader public understanding, thus serving the interests of the lay society, too.

Dedication to Quality

Each Frontiers article is a landmark of the highest quality, thanks to genuinely collaborative interactions between authors and review editors, who include some of the world's best academicians. Research must be certified by peers before entering a stream of knowledge that may eventually reach the public - and shape society; therefore, Frontiers only applies the most rigorous and unbiased reviews.
Frontiers revolutionizes research publishing by freely delivering the most outstanding research, evaluated with no bias from both the academic and social point of view. By applying the most advanced information technologies, Frontiers is catapulting scholarly publishing into a new generation.

What are Frontiers Research Topics?

Frontiers Research Topics are very popular trademarks of the Frontiers Journals Series: they are collections of at least ten articles, all centered on a particular subject. With their unique mix of varied contributions from Original Research to Review Articles, Frontiers Research Topics unify the most influential researchers, the latest key findings and historical advances in a hot research area! Find out more on how to host your own Frontiers Research Topic or contribute to one as an author by contacting the Frontiers Editorial Office: frontiersin.org/about/contact

CRANIAL PLACODES AND NEURAL CREST INTERACTIONS IN CRANIOFACIAL DEVELOPMENT

Topic Editors:
Jean-Pierre Saint-Jeannet, New York University, United States
Lisa Taneyhill, University of Maryland, College Park, United States
Patrick Blader, FR3743 Centre de Biologie Intégrative (CBI), France

Citation: Saint-Jeannet, J.-P., Taneyhill, L., Blader, P., eds. (2021). Cranial Placodes and Neural Crest Interactions in Craniofacial Development.
Lausanne: Frontiers Media SA. doi: 10.3389/978-2-88966-882-3

Table of Contents

frontiers in Physiology

EDITORIAL
published: 22 April 2021
doi: 10.3389/fphys.2021.681397

Editorial: Cranial Placodes and Neural Crest Interactions in Craniofacial Development

Jean-Pierre Saint-Jeannet[1]*, *Patrick Blader*[2]* and *Lisa A. Taneyhill*[3]*

[1] Department of Molecular Pathobiology, College of Dentistry, New York University, New York, NY, United States, [2] Unité de Biologie Moleculaire, Cellulaire et du Développement (MCD, UMR5077), Centre de Biologie Intégrative (CBI, FR 3743), Université de Toulouse, CNRS, UPS, Toulouse, France, [3] Department of Animal and Avian Sciences, University of Maryland, College Park, MD, United States

Keywords: neural crest, placodes, craniofacial, vertebrates, sensory ganglia, skeleton

Edited by:
Thimios Mitsiadis, University of Zurich, Switzerland

Reviewed by:
Paul Trainor, Stowers Institute for Medical Research, United States
Igor Adameyko, Karolinska Institutet (KI), Sweden

***Correspondence:**
Jean-Pierre Saint-Jeannet
jsj4@nyu.edu
Patrick Blader
patrick.blader@univ-tlse3.fr
Lisa A. Taneyhill
ltaney@umd.edu

Specialty section:
This article was submitted to Craniofacial Biology and Dental Research, a section of the journal Frontiers in Physiology

Received: *16 March 2021*
Accepted: *26 March 2021*
Published: *22 April 2021*

Citation:
Saint-Jeannet J-P, Blader P and Taneyhill LA (2021) Editorial: Cranial Placodes and Neural Crest Interactions in Craniofacial Development. Front. Physiol. 12:681397. doi: 10.3389/fphys.2021.681397

Editorial on the Research Topic

Cranial Placodes and Neural Crest Interactions in Craniofacial Development

The vertebrate head is characterized by a complex craniofacial skeleton and paired sensory organs. These structures are derived from two adjacent embryonic cell populations, the neural crest and cranial placodes. The neural crest contributes to the craniofacial skeleton and a subset of cranial ganglia, while cranial placodes form the anterior pituitary, optic lens, inner ear, olfactory epithelium and several cranial ganglia. Defects in cranial neural crest and placode development can cause a wide array of human congenital malformations ranging from craniofacial disorders to hormone imbalance and sensory deficits. Throughout head development, reciprocal interactions between neural crest and placode cells are essential to drive the coordinated morphogenesis of multiple craniofacial structures. For this Research Topic, we have collected 14 research articles and reviews, analyzing and discussing at the cellular, molecular and genetic levels the role of the neural crest and cranial placodes in craniofacial development, and the importance of their interactions to organize the orofacial complex.

Neural crest and placode cells are truly evolutionary marvels. Together, they build much of the peripheral nervous system and sense organs that reside in the vertebrate head. Notably, the intricate interactions that occur between these two cell types endow vertebrates with features that distinguish them from their invertebrate ancestors. Indeed, comparative studies between jawless and jawed vertebrates have revealed molecular signatures of neural crest and placode cells, shedding light on the gene products and developmental signaling pathways that are involved in mediating neural crest-placode cell interactions in these distinct vertebrate lineages. York et al. discusses the origin of, and associations between, neural crest and placode cells in the jawed vertebrate head. Here, the authors delineate the gene regulatory networks (GRNs) that control neural crest and placode cell development and highlight how the coordinated movement and coalescence of neural crest and placode cells during embryogenesis is essential to yield functional sensory structures such as the cranial ganglia. These findings are reviewed in the context of jawed and jawless vertebrates, the latter relying on seminal results obtained from lamprey and hagfish. Importantly, recent studies demonstrate both evolutionary conservation and differences between jawed and jawless vertebrates with respect to the assembly of the cranial ganglia from neural crest and placode cells, generating a testable model for how these critical cell types appeared and worked in concert in ancestral vertebrates to pattern the craniofacial apparatus.

At the end of gastrulation, neural crest and cranial placodes arise from a narrow domain of the embryonic ectoderm immediately adjacent to the prospective neural plate, the neural plate border.

In a pair of reviews, Thawani and Groves and Seal and Monsoro-Burq describe the major signaling molecules and transcription factors controlling the inductive and patterning events that elicit the development of these lineages at the neural plate border. Despite a growing understanding of the early GRN that controls the formation of the neural plate border during early embryonic stages, both reviews highlight important gaps in knowledge that will need to be resolved to understand how these two cell populations are established given their close proximity and similar developmental timeframe. The authors also consider outstanding questions in the field and how recent advances in transcriptomic analyses may help address these unresolved issues.

As discussed by Thawani and Groves and Seal and Monsoro-Burq, the neural plate border is defined by a unique signature of transcription factors among which Sox proteins are key players. Mutations in genes encoding SOX proteins have been linked to pathologies, often affecting multiple organ systems including the orofacial complex. Schock and LaBonne summarize the major classes of Sox factors and their role in the regulation of various aspects of neural crest development, including specification, multipotency retention, migration and differentiation. They highlight the importance of a subset of these genes in directing the development of neural crest- derived craniofacial structures through their unique ability to regulate craniofacial bone and cartilage formation, and drive palatogenesis, odontogenesis and salivary gland development. Finally they describe the clinical and molecular features of several SOXopathies, a group of rare multisystem developmental disorders. The prevalence of craniofacial defects in SOXopathies underscores the critical roles these factors have in the development and evolution of the vertebrate craniofacial complex.

In the last decade, modules of the neural crest GRN have been characterized in multiple organisms. This information has significantly improved our understanding of the mechanisms underlying the complex developmental trajectory of the neural crest. In their review, Chong-Morrison and Sauka-Spengler discuss recent advances in the characterization of the cranial neural crest GRN through state-of-the-art multi-omics approaches. They summarize how parallel considerations of transcriptome, interactome, and epigenome data sets have substantially refined the roles of the key players identified during the pre-omics era. They also discuss key questions that can now be addressed through a multi-omics approach and the development of new, unbiased functional genomics integration tools.

Neural crest cell migration is a process essential for the correct anatomical positioning of neural crest derivatives within the developing embryo. As highlighted in Barriga and Theveneau, neural crest cells employ a variety of different mechanisms, or "mixotaxis," to ensure successful migration. Using *Xenopus* cranial neural crest cells as an example, the authors discuss different strategies that may be used by neural crest cells to accomplish migration. These include chemotaxis, in which cells respond to a gradient of soluble guidance factors, or haptotaxis, in which the cue is a bound signal; durotaxis, whereby cells move from softer to stiffer substrates; ratchetaxis, in which migratory cells are confined to a local route due to the presence of physical and/or chemical barriers; and galvanotaxis, whereby electric fields can influence cell migration. It is important to note that, with the preceding types of migratory mechanisms, it is often challenging to obtain *in vivo* data to support their existence due to the complex nature of the environmental milieu in the embryo, which directly impacts the migratory capacity of neural crest cells.

The molecules that mediate the formation, migration and differentiation of neural crest and placode cells have been the subject of investigation by many groups. In this Research Topic, Manohar et al. and Mo et al. tackle the former in the neural crest, identifying roles for Cadherin-11 and Platelet-Derived Growth Factor Receptors (PDGFRa and PDGRFb), respectively. While Cadherin-11 function in *Xenopus* neural crest cells (migration) and cancer cells (proliferation, survival, and migration) has been well-documented, studies by Manohar et al. in the chick embryo reveal that Cadherin-11 acts during neural crest cell specification. Cadherin-11 is first expressed in the neural plate, and is maintained throughout the formed neural tube and later observed in migratory neural crest cells. Knockdown of Cadherin-11 reduces the number of premigratory cranial neural crest cells and negatively impacts neural crest cell survival, in part, through activation of p53-mediated apoptosis. Ultimately this influences neural crest cell migration, as fewer neural crest cells are available to migrate, and those that do migrate do so poorly due to the absence of filopodia and lamellipodia. Collectively, these data point to multiple functions for Cadherin-11 in the forming neural crest.

Mo et al. investigated the role of receptor tyrosine kinase signaling in murine craniofacial development by ablating both *PDGFRa* and *PDGFRb* from the cranial neural crest. Through these studies, a genetic interaction could be identified between the two receptors and, notably, the presence of additional conditional alleles exacerbated phenotypes exhibited by the mutants. These phenotypes included increased distance between the nasal pits, facial hemorrhaging, misshapen fore- and/or midbrain, facial blebbing, and facial clefting. Further experiments revealed that PDGRa regulates the size and shape of the cranial neural crest cell migratory stream, with PDGFRb only contributing minimally. Both receptors, however, augment neural crest cell proliferation earlier in development, while during mid-gestation, PDGFRb signaling predominates with respect to controlling the proliferation of the craniofacial neural crest-derived mesenchyme. Interestingly, neither receptor functions during mid-gestation to control the survival of the cranial neural crest-derived mesenchyme. Taken together, these data reveal the roles of each PDGFR in the cranial neural crest and, subsequently, craniofacial development.

Canonical Wnt signaling is especially critical for neural plate border formation and craniofacial morphogenesis, and dysregulation of Wnt signaling has been linked to several craniofacial syndromes. To gain insights into these pathologies, Hutchins et al. sought to identify novel downstream targets of canonical Wnt signaling. To this end, they performed RNA-seq on sorted chick cranial neural crest cells overexpressing Draxin, a potent Wnt antagonist, which also interferes with the cranial neural crest epithelial-mesenchymal transition (EMT).

The authors identified and validated a novel Wnt-responsive gene, RHOB, a member of the Rho GTP-binding protein family. Because RHOB is a known BMP-responsive gene in the trunk neural crest, by electroporation of a BMP reporter construct they confirmed the lack of active BMP signaling in cranial neural crest post-EMT, and demonstrated RHOB activation by expression of a stabilized form of b-catenin. These results highlight the importance of crosstalk between signaling pathways and axial level-specific interactions in the regulation of cranial neural crest development and craniofacial morphogenesis.

The complexity of the vertebrate head, containing as it does a wide variety of distinct neural crest and placodal derivatives, pleads for the importance of a multitude of specific molecular mechanisms in its development. In a genetic screen for regulators of craniofacial development, Dash et al. identified a mutant they named *snouty* that exhibits abnormalities of the facial prominences, cranial nerves and vasculature. Surprisingly, rather than affecting a gene involved specifically in craniofacial development, *snouty* codes for *Med23*, a subunit of the Mediator complex of proteins required for the transcriptional control of genes in all tissues. The allele isolated in the study represents a partial loss of *Med23* function that can be rescued, in part, by attenuating Wnt signaling. The results highlight the importance of undertaking forward genetic screens, even in systems such as the mouse. Furthermore, they reinforce the idea that so called housekeeping factors can have very specific developmental roles depending on the context.

Cranial neural crest cells express specific combinations of *Hox* genes based on their origin in the hindbrain. As they populate the pharyngeal arches (PA), neural crest cells respond to signals from the pharyngeal surface ectoderm and endoderm, which will determine their fate. Zhang et al. investigate the role of nested expression domains of *Hox* genes in the pharyngeal epithelium in the control of PA morphogenesis and differentiation. Transgenic mouse embryos with ectopic expression of Hoxb3 in the ectoderm pharyngeal epithelium of PA2 have multiple cranial nerve and skeletal defects. This phenotype correlates with a regionalized up-regulation of *Jag1* expression, a Notch ligand, in the ectoderm epithelium of PA2. The authors demonstrate through *in vivo* chromatin immunoprecipitation and *in vitro* luciferase reporter assays that Hoxb3 can directly bind to a cis-acting regulatory region at the *Jag1* locus to transactivate its expression. The work highlights the importance of pharyngeal epithelial and cranial neural crest cell interactions and the interplay between *Hox* genes and signaling molecules to promote PA and craniofacial development.

With the appearance of neural crest cells and placode cells in vertebrates, complex structures could be formed, such as the craniofacial skeleton, peripheral nerves, and paired sense organs. In his recent review, LaMantia posits that neural crest cells act as "inductive ambassadors" to promote the differentiation of craniofacial tissue and to serve as an initial conduit between the former and the brain. Neural crest-derived mesenchymal cells participate in interactions with epithelia and also directly supply signals to orchestrate tissue morphogenesis and differentiation. Using examples from normal embryogenesis (e.g., olfactory development) and various diseases possessing physical anomalies, cardiovascular defects and behavioral deficits (e.g., DiGeorge's Syndrome), data is put forth supporting the notion that the inductive cues provided by neural crest cells, along with neural crest-derived mesenchymal/epithelial interactions, are vital in driving tissue morphogenesis at sites outside of the face, such as the limbs and heart, and in forming proper neural circuits. Importantly, these studies have revealed signaling pathways and causative genes, the latter of which are expressed both in the brain and at sites of neural crest-derived mesenchymal/epithelial interactions in the developing embryo. Collectively, this review further underscores the intricate relationship and inherent cross-talk between the brain/neural tube, which initially possesses neural crest cells, and the face and other structures to which neural crest cells give rise.

The olfactory placodes form several cell types within the olfactory system such as gonadotropin releasing hormone-1 (GnRH-1) neurons, the first neuronal population present in the developing olfactory pit. However, the olfactory pit houses multiple neurons, including those expressing the transcription factor Islet1 (Isl1). To determine the role of Isl1 in GnRH development in the mouse, Taroc et al. document Isl1 expression, characterize the Isl1 lineage, and evaluate the phenotypes of GnRH neurons lacking Isl1. Isl1 is expressed in proliferating epithelial precursors that will give rise to neurons and later is noted in almost 90% of GnRH1-positive neurons in the olfactory pit. Lineage tracing of Isl1-expressing cells through the use of a tamoxifen inducible or constitutive *Cre* line results in the labeling of many different cell types. Finally, conditional knockout of *Isl1* in GnRH1 neurons revealed that Isl1 is not required for the migration of GnRH1 neurons nor expression of GnRH itself. In summary, these results raise the question as to the role of Isl1 in GnRH neuron development and point to the need for additional postnatal studies to shed light on Isl1 function.

Finally, Cheung et al. present the characterization of a rare cell type in the olfactory epithelium of the zebrafish. Olfactory rod cells display a prominent actin-rich projection at their apical surface. While not previously described in zebrafish, these cells have already been reported in other teleost but whether they represent artifacts of fixation has until now remained a possibility. In the present study, live imaging was used to verify the presence of an actin-rich rod unequivocally. Although the function of these rare cells remains a mystery, possibilities range from odor-sensing to a role in immunity, in a manner similar to brush or tuft cells described in mammals. Future studies will be needed to address these possibilities, and to determine the developmental origin of this intriguing cell type.

PERSPECTIVES

As illustrated by these contributions, cranial placode and neural crest cells are engaged in reciprocal interactions throughout their developmental history that influence their fate, behavior and ultimate differentiation. While much has been learned in the past decade on the importance of these interactions during vertebrate head development, it remains a burgeoning field. With the introduction of multi-omic and single cell analyses, the

next decade is expected to bring a wealth of new information on the development of these two cell types. One important challenge moving forward is to further refine the hierarchy of signaling molecules and downstream transcriptional regulators that form the basis of the placode and neural crest GRNs in order to understand how these adjacent cell populations are independently established at the neural plate border. It is especially critical to validate functionally the direct vs. indirect regulations among these factors. Another unresolved question relates to the molecular bases of placode and neural crest multipotency, a topic that is still under active debate. Through deployment of a wide array of signaling cues, placode and neural crest cells cross-regulate their respective migration and differentiation, but how these cells integrate inputs from multiple sources, both spatially and temporally, to build the craniofacial complex remains obscure and is essential to investigate. These are just a handful of questions and challenges that the craniofacial biology community will likely face in the upcoming years. We are extremely grateful to all the authors and reviewers who made this collection possible. We hope these articles will stimulate further interest and inspire young scientists to tackle some of these and other outstanding questions in the field.

AUTHOR CONTRIBUTIONS

All authors listed have made a substantial, direct and intellectual contribution to the work, and approved it for publication.

FUNDING

Work in the Saint-Jeannet lab was funded by NIH R01DE025806 and NIH R01DE025468. Work in the Blader lab was funded by the Agence National de la Recherche, ANR-16-CE13-0013-01. Work in the Taneyhill lab was funded by NIH R01DE024217, NIH R56DE028253, and NSF IOS-1947169.

Conflict of Interest: The authors declare that the research was conducted in the absence of any commercial or financial relationships that could be construed as a potential conflict of interest.

frontiers in Physiology

REVIEW
published: 13 August 2020
doi: 10.3389/fphys.2020.00986

Evolutionary and Developmental Associations of Neural Crest and Placodes in the Vertebrate Head: Insights From Jawless Vertebrates

*Joshua R. York[1], Tian Yuan[2] and David W. McCauley[1]**

[1]Department of Biology, University of Oklahoma, Norman, OK, United States, [2]Oklahoma Center for Neuroscience, University of Oklahoma Health Sciences Center, Oklahoma City, OK, United States

Neural crest and placodes are key innovations of the vertebrate clade. These cells arise within the dorsal ectoderm of all vertebrate embryos and have the developmental potential to form many of the morphological novelties within the vertebrate head. Each cell population has its own distinct developmental features and generates unique cell types. However, it is essential that neural crest and placodes associate together throughout embryonic development to coordinate the emergence of several features in the head, including almost all of the cranial peripheral sensory nervous system and organs of special sense. Despite the significance of this developmental feat, its evolutionary origins have remained unclear, owing largely to the fact that there has been little comparative (evolutionary) work done on this topic between the jawed vertebrates and cyclostomes—the jawless lampreys and hagfishes. In this review, we briefly summarize the developmental mechanisms and genetics of neural crest and placodes in both jawed and jawless vertebrates. We then discuss recent studies on the role of neural crest and placodes—and their developmental association—in the head of lamprey embryos, and how comparisons with jawed vertebrates can provide insights into the causes and consequences of this event in early vertebrate evolution.

Keywords: cyclostomes, lamprey, hagfish, CRISPR/Cas9, evo-devo

OPEN ACCESS

Edited by:
Lisa Taneyhill,
University of Maryland,
College Park, United States

Reviewed by:
Gerhard Schlosser,
National University of Ireland Galway, Ireland
Robert Cerny,
Charles University, Czechia

****Correspondence:***
David W. McCauley
dwmccauley@ou.edu

Specialty section:
This article was submitted to Embryonic and Developmental Physiology, a section of the journal Frontiers in Physiology

Received: *10 June 2020*
Accepted: *20 July 2020*
Published: *13 August 2020*

Citation:
York JR, Yuan T and McCauley DW (2020) Evolutionary and Developmental Associations of Neural Crest and Placodes in the Vertebrate Head: Insights From Jawless Vertebrates. Front. Physiol. 11:986. doi: 10.3389/fphys.2020.00986

INTRODUCTION

The vertebrate head is a complex tapestry of morphological features woven together during embryonic development from a varied array of specialized cell types. Although some of the features in the vertebrate head are derived from populations of cells that are evolutionarily ancient, and hence not unique to vertebrates (e.g., mesoderm and endoderm), there are two notable exceptions to this observation—the neural crest and placodes (Gans and Northcutt, 1983; Couly et al., 1993; Santagati and Rijli, 2003; Kuratani, 2008; Square et al., 2016b; Hall, 2018; Kuratani and Ahlberg, 2018; Cheung et al., 2019). Both neural crest cells and placodes are found only in vertebrate animals and they are responsible for constructing many of the traits that uniquely define the vertebrate clade (**Figure 1**), including the cartilage and bone of the head and jaw skeleton, neurons and glia of the peripheral sensory nervous system, colorful patterns of pigmentation, and much more (Green et al., 2015; Ziermann et al., 2018; Fish, 2019; Martik et al., 2019; Vandamme and Berx, 2019; York and McCauley, 2020b).

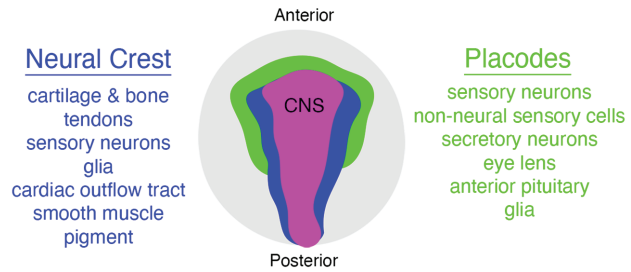

FIGURE 1 | Relationships between neural crest (blue), placode (green), and central nervous system (CNS; pink) populations in vertebrates, with some neural crest and placode derivatives listed on either side. Embryo is viewed from the dorsal aspect.

Given the developmental and evolutionary significance of neural crest and placodes, it should be no surprise that they have remained some of the most intensively studied and scrutinized populations of cells by vertebrate embryologists since their discovery over 150 years ago (His, 1868; Van Wijhe, 1883; Froriep, 1885; von Kupffer, 1891, 1893; Platt, 1894; Conel, 1942; Damas, 1943; Yntema, 1944). Most contemporary researchers in the fields of neural crest and placode "evo-devo" have directed their efforts and expertise toward the study of either neural crest or placodes in isolation, the inevitable result of specialization that characterizes modern scientific research. But it is important to recognize that the "origin story" of the vertebrates cannot be told from the perspective of either cell population alone. Rather, it was and is the intimate association of both neural crest and placodes in the head of vertebrate embryos that came to distinguish the vertebrates from their invertebrate chordate relatives, a point emphasized by Gans and Northcutt almost four decades ago (Gans and Northcutt, 1983; Northcutt and Gans, 1983). Thus, to understand the origin of the vertebrates is to understand how these cell populations became developmentally and evolutionarily coupled in our earliest vertebrate ancestors.

Here, we review the evolution of the developmental association of neural crest and placodes from the perspective of the jawless (cyclostome or "agnathan") vertebrate lineage. We describe shared and derived patterns of neural crest and placode development in these animals and compare them to well-studied examples from traditional jawed vertebrate model systems. We then focus on recent work describing the developmental association of neural crest and placodes in the head of jawless vertebrate embryos and how these studies, when placed within a comparative embryology framework, can provide important clues as to how the intimate relationship between these unique cell populations first evolved in early vertebrates.

DEVELOPMENT OF NEURAL CREST AND PLACODES IN JAWED VERTEBRATES

The jawed, or gnathostome, vertebrates are a monophyletic group that includes representatives of all but two extant lineages of vertebrate animals that diversified from a common ancestor nearly 475 million years ago (Brazeau and Friedman, 2015; Nelson et al., 2016). Jawed vertebrates are comprised of groups such as aquatic "fishes" (quotations denote a paraphyletic assemblage), as well as "amphibians," "reptiles," birds, and mammals that share traits including articulated jaws with teeth, paired fins, and paired nasal openings (diplorhiny), among others (Brazeau and Friedman, 2014, 2015). Much of our understanding of the development and evolution of neural crest and placodes has been informed by "traditional" model systems belonging to the jawed vertebrate lineage (e.g., mouse, *Xenopus*, and zebrafish). This is due in part to convenience as many jawed vertebrate models are relatively easy to obtain and rear in standard laboratory conditions, have publicly available and well-annotated genomes and transcriptomes, and are amenable either to the propagation of stable genetic lines and/or modern genome editing, and high-throughput molecular techniques. Below, we describe briefly the developmental mechanisms and genetic control of neural crest and placode development in jawed vertebrates.

Neural Crest

The neural crest is a migratory, embryonic stem cell population that gives rise to diverse tissues and structures throughout the vertebrate head and trunk, including much of the cartilage and bone of the craniofacial skeleton, melanocytes, many of the sensory neurons and glia of the peripheral nervous system, endocrine cells, as well as tooth and heart primordia (**Figure 1**; Le Douarin and Kalcheim, 1999; Hall, 2008; Trainor, 2013; York and McCauley, 2020b). Moreover, it has been shown recently that the trunk skeletal tissue in extant cartilaginous fishes such as sharks is also derived from neural crest cells, a feature likely homologous to the body armor of long-extinct fishes such as the "ostracoderms" and "placoderms" (Gillis et al., 2017).

Neural crest cells arise in the neural plate border, a region positioned between the medial neural plate (presumptive central nervous system, CNS) and lateral non-neural ectoderm (comprised of presumptive placodes and epidermis; Le Douarin and Kalcheim, 1999; Hall, 2008; Trainor, 2013). During neurulation, the neural plate borders elevate and fuse at the dorsal midline (i.e., the "crest") of the neural tube (His, 1868; Le Douarin and Kalcheim, 1999; Hall, 2008; Trainor, 2013). Soon thereafter, these cells delaminate from the neural tube, undergo an epithelial-to-mesenchyme transition (EMT), and then embark on long-distance migrations throughout the head and trunk. In the head, cranial neural crest cells typically migrate in streams of aggregated cells, whereas trunk neural crest cells often migrate as individual cells or small groups of cells (Vega-Lopez et al., 2017; Szabó and Mayor, 2018; Li et al., 2019; Goldberg et al., 2020). After tracking along specific routes throughout the embryo, which are shaped in large part by cell-cell guidance systems, neural crest cells finally reach their destination and differentiate into a specific cell type.

As with any other process in the embryo, neural crest development proceeds by the activities of a gene regulatory network (GRN), a complex and organized set of genetic interactions

and intercellular signaling pathways that progressively define the regulatory state of these cells from their earliest stages in the neural plate border to their differentiation into cartilage, bone, neurons, and pigment (Bronner, 2014; Simões-Costa and Bronner, 2015; Williams et al., 2019). The neural crest GRN is a spatial and temporal continuum of gene regulatory interactions from start to finish, and cannot therefore, be broken down into completely separable units for each stage of development. We can, however, recognize and study unique GRN "subcircuits"—a set of common gene regulatory interactions that govern similar mechanisms of neural crest development across highly divergent groups (e.g., mouse and fish; Meulemans and Bronner-Fraser, 2004; Sauka-Spengler et al., 2007; Simões-Costa and Bronner, 2015; Hockman et al., 2019; Parker et al., 2019).

The first of these GRN subcircuits is involved in neural crest induction. This is controlled by intercellular signaling systems that are evolutionarily conserved across metazoans, including members of the *Bmp*, *Wnt*, *Fgf*, and *Delta-Notch* families (Milet and Monsoro-Burq, 2012; Simões-Costa and Bronner, 2015). These signaling systems are activated in the neural plate, mesoderm and non-neural ectoderm, and converge on regulatory targets in the neural plate border, such as *Pax3/7*, *Msx1/2*, *Zic1/2*, and *Prdm1* (Milet and Monsoro-Burq, 2012; Pla and Monsoro-Burq, 2018). These so-called neural plate border specifiers in turn regulate expression of neural crest specifiers in the dorsal neural tube (*SoxE*-family, *FoxD3*, *Tfap2a*, *Myc*, *Twist*, *Snai1*/*Snai2*, *Id*, and *EdnrB*), which endow the neural crest with a distinct "molecular anatomy" that enables these cells to detach from the neural tube, undergo EMT and migrate, and generate specific precursors (Martik and Bronner, 2017; Lukoseviciute et al., 2018; Ling and Sauka-Spengler, 2019; Soldatov et al., 2019; Rothstein and Simões-Costa, 2020). Neural crest cell differentiation involves the deployment of gene batteries such as *Sox9*, *Sox5/6*, and *Col2a1* for cartilage, *Sox10*, *Mitf*, and *Tyr* for melanocytes, and *Phox2*, *Ascl*, and *Hand2* for sympathetic neurons (Simões-Costa and Bronner, 2015).

Placodes

Placodes arise as localized thickenings of ectoderm that in turn give rise to cells that make up many of the sensory components in the vertebrate head, such as cranial ganglia and organs of special sense (**Figure 1**; Schlosser, 2005, 2006, 2010; Patthey et al., 2014). Although there are slight variations across different jawed vertebrate groups, cranial placodes can be categorized broadly into adenohypophyseal, olfactory, lens, trigeminal (ophthalmic = V1, maxillary = V2, and mandibular = V3 divisions), epibranchial, and lateral line placodes (Schlosser and Northcutt, 2000; Xu et al., 2008; Patthey et al., 2014; Piotrowski and Baker, 2014). All of these, with the exception of the adenohypophyseal and lens placodes, produce various types of sensory and/or secretory cells (Schlosser and Ahrens, 2004; Schlosser, 2006, 2010). In addition to variation in the number and/or types of placodes present in different lineages, some placodes have been lost during evolution, such as that of the lateral line placodes eliminated in amniotes during the water-to-land transition (Schlosser, 2005; Washausen and Knabe, 2018).

Placodes arise in the non-neural ectoderm just lateral to the neural plate border, a region known as the pre-placodal ectoderm (PPE; Saint-Jeannet and Moody, 2014; Moody and LaMantia, 2015). The PPE is shaped like a horse-shoe, which wraps peripherally around the anterior neural plate and neural plate border and subsequently fractures into smaller clusters that represent the progenitors of each placode (Saint-Jeannet and Moody, 2014; Moody and LaMantia, 2015). These progenitors will then undergo invagination and/or delamination before differentiating into various types of sensory cells.

The GRN controlling placode developmental in jawed vertebrates has been less intensively studied than that of neural crest cells, but there are still several important conclusions that can be drawn. Induction of the PPE occurs by some of the same intercellular signaling systems that induce neural crest cells (e.g., *Fgf*, *Bmp*, *Wnt*, and retinoic acid; Baker and Bronner-Fraser, 2001; Lassiter et al., 2014; Singh and Groves, 2016). Placode specification occurs *via Six* and *Eya* (*Six1*, *Six4*, *Eya1*, and *Eya2*) factors, which can be viewed as "master regulators" of placode development, in the sense that they are some of the earliest expressed genes in the PPE, they are often continually expressed throughout development in most placodes, and they are functionally required for placode formation in numerous contexts (Sullivan et al., 2019). For example, in *Xenopus*, several transcriptional regulators of neural crest and placode development expressed in the neural (*Pax3*, *Hairy2b*, and *Zic1*) and non-neural (*Tfap2a*, *Msx1*, *Dlx3*) ectoderm are themselves regulated by *Six1* and *Eya1* (Maharana and Schlosser, 2018). Recent transcriptomic analyses have identified hundreds of putative regulatory targets of *Six1* and *Eya1*, including those involved in production of neural progenitors, such as *Sox2* and *Hes8*, and in sensory cell/neural differentiation *via Ngn1* and *Atoh1* (Riddiford and Schlosser, 2016). Additionally, a handful of transcription factors that are important in development of the ectoderm generally, and neural crest specifically, also have overlapping functions in early placode development (e.g., *Dlx*, *Msx*, *Pax*, *Zic* families, *Tfap2a*, *Gata*, and *Foxi*). Of these, there is evidence that a "*Pax* code" involving *Pax6*, *Pax3/7*, and *Pax2/5/8* may pattern placodes along the anterior-posterior axis (Mansouri et al., 1996; Dahl et al., 1997; Baker and Bronner-Fraser, 2000; Modrell et al., 2014). Finally, cell type differentiation of placodes requires the activity of transcription factors known to regulate neural and sensory cell differentiation in deuterostomes and bilaterians, including homologs of *atonal* (*Ath1* or *Math1* in mouse) and *achaete-scute* (*Ash1* or *Mash1* in mouse), as well as *NeuroD*, *Islet1*, *Phox2a*, *Phox2b*, *Brn3a*, and *Brn3c* (Schlosser, 2006).

INTERACTIONS OF NEURAL CREST AND PLACODES IN THE JAWED VERTEBRATE HEAD

Neural crest and placodes are both vertebrate novelties, but they are also distinct in several ways. Perhaps the most obvious difference is that neural crest cells are capable of generating both ectomesenchyme (e.g., cartilage and bone) and non-ectomesenchyme (e.g., neurons, glia, pigment, and secretory cells), and form

throughout the head and trunk. Placodes, by contrast, can only give rise to non-ectomesenchyme and arise exclusively in the head (Baker and Bronner-Fraser, 1997, 2001; Patthey et al., 2014). Another key difference is that whereas EMT and migration are a *sine qua non* of neural crest development, placodes may instead simply invaginate (e.g., lens, adenohypophyseal, and otic placodes) without migrating far from their site of origin (Schlosser, 2002, 2006, 2010). Finally, although they develop as adjacent cell populations in the ectoderm, neural crest and placodes in most jawed vertebrates, with a few notable exceptions, have relatively divergent GRNs that orchestrate their development, even though they likely share a common evolutionary origin (Grocott et al., 2012; Moody and LaMantia, 2015; Riddiford and Schlosser, 2016; Maharana et al., 2017; Martik and Bronner, 2017; Plouhinec et al., 2017; Horie et al., 2018; Maharana and Schlosser, 2018; Streit, 2018).

Despite these differences, there is a crucial, but often neglected aspect shared by both neural crest and placodes when discussing the issue of vertebrate origins: these cells work together during development to coordinately generate important structures in the vertebrate head (Grocott et al., 2012; Steventon et al., 2014). The clearest example of this is the creation of the paired sensory ganglia of the cranial peripheral nervous system—structures that are thought to have enabled the transition from passive filter feeding to active predation in early vertebrates (**Figure 2**; Gans and Northcutt, 1983; Northcutt and Gans, 1983; Northcutt, 2005). Several cranial sensory ganglia are a mosaic of neural crest and placodes, and both cell types must not only be organized together into morphologically and functionally coherent structures, but these structures must in turn form and maintain appropriate connections with the embryonic CNS (**Figure 2**). For example, placode-derived and neural crest-derived cells in amniotes contribute to distinct proximal and distal components, respectively, of the facial (VII), glossopharyngeal (IX), and vagus (X) nerves (**Figure 2**; D'Amico-Martel and Noden, 1983; Barlow, 2002; Steventon et al., 2014). In the trigeminal ganglion placodes generate sensory neurons mostly within the distal aspect, whereas neural crest cells produce neurons within the proximal aspect and glia in both aspects (Hamburger, 1961; Lwigale, 2001).

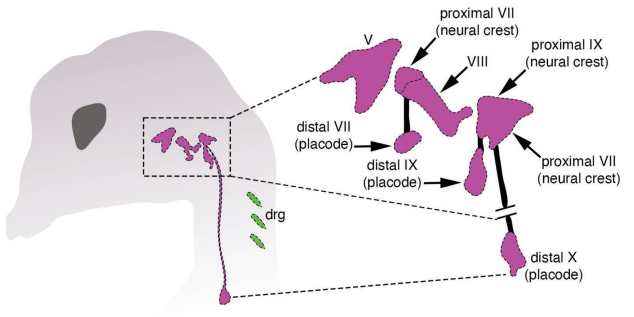

FIGURE 2 | Organization of cranial sensory ganglia in a jawed vertebrate (chicken). Cranial ganglia are pink and dorsal root sensory ganglia (drg) are green. The image on the right shows the distinct proximal and distal ganglion compartments that are formed by neural crest and placodes, respectively, modified from Barlow (2002).

Throughout vertebrate craniofacial development, neural crest and placodes are physically associated, and their mutual interactions coordinate the formation of cranial sensory ganglia (Steventon et al., 2014). During early development, placodes delaminate and migrate slightly earlier than neural crest cells. In cases where both cell populations contribute to ganglia (e.g., epibranchial), earlier-migrating placode cells are usually followed closely behind by cranial neural crest, whereas other placodes, such as the otic, may act as barriers that shape the migratory paths of cranial neural crest originating from the hindbrain *en route* to the pharyngeal arches (Steventon et al., 2014). Although not all cranial neural crest cells contribute to cranial ganglia, there is evidence that they may physically segregate and individuate placode-derived ganglionic clusters during migration, a phenomenon which may be reciprocated by placodes to enable the formation of neural crest streaming in the head (Theveneau et al., 2013; Szabó et al., 2019). These types of intercellular interactions can occur quite early in development, with neural crest and placodes each appearing to be required for the other to undergo migration and morphogenesis of craniofacial structures in a "chase-and-run" model whereby early migrating placodes chemoattract (*via Sdf*) trailing neural crest cells that express the corresponding receptor (*CXCR4*; Theveneau et al., 2010, 2013). Upon physical contact, the neural crest cell then repels the placode cell away. These repeated sets of interactions are thought to bring about the proper migration and shaping of each cell population into ganglia (Steventon et al., 2014).

The close developmental association of neural crest and placodes continues throughout vertebrate craniofacial development, with both modern and classical embryological experiments demonstrating an interdependence of the two populations for proper patterning of the cranial PNS (Steventon et al., 2014). In many of these studies, ablation of the neural crest did not lead to an obvious loss of cranial ganglia *per se*, but rather inappropriate positioning and morphology of the ganglion concomitant with abnormal or absent projections to the CNS (Yntema, 1944; Begbie and Graham, 2001). Additionally, development of distal ganglia can occur in absence of the proximal components (Kuratani et al., 1991). Genetic ablation of the neural crest or perturbation of proper neural crest migration can lead to inappropriate fusions of otherwise physically separated ganglia (Gassmann et al., 1995; Golding et al., 2004; Osborne et al., 2005; Schwarz et al., 2008). Finally, there is evidence that cranial neural crest cells actively form "corridors" that actually guide the migration and orchestrate patterning of sensory neurons derived from placodes (Freter et al., 2013). These results all point to an important role in the interaction of neural crest and placodes to form cranial sensory ganglia in the head of jawed vertebrates.

CYCLOSTOMES AND THE EVOLUTIONARY ANALYSIS OF NEURAL CREST AND PLACODES

The accurate reconstruction of ancestral vertebrate conditions, including the developmental association of neural crest and placodes in the vertebrate head, requires the careful choice of study systems within a comparative (evolutionary) framework.

Embryological studies of model systems from the jawed vertebrate lineage, no matter how carefully or elegantly done, tell us little about ancestral conditions. To do that requires that we compare developmental mechanisms *between* the two major lineages of vertebrates—the jawed and jawless clades—as well as a suitable outgroup, such as the invertebrate chordates. It is this simple but powerfully informative methodology that allows us to infer how developmental associations between neural crest and placodes evolved in the last common ancestor of vertebrates (Shimeld and Donoghue, 2012; York and McCauley, 2020a).

The extant jawless vertebrates, also known as the cyclostomes (**Figure 3**), are a monophyletic group of animals, and are the sole survivors of a diverse assemblage of jawless fishes that were among the first of their kind to evolve on this planet over 500 million years ago (Hardisty, 1979; Heimberg et al., 2010; Miyashita et al., 2019; York and McCauley, 2020a). They are represented by only two extant groups, the lampreys and hagfishes, which diverged from one another not too long after the cyclostome-gnathostome split. The importance of cyclostomes in understanding vertebrate origins resides in their phylogenetic position as the closest living relatives (i.e., sister group) of the jawed vertebrates (Heimberg et al., 2010). This means that developmental comparisons between jawed and jawless vertebrates allow us, in essence, to work backwards in time and infer how neural crest and placodes became associated in the embryonic head of our vertebrate ancestors, and how subsequent vertebrate lineages elaborated upon these ancestral conditions.

DEVELOPMENT OF LAMPREY NEURAL CREST AND PLACODES

For those interested in comparative vertebrate embryology, lampreys have been the cyclostome study system of choice for quite some time (Green and Bronner, 2014; McCauley et al., 2015; York et al., 2019a). This owes largely to the fact that lamprey adults and their embryos are relatively easy to obtain and rear in simple laboratory settings, at least compared to hagfish (York et al., 2019a; described below). Moreover, accessibility to annotated genomes and transcriptomes, as well as the application of modern molecular genetic techniques such as cell lineage tracing, overexpression of DNAs and RNAs, and knockdown/knockout experiments such as morpholinos and CRISPR/Cas9 genome editing has allowed researchers to address long-standing hypotheses concerning the origin and evolution of vertebrate traits, including neural crest and placodes (McCauley and Bronner-Fraser, 2006; Smith et al., 2013, 2018; Parker et al., 2014; Square et al., 2015; Zu et al., 2016; Hockman et al., 2019; York et al., 2019a; York and McCauley, 2020a).

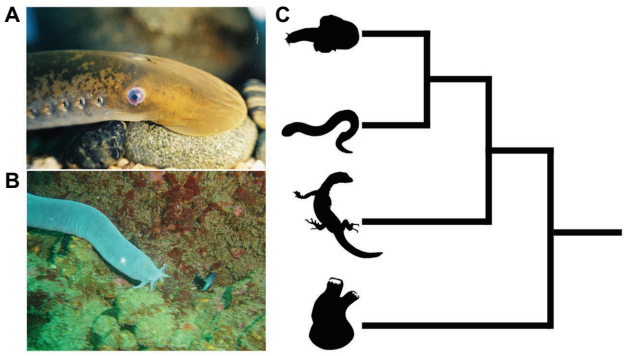

FIGURE 3 | Lampreys **(A)** and hagfish **(B)** are the only extant jawless vertebrates. **(C)** Phylogenetic tree showing relationships among vertebrates and invertebrate chordates. Hagfish and lamprey are on top forming the jawless cyclostome clade, with the jawed vertebrates below. The closest living relatives to the vertebrates are the tunicates, a lineage of invertebrate chordates (bottom). Images from panels **(A)** and **(B)** were used with permission from Wikipedia Commons.

Neural Crest

Lampreys, like all other vertebrates, have bona fide neural crest cells. They first arise in the neural plate border and are then brought by neurulation to the dorsal neural tube. From there, they delaminate and undergo an EMT before migrating throughout the head and trunk, where they will eventually reach their target destinations and help generate many morphological features shared with the jawed vertebrates, including a cartilaginous head skeleton, sensory neurons and glia of the peripheral nervous system, and melanocytes (Newth, 1950, 1951, 1956; Nyut, 1955; Langille and Hall, 1988; Horigome et al., 1999; McCauley and Bronner-Fraser, 2003). However, lampreys also lack several of the neural crest-derived structures found in their jawed vertebrate relatives. Included among these are jaws, the myelin sheath surrounding neurons, and sympathetic chain ganglia (Bullock et al., 1984; Shigetani et al., 2002; Häming et al., 2011; Green and Bronner, 2014; Yuan et al., 2018).

The genetic control of neural crest development in lampreys is also very similar to that of jawed vertebrates. The total set of genetic interactions that unfold during neural crest embryogenesis in lampreys, like other vertebrates, is structured into a GRN. This GRN can be broken down into "subcircuits" that direct control of neural crest induction (*Wnt*, *Delta-Notch*, and *Bmp* signaling), establishment of the neural plate border (expression of *DlxB*, *Pax3/7*, *MsxA*, *ZicA*, and *Prdm1*), as well as specification and migration from the dorsal neural tube (expression of *Snail*, *SoxE1*, *SoxE2*, *Id*, *EdnrB*, *Myc*, *Tfap2a*, *Sip1/Zeb2*, *Zeb1*, *type II cadherins*, and many of the neural plate border specifiers; Meulemans and Bronner-Fraser, 2002; Meulemans et al., 2003; Sauka-Spengler et al., 2007; Sauka-Spengler and Bronner-Fraser, 2008; Lakiza et al., 2011; Nikitina et al., 2011; Square et al., 2016a; York et al., 2017). These similarities extend beyond expression patterns. Studies involving gene knockdown/knockout, enhancer analysis, and chromatin profiling have revealed that many of the regulatory interactions at multiple tiers in the neural crest GRN are also shared between lampreys and jawed vertebrates (Sauka-Spengler et al., 2007; Nikitina et al., 2008; Lakiza et al., 2011; York et al., 2017, 2018, 2019b; Hockman et al., 2019; Parker et al., 2019; Yuan et al., 2020). There is also evidence that the production of several neural crest cell types shared between lampreys and jawed vertebrates relies upon a common gene regulatory logic. For example, both groups deploy *Fgf* signaling and *SoxE*-group

genes for production of cartilage and melanocytes, and *Phox2* in precursors of neural crest-derived enteric neurons (McCauley and Bronner-Fraser, 2006; Cattell et al., 2011; Lakiza et al., 2011; Jandzik et al., 2014; Green et al., 2017).

Placodes

Compared to the study of neural crest cells, the body of work on placode development in lampreys has been rather limited. Until recently, almost all of our understanding of placode biology in this group had been limited to a handful of papers describing gene expression patterns, histology, and comparative anatomy. In general, lampreys have homologs of many of the same placodes and placode-derived structures as present in jawed vertebrates, including, olfactory, adenohypophyseal, lens, trigeminal, otic, epibranchial, and lateral line (McCauley and Bronner-Fraser, 2002, 2003; Modrell et al., 2014). There are a few differences between lampreys and jawed vertebrates as well. For example, whereas in jawed vertebrates, the olfactory and adenohypophyseal placodes originate as separate primordia, lampreys have a singular nasohypophyseal placode that forms in the anterior-ventral midline of the head. The fused adenohypophyseal placode in lampreys produces the monorhine state of jawless vertebrates compared to that of diplorhiny in jawed vertebrates, and its separation into separate primordia may have precipitated the evolution of articulated jaws in gnathostomes (Murakami et al., 2001; Oisi et al., 2013b). Another difference, revealed by fate-mapping experiments, was that the separate upper lip and lower lip (velum) innervation patterns by neurons of trigeminal maxillomandibular (mmV) origin in the lamprey mouth may result from these placodes arising as distinct primordia early in development (Modrell et al., 2014).

The developmental mechanisms underlying formation of the PPE in lampreys are almost entirely unknown, with the exception of *DlxB* expression uniquely defining this region, along with overlapping expression of *MsxA* and *Tfap2a*, among others (Sauka-Spengler et al., 2007). It is unknown if the placode specification factors *Six1/2* and *Eya* are expressed in the lamprey PPE, making basic comparisons of early placode development between jawed and jawless vertebrates difficult. Similarly, almost nothing is known regarding the early delamination and migration patterns of placodes in lampreys and how this relates to early neural crest migration.

In terms of functional genetics, knockdown or knockout of early placode specification factors such as *Six*, *Eya*, and *Dlx* have not been performed in lampreys. Again, this leaves considerable uncertainty surrounding the conservation and divergence of gene regulatory interactions orchestrating placode development across vertebrates. Recent work on *Snail* has revealed an early role for this transcription factor during placode development in lamprey. It was found that a single *Snail* ortholog in lamprey was expressed simultaneously in the neural plate border and PPE (York et al., 2019b). There is also evidence that *Snail* is essential for early placode development because CRISPR/Cas9 knockout of *Snail* leads to near-total loss of *DlxB* expression in the pre-placodal domain, with subsequent elimination of placode-derived elements of cranial sensory ganglia that express *Six1/2*, *Pax3/7*, and *Phox2* (York et al., 2019b).

Later during lamprey craniofacial development, the combinatorial expression of several placode markers suggests a high degree of evolutionary conservation across vertebrates. For example, like jawed vertebrates, lamprey placode derivatives express multiple *Pax* genes in the form of a "*Pax* code" along the anterior-posterior axis, with orthologs of *Pax6* expressed in the lens, olfactory, and nasohypophyseal placodes, *Pax3/7* expressed in the ophthalmic division of the trigeminal placode, and *Pax2/5/8* expressed in otic, posterior lateral line, and epibranchial placodes (Murakami et al., 2001; McCauley and Bronner-Fraser, 2002; Modrell et al., 2014). Combinatorial expression of *Dlx* cognates is observed in some placodes as well with *DlxA*, *DlxB*, and *DlxC* in the otic vesicle and *DlxA*, *DlxC*, and *DlxD* in the nasohypophyseal placode (Cerny et al., 2010; Kuraku et al., 2010). Similar to that described in multiple jawed vertebrate model systems, lampreys express orthologs of *Six1/2* in the otic vesicle, posterior lateral line, and epibranchial placodes and *Phox2* in epibranchial ganglia, which are presumably derived in part from placodes (Häming et al., 2011; Green et al., 2017; Hockman et al., 2017; York et al., 2019b).

DEVELOPMENT OF HAGFISH NEURAL CREST AND PLACODES

Compared to lampreys, hagfishes are much more difficult to work with, especially within the context of comparative embryology. Hagfishes live in relatively deep waters and have an obscure reproductive physiology. Moreover, work from the past 100 years has shown that it is no simple matter to culture them in the laboratory (Holland, 2007; Ota and Kuratani, 2008). Consequently, much of our knowledge of hagfish embryology has historically been limited to descriptive embryology. Although advances in laboratory culture methods have enabled a critical re-examination of hagfish development, the unusually slow development of hagfishes has restricted molecular analysis of hagfish embryology to routine gene expression analysis by *in situ* hybridization. Work over the past several decades has revealed that hagfish have neural crest cells and placodes as other vertebrates do and that the developmental mechanisms and regulatory gene expression patterns are reminiscent of what has been described in lampreys and jawed vertebrates (Ota et al., 2007; Kuratani and Ota, 2008).

Neural Crest

Early investigations into hagfish embryology raised doubts concerning whether or not the development of neural crest cells in these animals was similar to that described in other vertebrates. For example, Conel (1942) suggested that the hagfish neural crest may arise as epithelial pouches that did not delaminate and migrate as mesenchyme, a result which, if confirmed, would suggest a very different route taken by hagfish in the development of this important cell population (Conel, 1942; Ota et al., 2007; Kuratani and Ota, 2008). The matter was settled in 2007 when a report described neural crest development in hagfish as being more or less identical to that described in other vertebrates. Hagfish neural crest cells arise

in the dorsal neural tube, express a common suite of neural crest regulatory genes (e.g., *SoxE* and *Pax3/7*), and delaminate and migrate throughout the head and trunk (Ota et al., 2007). Hagfish also share with other vertebrates structures which are presumably derived from neural crest cells, including elements of the cartilaginous head skeleton and cranial sensory and dorsal root ganglia (Wicht and Northcutt, 1995; Braun and Northcutt, 1997; Zhang and Cohn, 2006; Ota et al., 2007; Oisi et al., 2013a). However, despite the overall similarity in neural crest development between hagfish and other vertebrates, there is still much to be learned, an issue that will be difficult to overcome because of the lengthy and complicated development of these animals. Standard techniques in the developmental biologist's toolkit, including long-term cell lineage tracing and gene knockdown/knockout, are not feasible and this obviously limits the scope of investigation into the developmental genetics of hagfish neural crest and placodes (see below).

Placodes

Descriptive embryology of the hagfish head has suggested that there are several cranial placode primordia, including, among others, those of epibranchial, otic, trigeminal, lens, and lateral line origin, as well as a singular adenohypophyseal placode as observed in lampreys (Wicht and Northcutt, 1995; Braun and Northcutt, 1997; Wicht and Tusch, 1998; Oisi et al., 2013b). The placode primordia in hagfishes seemingly form as a contiguous, horseshoe-shaped PPE that encompasses the domains from which peripheral cranial nerves will emerge, although it is difficult to say if individual placodes can be observed in isolation early in development as in gnathostomes (Schlosser, 2005, 2017; Ota and Kuratani, 2007; Oisi et al., 2013b). Sensory innervation by some placodes has been described for the trigeminal, facial, glossopharyngeal, and vagus nerves, although there are some differences between Eptatretid and Myxinid lineages (von Kupffer, 1900; Wicht and Northcutt, 1995; Braun and Northcutt, 1997; Ota and Kuratani, 2007; Baker et al., 2008). Molecular analyses have revealed that some cranial placodes in hagfishes express a suite of transcription factors and signaling molecules similar to that of both jawed vertebrates and lampreys, including expression of *Sox9* in the otic vesicle, and combined expression of *EbFgf8/17*, *EbSoxB1*, *EbPitxA*, and *EbLhx3/4A* in the nasohypophyseal region (Ota et al., 2007; Oisi et al., 2013b).

INTERACTION OF NEURAL CREST AND PLACODES IN CYCLOSTOMES

Studies over the past several decades have found that neural crest cells and placodes in cyclostomes follow—with a few notable exceptions—a fairly typical course of development for vertebrates. Although we are now starting to get a deeper understanding of how neural crest and placodes develop in cyclostomes, it has remained unclear how these cells associate together within the embryonic cyclostome head to generate novel features such as cranial sensory ganglia (**Figure 4**) and how this compares to what we know about similar processes in jawed vertebrates. In this section, we discuss recent work

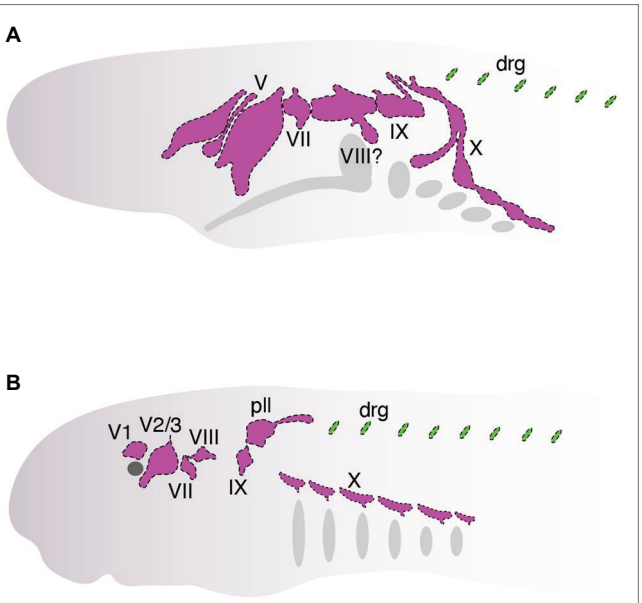

FIGURE 4 | Organization of cranial sensory ganglia in hagfish (**A**, ~between stages. E. VIII and E. IX, modified from von Kupffer, 1900) and lamprey (**B**, Tahara stage 26, modified from Yuan et al., 2020). Cranial ganglia are colored pink and dorsal root ganglia are colored green. Ganglia are shown that can be homologized with those in jawed vertebrates **(Figure 2)**.

that has begun to shed light on the matter specifically as it relates to the development of the cranial sensory ganglia in these animals (**Figure 4**). As noted above, in-depth cell lineage tracing and functional genetic analysis of neural crest and placodes is, for the most part, not feasible in hagfish. Consequently, almost all of our current understanding of neural crest and placode associations during cyclostome craniofacial development has come from data obtained from lampreys, given the relative ease with which their adults and embryos may be obtained and experimentally manipulated.

Cell lineage tracing by injection of vital lipophilic fluorescent dyes (DiI, DiO) has been a simple but powerful tool used in the lamprey embryological community for studying the origin, migration, and contributions of neural crest cells and placodes during development (Horigome et al., 1999; McCauley and Bronner-Fraser, 2003; Martin et al., 2009; Häming et al., 2011; Green et al., 2017). One early study by McCauley and Bronner-Fraser traced the contributions of neural crest cells to the lamprey head (McCauley and Bronner-Fraser, 2003). They found that DiI-labeled neural crest cells in the dorsal neural tube migrated in patterns similar to that of jawed vertebrates (McCauley and Bronner-Fraser, 2003). They observed cells migrating along dorsal-lateral and ventral pathways in the embryonic head and that colonized tissues that give rise to the oral and pharyngeal skeleton, as described in other vertebrates. The authors also revealed that lamprey cranial neural crest cells, particularly in the hindbrain, show very little restraint in their migration along the anterior-posterior axis, with cells often migrating far rostrally and/or caudally from their origin. Although the significance of this has remained

unclear, one possibility is that hindbrain neural crest cells are free to colonize any one of the posterior pharyngeal arches because many of the cartilage elements in this region are almost identical along the anterior-posterior axis.

In addition to the head skeleton, which is almost entirely derived from cranial neural crest cells, it was found that neural crest cells also appeared to contribute to a subset of cranial sensory ganglia, which are derived uniquely from both neural crest and placodes. DiI-labeled neural crest cells were observed to colonize the ophthalmic and maxillomandibular lobes of the trigeminal ganglion and posterior lateral line ganglion (McCauley and Bronner-Fraser, 2003). Importantly, however, DiI experiments and immunostaining with a mouse *Sox10* antibody revealed that these neural crest cells seemingly surrounded—but were excluded from—the main core of each ganglion. This is unlike the condition in jawed vertebrates in which *Sox10*-positive neural crest cells colonize the core of several cranial sensory ganglia, where they give rise to cells of glial and/or neural origin. This peculiar feature of lamprey cranial ganglion development raised some important evolutionary questions. What is the functional role of neural crest cells in and their precise contributions to the development of a key vertebrate structure such as cranial sensory ganglia? How do these contributions compare to that of another vertebrate innovation, cranial placodes, and how do these cell populations interact together during head development to drive the formation of cranial sensory ganglia?

Partial answers to these questions have been provided recently by studies examining the roles of both neural crest and placodes during the development of cranial sensory ganglia in lampreys. Fate mapping of lamprey cranial ganglia by Modrell et al. (2014) has provided key insights into the relative contributions of neural crest and placode populations to these structures in jawless vertebrates (Modrell et al., 2014). Using a combination of immunohistochemistry and DiI labeling, Modrell et al. (2014) made some important observations. First, they found that placode-labeled cells in the ectoderm were internalized and eventually differentiated into neurons occupying the core of cranial ganglia, a result consistent with that described in jawed vertebrates. Second, they found that the cranial sensory ganglia of lampreys, unlike like that first described by McCauley and Bronner-Fraser, did indeed contain a complement of both neural crest and placodes, another result quite similar to that of jawed vertebrates. This discrepancy is likely related to the fact that the labeling experiments performed by Modrell et al. (2014) were done very early in development and they may have therefore labeled some of the early-delaminating placodes that could have been missed from earlier experiments. Somewhat surprisingly, however, the neural crest cells that colonized cranial ganglia never seemed to express genetic markers characteristic of differentiated neurons and were therefore considered to be of potential glial origin. Thus, unlike the case in jawed vertebrates, neural crest cells in lamprey did not seem to be a major contributor of sensory neurons to cranial ganglia, raising questions regarding the functional roles of the neural crest during cranial ganglion development in jawless vertebrates.

To address these issues, Yuan et al. (2020) combined *in situ* hybridization, immunohistochemistry, functional analysis by CRISPR/Cas9 genome editing, and two different fluorescent vital dyes to track the development of both neural crest (DiO) and placodes (DiI) simultaneously during lamprey development to: (1) identify how each cell population physically associated within cranial ganglia and (2) characterize the functional roles of neural crest and placodes during ganglion development. The results from this study were similar to those of Modrell et al. (2014) by demonstrating that cranial placodes were a major source of sensory neurons in the core of cranial ganglia. Another result shared between these two studies was the apparent absence of a prominent neuronal contribution by neural crest cells to the core of the cranial ganglia studied. Neural crest cells were observed to migrate and then surround and eventually envelop the core of placode-derived neurons in the ophthalmic and maxillomandibular lobes of the trigeminal ganglia, geniculate (facial) ganglion, and epibranchial (nodose) ganglia. These results were corroborated by gene expression analyses which revealed that the neural crest markers *TwistA* and *SoxE2* (Sauka-Spengler et al., 2007), rather than being expressed in the neuronal core of ganglia, were instead expressed in cells surrounding each ganglion. This situation is different from that of jawed vertebrates in which neural crest cells are a major source of sensory neurons within cranial ganglia. That said, it is important to emphasize that neither of the studies described here conclusively demonstrates a lack of any sensory neuron contributions of neural crest cells to cranial ganglia, given differences in the timing of dye labeling and the specific ganglia analyzed. At the very least, however, both studies did not identify a prominent role for cranial neural crest cells in this capacity in lamprey.

Finally, to tease apart the functional roles of both neural crest and placodes in lamprey cranial ganglion development, Yuan et al. (2020) used CRISPR/Cas9 genome editing to knock out the neural crest (*SoxE1* and *FoxD-A* mutants) and placodes (*DlxB* mutants) separately and then examined for defects in gangliogenesis. These experiments showed that genetic ablation of the neural crest did not impair the specification or migration of placodes. Rather, they found that all of the cranial sensory ganglia had abnormal morphologies, including inappropriate fusions of otherwise separate ganglia and, conversely, broken clusters of ganglia that are fused during normal development. Notably, none of the neural crest knockouts revealed any obvious loss of sensory neurons or ganglia. On the other hand, placode-specific knockouts (*DlxB*) consistently resulted in total or near-total loss of cranial ganglia (Yuan et al., 2020), although whether this effect is direct or indirect remains unknown. These results together suggest a patterning role for neural crest and a neurogenic role for placodes.

These recent studies have revealed some interesting similarities and differences regarding the developmental association of neural crest and placodes during lamprey craniofacial development relative to what has been described in jawed vertebrates. First, there is certainly evidence of deep evolutionary conservation regarding the overall developmental and genetic programs that guide the interaction of neural crest and placodes in the vertebrate head. For example, both lampreys and jawed vertebrates have more or less the same complement of cranial sensory ganglia, and both neural crest and placodes are each required for proper development of these structures. Additionally, there is evidence of evolutionary conservation of gene expression

patterns in homologous placodes (e.g., *Six*, *Sox*, *Phox*, *Pax*, and *Dlx* expression in/around ganglia), with knockout experiments revealing that some of these genes are required for proper ganglion development across jawed and jawless vertebrate lineages (McCauley and Bronner-Fraser, 2002; Cerny et al., 2010; Modrell et al., 2014; Yuan et al., 2020).

In contrast to evolutionary conservation, there are also clear differences in the developmental associations of neural crest and placodes in the heads of jawed and jawless vertebrates. Most notably, a prominent neural crest contribution of sensory neurons to the core of cranial ganglia is conspicuously absent during stages of lamprey development that have been examined. Instead, cranial sensory neurons in the lamprey head seem to be derived almost entirely from placodes. Although there is marked variation in the extent to which neural crest cells do (maxillomandibular trigeminal) or do not (ophthalmic trigeminal) contribute sensory neurons to cranial ganglia in jawed vertebrates, lampreys are the only vertebrates, to our knowledge, that appear to lack any neural crest contribution of sensory neurons in cranial ganglia (Modrell et al., 2014; Yuan et al., 2020). Instead, cranial neural crest cells in lampreys may play important functional roles in cranial ganglion morphogenesis, in which placodes condense into clusters of differentiated neurons that become enveloped by migratory cranial neural crest cells to shape the functional morphology of these neuronal clusters. A similar role has also been described in jawed vertebrates in which neural crest cells form "corridors" that guide and physically shape placode-derived sensory neurons in the head (Freter et al., 2013). The molecular mechanisms of these types of interactions in jawed vertebrates seem to involve intercellular signaling pathways and adhesion proteins (Shiau et al., 2008; Wu et al., 2014; Shah and Taneyhill, 2015; Wu and Taneyhill, 2019), which have been shown recently to influence the patterning of cranial ganglia in lampreys (York et al., 2018).

By comparing neural crest and placode development across jawed and jawless vertebrates, we can begin to make some inferences regarding how these cell populations may have become associated in ancestral vertebrates to coordinate the development of key craniofacial structures (**Figure 5**). First, we can be fairly certain that early jawless vertebrates had both neural crest cells and placodes. Second, we can also be confident that the developmental mechanisms of each cell population were likely similar to that of extant vertebrates. Third, ancestral vertebrates possessed cranial sensory ganglia that were likely shaped by the developmental coordination of both neural crest and placodes. Finally, comparative embryology studies have shown no evidence that the cranial sensory ganglia of jawless vertebrates are compartmentalized into the morphologically or functionally distinct neural crest-derived (proximal) and placode-derived (distal) components that is characteristic of gnathostomes (Kuratani et al., 1997; Modrell et al., 2014; Pombal and Megías, 2019).

The recent work on neural crest and placode interactions in lamprey embryos compared with our current understanding of this process in jawed vertebrates, allows us to infer what might have been the ancestral vertebrate condition. One possibility is that cranial neural crest cells in the first vertebrates would have likely played a very minor role, if any, in the contribution of sensory neurons to the core of cranial ganglia, a role fulfilled instead by neurogenic placodes. Rather, cranial neural crest cells in ancestral vertebrates would have been important in patterning and shaping the morphology of the placode-derived sensory neurons occupying the core of cranial ganglia, with this feature still being retained in jawed vertebrates. This model suggests that the functional roles of neural crest and placodes in early jawless vertebrates were distinct and that the dual neural crest and placode origin of sensory neurons in cranial ganglia would have likely evolved along stem lineages leading to crown group jawed vertebrates (**Figure 5**). Thus, the overall trend in vertebrate evolution would have been the gradual mixing and integration of sensory neurons of both placode and neural crest origin, with a subset of ganglia (e.g., VII, IX, and X) incorporating neural crest and placodes into distinct proximal and distal aspects, respectively. It is important to point out that this scenario takes into account only information available from one lineage of extant jawless vertebrates, the lampreys. Detailed analysis of neural crest and placode contributions—and their interactions—in hagfish will be important for determining the polarity of character evolution and to better understand the roles of neural crest and placode interactions in the evolution of vertebrate craniofacial development.

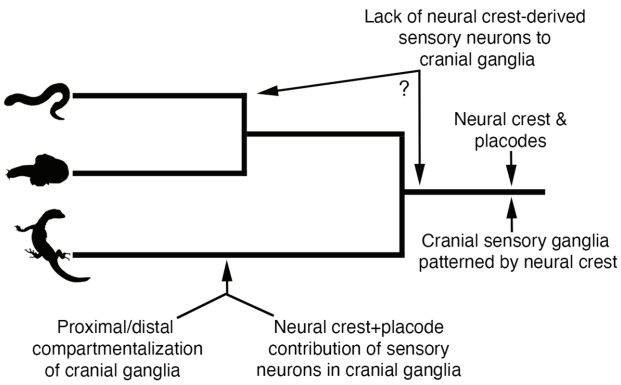

FIGURE 5 | Model for evolution of neural crest and placode associations during craniofacial development in vertebrates. Phylogenetic relationships are depicted for lampreys **(top panel)**, hagfishes **(middle panel)**, and jawed vertebrates **(bottom panel)**.

AUTHOR CONTRIBUTIONS

JY wrote the manuscript. DM, TY, and JY edited the manuscript. All authors contributed to the article and approved the submitted version.

FUNDING

This manuscript was supported through internal funding from the University of Oklahoma to DM.

REFERENCES

Baker, C. V. H., and Bronner-Fraser, M. (1997). The origins of the neural crest. Part I: embryonic induction. *Mech. Dev.* 69, 3–11. doi: 10.1016/s0925-4773(97)00132-9

Baker, C. V. H., and Bronner-Fraser, M. (2000). Establishing neuronal identity in vertebrate neurogenic placodes. *Development* 127, 3045–3056.

Baker, C. V. H., and Bronner-Fraser, M. (2001). Vertebrate cranial placodes I. embryonic induction. *Dev. Biol.* 232, 1–61. doi: 10.1006/dbio.2001.0156

Baker, C. V. H., O'neill, P., and Mccole, R. B. (2008). Lateral line, otic and epibranchial placodes: developmental and evolutionary links? *J. Exp. Zool. B Mol. Dev. Evol.* 310, 370–383. doi: 10.1002/jez.b.21188

Barlow, L. A. (2002). Cranial nerve development: placodal neurons ride the crest. *Curr. Biol.* 12, R171–R173. doi: 10.1016/S0960-9822(02)00734-0

Begbie, J., and Graham, A. (2001). Integration between the epibranchial placodes and the hindbrain. *Science* 294, 595–598. doi: 10.1126/science.1062028

Braun, C. B., and Northcutt, R. G. (1997). The lateral line system of hagfishes (Craniata: Myxinoidea). *Acta Zool.* 78, 247–268. doi: 10.1111/j.1463-6395.1997.tb01010.x

Brazeau, M. D., and Friedman, M. (2014). The characters of Palaeozoic jawed vertebrates. *Zool. J. Linnean Soc.* 170, 779–821. doi: 10.1111/zoj.12111

Brazeau, M. D., and Friedman, M. (2015). The origin and early phylogenetic history of jawed vertebrates. *Nature* 520, 490–497. doi: 10.1038/nature14438

Bronner, M. (2014). Migrating into genomics with the neural crest. *Adv. Biol.* 2014, 1–8. doi: 10.1155/2014/264069

Bullock, T. H., Moore, J. K., and Fields, R. D. (1984). Evolution of myelin sheaths: both lamprey and hagfish lack myelin. *Neurosci. Lett.* 48, 145–148. doi: 10.1016/0304-3940(84)90010-7

Cattell, M., Lai, S., Cerny, R., and Medeiros, D. M. (2011). A new mechanistic scenario for the origin and evolution of vertebrate cartilage. *PLoS One* 6:e22474. doi: 10.1371/journal.pone.0022474

Cerny, R., Cattell, M., Sauka-Spengler, T., Bronner-Fraser, M., Yu, F. Q., and Medeiros, D. M. (2010). Evidence for the prepattern/cooption model of vertebrate jaw evolution. *Proc. Natl. Acad. Sci. U. S. A.* 107, 17262–17267. doi: 10.1073/pnas.1009304107

Cheung, M., Tai, A., Lu, P. J., and Cheah, K. S. (2019). Acquisition of multipotent and migratory neural crest cells in vertebrate evolution. *Curr. Opin. Genet. Dev.* 57, 84–90. doi: 10.1016/j.gde.2019.07.018

Conel, J. L. (1942). The origin of the neural crest. *J. Comp. Neurol.* 76, 191–215. doi: 10.1002/cne.900760202

Couly, G. F., Coltey, P. M., and Le Douarin, N. M. (1993). The triple origin of skull in higher vertebrates: a study in quail-chick chimeras. *Development* 117, 409–429.

Dahl, E., Koseki, H., and Balling, R. (1997). Pax genes and organogenesis. *BioEssays* 19, 755–765. doi: 10.1002/bies.950190905

Damas, H. (1943). *Recherches sur le développement de Lampetra fluviatilis L.: contribution à l'étude de la Céphalogenèse des Vertébrés*. Paris: H. Vaillant-Carmanne.

D'amico-Martel, A., and Noden, D. M. (1983). Contributions of placodal and neural crest cells to avian cranial peripheral ganglia. *Am. J. Anat.* 166, 445–468. doi: 10.1002/aja.1001660406

Fish, J. L. (2019). Evolvability of the vertebrate craniofacial skeleton. *Semin. Cell Dev. Biol.* 91, 13–22. doi: 10.1016/j.semcdb.2017.12.004

Freter, S., Fleenor, S. J., Freter, R., Liu, K. J., and Begbie, J. (2013). Cranial neural crest cells form corridors prefiguring sensory neuroblast migration. *Development* 140, 3595–3600. doi: 10.1242/dev.091033

Froriep, A. (1885). *Ueber Anlagen von Sinnesorganen am Facialis, Glossopharyngeus und Vagus, über die genetische Stellung des Vagus zum Hypoglossus, und über die Herkunft der Zungenmuskulatur: Beitrag zur Entwickelungsgeschichte des Säugethierkopfes*. Leipzig: éditeur inconnu.

Gans, C., and Northcutt, R. G. (1983). Neural crest and the origin of vertebrates: a new head. *Science* 220, 268–274. doi: 10.1126/science.220.4594.268

Gassmann, M., Casagranda, F., Orioli, D., Simon, H., Lai, C., Klein, R., et al. (1995). Aberrant neural and cardiac development in mice lacking the ErbB4 neuregulin receptor. *Nature* 378, 390–394. doi: 10.1038/378390a0

Gillis, J. A., Alsema, E. C., and Criswell, K. E. (2017). Trunk neural crest origin of dermal denticles in a cartilaginous fish. *Proc. Natl. Acad. Sci. U. S. A.* 114, 13200–13205. doi: 10.1073/pnas.1713827114

Goldberg, S., Venkatesh, A., Martinez, J., Dombroski, C., Abesamis, J., Campbell, C., et al. (2020). The development of the trunk neural crest in the turtle *Trachemys scripta*. *Dev. Dyn.* 249, 125–140. doi: 10.1002/dvdy.119

Golding, J. P., Sobieszczuk, D., Dixon, M., Coles, E., Christiansen, J., Wilkinson, D., et al. (2004). Roles of erbB4, rhombomere-specific, and rhombomere-independent cues in maintaining neural crest-free zones in the embryonic head. *Dev. Biol.* 266, 361–372. doi: 10.1016/j.ydbio.2003.11.003

Green, S. A., and Bronner, M. E. (2014). The lamprey: a jawless vertebrate model system for examining origin of the neural crest and other vertebrate traits. *Differentiation* 87, 44–51. doi: 10.1016/j.diff.2014.02.001

Green, S. A., Simões-Costa, M., and Bronner, M. E. (2015). Evolution of vertebrates as viewed from the crest. *Nature* 520, 474–482. doi: 10.1038/nature14436

Green, S. A., Uy, B. R., and Bronner, M. E. (2017). Ancient evolutionary origin of vertebrate enteric neurons from trunk-derived neural crest. *Nature* 544, 88–91. doi: 10.1038/nature21679

Grocott, T., Tambalo, M., and Streit, A. (2012). The peripheral sensory nervous system in the vertebrate head: a gene regulatory perspective. *Dev. Biol.* 370, 3–23. doi: 10.1016/j.ydbio.2012.06.028

Hall, B. K. (2008). *The neural crest and neural crest cells in vertebrate development and evolution*. New York: Springer.

Hall, B. K. (2018). Germ layers, the neural crest and emergent organization in development and evolution. *Genesis* 56:e23103. doi: 10.1002/dvg.23103

Hamburger, V. (1961). Experimental analysis of the dual origin of the trigeminal ganglion in the chick embryo. *J. Exp. Zool.* 148, 91–123. doi: 10.1002/jez.1401480202

Häming, D., Simões-Costa, M., Uy, B., Valencia, J., Sauka-Spengler, T., and Bronner-Fraser, M. (2011). Expression of sympathetic nervous system genes in lamprey suggests their recruitment for specification of a new vertebrate feature. *PLoS One* 6:e26543. doi: 10.1371/journal.pone.0026543

Hardisty, M. W. (1979). *Biology of the cyclostomes*. USA: Springer.

Heimberg, A. M., Cowper-Sal-Lari, R., Sémon, M., Donoghue, P. C. J., and Peterson, K. J. (2010). microRNAs reveal the interrelationships of hagfish, lampreys, and gnathostomes and the nature of the ancestral vertebrate. *Proc. Natl. Acad. Sci. U. S. A.* 107, 19379–19383. doi: 10.1073/pnas.1010350107

His, W. (1868). *Untersuchungen über die erste Anlage des Wirbelthierleibes: die erste Entwickelung des Hühnchens im Ei*. Leipzig: FCW Vogel.

Hockman, D., Burns, A. J., Schlosser, G., Gates, K. P., Jevans, B., Mongera, A., et al. (2017). Evolution of the hypoxia-sensitive cells involved in amniote respiratory reflexes. *Elife* 6:e21231. doi: 10.7554/eLife.21231

Hockman, D., Chong-Morrison, V., Green, S. A., Gavriouchkina, D., Candido-Ferreira, I., Ling, I. T., et al. (2019). A genome-wide assessment of the ancestral neural crest gene regulatory network. *Nat. Commun.* 10:4689. doi: 10.1038/s41467-019-12687-4

Holland, N. D. (2007). Hagfish embryos again—the end of a long drought. *BioEssays* 29, 833–836. doi: 10.1002/bies.20620

Horie, R., Hazbun, A., Chen, K., Cao, C., Levine, M., and Horie, T. (2018). Shared evolutionary origin of vertebrate neural crest and cranial placodes. *Nature* 560, 228–232. doi: 10.1038/s41586-018-0385-7

Horigome, N., Myojin, M., Ueki, T., Hirano, S., Aizawa, S., and Kuratani, S. (1999). Development of cephalic neural crest cells in embryos of *Lampetra japonica*, with special reference to the evolution of the jaw. *Dev. Biol.* 207, 287–308. doi: 10.1006/dbio.1998.9175

Jandzik, D., Hawkins, M. B., Cattell, M. V., Cerny, R., Square, T. A., and Medeiros, D. M. (2014). Roles for FGF in lamprey pharyngeal pouch formation and skeletogenesis highlight ancestral functions in the vertebrate head. *Development* 141, 629–638. doi: 10.1242/dev.097261

Kuraku, S., Takio, Y., Sugahara, F., Takechi, M., and Kuratani, S. (2010). Evolution of oropharyngeal patterning mechanisms involving dlx and endothelins in vertebrates. *Dev. Biol.* 341, 315–323. doi: 10.1016/j.ydbio.2010.02.013

Kuratani, S. (2008). Is the vertebrate head segmented?—evolutionary and developmental considerations. *Integr. Comp. Biol.* 48, 647–657. doi: 10.1093/icb/icn015

Kuratani, S., and Ahlberg, P. E. (2018). Evolution of the vertebrate neurocranium: problems of the premandibular domain and the origin of the trabecula. *Zool. Lett.* 4:1. doi: 10.1186/s40851-017-0083-6

Kuratani, S. C., Miyagawa-Tomita, S., and Kirby, M. L. (1991). Development of cranial nerves in the chick embryo with special reference to the alterations

of cardiac branches after ablation of the cardiac neural crest. *Anat. Embryol.* 183, 501–514. doi: 10.1007/BF00186439

Kuratani, S., and Ota, K. G. (2008). Hagfish (Cyclostomata, vertebrata): searching for the ancestral developmental plan of vertebrates. *BioEssays* 30, 167–172. doi: 10.1002/bies.20701

Kuratani, S., Ueki, T., Aizawa, S., and Hirano, S. (1997). Peripheral development of cranial nerves in a cyclostome, *Lampetra japonica*: morphological distribution of nerve branches and the vertebrate body plan. *J. Comp. Neurol.* 384, 483–500. doi: 10.1002/(SICI)1096-9861(19970811)384:4<483::AID-CNE1>3.0.CO;2-Z

Lakiza, O., Miller, S., Bunce, A., Lee, E. M. J., and Mccauley, D. W. (2011). SoxE gene duplication and development of the lamprey branchial skeleton: insights into development and evolution of the neural crest. *Dev. Biol.* 359, 149–161. doi: 10.1016/j.ydbio.2011.08.012

Langille, R. M., and Hall, B. K. (1988). Role of the neural crest in development of the trabeculae and branchial arches in embryonic sea lamprey, *Petromyzon marinus*. *Development* 102, 301–310.

Lassiter, R. N., Stark, M. R., Zhao, T., and Zhou, C. J. (2014). Signaling mechanisms controlling cranial placode neurogenesis and delamination. *Dev. Biol.* 389, 39–49. doi: 10.1016/j.ydbio.2013.11.025

Le Douarin, N., and Kalcheim, C. (1999). *The neural crest*. New York: Cambridge University Press.

Li, Y., Vieceli, F. M., Gonzalez, W. G., Li, A., Tang, W., Lois, C., et al. (2019). In vivo quantitative imaging provides insights into trunk neural crest migration. *Cell Rep.* 26, 1489.e1483–1500.e1483. doi: 10.1016/j.celrep.2019.01.039

Ling, I. T., and Sauka-Spengler, T. (2019). Early chromatin shaping predetermines multipotent vagal neural crest into neural, neuronal and mesenchymal lineages. *Nat. Cell Biol.* 21, 1504–1517. doi: 10.1038/s41556-019-0428-9

Lukoseviciute, M., Gavriouchkina, D., Williams, R. M., Hochgreb-Hagele, T., Senanayake, U., Chong-Morrison, V., et al. (2018). From pioneer to repressor: bimodal foxd3 activity dynamically remodels neural crest regulatory landscape in vivo. *Dev. Cell* 47, 608.e606–628.e606. doi: 10.1016/j.devcel.2018.11.009

Lwigale, P. Y. (2001). Embryonic origin of avian corneal sensory nerves. *Dev. Biol.* 239, 323–337. doi: 10.1006/dbio.2001.0450

Maharana, S. K., Riddiford, N., and Schlosser, G. (2017). Gene regulatory networks for cranial placode development up-and downstream of Six1 and Eya1. *Mech. Dev.* 145:S140. doi: 10.1016/j.mod.2017.04.393

Maharana, S. K., and Schlosser, G. (2018). A gene regulatory network underlying the formation of pre-placodal ectoderm in *Xenopus laevis*. *BMC Biol.* 16:79. doi: 10.1186/s12915-018-0540-5

Mansouri, A., Hallonet, M., and Gruss, P. (1996). Pax genes and their roles in cell differentiation and development. *Curr. Opin. Cell Biol.* 8, 851–857. doi: 10.1016/S0955-0674(96)80087-1

Martik, M. L., and Bronner, M. E. (2017). Regulatory logic underlying diversification of the neural crest. *Trends Genet.* 33, 715–727. doi: 10.1016/j.tig.2017.07.015

Martik, M. L., Gandhi, S., Uy, B. R., Gillis, J. A., Green, S. A., Simoes-Costa, M., et al. (2019). Evolution of the new head by gradual acquisition of neural crest regulatory circuits. *Nature* 574, 675–678. doi: 10.1038/s41586-019-1691-4

Martin, W. M., Bumm, L. A., and Mccauley, D. W. (2009). Development of the viscerocranial skeleton during embryogenesis of the sea lamprey, *Petromyzon marinus*. *Dev. Dyn.* 238, 3126–3138. doi: 10.1002/dvdy.22164

McCauley, D. W., and Bronner-Fraser, M. (2002). Conservation of Pax gene expression in ectodermal placodes of the lamprey. *Gene* 287, 129–139. doi: 10.1016/S0378-1119(01)00894-0

McCauley, D. W., and Bronner-Fraser, M. (2003). Neural crest contributions to the lamprey head. *Development* 130, 2317–2327. doi: 10.1242/dev.00451

McCauley, D. W., and Bronner-Fraser, M. (2006). Importance of SoxE in neural crest development and the evolution of the pharynx. *Nature* 441, 750–752. doi: 10.1038/nature04691

McCauley, D. W., Docker, M. F., Whyard, S., and Li, W. (2015). Lampreys as diverse model organisms in the genomics era. *Bioscience* 65, 1046–1056. doi: 10.1093/biosci/biv139

Meulemans, D., and Bronner-Fraser, M. (2002). Amphioxus and lamprey AP-2 genes: implications for neural crest evolution and migration patterns. *Development* 129, 4953–4962.

Meulemans, D., and Bronner-Fraser, M. (2004). Gene-regulatory interactions in neural crest evolution and development. *Dev. Cell* 7, 291–299. doi: 10.1016/j.devcel.2004.08.007

Meulemans, D., Mccauley, D., and Bronner-Fraser, M. (2003). Id expression in amphioxus and lamprey highlights the role of gene cooption during neural crest evolution. *Dev. Biol.* 264, 430–442. doi: 10.1016/j.ydbio.2003.09.006

Milet, C., and Monsoro-Burq, A. H. (2012). Neural crest induction at the neural plate border in vertebrates. *Dev. Biol.* 366, 22–33. doi: 10.1016/j.ydbio.2012.01.013

Miyashita, T., Coates, M. I., Farrar, R., Larson, P., Manning, P. L., Wogelius, R. A., et al. (2019). Hagfish from the cretaceous Tethys Sea and a reconciliation of the morphological—molecular conflict in early vertebrate phylogeny. *Proc. Natl. Acad. Sci. U. S. A.* 116, 2146–2151. doi: 10.1073/pnas.1814794116

Modrell, M. S., Hockman, D., Uy, B., Buckley, D., Sauka-Spengler, T., Bronner, M., et al. (2014). A fate-map for cranial sensory ganglia in the sea lamprey. *Dev. Biol.* 385, 405–416. doi: 10.1016/j.ydbio.2013.10.021

Moody, S. A., and Lamantia, A. -S. (2015). Transcriptional regulation of cranial sensory placode development. *Curr. Top. Dev. Biol.* 111, 301–350. doi: 10.1016/bs.ctdb.2014.11.009

Murakami, Y., Ogasawara, M., Sugahara, F., Hirano, S., Satoh, N., and Kuratani, S. (2001). Identification and expression of the lamprey Pax6 gene: evolutionary origin of the segmented brain of vertebrates. *Development* 128, 3521–3531.

Nelson, J. S., Grande, T. C., and Wilson, M. V. (2016). *Fishes of the world*. Hoboken, New Jersey: John Wiley and Sons.

Newth, D. R. (1950). Fate of the neural crest in lampreys. *Nature* 165, 284–284. doi: 10.1038/165284a0

Newth, D. R. (1951). Experiments on the neural crest of the lamprey embryo. *J. Exp. Biol.* 28, 247–260.

Newth, D. R. (1956). On the neural crest of the lamprey embryo. *J. Embryol. Exp. Morpholog.* 4, 358–375.

Nikitina, N., Sauka-Spengler, T., and Bronner-Fraser, M. (2008). Dissecting early regulatory relationships in the lamprey neural crest gene network. *Proc. Natl. Acad. Sci. U. S. A.* 105, 20083–20088. doi: 10.1073/pnas.0806009105

Nikitina, N., Tong, L., and Bronner, M. (2011). Ancestral network module regulating prdm1 expression in the lamprey neural plate border. *Dev. Dyn.* 240, 2265–2271. doi: 10.1002/dvdy.22720

Northcutt, R. G. (2005). The new head hypothesis revisited. *J. Exp. Zool. B Mol. Dev. Evol.* 304B, 274–297. doi: 10.1002/jez.b.21063

Northcutt, R. G., and Gans, C. (1983). The genesis of neural crest and epidermal placodes: a reinterpretation of vertebrate origins. *Q. Rev. Biol.* 58, 1–28. doi: 10.1086/413055

Nyut, D. R. (1955). The neural crest and the head skeleton of lampreys. *Dokl. Akad. Nauk SSSR* 102, 653–656.

Oisi, Y., Ota, K. G., Fujimoto, S., and Kuratani, S. (2013a). Development of the chondrocranium in hagfishes, with special reference to the early evolution of vertebrates. *Zool. Sci.* 30, 944–961. doi: 10.2108/zsj.30.944

Oisi, Y., Ota, K. G., Kuraku, S., Fujimoto, S., and Kuratani, S. (2013b). Craniofacial development of hagfishes and the evolution of vertebrates. *Nature* 493, 175–180. doi: 10.1038/nature11794

Osborne, N. J., Begbie, J., Chilton, J. K., Schmidt, H., and Eickholt, B. J. (2005). Semaphorin/neuropilin signaling influences the positioning of migratory neural crest cells within the hindbrain region of the chick. *Dev. Dyn.* 232, 939–949. doi: 10.1002/dvdy.20258

Ota, K. G., Kuraku, S., and Kuratani, S. (2007). Hagfish embryology with reference to the evolution of the neural crest. *Nature* 446, 672–675. doi: 10.1038/nature05633

Ota, K. G., and Kuratani, S. (2007). Cyclostome embryology and early evolutionary history of vertebrates. *Integr. Comp. Biol.* 47, 329–337. doi: 10.1093/icb/icm022

Ota, K. G., and Kuratani, S. (2008). Developmental biology of hagfishes, with a report on newly obtained embryos of the Japanese inshore hagfish, *Eptatretus burgeri*. *Zool. Sci.* 25, 999–1011. doi: 10.2108/zsj.25.999

Parker, H. J., De Kumar, B., Green, S. A., Prummel, K. D., Hess, C., Kaufman, C. K., et al. (2019). A Hox-TALE regulatory circuit for neural crest patterning is conserved across vertebrates. *Nat. Commun.* 10:1189. doi: 10.1038/s41467-019-09197-8

Parker, H. J., Sauka-Spengler, T., Bronner, M., and Elgar, G. (2014). A reporter assay in lamprey embryos reveals both functional conservation and elaboration of vertebrate enhancers. *PLoS One* 9:e85492. doi: 10.1371/journal.pone.0085492

Patthey, C., Schlosser, G., and Shimeld, S. M. (2014). The evolutionary history of vertebrate cranial placodes–I: cell type evolution. *Dev. Biol.* 389, 82–97. doi: 10.1016/j.ydbio.2014.01.017

Piotrowski, T., and Baker, C. V. (2014). The development of lateral line placodes: taking a broader view. *Dev. Biol.* 389, 68–81. doi: 10.1016/j.ydbio.2014.02.016

Pla, P., and Monsoro-Burq, A. H. (2018). The neural border: induction, specification and maturation of the territory that generates neural crest cells. *Dev. Biol.* 444, S36–S46. doi: 10.1016/j.ydbio.2018.05.018

Platt, J. B. (1894). Ectodermic origin of the cartilages of the head. *Anat. Anz.* 1893, 506–509.

Plouhinec, J. -L., Medina-Ruiz, S., Borday, C., Bernard, E., Vert, J. -P., Eisen, M. B., et al. (2017). A molecular atlas of the developing ectoderm defines neural, neural crest, placode, and nonneural progenitor identity in vertebrates. *PLoS Biol.* 15:e2004045. doi: 10.1371/journal.pbio.2004045

Pombal, M. A., and Megías, M. (2019). Development and functional organization of the cranial nerves in lampreys. *Anat. Rec.* 302, 512–539. doi: 10.1002/ar.23821

Riddiford, N., and Schlosser, G. (2016). Dissecting the pre-placodal transcriptome to reveal presumptive direct targets of Six1 and Eya1 in cranial placodes. *Elife* 5:e17666. doi: 10.7554/eLife.17666

Rothstein, M., and Simões-Costa, M. (2020). Heterodimerization of TFAP2 pioneer factors drives epigenomic remodeling during neural crest specification. *Genome Res.* 30, 35–48. doi: 10.1101/gr.249680.119

Saint-Jeannet, J. -P., and Moody, S. A. (2014). Establishing the pre-placodal region and breaking it into placodes with distinct identities. *Dev. Biol.* 389, 13–27. doi: 10.1016/j.ydbio.2014.02.011

Santagati, F., and Rijli, F. M. (2003). Cranial neural crest and the building of the vertebrate head. *Nat. Rev. Neurosci.* 4, 806–818. doi: 10.1038/nrn1221

Sauka-Spengler, T., and Bronner-Fraser, M. (2008). Insights from a sea lamprey into the evolution of neural crest gene regulatory network. *Biol. Bull.* 214, 303–314. doi: 10.2307/25470671

Sauka-Spengler, T., Meulemans, D. M., Jones, M., and Bronner-Fraser, M. (2007). Ancient evolutionary origin of the neural crest gene regulatory network. *Dev. Cell* 13, 405–420. doi: 10.1016/j.devcel.2007.08.005

Schlosser, G. (2002). Development and evolution of lateral line placodes in amphibians I. Development. *Zoology* 105, 119–146. doi: 10.1078/0944-2006-00058

Schlosser, G. (2005). Evolutionary origins of vertebrate placodes: insights from developmental studies and from comparisons with other deuterostomes. *J. Exp. Zool. B Mol. Dev. Evol.* 304, 347–399. doi: 10.1002/jez.b.21055

Schlosser, G. (2006). Induction and specification of cranial placodes. *Dev. Biol.* 294, 303–351. doi: 10.1016/j.ydbio.2006.03.009

Schlosser, G. (2010). "Making senses: development of vertebrate cranial placodes" in *International review of cell and molecular biology*. ed. K. Jeon (Cambridge: Elsevier), 129–234.

Schlosser, G. (2017). From so simple a beginning–what amphioxus can teach us about placode evolution. *Int. J. Dev. Biol.* 61, 633–648. doi: 10.1387/ijdb.170127gs

Schlosser, G., and Ahrens, K. (2004). Molecular anatomy of placode development in *Xenopus laevis*. *Dev. Biol.* 271, 439–466. doi: 10.1016/j.ydbio.2004.04.013

Schlosser, G., and Northcutt, R. G. (2000). Development of neurogenic placodes in *Xenopus laevis*. *J. Comp. Neurol.* 418, 121–146. doi: 10.1002/(SICI)1096-9861(20000306)418:2<121::AID-CNE1>3.0.CO;2-M

Schwarz, Q., Vieira, J. M., Howard, B., Eickholt, B. J., and Ruhrberg, C. (2008). Neuropilin 1 and 2 control cranial gangliogenesis and axon guidance through neural crest cells. *Development* 135, 1605–1613. doi: 10.1242/dev.015412

Shah, A., and Taneyhill, L. A. (2015). Differential expression pattern of Annexin A6 in chick neural crest and placode cells during cranial gangliogenesis. *Gene Expr. Patterns* 18, 21–28. doi: 10.1016/j.gep.2015.05.001

Shiau, C. E., Lwigale, P. Y., Das, R. M., Wilson, S. A., and Bronner-Fraser, M. (2008). Robo2-Slit1 dependent cell-cell interactions mediate assembly of the trigeminal ganglion. *Nat. Neurosci.* 11, 269–276. doi: 10.1038/nn2051

Shigetani, Y., Sugahara, F., Kawakami, Y., Murakami, Y., Hirano, S., and Kuratani, S. (2002). Heterotopic shift of epithelial-mesenchymal interactions in vertebrate jaw evolution. *Science* 296, 1316–1319. doi: 10.1126/science.1068310

Shimeld, S. M., and Donoghue, P. C. J. (2012). Evolutionary crossroads in developmental biology: cyclostomes (lamprey and hagfish). *Development* 139, 2091–2099. doi: 10.1242/dev.074716

Simões-Costa, M., and Bronner, M. E. (2015). Establishing neural crest identity: a gene regulatory recipe. *Development* 142, 242–257. doi: 10.1242/dev.105445

Singh, S., and Groves, A. K. (2016). The molecular basis of craniofacial placode development. *Wiley Interdiscip. Rev. Dev. Biol.* 5, 363–376. doi: 10.1002/wdev.226

Smith, J. J., Kuraku, S., Holt, C., Sauka-Spengler, T., Jiang, N., Campbell, M. S., et al. (2013). Sequencing of the sea lamprey (*Petromyzon marinus*) genome provides insights into vertebrate evolution. *Nat. Genet.* 45, 415–421. doi: 10.1038/ng.2568

Smith, J. J., Timoshevskaya, N., Ye, C., Holt, C., Keinath, M. C., Parker, H. J., et al. (2018). The sea lamprey germline genome provides insights into programmed genome rearrangement and vertebrate evolution. *Nat. Genet.* 50, 270–277. doi: 10.1038/s41588-017-0036-1

Soldatov, R., Kaucka, M., Kastriti, M. E., Petersen, J., Chontorotzea, T., Englmaier, L., et al. (2019). Spatiotemporal structure of cell fate decisions in murine neural crest. *Science* 364:eaas9536. doi: 10.1126/science.aas9536

Square, T., Jandzik, D., Cattell, M., Hansen, A., and Medeiros, D. M. (2016a). Embryonic expression of endothelins and their receptors in lamprey and frog reveals stem vertebrate origins of complex Endothelin signaling. *Sci. Rep.* 6:34282. doi: 10.1038/srep34282

Square, T., Jandzik, D., Romášek, M., Cerny, R., and Medeiros, D. (2016b). The origin and diversification of the developmental mechanisms that pattern the vertebrate head skeleton. *Dev. Biol.* 427, 219–229. doi: 10.1016/j.ydbio.2016.11.014

Square, T., Romasek, M., Jandzik, D., Cattell, M. V., Klymkowsky, M., and Medeiros, D. M. (2015). CRISPR/Cas9-mediated mutagenesis in the sea lamprey *Petromyzon marinus*: a powerful tool for understanding ancestral gene functions in vertebrates. *Development* 142, 4180–4187. doi: 10.1242/dev.125609

Steventon, B., Mayor, R., and Streit, A. (2014). Neural crest and placode interaction during the development of the cranial sensory system. *Dev. Biol.* 389, 28–38. doi: 10.1016/j.ydbio.2014.01.021

Streit, A. (2018). Specification of sensory placode progenitors: signals and transcription factor networks. *Int. J. Dev. Biol.* 62, 195–205. doi: 10.1387/ijdb.170298as

Sullivan, C. H., Majumdar, H. D., Neilson, K. M., and Moody, S. A. (2019). Six1 and Irx1 have reciprocal interactions during cranial placode and otic vesicle formation. *Dev. Biol.* 446, 68–79. doi: 10.1016/j.ydbio.2018.12.003

Szabó, A., and Mayor, R. (2018). Mechanisms of neural crest migration. *Annu. Rev. Genet.* 52, 43–63. doi: 10.1146/annurev-genet-120417-031559

Szabó, A., Theveneau, E., Turan, M., and Mayor, R. (2019). Neural crest streaming as an emergent property of tissue interactions during morphogenesis. *PLoS Comput. Biol.* 15:e1007002. doi: 10.1371/journal.pcbi.1007002

Theveneau, E., Marchant, L., Kuriyama, S., Gull, M., Moepps, B., Parsons, M., et al. (2010). Collective chemotaxis requires contact-dependent cell polarity. *Dev. Cell* 19, 39–53. doi: 10.1016/j.devcel.2010.06.012

Theveneau, E., Steventon, B., Scarpa, E., Garcia, S., Trepat, X., Streit, A., et al. (2013). Chase-and-run between adjacent cell populations promotes directional collective migration. *Nat. Cell Biol.* 15, 763–772. doi: 10.1038/ncb2772

Trainor, P. A. (2013). *Neural crest cells: Evolution, development and disease*. Cambridge: Academic Press.

Van Wijhe, J. W. (1883). *Ueber die Mesodermsegmente und die Entwickelung der Nerven des Selachierkopfes*. Amsterdam: de Waal.

Vandamme, N., and Berx, G. (2019). From neural crest cells to melanocytes: cellular plasticity during development and beyond. *Cell. Mol. Life Sci.* 76, 1919–1934. doi: 10.1007/s00018-019-03049-w

Vega-Lopez, G. A., Cerrizuela, S., and Aybar, M. J. (2017). Trunk neural crest cells: formation, migration and beyond. *Int. J. Dev. Biol.* 61, 5–15. doi: 10.1387/ijdb.160408gv

von Kupffer, C. (1891). The development of the cranial nerves of vertebrates. *J. Comp. Neurol.* 1, 246–264. doi: 10.1002/cne.910010306

von Kupffer, C. (1893). *Studien zur vergleichenden Entwicklungsgeschichte des Kopfes der Kranioten*. München: JF Lehmann.

von Kupffer, C. (1900). *Zur Kopfentwicklung von Bdellostoma. Studien zur vergleichenden Entwicklungsgeschichte des Kopfes der Kranioten, Heft 4*. München: Lehman.

Washausen, S., and Knabe, W. (2018). Lateral line placodes of aquatic vertebrates are evolutionarily conserved in mammals. *Biol. Open* 7:bio031815. doi: 10.1242/bio.031815

Wicht, H., and Northcutt, R. G. (1995). Ontogeny of the head of the Pacific hagfish (*Eptatretus stouti*, Myxinoidea): development of the lateral line system.

Philos. Trans. R. Soc. Lond. Ser. B Biol. Sci. 349, 119–134. doi: 10.1098/rstb.1995.0098

Wicht, H., and Tusch, U. (1998). "Ontogeny of the head and nervous system of myxinoids" in *The biology of hagfishes*. eds. J. M. Jørgensen, J. P. Lomholt, R. E. Weber and H. Malte (Dordrecht, Netherlands: Springer), 431–451.

Williams, R. M., Candido-Ferreira, I., Repapi, E., Gavriouchkina, D., Senanayake, U., Ling, I. T., et al. (2019). Reconstruction of the global neural crest gene regulatory network in vivo. *Dev. Cell* 51, 255.e257–276.e257. doi: 10.1016/j.devcel.2019.10.003

Wu, C. -Y., Hooper, R. M., Han, K., and Taneyhill, L. A. (2014). Migratory neural crest cell αN-catenin impacts chick trigeminal ganglia formation. *Dev. Biol.* 392, 295–307. doi: 10.1016/j.ydbio.2014.05.016

Wu, C. Y., and Taneyhill, L. A. (2019). Cadherin-7 mediates proper neural crest cell–placodal neuron interactions during trigeminal ganglion assembly. *Genesis* 57:e23264. doi: 10.1002/dvg.23264

Xu, H., Dude, C. M., and Baker, C. V. (2008). Fine-grained fate maps for the ophthalmic and maxillomandibular trigeminal placodes in the chick embryo. *Dev. Biol.* 317, 174–186. doi: 10.1016/j.ydbio.2008.02.012

Yntema, C. L. (1944). Experiments on the origin of the sensory ganglia of the facial nerve in the chick. *J. Comp. Neurol.* 81, 147–167. doi: 10.1002/cne.900810204

York, J. R., Lee, E. M., and Mccauley, D. W. (2019a). "The lamprey as a model vertebrate in evolutionary developmental biology" in *Lampreys: Biology, conservation and control*. ed. M. F. Docker (Dordecht, Netherlands: Springer), 481–526.

York, J. R., and McCauley, D. W. (2020a). Functional genetic analysis in a jawless vertebrate, the sea lamprey: insights into the developmental evolution of early vertebrates. *J. Exp. Biol.* 223:jeb206433. doi: 10.1242/jeb.206433

York, J. R., and McCauley, D. W. (2020b). The origin and evolution of neural crest cells. *Open Biol.* 10:190285. doi: 10.1098/rsob.190285

York, J. R., Yuan, T., Lakiza, O., and McCauley, D. W. (2018). An ancestral role for semaphorin3F-neuropilin signaling in patterning neural crest within the new vertebrate head. *Development* 145:dev164780. doi: 10.1242/dev.164780

York, J. R., Yuan, T., Zehnder, K., and McCauley, D. W. (2017). Lamprey neural crest migration is snail-dependent and occurs without a differential shift in cadherin expression. *Dev. Biol.* 428, 176–187. doi: 10.1016/j.ydbio.2017.06.002

York, J. R., Zehnder, K., Yuan, T., Lakiza, O., and McCauley, D. W. (2019b). Evolution of snail-mediated regulation of neural crest and placodes from an ancient role in bilaterian neurogenesis. *Dev. Biol.* 453, 180–190. doi: 10.1016/j.ydbio.2019.06.010

Yuan, T., York, J. R., and McCauley, D. W. (2018). Gliogenesis in lampreys shares gene regulatory interactions with oligodendrocyte development in jawed vertebrates. *Dev. Biol.* 441, 176–190. doi: 10.1016/j.ydbio.2018.07.002

Yuan, T., York, J. R., and McCauley, D. W. (2020). Neural crest and placode roles in formation and patterning of cranial sensory ganglia in lamprey. *Genesis* 58:e23356. doi: 10.1002/dvg.23356

Zhang, G., and Cohn, M. J. (2006). Hagfish and lancelet fibrillar collagens reveal that type II collagen-based cartilage evolved in stem vertebrates. *Proc. Natl. Acad. Sci. U. S. A.* 103:16829. doi: 10.1073/pnas.0605630103

Ziermann, J. M., Diogo, R., and Noden, D. M. (2018). Neural crest and the patterning of vertebrate craniofacial muscles. *Genesis* 56:e23097. doi: 10.1002/dvg.23097

Zu, Y., Zhang, X., Ren, J., Dong, X., Zhu, Z., Jia, L., et al. (2016). Biallelic editing of a lamprey genome using the CRISPR/Cas9 system. *Sci. Rep.* 6:23496. doi: 10.1038/srep23496

Conflict of Interest: The authors declare that the research was conducted in the absence of any commercial or financial relationships that could be construed as a potential conflict of interest.

frontiers in Physiology

ORIGINAL RESEARCH
published: 21 October 2020
doi: 10.3389/fphys.2020.601923

Identifying Isl1 Genetic Lineage in the Developing Olfactory System and in GnRH-1 Neurons

*Ed Zandro M. Taroc, Raghu Ram Katreddi and Paolo E. Forni**

Department of Biological Sciences, The RNA Institute, and the Center for Neuroscience Research, University at Albany, State University of New York, Albany, NY, United States

During embryonic development, symmetric ectodermal thickenings [olfactory placodes (OP)] give rise to several cell types that comprise the olfactory system, such as those that form the terminal nerve ganglion (TN), gonadotropin releasing hormone-1 neurons (GnRH-1ns), and other migratory neurons in rodents. Even though the genetic heterogeneity among these cell types is documented, unidentified cell populations arising from the OP remain. One candidate to identify placodal derived neurons in the developing nasal area is the transcription factor Isl1, which was recently identified in GnRH-3 neurons of the terminal nerve in fish, as well as expression in neurons of the nasal migratory mass (MM). Here, we analyzed the Isl1 genetic lineage in chemosensory neuronal populations in the nasal area and migratory GnRH-1ns in mice using *in situ* hybridization, immunolabeling a Tamoxifen inducible Isl1Cre^{ERT} and a constitutive Isl1^{Cre} knock-in mouse lines. In addition, we also performed conditional Isl1 ablation in developing GnRH neurons. We found Isl1 lineage across non-sensory cells of the respiratory epithelium and sustentacular cells of OE and VNO. We identified a population of transient embryonic Isl1 + neurons in the olfactory epithelium and sparse Isl1 + neurons in postnatal VNO. Isl1 is expressed in almost all GnRH neurons and in approximately half of the other neuron populations in the MM. However, Isl1 conditional ablation alone does not significantly compromise GnRH-1 neuronal migration or GnRH-1 expression, suggesting compensatory mechanisms. Further studies will elucidate the functional and mechanistic role of Isl1 in development of migratory endocrine neurons.

Keywords: olfactory neurons, vomeronasal sensory neurons, GnRH neurons, Islet-1/Isl1, Isl1 conditional knock-out, genetic lineage tracing, olfactory placode, neural crest

OPEN ACCESS

Edited by:
Lisa Taneyhill, University of Maryland, College Park, United States

Reviewed by:
Anna Cariboni, University of Milan, Italy
Vincent Prevot, Institut National de la Santé et de la Recherche Médicale (INSERM), France

***Correspondence:**
Paolo E. Forni
pforni@albany.edu

Specialty section:
This article was submitted to Craniofacial Biology and Dental Research, a section of the journal Frontiers in Physiology

Received: *02 September 2020*
Accepted: *30 September 2020*
Published: *21 October 2020*

Citation:
Taroc EZM, Katreddi RR and Forni PE (2020) Identifying Isl1 Genetic Lineage in the Developing Olfactory System and in GnRH-1 Neurons. Front. Physiol. 11:601923. doi: 10.3389/fphys.2020.601923

INTRODUCTION

Cranial placodes are specialized regions of ectoderm, that give rise to the pituitary gland, sensory organs, and ganglia of the vertebrate head (Brugmann and Moody, 2005; Schlosser, 2006). They form as a result of specific expression patterns of transcription factors in pre-placodal ectoderm surrounding the anterior neural plate (Brugmann and Moody, 2005; Bailey and Streit, 2006). In mice, the olfactory placodes (OPs) are morphologically identifiable at embryonic day 9.5 (E9.5), as a bilateral ectoderm thickening in the antero-lateral region of the head (**Figure 1**). The transcription

factors Oct1, Sox2, Pou2f1, Pax6, Eya1, Six1, Six4, Ngnr1,Hes1, Hes5, MASH1/Ascl1, Ngn1, and Gli3 have been identified to control various steps of OP induction/formation, neurogenesis, neuronal development, and expression of olfactory specific genes (Cau et al., 1997, 2002; Zou et al., 2004; Donner et al., 2007; Schlosser et al., 2008; Chen et al., 2009; Riddiford and Schlosser, 2016).

The olfactory pit of vertebrates generates neurogenic and non-neurogenic progenitors. The non-neurogenic portions of the olfactory pit give rise to the respiratory epithelium, which is located in the rostral olfactory pit, while the neurogenic portions give rise to specific neuronal and glial/support cells (**Figures 1**, **2**). The respiratory epithelium, which is the main source of Fgf8, controls the development of the neural crest derived nasal mesenchyme and bones (Forni et al., 2013). Neurogenic waves in the olfactory pit of mice first gives rise to mostly migratory neurons (Fornaro et al., 2003; Forni et al., 2013) such as early pioneer olfactory neurons, neurons of the terminal nerve, including Gonadotropin releasing hormone-1 neurons (GnRH-1ns), NPY positive migratory neurons, and other neurons with unknown identity and function or neurons of the migratory mass (MM) (Schwanzel-Fukuda and Pfaff, 1989; Wray et al., 1989; Hilal et al., 1996; Fornaro et al., 2007). The nasal area of mice contains several other neuronal cell types that include specialized olfactory sensory neurons (OSNs) such as the guanylyl cyclase-D (GC-D) neurons of the necklace olfactory system (Luo, 2008; Mori et al., 2014; Greer et al., 2016), microvillar cells (MVCs) (Pfister et al., 2012), sensory neurons of the septal organ (SO) (Ma et al., 2003), the Grueneberg ganglion (GG) (Gruneberg, 1973; Schmid et al., 2010; Mamasuew et al., 2011; Matsuo et al., 2012; Moine et al., 2018), and cells forming the terminal nerve ganglion (TN) (Larsell, 1950; Brown, 1987; Jennes, 1987; Oelschlager et al., 1987; Schwanzel-Fukuda et al., 1987; Wirsig-Wiechmann, 2004; Taroc et al., 2017; Jin et al., 2019) including the GnRH-1ns (Schwanzel-Fukuda and Pfaff, 1989; Wray et al., 1989). The mechanisms and molecules that drive progenitors of the developing olfactory pit into early migratory cells types remain largely unknown.

Between E9.5 and E10.5, the OPs begin to ingress to form the olfactory pits that give rise to various cellular components of the nose during development (Cuschieri and Bannister, 1975b; Chen et al., 2009). The olfactory pit is largely populated by proliferative progenitors expressing the transcription factors Hes1 + /Hes5. These early progenitors undergo mitosis in the apical portion of the epithelium and give rise over time to neurogenic progenitors positive for the bHLH transcription factor Ascl-1 (Cuschieri and Bannister, 1975a,b; Cau et al., 2000; Taroc et al., 2020). Gli3 influences proliferative Hes1 + positive progenitors to give rise to Ascl-1 + neurogenic progenitors that eventually generate OSNs and vomeronasal sensory neurons (VSNs) (Cau et al., 2000; Taroc et al., 2020). Notably, Gli3 loss of function does not prevent neurogenesis of GnRH-1ns, suggesting that these have a distinct lineage from the olfactory neurons.

GnRH-1ns are the initial neuronal population to form in the developing olfactory pit (Wray et al., 1989; Fornaro et al., 2003). During embryonic development, GnRH-1ns migrate along the axons of the terminal nerve (Taroc et al., 2017) from the nasal area to the basal forebrain. Once in brain the GnRH-1ns control the release of gonadotropins from the pituitary gland (Forni and Wray, 2015). Aberrant development or function of GnRH-1ns causes hypogonadotropic hypogonadism (HH) (Cattanach et al., 1977), that can lead to a spectrum of reproductive disorders (Balasubramanian et al., 2010). GnRH-1 neuronal migration strictly depends on correct development and maturation of the neural crest derived olfactory ensheathing cells (Barraud et al., 2013; Pingault et al., 2013; Zhou et al., 2017; Wang et al., 2018). Cre genetic lineage tracing and BAC transgenic reporters have revealed extensive genetic heterogeneity among neurons that originate in the olfactory area of mice including the GnRH-1ns, suggesting a potential integration of neural crest cells in the developing OP (Forni et al., 2011b; Katoh et al., 2011; Suzuki and Osumi, 2015; Taroc et al., 2017; Shan et al., 2020). However, the mechanisms that give rise to the GnRH neurons and the required transcription factors for these regulatory processes remain unresolved.

The LIM-homeodomain transcription factor Isl1 has been recently identified in subsets of neuronal derivatives forming from the OP (Aguillon et al., 2018; Palaniappan et al., 2019; Shan et al., 2020). Isl1/2 expression occurs in GnRH expressing neurons and other putative neurons of the terminal nerve (Aguillon et al., 2018; Palaniappan et al., 2019; Lund et al., 2020; Shan et al., 2020) in chick, zebrafish, mouse, and humans. In zebrafish (Aguillon et al., 2018), Isl1/2 is expressed in terminal nerve GnRH-3 neurons associated with the olfactory epithelium. These neuro-modulatory cells, which are non-migratory in fish, exert the same physiological function as migratory GnRH-1ns in mice (Forni and Wray, 2015). The terminal nerve and MM in birds contains heterogeneous populations of (1) cells that express GnRH-1 but are negative for Isl1/2 and Lhx2, (2) cells only expressing Lhx2, (3) cells only positive for Isl1, and (4) cells that co-express Lhx2, Isl1/2, GnRH-1 (Palaniappan et al., 2019). In birds, cells from the TN are also positive for Isl1 and Lhx2 that differ from the GnRH-1ns. A third study in mouse (Shan et al., 2020) also confirmed Isl1/2 immuno-reactivity on GnRH-1ns at early stages of GnRH neuronal development (E11.5). A subset of GnRH-1ns, positive for Wnt1Cre genetic lineage (Forni et al., 2011b), were negative for Isl1 immunoreactivity.

One prediction is that Wnt1Cre tracing, a controversial neural crest marker, and Isl1 immunoreactivity define two distinct embryonic lineages for GnRH-1ns. The rival hypothesis is that the Wnt1Cre positive subpopulation of GnRH-1ns differ in its timing and/or expression levels of Isl1 from the majority of GnRH-1ns (Forni et al., 2011b; Shan et al., 2020). Understanding the molecular cascade that establishes the genetic lineage of different cell types is a fundamental step to identify potential cellular differences between cell types and to unravel the molecular mechanisms underlying neurodevelopmental pathologies. Here, we examined which regions in the OP express Isl1/2 and analyzed Isl1 genetic lineage in different neuronal types in the nasal area of mice. We further

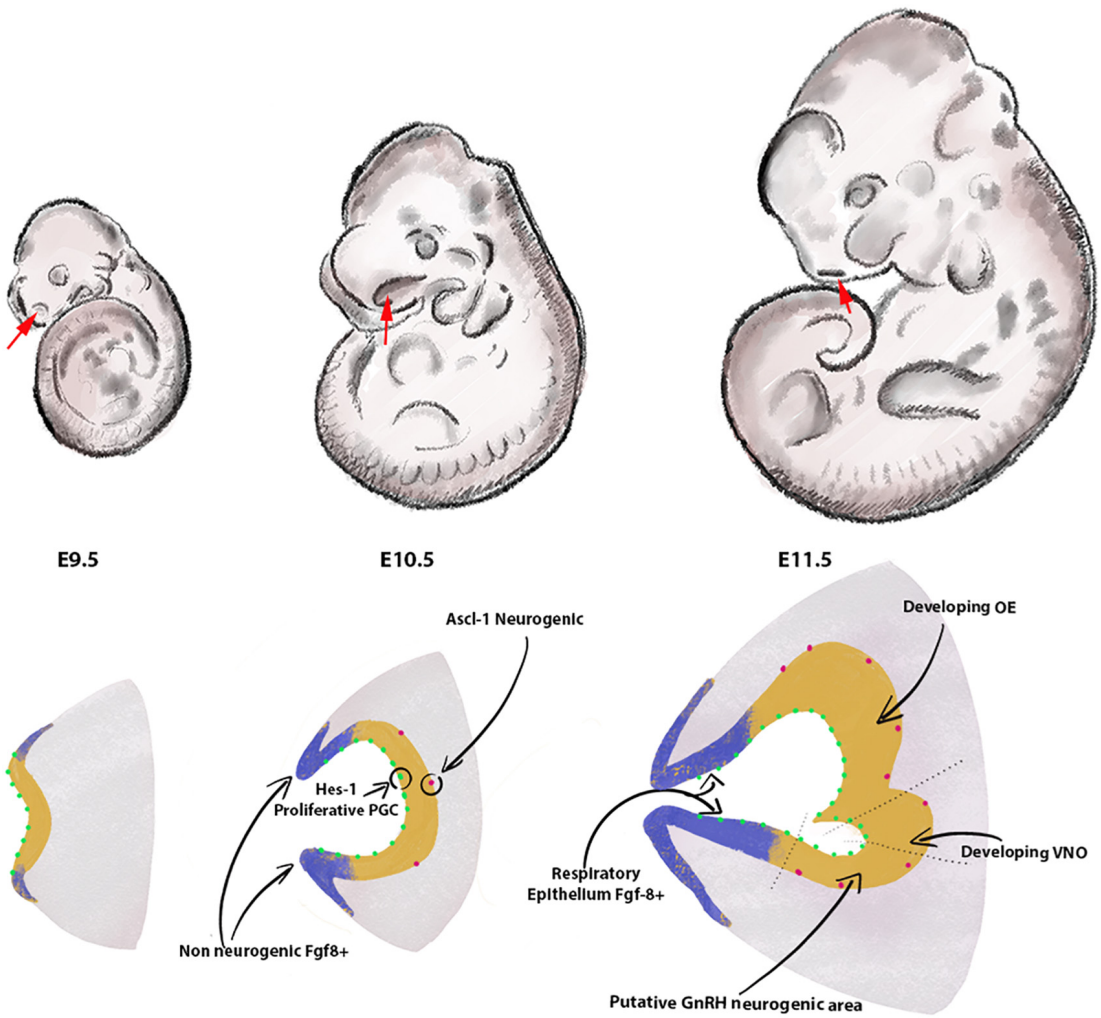

FIGURE 1 | Formation of the olfactory pit. Drawings depict developing embryos between E9.5 and E11.5. The frontonasal areas where the olfactory placodes/pits form are indicated with red arrows. Cartoons in the lower row illustrate the olfactory placode ingression between E9.5 and E10.5 (chronal view) and a parasagittal view of the olfactory pit at E11.5. The lateral and rostral portions of the invaginating olfactory placode (blue) act as the main source of FGF8. These Fgf8 + areas progressively differentiate into respiratory epithelium. In the neurogenesis portion of the olfactory placode (yellow), proliferative Hes-1 + progenitors (green) give rise over time to neurogenic Ascl-1 neuronal progenitors. Arrows show the vomeronasal organ [olfactory epithelium (OE)] and putative neurogenic area of the GnRH-1ns at E11.5 in the developing OE. The size of the pit and cells is arbitrary and does not reflect natural proportions.

generated Isl1 conditional KO mice to study the role of Isl1 in GnRH development.

MATERIALS AND METHODS

Animals

Isl1^{flox}(Isl1tm2Sev/J) (Sun et al., 2008), Isl1^{CreERT}(Isl1tm1(cre/Esr1*)Krc/SevJ) (Laugwitz et al., 2005), Isl1Cre (Isl1tm1(cre)Sev/J) (Yang et al., 2006), Rosa26tdTomato (B6.Cg-Gt(ROSA)26Sortm14(CAG-tdTomato)Hze/J) (Madisen et al., 2010), and GnRH-Cre (Gnrh1-cre 1Dlc/J) (Yoon et al., 2005) mouse lines were all purchased from JAX. Genotyping was conducted following the suggested primers and protocols from JAX. Mice of either sex were used for ISH and IHC experiments. All experiments involving mice were approved by the University at Albany Institutional Animal Care and Use Committee (IACUC).

Tamoxifen Treatment

Tamoxifen (Sigma–Aldrich), CAS # 10540−29−1, was dissolved in Corn Oil. Tamoxifen was administered once via intraperitoneal injection at indicated developmental stages. Tamoxifen was administered at 180 mg/kg based on the weight of the pregnant dam on the day of injection.

Tissue Preparation

Embryos were collected from time-mated dams where the emergence of the copulation plug was taken as E0.5. Collected

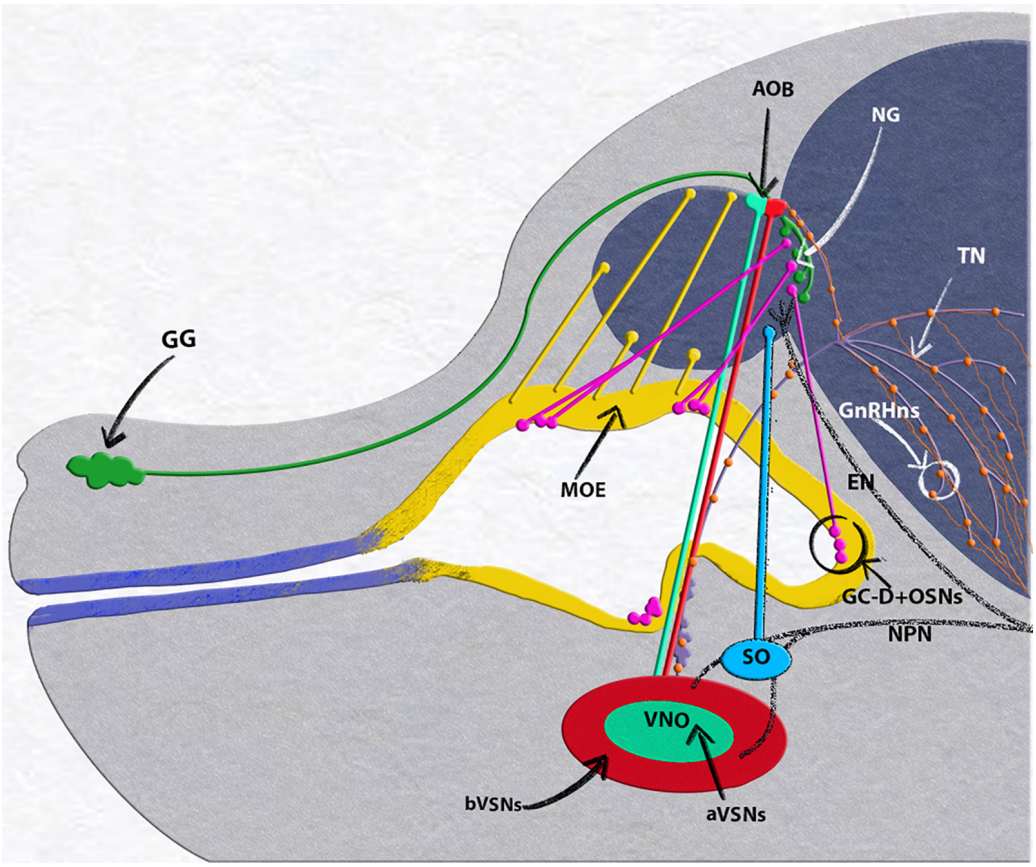

FIGURE 2 | E15.5 mouse embryo, neuronal populations in the nasal area. Grueneberg ganglion (GG, green) and GC-D+/necklace (OSNs, magenta) project to the necklace glomeruli (NG). Olfactory neurons of the main olfactory epithelium (MOE, yellow) projecting to the main olfactory bulb (MOB). Vomeronasal organ (VNO), composed of basal (bVSNs, green) and apical (a-VSNs, red), projecting to anterior and posterior portions of the accessory olfactory bulb (AOB). Septal organ (SO, light blue) projecting to the ventral OB. Terminal nerve (TN, purple) projecting to the basal forebrain, GnRH-1ns, orange, scattered along the terminal nerve fibers from the vomeronasal area to the basal forebrain. Trigeminal nasopalatine (NPN) and ethmoidal nerve projections (EN) drawn in dark gray.

embryos were immersion-fixed in 3.7% formaldehyde/PBS at 4°C for 3–5 h. Postnatal animals were perfused with 3.7% formaldehyde/PBS. All samples were then cryoprotected in 30% sucrose overnight, then frozen in O.C.T (Tissue-TeK), and stored at −80°C. Samples were cryosectioned using CM3050S Leica cryostat and collected on Superfrost plus slides (VWR) at 14 μm thickness for embryo's and 16 μm for post-natal tissue.

Immunohistochemistry

Primary antibodies and dilutions used in this study were: rabbit- α-Isl1(1:1000, Abcam), mouse-α-Isl1/2 (1:100, DSHB), SW rabbit-α-GnRH-1 (1:6000, Susan Wray, NIH), goat-α olfactory marker protein (OMP; 1:4000, WAKO), rabbit-α-phospho-Histone-H3 (1:400, Cell Signaling), goat-α-Sox2 (1:400, R & D systems), rat-α-phospho-Histone-H3 (1:500, Abcam), mouse-α-Ki67 (1:500, Cell Signaling), rabbit-α-DsRed (1:1000, Clontech), goat-DsRed (1:1000, Rockland), HuC/D 8 μg/ml (Molecular Probes). Antigen retrieval was performed in a citrate buffer prior to incubation with rabbit-α-Isl1, mouse-α-Isl1/2, rabbit-α-phospho-Histone-H3, rat-α-phospho-Histone-H3, mouse-α-Ki67. For immunoperoxidase staining procedures, slides were processed using standard protocols (Forni et al., 2013) and staining was visualized (Vectastain ABC Kit, Vector) using diaminobenzidine (DAB) in a glucose solution containing glucose oxidase to generate hydrogen peroxide; sections were counterstained with methyl green. For immunofluorescence, species-appropriate secondary antibodies were conjugated with Alexa-488, Alexa-594, or Alexa-568 (Molecular Probes and Jackson Laboratories) as specified in the legends. Sections were counterstained with 4',6'-diamidino-2-phenylindole (1:3000; Sigma–Aldrich) and coverslips were mounted with Fluoro Gel (Electron Microscopy Services). Confocal microscopy pictures were taken on a Zeiss LSM 710 microscope. Epifluorescence pictures were taken on a Leica DM4000 B LED fluorescence microscope equipped with a Leica DFC310 FX camera. Images were further analyzed using FIJ/ImageJ software. To remove auto-fluorescent blood cells in **Figure 9**, FIJ/ImageJ function image calculator was used. Each staining was replicated on at least three different animals for each genotype.

In situ Hybridization

Digoxigenin-labeled cRNA probes were prepared by *in vitro* transcription (DIG RNA labeling kit; Roche Diagnostics) from the following templates: Isl1 from Allen Brain Atlas (Probe RP_080807_04_G12). *In situ* hybridization was performed as described (Lin et al., 2018) and visualized by immunostaining with an alkaline phosphatase conjugated anti-DIG (1:500), and NBT/BCIP developer solution (Roche Diagnostics).

Cell Quantifications

GnRH-1/Isl1 double IHC quantifications were performed at E11.5 and E15.5 parasagittal non-serial sections on a single slide using the Rabbit-α-GnRH-1 primary and Mouse-α-Isl1/2 primary antibodies. Embryonic co-localized cell counts on Isl1Cre or Isl1Cre^{ERT} lineage traced animals were done on E14.5 and E15.5, respectively, parasagittal non-serial whole head sections within the nasal region on a single slide where we see co-localization of both markers indicated (DsRed/tdTomato GnRH-1, or HuCD). Post-natal OMP cell counts were done on P8 coronal nose sections. To get the density of mature OSNs positive for constitutive Isl1 lineage tracing at P8, number of OMP positive neurons colocalized for tdTom were counted in the caudal olfactory epithelium and calculated the area of the OMP positive cells within the traced epithelium. In VNO, to get the percentage of mature VSNs positive for constitutive Isl1 lineage tracing, first OMP positive cells colocalized for tdTom were counted. To get the total OMP positive cells in VNO section, density of OMP cells in smaller areas of VNO was determined and extended to the total area of OMP positive cells in the VNO.

GnRH-1 cell counts were performed on GnRH-1Cre/Islet1$^{flox/flox}$, Isl1$^{CreERT/flox}$, and control at E15.5 on two immunostained non-serial slides.

Validation of Conditional Isl1 Knockout

The Isl1^{flox} animals have the lox-p sites flanking exon 4 of the Isl1 gene which codes for the homeodomain and consists of the amino acids in positions 181–240. To detect conditional loss of Isl1^{flox} in GnRHCre/Isl1$^{flox/flox}$ mutants, we performed immunolabeling using the mouse anti-Isl1/2 (DSHB) primary antibody. This antibody recognizes the amino acids 178–349 of the Isl1 protein and was previously shown to be unable to detect Isl1^{flox} (Isl1tm2Sev/J) mice, after Cre mediated recombination (Sun et al., 2008). However, in Isl1^{CreERT} [Isl1tm1(cre/Esr1*)Krc/SevJ] which is null mouse model, the amino acids in positions 181–240 are maintained, therefore this null protein is still detectable in Isl1 null cells. Since Isl1^{CreERT} (Laugwitz et al., 2005) and Isl1^{flox} alleles (Sun et al., 2008) have been targeted in different gene regions, we could not validate recombination efficiency of Isl1$^{CreERT/flox}$ cKOs.

Statistical Analyses

All statistical analyses were carried out using GraphPad Prism7 software. All cell counts were averaged ± standard error (SE) among animals of the same age and genotype. Means ± SEs were calculated on at least three animals per genotype. The statistical difference between genotypes and groups was determined using an unpaired student's *t*-test.

RESULTS

Isl1 Expression in Proliferative Progenitors and Neurons During Early Development of the Olfactory Pit

Using *in situ* hybridization at E11.5, we found Isl1 mRNA expression in the more caudal region of the putative developing olfactory epithelium and proximal to the developing VNO (**Figure 3A**). We previously described the latter as the region where GnRH-1ns likely form and become immunoreactive (**Figure 3B**) (Forni et al., 2013). By pairing immunohistochemistry against Isl1/2 and the mitotic marker phospho-histone-3 (PHH3) at E11.5, we found (**Figures 3C,C'**) some proliferative progenitors in the apical regions of the developing pit that were also positive for Isl1. Isl1/2 protein expression was consistent with the mRNA expression pattern (**Figures 3A,C**). However, strong Isl1/2 immunoreactivity appeared localized in sparse nuclei ventral to the developing VNO and the putative respiratory epithelium (**Figures 3C,D**). Immunolabeling with anti Isl1/2 and GnRH-1 at E11.5, E13.5, and E15.5 (**Figures 3D–F'''**) indicated a dynamic Isl1/2 expression across GnRH-1ns (Shan et al., 2020). In fact, we could identify at E11.5 approximately 89% (SE ± 3.33%) of GnRH-1 + cells positive for Isl1/2 immunoreactivity (**Figures 3D–D"**).

Differential Lineage Among Olfactory, Vomeronasal, and GnRH-1 Neurons

As we observed sparse and a heterogeneous distribution of Isl1 mRNA and protein expression in the developing olfactory pit at E11.5 (**Figure 3**) and found Isl1/2 protein expression with the proliferative cell marker PHH3, we decided to investigate which cells formed from the Isl1/2 + proliferative cells. We utilized a tamoxifen inducible Isl1Cre^{ERT} knock-in mouse line (Laugwitz et al., 2005) mated with a sensitive Rosa-reporter (Madisen et al., 2010). Isl1Cre^{ERT} allows temporal control and restricts Cre mediated recombination to the time of Tamoxifen injection. Pregnant dams were treated with a single injection of Tamoxifen (180 mg/kg) at E11.5 and embryos were analyzed 4 days later (**Figure 4A**). At E15.5, we observed Isl1 recombination in trigeminal nerve, inner ear, Rathke's pouch, and oral mucosa (**Figures 4B,C**) (Hutchinson and Eisen, 2006; Sjodal and Gunhaga, 2008; Tanaka et al., 2011; Huang et al., 2013). We also found Isl1 tracing in the developing nasal area (**Figures 4D–E"**) in sparse OMP + sensory neurons of both the main olfactory and vomeronasal epithelium. Notably, Isl1Cre + neurons positive for the pan neuronal marker HuC/D were found at the border between the respiratory epithelium and sensory epithelium (**Figures 4E,E'**). We found extensive

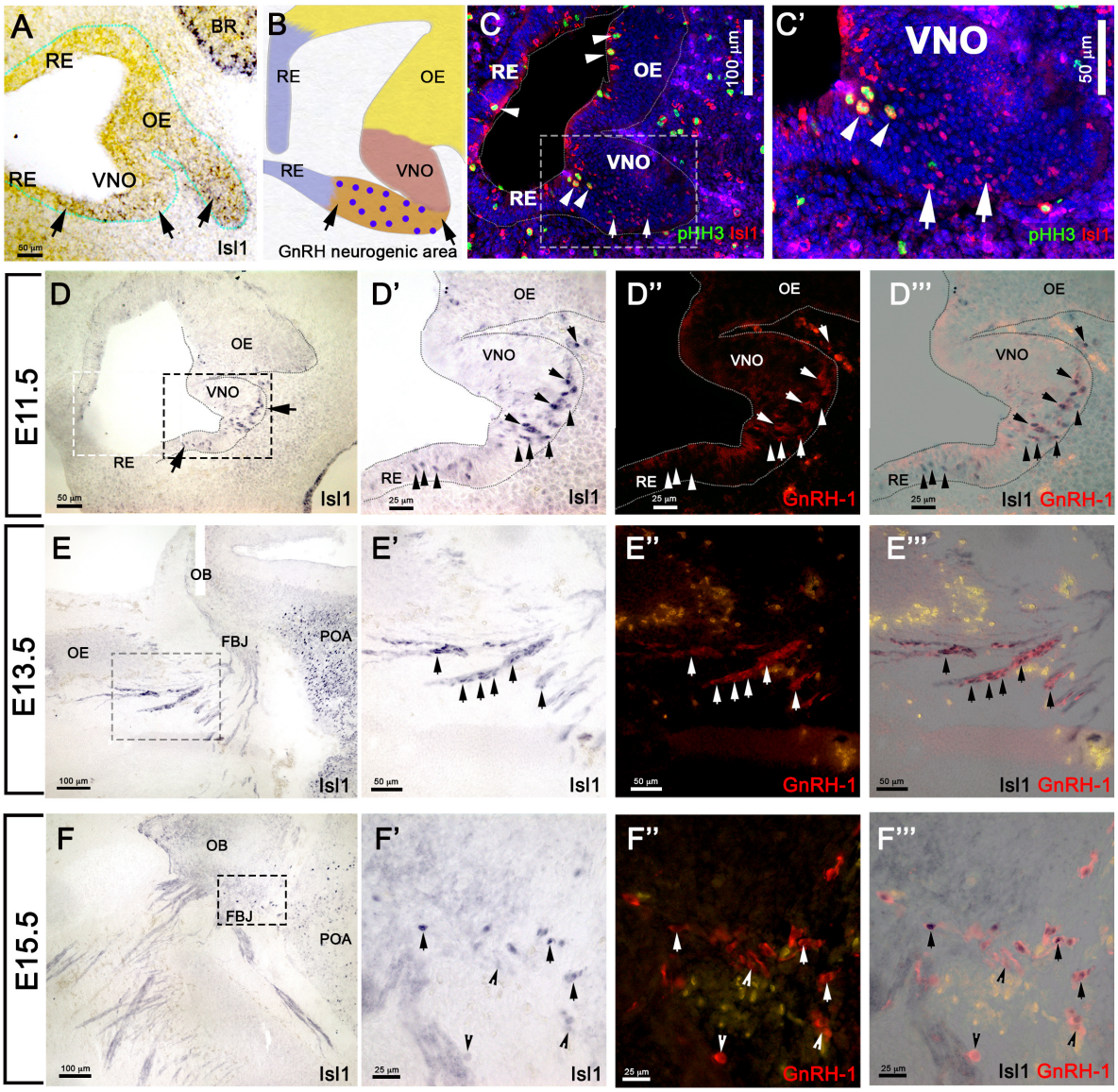

FIGURE 3 | Isl1 expression in the OP is restricted to GnRH neurons and a few other cells types. **(A)** E11.5 *in situ* hybridization anti-Isl1 mRNA shows Isl1 expression in the ventral portion of the developing olfactory pit proximal to the VNO. Arrows indicate putative GnRH neurogenic area. Only spare cells positive for Ilset1 could be detected in the OE (arrowhead). **(B)** Cartoon illustrating the putative areas giving rise to RE, OE, VNO, and the putative GnRH neurogenic area. Blue dots indicate GnRH-1ns. **(C,C')** Immunostaining anti-Isl1 (red) and the mitotic marker pHH3 (green) shows Ilset1 expression in sparse proliferative cells in the apical portion of the OP (arrowheads) and in cells in the putative GnRH neurogenic area ventral to the VNO (boxed) compared to **(A,B)**. **(D)** Isl1 immunoreactivity in the putative GnRH neurogenic area (arrows, compared to **(A,B,C)**. **(D'–D''')** Isl1 expression (black) in newly formed GnRH neurons(arrows) and in GnRH-1 negative cells (arrowheads). Isl1 expression (black) in migrating GnRH-1ns in the (arrows) in the nasal area at E13.5 **(E–E''')** and in the brain at E15.5 **(F–F''')**. OE, olfactory epithelium; OB, olfactory bulb; FBJ, forebrain junction; POA, preoptic area; RE, respiratory epithelium; VNO, vomeronasal organ; BR, brain.

Cre recombination penetrance throughout the nasal respiratory epithelium (**Figures 4D,D'**).

We detected putative nasopalatine and ethmoidal trigeminal axons positive for Isl1 throughout the nasal area and tangential to the olfactory bulb (**Figures 4B–D'**). By analyzing the olfactory projections via OMP and Peripherin immunostaining in combination with anti tdTomato staining, we confirmed that Isl1Cre recombination occurred in neurons that appeared to bundle with the olfactory neurons. Notably, most Isl1Cre^{ERT} traced axons did not appear to project to the main or accessory olfactory bulb (**Figures 4D,D'**). Analysis of the olfactory epithelium showed a very sparse colocalization between OMP and Isl1Cre mediated recombination. However, immunostaining against the pan neuronal marker HuC/D showed the presence of Isl1 + neurons within the developing olfactory epithelia (**Figures 4E,E'**). Triple immunostaining against GnRH-1, tdTomato, and the pan neuronal protein HuC/D showed that temporally controlled Isl1Cre^{ERT} recombination at

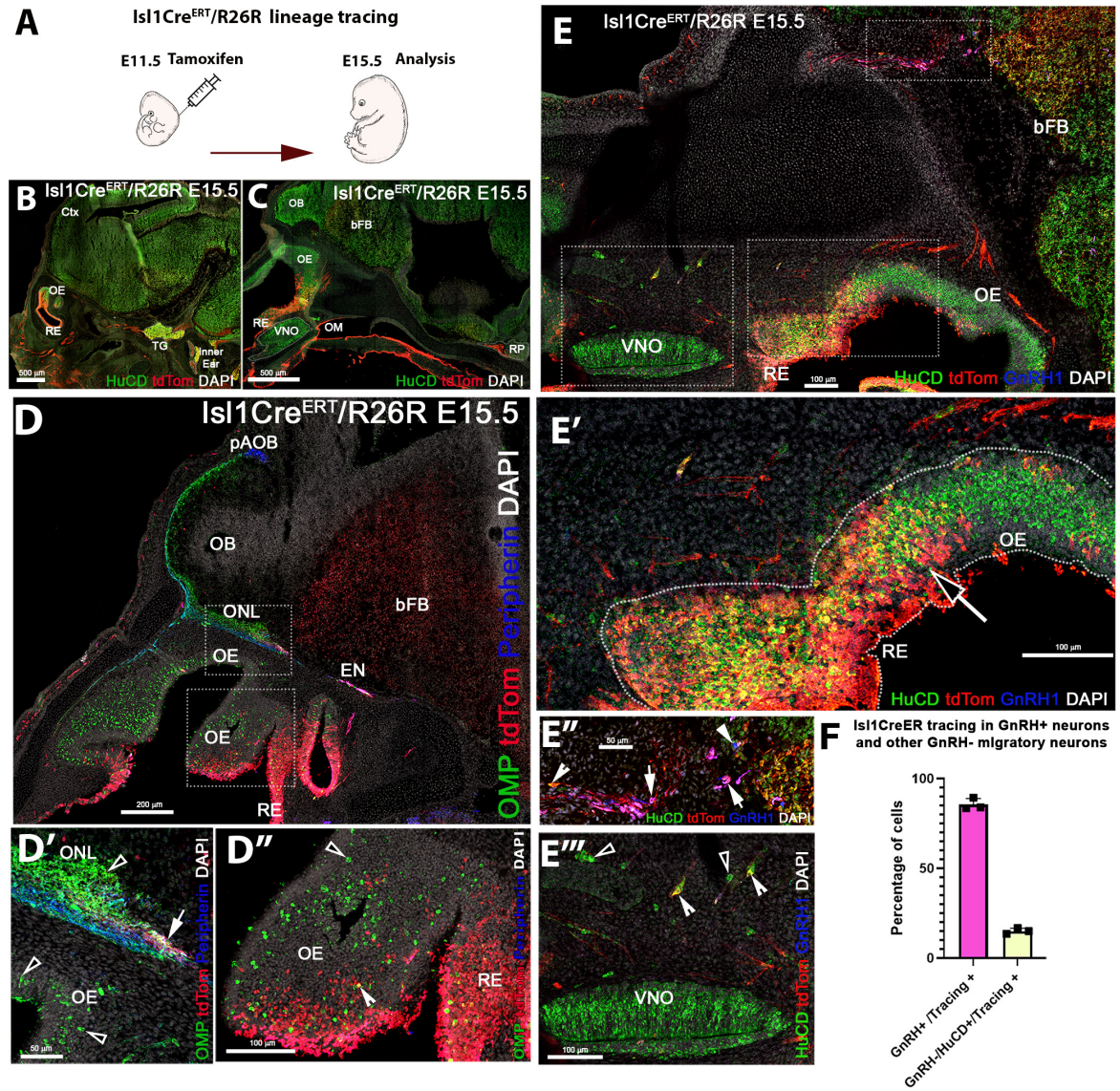

FIGURE 4 | Temporally controlled Isl1 lineage tracing at E11.5 primarily highlights cells of the respiratory epithelium and GnRH-1ns. **(A)** Cartoon illustrating experiential strategy for Iset-1CreERT/R26RTdTomato lineage tracing. Tamoxifen induction of Cre recombiantion at E11.5, analysis at E.15.5. **(B,C)** HuC/D/DsRed double immunostaining shows recombination (tdTomato) in the trigeminal ganglion (TG), the inner ear as well as in cells of the Rathke's pouch (RP). **(D–D")** In the developing nose recombination appears to be mostly restricted to the respiratory epithelium (RE) and ethmoidal (EN) trigeminal projections. **(D–D")** Anti tdTomato; OMP; Peripherin immunostaining showed that OMP positive olfactory projections of the main olfactory bulb. Peripherin positive projections to the accessory olfactory bulb appear negative for td Tomato expression. However, tdTomato positive fibers (**D'** white arrow), likely belonging to the trigeminal/ethmoid nerve (see EN in **D**), appeared to project to the ventral OB. **(D")** OMP and tdTomato immunoreactivity showed nearly complete absence of OSNs positive for Isl1 tracing. Neurons in the olfactory area appeared mostly negative for Isl1 lineage **D"**, sparse OMP + tdTomato + cells (Notched arrowhead) could be detected at the border between olfactory and respiratory epithelium, boxed area see **D'**. Pan neuronal marker HuC/D shows neurons of the developing vomeronasal organ (VNO), mostly negative for Isl1 lineage **(E')**. HuC/D + neurons at the border between OE and RE **(E')** migratory neurons, GnRH-1ns **(E")** and HuC/D + only **(E"')** were positive for Isl1 tracing. **(F)** Quantification of recombination in migratory GnRH-1 + and HuC/D GnRH-1 negative neurons. OM, oral mucosa; RP, Rathke's Pouch; Ctx, cortex; OB, olfactory bulb; bFB, basal Fore Brain; pAOB, putative Accessory Olfactory Bulb.

E11.5 yielded 85% (SE ± 1.88%) of GnRH-1ns, while only 15%(SE ± 0.91) of the migratory (HuC/D + /GnRH−) cells were Isl1 positive. These data suggest that Isl1 expression at E11.5 (**Figures 3A–C**) is mostly limited to progenitors or precursors of GnRH-1ns and the subsets of other neurons of the MM.

Analysis of Constitutive Isl1 Cre Genetic Lineage Tracing at E14.5

Tamoxifen controlled Cre recombination at E11.5 indicated that few neuronal progenitors and sparse neurons in the OE and VNO were positive for Isl1 as the olfactory pit forms, while the respiratory epithelium, oral mucosa, and the

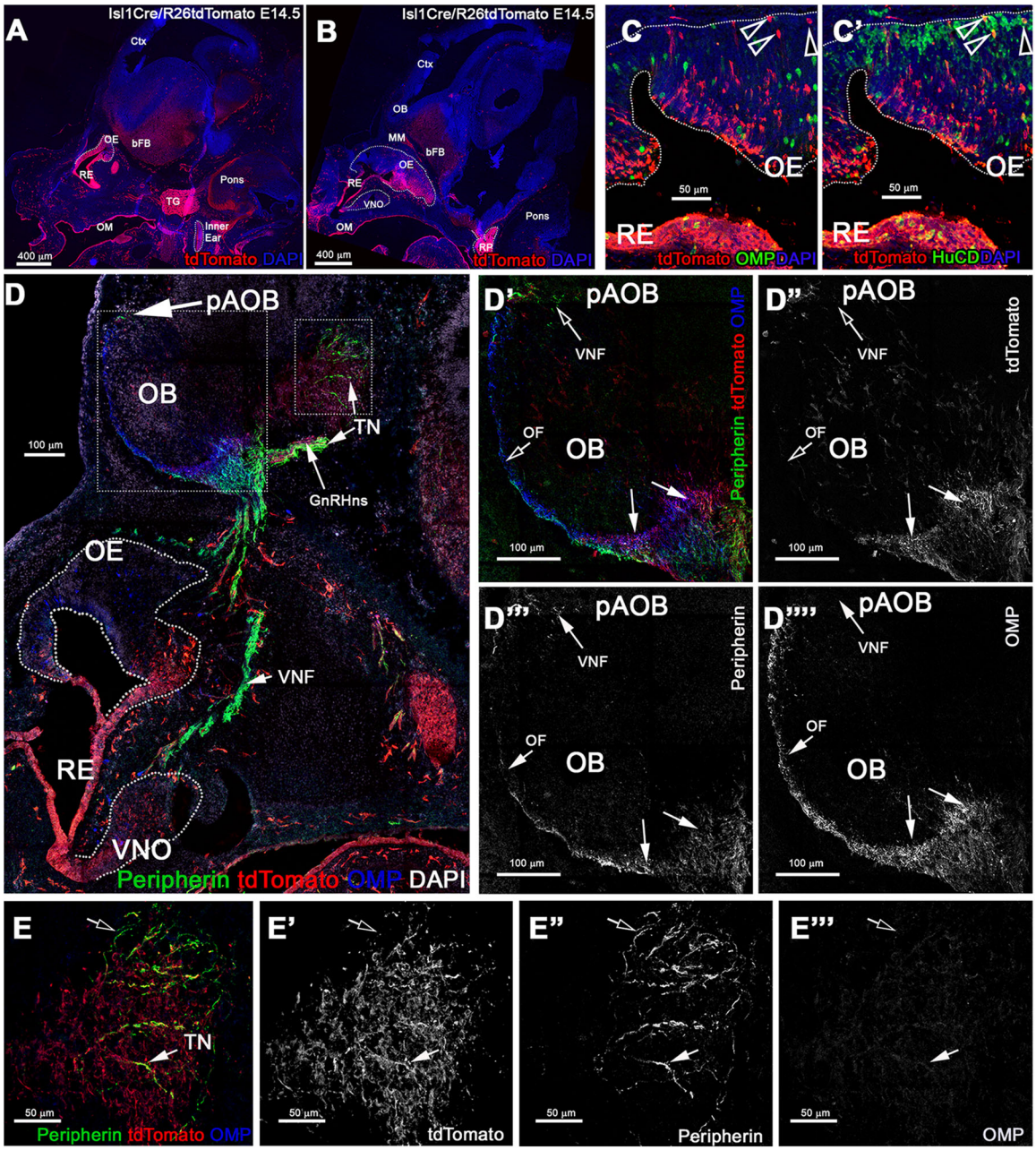

FIGURE 5 | Constitutive Isl1 lineage tracing highlights: sparse neurons the OE, VNO, neuronal projections to the ventral OB, GnRH neurons, and some TN fibers. **(A,B)** Immunostaining against tdTomato of Isl1Cre/R26tdTomato lineage traced embryos at E14.5, showing recombination the trigeminal ganglion (TG), inner ear, Rathke's pouch (RP), the oral mucosa (OM), respiratory epithelium (RE), and in sparse cells in the OE and VNO. **(C)** Anti-tdTomato; OMP and **(C')** anti-tdTomato; HuC/D staining shows that though almost all the OMP + cells were negative for tracing (arrowheads) **(C)**, those were neurons positive for HuC/D (arrowhead). **(D–E''')** Immunostaining against tdTomato, OMP, and Peripherin to highlight the projections of the developing olfactory system reveal that Isl1 tracing **(D'–D'''')** is mostly absent in the OMP + olfactory fibers (OF) and Peripherin + vomeronasal fibers (VNF) innervating the olfactory bulb (OB). GnRH-1 and other cells of the migratory mass positive for the tracing were detected invading the brain along the terminal nerve (TN). **(E–E''')** Peripherin positive TN fibers in the brain. Some fibers appear positive for the tracing (solid arrow) while other Peripherin fibers appear to be negative (empty arrow). MM, migratory mass; bFB, basal Fore Brain; OE, Olfactory Epithelium; VNO, Vomeronasal Organ.

majority of the GnRH-1ns resulted expressing Isl1. To further perform a temporally unbiassed lineage tracing for Isl1, we exploited a traditional Isl1Cre knock-in mouse line. In these mice recombination is expected to occur whenever Isl1 is expressed (Yang et al., 2006). We performed a Cre/Rosa reporter lineage analysis $Isl1^{Cre\pm}/R26^{tdTomato\pm}$ at E14.5 and P8. After temporally controlled recombination (**Figure 4**), constitutively active Isl1 Cre at E14.5 (**Figure 5**) showed recombination in

the trigeminal nerve, cells of the inner ear (Radde-Gallwitz et al., 2004), the Rathke's pouch forming the anterior pituitary gland (Castinetti et al., 2015), the oral mucosa, and the nasal respiratory epithelium.

During gross visual observation, we noticed that more cells positive for Isl1 lineage occurred in both olfactory and vomeronasal epithelia compared to that after temporally controlled Cre activation (compared **Figures 4**, **5**).

Isl1 Cre Recombination in GnRH and Terminal Nerve Neurons

At E14.5 we performed OMP, Peripherin, and tdTomato immunostaining. We observed labeled olfactory and terminal axonal projections (**Figures 5D–E**"'). In the olfactory system, we noticed that Isl1 Cre tracing could be seen in fibers forming bundles with the olfactory neurons after temporally controlled Isl1 Cre recombination (**Figures 5D'–D"'**). However, most axons positive for recombination at this stage appeared to project only to the ventral portions of the olfactory bulb with some verging on invading the basal forebrain (**Figures 5E–E**"'). The terminal nerve enters the brain ventral to the olfactory bulb (Taroc et al., 2017). Fibers of the putative terminal nerve associated with Isl1 + migratory GnRH-1ns. Using immunostaining against peripherin and tdTomato, we visualized Isl1 + positive cell somas and fibers of GnRH-1ns migrating on peripherin positive axons of the TN. Some putative TN's axons showed sparse positivity for tracing (**Figures 5E–E**""). To confirm Isl1 Cre tracing in cells of the terminal nerve, we immunostained against the antigen Robo3, which is selectively expressed by these cells (Taroc et al., 2017). Robo3/tdTomato staining confirmed the presence of cell bodies from putative TN cells, proximal and within the developing vomeronasal organ, some of these appeared to be positive for Isl1 lineage. We also observed TN fibers, positive for Robo3, in the brain (data not shown). GnRH-1, tdTomato, and HuC/D (**Figures 6D–D**"') immunostaining confirmed Isl1 lineage in virtually all GnRH-1ns (95%) (SE ± 0.68), while 55% (SE ± 4.63) of the HuC/D migratory neurons that were negative for GnRH-1, were actually positive for Islet1 tracing (**Figure 6E**).

Postnatal Analyses of Isl1Cre Lineage in the Nasal Cavity

During embryonic development, we observed Isl1 recombination in neurons in both olfactory and vomeronasal epithelia. So, we analyzed the pattern of constitutive Isl1 Cre recombination in postnatal animals. We performed double immunostaining against tdTomato and OMP at postnatal day 8 and noticed that most olfactory epithelium neurons did not express OMP and Isl1. However, we did find sparse neurons positive for Isl1 tracing in the most caudal ethmoid turbinates [0.12 (±0.03 SEM) cells/1000 μm^2] (**Figures 7D–D**"'). Isl1Cre positive sustentacular cells were found close to the border between the respiratory epithelium and sensory olfactory epithelium in the ventral–lateral zones of the OE and along the nasal septum (S) in all the sections from rostral to caudal. At visual gross observation, we noticed more pronounced Isl1 + lineage in sustentacular cells in the caudal OE along the lateral ethmoid turbinates (**Figures 7A–C**). These data imply spatial/regional heterogeneity in gene expression among sustentacular cells (Brann et al., 2020).

Analysis of postnatal vomeronasal epithelia showed a different scenario from that in the OE. Immunostaining against TdTom indicated Isl1 tracing in both non-sensory epithelium (NSE) and sensory epithelium of the VNO. In the sensory epithelium, staining against OMP and tdTom showed that sparse recombination in 3.74% (±1.06 SEM) of the neurons (**Figures 7F–F**"). The vomeronasal neurons positive for tracing were variously distributed in apical and basal regions. Sox2 and tdTomato immunostaining revealed, as observed in the OE (**Figures 7E–E**"'), that Islet1 tracing was detectable in sustentacular cells (**Figures 7G–G**"). Since constitutive Isl1 lineage showed cells positive in olfactory and vomeronasal epithelia, we further investigated if Isl1 recombination also occurred in neurons of the SO and Gruenberg ganglion (GG). By performing immunostaining anti-OMP in postnatal animals, we found that both neuronal populations were negative for lineage tracing (**Figure 8**). Immunostaining with anti-CART and -PDE2A antibodies also revealed an absence of Isl1 expression in Necklace glomeruli cells (NGCs) (data not shown).

Conditional Isl1 Loss of Function in GnRH-1ns

Isl1 is important for differentiation, cell migration, survival, and axonal targeting of neurons of the peripheral nervous system (Thor et al., 1991; Thaler et al., 2004; Sun et al., 2008). Our data revealed strong Isl1/2 expression in developing migrating GnRH-1ns (**Figures 3**, **4**, **6**). To test if Isl1 plays a role in GnRH-1ns migration or controls GnRH expression, we generated GnRH-1Cre/$Isl^{flox/flox}$ conditional mutants. Embryos were analyzed at E15.5, which is the stage at which the majority of the GnRH-1ns have already migrated in the brain (Forni et al., 2011a). Double immunostaining against Isl1/2 and GnRH confirmed detectable Isl1 ablation in 38% (SE ± 5.28%) of GnRH-1ns (**Figures 9A–B**'), while Isl1 in controls was detectable in virtually all migratory GnRH-1ns. In GnRH-1Cre/$Isl^{flox/flox}$ conditional mutants, GnRH-1ns negative for Isl1 immunoreactivity were found in the nasal area, forebrain junction, and the brain. These data suggest that Isl1 expression is not required for GnRH-1 peptide expression nor GnRH-1 neuronal migration. Quantification of GnRH-1ns distribution in nasal area, forebrain junction, and brain indicated an overall distribution of GnRH-1ns comparable with the one of controls (**Figure 9E**).

DISCUSSION

Cellular derivatives of the OPs play central roles in respiration, chemosensory detection, sexual development, fertility, and inter- and intra-species social behaviors. Understanding the basic mechanisms that define cellular diversity and underly normal and pathological development of the OP derivatives is of high clinical importance. Isl1 expression can occur in various neurogenic placodes (Begbie et al., 2002; Zhuang et al., 2013); however, a comprehensive analysis of Isl1 expression

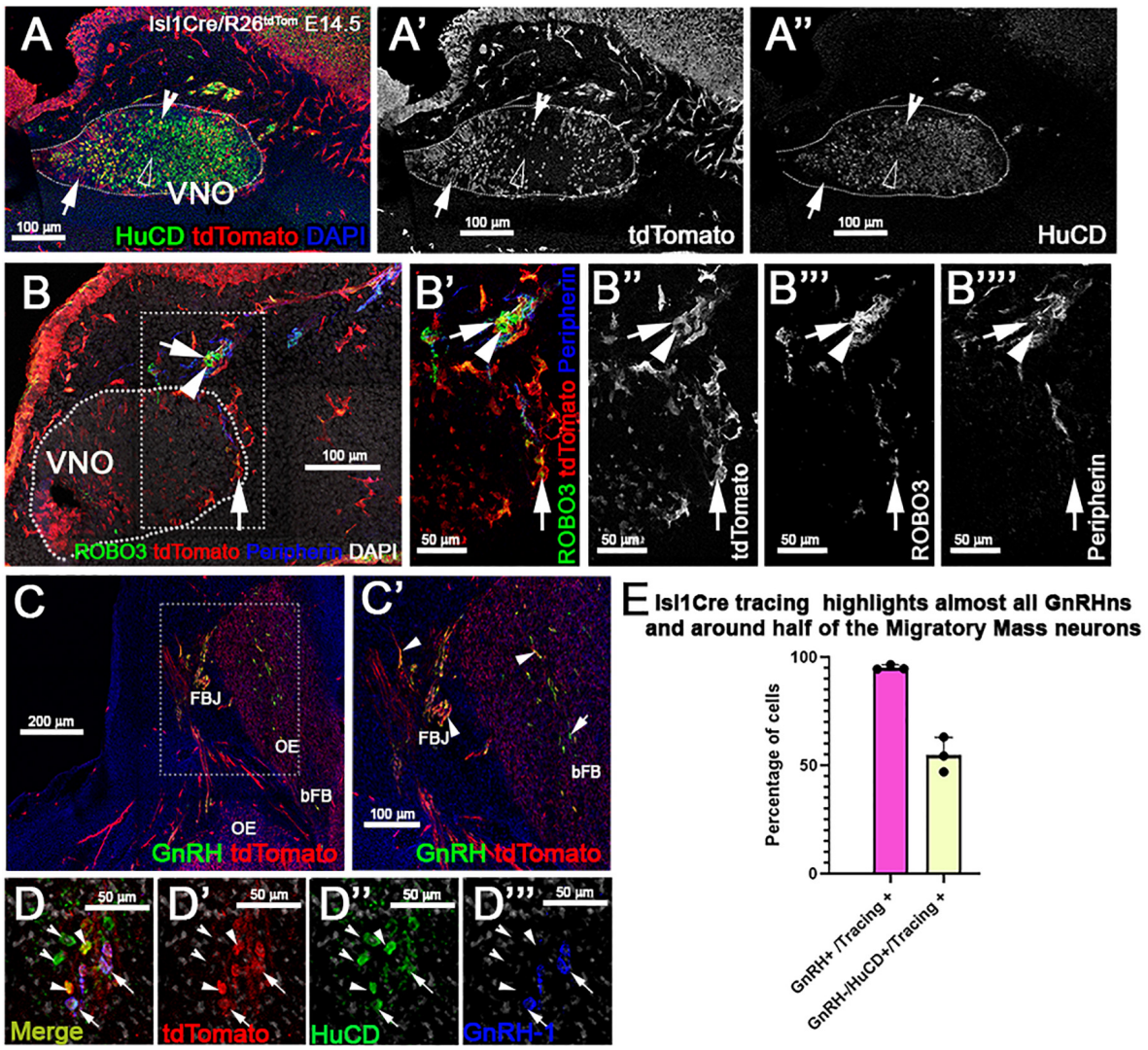

FIGURE 6 | Isl1 constitutive lineage tracing highlights GnRH-1ns, some cell bodies of the TN, and other migratory neurons. **(A–A")** HuC/D and tdTomato immunostaining of Isl1Cre$^{\pm}$/R26tdTomato VNO at E14.5 show some neurons within the VNO positive (empty arrowhead) and negative (notched arrowhead) for Isl1 recombination. Population of tdTomato + non-neuronal cells positive for tracing (arrow). **(B–B"")** Anti-Robo3; tdTomato and Peripherin labeling shows that a portion of putative terminal nerve cell bodies located within and proximal to the VNO are highlighted by Isl1 recombination (arrow) while a portion do not (arrowhead). **(C–C')** GnRH and tdTomato staining shows recombination in the majority of the GnRH-1ns (arrowheads). **(D–D"")** Recombination in ∼ half of the (GnRH−;HuC/D +) migratory neurons (arrows). **(E)** Quantification of Isl1Cre recombination in migratory GnRH + and HuC/D GnRH-1 negative neurons. VNO, vomeronasal organ; OE, olfactory epithelium; FBJ, fore brain junction; bFB, basal fore brain.

remains unknown. Isl1, which is important for differentiation, cell migration, survival, and axonal targeting of neurons in the peripheral nervous system (Thor et al., 1991; Thaler et al., 2004; Sun et al., 2008), has a very high upregulation during GnRH-1 neuronal differentiation (Lund et al., 2020). So, Isl1 remained a potential suitable genetic marker to label derivatives of the OP (Shan et al., 2020). Here, we sought to trace Isl1 expression and lineage in the developing nasal area using *in situ* hybridization, immunohistochemistry (**Figure 3**), temporally controlled Is1CreRT recombination (**Figure 4**), and constitutive Isl1Cre^{ERT} genetic lineage tracing (**Figures 5–8**).

GnRH-1 Lineage Tracing in the Developing Nasal Area

Using *in situ* hybridization and immunohistochemistry, we detected Isl1 expression at E11.5 in the putative GnRH neurogenic area, ventral to the developing VNO (**Figures 3A–D**), in newly formed GnRH-1ns and the developing olfactory epithelium (**Figures 3D–F**"'). At E11.5, Isl1 immunoreactivity occurred in 89%(±3.33%) of GnRH cells, in line with published reports (Shan et al., 2020). However, histochemistry at E13.5 and E15.5 showed strong Isl1/2 immunoreactivity in virtually all GnRH-1ns, suggesting that Isl1 expression is not limited to specific subpopulations of GnRH cells (Shan et al., 2020). These

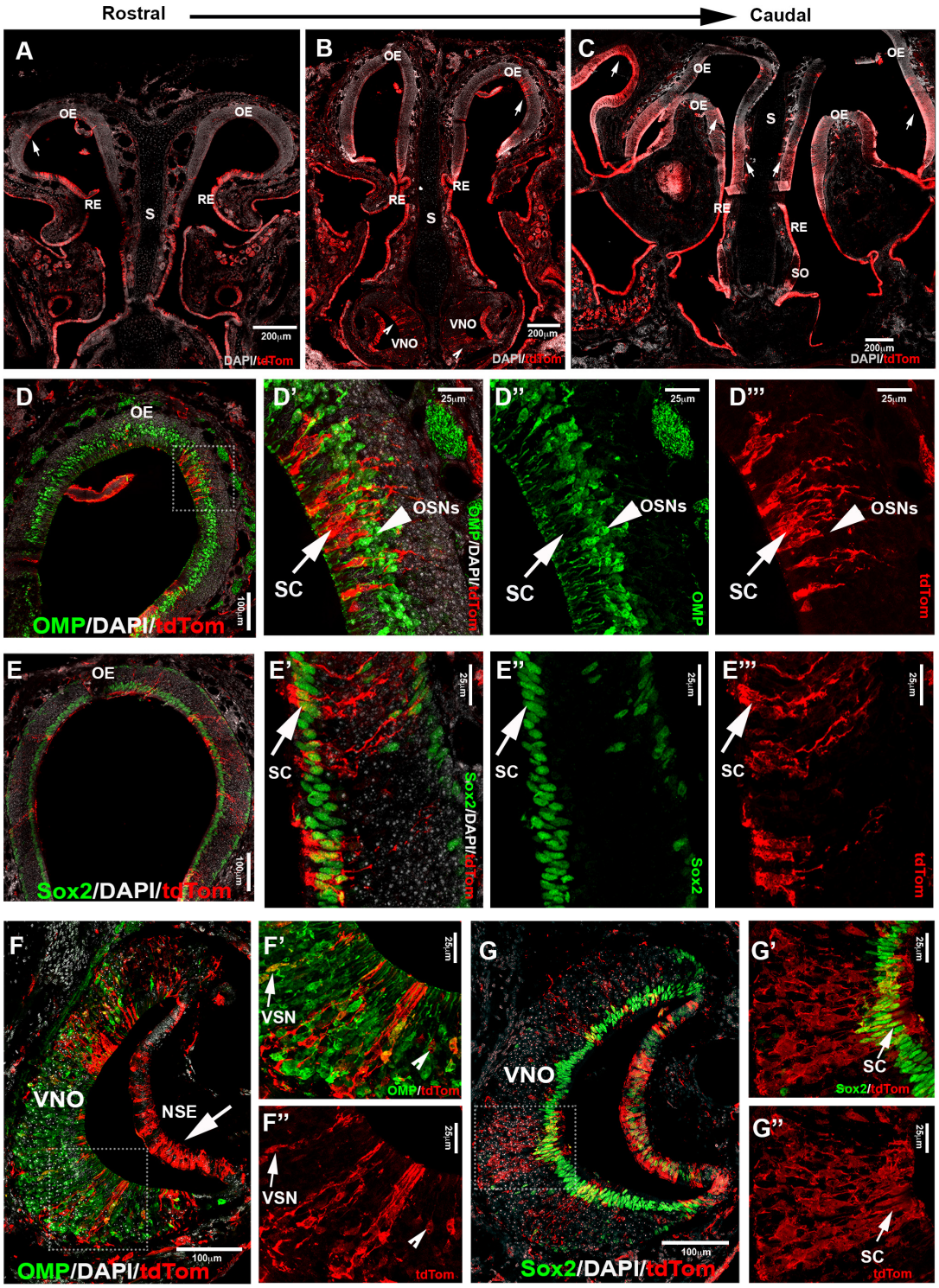

FIGURE 7 | Lineage tracing of Isl1 positive cells postnatally highlights neuronal and non-neuronal cells in OE and VNE. **(A–C)** Immunofluorescence against tdTom showing Isl1 tracing in olfactory epithelium (OE) from rostral toward the caudal ethmoid turbinates. Arrows **(A,B,C)** show tracing in OE. **(B)** Notched arrowheads show tracing in VNO. **(D–D''')** Double immunofluorescence against OMP (green) and tdTom (red) shows no colocalization in neurons of the OE. **(E–E''')** Double immunofluorescence against Sox2 (green) and tdTom (red) shows Isl1Cre tracing (arrow marks) in the sustentacular cells of the OE. Sox2 is present in both globose basal cells that are present in the base of the OE and sustentacular cells in the upper layers of the OE. **(F)** Double immunofluorescence against OMP (green) and tdTom (red) shows Isl1 tracing in both non-sensory epithelium (NSE—arrow mark) and sensory epithelium of the VNO. **(F',F'')** Arrow marks show colocalized mature vomeronasal neurons (VSNs) and notched arrow heads show traced neurons that are not labeled with OMP. **(G–G'')** Double immunofluorescence against Sox2 (green) and tdTom (red) shows Isl1 tracing in sustentacular cells in the VNO. S, septum; SO, septal organ; SC, sustentacular cells; OSNs, olfactory sensory neurons.

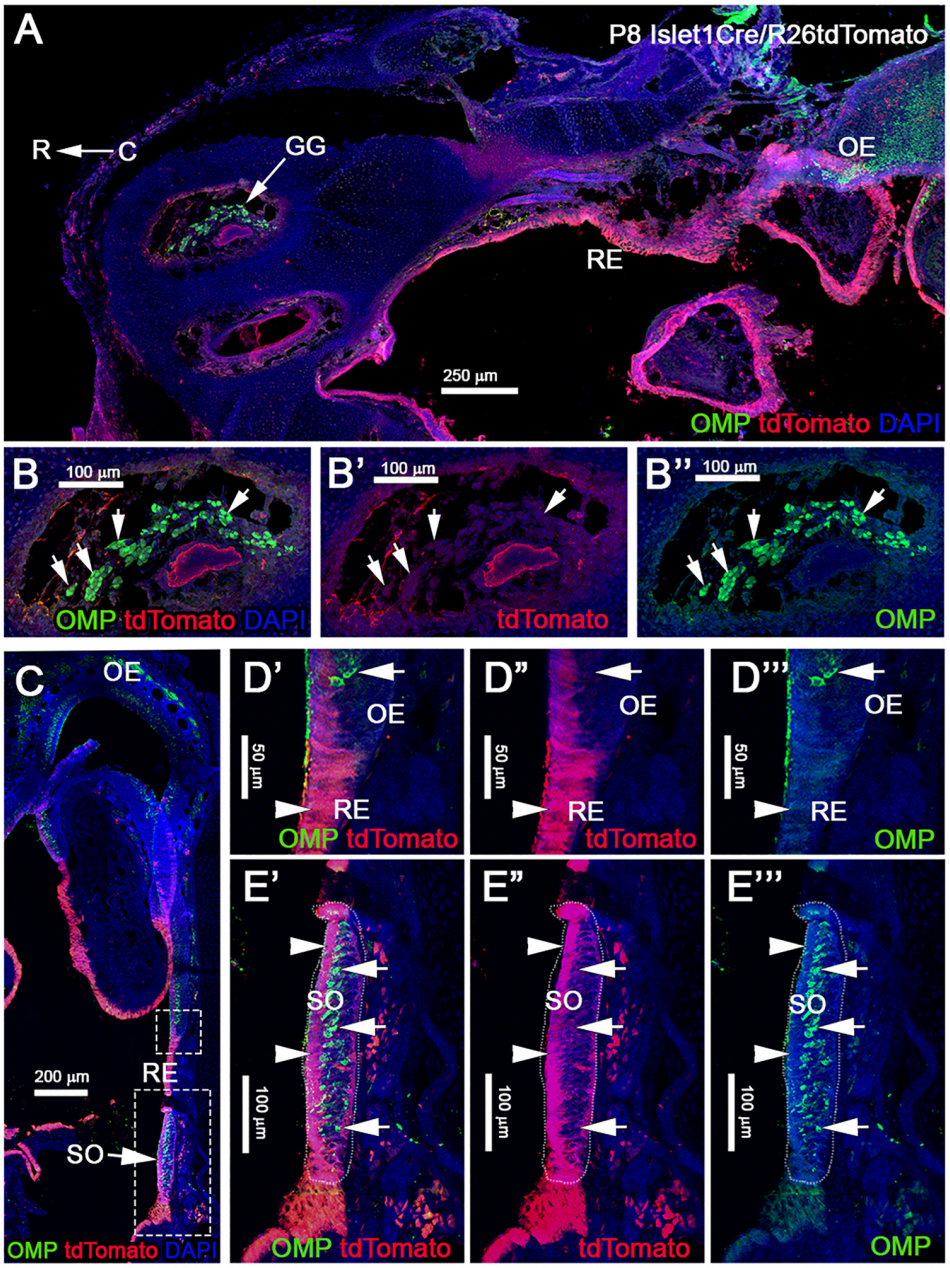

FIGURE 8 | Post-natal Isl1 constitutive lineage tracing is not expressed in other nasal sensory neurons. **(A)** Isl1Cre/R26tdTomato P8 parasagittal section of the nose immunostained against OMP and tdTomato shows that Isl1 recombination is limited to the respiratory epithelium even in post-natal stages. Neuronal sensory populations, such as the Gruenberg Ganglion (GG) **(B–B")**, is negative for recombination. **(C)** Coronal view of Isl1Cre/R26tdTomato at P8, stained against OMP and tdTomato shows Isl1 tracing restricted to the non-sensory cells and cells of the respiratory epithelium. **(D–D"')** Magnification from **C** of the border between olfactory and respiratory epithelium shows Isl1Cre tracing restricted to the respiratory epithelium (arrowhead), while OMP + neurons are negative (arrow). **(E–E"')** Septal organ (SO) from **C** indicates Isl1 recombination is restricted to the non-sensory (arrowheads) cells, while OMP + neurons are negative (arrows). R, rostral; C, caudal; RE, respiratory epithelium; OE, olfactory epithelium.

data suggest a dynamic expression of Isl1 with more GnRH-1 cells positive across development.

At E11.5 we also found the existence of proliferative cells positive for Isl1 in the developing olfactory pit. Tamoxifen controlled Isl1Cre^{ERT} tracing at E11.5 showed Isl1 lineage in putative GnRH progenitors/newly formed GnRH-1ns, cells of the respiratory epithelium, few proliferative progenitors in the developing olfactory pit, neurons at the border between respiratory epithelium and developing olfactory epithelium and sparse neuronal (HuC/D+) cells in the OE and VNO. Notably in this experiment we analyzed Isl1Cre^{ERT}/R26R recombination 4 days after Tam treatment. This means that,

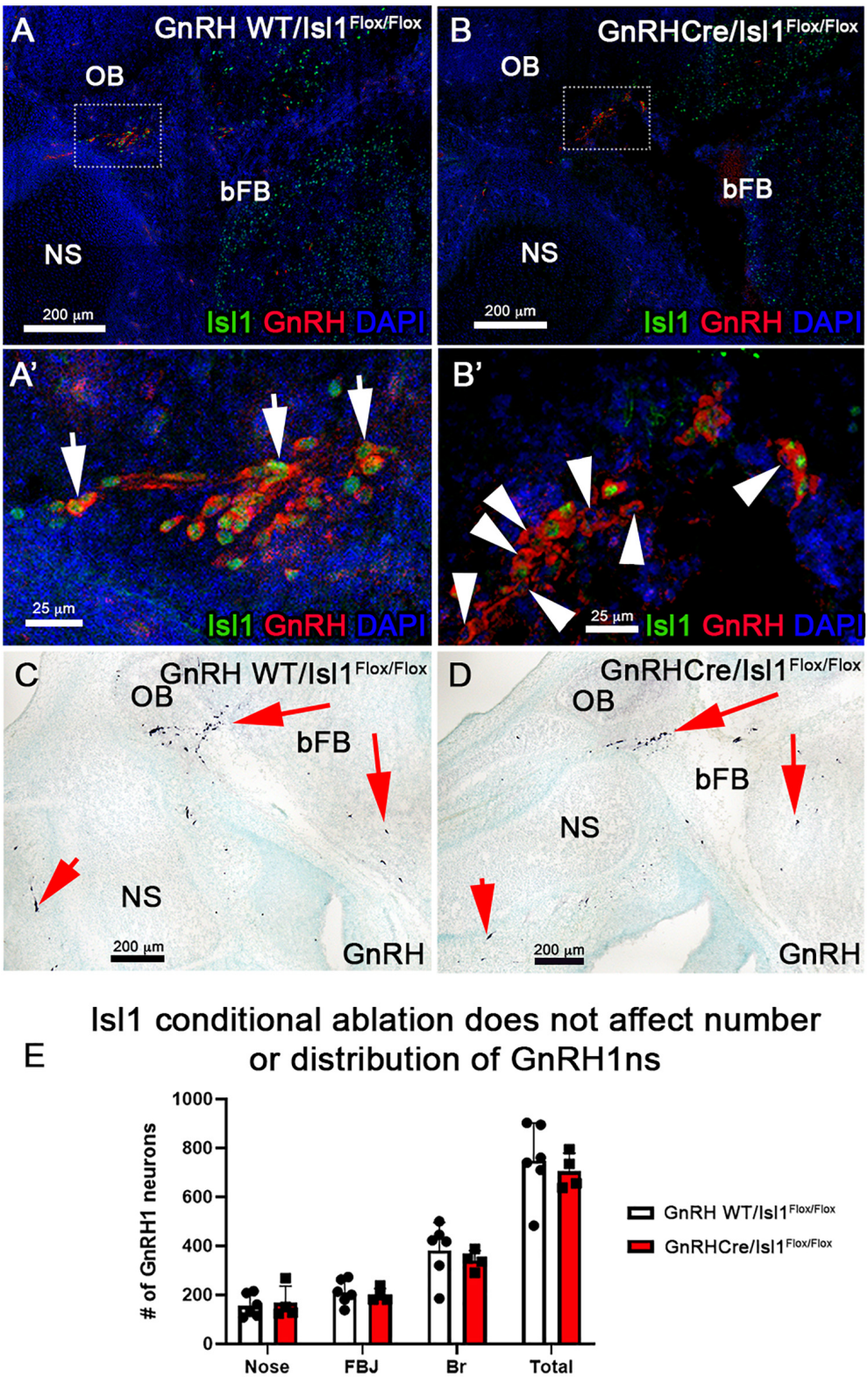

FIGURE 9 | Conditional loss of Isl1 in GnRH-1ns has no effect in their migration or development. Isl1/2 and GnRH double IF on E15.5 WT **(A–A')**, where all GnRH-1ns express Isl1/2 (arrows) and cKO **(B–B')** sections show that some GnRH-1ns lose the expression of Isl1 (arrowheads). **(C,D)** Immunohistochemistry of GnRH-1 on WT and cKO sections shows comparable distribution of cells positive for GnRH-1ns. **(E)** Quantification of cKO shows no changes in the number or distribution of GnRH-1ns. NS, nasal septum; OB, olfactory bulb; bFB, basal forebrain.

when we observed the histological samples, we identified either cells that expressed Isl1 at the moment of Tam injection or cells that derived from progenitors expressing Isl1 at time of Tam injection.

In line with what observed after temporally Tam controlled recombination at E11.5, constitutively active Isl1Cre recombination showed that, during embryonic development (**Figures 5**, **6**), Isl1 tracing highlights neurons in OE proximal to the border with RE, neurons in the vomeronasal organ, cells of the RE, GnRH-1ns, migratory neurons negative for GnRH, and sustentacular cells in olfactory and vomeronasal organ.

These data indicate that Isl1 expression/lineage is limited to specific subsets of olfactory placodal derivatives. In contrast to prior observations during embryonic development, Isl1Cre recombination analysis of postnatal Isl1Cre/R26R mice showed only sparse neurons positive for Isl1 tracing in the most caudal regions of the olfactory sensory epithelium, while cells positive for Isl1 tracing were still found in the VNO, respiratory epithelium, and in sustentacular cells of both OE and VNO (**Figure 7**). No Isl1 expression or lineage was in GC neurons and GG (**Figure 8**). These data suggest that Isl1 positive neurons in the OE at the border with the RE during embryonic development (**Figures 4**, **5**) either migrated out of the epithelium as a part of the MM or died, even though we could still detect Isl1 expression/lineage in some vomeronasal organ neurons (**Figures 7F–F**"). So, we further defined the fate of the Isl1 neurons detectable in the OE during embryonic development. During embryonic development, we could also detect axonal projections positive for Isl1 traversing through the nasal area (**Figures 4**, **5**). Some axonal projections likely belonged to the nasopalatine projections of the trigeminal nerve (**Figures 3–5**). Although both Isl1^{CreERT} and Isl1Cre induced recombination in Peripherin + fibers projected to the ventral OB, the majority of OMP + fibers projecting to the MOB and AOB appeared negative for Isl1 tracing (**Figures 4**, **5**). We did not pursue a detailed analysis of olfactory projections in postnatal animals, due to technical challenges in tracing Isl1 recombination in mitral cells of the MOB.

Isl1 in the GnRH-1 System

During embryonic development, GnRH-1ns migrate from the developing olfactory pit into the hypothalamus. Once in the preoptic area, GnRH neurons (GnRH-1ns) control the hypothalamic–pituitary–gonadal hormonal axis and reproductive development. Defective GnRH-1 release is the cause of HH, a condition that negatively impacts normal body development, social interactions, the ability to procreate, and physical performances (Burmeister et al., 2005; Yin and Gore, 2006; Maruska and Fernald, 2011; Zhang et al., 2013). HH associated with congenital anosmia (impairment of the sense of smell) is clinically defined as Kallmann syndrome (Kallmann, 1944; Legouis et al., 1991; Guioli et al., 1992; Hardelin et al., 1992; Incerti et al., 1992; Dode et al., 2003; Pitteloud et al., 2007). Though postnatal development of the olfactory system has been extensively studied, we still ignore many aspects regarding early development of the olfactory pit derivatives.

Previous studies in chick and mice indicate that soon after the OPs form they give rise to migratory olfactory pioneer neurons, and to several other neuronal populations including the terminal nerve cells and the GnRH-1ns. Placodal derived migratory neurons and the neural crest derived olfactory ensheathing cells form the MM (Barraud et al., 2013, 2010).

We previously showed that the fibers of the terminal nerve, upon which the GnRH-1ns migrate, are distinct from the OSN and VSN (Taroc et al., 2017, 2019, 2020). What progenitors give rise to the GnRH neurons, and what transcription factors control their onset are still open questions. Moreover, if what we define as GnRH neurons is one homogenous neuronal population is also a matter of debate.

Lineage tracing at different developmental stages suggests strong and consistent Isl1 expression in GnRH-1ns and cells of the MM (**Figures 3**, **4**, **6**). While the terminal nerve that projects from the vomeronasal area to the basal forebrain appeared to have heterogeneous Isl1 expression/genetic lineage tracing (**Figure 6**), Isl1 has been reported to be important in neuronal differentiation, cell migration, survival, and axonal targeting of various neuronal types (Thor et al., 1991; Thaler et al., 2004; Sun et al., 2008). The consistent Isl1/2 expression in developing and migratory GnRH-1ns (**Figures 3**, **4**, **6**), which is conserved from fish to humans prompted us to test its developmental role.

We first made an attempt to conditionally KO Isl1, which as a whole KO is embryonic lethal, by mating Isl1^{CreERT} mice (**Figure 4**), which are Isl1^{null} heterozygous, with Isl1^{flox}. After Tamoxifen injection at E11.5, we analyzed Isl1$^{CreERT/flox}$ mice and controls at E15.5 (as in **Figure 4**). After Tamoxifen treatment, Isl1^{CreERT} extensively recombines in the developing GnRH-1ns (**Figure 4**). Surprisingly Tam + Isl1^{CreERT}/Isl1^{flox} embryos did not show any obvious phenotype related to GnRH-1ns (**Supplementary Material**). However, for this model, we could not verify the efficiency of recombination because antibodies unable to detect the floxed Isl1 truncated protein were still recognizing the Isl1^{CreERT} protein product (see section "Materials and Methods"). For this reason, we report these as supplementary observations. In order to further test the role of Isl1 in GnRH-1 neuronal development, we generated GnRH-1Cre/Isl1$^{flox/flox}$ conditional mutants. Here, we could document complete loss of Isl1 immunoreactvity in around ∼40% of GnRH-1ns (**Figure 9**). Notably most of the anti Isl1 Abs have some level of cross reactivity with Isl2, therefore we performed *in situ* hybridization against exon 4 of Isl1 paired with anti GnRH-1 immunofluorescent staining (not shown). These experiments suggest similar penetrance of recombination as indicated by IF. Notably, also in GnRH-1Cre/Isl1$^{flox/flox}$ mutants, we did not observe obvious defects in GnRH-1 neuronal migration nor in GnRH-1 expression (**Figure 9**). In fact, GnRH-1ns negative for Isl1 were found in both nasal area and brain. Total number and overall distribution of GnRH-1 was comparable to controls. These data suggest that Isl1 alone is not necessary for GnRH-1 expression or neuronal migration. We believe that our conditional Isl1KO might partially compensate Isl1 loss-of-function through Isl2 expression. Notably, Isl1 and Isl2 have been shown to be required for the expression of neuropilin-1

(Nrp1) (Lee et al., 2015). Moreover, it was recently demonstrated that selective loss of Nrp1 in GnRH-1ns leads to a total increase in the number of GnRH-1ns in mouse (Vanacker et al., 2020). In line with these observations in our $Isl1^{CreERT/Flox}$ cKO embryos, we observed a trend with an increase in the total number of immunoreactive GnRH-1ns (**Supplementary Figure S1**). Since loss of Nrp1 expression is more dramatic in Isl1/Isl2 double knockouts (Lee et al., 2015), we predict that Isl1/Isl2 double knockouts could have increased number of GnRH-1ns as reported for Nrp1 null mice (Vanacker et al., 2020).

CONCLUSION

Our data indicate very selective expression of Isl1 in neurons forming in the OP including the GnRH-1ns, various migratory neuronal populations and some cells in the VNO, terminal nerve and sustentacular cells on the more medial and lateral portions of the OE. Isl-1 immunoreactivity and genetic tracing suggest that Isl-1 expression, though dynamic, is common feature for virtually all GnRH-1ns (Shan et al., 2020) and several other neurons of the MM. If all these early migratory neurons derive from similar pre-placodal subregions should be further investigated. Performing GnRH-1ns specific Isl1 ablation in GnRH-1ns we did not detect obvious cell specification, differentiation, survival, or migratory defects (Shan et al., 2020) at embryonic development stages suggesting a dispensable role for Isl1 in GnRH neurons.

Our results leave open the question of what is the physiological role of this transcription factor in murine GnRH-1ns development and function. Further studies focused on Isl1 role in postnatal developmental and fertility can give definitive insights.

DATA AVAILABILITY STATEMENT

All datasets presented in this study are included in the article/**Supplementary Material**.

ETHICS STATEMENT

The animal study was reviewed and approved by the Institutional Animal Care and Use Committee (IACUC).

AUTHOR CONTRIBUTIONS

ET set the mouse mating, collected samples, prepared histological samples, performed immunostaining and imaging, and analyzed data at embryonic developmental stages. RK prepared histological samples and performed immunostaining and analyses of postnatal animals. ET and PF designed the experiments, wrote the article, and prepared figure panels. All authors contributed to the article and approved the submitted version.

FUNDING

Research reported in this publication was supported by the Eunice Kennedy Shriver National Institute of Child Health and Human Development of the National Institutes of Health under the Awards R15-HD096411 (PF) and R01-HD097331/HD/NICHD (PF), and by the National Institute of Deafness and Other Communication Disorders of the National Institutes of Health under the Award R01-DC017149 (PF).

SUPPLEMENTARY MATERIAL

The Supplementary Material for this article can be found online at: https://www.frontiersin.org/articles/10.3389/fphys.2020.601923/full#supplementary-material

Supplementary Figure 1 | $Isl1Cre^{ERT}/Isl1^{Flx}$ conditional knockout at E11.5 does not affect GnRH1ns. GnRH IHC on WT **(A)** and cKO **(B)** sections show that between each genotype the distribution of GnRH-1ns looks similar. **(C)** Quantification of the number of GnRH-1ns in whole embryo heads shows no significant regional changes or in total cell number.

REFERENCES

Aguillon, R., Batut, J., Subramanian, A., Madelaine, R., Dufourcq, P., Schilling, T. F., et al. (2018). Cell-type heterogeneity in the early zebrafish olfactory epithelium is generated from progenitors within preplacodal ectoderm. *eLife* 7:e32041. doi: 10.7554/eLife.32041

Bailey, A. P., and Streit, A. (2006). Sensory organs: making and breaking the pre-placodal region. *Curr. Top. Dev. Biol.* 72, 167–204. doi: 10.1016/s0070-2153(05)72003-2

Balasubramanian, R., Dwyer, A., Seminara, S. B., Pitteloud, N., and Kaiser, U. B. (2010). Human GnRH deficiency: a unique disease model to unravel the ontogeny of GnRH neurons. *Neuroendocrinology* 92, 81–99. doi: 10.1159/000314193

Barraud, P., Seferiadis, A. A., Tyson, L. D., Zwart, M. F., Szabo-Rogers, H. L., Ruhrberg, C., et al. (2010). Neural crest origin of olfactory ensheathing glia. *Proc. Natl. Acad. Sci. U.S.A.* 107, 21040–21045. doi: 10.1073/pnas.1012248107

Barraud, P., St John, J. A., Stolt, C. C., Wegner, M., and Baker, C. V. (2013). Olfactory ensheathing glia are required for embryonic olfactory axon targeting and the migration of gonadotropin-releasing hormone neurons. *Biol. Open* 2, 750–759. doi: 10.1242/bio.20135249

Begbie, J., Ballivet, M., and Graham, A. (2002). Early steps in the production of sensory neurons by the neurogenic placodes. *Mol. Cell. Neurosci.* 21, 502–511. doi: 10.1006/mcne.2002.1197

Brann, D. H., Tsukahara, T., Weinreb, C., Lipovsek, M., Van den Berge, K., Gong, B., et al. (2020). Non-neuronal expression of SARS-CoV-2 entry genes in the olfaory system suggests mechanisms underlying COVID-19-associated anosmia. *Sci. Adv.* 6:eabc5801. doi: 10.1126/sciadv.abc5801

Brown, J. W. (1987). The nervus terminalis in insectivorous bat embryos and notes on its presence during human ontogeny. *Ann. N.Y. Acad. Sci.* 519, 184–200. doi: 10.1111/j.1749-6632.1987.tb36297.x

Brugmann, S. A., and Moody, S. A. (2005). Induction and specification of the vertebrate ectodermal placodes: precursors of the cranial sensory organs. *Biol. Cell.* 97, 303–319. doi: 10.1042/bc20040515

Burmeister, S. S., Jarvis, E. D., and Fernald, R. D. (2005). Rapid behavioral and genomic responses to social opportunity. *PLoS Biol.* 3:e363. doi: 10.1371/journal.pbio.0030363

Castinetti, F., Brinkmeier, M. L., Mortensen, A. H., Vella, K. R., Gergics, P., Brue, T., et al. (2015). ISL1 is necessary for maximal thyrotrope response to hypothyroidism. *Mol. Endocrinol.* 29, 1510–1521. doi: 10.1210/me.2015-1192

Cattanach, B. M., Iddon, C. A., Charlton, H. M., Chiappa, S. A., and Fink, G. (1977). Gonadotrophin-releasing hormone deficiency in a mutant mouse with hypogonadism. *Nature* 269, 338–340. doi: 10.1038/269338a0

Cau, E., Casarosa, S., and Guillemot, F. (2002). Mash1 and Ngn1 control distinct steps of determination and differentiation in the olfactory sensory neuron lineage. *Development* 129, 1871–1880.

Cau, E., Gradwohl, G., Casarosa, S., Kageyama, R., and Guillemot, F. (2000). Hes genes regulate sequential stages of neurogenesis in the olfactory epithelium. *Development* 127, 2323–2332.

Cau, E., Gradwohl, G., Fode, C., and Guillemot, F. (1997). Mash1 activates a cascade of bHLH regulators in olfactory neuron progenitors. *Development* 124, 1611–1621.

Chen, B., Kim, E. H., and Xu, P. X. (2009). Initiation of olfactory placode development and neurogenesis is blocked in mice lacking both Six1 and Six4. *Dev. Biol.* 326, 75–85. doi: 10.1016/j.ydbio.2008.10.039

Cuschieri, A., and Bannister, L. H. (1975a). The development of the olfactory mucosa in the mouse: electron microscopy. *J. Anat.* 119, 471–498.

Cuschieri, A., and Bannister, L. H. (1975b). The development of the olfactory mucosa in the mouse: light microscopy. *J. Anat.* 119, 277–286.

Dode, C., Levilliers, J., Dupont, J. M., De Paepe, A., Le Du, N., Soussi-Yanicostas, N., et al. (2003). Loss-of-function mutations in FGFR1 cause autosomal dominant Kallmann syndrome. *Nat. Genet.* 33, 463–465. doi: 10.1038/ng1122

Donner, A. L., Episkopou, V., and Maas, R. L. (2007). Sox2 and Pou2f1 interact to control lens and olfactory placode development. *Dev. Biol.* 303, 784–799. doi: 10.1016/j.ydbio.2006.10.047

Fornaro, M., Geuna, S., Fasolo, A., and Giacobini-Robecchi, M. G. (2003). HuC/D confocal imaging points to olfactory migratory cells as the first cell population that expresses a post-mitotic neuronal phenotype in the chick embryo. *Neuroscience* 122, 123–128. doi: 10.1016/j.neuroscience.2003.07.004

Fornaro, M., Raimondo, S., Lee, J. M., and Giacobini-Robecchi, M. G. (2007). Neuron-specific Hu proteins sub-cellular localization in primary sensory neurons. *Ann. Anat.* 189, 223–228. doi: 10.1016/j.aanat.2006.11.004

Forni, P. E., Bharti, K., Flannery, E. M., Shimogori, T., and Wray, S. (2013). The indirect role of fibroblast growth factor-8 in defining neurogenic niches of the olfactory/GnRH systems. *J. Neurosci.* 33, 19620–19634. doi: 10.1523/jneurosci.3238-13.2013

Forni, P. E., Fornaro, M., Guenette, S., and Wray, S. (2011a). A role for FE65 in controlling GnRH-1 neurogenesis. *J. Neurosci.* 31, 480–491. doi: 10.1523/jneurosci.4698-10.2011

Forni, P. E., Taylor-Burds, C., Melvin, V. S., Williams, T., and Wray, S. (2011b). Neural crest and ectodermal cells intermix in the nasal placode to give rise to GnRH-1 neurons, sensory neurons, and olfactory ensheathing cells. *J. Neurosci.* 31, 6915–6927. doi: 10.1523/jneurosci.6087-10.2011

Forni, P. E., and Wray, S. (2015). GnRH, anosmia and hypogonadotropic hypogonadism–where are we? *Front. Neuroendocrinol.* 36:165–177. doi: 10.1016/j.yfrne.2014.09.004

Greer, P. L., Bear, D. M., Lassance, J. M., Bloom, M. L., Tsukahara, T., Pashkovski, S. L., et al. (2016). A family of non-GPCR chemosensors defines an alternative logic for mammalian olfaction. *Cell* 165, 1734–1748. doi: 10.1016/j.cell.2016.05.001

Gruneberg, H. (1973). A ganglion probably belonging to the N. terminalis system in the nasal mucosa of the mouse. *Z. Anat. Entwicklungsgesch.* 140, 39–52. doi: 10.1007/bf00520716

Guioli, S., Incerti, B., Zanaria, E., Bardoni, B., Franco, B., Taylor, K., et al. (1992). Kallmann syndrome due to a translocation resulting in an X/Y fusion gene. *Nat. Genet.* 1, 337–340. doi: 10.1038/ng0892-337

Hardelin, J. P., Levilliers, J., del Castillo, I., Cohen-Salmon, M., Legouis, R., Blanchard, S., et al. (1992). X chromosome-linked Kallmann syndrome: stop mutations validate the candidate gene. *Proc. Natl. Acad. Sci. U.S.A.* 89, 8190–8194. doi: 10.1073/pnas.89.17.8190

Hilal, E. M., Chen, J. H., and Silverman, A. J. (1996). Joint migration of gonadotropin-releasing hormone (GnRH) and neuropeptide Y (NPY) neurons from olfactory placode to central nervous system. *J. Neurobiol.* 31, 487–502. doi: 10.1002/(sici)1097-4695(199612)31:4<487::aid-neu8>3.0.co;2-5

Huang, M., Kantardzhieva, A., Scheffer, D., Liberman, M. C., and Chen, Z. Y. (2013). Hair cell overexpression of Islet1 reduces age-related and noise-induced hearing loss. *J. Neurosci.* 33, 15086–15094. doi: 10.1523/jneurosci.1489-13.2013

Hutchinson, S. A., and Eisen, J. S. (2006). Islet1 and Islet2 have equivalent abilities to promote motoneuron formation and to specify motoneuron subtype identity. *Development* 133, 2137–2147. doi: 10.1242/dev.02355

Incerti, B., Guioli, S., Pragliola, A., Zanaria, E., Borsani, G., Tonlorenzi, R., et al. (1992). Kallmann syndrome gene on the X and Y chromosomes: implications for evolutionary divergence of human sex chromosomes. *Nat. Genet.* 2, 311–314. doi: 10.1038/ng1292-311

Jennes, L. (1987). The nervus terminalis in the mouse: light and electron microscopic immunocytochemical studies. *Ann. N.Y. Acad. Sci.* 519, 165–173. doi: 10.1111/j.1749-6632.1987.tb36295.x

Jin, Z. W., Cho, K. H., Shibata, S., Yamamoto, M., Murakami, G., and Rodriguez-Vazquez, J. F. (2019). Nervus terminalis and nerves to the vomeronasal organ: a study using human fetal specimens. *Anat. Cell. Biol.* 52, 278–285. doi: 10.5115/acb.19.020

Kallmann, F. J. (1944). The genetic aspects of primary eunuchoidism. *J. Ment. Defic.* 48, 203–236.

Katoh, H., Shibata, S., Fukuda, K., Sato, M., Satoh, E., Nagoshi, N., et al. (2011). The dual origin of the peripheral olfactory system: placode and neural crest. *Mol. Brain* 4:34. doi: 10.1186/1756-6606-4-34

Larsell, O. (1950). The nervus terminalis. *Ann. Otol. Rhinol. Laryngol.* 59, 414–438.

Laugwitz, K. L., Moretti, A., Lam, J., Gruber, P., Chen, Y., Woodard, S., et al. (2005). Postnatal isl1+ cardioblasts enter fully differentiated cardiomyocyte lineages. *Nature* 433, 647–653. doi: 10.1038/nature03215

Lee, H., Kim, M., Kim, N., Macfarlan, T., Pfaff, S. L., Mastick, G. S., et al. (2015). Slit and Semaphorin signaling governed by Islet transcription factors positions motor neuron somata within the neural tube. *Exp. Neurol.* 269, 17–27. doi: 10.1016/j.expneurol.2015.03.024

Legouis, R., Hardelin, J. P., Levilliers, J., Claverie, J. M., Compain, S., Wunderle, V., et al. (1991). The candidate gene for the X-linked Kallmann syndrome encodes a protein related to adhesion molecules. *Cell* 67, 423–435. doi: 10.1016/0092-8674(91)90193-3

Lin, J. M., Taroc, E. Z. M., Frias, J. A., Prasad, A., Catizone, A. N., Sammons, M. A., et al. (2018). The transcription factor Tfap2e/AP-2epsilon plays a pivotal role in maintaining the identity of basal vomeronasal sensory neurons. *Dev. Biol.* 441, 67–82. doi: 10.1016/j.ydbio.2018.06.007

Lund, C., Yellapragada, V., Vuoristo, S., Balboa, D., Trova, S., Allet, C., et al. (2020). Characterization of the human GnRH neuron developmental transcriptome using a GNRH1-TdTomato reporter line in human pluripotent stem cells. *Dis. Model. Mech.* 13:dmm040105. doi: 10.1242/dmm.040105

Luo, M. (2008). The necklace olfactory system in mammals. *J. Neurogenet.* 22, 229–238. doi: 10.1080/01677060802340228

Ma, M., Grosmaitre, X., Iwema, C. L., Baker, H., Greer, C. A., and Shepherd, G. M. (2003). Olfactory signal transduction in the mouse septal organ. *J. Neurosci.* 23, 317–324. doi: 10.1523/jneurosci.23-01-00317.2003

Madisen, L., Zwingman, T. A., Sunkin, S. M., Oh, S. W., Zariwala, H. A., Gu, H., et al. (2010). A robust and high-throughput Cre reporting and characterization system for the whole mouse brain. *Nat. Neurosci.* 13, 133–140. doi: 10.1038/nn.2467

Mamasuew, K., Hofmann, N., Breer, H., and Fleischer, J. (2011). Grueneberg ganglion neurons are activated by a defined set of odorants. *Chem. Senses.* 36, 271–282. doi: 10.1093/chemse/bjq124

Maruska, K. P., and Fernald, R. D. (2011). Social regulation of gene expression in the hypothalamic-pituitary-gonadal axis. *Physiology* 26, 412–423. doi: 10.1152/physiol.00032.2011

Matsuo, T., Rossier, D. A., Kan, C., and Rodriguez, I. (2012). The wiring of Grueneberg ganglion axons is dependent on neuropilin 1. *Development* 139, 2783–2791. doi: 10.1242/dev.077008

Moine, F., Brechbuhl, J., Nenniger Tosato, M., Beaumann, M., and Broillet, M. C. (2018). Alarm pheromone and kairomone detection via bitter taste receptors in the mouse *Grueneberg ganglion*. *BMC Biol.* 16:12.

Mori, K., Manabe, H., and Narikiyo, K. (2014). Possible functional role of olfactory subsystems in monitoring inhalation and exhalation. *Front. Neuroanat.* 8:107.

Oelschlager, H. A., Buhl, E. H., and Dann, J. F. (1987). Development of the nervus terminalis in mammals including toothed whales and

humans. *Ann. N.Y. Acad. Sci.* 519, 447–464. doi: 10.1111/j.1749-6632.1987.tb36316.x

Palaniappan, T. K., Slekiene, L., Gunhaga, L., and Patthey, C. (2019). Extensive apoptosis during the formation of the terminal nerve ganglion by olfactory placode-derived cells with distinct molecular markers. *Differentiation* 110, 8–16. doi: 10.1016/j.diff.2019.09.003

Pfister, S., Dietrich, M. G., Sidler, C., Fritschy, J. M., Knuesel, I., and Elsaesser, R. (2012). Characterization and turnover of CD73/IP(3)R3-positive microvillar cells in the adult mouse olfactory epithelium. *Chem. Senses.* 37, 859–868. doi: 10.1093/chemse/bjs069

Pingault, V., Bodereau, V., Baral, V., Marcos, S., Watanabe, Y., Chaoui, A., et al. (2013). Loss-of-function mutations in SOX10 cause Kallmann syndrome with deafness. *Am. J. Hum. Genet.* 92, 707–724. doi: 10.1016/j.ajhg.2013.03.024

Pitteloud, N., Zhang, C., Pignatelli, D., Li, J. D., Raivio, T., Cole, L. W., et al. (2007). Loss-of-function mutation in the prokineticin 2 gene causes Kallmann syndrome and normosmic idiopathic hypogonadotropic hypogonadism. *Proc. Natl. Acad. Sci. U.S.A.* 104, 17447–17452. doi: 10.1073/pnas.0707173104

Radde-Gallwitz, K., Pan, L., Gan, L., Lin, X., Segil, N., Chen, P., et al. (2004). Expression of Islet1 marks the sensory and neuronal lineages in the mammalian inner ear. *J. Comp. Neurol.* 477, 412–421. doi: 10.1002/cne.20257

Riddiford, N., and Schlosser, G. (2016). Dissecting the pre-placodal transcriptome to reveal presumptive direct targets of Six1 and Eya1 in cranial placodes. *eLife* 5:e17666.

Schlosser, G. (2006). Induction and specification of cranial placodes. *Dev. Biol.* 294, 303–351. doi: 10.1016/j.ydbio.2006.03.009

Schlosser, G., Awtry, T., Brugmann, S. A., Jensen, E. D., Neilson, K., Ruan, G., et al. (2008). Eya1 and Six1 promote neurogenesis in the cranial placodes in a SoxB1-dependent fashion. *Dev. Biol.* 320, 199–214. doi: 10.1016/j.ydbio.2008.05.523

Schmid, A., Pyrski, M., Biel, M., Leinders-Zufall, T., and Zufall, F. (2010). Grueneberg ganglion neurons are finely tuned cold sensors. *J. Neurosci.* 30, 7563–7568. doi: 10.1523/jneurosci.0608-10.2010

Schwanzel-Fukuda, M., Garcia, M. S., Morrell, J. I., and Pfaff, D. W. (1987). Distribution of luteinizing hormone-releasing hormone in the nervus terminalis and brain of the mouse detected by immunocytochemistry. *J. Comp. Neurol.* 255, 231–244. doi: 10.1002/cne.902550207

Schwanzel-Fukuda, M., and Pfaff, D. W. (1989). Origin of luteinizing hormone-releasing hormone neurons. *Nature* 338, 161–164. doi: 10.1038/338161a0

Shan, Y., Saadi, H., and Wray, S. (2020). Heterogeneous origin of gonadotropin releasing hormone-1 neurons in mouse embryos detected by islet-1/2 expression. *Front. Cell. Dev. Biol.* 8:35.

Sjodal, M., and Gunhaga, L. (2008). Expression patterns of Shh, Ptc2, Raldh3, Pitx2, Isl1, Lim3 and Pax6 in the developing chick hypophyseal placode and Rathke's pouch. *Gene Exp. Patterns* 8, 481–485. doi: 10.1016/j.gep.2008.06.007

Sun, Y., Dykes, I. M., Liang, X., Eng, S. R., Evans, S. M., Turner, E. E., et al. (2008). A central role for Islet1 in sensory neuron development linking sensory and spinal gene regulatory programs. *Nat. Neurosci.* 11, 1283–1293. doi: 10.1038/nn.2209

Suzuki, J., and Osumi, N. (2015). Neural crest and placode contributions to olfactory development. *Curr. Top. Dev. Biol.* 111, 351–374. doi: 10.1016/bs.ctdb.2014.11.010

Tanaka, H., Nojima, Y., Shoji, W., Sato, M., Nakayama, R., Ohshima, T., et al. (2011). Islet1 selectively promotes peripheral axon outgrowth in Rohon-Beard primary sensory neurons. *Dev. Dyn.* 240, 9–22. doi: 10.1002/dvdy.22499

Taroc, E. Z. M., Lin, J. M., Tulloch, A. J., Jaworski, A., and Forni, P. E. (2019). GnRH-1 neural migration from the nose to the brain is independent from Slit2, Robo3 and NELL2 signaling. *Front. Cell Neurosci.* 13:70.

Taroc, E. Z. M., Naik, A. S., Lin, J. M., Peterson, N. B., Keefe, D. L. Jr., Genis, E., et al. (2020). Gli3 regulates vomeronasal neurogenesis, olfactory ensheathing cell formation, and GnRH-1 neuronal migration. *J. Neurosci.* 40, 311–326. doi: 10.1523/jneurosci.1977-19.2019

Taroc, E. Z. M., Prasad, A., Lin, J. M., and Forni, P. E. (2017). The terminal nerve plays a prominent role in GnRH-1 neuronal migration independent from proper olfactory and vomeronasal connections to the olfactory bulbs. *Biol. Open* 6, 1552–1568. doi: 10.1242/bio.029074

Thaler, J. P., Koo, S. J., Kania, A., Lettieri, K., Andrews, S., Cox, C., et al. (2004). A postmitotic role for Isl-class LIM homeodomain proteins in the assignment of visceral spinal motor neuron identity. *Neuron* 41, 337–350. doi: 10.1016/s0896-6273(04)00011-x

Thor, S., Ericson, J., Brannstrom, T., and Edlund, T. (1991). The homeodomain LIM protein Isl-1 is expressed in subsets of neurons and endocrine cells in the adult rat. *Neuron* 7, 881–889. doi: 10.1016/0896-6273(91)90334-v

Vanacker, C., Trova, S., Shruti, S., Casoni, F., Messina, A., Croizier, S., et al. (2020). Neuropilin-1 expression in GnRH neurons regulates prepubertal weight gain and sexual attraction. *EMBO J.* 39:e104633.

Wang, F., Zhao, S., Xie, Y., Yang, W., and Mo, Z. (2018). De novo SOX10 nonsense mutation in a patient with kallmann syndrome, deafness, iris hypopigmentation, and hyperthyroidism. *Ann. Clin. Lab. Sci.* 48, 248–252.

Wirsig-Wiechmann, C. R. (2004). Introduction to the anatomy and function of the nervus terminalis. *Microsc. Res. Tech.* 65:1. doi: 10.1002/jemt.20115

Wray, S., Grant, P., and Gainer, H. (1989). Evidence that cells expressing luteinizing hormone-releasing hormone mRNA in the mouse are derived from progenitor cells in the olfactory placode. *Proc. Natl. Acad. Sci. U.S.A.* 86, 8132–8136. doi: 10.1073/pnas.86.20.8132

Yang, L., Cai, C. L., Lin, L., Qyang, Y., Chung, C., Monteiro, R. M., et al. (2006). Isl1Cre reveals a common Bmp pathway in heart and limb development. *Development* 133, 1575–1585. doi: 10.1242/dev.02322

Yin, W., and Gore, A. C. (2006). Neuroendocrine control of reproductive aging: roles of GnRH neurons. *Reproduction* 131, 403–414. doi: 10.1530/rep.1.00617

Yoon, H., Enquist, L. W., and Dulac, C. (2005). Olfactory inputs to hypothalamic neurons controlling reproduction and fertility. *Cell* 123, 669–682. doi: 10.1016/j.cell.2005.08.039

Zhang, G., Li, J., Purkayastha, S., Tang, Y., Zhang, H., Yin, Y., et al. (2013). Hypothalamic programming of systemic ageing involving IKK-beta, NF-kappaB and GnRH. *Nature* 497, 211–216. doi: 10.1038/nature12143

Zhou, X., Li, W. W., Wu, Q. Y., Yu, M. M., and Xia, X. Y. (2017). [Kallmann syndrome with deafness caused by SOX10 mutation: advances in research]. *Zhonghua Nan Ke Xue* 23, 838–841.

Zhuang, S., Zhang, Q., Zhuang, T., Evans, S. M., Liang, X., Sun, Y., et al. (2013). Expression of Isl1 during mouse development. *Gene Exp. Patterns* 13, 407–412. doi: 10.1016/j.gep.2013.07.001 widen

Zou, D., Silvius, D., Fritzsch, B., and Xu, P. X. (2004). Eya1 and Six1 are essential for early steps of sensory neurogenesis in mammalian cranial placodes. *Development* 131, 5561–5572. doi: 10.1242/dev.01437

Conflict of Interest: The authors declare that the research was conducted in the absence of any commercial or financial relationships that could be construed as a potential conflict of interest.

frontiers in Physiology

ORIGINAL RESEARCH
published: 22 October 2020
doi: 10.3389/fphys.2020.531933

The Mediator Subunit, Med23 Is Required for Embryonic Survival and Regulation of Canonical WNT Signaling During Cranial Ganglia Development

Soma Dash[1†], Shachi Bhatt[1,2†], Lisa L. Sandell[3], Christopher W. Seidel[1], Youngwook Ahn[1], Robb E. Krumlauf[1,2] and Paul A. Trainor[1,2]*

[1] Stowers Institute for Medical Research, Kansas City, MO, United States, [2] Department of Anatomy and Cell Biology, University of Kansas Medical Center, Kansas City, KS, United States, [3] Department of Oral Immunology and Infectious Diseases, School of Dentistry, University of Louisville, Louisville, KY, United States

OPEN ACCESS

Edited by:
Patrick Blader,
FR3743 Centre de Biologie Intégrative (CBI), France

Reviewed by:
Pierfrancesco Pagella,
University of Zurich, Switzerland
Trevor Williams,
University of Colorado Anschutz Medical Campus, United States

***Correspondence:**
Paul A. Trainor
pat@stowers.org

[†] These authors have contributed equally to this work

Specialty section:
This article was submitted to Craniofacial Biology and Dental Research, a section of the journal Frontiers in Physiology

Received: 02 February 2020
Accepted: 16 September 2020
Published: 22 October 2020

Citation:
Dash S, Bhatt S, Sandell LL, Seidel CW, Ahn Y, Krumlauf RE and Trainor PA (2020) The Mediator Subunit, Med23 Is Required for Embryonic Survival and Regulation of Canonical WNT Signaling During Cranial Ganglia Development. Front. Physiol. 11:531933. doi: 10.3389/fphys.2020.531933

Development of the vertebrate head is a complex and dynamic process, which requires integration of all three germ layers and their derivatives. Of special importance are ectoderm-derived cells that form the cranial placodes, which then differentiate into the cranial ganglia and sensory organs. Critical to a fully functioning head, defects in cranial placode and sensory organ development can result in congenital craniofacial anomalies. In a forward genetic screen aimed at identifying novel regulators of craniofacial development, we discovered an embryonically lethal mouse mutant, *snouty,* which exhibits malformation of the facial prominences, cranial nerves and vasculature. The *snouty* mutation was mapped to a single nucleotide change in a ubiquitously expressed gene, *Med23*, which encodes a subunit of the global transcription co-factor complex, Mediator. Phenotypic analyses revealed that the craniofacial anomalies, particularly of the cranial ganglia, were caused by a failure in the proper specification of cranial placode neuronal precursors. Molecular analyses determined that defects in cranial placode neuronal differentiation in *Med23*$^{sn/sn}$ mutants were associated with elevated WNT/β-catenin signaling, which can be partially rescued through combined *Lrp6* and *Wise* loss-of-function. Our work therefore reveals a surprisingly tissue specific role for the ubiquitously expressed mediator complex protein Med23 in placode differentiation during cranial ganglia development. This highlights the importance of coupling general transcription to the regulation of WNT signaling during embryogenesis.

Keywords: MED23, Wnt signaling, cranial placodes, cranial ganglia, neural crest cells

INTRODUCTION

1% of all live human births exhibit a developmental anomaly, and of those, about one-third affect the head and face. Although jaw and skull anomalies are the most common, defects in cranial nerve development also frequently occur, underscoring their importance for development and survival. Mammals have 12 cranial nerves that control various functions, including jaw movement for talking

and eating, facial expression, gathering and transmitting information through the sense organs, as well as regulating heart rate and gut peristalsis. The cranial nerves and their associated ganglia are typically composed of two ectodermally-derived cell populations, neural crest cells and cranial placode cells, which collectively give rise to neurons and glia (D'Amico-Martel and Noden, 1983).

Neural crest cells comprise a migratory stem and progenitor cell population and are derived from the neural ectoderm. Neural crest cells contribute to a diverse array of cells and tissues throughout vertebrate embryos, including much of the bone, cartilage and connective tissue of the craniofacial skeleton, smooth muscle cells and pericytes of the vasculature, melanocytes or pigment cells in the skin, as well as neurons and glia of the peripheral nervous system (Crane and Trainor, 2006; Sandell and Trainor, 2006; Bhatt et al., 2013; Trainor, 2016). Meanwhile, the cranial placodes originate from a single pre-placodal region (PPR) of non-neural ectoderm, which then segregates into individual cranial placode territories as embryogenesis progresses (Baker and Bronner-Fraser, 2001). Some of the placodes are neurogenic and differentiate into cranial nerves, while others as their names suggest differentiate into the paired olfactory, optic and otic sense organs, or the hormone secreting anterior pituitary gland (Harvard Stem Cell Institute, 2008; Saint-Jeannet and Moody, 2014).

To identify, in an unbiased manner, novel genes that play important roles in neural crest, placode and craniofacial development, we performed a three generation forward genetic screen in mice via *N*-ethyl-*N*-nitrosourea (ENU) induced mutagenesis (Sandell et al., 2011). From this screen we identified a mouse mutant, which was termed *snouty*, due to the hypoplastic malformed shape of its frontonasal tissues. Subsequently, we identified a point mutation in *Med23* underlying the etiology of the *snouty* phenotype. *Med23* encodes a subunit of Mediator, which is essential for general and activated transcription (Allen and Taatjes, 2015). In mammals, the Mediator complex consists of about 30 subunits, which are arranged into four modules, Head, Middle, Tail and Kinase, and Med23 is a member of the Tail module (Conaway et al., 2005). These subunits interact with components of the RNA Polymerase II complex as well as diverse transcription factors, thereby coordinating development and cell fate determination (Risley et al., 2010; Li et al., 2015; Ranjan and Ansari, 2018).

In this study, we show that Med23 is essential for embryo survival, and plays a novel critical role in cranial ganglia development. Med23 regulates canonical WNT signaling during cranial placode development, the perturbation of which results in defects in cranial ganglia neuronal differentiation. Consistent with this model, we demonstrate that genetically modulating WNT signaling in *snouty* embryos can ameliorate the neuronal defects in cranial ganglia development. Our work therefore has uncovered an important link between the Mediator complex and WNT signaling, which links the general transcription co-factor machinery to modulation of a major highly conserved signaling pathway important in development, tissue homeostasis and disease.

MATERIALS AND METHODS

Animals

The *snouty* mouse line (*Med23*^{sn}) used in this study was generated as previously described (Sandell et al., 2011). DNA from *snouty* mutants and founders was collected and subjected to mapping with microsatellites polymorphic between the mixed C57/BL6 and 129/Sv background of our mutagenized animals and the FVB strain to which they were bred (Sandell et al., 2007, 2011). The *snouty* mutation was initially mapped to proximal region of chromosome 10 and then through single nucleotide polymorphism refinement, was identified as a single T-A base pair change in exon 22 of *Med23*. Genotyping was performed by Transnetyx with the following Taqman probes:

Forward Primer: CAACGACATGGTGTGGAAGTACA
Reverse Primer: TCTTACCAGGCAGAGAATGAGTCT
Reporter 1: CCAGCGTGACAATGT (mutant)
Reporter 2: TCCAGCGTGTCAATGT (wild-type)

The *Med23*$^{bgeo/+}$ and *Med23*$^{flox/+}$ allele mice were derived from ES cells generated through the Knockout Mouse Project (KOMP) consortium. These mice and their derivatives were genotyped via Transnetyx. *Cre-ER*^{T2} [B6.129 – *Gt(ROSA)26Sor*$^{TM1(Cre-ERT2)Tyj}$*/J*, Jax stock cat# 008463], *Tek-Cre* [B6.Cg-Tg(Tek-cre)1Ywa/J, Jax Stock cat# 008863], and *Wnt1-Cre* [*H2afv*$^{Tg(Wnt1-cre)11Rth}$ Tg(Wnt1-GAL4)11Rth/J, Jax stock cat# 003829] mice were obtained from the Jackson Laboratory and maintained as previously described (Chai et al., 2000; Jiang et al., 2000; Kisanuki et al., 2001). *Med23*$^{flox/flox}$ mice were crossed with Cre driver mice in order to delete *Med23* in neural crest cells (*Wnt1-Cre*), in endothelial cells (*Tek-Cre*) or in all cells following treatment with 2 mg of tamoxifen and 0.4 mg progesterone (*Cre-ER*^{T2}). *Lrp6*$^{+/-}$ and *Wise*$^{+/-}$ mice were generated and maintained as previously described (Ahn et al., 2010, 2013). For embryonic staging, the morning of identification of the vaginal plug was defined as embryonic day (E)0.5. All procedures were performed in compliance with Stowers Institute of Medical Research (SIMR) IACUC approved protocols (2019-094 and 2019-097).

Western Blotting

Total protein was extracted from three control and three mutant embryos. Protein concentration was estimated by a BCA assay. A standard western blot was performed using the following primary antibodies: Med23 at 1:500 (LifeSpan BioSciences, cat# LS-C193128) and a-Tubulin at 1:1000 (Life Technologies, cat# MA1-19162).

Whole Mount Immunostaining

Embryos were harvested in 1X PBS and fixed in 4%PFA in PBS at 4°C overnight. Standard whole embryo immunostaining was performed as previously described (Inman et al., 2013; Sandell et al., 2014). Primary antibodies against the following proteins were used: β-tubulin III (TuJ1) at 1:1000 dilution (Covance Research products, cat# MMS-435P), PECAM1/CD31 at 1:400 dilution (BD Pharminogen, cat# 553370), cleaved

caspase 3 at 1:1000 dilution (Cell Signaling Technology, cat# 9661S) and Sox10 at 1:500 dilution (Abcam, cat# 155279). Secondary antibodies used were: Goat anti-Mouse IgM (Invitrogen/Molecular Probes, cat# A-21042), Goat anti-Rabbit IgM (Invitrogen/Molecular Probes, cat# A-11034) and Peroxidase AffiniPure Donkey Anti-Rat IgG (H + L) (Jackson ImmunoResearch, cat# 712-035-153) at 1:500 dilution. Immunostained embryos were mounted in Vectashield Antifade Mounting Media (Vectorlabs, cat# H-1000) and imaged using an upright confocal microscope. Except for Pecam1 staining in **Figure 1**, control and mutant embryos were imaged with the same magnification.

X-Gal Staining

For whole mount X-Gal staining, the embryos were dissected in Tyrode's solution and fixed in 2% PFA/0.2% Glutaraldehyde in PBS on ice for varying time periods depending on their embryonic stage (E7.5–15, E8.5–30, E9.5–45 min). Following fixation, the embryos were stained using the X-gal staining kit from Millipore corporation, cat# BG-6-B according to the manufacturer's protocol.

RNA *in situ* Hybridization

The embryos were harvested in 1X PBS/0.1% DEPC and fixed in 4% PFA in 1X PBS/0.1% DEPC overnight at 4°C. *In Situ* hybridization was performed using a standard protocol as previously described (Behringer et al., 2014). Control and mutant embryos were imaged at the same magnification using a Nikon camera. Images were processed using Adobe Photoshop.

Microarray

Mouse Exonic Evidence Based Oligonucleotide (MEEBO) arrays[1] were printed on poly-L-lysine coated slides using a High-Speed Linear Servo Arrayer. The concentration of oligonucleotides was 40 μM in 3X SSC buffer. Following printing, slides were blocked with succinic anhydride. Microarrays were performed on total RNA isolated from individual E9.5 wild-type and *snouty* mutant littermate embryos using the RNeasy Mini Kit (Qiagen). Aliquots of total RNA were tested for integrity and concentration using the RNA 6000 Nano Assay and RNA LabChips on the Agilent Bioanalyzer 2100. ArrayControl RNA Spikes (Thermo Fisher, cat# AM1780) were mixed with 1 μg of high integrity total RNA before undergoing amplification using the AminoAllyl MessageAmp II aRNA Amplification Kit (Thermo Fisher, cat# AM1753) according to the corresponding instruction manual.

Labeling and hybridization of aRNA was carried out essentially as described previously but with a few modifications (Bozdech et al., 2003). Briefly, 3 μg amplified aRNA was coupled with Cy dyes (CyDye Post-Labeling Reactive Dye Pack, GE Healthcare, RPN 5661). Labeling reactions were quenched with hydroxylamine, and uncoupled dye material removed using cleanup columns following the AminoAllyl MessageAmp II aRNA Amplification Kit instructions (Thermo Fisher, cat# AM1753). Fragmentation of aRNA to between 60 and 200 nt was conducted using (Ambion) RNA Fragmentation Reagents (Thermo Fisher, cat# AM8740) according to the manufacturer's instructions. Slides were hybridized with a mixture of Cy3 and Cy5 labeled probes. Hybridizations were performed at 63°C overnight under standard conditions (3X SSC, 0.2 mg/ml Poly-dA15, 25 mM HEPES, 0.25% SDS). Slides were then washed at room temperature successively with 0.6X SSC/0.03% SDS and then 0.06X SSC prior to scanning.

Microarray images were acquired with a GenePix 4000B scanner (Axon Instruments, Foster City, CA, United States). Image analysis was performed using GenePix Pro 6.0 software (Axon Instruments). Differentially expressed genes were identified at a significant p-value < 0.05 and fold change cut-off of $\pm$ 1.2. Microarray data has been deposited in NCBI's Gene Expression Omnibus and is available through GEO Series accession number GSE144327[2]. Pathway analysis was performed using Ingenuity Pathway Analysis (IPA®). Cytoscape was used to perform network analyses.

qRT-PCR

Total RNA was isolated from the heads of individual E9.5 wild-type, *Med23*$^{sn/sn}$, *Med23*$^{sn/sn}$;*Lrp6*$^{+/-}$, *Med23*$^{sn/sn}$;*Wise*$^{+/-}$ and *Med23*$^{sn/sn}$;*Lrp6*$^{+/-}$;*Wise*$^{+/-}$ embryos using the RNeasy Mini Plus Kit (Qiagen). cDNA synthesis and RT-qPCR were performed as described on an ABI7300 Real-Time PCR system using Power Sybr Green PCR master mix (Invitrogen Life Technologies, Carlsbad, CA, United States). For each sample, differential expression was determined using the ΔΔCT method and a t-test was used for statistical analysis. The following primers were used for qRT-PCR: *Med23* Forward: 5′-ATTACAAGGGTGTTCGAGA-3′; *Med23* Reverse 5′-TATAACCTCTCTTGCTGCCAGA-3′; *Dkk1* Forward: 5′-CA ACTACCAGCCCTACCCTTG-3′, *Dkk1* Reverse: 5′-GAGCCT TCTTGTCCTTTGGTGTGA-3′, *Ccnd1* Forward: 5′-TGGATG CTGGAGGTCTGTG-3′, *Ccnd1* Reverse: 5′-ACTTCACATCTG TGGCA-3′, *Ngn1* Forward: 5′-CAAGCCCATTCACTCCCTGA-3′, *Ngn1* Reverse: 5′-CAAGCCCATTCACTCCCTGA-3′, *Ngn2* Forward: 5′-GAGCCGCGTAGGATGTTCGTCA-3′, *Ngn2* Reverse: 5′-CCTGCCCGGCTTCCGCTCCA-3′, *NeuroD1* Forward: 5′-GCTGTTTGAGATGTGATGCTGG-3′, and *NeuroD1* Reverse: 5′-AGACGTTGATCCTCCTCGCT-3′. Primers to detect *Med23* transcripts were designed based on the exon–exon junction of exons 1–2 and exons 3–4 of the *Med23* gene.

RESULTS

snouty Embryos Exhibit Defects in Craniofacial, Cranial Ganglia, and Vascular Development

We identified 10 distinct recessive mutants in our ENU mutagenesis screen, each of which presented with craniofacial dysmorphogenesis at E9.5-E10.5 (Sandell et al., 2011). One mutant was termed *snouty* due to the characteristic hypoplasia

[1]https://microarray.org/sfgf/meebo.do

[2]https://www.ncbi.nlm.nih.gov/geo/query/acc.cgi?acc=GSE144327

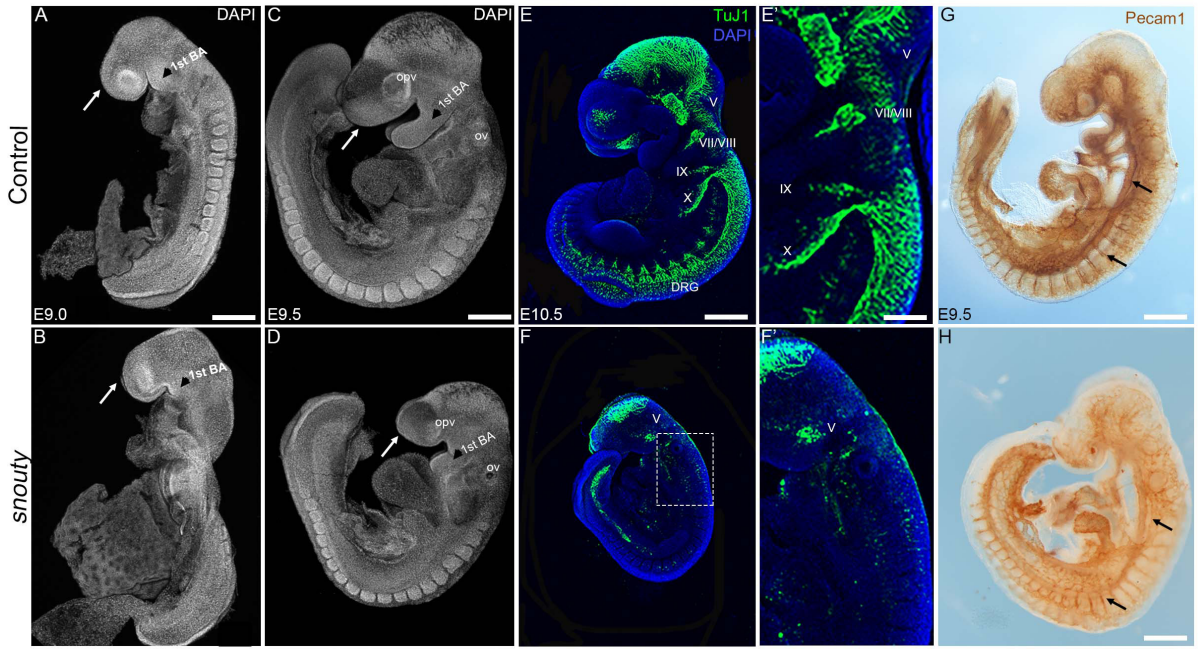

FIGURE 1 | *snouty* embryos exhibit small body size and craniofacial defects at E9.5. **(A–D)** Control and *snouty* mouse embryo littermates at E9.0 and E9.5 were stained with DAPI and imaged with a confocal microscope demonstrating the smaller body size and shortened frontonasal prominences (arrows) in *snouty* embryos. **(E–F′)** Neuronal marker TuJ1 staining of control and *snouty* embryos at E9.5 suggests that *snouty* embryos exhibit disrupted cranial ganglia. **(E′,F′)** Are higher magnification images of **(E,F)**. **(G,H)** PECAM1 immunostaining of E9.5 control and *snouty* embryos reveal abnormal development of the vascular tree like network in the head and epibranchial regions of *snouty* mutants. Intersomitic vessel formation (arrow, **G,H**) is not affected.opv, optic vesicle; ov, otic capsules; BA, branchial arch; DRG, dorsal root ganglia. Scale bars for **(A–D)** is 300 um, **(E,F)** is 350 um, **(G)** is 300 um, **(H)** is 200 um.

of its frontonasal prominence and pharyngeal arches, which was evident as early as E9.0 (**Figures 1A,B**). By E9.5, *snouty* embryos exhibit defects in overall growth compared to littermate controls with progressively worsening craniofacial abnormalities, including malformed frontonasal prominences, pharyngeal arches, otic and optic vesicles (**Figures 1C,D**). Relative to control littermates, *snouty* embryos are also slightly developmentally delayed at this stage, by about 4 h, as measured by their difference in somite number. *snouty* embryos are embryonic lethal around E10.5.

The nervous and vascular systems are two precisely patterned networks that develop in close proximity to each other during embryogenesis. Perturbation of either system or their integration can lead to neurovascular disorders, which are a major cause of embryonic lethality (Shalaby et al., 1995; Lim et al., 2000, 3; Ruhrberg and Bautch, 2013). Therefore, as a first step toward understanding the mechanistic origin of the craniofacial defects and the lethality observed in *snouty* embryos, we examined whether neurovascular development occurred normally in *snouty* embryos. Using β-tubulin III (TuJ1) which labels developing neurons and their axons in the central and peripheral nervous systems (CNS and PNS), we observed that a complex neuronal network forms in the midbrain (CNS) of wild-type embryos by E10.5 (**Figures 1E,E′**). Furthermore, β-tubulin III demarcates developing neurons of the cranial sensory nervous system, including the trigeminal (V), facial/vestibulo-acoustic (VII/VIII), glossopharyngeal (IX) and vagal (X) nerves, as well as dorsal root ganglia (DRG) in the trunk. In contrast, in *snouty* mutant embryos, although a midbrain neuronal plexus is formed, β-tubulin III immunostaining revealed that the network was hypoplastic, and furthermore that there was a paucity of neurons in the cranial sensory ganglia, with respect to the trigeminal, facial, and glossopharyngeal nerves (**Figures 1F,F′**). Thus, *snouty* embryos exhibit major perturbations in nervous system development, particularly the PNS when compared to control littermates, and this may underpin their early embryonic lethality (**Figures 1E,F**).

Defective vascular development is also a frequent cause of embryonic lethality and platelet endothelial cell adhesion molecule (PECAM1/CD31), which labels endothelial cells amongst others, illustrates the complexity of the developing vascular network during embryogenesis (**Figures 1G,H**). Similar to wild-type embryos, PECAM1 immunostaining revealed a well-developed network of embryonic blood vessels in *snouty* mutant embryos. This is evident in the dorsal aorta and intersomitic vessels. However, the complexity and density of the vessel pattern, particularly in the midbrain and pharyngeal arch arteries were noticeably reduced (**Figures 1G,H**). Perturbation of the vascular network was not perceived to be as severe as that of the neural network, suggesting the gene mutated in *snouty* embryos played a predominant role in regulating cranial sensory nervous system development.

snouty Carries a Single Point Mutation in *Med23*, Which Encodes a Ubiquitously Expressed Subunit of the Mediator Complex and Is Essential for Embryo Survival

To identify the DNA mutation associated with the *snouty* phenotype, we used a panel of microsatellite markers polymorphic between the mixed C57/BL6 and 129/Sv background of our mutagenized animals and the FVB strain to which they were bred (Sandell et al., 2007, 2011). The *snouty* mutation was initially mapped to chromosome 10 and then through single nucleotide polymorphism refinement, was identified as a single T-A base pair change in exon 22 of *Med23* (**Figure 2A**). *Med23* encodes a subunit of the transcription co-factor complex, Mediator. The missense base pair change which maps to the core of Med23, led to a single amino acid change from Valine to Aspartic acid (V to D) in the 6-HEAT motif that contributes to the arch-shaped structure or conformation of Med23 (Monté et al., 2018). Western blotting indicated that Med23 is essentially absent in *snouty* mutant embryos (**Figure 2B**). The reduced protein level is consistent with a potential conformational change rendering the mutant Med23 protein unstable.

To definitively prove that *Med23* loss-of-function was responsible for the *snouty* phenotype, we performed a complementation test with a null allele of *Med23* generated from ES cells obtained through the Knock-out Mouse Project (KOMP) consortium. The ES cells contained a splice acceptor-lacZ genetrap construct inserted between exons 12 and 13 of *Med23* (**Supplementary Figure S1A**). The 5′ splice acceptor site and 3′ polyA tail were designed to produce a null allele by disrupting the endogenous *Med23* transcript through expression of a reporter lacZ fusion transcript. Mice carrying the genetrap allele were designated $Med23^{bgeo/+}$. $Med23^{bgeo/bgeo}$ homozygous embryos displayed similar developmental defects to *snouty* (hereafter referred to as $Med23^{sn/sn}$) embryos and did not survive beyond E10.5 (**Supplementary Figures S1B,C**). $Med23^{bgeo/bgeo}$ embryos were also developmentally delayed relative to control littermates, and perhaps slightly more so than $Med23^{sn/sn}$ embryos. This is likely due to the complete loss of function of Med23 in $Med23^{bgeo/bgeo}$ embryos as well as the C57BL/6 background of the $Med23^{bgeo/bgeo}$ embryos compared to FVB background for $Med23^{sn/sn}$ embryos.

For the complementation test, we generated $Med23^{sn/bgeo}$ embryos and compared their phenotype to $Med23^{sn/sn}$ and $Med23^{bgeo/bgeo}$ embryos (**Supplementary Figure S2**). Similar to $Med23^{sn/sn}$ and $Med23^{bgeo/bgeo}$ embryos, $Med23^{sn/bgeo}$ embryos also do not survive beyond E10.5, and display craniofacial, neuronal and vascular development defects that are similar to $Med23^{sn/sn}$ and $Med23^{bgeo/bgeo}$ embryos (**Supplementary Figures S2A–F**). The failure of the $Med23^{bgeo}$ allele to complement the $Med23^{sn}$ allele provided genetic confirmation that Med23 loss-of-function is responsible for the $Med23^{sn/sn}$ phenotype and furthermore that $Med23^{sn}$ is likely a null allele similar to $Med23^{bgeo}$.

Because *Med23* has been previously identified as a candidate gene for placental defects (Perez-Garcia et al., 2018), we examined the placentas of wild-type and $Med23^{sn/sn}$ embryos at E9.5 by histology. The primary layers, trophoblast giant cell layer, chorion and allantois, appear to be present in $Med23^{sn/sn}$ placenta and in similar proportions compared to wild-type placenta. This suggest that there are no gross morphological defects in placenta development in $Med23^{sn/sn}$ embryos (**Supplementary Figure S3**). This could be because the *snouty* point mutation in *Med23* does not affect placental development as opposed to the *bgeo* insertional deletion of *Med23*. Another possibility is that genetic background affects placental development (Dackor et al., 2009). $Med23^{sn/sn}$ embryos are on an FVB background in contrast to the C57Bl/6N background in which the placental defects were previously described.

Therefore, to begin to understand the mechanistic origins and pathogenesis of the craniofacial, neuronal and vascular defects observed in the allelic series of *Med23* embryos, we characterized the spatiotemporal expression of *Med23* during normal embryogenesis. Using the lacZ fusion transcript as a reporter for Med23 activity, X-gal staining of $Med23^{bgeo/+}$ embryos revealed that *Med23* is expressed ubiquitously in all embryonic tissues during post-implantation development from E7.5 to 10.5 (**Figure 2C**).

Cranial Ganglia Defects in $Med23^{sn/sn}$ Embryos Occur Predominantly Due to Defects in Cranial Placode Development

$Med23^{sn/sn}$ embryos are characterized primarily by hypoplastic frontonasal prominences and pharyngeal arches as well as a malformed peripheral nervous system, particularly of the cranial sensory ganglia (**Figure 1**). Previous studies have shown that the cranial ganglia are derived from two distinct ectodermal cell populations; neural crest cells and placode cells (D'Amico-Martel and Noden, 1983). Cranial neural crest cells contribute neurons and glia, whereas the ectodermal placodes only contribute neurons of the cranial ganglia. However, cellular interactions between neural crest cells and placodes are also essential for proper cranial nerve development (Shiau et al., 2008; Freter et al., 2013; Sandell et al., 2014; Kurosaka et al., 2015). In order to determine whether Med23 was required in neural crest cells and/or cranial placode cells, for proper cranial sensory ganglia development, we analyzed their contributions with cell specific markers via RNA *in situ* hybridization in wild-type and $Med23^{sn/sn}$ littermate embryos. *Sox10* labels migrating neural crest cells as they delaminate from the neuroepithelium beginning around E8.25–8.5, and becomes progressively restricted to neural crest cells destined for neurogliogenic fates around E9.0–E9.5 (Britsch et al., 2001). *Sox10* expression is observed in neural crest cells populating the cranial ganglia in E8.5–9.5 wild-type and $Med23^{sn/sn}$ littermate embryos (**Figures 3A–D**). However, E9.5 $Med23^{sn/sn}$ embryos display a slight reduction in $Sox10^{+}$ cells in the head (**Figures 3B,D**). *Crabp1* labels the neuroepithelium, midbrain neuronal plexus, and migrating neural crest cells that colonize the pharyngeal

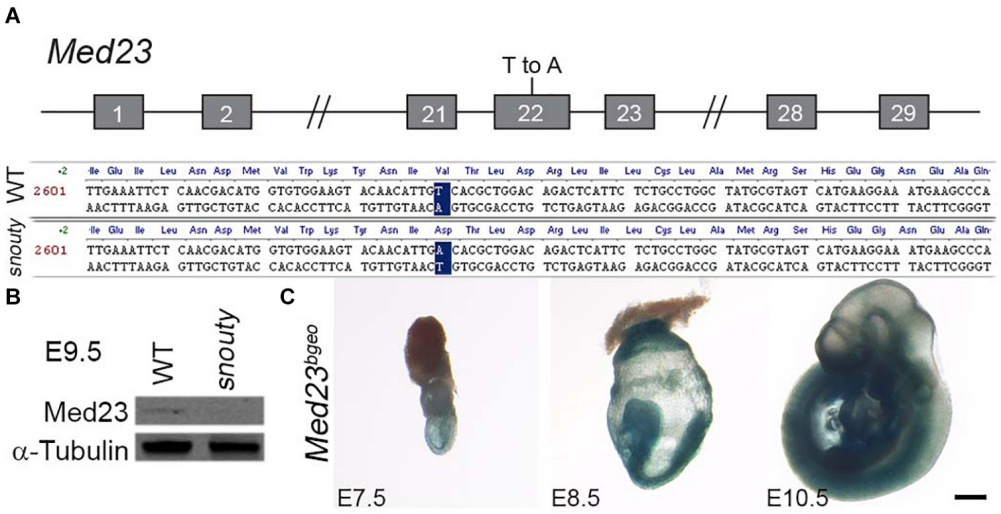

FIGURE 2 | *snouty* mutant mice have a mutation in the *Med23* gene. **(A)** The *snouty* mouse mutant phenotype was determined to be caused by a single base pair mutation in Exon 22 of the *Med23* gene, which leads to a valine to aspartic acid amino acid change in the protein. Chromosome position of the mutation is noted based on mm10 mouse assembly. **(B)** Western blot against Med23 shows a drastic reduction of Med23 protein levels in *snouty* mutant embryos. **(C)** Ubiquitous expression of LacZ throughout E7.5 to E10.5 embryos is indicative of the Med23 expression. Scale bar is 250 um.

arches in E9.0–9.5 control embryos (Dencker et al., 1990). Although the levels of *Crabp1* expression are comparable, the domains are somewhat reduced in *Med23*$^{sn/sn}$ mutant embryos (**Figures 3E,F**). Collectively, the expression of *Sox10* and *Crabp1* in *Med23*$^{sn/sn}$ embryos relative to controls indicates that Med23 is not required for the induction or migration of cranial neural crest cells. Thus, defects in neural crest cell development are unlikely to cause the cranial peripheral nervous system defects observed in *Med23*$^{sn/sn}$ embryos.

Therefore, we turned our attention to cranial placode development, the perturbation of which could underlie the malformed cranial sensory ganglia observed in *Med23*$^{sn/sn}$ embryos (**Figure 1**). Each stage of cranial sensory development, from specification of the pre-placode territory to neuronal differentiation of cranial placode cells, can be delineated via spatiotemporal gene expression (Schlosser, 2006; Saint-Jeannet and Moody, 2014). Cranial placode development begins with the formation of a single ectodermal-cell population called the pre-placodal region. *Six* and *Eya* gene family members are expressed at the time of pre-placodal region specification and their expression is maintained as the pre-placodal region segregates and differentiates into specific placodes (Zou et al., 2004). At E9.5, *Eya2*$^{+}$ cells are observed in the trigeminal and epibranchial placodes of wild-type embryos (**Figure 3G**). In contrast, *Med23*$^{sn/sn}$ embryos display a reduced domain of *Eya2*$^{+}$ cells in the developing trigeminal placode and forming epibranchial placodes (**Figure 3H**). Interestingly, *Eya2*$^{-/-}$ mutant mice present with no obvious external phenotype and are viable and fertile (Grifone et al., 2007), indicating that loss of *Eya2* expression cannot explain the cranial ganglia neurogenesis defects in *Med23*$^{sn/sn}$ embryos. This led us to hypothesize that Med23 is specifically required during later stages of cranial sensory nervous system development, namely segregation and/or differentiation.

To further understand the function of Med23 during cranial placode development, we next examined whether the placodes are appropriately specified in *Med23*$^{sn/sn}$ embryos. More specifically, we characterized the expression of *Pax2* and *Pax8*, which have been shown to demarcate the newly specified epibranchial and otic placodes in mouse embryos (Baker and Bronner-Fraser, 2001; Bouchard et al., 2004; Ohyama and Groves, 2004). In E9.5 wild-type embryos, *Pax2*$^{+}$ cells were observed in the nasal, optic and otic placodes, and in the epibranchial region and isthmus (**Figure 3I**). A similar pattern of *Pax2* expression was also found in *Med23*$^{sn/sn}$ embryos (**Figure 3J**). *Pax8* is expressed in the epibranchial and otic placodes as well as in the isthmus of E9.5 wild-type mouse embryos (**Figure 3K**), and this pattern remained largely unchanged in *Med23*$^{sn/sn}$ littermate embryos (**Figure 3L**), except that *Pax8*$^{+}$ cells in the developing epibranchial placodes do not seem to coalesce as well in the mutant embryos as they do in wild-type controls. Nonetheless, the presence of *Pax2*$^{+}$ and *Pax8*$^{+}$ cells in the epibranchial region suggests that the epibranchial placodes are being specified in *Med23*$^{sn/sn}$ embryos. The persistence of *Eya2*$^{+}$ cells in both wild-type and *Med23*$^{sn/sn}$ embryos, and proper specification of epibranchial placodes (presence of *Pax2*$^{+}$ and *Pax8*$^{+}$ cells in the epibranchial region) in *Med23*$^{sn/sn}$ embryos, suggests that Med23 is required during later stages of cranial placode development, namely segregation and/or differentiation. Collectively, these results imply that malformation of the cranial sensory nervous system in *Med23*$^{sn/sn}$ embryos possibly occurs during the stage of neuronal progenitor cell specification and delamination, which precedes the later differentiation and maturation of the cranial sensory ganglia.

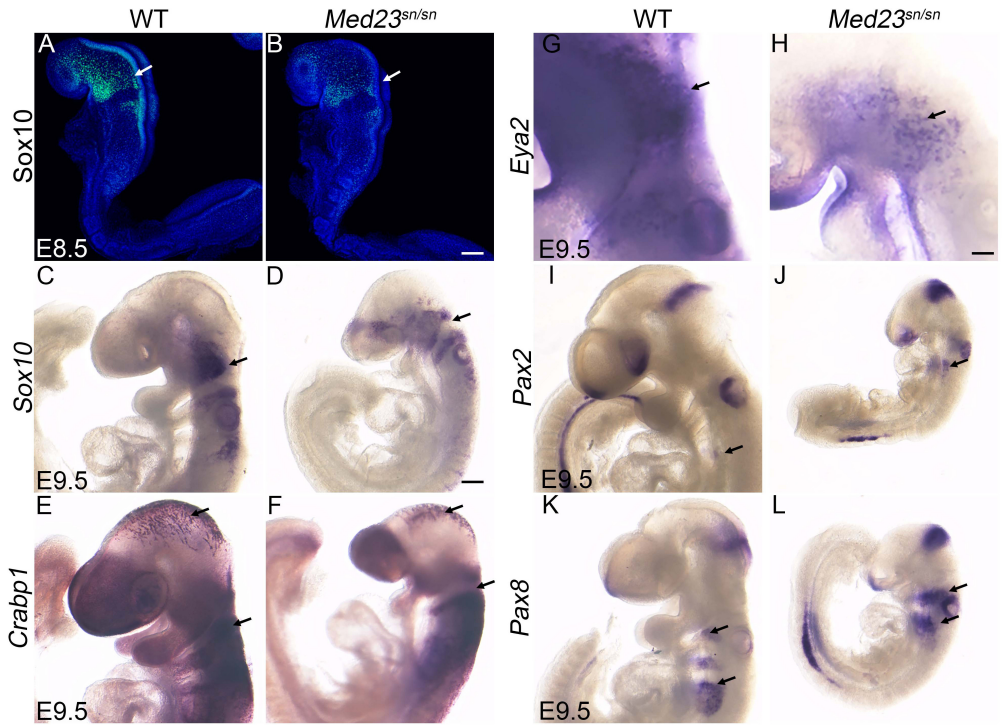

FIGURE 3 | *Med23*$^{sn/sn}$ mutants display neural crest cell and placodal defects. **(A–D)** Sox10 expression in E8.5 and E9.5 control and *Med23*$^{sn/sn}$ embryos shows reduced *Sox10* + cells entering the cranial ganglia region near the 1st branchial arch and around the otic vesicle in *Med23*$^{sn/sn}$ embryos. **(E,F)** *Crabp1* ISH reveals proper neural crest cell migration in the cranial and trunk regions of E9.5 control and *Med23*$^{sn/sn}$ embryos. **(G,H)** *Eya2* expression in control and *Med23*$^{sn/sn}$ embryos shows proper formation of anterior pre-placodal area. However, very few *Eya2*$^{+}$ cells are observed in the trigeminal and epibranchial regions of *Med23*$^{sn/sn}$ embryos (arrow, **H**). **(I,J)** *Pax2*$^{+}$ cells are present in the optic, otic, and isthmus of both control and *Med23*$^{sn/sn}$ embryos. **(K,L)** *Pax8*$^{+}$ cells are present but loosely organized in the epibranchial region, otic placode and isthmus of *Med23*$^{sn/sn}$ embryos in comparison to controls. Scale bar for **(A,B)** is 120 um, **(C–F,I–L)** is 300 um, and **(G–H)** is 150 um.

To delineate the role of Med23 in neuronal specification of cranial placodes cells, we next analyzed the expression of *Neurogenin1* (*Ngn1*) and *Neurogenin2* (*Ngn2*), which are vertebrate neurogenesis determination genes (Fode et al., 1998; Ma et al., 1998). *Ngn1* and *Ngn2* are expressed in the placodal ectoderm prior to neuroblast delamination where they define complementary subsets of cranial sensory neuron precursors. *Ngn1* loss-of-function was previously shown to prevent development of the "proximal" subset of cranial sensory ganglia, whose neurons derive from cranial neural crest, trigeminal, or otic placode precursors (Ma et al., 1998). In contrast, loss of *Ngn2* prevents development of the complementary "distal" subset of ganglia, whose precursors derive from posterior epibranchial placodes (Fode et al., 1998). In E9.5 wild-type embryos, *Ngn1* is primarily expressed in the developing trigeminal placode, but can also be found in the developing epibranchial placodes (**Figure 4A**). In contrast, very few cells in the developing trigeminal placode of *Med23*$^{sn/sn}$ littermate embryos express *Ngn1,* and no cells in the epibranchial placode region were observed to be *Ngn1*$^{+}$ (**Figure 4B**). Similar results were observed with respect to *Ngn2*. In E9.5 wild-type embryos, numerous *Ngn2*$^{+}$ cells are present in the epibranchial placodes (**Figure 4C**), however, in *Med23*$^{sn/sn}$ littermate embryos the region of *Ngn2*$^{+}$ cells in the developing epibranchial placodes was drastically reduced (**Figure 4D**). We confirmed the downregulation of *Ngn1* and *Ngn2* transcript levels in E9.5 *Med23*$^{sn/sn}$ embryonic heads by qPCR (**Figure 4I**). These data imply that cranial placode neuronal precursors fail to be specified or delaminate during cranial sensory nervous system development in *Med23*$^{sn/sn}$ embryos.

Ngn1 and Ngn2 directly regulate *Neurod1* expression in the trigeminal and epibranchial ganglia respectively during cranial sensory nervous system development (Sun et al., 2001; Mattar et al., 2004). *Neurod1*, which is a well-established indicator of neuronal differentiation, is expressed in neurogenic cranial placodal cells in the trigeminal and epibranchial ganglia of wild-type embryos at E9.5 (**Figure 4E**). *Med23*$^{sn/sn}$ embryos display an almost complete absence of *Neurod1* expression in the developing cranial ganglia (**Figure 4F**), which we confirmed by qPCR (**Figure 4I**). The few cells in the trigeminal ganglion that still express *Neurod1* in *Med23*$^{sn/sn}$ embryos correlate with the small number of β-tubulin III^{+} cells observed in the trigeminal ganglion (**Figure 1F**). In addition, a higher number of cells in *Med23*$^{sn/sn}$ embryos, especially in the trigeminal and the frontonasal prominence are cleaved Caspase 3 positive indicating that cell death is elevated in *Med23*$^{sn/sn}$ embryos compared to controls (**Figures 4G,H**).

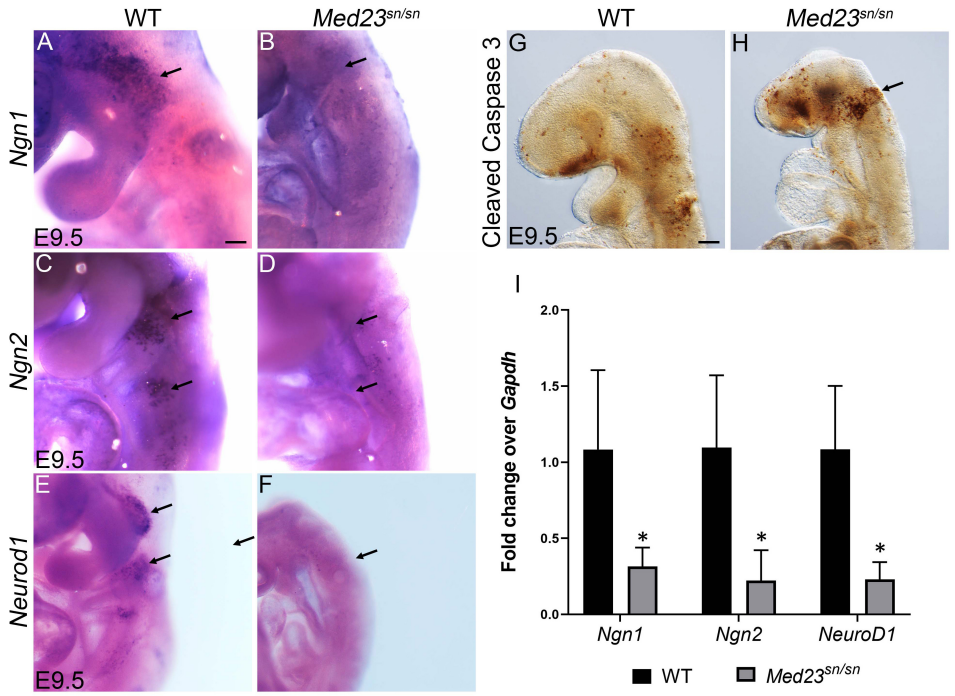

FIGURE 4 | *Med23*$^{sn/sn}$ mutants display defects in neuronal differentiation. **(A,B)** *Ngn1* is expressed in trigeminal (arrow) and epibranchial cells in control embryos, however is downregulated or lost in *Med23*$^{sn/sn}$ embryos. **(C,D)** *Ngn2*$^{+}$ cells are observed in the epibranchial ganglia of control embryos (arrows, **C**). *Ngn2*$^{+}$ cell number is drastically reduced in the epibranchial ganglia of *Med23*$^{sn/sn}$ embryos (arrows, **D**). **(E,F)** *Neurod1*$^{+}$ cells are considerably reduced in the developing trigeminal and epibranchial ganglia of *Med23*$^{sn/sn}$ embryos at E9.5 compared to controls. **(G,H)** A higher number of cleaved Caspase 3 positive cells are observed in the developing trigeminal and frontonasal prominence of E9.5 *Med23*$^{sn/sn}$ embryos compared to controls. **(I)** qPCR analyses of E9.5 wild-type and *Med23*$^{sn/sn}$ littermate embryos revealed downregulation of *Ngn1*, *Ngn2,* and *NeuroD1* transcripts in the mutants. Statistical analysis was performed using ANOVA and * denotes a p-value < 0.05. Scale bar for **(A–F)** is 150 um, **(G,H)** is 300 um. *$p < 0.05$.

Therefore, our analyses have revealed a requirement for Med23 during multiple steps of cranial placode development, and that a failure in neuronal differentiation and maturation together with apoptosis underlies abnormal development of the cranial sensory nervous system in *Med23*$^{sn/sn}$ embryos.

Med23 Regulates WNT Signaling During Cranial Ganglia Differentiation

To determine how Med23 regulates differentiation of the trigeminal and epibranchial placodes during cranial sensory nervous system development, we undertook comparative transcriptome analyses of E9.5 *Med23*$^{sn/sn}$ embryos and their control littermates. Consistent with our spatiotemporal analyses of gene expression, *NeuroD1* was downregulated. More importantly, Ingenuity Pathway Analysis (IPA®) and a Cytoscape network plot revealed that the differential expression of multiple genes in *Med23*$^{sn/sn}$ embryos was associated with the canonical WNT/β-catenin signaling pathway (**Supplementary Table S1** and **Supplementary Figure S7**). Differentially expressed genes include the WNT inhibitor *Dkk1*, and WNT target, *Ccnd1*, both of which were downregulated. We confirmed the downregulation of *Dkk1 and Ccnd1* transcripts in concert with *Med23* loss-of-function using qPCR (**Figure 5A**), which led us to hypothesize that WNT signaling may be mis-regulated in *Med23*$^{sn/sn}$ embryos. To test this hypothesis, we bred the *BATGal* transgenic reporter into the background of *Med23*$^{sn/sn}$ embryos. *BATGal* reporter mice express *lacZ* under the regulation of β-catenin responsive elements, such that *lacZ* expression serves as a proxy for spatiotemporal WNT signaling (Ahn et al., 2010, 2013). WNT/β-catenin signaling levels, as evidenced by the intensity and spatial distribution of lacZ activity, were increased in the pharyngeal/epibranchial region (dotted box) and lateral frontonasal processes (asterisk) of *Med23*$^{sn/sn}$ embryos, coinciding with the anatomical regions most disrupted (**Figures 5B–E′**). This suggests that elevated WNT signaling is associated with abnormal morphological development in *Med23*$^{sn/sn}$ embryos.

Genetic Modulation of WNT Signaling in *Med23*$^{sn/sn}$ Embryos Results in Partial Restoration of Cranial Sensory Neuron Differentiation

WNT/β-catenin signaling is well-known for regulating crucial aspects of mammalian embryonic development (Wodarz and Nusse, 1998), and is associated with ectodermal placode formation (Ahn, 2015). WNT/β-catenin signaling requires interaction between Wnt ligands, Frizzled receptors and WNT co-receptors, Lrp5 and Lrp6 that leads to stabilization and nuclear localization of β-catenin (MacDonald et al., 2009). In contrast,

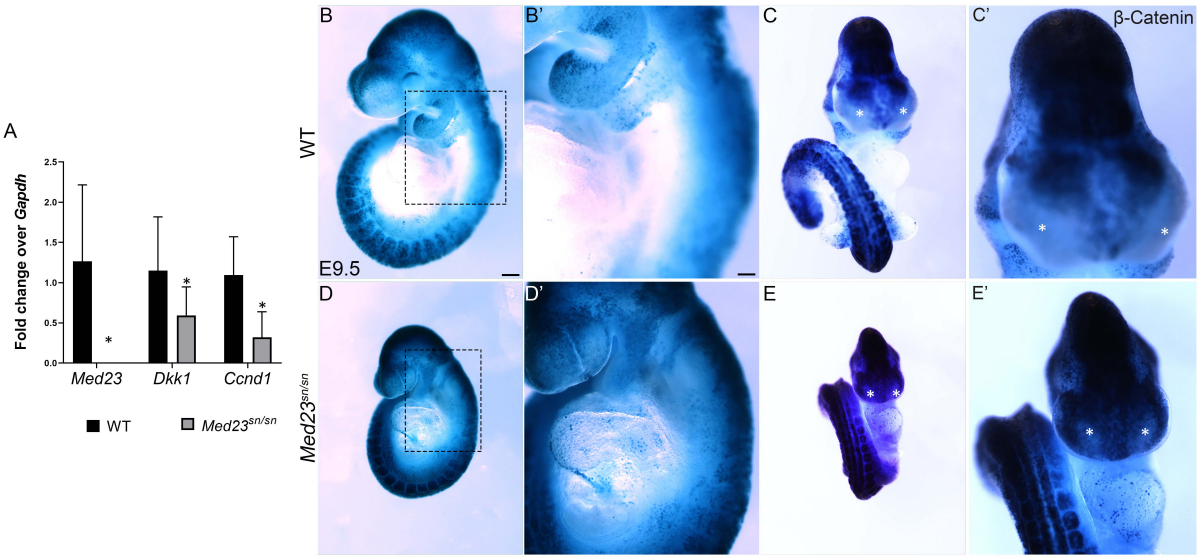

FIGURE 5 | WNT signaling is upregulated and ectopically expressed in the lateral nasal processes of *Med23*$^{sn/sn}$ embryos. **(A)** qPCR analysis of cDNA obtained from E9.5 wild-type and *Med23*$^{sn/sn}$ littermate embryos shows a reduction in the levels of *Med23*, *Dkk1,* and *Ccnd1*. **(B–E′)** Lateral and frontal images of control BATGal and *Med23*$^{sn/sn}$;BATGal embryos reveal an increase in WNT signaling in the frontonasal processes at E9.5. The lateral nasal processes, which are usually devoid of active WNT signaling (*, asterisk, control) exhibit positive LacZ staining (WNT activity) in *Med23*$^{sn/sn}$ embryos (*, asterisk, *Med23*$^{sn/sn}$). **(B′–E′)** are high magnification images of **(B–E)**. Scale bar for **(B–E)** is 450 um, **(B′–E′)** is 100 um.

Wise (also known as Sostdc1) modulates WNT/β-catenin signaling by binding to WNT agonists, Lrp5 and Lrp6 and WNT antagonist, Lrp4 (Itasaki et al., 2003; Ahn et al., 2013, 2017). We hypothesized that an up-regulation of WNT/β-catenin signaling was responsible for pathogenesis of the *Med23*$^{sn/sn}$ embryo phenotype and furthermore that genetically modulating WNT signaling might ameliorate the anomalies observed in *Med23*$^{sn/sn}$ mutant embryos. To test this hypothesis, we bred loss-of-function alleles of *Lrp6* and *Wise*, into the background of *Med23*$^{sn/sn}$ embryos. In control experiments, we first confirmed that loss of a single allele of *Lrp6* or *Wise* did not affect craniofacial or neuronal development in E10.5 *Lrp6*$^{+/-}$ and *Wise*$^{+/-}$ embryos (**Supplementary Figures S4A–C**). Then we ascertained that *Med23*$^{sn/sn}$ embryos do not display any gross aberration in *Lrp6* or *Wise* expression (**Supplementary Figures S4D–G**).

Interestingly, although compound *Med23*$^{sn/sn}$;*Lrp6*$^{+/-}$, *Med23*$^{sn/sn}$;*Wise*$^{+/-}$ and *Med23*$^{sn/sn}$;*Lrp6*$^{+/-}$;*Wise*$^{+/-}$ embryos do not exhibit any gross morphological rescue of craniofacial defects or embryonic lethality (**Figures 6A–E**), the *Med23*$^{sn/sn}$; *Lrp6*$^{+/-}$; *Wise*$^{+/-}$ compound mutants display a partial restoration of cranial ganglia neurogenesis (**Figures 6F–K**). More specifically, E9.5 *Med23*$^{sn/sn}$; *Lrp6*$^{+/-}$; *Wise*$^{+/-}$ embryos exhibit considerable β-tubulin III + staining of the trigeminal (V), facial/vestibulo-acoustic (VII/VIII), glossopharyngeal (IX) and vagal (X) nerves, as well as within the epibranchial region, which is in striking contrast to control, *Med23*$^{sn/sn}$ littermate embryos that show little to no β-tubulin III staining in the equivalent tissues and regions (**Figure 6G**). This demonstrates that a reduction in the levels of WNT signaling is sufficient to partially rescue some of the defects in cranial placode neuronal differentiation. In addition, we observed a rescue in the expression of *Dkk1 and Ccnd1* transcripts in *Med23*$^{sn/sn}$;*Lrp6*$^{+/-}$;*Wise*$^{+/-}$ compared to *Med23*$^{sn/sn}$ embryos using qPCR (**Figure 6L**).

Med23 Is Not Intrinsically Required in Neural Crest Cells or Endothelial Cells During Cranial Ganglia Development

Our analyses point toward a role for Med23 in regulating WNT/β-catenin signaling during cranial placode development, the perturbation of which results in defects in cranial ganglia formation. However, in addition to placode cells, cranial ganglia also receive a major contribution from another ectodermal cell population, the neural crest. Neural crest cells have been shown to be important for proper cranial placode development and neuronal differentiation (Begbie and Graham, 2001). Because *Med23* is ubiquitously expressed in all cell types, including neural crest cells, we hypothesized that Med23 might also be required in neural crest cells for proper cranial sensory nervous system development, and that the deficiencies observed in cranial placodogenesis in *Med23*$^{sn/sn}$ embryos were a secondary consequence of perturbed neural crest cell development. To test this idea, we generated *Med23*$^{fx/lx}$ animals where exons 12 and 13 of *Med23* were flanked by *loxP* sites. We then conditionally deleted *Med23* specifically in neural crest cell progenitors and their descendants using the *Wnt1-Cre* transgenic line that expresses Cre recombinase in the dorsal neural tube, which encompasses progenitor neural crest cells (**Figure 7**). *Med23*$^{fx/fx}$;*Wnt1-Cre* embryos survive until postnatal day (P)0 and exhibit micrognathia (**Figures 7A,B**). However, these embryos do not display any overt defects in facial prominence, pharyngeal arch or in cranial ganglia development at E10.5 (**Figures 7C,D**), a time-point when *Med23*$^{sn/sn}$ embryos exhibit

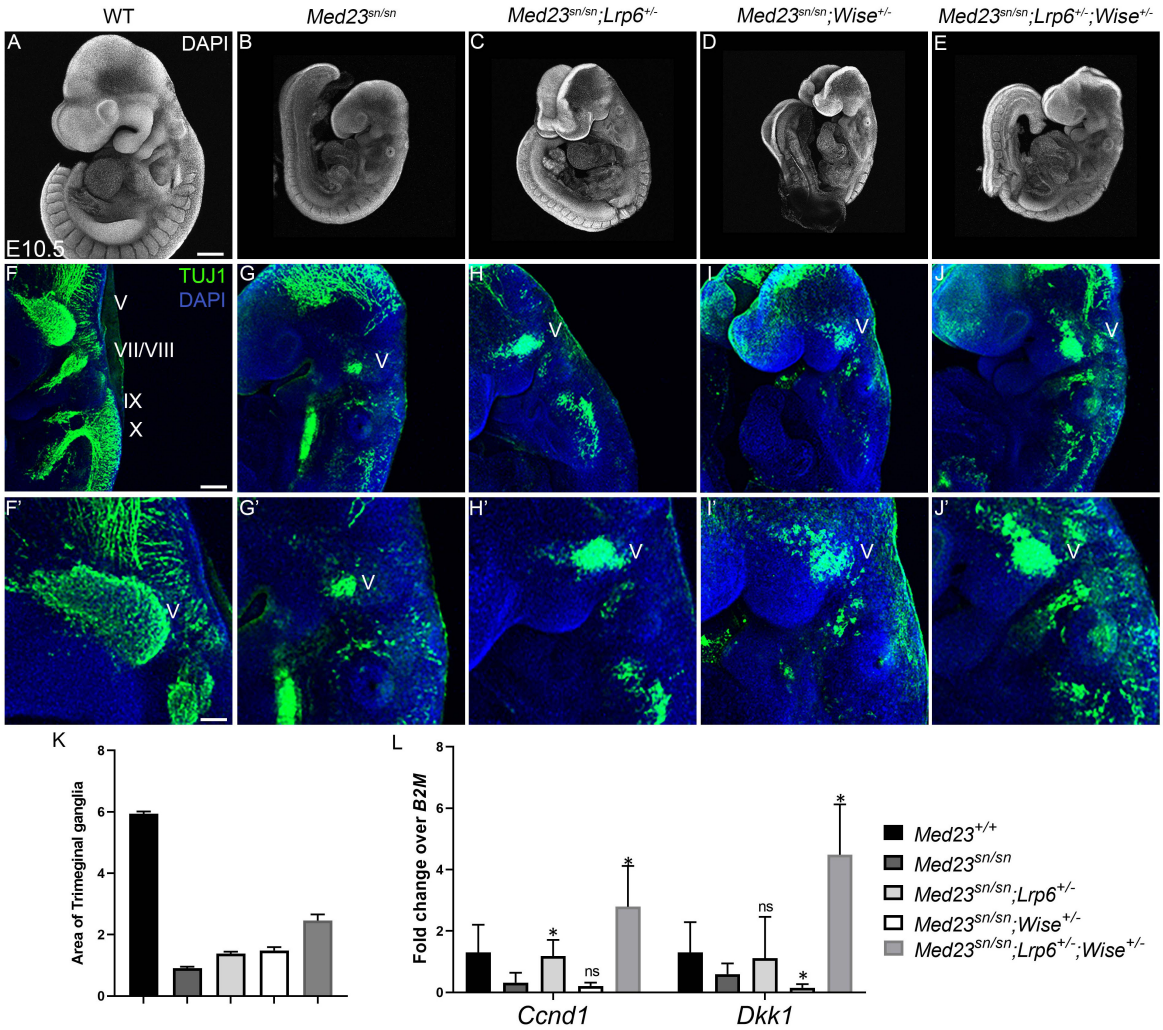

FIGURE 6 | Rescue of the *Med23*$^{sn/sn}$ phenotype by modulating WNT signaling. DAPI stained E9.5 **(A)** wild-type, **(B)** *Med23*$^{sn/sn}$, **(C)** *Med23*$^{sn/sn}$; *Lrp6*$^{+/-}$, **(D)** *Med23*$^{sn/sn}$; *Wise*$^{+/-}$ and **(E)** *Med23*$^{sn/sn}$; *Lrp6*$^{+/-}$; *Wise*$^{+/-}$ embryos. TuJ1 immunostained (green) E9.5 **(F)** wild-type **(G)** *Med23*$^{sn/sn}$ **(H)** *Med23*$^{sn/sn}$; *Lrp6*$^{+/-}$, **(I)** *Med23*$^{sn/sn}$; *Wise*$^{+/-}$ and **(J)** *Med23*$^{sn/sn}$; *Lrp6*$^{+/-}$; *Wise*$^{+/-}$, embryos. Combinatorial loss of *Lrp6* and *Wise* restores neuronal differentiation in the epibranchial region of *Med23*$^{sn/sn}$ embryos. **(F′–J′)** are higher magnification images of **(F–J)** focused on the trigeminal ganglia. **(K)** Quantification of the area of Tuj1 staining in the trigeminal ganglia is shown as a ratio of the length of the embryo for wild-type, *Med23*$^{sn/sn}$, *Med23*$^{sn/sn}$; *Lrp6*$^{+/-}$, *Med23*$^{sn/sn}$; *Wise*$^{+/-}$ and *Med23*$^{sn/sn}$; *Lrp6*$^{+/-}$; *Wise*$^{+/-}$ **(L)** qPCR analysis of cDNA obtained from E9.5 wild-type, *Med23*$^{sn/sn}$, *Med23*$^{sn/sn}$; *Lrp6*$^{+/-}$, *Med23*$^{sn/sn}$; *Wise*$^{+/-}$, and *Med23*$^{sn/sn}$; *Lrp6*$^{+/-}$; *Wise*$^{+/-}$ embryos indicates a significant increase in *Ccnd1* and *Dkk1* transcripts in *Med23*$^{sn/sn}$; *Lrp6*$^{+/-}$; *Wise*$^{+/-}$ embryos compared to WT and *Med23*$^{sn/sn}$. Statistical analysis was performed using Students *t*-test with *Med23*$^{sn/sn}$ as one of the nominal variables. Scale bars for **(A–E)** is 300 um, **(F–J)** is 200 um, **(F′–J′)** is 50 um. *$p < 0.05$.

severe craniofacial defects, prior to lethality. This is in stark contrast to *Med23*$^{sn/sn}$ embryos, which display considerable diminishment of neurogenesis in the cranial ganglia (**Figure 1**). Collectively, this suggests that Med23 is not required in neural crest cells for their contribution to cranial ganglia, which supports our original hypothesis that the predominant role for Med23 in cranial sensory nervous system development lies in regulating WNT/β-catenin signaling during cranial placode maturation and neuronal differentiation, the perturbation of which results in defects in cranial ganglia development.

Mid-gestation lethality, together with abnormal vascular development and diminished growth are recognizable and consistent features of *Med23*$^{sn/sn}$ embryos relative to control littermates (**Figure 1**). Because proper vascular network formation and remodeling is critical for embryo survival, we posited that Med23 may be specifically required in endothelial cells for proper neurovascular formation, embryo growth and survival. To test this hypothesis, we conditionally deleted *Med23* in endothelial cells beginning around E8.5 with *Tek-Cre* (*Tie2-Cre*) (Kisanuki et al., 2001; Proctor et al., 2005). *Med23*$^{fx/fx}$*;Tek-Cre* embryos exhibit embryonic lethality at E16.5 in association with vascular defects including blood hemorrhaging and edema (**Figures 8A,B**). Surprisingly, *Med23*$^{fx/fx}$*;Tek-Cre* embryos did not exhibit any obvious

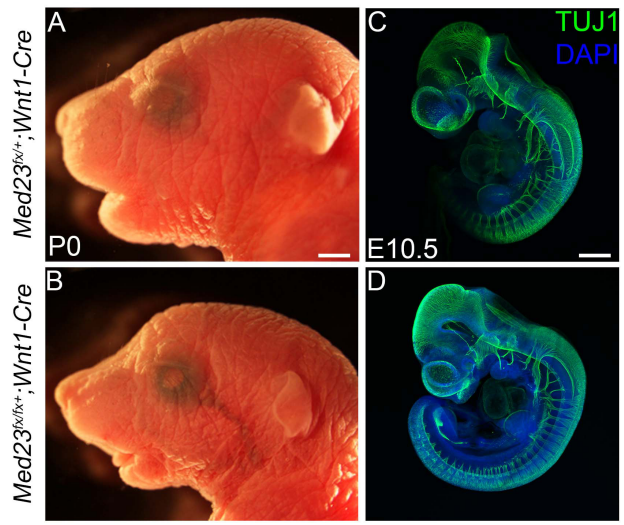

FIGURE 7 | Conditional deletion of *Med23* in neural crest cells. **(A,B)** Brightfield images of P0 *Med23*$^{fx/+}$*;Wnt1-Cre* and *Med23*$^{fx/fx}$*;Wnt1-Cre* embryos indicate that the mutants exhibit micrognathia. **(C,D)** TuJ1 staining of E10.5 *Med23*$^{fx/+}$*;Wnt1-Cre* and *Med23*$^{fx/fx}$*;Wnt1-Cre* embryos however revealed proper formation of the cranial ganglia in mutant embryos. Scale bars for **(A,B)** is 450 um, **(C,D)** is 375 um.

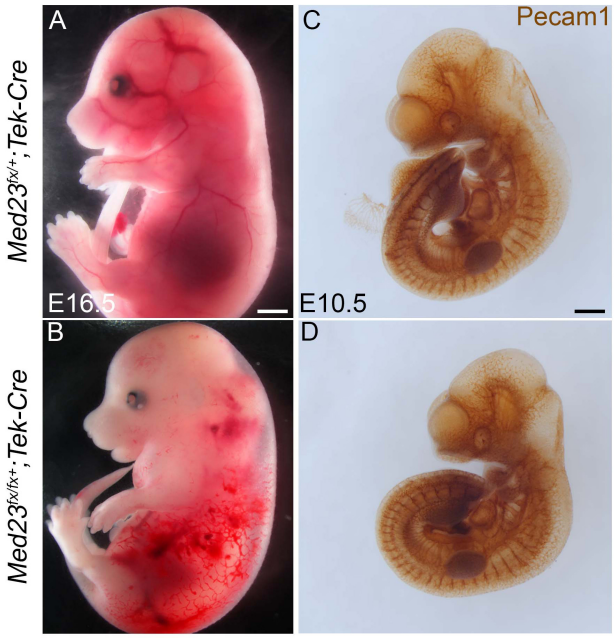

FIGURE 8 | Conditional deletion of Med23 in endothelial cells. **(A,B)** Brightfield images of E16.5 *Med23*$^{fx/+}$*;Tek-Cre* and *Med23*$^{fx/fx}$*;Tek-Cre* embryos indicate that the mutant embryos exhibit severe hemorrhaging and edema, probably resulting in lethality. **(C,D)** Immunostaining for endothelial cells using PECAM1 suggests development in *Med23*$^{fx/fx}$*;Tek-Cre* embryos is normal. Scale bars for **(A,B)** is 450 um, **(C,D)** is 300 um.

gross craniofacial, or vascular defects at E10.5 (**Figures 8C,D**). Therefore, Med23 is not required in endothelial cells for early embryonic survival. Instead, Med23 appears to be required later in mid-gestation for proper vascular development and maintenance, and also for embryo growth and survival.

Med23 Is Required at E6.5 for Embryonic Survival and Growth

To determine the developmental stage at which Med23 is required for embryo growth and survival, we deleted *Med23* in a temporal manner using *Cre-ER*^{T2} transgenic mice in conjunction with tamoxifen induction. Ubiquitous deletion of *Med23* in E8.5 mouse embryos elicits no gross defects in cranial ganglia or vascular development at E10.5, and mutant embryos survive until birth (**Supplementary Figure S5**). Deletion of *Med23* a day earlier at E7.5 results in embryos that are smaller compared to controls. However, the cranial ganglia and vascular network appear to be properly formed and patterned by E10.5 (**Supplementary Figure S6**). In contrast tamoxifen gavage at E5.5, leading to *Med23* deletion by E6.5 results in defects in both cranial ganglia as well as vascular development (**Figures 9C–F**). Furthermore, these embryos die by E10.5 similar to *Med23*$^{sn/sn}$ mutants (**Figure 9**). This indicates that Med23 is critically required by E6.5 for normal cranial ganglia and vascular network formation and patterning along with mouse embryo growth, development and survival.

DISCUSSION

Mediator is a multi-protein complex that has been identified in eukaryotic organisms, from yeast to human (Conaway et al., 2005), and which transmits information from transcription factors to RNA polymerase II (Pol II) to regulate transcription. Med23 and some other subunits of the Mediator complex, are however a metazoan innovation (Malik and Roeder, 2000), and their appearance coincides with the evolution of multi-cellular and multi-tissue complex organisms whose embryonic development requires precise control of cell specification, commitment and differentiation.

The cranial ganglia and their associated 12 sensory-motor nerves are vital for proper functioning of the head, face and neck in adult animals. Their development is governed by the reiterated use of key signaling pathways including WNT signaling (Lassiter et al., 2014; Saint-Jeannet and Moody, 2014; Singh and Groves, 2016). In this study, we describe a novel role for the mediator subunit Med23 in craniofacial and cranial ganglia development. More specifically we show that Med23 is essential for embryonic growth and survival and, also that it regulates canonical WNT signaling during cranial placode development, the perturbation of which results in defects in sensory neuron differentiation in the trigeminal and epibranchial ganglia.

Neurons within the trigeminal ganglion are of a dual neural crest or cranial placode origin. In contrast, neurons in the distal epibranchial ganglia are derived from placode cells, while the neural crest cells primarily form glia. Although the origin and development of sensory neurons within the cranial ganglia have been well-described, our understanding of how placodal ectoderm cells are induced to differentiate into sensory neurons

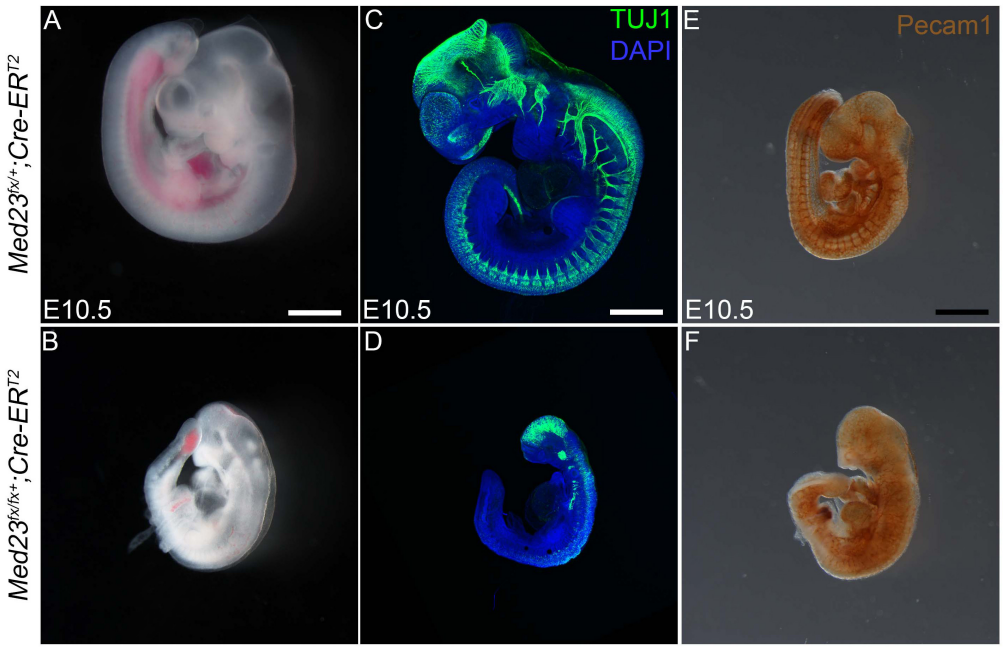

FIGURE 9 | Temporal systemic deletion of Med23 at E6.5 phenocopies *Med23*$^{sn/sn}$ embryos. **(A,B)** *Med2*$^{fx/fx}$*;Cre-ER*^{T2} embryos treated with tamoxifen at E5.5 are small in size compared to *Med2*$^{fx/+}$*;Cre-ER*^{T2} embryos. These embryos also display a shortened frontonasal prominence similar to *Med23*$^{sn/sn}$ embryos. **(C,D)** TuJ1 staining revealed severely hypoplastic cranial as well as vagal ganglia in *Med2*$^{fx/fx}$*;Cre-ER*^{T2} embryos. **(E,F)** PECAM1 staining revealed that endothelial cells are disorganized in the *Med2*$^{fx/fx}$*;Cre-ER*^{T2} embryos compared to control *Med2*$^{fx/+}$*;Cre-ER*^{T2} embryos. Scale bars for **(A,B)** is 250 um, **(C,D)** is 375 um, **(E,F)** is 300 um.

during cranial ganglia formation, and the molecular mechanisms that direct this process are not fully understood.

In the absence of Med23, *Ngn1, Ngn2,* and *NeuroD1* positive cells are diminished or absent in the trigeminal and epibranchial regions of *Med23*$^{sn/sn}$ embryos. This illustrates an important role for Med23 specifically in cranial placode sensory neuron differentiation (**Figure 10**). Cellular interactions between neural crest cells and placode cells are essential for proper cranial nerve patterning (Shiau et al., 2008; Freter et al., 2013; Theveneau et al., 2013), however, the conditional deletion of *Med23* specifically in neural crest cells did not result in defects in cranial ganglia development in *Med23*$^{fx/fx}$*;Wnt1-Cre* conditional mutant embryos. This argues against an intrinsic role for Med23 in neural crest cells during their differentiation into trigeminal neurons. However, we cannot completely rule out the possibility that the loss of placode derived neurons within the trigeminal ganglion of *Med23*$^{sn/sn}$ embryos secondarily influences the neurogenic differentiation of neural crest cells that populate the trigeminal ganglion. Nonetheless, our data collectively supports a primary role for Med23 in placode cells during cranial sensory neuron differentiation.

Currently, the role of distinct Mediator subunits in general transcription versus transcription stimulated by specific signaling pathways is poorly understood. However, our transcriptome analyses of *Med23*$^{sn/sn}$ embryos demonstrated that loss of Med23 resulted in an enhancement of WNT signaling. Furthermore, we showed that the regulation of canonical WNT signaling by Med23 is required to initiate and/or maintain the cascade of neurogenic differentiation in the trigeminal and epibranchial placodal regions. Consistent with this observation, we demonstrated that genetically modulating WNT signaling could partially ameliorate the defects in cranial ganglia development in *Med23*$^{sn/sn}$ embryos. Our work therefore has uncovered an important link between the Mediator complex and WNT signaling which integrates the general transcription co-factor machinery with modulation of a major highly conserved signaling pathway important in development, tissue homeostasis and disease.

Interestingly, a similar enhancement in WNT signaling was observed in zebrafish embryos in response to Med10, Med12 or Med13 loss-of-function (Lin et al., 2007). Taken together with our Med23 loss-of-function results, this collectively illustrates the important roles that Mediator and its subunits play in transducing WNT signaling during embryogenesis. However, the role of Med23 and other Mediator subunits, and their effects are context dependent. For example, our results indicate that Med23 promotes cranial placode sensory neuron differentiation through inhibition of WNT signaling. In contrast, Med23 inhibits primitive neural determination of murine embryonic stem cells via the activation of BMP signaling (Zhu et al., 2015). Cross-talk between WNT and BMP signaling has been implicated in many biological events during embryogenesis including neural development, and Wise has been shown to modulate both WNT and BMP signaling (Itasaki et al., 2003). Furthermore, Wise modulates WNT signaling through an interaction with the WNT co-receptor LRP6 (Guidato and Itasaki, 2007; Lintern et al., 2009). This is important because we demonstrated that the

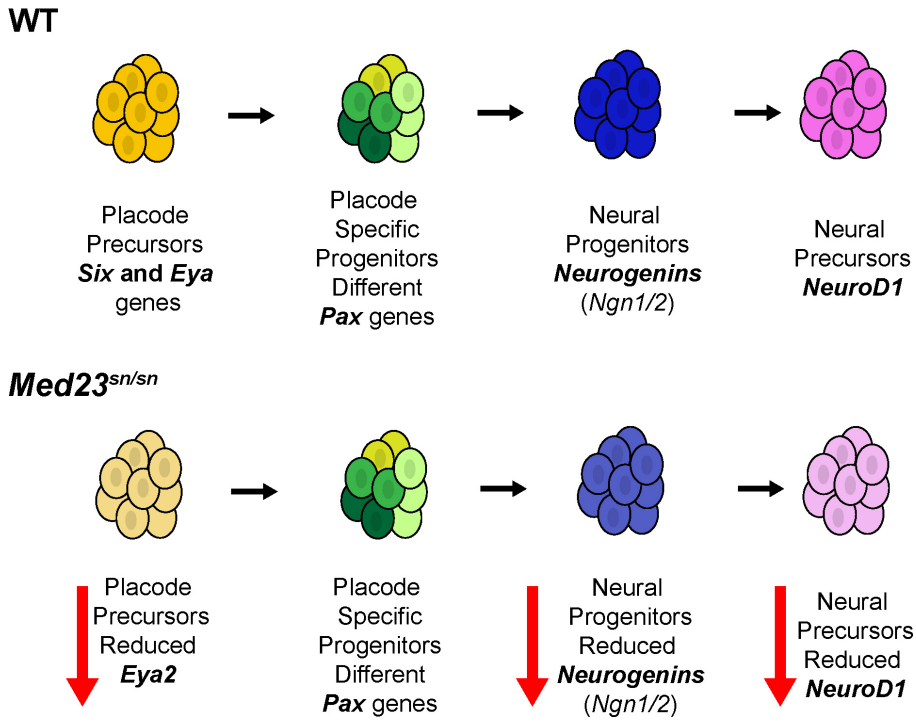

FIGURE 10 | Model for Med23-mediated regulation of cranial placode development. In wild-type embryos, placode precursors express *Six* and *Eya* genes. Their subsequent expression of different *Pax* genes defines them as placode specific progenitor cells. Some of these cells then express *Ngn1* and *Ngn2* thus becoming neural progenitor cells. Ngn1 and Ngn2 regulate the expression of *NeuroD1* which then defines these cells as neural precursors. However, in *Med23*$^{sn/sn}$ embryos, placode precursors exhibit reduced *Eya2* expression, and although Pax genes are similarly expressed in *Med23*$^{sn/sn}$ embryos as they are in wild-type embryos, *Ngn1*, *Ngn2,* and *NeuroD1* are downregulated. Collectively, this reduces the number of neural precursors resulting in defects in cranial ganglia development in *Med23*$^{sn/sn}$ embryos.

defects in cranial sensory neuron differentiation observed in the trigeminal and epibranchial ganglia of *Med23*$^{sn/sn}$ embryos can be ameliorated through combined allelic loss of *Wise* and *Lrp6*.

Wise has also been reported to promote the coalescence of placode cells and neural crest cells during formation and differentiation of the cranial ganglia (Shigetani et al., 2008) and it is interesting to note that despite partial restoration of cranial ganglia sensory neuron differentiation in *Med23*$^{sn/sn}$;*Wise*$^{+/-}$ and *Med23*$^{sn/sn}$;*Lrp6*$^{+/-}$ embryos, the sensory neurons were diffusely and incompletely organized into trigeminal and epibranchial ganglia. Although the defects in cranial ganglia sensory neuron differentiation appear to be primarily associated with perturbation of WNT signaling, we cannot rule out an additional role for Med23 in modulating BMP during cranial placode neurogenesis. However, our transcriptome analyses of *Med23*$^{sn/sn}$ embryos did not reveal mis-regulation of *Bmp4* itself or characteristic downstream targets of BMP signaling.

A key question that emerges from our work is how a ubiquitously expressed transcriptional co-factor subunit can play tissue specific differentiation roles during embryogenesis. A number of Mediator subunits have previously been shown to exhibit tissue specific roles or effects (Yin and Wang, 2014), and one possibility is that the composition of the Mediator complex may be quite dynamic and comprise a different number and combination of subunits at different times and in different tissues during embryogenesis and adult homeostasis. This hypothesis assumes that the subunits that are required for core Mediator functionality (e.g., Pol II binding) are always present within the complex, while others, that perhaps exist in the tail of Mediator such as Med23, are only present at specific times or in specific tissues. *Med23* loss-of-function in mouse embryos does not disrupt preimplantation development or germ layer specification during gastrulation, when WNT signaling through the Lrp5 and Lrp6 co-receptors is known to be required (Kelly et al., 2004). Hence Med23 does not uniformly impact levels of WNT signaling in all contexts where it is expressed. It is only around E9.5 that developmental anomalies become apparent in *Med23*$^{sn/sn}$ embryos. We propose therefore that Med23 may be dynamically required for the regulation of specific genes in specific cells and that there is some degree of context-dependence in its ability to exert its regulatory activity. In support of this idea, the response of transcription factors such as Egr1 to *Med23* loss-of-function is different in embryonic stem cells versus fibroblasts (Balamotis et al., 2009).

A precedent for the differential and dynamic role of Med23 exists with respect to adipocyte and smooth muscle cells (Yin et al., 2012), in osteoblast differentiation and bone development (Liu et al., 2016), in melanocytes (Xia et al., 2017) and in invariant natural killer T cells (Xu et al., 2018). More specifically, Med23 has been shown to directly interact with the ETS1 family

member, phospho-Elk1, which is central to the transcriptional activation of *Egr2* during adipocyte differentiation (Wang et al., 2009). In addition, MED23 favors ELK1-SRF binding to smooth muscle cell gene promoters to repress gene activity, whereas the absence of MED23 promotes MAL-SRF binding to smooth muscle cell gene promoters resulting in gene activation. Med23 also binds to Runx2 and co-operates with Runx2 to promote osteoblast differentiation (Liu et al., 2016). Lastly, Med23 loss-of-function in thymocytes blocks invariant natural killer cell development by regulating the expression of c-Jun (Xu et al., 2018). Taken together with our data, this highlights the context-dependent nature and importance of Med 23 – transcription factor interactions during development.

Our analysis of Med23 expression during murine embryogenesis revealed that Med23 is ubiquitously expressed (**Figure 2**). This combined with the relatively late onset of a developmental phenotype in *Med23*$^{sn/sn}$ embryos at around E9.5, is suggestive of functional redundancy among the Mediator subunits, and interestingly, knockouts of currently known Med23 binding partners do not recapitulate the phenotype of *Med23*$^{sn/sn}$ embryos (Screpanti et al., 1996; Cesari et al., 2004; Oqani et al., 2016). This implies the existence of other as yet unknown Med23 binding partners, the interactions of which are likely crucial for eliciting Med23's role in regulating WNT signaling during sensory neuron differentiation in the trigeminal and epibranchial placodes.

Med23 has been shown to be important for gene expression and tissue development in *C. elegans, Drosophila,* zebrafish and mouse embryos (Singh and Han, 1995; Stevens et al., 2002; Kim and Lis, 2005; Wang et al., 2005, 2009; Yin and Wang, 2014; Liu et al., 2016), and interestingly, mutations in *MED23* in humans have been linked to intellectual disability, microcephaly and cardiovascular anomalies together with overall growth retardation defects (Lüneburg et al., 2014; Lionel et al., 2016; Hashemi-Gorji et al., 2019). Our work on *Med23*$^{sn/sn}$ embryos has uncovered a previously unexplored role for Med23-containing Mediator in craniofacial and cranial ganglia development and it is tempting to speculate that a similar effect on WNT signaling and neuronal development may contribute to the pathogenesis of the neurological phenotypes observed in humans.

Protein binding studies have shown that the Mediator complex, through its various subunit interactions, acts as a hub for integrating cellular signaling cascades, transcription factors and the RNA Pol II machinery (Poss et al., 2013; Yin and Wang, 2014). Mediator regulates various transcriptional processes, including, but not limited to, the assembly of the pre-initiation complex (PIC) at the transcription initiation site, transcript elongation and termination, mRNA processing, and chromatin architecture. Furthermore, the differential interaction of specific mediator subunits with distinct transcription factors is critical to Mediator function. Potentially, a single transcription factor or activator can interact with multiple Mediator-binding sites and thus activate transcription from the same promoter differently in distinct cell types depending on which contacts are made. For example, the transcriptional activator Gcn4 binds to a Mediator subcomplex consisting of MED2, MED3, and MED15 (Park et al., 2000; Zhang et al., 2004). In contrast, the mammalian glucocorticoid receptor interacts with a distinct set of Mediator subunits including MED1 (Chen and Roeder, 2007), MED14 (Chen et al., 2006), and MED15 (Kim et al., 2008). Similar differential and dynamic roles for other Mediator subunits such as Med26 or the Mediator associated sub-complex CDK8, have also been reported (Yin and Wang, 2014). As might be expected from its central role in transcription regulation, Mediator and its subunits are crucial for gene expression and cellular differentiation during embryonic development. Consequently, it will be interesting in the future to determine the stoichiometric composition of subunits of Mediator, together with their compete repertoire of subunit-transcription factor interactions as well DNA-binding capabilities within various cell types and tissues and at different times, to understand their relative importance in embryo development and adult homeostasis.

DATA AVAILABILITY STATEMENT

The datasets generated for this study can be found in the GEO Series, accession number GSE144327.

ETHICS STATEMENT

The animal study was reviewed and approved by the Stowers Institute of Medical Research (SIMR) IACUC protocols (2019-094 and 2019-097).

AUTHOR CONTRIBUTIONS

All authors listed have made a substantial, direct and intellectual contribution to the work, and approved it for publication.

FUNDING

This work was supported by the Stowers Institute for Medical Research (PAT and REK). Original data underlying this manuscript can be accessed from the Stowers Original Data Repository at http://www.stowers.org/research/publications/LIBPB-1503.

ACKNOWLEDGMENTS

We thank members of the Trainor lab for their insights and discussions. We greatly appreciate Melissa Childers for her expertise in breeding, maintaining, and caring for the mice used in this project, and acknowledge Rodney McCay, Lacey Ellington, and the Stowers Institute ES Cell and Transgenic Core for generating the *Med23*^{bgeo} mice. We thank Karin Zueckert-Gaudenz and Allison Peak for performing the custom microarrays.

SUPPLEMENTARY MATERIAL

The Supplementary Material for this article can be found online at: https://www.frontiersin.org/articles/10.3389/fphys.2020.531933/full#supplementary-material

Supplementary Figure 1 | *Med23*$^{bgeo/bgeo}$ embryos exhibit developmental delay. **(A)** Generation of the *Med23*^{bgeo} allele **(B,C)** DAPI stained E9.5 control and *Med23*$^{bgeo/bgeo}$ littermate embryos reveal developmental delay in *Med23*$^{bgeo/bgeo}$ embryos, in concert with a failure to undergo axial turning. Scale bar is 100 um.

Supplementary Figure 2 | Complementation cross indicates *snouty* is a null allele of *Med23*. Wild-type **(A,C,E)** and *Med23*$^{bgeo/sn}$ **(B,D,F)** littermate embryos stained with DAPI **(A,B)**, immunostained with TuJ1 **(C,D)**, or PECAM1 **(E,F)**. Morphological, neural and vascular defects in *Med23*$^{bgeo/sn}$ embryos are similar to *Med23*$^{sn/sn}$ embryos suggesting that *snouty* is likely a null allele of *Med23*. Scale bar is 100 um.

Supplementary Figure 3 | Placental development is not affected in *Med23*$^{sn/sn}$ embryos. **(A–D)** Wild-type and *Med23*$^{sn/sn}$ placentas sectioned along two separate planes and stained with hematoxylin and eosin shows that the trophoblast and allantois layers are appropriately formed in both wild-type and *Med23*$^{sn/sn}$ placenta. The dotted line denotes the separation of the maternal decidua to the placenta. MD, maternal deciduas; T, trophoblast; AL, allantois. Scale bar for **(A,C)** is 200 um and **(B–D)** and 150 um.

Supplementary Figure 4 | Peripheral nervous system formation is not affected by loss of one copy of *Lrp6* or *Wise*. **(A–C)** TuJ1 immunostaining of E9.5 *Lrp6*$^{+/-}$ and *Wise*$^{+/-}$ embryos revealed proper formation of the cranial and trunk peripheral nervous systems, as well as midbrain neuron differentiation. **(D,E)** Intercrossing the *Lrp6*^{lacZ} mouse line demonstrated that E9.5 wild-type and *Med23*$^{sn/sn}$ embryos display similar *Lrp6* expression as evidenced by X-gal staining. **(F,G)** Intercrossing the *Wise*^{lacZ} mouse line demonstrated that wild-type and *Med23*$^{sn/sn}$ embryos display similar patterns of *Wise* activity as evidenced by X-gal staining. Scale bar is 300 um.

Supplementary Figure 5 | Temporal systemic deletion of Med23 at E8.5 does not affect cranial ganglia development. **(A,B)** *Med2*$^{fx/fx}$*;Cre-ER*^{T2} embryos treated with tamoxifen at E7.5 survive until P0 with no discernable defects. **(C,D)** TuJ1 staining indicates proper patterning of cranial ganglia in *Med2*$^{fx/fx}$*;Cre-ER*^{T2} embryos. **(E,F)** PECAM1 staining reveals that endothelial cells are properly formed and organized into networks in *Med2*$^{fx/fx}$*;Cre-ER*^{T2} embryos compared to *Med2*$^{fx/+}$*;Cre-ER*^{T2} controls. Scale bar for **(A,B)** is 500 um, **(C,D)** is 375 um, **(C–F)** is 300 um.

Supplementary Figure 6 | Temporal systemic deletion of Med23 at E7.5 leads to a mild cranial ganglia patterning defects. **(A,B)** *Med2*$^{fx/fx}$*;Cre-ER*^{T2} embryos treated with tamoxifen at E6.5 survive until E15.5. However, at E14.5, they are smaller in size compared to *Med2*$^{fx/+}$*;Cre-ER*^{T2} embryos. **(C,D)** TuJ1 staining revealed mild patterning defects in the cranial ganglia of *Med2*$^{fx/fx}$*;Cre-ER*^{T2} embryos. **(E,F)** PECAM1 staining showed that endothelial cells are unaffected in *Med2*$^{fx/fx}$*;Cre-ER*^{T2} embryos compared to *Med2*$^{fx/+}$*;Cre-ER*^{T2} controls. Scale bar for **(A,B)** is 500 um, **(C,D)** is 375 um, **(C–F)** is 300 um.

Supplementary Figure 7 | Pathway analysis of genes differentially regulated in *Med23*$^{sn/sn}$ embryos compared to wild-type. Cytoscape network plot of results from Ingenuity Pathway Analysis illustrating the association of the canonical WNT/β-catenin signaling pathway with the differential expression of multiple genes in *Med23*$^{sn/sn}$ embryos compared to controls.

Supplementary Table 1 | Examples of genes with downregulated expression in *Med23*$^{sn/sn}$ embryos compared to wild-type littermate controls.

Supplementary Table 2 | List of genes differentially regulated in *Med23*$^{sn/sn}$ embryos compared to wild-type with $p < 0.01$.

REFERENCES

Ahn, Y. (2015). Signaling in tooth, hair, and mammary placodes. *Curr. Top. Dev. Biol.* 111, 421–459. doi: 10.1016/bs.ctdb.2014.11.013

Ahn, Y., Sanderson, B. W., Klein, O. D., and Krumlauf, R. (2010). Inhibition of Wnt signaling by Wise (Sostdc1) and negative feedback from Shh controls tooth number and patterning. *Development* 137, 3221–3231. doi: 10.1242/dev.054668

Ahn, Y., Sims, C., Logue, J. M., Weatherbee, S. D., and Krumlauf, R. (2013). Lrp4 and Wise interplay controls the formation and patterning of mammary and other skin appendage placodes by modulating Wnt signaling. *Development* 140, 583–593. doi: 10.1242/dev.085118

Ahn, Y., Sims, C., Murray, M. J., Kuhlmann, P. K., Fuentes-Antrás, J., Weatherbee, S. D., et al. (2017). Multiple modes of Lrp4 function in modulation of Wnt/β-catenin signaling during tooth development. *Development* 144, 2824–2836. doi: 10.1242/dev.150680

Allen, B. L., and Taatjes, D. J. (2015). The Mediator complex: a central integrator of transcription. *Nat. Rev. Mol. Cell Biol.* 16, 155–166. doi: 10.1038/nrm3951

Baker, C. V., and Bronner-Fraser, M. (2001). Vertebrate cranial placodes I. Embryonic induction. *Dev. Biol.* 232, 1–61. doi: 10.1006/dbio.2001.0156

Balamotis, M. A., Pennella, M. A., Stevens, J. L., Wasylyk, B., Belmont, A. S., and Berk, A. J. (2009). Complexity in transcription control at the activation domain–mediator interface. *Sci. Signal.* 2:ra20. doi: 10.1126/scisignal.1164302

Begbie, J., and Graham, A. (2001). Integration between the epibranchial placodes and the hindbrain. *Science* 294, 595–598. doi: 10.1126/science.1062028

Behringer, R. R., Gertsenstein, M., Nagy, K. V., and Nagy, A. (2014). *Manipulating the Mouse Embryo: A Laboratory Manual*, 4th Edn. Cold Spring Harbor, NY: Cold Spring Harbor Laboratory.

Bhatt, S., Diaz, R., and Trainor, P. A. (2013). Signals and switches in mammalian neural crest cell differentiation. *Cold Spring Harb. Perspect. Biol.* 5:a008326. doi: 10.1101/cshperspect.a008326

Bouchard, M., Souabni, A., and Busslinger, M. (2004). Tissue-specific expression of cre recombinase from the Pax8 locus. *Genesis* 38, 105–109. doi: 10.1002/gene.20008

Bozdech, Z., Zhu, J., Joachimiak, M. P., Cohen, F. E., Pulliam, B., and DeRisi, J. L. (2003). Expression profiling of the schizont and trophozoite stages of Plasmodium falciparum with a long-oligonucleotide microarray. *Genome Biol.* 4:R9. doi: 10.1186/gb-2003-4-2-r9

Britsch, S., Goerich, D. E., Riethmacher, D., Peirano, R. I., Rossner, M., Nave, K. A., et al. (2001). The transcription factor Sox10 is a key regulator of peripheral glial development. *Genes Dev.* 15, 66–78. doi: 10.1101/gad.186601

Cesari, F., Brecht, S., Vintersten, K., Vuong, L. G., Hofmann, M., Klingel, K., et al. (2004). Mice deficient for the ets transcription factor elk-1 show normal immune responses and mildly impaired neuronal gene activation. *Mol. Cell. Biol.* 24, 294–305. doi: 10.1128/mcb.24.1.294-305.2004

Chai, Y., Jiang, X., Ito, Y., Bringas, P., Han, J., Rowitch, D. H., et al. (2000). Fate of the mammalian cranial neural crest during tooth and mandibular morphogenesis. *Development* 127, 1671–1679.

Chen, W., and Roeder, R. G. (2007). The Mediator subunit MED1/TRAP220 is required for optimal glucocorticoid receptor-mediated transcription activation. *Nucleic Acids Res.* 35, 6161–6169. doi: 10.1093/nar/gkm661

Chen, W., Rogatsky, I., and Garabedian, M. J. (2006). MED14 and MED1 differentially regulate target-specific gene activation by the glucocorticoid receptor. *Mol. Endocrinol.* 20, 560–572. doi: 10.1210/me.2005-0318

Conaway, R. C., Sato, S., Tomomori-Sato, C., Yao, T., and Conaway, J. W. (2005). The mammalian Mediator complex and its role in transcriptional regulation. *Trends Biochem. Sci.* 30, 250–255. doi: 10.1016/j.tibs.2005.03.002

Crane, J. F., and Trainor, P. A. (2006). Neural crest stem and progenitor cells. *Annu. Rev. Cell Dev. Biol.* 22, 267–286. doi: 10.1146/annurev.cellbio.22.010305.103814

Dackor, J., Caron, K. M., and Threadgill, D. W. (2009). Placental and embryonic growth restriction in mice with reduced function epidermal growth factor receptor alleles. *Genetics* 183, 207–218. doi: 10.1534/genetics.109.104372

D'Amico-Martel, A., and Noden, D. M. (1983). Contributions of placodal and neural crest cells to avian cranial peripheral ganglia. *Am. J. Anat.* 166, 445–468. doi: 10.1002/aja.1001660406

Dencker, L., Annerwall, E., Busch, C., and Eriksson, U. (1990). Localization of specific retinoid-binding sites and expression of cellular retinoic-acid-binding protein (CRABP) in the early mouse embryo. *Development* 110, 343–352.

Fode, C., Gradwohl, G., Morin, X., Dierich, A., LeMeur, M., Goridis, C., et al. (1998). The bHLH protein NEUROGENIN 2 is a determination factor for epibranchial placode-derived sensory neurons. *Neuron* 20, 483–494. doi: 10.1016/s0896-6273(00)80989-7

Freter, S., Fleenor, S. J., Freter, R., Liu, K. J., and Begbie, J. (2013). Cranial neural crest cells form corridors prefiguring sensory neuroblast migration. *Development* 140, 3595–3600. doi: 10.1242/dev.091033

Grifone, R., Demignon, J., Giordani, J., Niro, C., Souil, E., Bertin, F., et al. (2007). Eya1 and Eya2 proteins are required for hypaxial somitic myogenesis in the mouse embryo. *Dev. Biol.* 302, 602–616. doi: 10.1016/j.ydbio.2006.08.059

Guidato, S., and Itasaki, N. (2007). Wise retained in the endoplasmic reticulum inhibits Wnt signaling by reducing cell surface LRP6. *Dev. Biol.* 310, 250–263. doi: 10.1016/j.ydbio.2007.07.033

Hashemi-Gorji, F., Fardaei, M., Tabei, S. M. B., and Miryounesi, M. (2019). Novel mutation in the MED23 gene for intellectual disability: A case report and literature review. *Clin Case Rep* 7, 331–335. doi: 10.1002/ccr3.1942

Inman, K. E., Purcell, P., Kume, T., and Trainor, P. A. (2013). Interaction between Foxc1 and Fgf8 during Mammalian Jaw Patterning and in the Pathogenesis of Syngnathia. *PLoS Genet* 9:e1003949. doi: 10.1371/journal.pgen.1003949

Itasaki, N., Jones, C. M., Mercurio, S., Rowe, A., Domingos, P. M., Smith, J. C., et al. (2003). Wise, a context-dependent activator and inhibitor of Wnt signalling. *Development* 130, 4295–4305. doi: 10.1242/dev.00674

Jiang, X., Rowitch, D. H., Soriano, P., McMahon, A. P., and Sucov, H. M. (2000). Fate of the mammalian cardiac neural crest. *Development* 127, 1607–1616.

Kelly, O. G., Pinson, K. I., and Skarnes, W. C. (2004). The Wnt co-receptors Lrp5 and Lrp6 are essential for gastrulation in mice. *Development* 131, 2803–2815. doi: 10.1242/dev.01137

Kim, D.-H., Kim, G. S., Yun, C. H., and Lee, Y. C. (2008). Functional Conservation of the Glutamine-Rich Domains of Yeast Gal11 and Human SRC-1 in the Transactivation of Glucocorticoid Receptor Tau 1 in Saccharomyces cerevisiae. *Mol. Cell. Biol.* 28, 913–925. doi: 10.1128/MCB.01140-07

Kim, Y.-J., and Lis, J. T. (2005). Interactions between subunits of Drosophila Mediator and activator proteins. *Trends Biochem. Sci.* 30, 245–249. doi: 10.1016/j.tibs.2005.03.010

Kisanuki, Y. Y., Hammer, R. E., Miyazaki, J., Williams, S. C., Richardson, J. A., and Yanagisawa, M. (2001). Tie2-Cre transgenic mice: a new model for endothelial cell-lineage analysis in vivo. *Dev. Biol.* 230, 230–242. doi: 10.1006/dbio.2000.0106

Kurosaka, H., Trainor, P. A., Leroux-Berger, M., and Iulianella, A. (2015). Cranial nerve development requires co-ordinated Shh and canonical Wnt signaling. *PLoS One* 10:e0120821. doi: 10.1371/journal.pone.0120821

Lassiter, R. N. T., Stark, M. R., Zhao, T., and Zhou, C. (2014). Signaling mechanisms controlling cranial placode neurogenesis and delamination. *Dev. Biol.* 389, 39–49. doi: 10.1016/j.ydbio.2013.11.025

Li, L., Walsh, R. M., Wagh, V., James, M. F., Beauchamp, R. L., Chang, Y.-S., et al. (2015). Mediator Subunit Med28 Is Essential for Mouse Peri-Implantation Development and Pluripotency. *PLoS One* 10:e0140192. doi: 10.1371/journal.pone.0140192

Lim, K. C., Lakshmanan, G., Crawford, S. E., Gu, Y., Grosveld, F., and Engel, J. D. (2000). Gata3 loss leads to embryonic lethality due to noradrenaline deficiency of the sympathetic nervous system. *Nat. Genet.* 25, 209–212. doi: 10.1038/76080

Lin, X., Rinaldo, L., Fazly, A. F., and Xu, X. (2007). Depletion of Med10 enhances Wnt and suppresses Nodal signaling during zebrafish embryogenesis. *Dev. Biol.* 303, 536–548. doi: 10.1016/j.ydbio.2006.11.034

Lintern, K. B., Guidato, S., Rowe, A., Saldanha, J. W., and Itasaki, N. (2009). Characterization of wise protein and its molecular mechanism to interact with both Wnt and BMP signals. *J. Biol. Chem.* 284, 23159–23168. doi: 10.1074/jbc.M109.025478

Lionel, A. C., Monfared, N., Scherer, S. W., Marshall, C. R., and Mercimek-Mahmutoglu, S. (2016). MED23-associated refractory epilepsy successfully treated with the ketogenic diet. *Am. J. Med. Genet. A* 170, 2421–2425. doi: 10.1002/ajmg.a.37802

Liu, Z., Yao, X., Yan, G., Xu, Y., Yan, J., Zou, W., et al. (2016). Mediator MED23 cooperates with RUNX2 to drive osteoblast differentiation and bone development. *Nat. Commun.* 7:11149. doi: 10.1038/ncomms11149

Lüneburg, N., Lieb, W., Zeller, T., Chen, M.-H., Maas, R., Carter, A. M., et al. (2014). Genome-wide association study of L-arginine and dimethylarginines reveals novel metabolic pathway for symmetric dimethylarginine. *Circ. Cardiovasc. Genet.* 7, 864–872. doi: 10.1161/CIRCGENETICS.113.000264

Ma, Q., Chen, Z., del Barco Barrantes, I., de la Pompa, J. L., and Anderson, D. J. (1998). neurogenin1 is essential for the determination of neuronal precursors for proximal cranial sensory ganglia. *Neuron* 20, 469–482. doi: 10.1016/s0896-6273(00)80988-5

MacDonald, B. T., Tamai, K., and He, X. (2009). Wnt/beta-catenin signaling: components, mechanisms, and diseases. *Dev. Cell* 17, 9–26. doi: 10.1016/j.devcel.2009.06.016

Malik, S., and Roeder, R. G. (2000). Transcriptional regulation through Mediator-like coactivators in yeast and metazoan cells. *Trends Biochem. Sci.* 25, 277–283. doi: 10.1016/s0968-0004(00)01596-6

Mattar, P., Britz, O., Johannes, C., Nieto, M., Ma, L., Rebeyka, A., et al. (2004). A screen for downstream effectors of Neurogenin2 in the embryonic neocortex. *Dev. Biol.* 273, 373–389. doi: 10.1016/j.ydbio.2004.06.013

Monté, D., Clantin, B., Dewitte, F., Lens, Z., Rucktooa, P., Pardon, E., et al. (2018). Crystal structure of human Mediator subunit MED23. *Nat. Commun.* 9:3389. doi: 10.1038/s41467-018-05967-y

Ohyama, T., and Groves, A. K. (2004). Generation of Pax2-Cre mice by modification of a Pax2 bacterial artificial chromosome. *Genesis* 38, 195–199. doi: 10.1002/gene.20017

Oqani, R. K., Lin, T., Lee, J. E., Kim, S. Y., Sa, S. J., Woo, J. S., et al. (2016). Inhibition of P-TEFb disrupts global transcription, oocyte maturation, and embryo development in the mouse. *Genesis* 54, 470–482. doi: 10.1002/dvg.22961

Park, J. M., Kim, H.-S., Han, S. J., Hwang, M.-S., Lee, Y. C., and Kim, Y.-J. (2000). In Vivo Requirement of Activator-Specific Binding Targets of Mediator. *Mol. Cell. Biol.* 20, 8709–8719. doi: 10.1128/MCB.20.23.8709-8719.2000

Perez-Garcia, V., Fineberg, E., Wilson, R., Murray, A., Mazzeo, C. I., Tudor, C., et al. (2018). Placentation defects are highly prevalent in embryonic lethal mouse mutants. *Nature* 555, 463–468. doi: 10.1038/nature26002

Poss, Z. C., Ebmeier, C. C., and Taatjes, D. J. (2013). The Mediator complex and transcription regulation. *Crit. Rev. Biochem. Mol. Biol.* 48, 575–608. doi: 10.3109/10409238.2013.840259

Proctor, J. M., Zang, K., Wang, D., Wang, R., and Reichardt, L. F. (2005). Vascular development of the brain requires beta8 integrin expression in the neuroepithelium. *J. Neurosci.* 25, 9940–9948. doi: 10.1523/JNEUROSCI.3467-05.2005

Ranjan, A., and Ansari, S. A. (2018). Therapeutic potential of Mediator complex subunits in metabolic diseases. *Biochimie* 144, 41–49. doi: 10.1016/j.biochi.2017.10.012

Risley, M. D., Clowes, C., Yu, M., Mitchell, K., and Hentges, K. E. (2010). The Mediator complex protein Med31 is required for embryonic growth and cell proliferation during mammalian development. *Dev. Biol.* 342, 146–156. doi: 10.1016/j.ydbio.2010.03.019

Ruhrberg, C., and Bautch, V. L. (2013). Neurovascular development and links to disease. *Cell. Mol. Life Sci.* 70, 1675–1684. doi: 10.1007/s00018-013-1277-5

Saint-Jeannet, J.-P., and Moody, S. A. (2014). Establishing the pre-placodal region and breaking it into placodes with distinct identities. *Dev. Biol.* 389, 13–27. doi: 10.1016/j.ydbio.2014.02.011

Sandell, L. L., Butler Tjaden, N. E., Barlow, A. J., and Trainor, P. A. (2014). Cochleovestibular nerve development is integrated with migratory neural crest cells. *Dev. Biol.* 385, 200–210. doi: 10.1016/j.ydbio.2013.11.009

Sandell, L. L., Iulianella, A., Melton, K. R., Lynn, M., Walker, M., Inman, K. E., et al. (2011). A phenotype-driven ENU mutagenesis screen identifies novel alleles with functional roles in early mouse craniofacial development. *Genesis* 49, 342–359. doi: 10.1002/dvg.20727

Sandell, L. L., Sanderson, B. W., Moiseyev, G., Johnson, T., Mushegian, A., Young, K., et al. (2007). RDH10 is essential for synthesis of embryonic retinoic acid and is required for limb, craniofacial, and organ development. *Genes Dev.* 21, 1113–1124. doi: 10.1101/gad.1533407

Sandell, L. L., and Trainor, P. A. (2006). Neural crest cell plasticity. size matters. *Adv. Exp. Med. Biol.* 589, 78–95. doi: 10.1007/978-0-387-46954-6_5

Schlosser, G. (2006). Induction and specification of cranial placodes. *Dev. Biol.* 294, 303–351. doi: 10.1016/j.ydbio.2006.03.009

Screpanti, I., Musiani, P., Bellavia, D., Cappelletti, M., Aiello, F. B., Maroder, M., et al. (1996). Inactivation of the IL-6 gene prevents development of multicentric

Castleman's disease in C/EBP beta-deficient mice. *J. Exp. Med.* 184, 1561–1566. doi: 10.1084/jem.184.4.1561

Shalaby, F., Rossant, J., Yamaguchi, T. P., Gertsenstein, M., Wu, X. F., Breitman, M. L., et al. (1995). Failure of blood-island formation and vasculogenesis in Flk-1-deficient mice. *Nature* 376, 62–66. doi: 10.1038/376062a0

Shiau, C. E., Lwigale, P. Y., Das, R. M., Wilson, S. A., and Bronner-Fraser, M. (2008). Robo2-Slit1 dependent cell-cell interactions mediate assembly of the trigeminal ganglion. *Nat. Neurosci.* 11, 269–276. doi: 10.1038/nn2051

Shigetani, Y., Howard, S., Guidato, S., Furushima, K., Abe, T., and Itasaki, N. (2008). Wise promotes coalescence of cells of neural crest and placode origins in the trigeminal region during head development. *Dev. Biol.* 319, 346–358. doi: 10.1016/j.ydbio.2008.04.033

Singh, N., and Han, M. (1995). sur-2, a novel gene, functions late in the let-60 ras-mediated signaling pathway during Caenorhabditis elegans vulval induction. *Genes Dev.* 9, 2251–2265. doi: 10.1101/gad.9.18.2251

Singh, S., and Groves, A. K. (2016). The molecular basis of craniofacial placode development. *Wiley Interdiscip. Rev. Dev. Biol.* 5, 363–376. doi: 10.1002/wdev.226

Harvard Stem Cell Institute (2008). *StemBook*. Cambridge, MA: Harvard Stem Cell Institute.

Stevens, J. L., Cantin, G. T., Wang, G., Shevchenko, A., Shevchenko, A., and Berk, A. J. (2002). Transcription control by E1A and MAP kinase pathway via Sur2 mediator subunit. *Science* 296, 755–758. doi: 10.1126/science.1068943

Sun, Y., Nadal-Vicens, M., Misono, S., Lin, M. Z., Zubiaga, A., Hua, X., et al. (2001). Neurogenin Promotes Neurogenesis and Inhibits Glial Differentiation by Independent Mechanisms. *Cell* 104, 365–376. doi: 10.1016/S0092-8674(01)00224-0

Theveneau, E., Steventon, B., Scarpa, E., Garcia, S., Trepat, X., Streit, A., et al. (2013). Chase-and-run between adjacent cell populations promotes directional collective migration. *Nat. Cell Biol.* 15, 763–772. doi: 10.1038/ncb2772

Trainor, P. A. (2016). Developmental biology: we are all walking mutants. *Curr. Top. Dev. Biol.* 117, 523–538. doi: 10.1016/bs.ctdb.2015.11.029

Wang, G., Balamotis, M. A., Stevens, J. L., Yamaguchi, Y., Handa, H., and Berk, A. J. (2005). Mediator requirement for both recruitment and postrecruitment steps in transcription initiation. *Mol. Cell* 17, 683–694. doi: 10.1016/j.molcel.2005.02.010

Wang, W., Huang, L., Huang, Y., Yin, J., Berk, A. J., Friedman, J. M., et al. (2009). Mediator MED23 links insulin signaling to the adipogenesis transcription cascade. *Dev. Cell* 16, 764–771. doi: 10.1016/j.devcel.2009.04.006

Wodarz, A., and Nusse, R. (1998). Mechanisms of Wnt signaling in development. *Annu. Rev. Cell Dev. Biol.* 14, 59–88. doi: 10.1146/annurev.cellbio.14.1.59

Xia, M., Chen, K., Yao, X., Xu, Y., Yao, J., Yan, J., et al. (2017). Mediator MED23 Links Pigmentation and DNA Repair through the Transcription Factor MITF. *Cell Rep.* 20, 1794–1804. doi: 10.1016/j.celrep.2017.07.056

Xu, Y., Sun, Y., Shen, H., Dai, Y., Liu, H., Li, R., et al. (2018). Regulation of the terminal maturation of iNKT cells by mediator complex subunit 23. *Nat. Commun.* 9:3875. doi: 10.1038/s41467-018-06372-1

Yin, J., Liang, Y., Park, J. Y., Chen, D., Yao, X., Xiao, Q., et al. (2012). Mediator MED23 plays opposing roles in directing smooth muscle cell and adipocyte differentiation. *Genes Dev.* 26, 2192–2205. doi: 10.1101/gad.192666.112

Yin, J., and Wang, G. (2014). The Mediator complex: a master coordinator of transcription and cell lineage development. *Development* 141, 977–987. doi: 10.1242/dev.098392

Zhang, F., Sumibcay, L., Hinnebusch, A. G., and Swanson, M. J. (2004). A Triad of Subunits from the Gal11/Tail Domain of Srb Mediator Is an In Vivo Target of Transcriptional Activator Gcn4p. *Mol. Cell Biol.* 24, 6871–6886. doi: 10.1128/MCB.24.15.6871-6886.2004

Zhu, W., Yao, X., Liang, Y., Liang, D., Song, L., Jing, N., et al. (2015). Mediator Med23 deficiency enhances neural differentiation of murine embryonic stem cells through modulating BMP signaling. *Development* 142, 465–476. doi: 10.1242/dev.112946

Zou, D., Silvius, D., Fritzsch, B., and Xu, P.-X. (2004). Eya1 and Six1 are essential for early steps of sensory neurogenesis in mammalian cranial placodes. *Development* 131, 5561–5572. doi: 10.1242/dev.01437

Conflict of Interest: The authors declare that the research was conducted in the absence of any commercial or financial relationships that could be construed as a potential conflict of interest.

frontiers in Physiology

ORIGINAL RESEARCH
published: 30 October 2020
doi: 10.3389/fphys.2020.563372

Cadherin-11 Is Required for Neural Crest Specification and Survival

Subrajaa Manohar[1†], Alberto Camacho-Magallanes[1†], Camilo Echeverria Jr.[2] and Crystal D. Rogers[2]*

[1]*Department of Biology, School of Math and Science, California State University Northridge, Northridge, CA, United States,*
[2]*Department of Anatomy, Physiology, and Cell Biology, UC Davis School of Veterinary Medicine, Davis, CA, United States*

Neural crest (NC) cells are multipotent embryonic cells that form melanocytes, craniofacial bone and cartilage, and the peripheral nervous system in vertebrates. NC cells express many cadherin proteins, which control their specification, epithelial to mesenchymal transition (EMT), migration, and mesenchymal to epithelial transition. Abnormal NC development leads to congenital defects including craniofacial clefts as well as NC-derived cancers. Here, we identify the role of the type II cadherin protein, Cadherin-11 (CDH11), in early chicken NC development. CDH11 is known to play a role in NC cell migration in amphibian embryos as well as cell survival, proliferation, and migration in cancer cells. It has also been linked to the complex neurocristopathy disorder, Elsahy-Waters Syndrome, in humans. In this study, we knocked down CDH11 translation at the onset of its expression in the NC domain during NC induction. Loss of CDH11 led to a reduction of *bonafide* NC cells in the dorsal neural tube combined with defects in cell survival and migration. Loss of CDH11 increased p53-mediated programmed-cell death, and blocking the p53 pathway rescued the NC phenotype. Our findings reveal an early requirement for CDH11 in NC development and demonstrated the complexity of the mechanisms that regulate NC development, where a single cell-cell adhesion protein simultaneous controls multiple essential cellular functions to ensure proper specification, survival, and transition to a migratory phase in the dorsal neural tube. Our findings may also increase our understanding of early cadherin-related NC developmental defects.

Keywords: Cadherin-11, neural crest, specification, apoptosis, survival, p53, caspase

OPEN ACCESS

Edited by:
Lisa Taneyhill, University of Maryland, College Park, United States

Reviewed by:
Dominique Alfandari, University of Massachusetts Amherst, United States
Clemens Martin Franz, Kanazawa University, Japan

***Correspondence:**
Crystal D. Rogers
crdrogers@ucdavis.edu

[†]These authors have contributed equally to this work

Specialty section:
This article was submitted to Craniofacial Biology and Dental Research, a section of the journal Frontiers in Physiology

Received: *18 May 2020*
Accepted: *06 October 2020*
Published: *30 October 2020*

Citation:
Manohar S, Camacho-Magallanes A, Echeverria C Jr and Rogers CD (2020) Cadherin-11 Is Required for Neural Crest Specification and Survival. Front. Physiol. 11:563372. doi: 10.3389/fphys.2020.563372

INTRODUCTION

Cadherin proteins are calcium dependent cell-cell adhesion molecules, which are essential for the development and maintenance of embryonic tissues (Giger and David, 2017; Taneyhill and Schiffmacher, 2017). Cadherins are single pass transmembrane proteins that contain a calcium-binding extracellular domain as well as a cytoplasmic domain which links with three catenin family proteins (α, β, and p120) and the actin cytoskeleton (Gul et al., 2017). Classical cadherins are divided into types I and II. Type I cadherins include epithelial cadherin (E-cadherin/CDH1) and neural cadherin (N-cadherin/CDH2) among others, which have been implicated in both central nervous system (CNS) development in chick and zebrafish embryos (Dady et al., 2012; Miyamoto et al., 2015), and neural crest (NC) specification and the epithelial to mesenchymal transition (EMT) in frog, fish, and chicks (Piloto and Schilling, 2010; Rogers et al., 2013, 2018; Huang et al., 2016). Type II cadherins include Cadherin 7 (CDH7),

Cadherin 11 (Osteoblast-cadherin/CDH11), and Cadherin-6B (CDH6), which have been linked to CNS patterning, NC cell delamination, EMT, and migration during embryonic development (Taneyhill et al., 2007; Liu et al., 2008; Kashef et al., 2009; Schiffmacher et al., 2014, 2016). With varied timing and onset of protein expression, the regulation and function of cadherin proteins is clearly important for normal development of the CNS, NC cells, and NC derivatives.

Here, we focus on identifying the role of Cadherin-11 (CDH11) during early avian embryogenesis. CDH11 has been identified as a Wnt signaling target and effector in developmental and disease systems (Hadeball et al., 1998; Chalpe et al., 2010; Satriyo et al., 2019). Originally defined as a mesenchymal marker with no expression in the undifferentiated neural tube in mouse embryos (Hoffmann and Balling, 1995), the transcript was subsequently reported in developing mouse neuroepithelia (Kimura et al., 1995, 1996), as well as migratory NC cells in chick and frog embryos (Vallin et al., 1998; Borchers et al., 2001; Chalpe et al., 2010). It has been identified as a major regulator of NC migration in *Xenopus* embryos (Vallin et al., 1998; Kashef et al., 2009; Abbruzzese et al., 2016; Langhe et al., 2016) and has been linked to tumor growth, cell survival, and EMT in disease models (Yoshioka et al., 2015; Piao et al., 2016; Row et al., 2016). Both reduced and increased levels of CDH11 are linked to patient survival and reduced metastasis in numerous cancers; however, its role is contrasting in different cancer cell types (Carmona et al., 2012; Lee et al., 2013). Specifically, high levels of CDH11 expression have been linked to poor prognosis in gastric cancer and triple-negative breast cancer (Chen et al., 2018; Satriyo et al., 2019), yet it maintains a pro-apoptotic tumor suppressor role in others (Marchong et al., 2010; Li et al., 2012). Although studies have linked CDH11 to NC migration its role in NC induction, specification, maintenance, or survival during premigratory stages has not been studied.

NC cells are a vertebrate-specific population of stem-like cells that form craniofacial bone, cartilage, pigment cells, and the peripheral and enteric nervous systems (Hutchins et al., 2018; Rogers and Nie, 2018). In avian embryos, NC cells begin as tightly adherent neuroepithelial cells in the dorsal neural tube. By going through an EMT, which is controlled by alterations in the expression of type I and II cadherin proteins (Taneyhill et al., 2007; Rogers et al., 2013; Scarpa et al., 2015), the NC cells detach from each other and the basal lamina and gain the ability to migrate. Abnormal NC development can cause congenital defects known as neurocristopathies, which include cleft palate, craniofacial abnormalities, albinism, and defects in the enteric and peripheral nervous systems among others (Reissmann and Ludwig, 2013; Lopez et al., 2018). Bi-allelic mutations in CDH11 have specifically been linked to Elsahy-Waters syndrome, which is a combination of abnormal craniofacial developmental morphologies including those likely induced by neurocristopathies (Harms et al., 2018). The processes of NC specification and EMT are tightly regulated at multiple levels by signaling molecules (Bhattacharya et al., 2018), epigenetic modifiers (Hu et al., 2012), transcription factors (Simoes-Costa et al., 2015), and adhesion molecules (Abbruzzese et al., 2016; Schiffmacher et al., 2016; Rogers et al., 2018) to prevent developmental defects. Previous studies showed that perturbation of factors involved in this process can directly affect the formation and migratory ability of NC cells. Studies also identified links between cadherin proteins and NC cell migration and differentiation; however, there is little known about how type I or II cadherin proteins regulate premigratory NC development. Our study focuses on the role of CDH11 during the time point it first emerges in the NC domain in the dorsal neural tube. We thoroughly define the spatiotemporal localization of CDH11 in the neural plate and neural tube as well as in the pre- and post-migratory NC cells in the chick embryo during early stages Hamburger Hamilton (HH) stages 4–12. Loss of CDH11 expression reduces the premigratory NC population marked by PAX7, SOX9, SNAI2, and SOX10, and increases membrane-associated CDH1, F-actin, p53 and p53-mediated apoptosis in the presumptive NC regions. Our results indicate that the upregulation of CDH11 in the dorsal neural tube prior to NC migration is necessary for NC cell specification, survival, EMT, and migration.

RESULTS

CDH11 Expression Starts in the Neural Tube Prior to NC Cell Formation

CDH11 function has been extensively examined during NC migration and EMT in amphibian embryos (Hadeball et al., 1998; Vallin et al., 1998; Borchers et al., 2001; Kashef et al., 2009; McCusker et al., 2009; Koehler et al., 2013; Abbruzzese et al., 2016), but less is known about its endogenous expression and role in amniotes, which encouraged us to begin by examining the spatiotemporal expression pattern of the CDH11 protein in the chicken embryo. First, protein lysate was collected at multiple developmental stages (HH4–6, HH8–10, and HH11–12) and western blot analysis was used to define the relevant stages. To test the antibody reactivity across species, we also used lysate from tailbud stage *Ambystoma mexicanum* (axolotl) whole embryos. Two antibodies against CDH11 were tested: a previously verified monoclonal mouse antibody against recombinant intracellular peptide of human CDH11 (Chalpe et al., 2010) and a rabbit polyclonal antibody directed against human CDH11 used previously in mouse tissue (Chang et al., 2017; **Supplementary Figure S1A**). The mouse antibody identified three bands (potentially different isoforms or posttranslationally modified versions of CDH11) between the sizes of 110–135 kD while the rabbit antibody identified only the mid-sized band and did not recognize axolotl CDH11. Further, the mouse antibody bound to an antigen in the non-neural ectoderm (**Supplementary Figures S1B–E'**, white arrow). Both antibodies show that CDH11 protein is expressed by stages HH4–6 through HH11–12 in chicken (**Supplementary Figures S1A–M'**). It is likely that the mouse antibody recognizes three versions of CDH11 (pro-, active full-length, cleaved) previously reported in *Xenopus* based on the absence of the smallest band from the early premigratory stages (McCusker et al., 2009). We also performed whole mount IHC using both antibodies, and although their expression profiles were similar in whole mount

(**Supplementary Figures S1B–M**), in section, the mouse antibody also bound to an epitope localized in non-neural ectoderm (**Supplementary Figures S1C'–E'**, arrows). Due to its specificity, we chose to use the rabbit antibody for the rest of our experiments. We also verified specificity of the antibody by performing CDH11 loss and gain of function experiments and visualizing reduction or exogenous expression of the protein in whole mount (**Supplementary Figures S2A–D,H–J, S3**) and transverse sections (**Supplementary Figures S2E–G,K–M, S3**).

To characterize the spatiotemporal localization of CDH11 in early avian development, we performed IHC using anti-CDH11 in conjunction with previously characterized markers of NC cells (PAX7 and HNK1; Del Barrio and Nieto, 2004; Basch et al., 2006). The results identify CDH11 expression in the neural plate of 1 somite stage (SS) embryos at HH7 (**Figures 1A–D,A'–D'**, **Supplementary Figures S1F–M'**), but is expressed at much lower levels in the neural plate border, which expresses PAX7 and CDH1 as NC cells are being induced (**Figures 1B–D,B'–D'**). As the neural tube begins to fuse at 5 SS (HH8). CDH11 expression is maintained throughout the neural tube, co-localizing with dorsal cells expressing CDH1 (**Figures 1E–H,E'–H'**). CDH11 expression starts to emerge in a subset of PAX7-positive cells in the dorsal neural tube (**Figures 1I–L,I'–L'**, **Supplementary Figures S1H–M**). At 7 SS (HH9), as NC cells begin to delaminate and undergo EMT, CDH11 is upregulated in the most proximal PAX7-positive cells (**Figures 1M–P,M'–P'**). As HNK1 expression begins in the early migrating NC cells, the leading cells co-express CDH11 (**Figures 1O,P,O',P'**). In 9 SS (late HH9) embryos, as NC cells begin to migrate away from the midline, and all migratory cells are positive for both CDH11 and PAX7 (**Figures 1Q-T,Q'–T'**), while the most lateral cells express HNK1 (**Figures 1S,T**). Focusing on CDH11-postive cells at 7 SS (**Figure 1M'**) and 9 SS (**Figure 1Q'**) shows that CDH11 appears membrane-localized as NC cells collectively migrate out of the neural tube. At 15 SS (HH11), CDH11 remains in the neural tube and the migratory NC cells, co-localizing with PAX7 (**Figures 1U–X,U'–X'**); however, the cellular localization in later migratory NC appears more punctate (**Figures 1Q'–T'**). Our results support previous studies in frog by demonstrating the endogenous expression of CDH11 in migrating chick NC cells (McCusker et al., 2009; Abbruzzese et al., 2016; Mathavan et al., 2017). These data confirm that CDH11 is expressed during NC cell EMT and migration, but introduce novel expression in epithelial premigratory NC cells suggesting that CDH11 may play an earlier role in NC development.

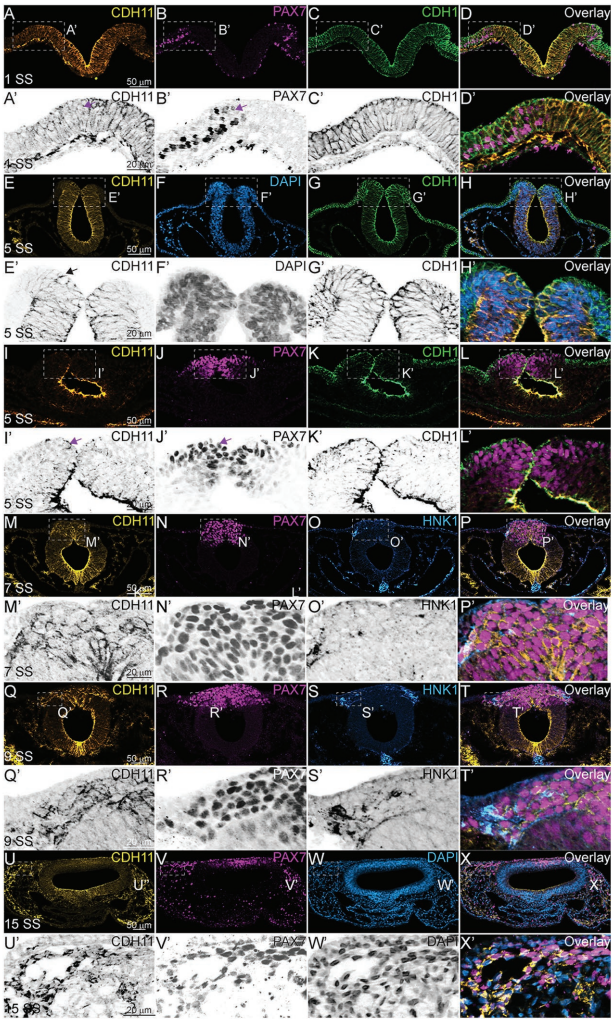

FIGURE 1 | CDH11 expression in NC cells starts during specification stages. **(A–X')** Immunohistochemistry (IHC) using antibodies against CDH11 (yellow), PAX7 (pink) to mark NC cells and neural plate border, CDH1 (green) to mark cell-cell junctions and epithelial tissues, and HNK1 (blue) to mark migratory NC cells as well as parts of the endoderm, mesoderm, and notochord, or stained with DAPI (blue) to mark nuclei. At **(A–D')** HH7[1 somite stage (SS)], when NC are induced at the neural plate border, CDH11 is expressed in the neural plate/tube, but is only expressed in a subset of border cells with PAX7. Examples of cells positive for both PAX7 and CDH11 are marked with pink arrows. **(E-H', I-L')** At HH8 (5 SS), CDH11 co-localizes with CDH1 in the developing neural tube. Black arrow marks cell in premigratory NC region positive for CDH11. **(M–P')** At HH9 (7 SS) is strongly upregulated in the premigratory NC cells marked by PAX7 and early migrating NC cells marked by HNK1. **(Q-T')** At late HH9 (9 SS) expression is maintained in the NC cells undergoing EMT and migrating out of the neural tube. **(U–X')** At HH11 (15 SS), CDH11 expression is weaker in the neural tube and is maintained in the migratory NC cells marked by PAX7. Dashed boxes indicate zoom regions depicted by grayscale images. Scale bars as indicated in first row.

CDH11 Is Necessary for NC Cell Population Maintenance During Specification

Next, to understand the stage at which CDH11 is necessary for NC cell development, and to determine whether CDH11 was required for induction, specification, or maintenance of the NC population, in addition to its role in migration, a time-course experiment was performed. We used a translation-blocking CDH11MO, which effectively reduced CDH11 fluorescence intensity on the injected side of the embryo compared to the uninjected side by approximately 50% (**Supplementary Figures S2A–G, S3**). CDH11 expression was inhibited at gastrula stage (HH4), prior to the expression of the neural plate border marker, PAX7. After injection, embryos were collected at stages HH5 and HH7 and IHC for PAX7 was performed. We next counted the number of PAX7-positive

cells and measured fluorescence intensity on the morpholino-injected side compared to the uninjected side. As expected, at NC induction and early specification stages prior to the onset of CDH11 expression upregulation (HH5- HH8-), the number of PAX7-positive NC progenitors in the neural plate border was unchanged (**Figures 2A–B',I**, $n = 14$, $p = 0.94$). In contrast, at 5 SS (HH8), when CDH11 expression emerges in the dorsal neural tube, the number of PAX7-positive NC cells was reduced by 40% (**Figures 2C–D'**, $n = 19$, $p = 0.0005$). At 10 SS (HH10), there continued to be 35% less PAX7-positive cells on the CDH11MO-injected side, suggesting that the NC cells did not recover prior to migration (**Figures 2E–F',I**, $n = 7$, $p = 0.01$). Embryos injected with a non-specific control morpholino (ContMO), did not exhibit significant differences in the number of PAX7-positive cells between the injected and uninjected sides (**Figures 2G–H'**, $n = 14$, $p = 0.74$). We additionally assessed the changes in fluorescence intensity at each stage after CDH11 knockdown and although the fluorescence was

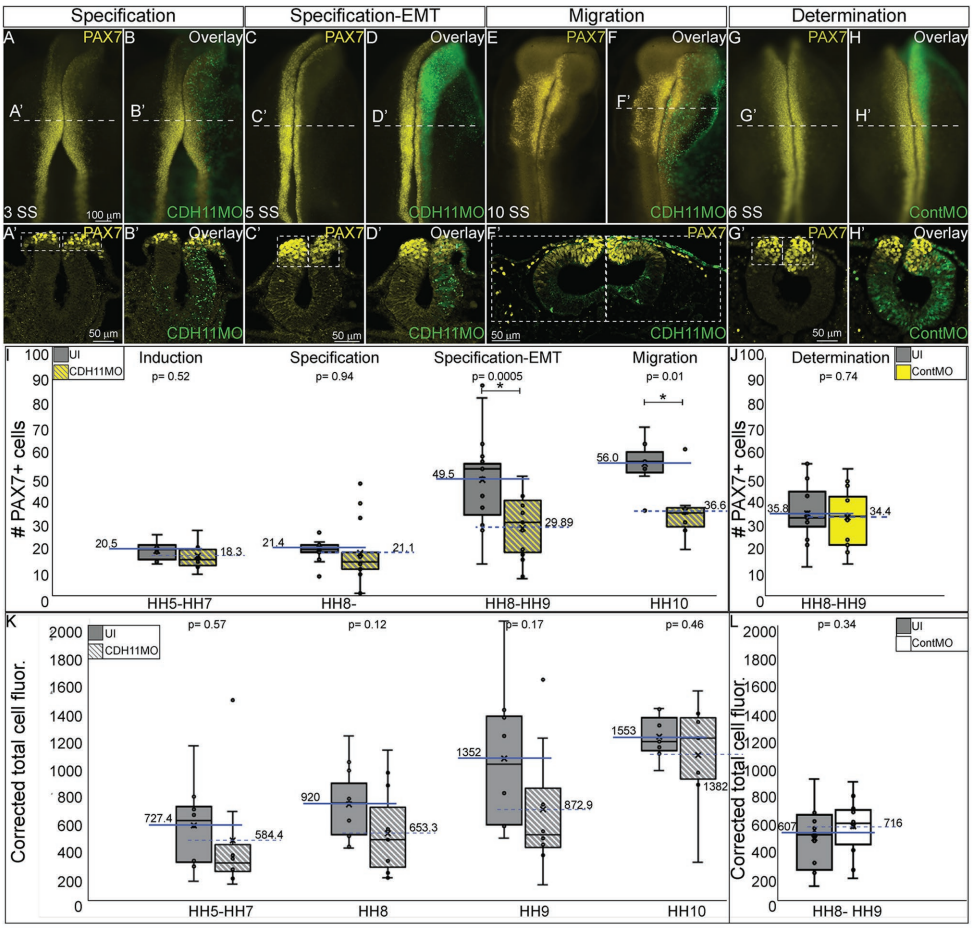

FIGURE 2 | CDH11 is required for NC cell population specification. Embryos were injected at HH4 and collected at multiple stages to analyze NC progenitor marker, PAX7. **(A-F')** IHC for PAX7 on embryos injected with CDH11MO and collected between 3 SS and 10 SS. **(G–H')** IHC for Pax7 in embryo injected with ContMO and collected at 6 SS. **(I,J)** Actual PAX7+ cell counts of uninjected and morpholino-injected sides. **(K)** Corrected total cell fluorescence of PAX7 expression in section images injected with either CDH11MO or ContMO. **(A)** Whole mount IHC for PAX7 in HH8- (3 SS) embryo with **(B)** overlay with CDH11MO (green). **(A',B')** Transverse section of **(A,B)** with PAX7-positive NC cells circled. Mean number of cells at HH8- is 21.43 on uninjected and 21.14 on CDH11MO-injected side, $p = 0.94$, $n = 14$. **(C)** Whole mount IHC for PAX7 in HH8 embryo with **(C)** overlay with CDH11MO (green). **(C',D')** Transverse section of **(C,D)** with PAX7-positive NC cells boxed. Mean number of cells at HH8 is 49.53 on uninjected and 29.89 on CDH11MO-injected side, $p = 0.0005$, $n = 19$. **(E)** Whole mount IHC for PAX7 in HH10 embryo with **(F)** overlay with CDH11MO (green). **(F')** Transverse section of **(F)** with PAX7-positive NC cells. Mean number of cells at HH10 is 56.00 on uninjected and 36.57 on CDH11MO-injected side, $p = 0.01$, $n = 7$. **(G)** Whole mount IHC for PAX7 in HH8 embryo with **(H)** overlay with ContMO (green). **(G',H')** Transverse sections of **(G,H)** with PAX7-positive NC cells circled. Mean number of cells on uninjected side is 35.8 and on ContMO-injected side is 34.4, $p = 0.74$, $n = 14$. Dashed boxes were drawn around NC cell population from uninjected side and are mirrored on injected sides to demonstrate changes in the NC cell population density. At 5 SS the NC cell population is less dense in the CDH11MO-side compared to uninjected when compared to 3 SS and ContMO-injected embryos. **(K,L)** Fluorescence intensity calculated using NIH ImageJ (see methods) from HH5 ($n = 8$, $p = 0.57$), HH8 ($N = 11$, $p = 0.11$), HH9 ($n = 8$, $p = 0.17$), HH10 ($n = 7$, $p = 0.46$), and ContMO HH8–9 ($n = 12$, $p = 0.34$). Scale bars are as marked (100 µm for whole mount and 50 µm for sections). Anterior to top in all whole mount images, dorsal to top in all sections. Loss of CDH11 reduces the PAX7-positive NC cell population after induction (**I**, HH5-3SS) and at a point between specification and determination (5 SS).

reduced in the injected vs. uninjected sides, due to variability in the NC population responses to CDH11MO, the changes in fluorescence were not significant (**Figure 2K**, $p > 0.05$). Taken together, loss of CDH11 significantly reduced PAX7+ NC cells after induction during the stages at which NC specifier genes and proteins are normally upregulated suggesting a role for CDH11 specifically in NC specification or maintenance in preparation for EMT, prior to its role in NC migration.

Loss of CDH11 Reduces Expression of NC Specifiers SNAI2, SOX9, and SOX10

As reported by multiple groups, in the NC gene regulatory network (GRN) the factors in the neural plate border (i.e., PAX7, PAX3) drive the expression of bonafide NC markers (SNAI2, SOX9, SOX10, etc.) as neurulation proceeds (Basch et al., 2006; Plouhinec et al., 2014; Williams et al., 2019). These factors are then responsible for altering the expression of specific cadherin proteins and allowing for NC cell EMT and migration (Taneyhill et al., 2007; Huang et al., 2016; Taneyhill and Schiffmacher, 2017). To determine if loss of CDH11 universally reduced the NC cell population by reducing definitive NC cells, embryos were unilaterally injected with CDH11MO, electroporated at HH4, and IHC was used to detect bonafide NC cell markers (SOX9, SNAI2, SOX10) at HH8–9 (5 SS to 7 SS). Loss of CDH11 significantly reduced SOX9-postive NC cells by 41% (**Figures 3A–C**, $n = 11$, $p = 0.04$). SNAI2-positive cells were reduced by 34% (**Figures 3D–F**, $n = 16$, $p = 0.001$) and SOX10-positive NC cells were reduced by 41.7% (**Figures 3G–I**, $n = 19$, $p = 0.01$). We next knocked down CDH11 and performed IHC for PAX7, SOX9, and SOX10 in the same embryos to confirm that the loss of CDH11 was affecting both NC cell progenitors and the premigratory *bonafide* NC population. We identified that both cell populations were reduced in the absence of CDH11 (**Figures 3J–M'**, $n = 8/9$). Finally, we wanted to determine if the CDH11-knockdown phenotype was NC-specific or if loss of CDH11 affected all ectodermal derivatives. Therefore, we analyzed the expression of SOX2, a neural tube progenitor marker, which was unaffected in the CDH11MO-innjected side compared to the UI-side (**Figures 3N–P**, $n = 5$, $p = 0.9$).

The loss of CDH11 thus reduces the amount of progenitors and definitive NC cells prior to NC cell migration. However, each NC specifier protein drives specific programs with regards to NC cell development. SNAI2 inhibits *Cdh6B* and *Cdh1* expression to drive cell migration (Taneyhill et al., 2007; Tien et al., 2015) and it is also linked to the inhibition of apoptotic activity in NC cells (Tribulo et al., 2004), while the SOXE proteins, SOX9 and SOX10 are linked with the progression of NC cell migration (Cheung and Briscoe, 2003). To determine the mechanisms downstream of CDH11 knockdown that led to a reduction in the NC population, we next analyzed the impact on cell death and proliferation.

CDH11 Is Required for NC Cell Survival

The reduction in NC cells after CDH11 knockdown could be caused by two cellular responses. To determine if this phenotype was a result of increased cell death (or reduced

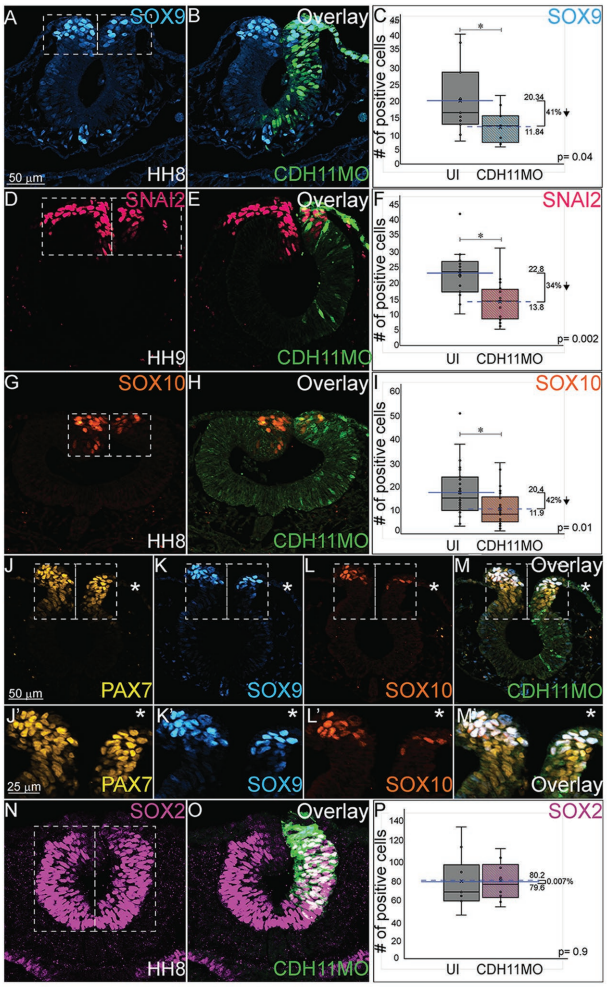

FIGURE 3 | Loss of CDH11 reduces definitive NC cells. To determine if loss of CDH11 affected neural progenitors and definitive NC cells in addition to NC progenitors, embryos were injected with CDH11MO or ContMO and electroporated, and IHC was performed for definitive NC cells (SOX9, SNAI2, SOX10) and neural progenitors (SOX2). **(A)** IHC for SOX9 in transverse section from HH8 embryo with **(B)** overlay with CDH11MO (green). **(C)** Graph showing difference between uninjected and CDH11MO-injected sides. Mean number of SOX9+ cells is 20.34 on uninjected and 11.85 on CDH11MO-injected side, $p = 0.04$, $n = 11$. **(D)** IHC for SNAI2 in transverse section from HH9 embryo with **(E)** overlay with CDH11MO (green). **(F)** Graph showing difference between uninjected and CDH11MO-injected sides. Mean number of SNAI2+ cells is 22.75 on uninjected and 13.75 on CDH11MO-injected side, $p = 0.001$, $n = 16$. **(G)** IHC for SOX10 in transverse section from HH8 embryo with **(H)** overlay with CDH11MO (green). **(I)** Graph showing difference between uninjected and CDH11MO-injected sides. Mean number of SOX10+ cells is 20.35 on uninjected and 11.87 on CDH11MO-injected side, $p = 0.01$, $n = 18$. **(J–M')** Overlay from the same embryo to demonstrate reduction in NC progenitors (PAX7) and definitive NC cells (SOX9, SOX10) after CDH11 MO-injection ($n = 8/9$ embryos with reduced cells). **(N)** IHC for SOX2 in transverse section from HH8 embryo with **(O)** overlay with CDH11MO (green). **(P)** Graph showing difference between uninjected and CDH11MO-injected sides. Mean number of SOX2+ cells is 80.20 on uninjected and 79.50 on CDH11MO-injected side, $p = 0.90$, $n = 5$. All graphs show mean (indicated on graph) and median (line within graph). Scale bar for **(A,B,D,E,G,H,N,O)** indicated in **(A)** and scale bar for **(J-M')** indicated in **(J)**. Reducing CDH11 significantly reduces the entire population of premigratory NC cells without affecting the SOX2-positive neural tube progenitors.

cell survival) or of a reduction NC cell proliferation (or reduced population growth), we unilaterally injected chicken embryos with CDH11MO or ContMO, electroporated at HH4, and performed IHC for markers of cell death and cell proliferation. To determine the requirement for CDH11 in NC cell survival, IHC was performed for tumor protein p53 (p53) as previous work in chicken NC cells demonstrated that p53 plays a role in NC cell EMT and that excess p53 reduces the premigratory NC cell population (Rinon et al., 2011). The fluorescence intensity of p53 expression was measured in the dorsal region of the neural tube, and in the absence of CDH11, p53 expression was increased in the CDH11MO-injected side of the neural tube compared to the uninjected side (**Figures 4A–C**, $n = 17$, $p = 0.02$, **Supplementary Figures S4A–D**). We next analyzed expression of the p53-mediated apoptosis effector protein, activated Caspase-3 (*Casp3) together with PAX7 (Zou et al., 1999). After CDH11 knockdown, the total number of *Casp3-positive cells was counted in the injected and uninjected sides of each embryo. Expression of *Casp3 was significantly increased by 71.5% in CDH11MO-injected sides compared with the uninjected side (**Figures 4D,D',G,H**, $n = 14$, $p = 0.04$), concurrent with a reduction in PAX7-positive cells (**Figures 4E,E',G,G'**). However, embryos injected with ContMO showed no significant difference in *Casp3 or PAX7 between the injected versus uninjected sides (**Figures 4I-M**, $n = 14$, $p = 0.97$). We also performed terminal deoxynucleotidyl transferase dUTP nick end labeling (TUNEL) analysis to further confirm the presence of apoptotic cells in the neural tube after CDH11 knockdown. We identified an increase in fluorescence intensity of the TUNEL staining in the injected side of CDH11MO-injected neural tubes compared to the uninjected side (**Supplementary Figures S4E–H,J**, $n = 12$, $p = 0.02$) while ContMO-injected embryos had no significant difference in TUNEL staining between the injected and uninjected sides (**Supplementary Figure S4I**, $n = 5$, $p = 0.53$). Loss of CDH11 is thus correlated with an increase in cell death and CDH11 may be necessary for NC cell survival.

Previous results in *Xenopus* embryos linked loss of CDH11 to increased Wnt-dependent cell cycling and suggested that loss of CDH11 was positively correlated with NC cell proliferation (Koehler et al., 2013). To determine if NC cell proliferation was altered after CDH11 knockdown at the premigratory stage, we injected and electorporated CDH11MO or ContMO unilaterally at HH4 and performed IHC for phosphorylated histone H3 (PH3), a marker of mitotic cells (**Figures 4N–U**). We determined that neither CDH11MO (**Figures 4N–Q**, $n = 20$, $p = 0.57$) nor ContMO (**Figures 4R–U**, $n = 8$, $p = 0.54$) significantly changed the number of PH3-positive cells suggesting that there is no consistent role for CDH11 in NC proliferation. These data demonstrate a requirement for CDH11 in NC cell survival.

Blocking p53-Mediated Apoptosis Rescues NC Cells

Previous studies have identified both SNAI2 and SOX9 as factors that prevent apoptosis in NC cells in *Xenopus* and chick embryos, respectively (Tribulo et al., 2004; Cheung et al., 2005). Further, increased p53 expression has been linked to reduction

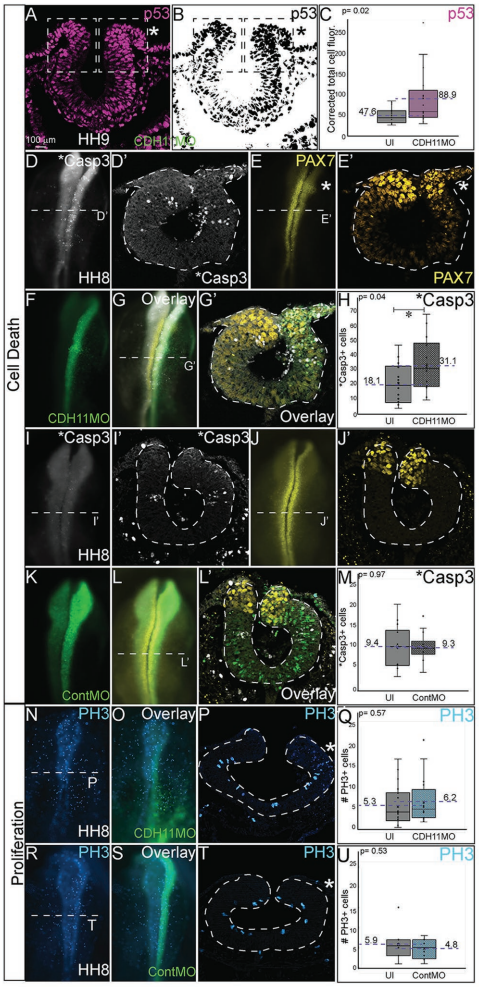

FIGURE 4 | Loss of CDH11 increases cell death. To determine the cause of reduced NC cell population after CDH11 knockdown, IHC was performed for **(A-C)** p53, **(D,D',G,G',I,I',L,L')** activated caspase 3 (*Casp3) to mark apoptotic cells, **(E,E',G,G',J,J',L,L')** PAX7, or **(N–U)** phosphorylated histone H3 (PH3) to mark mitotic cells. **(A,B)** IHC for p53 in transverse section. **(C)** Graph showing difference between fluorescence intensity on uninjected and CDH11MO-injected sides ($n = 17$, $p = 0.02$). **(D)** IHC for *Casp3 or **(E)** PAX7 in whole mount or for **(D')** *Casp3 or **(E')** PAX7 in transverse section, **(F)** CDH11MO in whole mount and **(G,G')** are overlays. **(H)** Graph showing increased number of *Casp3-positive cells on CDH11MO side. Mean number *Casp3+ apoptotic cells is 17.90 on uninjected and 31.86 on CDH11MO-injected side, $n = 14$, $p = 0.04$. **(I)** IHC for *Casp3 or **(J)** PAX7 in whole mount or for **(I')** *Casp3 or **(J')** PAX7 in transverse section, **(K)** ContMO in whole mount and **(L,L')** are overlays. **(M)** Graph showing difference between uninjected and ContMO-injected sides. Mean number of *Casp3+ apoptotic bodies is 9.36 on uninjected and 9.36 on ContMO-injected side, $p = 0.97$, $n = 14$. **(N)** IHC for PH3 in whole mount and **(O)** overlay with CDH11MO. **(P)** Transverse section from HH8 embryo injected with CDH11MO on right side (green). **(Q)** Graph showing difference between uninjected and CDH11MO-injected sides. Mean number of PH3+ cells is 6.20 on uninjected and 5.20 on CDH11MO-injected side, $p = 0.50$, $n = 20$. **(R)** IHC for PH3 in whole mount embryo injected with **(S)** ContMO. **(T)** Transverse section. **(U)** Graph showing difference between uninjected and ContMO-injected sides. Mean number of PH3+ cells is 5.88 on uninjected and 4.75 on ContMO-injected side, $p = 0.54$, $n = 8$. Loss of CDH11 increases cell death on injected side. All graphs show mean (indicated on graph) and median (line within graph). Scale bar whole mount images indicated in **(A)** and for sections in **(C)**. Asterisk indicates injected side in sections.

in SNAI2 protein expression and increased craniofacial defects in chick and mouse (Rinon et al., 2011). Due to the reduction in the expression of the NC specifier proteins and increased in p53 and *Casp3 expression after CDH11 knockdown, we hypothesized that blocking the p53-mediated apoptotic pathway would rescue the phenotype caused by reduction of CDH11. To confirm that the NC phenotype was specific to changes in CDH11 expression, we first compared embryos injected with CDH11MO alone to those co-injected with CDH11MO and full length CDH11-GFP rescue construct and performed IHC for PAX7 expression to examine NC development. As expected, whereas loss of CDH11 reduced PAX7-expressing cells at stages after HH8 significantly (**Figures 5A,K**, n = 18, p = 0.02), PAX7 expression was rescued by co-injection of CDH11-GFP (**Figures 5B,E,F,K**, n = 13, p = 0.15). We next co-injected CDH11MO with a p53 translation-blocking morpholino (p53MO) to rescue the loss of PAX7. Injection of p53MO alone had little effect on PAX7 expression (**Figure 5C**), but interestingly, co-injection of CDH11MO with p53MO was able to partially rescue the PAX7-positive cell population (**Figures 5D,G,H,K**, n = 16, p = 0.48). To confirm that the renewed PAX7 expression was caused by a reduction in CDH11-p53-mediated cell death, we verified the rescued phenotype by analyzing *Casp3 expression in CDH11MO and p53MO co-injected embryos (**Figures 5I,J,L**, n = 14, p = 0.04), injection of p53MO alone did not significantly change levels of *Casp3 in embryos (**Figure 5L**, n = 10, p = 0.71). However, blocking p53 was able to partially rescue the increased *Casp3 expression (**Figures 5I,J,L**, n = 12, p = 0.68). These data demonstrate that loss of CDH11 reduces NC cells due to increased p53-mediated cell death, and that blocking p53-mediated apoptosis can rescue the loss of NC cells.

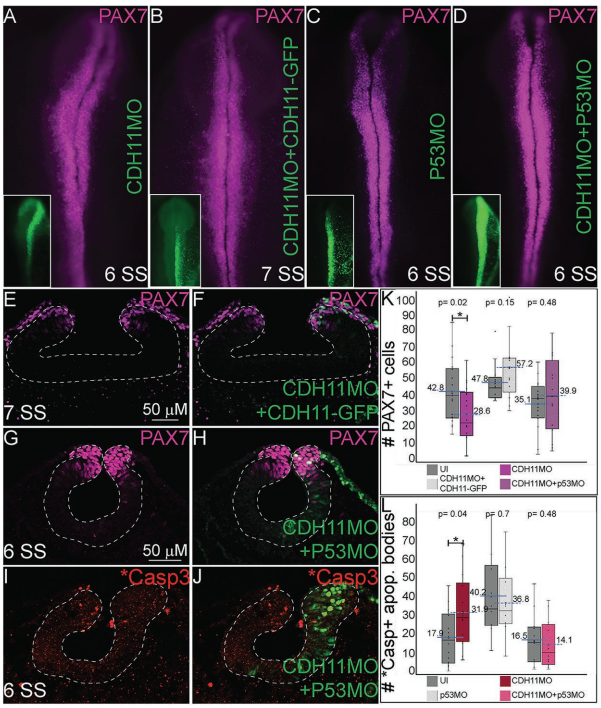

FIGURE 5 | Blocking p53-mediated apoptosis rescues the NC fate. To determine if the NC and *Casp3 phenotypes resulted from p53-mediated apoptosis, embryos were injected with multiple combinations of treatments to attempt to rescue the phenotype. **(A–D)** Whole mount IHC for PAX7 in HH8-HH9 embryos after **(A)** CDH11MO, **(B)** CDH11MO + CDH11-GFP, **(C)** p53MO, or **(D)** CDH11MO + p53MO. Inset shows treatment injection (green). **(E)** IHC for PAX7 in transverse section from HH9 embryo with **(F)** overlay with CDH11MO + CDH11-GFP (green). **(G)** IHC for PAX7 in transverse section from HH9 embryo with **(H)** overlay with CDH11MO + p53MO (green). **(I)** IHC for *Casp3 in transverse section from HH8 embryo with **(J)** overlay with CDH11MO + p53MO (green). **(K)** Graph showing difference in PAX7 expression between uninjected and injected sides. Mean number of PAX7+ cells is 42.8 on uninjected and 28.6 on CDH11MO-injected side, p = 0.02, n = 18. Mean number of PAX7+ cells is 47.77 on uninjected and 57.23 on CDH11MO + CDH11-GFP-injected side, p = 0.15, n = 13. Mean number of PAX7+ cells is 35.06 on uninjected and 39.94 on CDH11MO + p53MO-injected side, p = 0.48, n = 16. **(L)** Graph showing difference in *Casp3 expression between uninjected and injected sides. Mean number of *Casp3+ cells is 17.90 on uninjected and 31.86 on CDH11MO-injected side, p = 0.04, n = 14. Mean number of *Casp3 + cells is 40.20 on uninjected and 36.80 on CDH11MO + CDH11-GFP-injected side, p = 0.71, n = 10. Mean number of *Casp3 + cells is 16.50 on uninjected and 14.17 on CDH11MO + p53MO-injected side, p = 0.68, n = 12. All graphs show mean (indicated on graph) and median (line within graph). Phenotypes were rescued by co-injection with full length CDH11 as well as by blocking p53 translation suggesting that the NC phenotype is due to cell death after loss of CDH11. Scale bars for **(E,F)** are as marked in **(E)** and **(G-J)** are marked in **(G)**.

CDH11 Is Required for Normal NC Cell EMT, Morphology, and Migration

Finally, since cell adhesion molecules such as cadherins play a critical role in morphological changes during NC EMT and migration, we investigated how the NC cell features were affected by the early loss of CDH11 in the premigratory cells *in vivo*. To this end, we analyzed changes in the expression of E-cadherin/CDH1, a membrane-bound type I cadherin protein that has been linked to NC cell specification (Rogers et al., 2018) and to NC cell EMT and migration in both frog and chick embryos (Rogers et al., 2013; Huang et al., 2016). CDH11MO was unilaterally injected and electroporated at HH4, and cell morphology, CDH1 fluorescence intensity, and cell migration distance were measured in HH10 (10 SS) embryos. Loss of CDH1 enhanced CDH1 protein fluorescence in NC cells on the injected side (**Figures 6A–B'**, n = 11, p = 0.02), which resulted in defective migration while cells from the uninjected side had already migrated. We separately measured the distance from the midline that PAX7 and SOX9-positive cells traveled in CDH11MO-injected cells compared to uninjected sides because their expression differs in premigratory NC cell populations. CDH11MO-injected SOX9-positive cells migrated 31% less than the uninjected side (**Figures 6C–D',J**, n = 17, p = 0.026) and PAX7-positive cells migrated 43.8% less than the uninjected side (**Figure 6J**, n = 19, p = 0.029). Our results suggest that CDH11 is necessary for NC specification, survival, and EMT. As a result of the early phenotype, cell morphology and migration remain affected at migratory stages.

We also performed NC explant assays to better assess the morphology and migratory ability of the cells lacking CDH11 *ex vivo* to determine if the NC migration defects in embryos

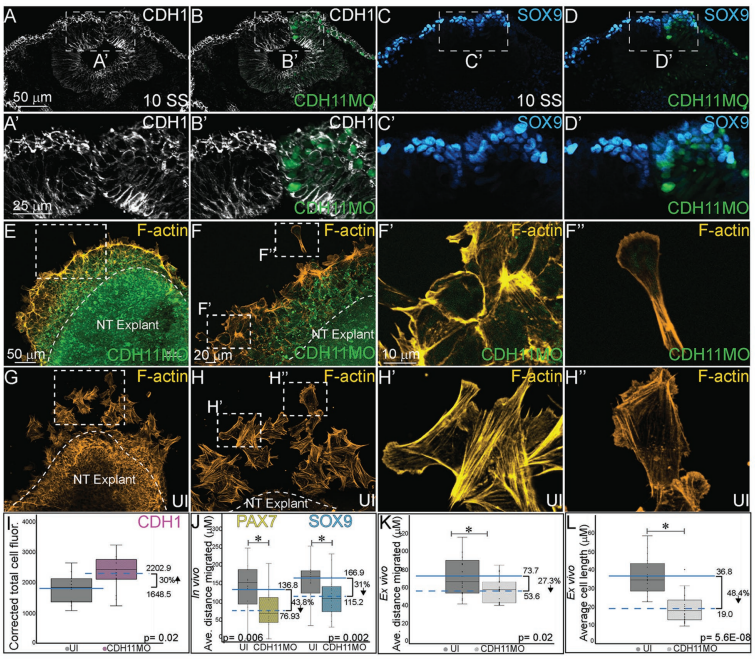

FIGURE 6 | CDH11 knockdown affects cell morphology and NC cell migration. To determine if the NC determination and cell death phenotype affects cell morphology *in vivo* **(A–D')** embryos were injected unilaterally with CDH11MO and electroporated at HH4, and IHC was performed for **(A–B')** CDH1 to mark epithelial cells and **(C–D')** SOX9 to mark definitive NC cells. Dashed boxes in **(A-D)** indicate location of zoom in from **(A'–D')**.To determine if the CDH11 knockdown phenotype affects cell morphology and migration *ex vivo* **(E–H")** neural tube explants were dissected from HH8 embryos, cultured on fibronectin coated slides, and stained for filamentous actin (F-actin). **(A)** IHC for CDH1 in transverse section from 10 SS embryo with **(B)** overlay with CDH11MO (green). **(A')** Zoom in of dashed box from **(A)** showing increased CDH1 expression in dorsal neural tube in CDH11MO-injected versus uninjected side. **(B')** Overlay with CDH11MO. **(C)** IHC for SOX9 in transverse section from the same 10 SS embryo from **(A)** with **(D)** overlay with CDH11MO (green) demonstrating reduced migration on CDH11-injected side. **(C',D')** Zoom in of dashed box from **(C,D)**. **(E-F")** Staining for F-actin in explant from embryo unilaterally injected with CDH11MO and electroporated at HH4, at **(E)** 20X and **(F)** 40X magnification. **(F')** Zoom in of single follower cell from CDH11MO-injected explant. **(F")** Zoom in of single leading cell from CDH11MO-injected explant. Both cells are significantly closer to epithelial explant and smaller than uninjected cells. **(G–H")** Staining for F-actin in explant from uninjected side at **(G)** 20X and **(H)** 40X magnification. **(H')** Zoom in of grouped follower cells from uninjected explant. **(H")** Zoom in of single leading cell from uninjected explant. **(I)** Graph showing *in vivo* difference in CDH1 between uninjected and CDH11MO-injected sides. Corrected mean total cell fluorescence of CDH1 in the dorsal neural tube is 1645.5 on uninjected and 2202.9 on CDH11MO-injected side, $p = 0.02$, $n = 11$. **(J)** Graph showing difference in migration *in vivo* from midline of PAX7 and SOX9-positive cells between uninjected and CDH11MO-injected sides. Average distance migrated away from midline by PAX7+ cells is 136.8 μm on uninjected and 76.93 μm on CDH11MO-injected side, $p = 0.006$, $n = 11$ cells. Average distance migrated away from midline by SOX9+ cells is 166.87 μm on uninjected and 115.22 μm on CDH11MO-injected side, $p = 0.002$, $n = 19$. **(K)** Graph showing average distance migrated *ex vivo* by cells from explant is 73.7 μm from uninjected explant and 53.6 μm from CDH11MO-injected explant, $p = 0.02$, $n = 17$ cells. **(L)** Graph showing average cell length is 36.8 μm in uninjected explants and 19.0 μm in CDH11MO-injected explants, $p = 5.6E-08$, $n = 23$ cells. Overall, loss of CDH11 significantly reduces NC cell population, affects their morphology, and reduces cell migration as a result. All graphs show mean (indicated on graph) and median (line within graph). Scale bars for **(A-D)** are as marked in **(A)**, **(A',B')** are marked in **(A')**, **(E,G)** are marked in **(E)**, **(F,H)** are marked in **(F)**, and **(F'–H")** are marked in **(F')**.

are due to intrinsic or extrinsic properties. Embryos were electroporated with CDH11MO at HH4 and neural tube explants were dissected from the embryos at HH8 (3 SS–6 SS), cultured for 8 h, and then stained for filamentous actin (F-actin). Explants were repeated in triplicate and both leading edge and follower cells were measured (distance and size) individually. Cells lacking CDH11 migrated away from the explant 27.3% less than uninjected cells (**Figures 6E–F",K**, $n = 17$, $p = 0.02$). The average migration distance from the epithelial explant by CDH11MO-injected cells was 53.6 μm while uninjected cells demonstrated a normal migratory ability, formed both lamellipodia and filopodia, and migrated approximately 73.7 μm from the explant (**Figures 6G–H",K**). Very few cells were physically able to detach from the collective group in CDH11MO-injected explants, and most remained strongly adherent to the epithelial explant (compare **Figures 6E,F'–G,H'**). In addition to exhibiting migration defects, cells lacking CDH11 were significantly smaller more rounded and lacked filopodia similar to *Xenopus* NC cells lacking CDH11 (Kashef et al., 2009; compare **Figures 6F',F"-H',H"**, $n = 23$ cells, $p = 5.6E-08$).

DISCUSSION

Defining the specific roles of cell adhesion proteins in early development is necessary as abnormal expression of these proteins is linked to cellular anomalies and congenital defects. With dynamic expression profiles, differential downstream signaling; and implications in cell survival, specification, and

migration, cadherin proteins are involved in multiple aspects of embryonic development. Here, we examined the localization and function of CDH11 protein in early avian NC cells. CDH11 is expressed in the neural tube prior to NC cell formation, is turned on in the NC cells at the premigratory stages, and is maintained in migratory NC cells. Loss of CDH11 reduced the number of specified cells (SNAI2, SOX9, SOX10-positive) that normally proceed to cell migration and reduced proteins that are crucial for NC cell survival (SNAI2, SOX9). Furthermore, loss of CDH11 increased levels of CDH1 in premigratory NC cells, which failed to migrate normally. In contrast to previous studies, loss of CDH11 had little effect on cell proliferation but increased p53 expression and p53-mediated cell death in the neural tube, which was either a result of losing SNAI2 and SOX9 or caused the reduction in those proteins. Inhibition of p53 in cells deficient for CDH11 partially rescued the loss of NC cells and the increase in *Casp3 (**Figure 7A**). Previous studies in frog embryos (Borchers et al., 2001; Kashef et al., 2009; Langhe et al., 2016) have reported that CDH11-deficient cells exhibit migratory and morphological defects. Our results shed light on the CDH11-mediated events in NC prior to migration and allows us to posit that at least some of the migratory defects may be secondarily caused by defects in cell specification and cell survival.

Critical Timing of CDH11 Function

NC cells are a dynamic population of cells controlled by multiple levels of secreted morphogens, transcription factors, epigenetic modifiers, and cell-cell adhesion molecules (Martik and Bronner, 2017). To understand the potential role of CDH11 in early development, we characterized the spatiotemporal expression and localization of the protein *in vivo* in stages earlier than those previously identified (Chalpe et al., 2010). Our data indicate that CDH11 protein is expressed in the neuroepithelium during neurulation and is specifically upregulated above its neuroepithelial levels in the *bonafide* NC cells (SOX9+, SNAI2+) prior to EMT (**Figure 1**). The bulk of previous work studying CDH11 function in NC cells focused on its necessity for normal NC cell migration including its post-translational processing (McCusker et al., 2009; Abbruzzese et al., 2016), the formation of focal adhesions, protrusive activity, and extracellular matrix dynamics (Kashef et al., 2009; Langhe et al., 2016; Row et al., 2016). Here, we focused on understanding the pre-migratory role of CDH11 in NC cell development. CDH11 is expressed at very low levels in the neural plate border cells during NC induction, and our results suggest that it is not necessary for NC induction (3 SS and earlier), but rather it is necessary for NC cell specification and survival (5 SS and later; **Figure 2**). In support of our results, previous studies in *Xenopus* embryos showed that both exogenous CDH11 and dominant negative CDH11 expression reduced the population of undifferentiated NC cells and inhibited NC cell migration without affecting neural plate specification (Borchers et al., 2001). Interestingly, the same study reported that NC cells gained neural cell identities in the presence of dominant negative CDH11, in line with our finding that CDH11 may be necessary for specification during premigratory stages. We believe that our results fill a gap in the previously reported phenotype. Loss of CDH11 reduces

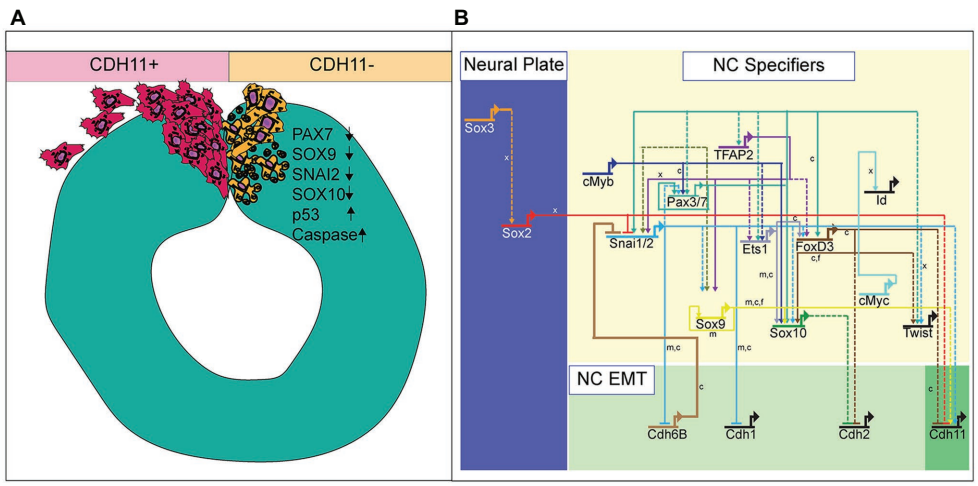

FIGURE 7 | Summary diagram of CDH11-knockdown phenotype. **(A)** Image depicting NC cell development in normal NC cells (CDH11+) and cells lacking CDH11 (CDH11-). Normal cells undergo EMT, exit the neural tube, migrate collectively, and then progressively mesenchymalize as development proceeds. Normal lamellipodial and filopodial projections form as the cells navigate through the extracellular matrix. In the absence of CDH11, NC cells are induced, but undergo p53-mediated apoptosis due to either (1) inability to complete EMT/migration or (2) altered intracellular signaling in the absence of CDH11. PAX7, SOX9, SNAI2, and SOX10 positive cells are all significantly reduced in the absence of CDH11 while p53 and *Casp3 are upregulated. **(B)** Simplified NC GRN identifying NC specifiers and multiple putative inputs into the CDH11 upstream regulatory region as identified by ATAC-seq performed on NC cells (Williams et al., 2019). Little is known about the downstream targets and effectors of most cadherin proteins in the NC GRN with the exception of CDH6B (Schiffmacher et al., 2016) and CDH11 in migratory NC cells (Kashef et al., 2009; Koehler et al., 2013), and therefore identifying their targets in premigratory NC cells is essential. Direct binding relationships are indicated with solid lines while putative regulatory relationships are indicated by dashed lines. Letters indicate species in which experiments were performed: *x* = *Xenopus*, *c* = chicken, *m* = mouse. GRN information sourced from Rogers and Nie (2018).

the definitive NC cell populations (**Figures 2, 3**) because without CDH11, these cells undergo p53-mediated cell death (**Figures 4, 5**). The timing of cell death occurs after induction but prior to NC cell EMT and migration. Our data suggest one of two possibilities; intracellular signaling downstream of CDH11 is necessary for the maintenance and survival of the premigratory NC cells, or that the cells require the presence of CDH11 for normal cell-cell adhesion-related EMT preparatory steps prior to migration, and without it they die. Future experiments are designed to test those hypotheses. Although CDH11 and other cadherins currently reside at the end of the NC GRN and are thought to function solely as regulators of NC EMT and migration downstream of NC specifiers, recent work that characterized all open enhancers in premigratory NC cells indeed identified putative binding sites in the CDH11 enhancer for SNAI2 and SOX9 (**Figure 7B**; Williams et al., 2019). Their enhancer analyses suggest that SNAI2 and SOX9 may drive CDH11 expression prior to EMT while FOXD3 and SOX2 may repress it. Future work will determine which of these factors functions upstream of CDH11 in the NC cells and whether the effects of CDH11 knockdown on cell specification and survival are direct (SOX9/SNAI2➔CDH11➔cell specification/survival) or indirect through changes in NC specifiers (CDH11➔SOX9/SNAI2➔cell specification/survival).

CDH11 and p53 Mediated Apoptosis

Our initial investigation into the role of CDH11 during early embryogenesis stemmed from its expression in developing NC cells and the varied accounts of its function in cancer cells. Previous studies in embryos demonstrated that CDH11 is necessary for NC migration (Vallin et al., 1998; Kashef et al., 2009; Abbruzzese et al., 2016; Langhe et al., 2016), but very few studies dissected its function in formation or survival *in vivo* (Borchers et al., 2001). Additionally, the role of CDH11 in cancer cells is variable. In murine retinoblastoma, CDH11 functions as a tumor suppressor, and overexpression of the gene in mouse models resulted in increased cell death (Marchong et al., 2010). This study relates to our data demonstrating that changes in CDH11 induces cell death or reduces NC cell survival; however, the mechanisms driving cell death downstream of gain and loss of CDH11 are likely unique in each situation. Both SLUG/SNAI2 (Tribulo et al., 2004) and SOX9 (Cheung et al., 2005) have demonstrated anti-apoptotic activity in NC cells, and their presence in the neural folds is correlated with reduced cell death. The previous studies paired with our data showing that loss of CDH11 reduces SOX9 and SNAI2 expression while concurrently increasing p53 expression (**Figures 3, 5**), suggests a link between CDH11 and the p53-mediated apoptotic pathway.

However, rather than driving cell death indirectly, it is possibly based on its requirement for CDH11 in NC migration. The loss of CDH11, whether through changes in cell-cell adhesion or intracellular signaling, drives cell death. Loss of CDH11 in the premigratory cells creates a defect in the mechanisms driving NC delamination and EMT. Western blot analysis using protein lysates from progressives stages of chicken embryos confirmed that chicken CDH11 undergoes processing and cleavage similar to *Xenopus* embryos (**Supplementary Figure S1A**), likely creating an extracellular fragment that would interact with the full length CDH11 to drive NC cell migration (McCusker et al., 2009). In our study, the NC cells have activated NC specifier proteins (SOX9, SNAI2, SOX10) and attempt to migrate, but cannot due to abnormal levels of CDH1 that prevent proper mesenchymalization (**Figure 6**; Rogers et al., 2013). Cells lacking CDH11 have increased F-actin cabling (**Figure 6**), which has previously been linked to the execution phase of cell death and is required for the formation of apoptotic bodies in embryonic carcinoma cells (Neradil et al., 2005). Additionally, actin-induced activation of the Ras signaling pathway has been previously linked to apoptosis (Gourlay and Ayscough, 2006). In contrast, overexpression of CDH11 may function to activate cell death *via* a Wnt-or Rho-dependent mechanism as previously described (Li et al., 2012; Row et al., 2016), and future experiments are designed to identify CDH11-specific apoptotic mechanisms.

Implications and Considerations for Disease Studies

Contrasting conclusions about the role of CDH11 in the disease state may be clarified if its function is assessed in the context of epithelial vs. mesenchymal cells. Loss of CDH11 prior to NC cell migration prevents the cells from leaving the neural tube efficiently, thereby activating the p53-mediated apoptotic pathway. The lack of specific expression in NC progenitors and generalized neural tube expression until just prior to the stage of migration suggests that CDH11 may play another role in the developing neuroepithelium. These data support a dual role for CDH11 during development. The upregulated expression of CDH11 in premigratory NC cells at 5 SS coincides with the wild type expression of SNAI2, SOX9, and SOX10, three proteins that are necessary for NC cell migration. It also coincides with the stage at which N-cadherin is reduced in the dorsal neural tube (Rogers et al., 2018). We believe that the functional type II cadherin complex is required for the completion of EMT and that loss of CDH11 leads to an increased tension on the cytoskeletal elements of the NC cells as evidenced by the increased CDH1 expression and F-actin localization causing activation of the p53-mediated apoptotic pathway. This hypothesis is supported by previous work demonstrating tightly controlled cadherin proteins in the NC EMT process (Coles et al., 2007; Rogers et al., 2013; Schiffmacher et al., 2014, 2016; Scarpa et al., 2015). In essence, the cells are programmed to migrate, but because they are unable, they are directed to die. As altering CDH11 affects cell survival, CDH11 may be functioning as it does in cancer cells, as pro-apoptotic stemness modulator that functions *via* the WNT and Rho pathways. Future experiments will focus on understanding the specific mechanisms downstream of CDH11 that regulate the NC cell population.

Possible Mechanisms Downstream of CDH11

In *Xenopus*, CDH11 controls filopodia and lamellipodia formation by binding to the guanine nucleotide exchange factor (GEF)

proteins. Overexpression of cdc42, Rac1, and RhoA in frog embryos lacking CDH11, rescues cranial NC cell migration (Kashef et al., 2009), and the GEF proteins specifically regulate NC cell protrusion and migration likely mediated by Rac1 (Kratzer et al., 2020). Therefore, loss of CDH11 may cause alterations in intracellular signaling and cytoskeletal rearrangements specifically linked to altered Rac/Rho signaling downstream of CDH11.

CDH11 also interacts with the proteoglycan, Syndecan-4, which maintains cell-substrate adhesion during cell migration. Loss of Syndecan-4 increased Rac activity, and inhibition of Rac1 by Syndecan-4 regulated the migration of NC cells (Matthews et al., 2008; Langhe et al., 2016). However, the non-canonical Wnt Planer Cell Polarity (PCP) Pathway promotes RhoA activity, which is necessary for NC cell migration, and inhibition of RhoA increased in Rac activation which can induce cell death (Matthews et al., 2008). It is possible that if the NC phenotype caused by loss of CDH11 is not directly related to cell-cell adhesion specific migration defects, rather, CDH11 may be a novel regulator that functions between Rac1 and RhoA, and loss of CDH11 may activate Rac1, preventing the cells from migrating and inducing apoptosis. Future studies will continue to investigate the mechanisms that cause a reduction in the NC cell population in CDH11-deficient cells, but it is clear from our studies and others that CDH11 plays a complex and important role in NC cell formation and survival prior to its role in migration.

Loss of CDH11 causes p53-mediated cell death and reduces the number of *bonafide* NC cells in addition to causing morphological and migratory defects both *in vivo* and *ex vivo*. Our analyses add new information to previous discoveries, demonstrating that CDH11 is not solely required for migration, but plays an important role prior to NC cell emigration from the neural tube.

MATERIALS AND METHODS

Chicken Embryos

Fertilized chicken eggs were obtained from local sources (Sunstate Ranch, CA and the UC Davis Hopkins Avian Facility) and incubated at 37°C to the desired stages according to the criteria of Hamburger and Hamilton (HH). Use and experiments on embryos was approved by the California State University Northridge IACUC protocol: 1516-012a, c and the UC Davis IACUC protocol #21448.

Microinjection and Electroporation

Translation blocking antisense fluorescein or biotin-labeled morpholinos to CDH11 (CDH11MO; 5'-TATTTTGTAGGCA CAGGAGTATCCA-3'), p53 (5'-CAATGGTTCCATCTCCTCC GCCATG-3') and a non-specific control morpholino (ContMO; 5'-CCTCTTACCTCAGTTACAATTTATA-3') were microinjected into the right side of a Hamburger-Hamilton stage 4–5 chicken embryo and platinum electrodes were placed vertically across the embryos and electroporated with five pulses of 6.3–6.8 V in 50 ms at 100 ms intervals. Injections of the morpholinos (0.5 mM^{-1} mM) were paired with 0.5–1.5 mg/ml of carrier plasmid DNA (Voiculescu et al., 2008) to enhance cell uptake of treatment. Injections were performed by air pressure using a glass micropipette targeted to the presumptive neural plate and neural plate border region. DNA plasmids pCAGGS-CDH11-IRES-GFP[1], Sirius-H2B-C-10 (injected as marker for CDH11MO) were a gift from Michael Davidson to Addgene (Addgene plasmid # 55226[2]; RRID:Addgene_55226) and were introduced in a similar manner to morpholinos described above. HH stage 4–5 electroporations were conducted on whole chick embryo explants placed ventral side up on filter paper rings.

Immunohistochemistry

Immunohistochemistry (IHC) was performed as described previously (Strobl-Mazzulla and Bronner, 2012; Rogers et al., 2013). Briefly, for IHC, chicken embryos were fixed on filter paper in 4% paraformaldehyde (PFA) in phosphate buffer for 15–25 min at room temperature. After fixation, embryos were washed in 1X TBS (500 mM Tris-HCl, pH 7.4, 1.5 M NaCl, and 10 mM $CaCl_2$) containing 0.1% Triton X-100 (TBST+ $Ca2^+$). Short fixation times and TBST+ $Ca2^+$ were used to enhance the IHC for cadherin proteins specifically. IHC using longer fixation or PBS + Triton without $Ca2^+$ resulted in much lower antigen signal. For blocking, embryos were incubated in TBST+ $Ca2^+$ and 10% donkey serum for 1 h at room temperature. Primary antibodies were diluted in blocking solution and incubated with embryos for 3 h at room temperature or for 24–48 h at 4°C. After incubation with primary antibodies, whole embryos were washed in TBST + Ca2+, incubated with AlexaFluor secondary antibodies diluted in blocking buffer (1,500) for 3 h at room temperature or 12–24 h at 4°C. They were then washed in TBST+ $Ca2^+$, and post-fixed in 4% PFA for 30 min^{-1} h at room temperature. Antibodies used in the study (**Table 1**): Rabbit α-Cadherin-11 (Cell Signaling Technologies, #4442), Mouse α-Cadherin-11 (Invitrogen, #5B2H5), Mouse α-E-cadherin (BD Transduction Laboratories, 61081), Rabbit α-Active Caspase-3 (R and D Systems, #AF835), Mouse α-PAX7 (DSHB), Rabbit α-SOX9 (EMD Millipore, #ab5535), Rabbit α-SOX2 (Abcam, #ab97959), Mouse α-SOX10 (Proteintech, #66786-1-Ig), Rabbit α-SLUG/SNAI2 (Cell Signaling Technology, #9585S), Mouse α-p53 (Millipore, CBL404), and Rabbit α-Phospho histone H3 (R7D Systems, #ab5176). After IHC all embryos were imaged in both whole mount and transverse section (after cryosectioning) using a Zeiss Imager M2 with Apotome capability and Zen optical processing software.

Western Blot

Embryo lysate was isolated from 10 to 20 manually dissected chicken embryos from stages HH4–6, HH8–10, and HH11–12 or tailbud stage axolotl embryos for Western blot analysis. Lysate was isolated using lysis buffer: 50 mM Tris-HCL pH

[1]VectorBuilder.com
[2]http://n2t.net/addgene:55226

TABLE 1 | Antibodies used in study.

Antibody	Dilution	SOURCE	IDENTIFIER
Mouse monoclonal anti-CDH11 (CDH11/Cadherin-OB) IgG1	1:250 IHC/1:10,000 WB	Invitrogen	5B2H5
Rabbit polyclonal anti-CDH11 (CDH11/OB Cadherin) IgG	1:200 IHC/1:10,000 WB	Cell Signaling Technologies	4442
Mouse anti-Pax7 IgG1	1:5	DSHB	PAX7
Mouse anti-HNK1 IgM	1:5	DSHB	3H5
Mouse anti-CDH1 IgG2a	1:500	BD Biosciences	610181
Rabbit anti-SOX2 IgG	1:250	Abcam	ab97959
Rabbit anti-SOX9	1:500	EMD Millipore	ab5535
Rabbit anti-SLUG (SNAI2)	1:250	Cell Signaling Technology	9585S
Mouse anti-SOX10 IgG2a	1:500	Proteintech	66786-1-Ig
Rabbit anti-Phospho histone H3	1:500	Abcam	ab5176
Mouse anti-p53	1:250	Millipore	CBL404
Rabbit anti-Active Caspase-3	1:500	R and D Systems	AF835

7.4 with 150 mM NaCl plus 1.0% NP-40 and EDTA-free protease inhibitor (Roche cOmplete, #11697498001). SDS page was run on precast 8–12% bis-tris gel (Invitrogen, #NP0321BOX) for 3 h at 60 V; gel was transferred to nitrocellulose using the Invitrogen iBlot2 Dry Blotting System. Nitrocellulose membranes were washed in TBST+ $Ca2^{+}$, blocked and incubated with primary antibody in TBST+ $Ca2^{+}$ with 5.0% milk or 5.0% BSA, were then incubated in (5%) milk protein in TBST+ $Ca2^{+}$ with secondary antibodies, and visualized using Prometheus ProSignal Femto ECL Reagent (#: 20-302B) and exposed to Prometheus ProSignal ECL Blotting Film, 5 × 7 in. (#: 30-507 L).

Imaging and Fluorescence Quantification

Fluorescence images were taken using Zeiss ImagerM2 with Apotome.2 and Zen software (Karl Zeiss). Fluorescence was quantified using NIH ImageJ by averaging the relative intensity of 1–6 images per embryo. Specifically, when multiple section images were available, intensity would be measured individually and then averaged over one individual. N's represent unique individuals. Background was subtracted uniformly across the images using the background subtraction function in NIH ImageJ with a rolling-ball radius of 50.00 pixels before quantitation (Hutchins and Szaro, 2013). For *Casp3, fluorescence was compared between half neural tubes while all other analyses compared fluorescence in the dorsal half of the neural tubes on the injected and uninjected sides. Half embryos injected with CDH11MO or ContMO were compared to the uninjected or control side.

Ex vivo Neural Tube Explants

For explant assays, embryos were electroporated with 0.75 mM CDH11MO plus Sirius carrier DNA on the right side of the embryo at HH4. Embryos were cultured until HH8 as described previously (Sauka-Spengler and Barembaum, 2008). At HH8, the neural tubes were dissected out of the embryo in Ringer's solution and subsequently placed in 8-well chamber slides (Millicell EZ SLIDE 8-well glass, sterile, # PEZGS0816) that were coated with 100 µg/ml fibronectin. The explants were cultured in DMEM with 10% FBS, 2 mM l-glutamine, and 100 units of penicillin with 0.1 mg/ml streptomycin at 37°C with 0.5% CO_2 for 8 h. After incubation, explants were fixed using 4% PFA, washed in TBST + Ca2+, and incubated with Phalloidin stain. Cytoskeletal stain was: Invitrogen Molecular Probes Alexa Fluor 568 Phalloidin (#A12380).

TUNEL Assay

For TUNEL assay, the Click-iT Plus TUNEL Alexa Fluor 488 and 647 were used. Protocol was as the manufacturer suggests. Briefly, embryos were fixed for 15 min in 4% PFA in phosphate buffer, washed in TBST + Ca2+, washed with deionized H2O, incubated with TdT reaction mix at 37°C, washed and incubated with Click-iT reaction for 30–60 min at room temperature.

Cell Counts and Statistical Analysis

All experiments were repeated three to four times. Cell counts and fluorescence intensity represented in box plots were either performed manually in Adobe Photoshop or were performed using NIH ImageJ. Cell counts were averaged from one to three sections per embryo. Mean, median, and standard deviation were calculated using Microsoft Excel across all biological replicates. The value of p was calculated in Microsoft excel using a Student's t-Test with a 2-tailed distribution with unequal variance between samples for stringency. p-values under 0.05 are considered statistically significant. All cell counts are availables in **Supplementary Tables 1–7**.

DATA AVAILABILITY STATEMENT

The original contributions presented in the study are included in the article/**Supplementary Material**, further inquiries can be directed to the corresponding author.

ETHICS STATEMENT

The animal study was reviewed and approved by California State University IACUC UC Davis IACUC.

AUTHOR CONTRIBUTIONS

Conceptualization: CR and AC-M. Data Curation: AC-M (functional experiments and imaging), SM (characterization, functional experiments, and imaging), CR (functional experiments, data analysis, and imaging), and CE (functional experiments and imaging). Formal Analysis (cell counts, statistics): AC-M,

SM, and CR. Funding Acquisition: CR (funds were provided either by NIH R15 HD092170-01 from the NICHD, CSUN startup funding, and UC Davis startup funding). Methodology: AC-M, SM, and CR. Supervision: CR. Writing: CR (wrote manuscript and performed editing), SM (wrote manuscript and performed editing), and AC-M (performed editing). All authors contributed to the article and approved the submitted version.

FUNDING

This research was supported in part by a National Institute of Health, NICHD grant to CR (R15HD092170-01) and startup funds from UC Davis.

ACKNOWLEDGMENTS

We thank our colleagues from the Rogers Lab at California State University Northridge in the Department of Biology and those at UC Davis in the Department of Anatomy, Physiology, and Cell Biology, who provided insight and expertise that greatly assisted the research.

SUPPLEMENTARY MATERIAL

The Supplementary Material for this article can be found online at: https://www.frontiersin.org/articles/10.3389/fphys.2020.563372/full#supplementary-material

REFERENCES

Abbruzzese, G., Becker, S. F., Kashef, J., and Alfandari, D. (2016). ADAM13 cleavage of cadherin-11 promotes CNC migration independently of the homophilic binding site. *Dev. Biol.* 415, 383–390. doi: 10.1016/j.ydbio.2015.07.018

Basch, M. L., Bronner-Fraser, M., and Garcia-Castro, M. I. (2006). Specification of the neural crest occurs during gastrulation and requires Pax7. *Nature* 441, 218–222. doi: 10.1038/nature04684

Bhattacharya, D., Rothstein, M., Azambuja, A. P., and Simoes-Costa, M. (2018). Control of neural crest multipotency by Wnt signaling and the Lin28/let-7 axis. *elife* 7:e40556. doi: 10.7554/eLife.40556

Borchers, A., David, R., and Wedlich, D. (2001). Xenopus cadherin-11 restrains cranial neural crest migration and influences neural crest specification. *Development* 128, 3049–3060.

Carmona, F. J., Villanueva, A., Vidal, A., Munoz, C., Puertas, S., Penin, R. M., et al. (2012). Epigenetic disruption of cadherin-11 in human cancer metastasis. *J. Pathol.* 228, 230–240. doi: 10.1002/path.4011

Chalpe, A. J., Prasad, M., Henke, A. J., and Paulson, A. F. (2010). Regulation of cadherin expression in the chicken neural crest by the Wnt/beta-catenin signaling pathway. *Cell Adhes. Migr.* 4, 431–438. doi: 10.4161/cam.4.3.12138

Chang, H. H., Moro, A., Takakura, K., Su, H. Y., Mo, A., Nakanishi, M., et al. (2017). Incidence of pancreatic cancer is dramatically increased by a high fat, high calorie diet in KrasG12D mice. *PLoS One* 12:e0184455. doi: 10.1371/journal.pone.0184455

Chen, P. F., Wang, F., Nie, J. Y., Feng, J. R., Liu, J., Zhou, R., et al. (2018). Co-expression network analysis identified CDH11 in association with progression and prognosis in gastric cancer. *Onco. Targets. Ther.* 11, 6425–6436. doi: 10.2147/OTT.S176511

Cheung, M., and Briscoe, J. (2003). Neural crest development is regulated by the transcription factor Sox9. *Development* 130, 5681–5693. doi: 10.1242/dev.00808

Cheung, M., Chaboissier, M. C., Mynett, A., Hirst, E., Schedl, A., and Briscoe, J. (2005). The transcriptional control of trunk neural crest induction, survival, and delamination. *Dev. Cell* 8, 179–192. doi: 10.1016/j.devcel.2004.12.010

Coles, E. G., Taneyhill, L. A., and Bronner-Fraser, M. (2007). A critical role for Cadherin6B in regulating avian neural crest emigration. *Dev. Biol.* 312, 533–544. doi: 10.1016/j.ydbio.2007.09.056

Dady, A., Blavet, C., and Duband, J. L. (2012). Timing and kinetics of E- to N-cadherin switch during neurulation in the avian embryo. *Dev. Dyn.* 241, 1333–1349. doi: 10.1002/dvdy.23813

Del Barrio, M. G., and Nieto, M. A. (2004). Relative expression of Slug, RhoB, and HNK-1 in the cranial neural crest of the early chicken embryo. *Dev. Dyn.* 229, 136–139. doi: 10.1002/dvdy.10456

Giger, F. A., and David, N. B. (2017). Endodermal germ-layer formation through active actin-driven migration triggered by N-cadherin. *Proc. Natl. Acad. Sci. U. S. A.* 114, 10143–10148. doi: 10.1073/pnas.1708116114

Gourlay, C. W., and Ayscough, K. R. (2006). Actin-induced hyperactivation of the Ras signaling pathway leads to apoptosis in *Saccharomyces cerevisiae*. *Mol. Cell. Biol.* 26, 6487–6501. doi: 10.1128/MCB.00117-06

Gul, I. S., Hulpiau, P., Saeys, Y., and van Roy, F. (2017). Evolution and diversity of cadherins and catenins. *Exp. Cell Res.* 358, 3–9. doi: 10.1016/j.yexcr.2017.03.001

Hadeball, B., Borchers, A., and Wedlich, D. (1998). Xenopus cadherin-11 (Xcadherin-11) expression requires the Wg/Wnt signal. *Mech. Dev.* 72, 101–113. doi: 10.1016/s0925-4773(98)00022-7

Harms, F. L., Nampoothiri, S., Anazi, S., Yesodharan, D., Alawi, M., Kutsche, K., et al. (2018). Elsahy-waters syndrome is caused by biallelic mutations in CDH11. *Am. J. Med. Genet. A* 176, 477–482. doi: 10.1002/ajmg.a.38568

Hoffmann, I., and Balling, R. (1995). Cloning and expression analysis of a novel mesodermally expressed cadherin. *Dev. Biol.* 169, 337–346. doi: 10.1006/dbio.1995.1148

Hu, N., Strobl-Mazzulla, P., Sauka-Spengler, T., and Bronner, M. E. (2012). DNA methyltransferase3A as a molecular switch mediating the neural tube-to-neural crest fate transition. *Genes Dev.* 26, 2380–2385. doi: 10.1101/gad.198747.112

Huang, C., Kratzer, M. C., Wedlich, D., and Kashef, J. (2016). E-cadherin is required for cranial neural crest migration in *Xenopus laevis*. *Dev. Biol.* 411, 159–171. doi: 10.1016/j.ydbio.2016.02.007

Hutchins, E. J., Kunttas, E., Piacentino, M. L., Howard, A. G. A. T., Bronner, M. E., and Uribe, R. A. (2018). Migration and diversification of the vagal neural crest. *Dev. Biol.* 444(Suppl. 1), S98–S109. doi: 10.1016/j.ydbio.2018.07.004

Hutchins, E. J., and Szaro, B. G. (2013). C-Jun N-terminal kinase phosphorylation of heterogeneous nuclear ribonucleoprotein K regulates vertebrate axon outgrowth via a posttranscriptional mechanism. *J. Neurosci.* 33, 14666–14680. doi: 10.1523/JNEUROSCI.4821-12.2013

Kashef, J., Kohler, A., Kuriyama, S., Alfandari, D., Mayor, R., and Wedlich, D. (2009). Cadherin-11 regulates protrusive activity in Xenopus cranial neural crest cells upstream of trio and the small GTPases. *Genes Dev.* 23, 1393–1398. doi: 10.1101/gad.519409

Kimura, Y., Matsunami, H., Inoue, T., Shimamura, K., Uchida, N., Ueno, T., et al. (1995). Cadherin-11 expressed in association with mesenchymal morphogenesis in the head, somite, and limb bud of early mouse embryos. *Dev. Biol.* 169, 347–358. doi: 10.1006/dbio.1995.1149

Kimura, Y., Matsunami, H., and Takeichi, M. (1996). Expression of cadherin-11 delineates boundaries, neuromeres, and nuclei in the developing mouse brain. *Dev. Dyn.* 206, 455–462. doi: 10.1002/(SICI)1097-0177(199608)206:4<455::AID-AJA11>3.0.CO;2-W

Koehler, A., Schlupf, J., Schneider, M., Kraft, B., Winter, C., and Kashef, J. (2013). Loss of Xenopus cadherin-11 leads to increased Wnt/beta-catenin signaling and up-regulation of target genes c-myc and cyclin D1 in neural crest. *Dev. Biol.* 383, 132–145. doi: 10.1016/j.ydbio.2013.08.007

Kratzer, M. C., Becker, S. F. S., Grund, A., Merks, A., Harnos, J., Bryja, V., et al. (2020). The Rho guanine nucleotide exchange factor Trio is required for neural crest cell migration and interacts with Dishevelled. *Development* 147:dev186338. doi: 10.1242/dev.186338

Langhe, R. P., Gudzenko, T., Bachmann, M., Becker, S. F., Gonnermann, C., Winter, C., et al. (2016). Cadherin-11 localizes to focal adhesions and promotes cell-substrate adhesion. *Nat. Commun.* 7:10909. doi: 10.1038/ncomms10909

Lee, Y. C., Bilen, M. A., Yu, G., Lin, S. C., Huang, C. F., Ortiz, A., et al. (2013). Inhibition of cell adhesion by a cadherin-11 antibody thwarts bone metastasis. *Mol. Cancer Res.* 11, 1401–1411. doi: 10.1158/1541-7786.MCR-13-0108

Li, L., Ying, J., Li, H., Zhang, Y., Shu, X., Fan, Y., et al. (2012). The human cadherin 11 is a pro-apoptotic tumor suppressor modulating cell stemness through Wnt/beta-catenin signaling and silenced in common carcinomas. *Oncogene* 31, 3901–3912. doi: 10.1038/onc.2011.541

Liu, Q., Marrs, J. A., Londraville, R. L., and Wilson, A. L. (2008). Cadherin-7 function in zebrafish development. *Cell Tissue Res.* 334, 37–45. doi: 10.1007/s00441-008-0664-y

Lopez, S. H., Avetisyan, M., Wright, C. M., Mesbah, K., Kelly, R. G., Moon, A. M., et al., (2018). Loss of Tbx3 in murine neural crest reduces enteric glia and causes cleft palate, but does not influence heart development or bowel transit. *Dev. Biol.* 444(Suppl. 1), S337–S351. doi: 10.1016/j.ydbio.2018.09.017

Marchong, M. N., Yurkowski, C., Ma, C., Spencer, C., Pajovic, S., and Gallie, B. L. (2010). Cdh11 acts as a tumor suppressor in a murine retinoblastoma model by facilitating tumor cell death. *PLoS Genet.* 6:e1000923. doi: 10.1371/journal.pgen.1000923

Martik, M. L., and Bronner, M. E. (2017). Regulatory logic underlying diversification of the neural crest. *Trends Genet.* 33, 715–727. doi: 10.1016/j.tig.2017.07.015

Mathavan, K., Khedgikar, V., Bartolo, V., and Alfandari, D. (2017). The ectodomain of cadherin-11 binds to erbB2 and stimulates Akt phosphorylation to promote cranial neural crest cell migration. *PLoS One* 12:e0188963. doi: 10.1371/journal.pone.0188963

Matthews, H. K., Marchant, L., Carmona-Fontaine, C., Kuriyama, S., Larrain, J., Holt, M. R., et al. (2008). Directional migration of neural crest cells in vivo is regulated by Syndecan-4/Rac1 and non-canonical Wnt signaling/RhoA. *Development* 135, 1771–1780. doi: 10.1242/dev.017350

McCusker, C., Cousin, H., Neuner, R., and Alfandari, D. (2009). Extracellular cleavage of cadherin-11 by ADAM metalloproteases is essential for Xenopus cranial neural crest cell migration. *Mol. Biol. Cell* 20, 78–89. doi: 10.1091/mbc.e08-05-0535

Miyamoto, Y., Sakane, F., and Hashimoto, K. (2015). N-cadherin-based adherens junction regulates the maintenance, proliferation, and differentiation of neural progenitor cells during development. *Cell Adhes. Migr.* 9, 183–192. doi: 10.1080/19336918.2015.1005466

Neradil, J., Veselska, R., and Svoboda, A. (2005). The role of actin in the apoptotic cell death of P19 embryonal carcinoma cells. *Int. J. Oncol.* 27, 1013–1021.

Piao, S., Inglehart, R. C., Scanlon, C. S., Russo, N., Banerjee, R., and D'Silva, N. J. (2016). CDH11 inhibits proliferation and invasion in head and neck cancer. *J. Oral Pathol. Med.* 46, 89–97. doi: 10.1111/jop.12471

Piloto, S., and Schilling, T. F. (2010). Ovo1 links Wnt signaling with N-cadherin localization during neural crest migration. *Development* 137, 1981–1990. doi: 10.1242/dev.048439

Plouhinec, J. L., Roche, D. D., Pegoraro, C., Figueiredo, A. L., Maczkowiak, F., Brunet, L. J., et al. (2014). Pax3 and Zic1 trigger the early neural crest gene regulatory network by the direct activation of multiple key neural crest specifiers. *Dev. Biol.* 386, 461–472. doi: 10.1016/j.ydbio.2013.12.010

Reissmann, M., and Ludwig, A. (2013). Pleiotropic effects of coat colour-associated mutations in humans, mice and other mammals. *Semin. Cell Dev. Biol.* 24, 576–586. doi: 10.1016/j.semcdb.2013.03.014

Rinon, A., Molchadsky, A., Nathan, E., Yovel, G., Rotter, V., Sarig, R., et al. (2011). p53 coordinates cranial neural crest cell growth and epithelial-mesenchymal transition/delamination processes. *Development* 138, 1827–1838. doi: 10.1242/dev.053645

Rogers, C. D., and Nie, S. (2018). Specifying neural crest cells: from chromatin to morphogens and factors in between. *Wiley Interdiscip. Rev. Dev. Biol.* 7:e322. doi: 10.1002/wdev.322

Rogers, C. D., Saxena, A., and Bronner, M. E. (2013). Sip1 mediates an E-cadherin-to-N-cadherin switch during cranial neural crest EMT. *J. Cell Biol.* 203, 835–847. doi: 10.1083/jcb.201305050

Rogers, C. D., Sorrells, L. K., and Bronner, M. E. (2018). A catenin-dependent balance between N-cadherin and E-cadherin controls neuroectodermal cell fate choices. *Mech. Dev.* 152, 44–56. doi: 10.1016/j.mod.2018.07.003

Row, S., Liu, Y., Alimperti, S., Agarwal, S. K., and Andreadis, S. T. (2016). Cadherin-11 is a novel regulator of extracellular matrix synthesis and tissue mechanics. *J. Cell Sci.* 129, 2950–2961. doi: 10.1242/jcs.183772

Satriyo, P. B., Bamodu, O. A., Chen, J. H., Aryandono, T., Haryana, S. M., Yeh, C. T., et al. (2019). Cadherin 11 inhibition downregulates beta-catenin, deactivates the canonical WNT Signalling pathway and suppresses the cancer stem cell-like phenotype of triple negative breast cancer. *J. Clin. Med.* 8:148. doi: 10.3390/jcm8020148

Sauka-Spengler, T., and Barembaum, M. (2008). Gain- and loss-of-function approaches in the chick embryo. *Methods Cell Biol.* 87, 237–256. doi: 10.1016/S0091-679X(08)00212-4

Scarpa, E., Szabo, A., Bibonne, A., Theveneau, E., Parsons, M., and Mayor, R. (2015). Cadherin switch during EMT in neural crest cells leads to contact inhibition of locomotion via repolarization of forces. *Dev. Cell* 34, 421–434. doi: 10.1016/j.devcel.2015.06.012

Schiffmacher, A. T., Padmanabhan, R., Jhingory, S., and Taneyhill, L. A. (2014). Cadherin-6B is proteolytically processed during epithelial-to-mesenchymal transitions of the cranial neural crest. *Mol. Biol. Cell* 25, 41–54. doi: 10.1091/mbc.E13-08-0459

Schiffmacher, A. T., Xie, V., and Taneyhill, L. A. (2016). Cadherin-6B proteolysis promotes the neural crest cell epithelial-to-mesenchymal transition through transcriptional regulation. *J. Cell Biol.* 215, 735–747. doi: 10.1083/jcb.201604006

Simoes-Costa, M., Stone, M., and Bronner, M. E. (2015). Axud1 integrates Wnt signaling and transcriptional inputs to drive neural crest formation. *Dev. Cell* 34, 544–554. doi: 10.1016/j.devcel.2015.06.024

Strobl-Mazzulla, P. H., and Bronner, M. E. (2012). A PHD12-Snail2 repressive complex epigenetically mediates neural crest epithelial-to-mesenchymal transition. *J. Cell Biol.* 198, 999–1010. doi: 10.1083/jcb.201203098

Taneyhill, L. A., Coles, E. G., and Bronner-Fraser, M. (2007). Snail2 directly represses cadherin6B during epithelial-to-mesenchymal transitions of the neural crest. *Development* 134, 1481–1490. doi: 10.1242/dev.02834

Taneyhill, L. A., and Schiffmacher, A. T. (2017). Should I stay or should I go? Cadherin function and regulation in the neural crest. *Genesis* 55:dvg.23028. doi: 10.1002/dvg.23028

Tien, C. L., Jones, A., Wang, H., Gerigk, M., Nozell, S., and Chang, C. (2015). Snail2/Slug cooperates with Polycomb repressive complex 2 (PRC2) to regulate neural crest development. *Development* 142, 722–731. doi: 10.1242/dev.111997

Tribulo, C., Aybar, M. J., Sanchez, S. S., and Mayor, R. (2004). A balance between the anti-apoptotic activity of Slug and the apoptotic activity of msx1 is required for the proper development of the neural crest. *Dev. Biol.* 275, 325–342. doi: 10.1016/j.ydbio.2004.07.041

Vallin, J., Girault, J. M., Thiery, J. P., and Broders, F. (1998). Xenopus cadherin-11 is expressed in different populations of migrating neural crest cells. *Mech. Dev.* 75, 171–174. doi: 10.1016/s0925-4773(98)00099-9

Voiculescu, O., Papanayotou, C., and Stern, C. D. (2008). Spatially and temporally controlled electroporation of early chick embryos. *Nat. Protoc.* 3, 419–426. doi: 10.1038/nprot.2008.10

Williams, R. M., Candido-Ferreira, I., Repapi, E., Gavriouchkina, D., Senanayake, U., Ling, I. T. C., et al. (2019). Reconstruction of the global neural crest gene regulatory network in vivo. *Dev. Cell* 51, 255–276e7. doi: 10.1016/j.devcel.2019.10.003

Yoshioka, R., Kita, Y., Nagahira, A., Manno, A., Makita, N., Tomita, U., et al. (2015). Quantitative analysis of cadherin-11 and beta-catenin signalling during proliferation of rheumatoid arthritis-derived synovial fibroblast cells. *J. Pharm. Pharmacol.* 67, 1075–1082. doi: 10.1111/jphp.12410

Zou, H., Li, Y., Liu, X., and Wang, X. (1999). An APAF-1.Cytochrome *c* multimeric complex is a functional apoptosome that activates procaspase-9. *J. Biol. Chem.* 274, 11549–11556. doi: 10.1074/jbc.274.17.11549

Conflict of Interest: The authors declare that the research was conducted in the absence of any commercial or financial relationships that could be construed as a potential conflict of interest.

frontiers in Physiology

ORIGINAL RESEARCH
published: 02 November 2020
doi: 10.3389/fphys.2020.588901

Pdgfra and *Pdgfrb* Genetically Interact in the Murine Neural Crest Cell Lineage to Regulate Migration and Proliferation

*Julia Mo, Robert Long and Katherine A. Fantauzzo**

Department of Craniofacial Biology, School of Dental Medicine, University of Colorado Anschutz Medical Campus, Aurora, CO, United States

Cranial neural crest cells (cNCCs) are migratory, multipotent cells that originate from the forebrain to the hindbrain and eventually give rise to the cartilage and bone of the frontonasal skeleton, among other derivatives. Signaling through the two members of the platelet-derived growth factor receptor (PDGFR) family of receptor tyrosine kinases, alpha and beta, plays critical roles in the cNCC lineage to regulate craniofacial development during murine embryogenesis. Further, the PDGFRs have been shown to genetically interact during murine craniofacial development at mid-to-late gestation. Here, we examined the effect of ablating both *Pdgfra* and *Pdgfrb* in the murine NCC lineage on earlier craniofacial development and determined the cellular mechanisms by which the observed phenotypes arose. Our results confirm a genetic interaction between the two receptors in this lineage, as phenotypes observed in an allelic series of mutant embryos often worsened with the addition of conditional alleles. The defects observed here appear to stem from aberrant cNCC migration, as well as decreased proliferation of the facial mesenchyme upon combined decreases in PDGFRα and PDGFRβ signaling. Importantly, we found that PDGFRα plays a predominant role in cNCC migration whereas PDGFRβ primarily contributes to proliferation of the facial mesenchyme past mid-gestation. Our findings provide insight into the distinct mechanisms by which PDGFRα and PDGFRβ signaling regulate cNCC activity and subsequent craniofacial development in the mouse embryo.

Keywords: Pdgfra, Pdgfrb, neural crest, craniofacial, migration, proliferation

OPEN ACCESS

Edited by:
Lisa Taneyhill, University of Maryland, United States

Reviewed by:
Rulang Jiang, Cincinnati Children's Research Foundation, United States
Patrick Blader, FR3743 Centre de Biologie Intégrative (CBI), France

****Correspondence:***
Katherine A. Fantauzzo
katherine.fantauzzo@cuanschutz.edu

Specialty section:
This article was submitted to Craniofacial Biology and Dental Research, a section of the journal Frontiers in Physiology

Received: *29 July 2020*
Accepted: *06 October 2020*
Published: *02 November 2020*

Citation:
Mo J, Long R and Fantauzzo KA (2020) Pdgfra and Pdgfrb Genetically Interact in the Murine Neural Crest Cell Lineage to Regulate Migration and Proliferation. Front. Physiol. 11:588901. doi: 10.3389/fphys.2020.588901

INTRODUCTION

The various populations of neural crest cells (NCCs) within the vertebrate embryo play critical roles in development and contribute to a wide array of derivatives. In mammals, these cells originate at the neural ectoderm border and undergo an epithelial-to-mesenchymal transition before delaminating from the cranial neural folds or dorsal neural tube. Cranial NCCs (cNCCs) are a subpopulation of NCCs that arise from the forebrain to the hindbrain and eventually contribute to the cartilage and bone of the frontonasal skeleton, as well as the cartilages of the jaw, middle ear, hyoid, and thyroid, among other derivatives (Trainor, 2005; Mayor and Theveneau, 2013). Craniofacial development in the mouse begins around embryonic day (E)

9.5 with the formation of five facial prominences populated by post-migratory cNCCs. These prominences include the frontonasal prominence and pairs of maxillary prominences (MxPs) and mandibular prominences (MdPs). The frontonasal prominence is divided into the lateral and medial nasal processes (MNPs) upon formation of the nasal pits. These nasal processes will eventually fuse to form the nostrils. An additional fusion event occurs between the MNPs and the MxPs resulting in formation of the upper lip. Concurrently, the secondary palatal shelves appear as outgrowths from the oral surface of the MxPs. The shelves grow downward from the MxPs and subsequently elevate to a horizontal position above the tongue. The palatal shelves grow toward one another and eventually fuse, generating a continuous palate that divides the nasal and oral cavities (Bush and Jiang, 2012). The complex morphogenetic process of craniofacial development requires a precise interplay of multiple cell and tissue types. As such, craniofacial development defects, such as cleft lip and palate, are among the most common birth defects in humans (Parker et al., 2010).

Signaling through the platelet-derived growth factor receptor (PDGFR) family of receptor tyrosine kinases plays a critical role in human craniofacial development. In mammals, there are four PDGF ligands, PDGF-A-D, which interact with two receptors, PDGFRα and PDGFRβ. The homodimers PDGF-AA and PDGF-CC solely activate PDGFRα signaling during mammalian development (Boström et al., 1996; Soriano, 1997; Ding et al., 2004), while the homodimer PDGF-BB exclusively activates PDGFRβ signaling (Levéen et al., 1994; Soriano, 1994). Ligand binding induces PDGFR dimerization and activation of tyrosine kinase domains in the cytoplasmic portion of the receptors. These domains in turn autophosphorylate cytoplasmic tyrosine residues, which are then bound by signaling molecules to activate various intracellular signaling pathways and effect downstream cellular responses (Heldin and Westermark, 1999). In humans, nonsyndromic cleft palate is associated with heterozygous missense mutations in the coding region of *PDGFRA* and single base-pair substitutions in the 3' untranslated region (Rattanasopha et al., 2012). Further, cleft lip and palate are associated with single-nucleotide polymorphisms in the regulatory region of *PDGFC* which reduce transcriptional activity of the promoter (Choi et al., 2009). Alternatively, heterozygous missense mutations in *PDGFRB* have been shown to cause Kosaki overgrowth syndrome (OMIM 616592) and Penttinen syndrome (OMIM 601812), the clinical features of which include facial dysmorphology (Johnston et al., 2015; Takenouchi et al., 2015).

The roles of PDGFRα and PDGFRβ in human craniofacial development are evolutionarily conserved in the mouse. *Pdgfra*-null mouse embryos die at mid-gestation and display facial clefting, subepidermal blebbing, hemorrhaging, edema, defects in the cardiac outflow tract, abnormal neural tube development, mispatterned somites, and extensive skeletal defects affecting cNCC derivatives in the frontonasal skeleton and non-NCC-derived axial skeletal elements (Soriano, 1997). Embryos lacking both *Pdgfa* and *Pdgfc* phenocopy the defects in *Pdgfra*-null embryos (Ding et al., 2004). *Pdgfra* is expressed in migrating cNCCs and in the cNCC-derived facial process mesenchyme during mid-gestation, among other sites, while the ligands *Pdgfa* and *Pdgfc* are expressed in the adjacent epithelium (Morrison-Graham et al., 1992; Orr-Urtreger and Lonai, 1992; Ding et al., 2000; Hamilton et al., 2003; He and Soriano, 2013; Fantauzzo and Soriano, 2016). Embryos in which *Pdgfra* has been conditionally ablated in the NCC lineage using the *Wnt1-Cre* driver (Danielian et al., 1998) exhibit a subset of the phenotypes found in null embryos, such as facial clefting, midline hemorrhaging, defects in the aortic arch, and thymus hypoplasia (Tallquist and Soriano, 2003; He and Soriano, 2013). These $Pdgfra^{fl/fl}$;$Wnt1\text{-}Cre^{+/Tg}$ embryos display delayed NCC migration into the frontonasal prominence at E9.5 and fewer NCCs in pharyngeal arches 3–6 at E10.5, with bifurcation of the streams entering these arches in a subset of embryos (He and Soriano, 2013). Additionally, these embryos have decreased proliferation in the frontonasal and medial nasal processes at E9.5 and E11.5, respectively (He and Soriano, 2013). Similarly, PDGFRα signaling regulates cell survival and proliferation of the cNCC-derived mesenchyme of the secondary palatal shelves at E13.5 (Fantauzzo and Soriano, 2014). Conditional ablation of *Pdgfra* specifically in cNCCs using the $Sox10ER^{T2}CreER^{T2}$ driver and following administration of tamoxifen at E7.5 likewise leads to fewer NCCs in the craniofacial region at E10.5, decreased proliferation in the MNP at E11.5, and eventual frontonasal dysplasia (He and Soriano, 2015). Interestingly, use of this driver revealed a novel requirement for PDGFRα in the mandible, as $Pdgfra^{fl/fl}$; $Sox10ER^{T2}CreER^{T2}$ embryos additionally exhibited decreased proliferation in the mandibular mesenchyme at E11.5 and mandibular hypoplasia at E16.5 (He and Soriano, 2015). Conversely, *Pdgfrb*- and *Pdgfb*-null mice die near birth and display hemorrhaging, edema, defects in the cardiac ventricular septum, kidney defects, thrombocytopenia, and anemia (Levéen et al., 1994; Soriano, 1994). *Pdgfrb*, like *Pdgfra*, is expressed in the craniofacial mesenchyme during embryogenesis (Soriano, 1994; Fantauzzo and Soriano, 2016; McCarthy et al., 2016) and conditional ablation of *Pdgfrb* in the NCC lineage results in a wider nasal septum (NS), delayed palatal shelf development, and facial subepidermal blebbing in a subset of embryos (Fantauzzo and Soriano, 2016). Though the etiology of these defects is currently unknown, $Pdgfrb^{fl/fl}$;$Wnt1\text{-}Cre^{+/Tg}$ embryos do not have obvious defects in cNCC migration at E8.5–E10.5 (Fantauzzo and Soriano, 2016).

The PDGFRs have been shown to genetically interact during murine craniofacial and heart development. A previous report analyzing the effect of simultaneously conditionally ablating *Pdgfra* and *Pdgfrb* in the NCC lineage observed that skeletal preparations of these double-homozygous mutant embryos did not have more severe frontonasal midline defects than those found in $Pdgfra^{fl/fl}$;$Wnt1\text{-}Cre^{+/Tg}$ embryos (McCarthy et al., 2016). However, malformations in bones at other locations at E17.5, including the basisphenoid, alisphenoid, and hyoid bones, as well as defects in various cardiac NCC derivatives at E14.5–E18.5, were observed that were more severe than those found in either *Pdgfra* or *Pdgfrb* single-homozygous mutant embryos (Richarte et al., 2007; McCarthy et al., 2016). The latter phenotype was shown to arise from cardiac NCC migration defects into the outflow tract as early as E10.5 and not from defects in proliferation nor survival of cells in the conotruncal

region between E10.5 and E12.5 (Richarte et al., 2007). Phosphatidylinositol 3-kinase (PI3K) has been identified as the main downstream effector of PDGFRα signaling during embryonic development in the mouse (Klinghoffer et al., 2002). Embryos homozygous for a constitutive autophosphorylation mutant knock-in allele (*Pdgfra*^{PI3K}) that renders PDGFRα unable to bind PI3K exhibit a cleft palate and die perinatally, among other defects (Klinghoffer et al., 2002; Fantauzzo and Soriano, 2014). This palatal clefting is less severe than the overt facial clefting phenotype found in *Pdgfra*-null and *Pdgfra*$^{fl/fl}$;*Wnt1-Cre*$^{+/Tg}$ embryos (Soriano, 1997; Tallquist and Soriano, 2003; He and Soriano, 2013). While *Pdgfra*$^{PI3K/PI3K}$ embryos do not exhibit NCC migration defects at E9.5–E10.5 (He and Soriano, 2013), primary mouse embryonic palatal mesenchyme (MEPM) cells derived from E13.5 *Pdgfra*$^{PI3K/PI3K}$ embryos fail to proliferate in response to PDGF-AA ligand treatment (He and Soriano, 2013; Fantauzzo and Soriano, 2014). When the *Pdgfra*^{PI3K} allele was combined with the *Pdgfrb*^{fl} allele and the *Wnt1-Cre* driver, E13.5 double-homozygous mutant embryos had a complete facial clefting phenotype not observed in either single-homozygous mutant (Fantauzzo and Soriano, 2016). Further, addition of a single *Pdgfrb*^{fl} allele worsened the midline defects found in *Pdgfra*$^{PI3K/PI3K}$ skeletons at E16.5; *Pdgfra*$^{PI3K/PI3K}$;*Pdgfrb*$^{+/fl}$; *Wnt1-Cre*$^{+/Tg}$ skeletons further exhibited nasal cartilage that was clefted and upturned, a widening of the space between the premaxilla bones and a broader skull (Fantauzzo and Soriano, 2016), similar to the frontonasal defects observed in *Pdgfra*$^{fl/fl}$; *Wnt1-Cre*$^{+/Tg}$ embryos (Tallquist and Soriano, 2003; He and Soriano, 2013). Importantly, however, it could not be determined from this study whether the double-homozygous mutant phenotypes observed past mid-gestation were more severe than those exhibited by single-homozygous mutant embryos because of cell-autonomous or non-cell-autonomous effects on the NCC lineage.

To examine the effect of ablating both *Pdgfra* and *Pdgfrb* in the murine NCC lineage on earlier craniofacial development and to determine the cellular mechanisms by which the observed phenotypes arise, we analyzed an allelic series of mutant embryos. Our results confirm a genetic interaction between the two receptors in this lineage and demonstrate that PDGFRα plays a predominant role in cNCC migration whereas PDGFRβ exerts its effect primarily through the regulation of proliferation in the facial mesenchyme past mid-gestation.

MATERIALS AND METHODS

Mouse Strains

All animal experimentation was approved by the Institutional Animal Care and Use Committee of the University of Colorado Anschutz Medical Campus. *Pdgfra*^{tm8Sor} mice (Tallquist and Soriano, 2003), referred to in the text as *Pdgfra*^{fl}; *Pdgfrb*^{tm11Sor} mice (Schmahl et al., 2008), referred to in the text as *Pdgfrb*^{fl}; *H2afv*$^{Tg(Wnt1-cre)11Rth}$ mice (Danielian et al., 1998), referred to in the text as *Wnt1-Cre*^{Tg}; and *Gt(ROSA)26Sor*$^{tm4(ACTB-tdTomato,-EGFP)Luo}$ mice (Muzumdar et al., 2007), referred to in the text as *ROSA26*^{mTmG}, were maintained on a 129S4 coisogenic genetic background. Statistical analyses of Mendelian inheritance were performed with the GraphPad QuickCalcs data analysis resource (GraphPad Software, Inc., La Jolla, CA, United States) using a χ^2 test. Statistical analyses of litter sizes were performed with Prism 8 (GraphPad Software, Inc.) using a two-tailed, unpaired *t*-test with Welch's correction.

Morphological Analysis

Embryos were dissected at multiple timepoints (day of plug considered 0.5 days) in 1x phosphate buffered saline (PBS) and fixed overnight at 4°C in 4% paraformaldehyde (PFA) in PBS. Embryos were photographed using an Axiocam 105 color digital camera (Carl Zeiss, Inc., Thornwood, NY, United States) fitted onto a Stemi 508 stereo microscope (Carl Zeiss, Inc.). Distances between nasal pits and heights of heads were measured using Photoshop software v 21.1.1 (Adobe, San Jose, CA, United States). The normalized distance between nasal pits was calculated by dividing the distance between nasal pits by the height of the head from the anterior surface of the forebrain to the posterior surface of pharyngeal arch 1. Statistical analyses were performed on all embryos represented in graphs, regardless of somite pair number, with Prism 8 (GraphPad Software, Inc.) using a two-tailed, unpaired *t*-test with Welch's correction and Welch and Brown-Forsythe ANOVA tests.

Whole-Mount DAPI Staining

Whole-mount 4',6-diamidino-2-phenylindole (DAPI) staining was performed according to a previously published protocol (Sandell et al., 2012), except that staining was performed with 10 μg/ml DAPI (Sigma-Aldrich Corp., St. Louis, MO, United States) for 1 h at room temperature. Embryos were photographed using an Axiocam 506 mono digital camera (Carl Zeiss, Inc.) fitted onto an Axio Observer 7 fluorescence microscope (Carl Zeiss, Inc.). For lateral views of NCC streams, embryos were positioned on their sides at identical angles in glass-bottom dishes. Images were acquired and analyzed from both sides of each embryo using identical lamp intensities and exposure times. Extended depth of focus was applied to z-stacks using ZEN Blue software (Carl Zeiss, Inc.) to generate images with the maximum depth of field. Anterior-posterior heights and dorsal-ventral lengths of NCC streams in at least three embryos per genotype per timepoint were measured using ZEN Blue software (Carl Zeiss, Inc.). NCC stream height was measured at the tallest part of the middle of the stream. NCC stream length was measured from the dorsal-most edge of the NCC stream where cell condensation was apparent to the dorsal border of each pharyngeal arch, as determined by pharyngeal pouch morphology. The normalized distance of NCC streams was calculated by dividing the stream height or length by the height of the head from the crown to the posterior surface of pharyngeal arch 1. NCC stream bifurcations were assessed per stream and defined as errant holes and/or forking in the stream. NCC stream intermingling was assessed between streams entering pharyngeal arches 1–2 and between streams entering pharyngeal arches 3–4, and defined as two streams joining abnormally as compared to streams in control embryos.

An Unsharp Mask was applied to select images of NCC streams at E10.5 using ImageJ software (version 2.0.0-rc-69/1.52p; National Institutes of Health) with radius 40 pixels and mask weight 0.90. For quantification of green fluorescent protein (GFP) intensity in the facial processes, embryos were positioned face-down at identical angles in 0.5% agarose-filled polystyrene dishes. Images were acquired using identical lamp intensities and exposure times. Extended depth of focus was applied to z-stacks using ZEN Blue software (Carl Zeiss, Inc.) to generate images with the maximum depth of field. GFP signal was measured in frontal views of at least three embryos per genotype per timepoint using ImageJ software (version 2.0.0-rc-69/1.52p; National Institutes of Health). For each embryo, the entire head was selected as the region of interest (ROI) to be measured. Values for integrated density for each ROI were recorded and normalized to the mean background value. For each embryo, the mean gray value for each of three separate regions surrounding but apart from the embryo were measured and averaged to obtain the mean background value. Relative fluorescence units were calculated using the following formula: corrected total fluorescence = integrated density – (ROI area × mean background). Statistical analyses were performed on all embryos represented in graphs, regardless of somite pair number, with Prism 8 (GraphPad Software, Inc.) using a two-tailed, unpaired *t*-test with Welch's correction and Welch and Brown-Forsythe ANOVA tests.

TUNEL Assay

Embryos were fixed in 4% PFA in PBS and infiltrated with 30% sucrose in PBS before being mounted in O.C.T. compound (Sakura Finetek United States Inc., Torrance, CA, United States). Sections (8 μm) were deposited on glass slides. Apoptotic cells were identified using the *In Situ* Cell Death Detection Kit, Fluorescein (Sigma-Aldrich Corp.) according to the manufacturer's instructions for the treatment of cryopreserved tissue sections. Sections were mounted in VECTASHIELD® Antifade Mounting Medium with DAPI (Vector Laboratories, Burlingame, CA, United States) and photographed using an Axiocam 506 mono digital camera (Carl Zeiss, Inc.) fitted onto an Axio Observed 7 fluorescence microscope (Carl Zeiss, Inc.). All positive signals were confirmed by DAPI staining. The percentage of terminal deoxynucleotidyl transferase-mediated dUTP nick end labeling (TUNEL)-positive cells was determined in three embryos per genotype per timepoint, with up to four sections analyzed per individual embryo. Analyzed sections within a given embryo were 5–10 sections apart, representing a distance of 40–80 μm. Graphed data represent averages from three independent embryos per timepoint. Statistical analyses were performed on values from individual sections with Prism 8 (GraphPad Software, Inc.) using a two-tailed, unpaired *t*-test with Welch's correction and Welch and Brown-Forsythe ANOVA tests.

Ki67 Immunofluorescence Analysis

Sections (8 μm) of PFA-fixed, sucrose-infiltrated, O.C.T.-mounted embryos were deposited on glass slides. Sections were fixed in 4% PFA in PBS with 0.1% Triton X-100 for 10 min and washed in PBS with 0.1% Triton-X 100. Sections were blocked for 1 h in 5% normal donkey serum (Jackson ImmunoResearch Inc., West Grove, PA, United States) in PBS and incubated overnight at 4°C in anti-Ki67 primary antibody (1:300; Invitrogen, Carlsbad, CA, United States) in 1% normal donkey serum in PBS. After washing in PBS, sections were incubated in Alexa Fluor 488-conjugated donkey anti-rabbit secondary antibody (1:1,000; Invitrogen) diluted in 1% normal donkey serum in PBS with 2 μg/ml DAPI (Sigma-Aldrich Corp.) for 1 h. Sections were mounted in Aqua Poly/Mount mounting medium (Polysciences, Inc., Warrington, PA, United States) and photographed using an Axiocam 506 mono digital camera (Carl Zeiss, Inc.) fitted onto an Axio Observer 7 fluorescence microscope (Carl Zeiss, Inc.). All positive signals were confirmed by DAPI staining. The percentage of Ki67-positive cells was determined in three embryos per genotype per timepoint, with up to four sections analyzed per individual embryo. Analyzed sections within a given embryo were 5–10 sections apart, representing a distance of 40–80 μm. Graphed data represent averages from three independent embryos per timepoint. Statistical analyses were performed on values from individual sections with Prism 8 (GraphPad Software, Inc.) using a two-tailed, unpaired *t*-test with Welch's correction and Welch and Brown-Forsythe ANOVA tests.

Cell Culture and Growth Assays

Primary MEPM cells were isolated from the palatal shelves of embryos dissected at E13.5 in PBS and cultured in medium [Dulbecco's modified Eagle's medium (GIBCO, Invitrogen) supplemented with 50 U/ml penicillin (GIBCO), 50 μg/ml streptomycin (GIBCO), and 2 mM L-glutamine (GIBCO)] containing 10% fetal bovine serum (FBS; HyClone Laboratories, Inc., Logan, UT, United States) as previously described (Bush and Soriano, 2010). For cell growth assays, 11,500 passage 2 MEPM cells were seeded into wells of a 24-well plate and cultured in medium containing 10% FBS. After 24 h, medium was aspirated and replaced with fresh medium containing 10% FBS (growth medium) or 0.1% FBS (starvation medium).

After 1, 2, 3, 4, and 6 total days in culture, cells were subsequently fixed in 4% PFA in PBS, stained with 0.1% crystal violet in 10% ethanol, extracted with 10% acetic acid, and the absorbance measured at 590 nm. Data represent results from three independent trials, each consisting of MEPM cells derived from one heterozygous embryo and at least one conditional knock-out littermate. Statistical analyses were performed with Prism 8 (GraphPad Software, Inc.) using a two-tailed, unpaired *t*-test with Welch's correction and Welch and Brown-Forsythe ANOVA tests.

RESULTS

Pdgfra and *Pdgfrb* Genetically Interact in the NCC Lineage

To examine the effect of ablating both *Pdgfra* and *Pdgfrb* in the NCC lineage on mid-gestation craniofacial development,

we intercrossed *Pdgfra*$^{fl/fl}$;*Pdgfrb*$^{fl/fl}$ mice with *Pdgfra*$^{+/fl}$;*Pdgfrb*$^{+/fl}$;*Wnt1-Cre*$^{+/Tg}$ mice and harvested the resulting progeny at E10.5 for gross morphological examination. Double-homozygous mutant embryos were recovered at Mendelian frequencies at this timepoint (16 embryos vs. 14 expected embryos out of 109 total, χ^2 two-tailed $p = 0.4915$; **Table 1**). A small percentage of embryos across several of the eight allele combinations from the intercrosses exhibited an abnormal head shape due to a misshapen forebrain and/or midbrain, blebbing of the surface ectoderm in the facial region and/or facial hemorrhaging (**Table 1**). Further, 18% of *Pdgfra*$^{fl/fl}$;*Pdgfrb*$^{+/fl}$;*Wnt1-Cre*$^{+/Tg}$ embryos displayed ventral body wall closure defects ($n = 11$; **Table 1**).

We next measured the distance between nasal pits, normalized to the height of the head, in E10.5 embryos as a readout of defects at the facial midline, revealing a significant difference in measurements across one control (*Pdgfra*$^{+/fl}$;*Pdgfrb*$^{+/fl}$;*Wnt1-Cre*$^{+/+}$) and the four experimental genotypes containing the *Wnt1-Cre* transgene (Welch's ANOVA test $p = 0.0390$; Brown-Forsythe ANOVA test $p = 0.0195$). The distance between nasal pits was significantly increased in *Pdgfra*$^{+/fl}$;*Pdgfrb*$^{fl/fl}$;*Wnt1-Cre*$^{+/Tg}$ embryos (0.6542 ± 0.04112, $p = 0.0095$), *Pdgfra*$^{fl/fl}$;*Pdgfrb*$^{+/fl}$;*Wnt1-Cre*$^{+/Tg}$ embryos (0.6648 ± 0.03722, $p = 0.0052$), and double-homozygous mutant embryos (0.6532 ± 0.05014, $p = 0.0155$) compared to control *Pdgfra*$^{+/fl}$;*Pdgfrb*$^{+/fl}$;*Wnt1-Cre*$^{+/+}$ embryos (0.4682 ± 0.04628; **Figure 1**). While double-heterozygous mutant embryos had a larger distance between nasal pits than control embryos, this difference was not statistically significant (**Figure 1**). Interestingly, the greatest distance between nasal pits was observed in *Pdgfra*$^{fl/fl}$;*Pdgfrb*$^{+/fl}$;*Wnt1-Cre*$^{+/Tg}$ embryos, though this distance was not significantly different between these and double-homozygous mutant embryos (**Figure 1**).

To determine whether the above craniofacial phenotypes persisted or worsened at later timepoints, embryos were harvested at E13.5 from the same intercrosses (**Figure 2**). While the presence of the *Wnt1-Cre* transgene always exacerbated E13.5 facial phenotypes, facial blebbing was detected in a subset of embryos upon combination of at least three out of four conditional alleles in the absence of the *Wnt1-Cre* transgene, reaching a prevalence of 83% in *Pdgfra*$^{fl/fl}$;*Pdgfrb*$^{+/fl}$;*Wnt1-Cre*$^{+/+}$ embryos ($n = 12$; **Table 2**; **Figures 2E,G**). Further, facial hemorrhaging was noted in approximately 15% of *Pdgfra*$^{fl/fl}$;*Pdgfrb*$^{+/fl}$;*Wnt1-Cre*$^{+/+}$ embryos ($n = 12$) and double-homozygous floxed embryos without Cre ($n = 14$; **Table 2**). These results indicate that one or both of the conditional alleles are hypomorphic. However, the fact that only 8% of *Pdgfra*$^{+/fl}$;*Pdgfrb*$^{fl/fl}$;*Wnt1-Cre*$^{+/+}$ embryos exhibited facial blebbing ($n = 13$), and none of these embryos exhibited facial hemorrhaging ($n = 13$), combined with the finding that the prevalence of these phenotypes was comparable between *Pdgfra*$^{fl/fl}$;*Pdgfrb*$^{+/fl}$;*Wnt1-Cre*$^{+/+}$ embryos and double-homozygous floxed embryos without Cre, in which 64% ($n = 14$) and 14% ($n = 14$) of embryos exhibited facial blebbing and hemorrhaging, respectively (**Table 2**), indicates that the *Pdgfrb*^{fl} allele is not hypomorphic. Double-homozygous mutant embryos were recovered at Mendelian frequencies at this timepoint as well (8 embryos vs. 12 expected embryos out of 93 total, χ^2 two-tailed $p = 0.2557$; **Table 2**). A fully-penetrant, overt facial clefting phenotype was observed in *Pdgfra*$^{fl/fl}$;*Pdgfrb*$^{+/fl}$;*Wnt1-Cre*$^{+/Tg}$ embryos (100%; $n = 12$; **Figure 2F'**) and double-homozygous mutant embryos (100%; $n = 8$; **Figure 2H'**), though not in any of the other six allele combinations from the intercrosses ($n = 73$; **Table 2**). Facial blebbing was detected in the majority of embryos among the four genotypes containing the *Wnt1-Cre* allele and was fully penetrant in *Pdgfra*$^{fl/fl}$;*Pdgfrb*$^{+/fl}$;*Wnt1-Cre*$^{+/Tg}$ embryos (100%; $n = 12$; **Table 2**; **Figures 2B,D,D',F,F',H,H'**).

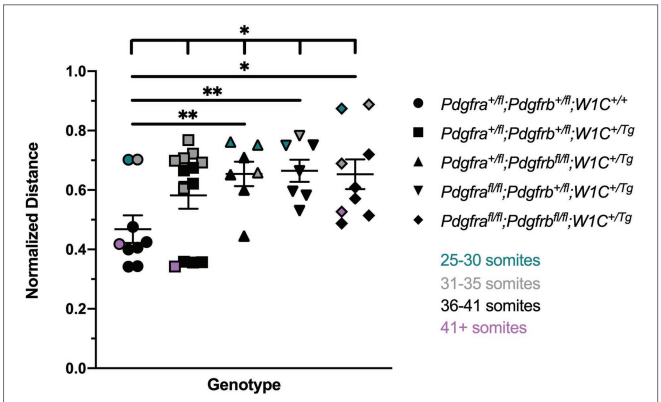

FIGURE 1 | Ablation of *Pdgfra* and *Pdgfrb* in the neural crest cell (NCC) lineage leads to increased distances between the nasal pits at mid-gestation. Scatter dot plot depicting the normalized distance between nasal pits across five genotypes at E10.5. Data are presented as mean ± SEM. *$p < 0.05$; **$p < 0.01$. Colors correspond to number of somite pairs in assayed embryos.

TABLE 1 | Phenotypes of E10.5 embryos from intercrosses of *Pdgfra*$^{fl/fl}$;*Pdgfrb*$^{fl/fl}$ mice with *Pdgfra*$^{+/fl}$;*Pdgfrb*$^{+/fl}$;*Wnt1-Cre*$^{+/Tg}$ mice.

Genotype	Expected	Observed	Normal	Dead	Abnormal head	Facial bleb	Facial hemorrhage	Body wall closure defects
$\alpha^{+/fl};\beta^{+/fl};W1C^{+/+}$	0.125	0.092	10/10	1	0/10	0/10	0/10	0/10
$\alpha^{+/fl};\beta^{+/fl};W1C^{+/Tg}$	0.125	0.192	19/21	2	0/21	2/21	0/21	0/21
$\alpha^{+/fl};\beta^{fl/fl};W1C^{+/+}$	0.125	0.117	13/14	0	1/14	0/14	0/14	0/14
$\alpha^{+/fl};\beta^{fl/fl};W1C^{+/Tg}$	0.125	0.075	7/9	0	1/9	0/9	1/9	0/9
$\alpha^{fl/fl};\beta^{+/fl};W1C^{+/+}$	0.125	0.142	14/14	3	0/14	0/14	0/14	0/14
$\alpha^{fl/fl};\beta^{+/fl};W1C^{+/Tg}$	0.125	0.117	8/11	3	1/11	1/11	1/11	2/11
$\alpha^{fl/fl};\beta^{fl/fl};W1C^{+/+}$	0.125	0.117	12/14	0	1/14	0/14	1/14	0/14
$\alpha^{fl/fl};\beta^{fl/fl};W1C^{+/Tg}$	0.125	0.150	13/16	2	1/16	1/16	1/16	0/16

TABLE 2 | Phenotypes of E13.5 embryos from intercrosses of *Pdgfra*$^{fl/fl}$;*Pdgfrb*$^{fl/fl}$ mice with *Pdgfra*$^{+/fl}$;*Pdgfrb*$^{+/fl}$;*Wnt1-Cre*$^{+/Tg}$ mice.

Genotype	Expected	Observed	Normal	Dead	Facial cleft	Facial bleb	Facial hemorrhage
$\alpha^{+/fl};\beta^{+/fl};W1C^{+/+}$	0.125	0.077	5/5	3	0/5	0/5	0/5
$\alpha^{+/fl};\beta^{+/fl};W1C^{+/Tg}$	0.125	0.173	5/16	2	0/16	10/16	2/16
$\alpha^{+/fl};\beta^{fl/fl};W1C^{+/+}$	0.125	0.135	12/13	1	0/13	1/13	0/13
$\alpha^{+/fl};\beta^{fl/fl};W1C^{+/Tg}$	0.125	0.154	2/13	3	0/13	11/13	9/13
$\alpha^{fl/fl};\beta^{+/fl};W1C^{+/+}$	0.125	0.125	2/12	1	0/12	10/12	2/12
$\alpha^{fl/fl};\beta^{+/fl};W1C^{+/Tg}$	0.125	0.115	0/12	0	12/12	12/12	9/12
$\alpha^{fl/fl};\beta^{fl/fl};W1C^{+/+}$	0.125	0.144	5/14	1	0/14	9/14	2/14
$\alpha^{fl/fl};\beta^{fl/fl};W1C^{+/Tg}$	0.125	0.077	0/8	0	8/8	7/8	8/8

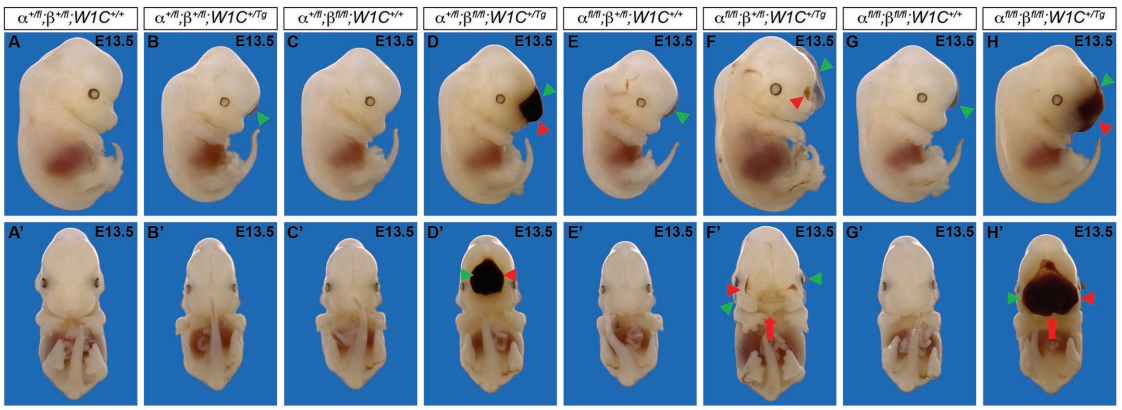

FIGURE 2 | Ablation of *Pdgfra* and *Pdgfrb* in the NCC lineage results in facial clefting, blebbing, and hemorrhaging at E13.5. **(A–H')** Gross morphology of E13.5 embryos resulting from intercrosses of *Pdgfra*$^{fl/fl}$;*Pdgfrb*$^{fl/fl}$ mice with *Pdgfra*$^{+/fl}$;*Pdgfrb*$^{+/fl}$;*Wnt1-Cre*$^{+/Tg}$ mice as viewed laterally **(A–H)** and frontally **(A'–H')**. *Pdgfra*$^{fl/fl}$;*Pdgfrb*$^{+/fl}$;*Wnt1-Cre*$^{+/Tg}$ and double-homozygous mutant embryos exhibited an overt facial cleft (red arrow). Facial blebbing (green arrowheads) and facial hemorrhaging (red arrowheads) were also detected among embryos possessing a variety of allele combinations.

Similarly, facial hemorrhaging was observed in the majority of embryos containing at least three out of four conditional alleles in combination with the *Wnt1-Cre* transgene and was fully penetrant in double-homozygous mutant embryos (100%, n = 8; **Table 2**; **Figures 2D,D'**,**F,F'**,**H,H'**). Together, these results demonstrate that *Pdgfra* and *Pdgfrb* genetically interact in the NCC lineage, with PDGFRα playing a more predominant role in NCC-mediated craniofacial development.

PDGFRα and, to a Lesser Extent, PDGFRβ Regulate cNCC Stream Size and Shape

We next introduced the *ROSA26*^{mTmG} double-fluorescent Cre reporter allele (Muzumdar et al., 2007) into the above intercrosses to examine the timing, extent, and pattern of NCC migration at E9.5–E10.5. Whereas streams entering pharyngeal arches 1 (PA1) and 2 (PA2) were readily apparent in all embryos assayed at E9.5 (**Figures 3A–E''**), there was a trend for the stream entering PA1 to be taller along the anterior-posterior axis in *Pdgfra*$^{+/fl}$;*Pdgfrb*$^{fl/fl}$;*Wnt1-Cre*$^{+/Tg}$ embryos and especially *Pdgfra*$^{fl/fl}$;*Pdgfrb*$^{+/fl}$;*Wnt1-Cre*$^{+/Tg}$ embryos than in control *Pdgfra*$^{+/+}$;*Pdgfrb*$^{+/+}$;*Wnt1-Cre*$^{+/Tg}$ embryos (**Figure 3F**). The dorsal-ventral length of the stream entering PA1 was significantly different across one control and the four experimental genotypes (Brown-Forsythe ANOVA test p = 0.0137). Further, the length of this stream was significantly longer in *Pdgfra*$^{+/fl}$;*Pdgfrb*$^{fl/fl}$;*Wnt1-Cre*$^{+/Tg}$ embryos (0.6069 ± 0.02081) compared to double-heterozygous mutant embryos (0.5252 ± 0.01524, p = 0.0252) and double-homozygous mutant embryos (0.5352 ± 0.004245, p = 0.0383), and in *Pdgfra*$^{fl/fl}$;*Pdgfrb*$^{+/fl}$;*Wnt1-Cre*$^{+/Tg}$ embryos (0.6511 ± 0.03018) compared to control *Pdgfra*$^{+/+}$;*Pdgfrb*$^{+/+}$;*Wnt1-Cre*$^{+/Tg}$ embryos (0.4907 ± 0.03919, p = 0.0304), double-heterozygous mutant embryos (0.5252 ± 0.01524, p = 0.0179), and double-homozygous mutant embryos (0.5352 ± 0.004245, p = 0.0298; **Figure 3F**). While the anterior-posterior height of the stream entering PA2 was not significantly different across genotypes, the dorsal-ventral length of the stream entering PA2 was significantly longer in *Pdgfra*$^{+/fl}$;*Pdgfrb*$^{fl/fl}$;*Wnt1-Cre*$^{+/Tg}$ embryos (0.3789 ± 0.01033, p = 0.0269) and *Pdgfra*$^{fl/fl}$;*Pdgfrb*$^{+/fl}$;*Wnt1-Cre*$^{+/Tg}$ embryos (0.3886 ± 0.009503, p = 0.0144) compared to double-heterozygous mutant embryos (0.3285 ± 0.01171; **Figure 3F**). These results demonstrate that combined decreases in PDGFRα and PDGFRβ signaling lead to longer cNCC streams along the dorsal-ventral axis entering PA1 and PA2 at E9.5.

At E10.5, whereas double-heterozygous mutant embryos (**Figures 4B–B'''**) and *Pdgfra*$^{+/fl}$;*Pdgfrb*$^{fl/fl}$;*Wnt1-Cre*$^{+/Tg}$ embryos (**Figures 4C–C'''**) appeared similar to control

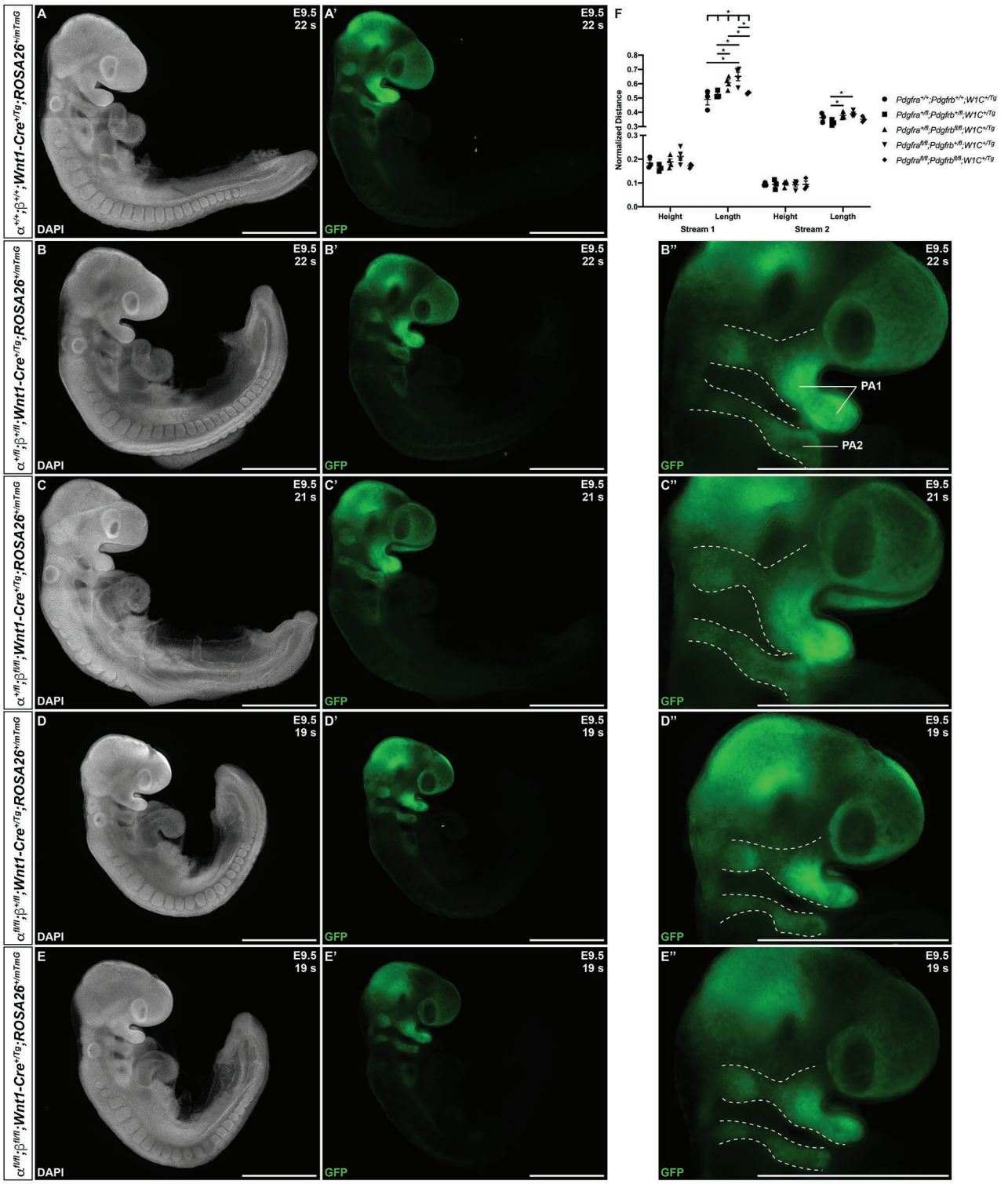

FIGURE 3 | Ablation of *Pdgfra* and *Pdgfrb* in the NCC lineage leads to longer cranial NCC (cNCC) streams entering pharyngeal arch 1 (PA1) and pharyngeal arch 2 (PA2) at E9.5. **(A–E')** Lateral, whole-mount fluorescence images of 4',6-diamidino-2-phenylindole (DAPI; **A–E**) and GFP **(A'–E')** expression across five genotypes at E9.5. **(B''–E'')** Zoomed-in images of GFP expression in cNCC streams (outlined by dotted lines) entering PA1 and PA2. PA1, pharyngeal arch 1; PA2, pharyngeal arch 2. **(F)** Scatter dot plot depicting the normalized anterior-posterior heights and dorsal-ventral lengths of cNCC streams entering PA1 and PA2 across five genotypes at E9.5. Data are presented as mean ± SEM. $^*p < 0.05$.

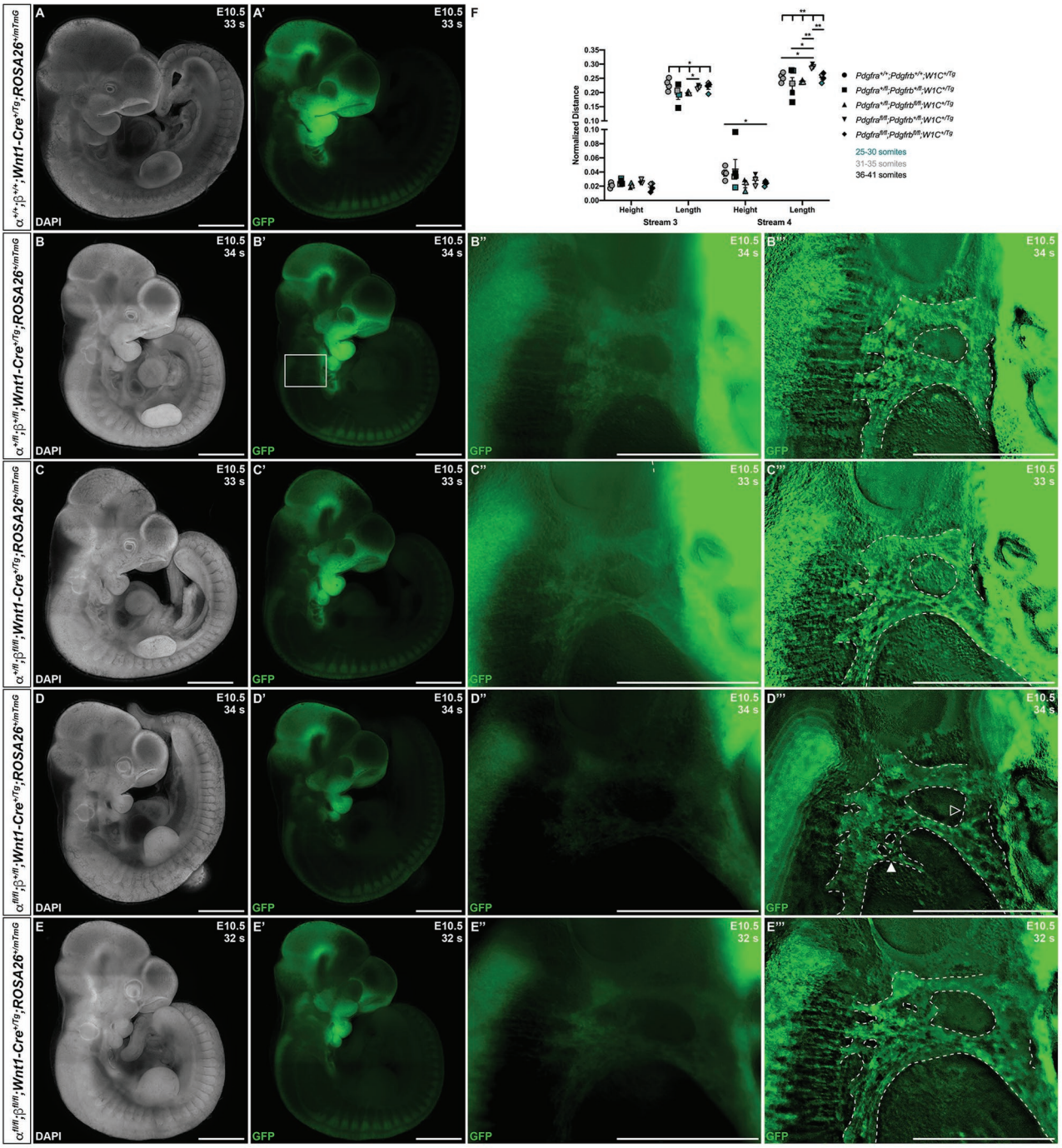

FIGURE 4 | Ablation of *Pdgfra* and *Pdgfrb* in the NCC lineage results in longer cNCC streams entering PA3 and PA4 at E10.5, with increased incidences of stream bifurcations and intermingling. **(A–E')** Lateral, whole-mount fluorescence images of DAPI **(A–E)** and GFP **(A'–E')** expression across five genotypes at E10.5. **(B''–E''')** Zoomed-in images of GFP expression in cNCC streams (outlined by dotted lines) entering PA3 and PA4. Filled arrowhead indicates an example of a bifurcated cNCC stream. Unfilled arrowhead indicates an example of intermingling cNCC streams. **(F)** Scatter dot plot depicting the normalized anterior-posterior heights and dorsal-ventral lengths of cNCC streams entering PA3 and PA4 across five genotypes at E10.5. Data are presented as mean ± SEM. $^{*}p < 0.05$; $^{**}p < 0.01$. Colors correspond to number of somite pairs in assayed embryos.

Pdgfra$^{+/+}$;*Pdgfrb*$^{+/+}$;*Wnt1-Cre*$^{+/Tg}$ embryos (**Figures 4A**,**A'**) with clearly delineated NCC streams entering pharyngeal arches 3 (PA3) and 4 (PA4), *Pdgfra*$^{fl/fl}$;*Pdgfrb*$^{+/fl}$;*Wnt1-Cre*$^{+/Tg}$ embryos had streams with reduced GFP intensity and noticeable bifurcations (**Figures 4D–D'''**). Interestingly, the double-homozygous embryo phenotype was again less severe than

that of *Pdgfra*$^{fl/fl}$;*Pdgfrb*$^{+/fl}$;*Wnt1-Cre*$^{+/Tg}$ embryos. Double-homozygous mutant embryos exhibited streams with intermediate GFP intensity and only mild bifurcations (**Figures 4E–E'''**). While the anterior-posterior height of the stream entering PA3 did not vary significantly across genotypes, the dorsal-ventral length of this stream was significantly different across one control and the four experimental genotypes (Welch's ANOVA test $p = 0.0403$; **Figure 4F**). Further, the length of the stream entering PA3 was longer in *Pdgfra*$^{fl/fl}$;*Pdgfrb*$^{+/fl}$;*Wnt1-Cre*$^{+/Tg}$ embryos (0.2181 ± 0.003919) compared to *Pdgfra*$^{+/fl}$;*Pdgfrb*$^{fl/fl}$;*Wnt1-Cre*$^{+/Tg}$ embryos (0.1990 ± 0.002382, $p = 0.0209$; **Figure 4F**). The height of the stream entering PA4 was significantly shorter in double-homozygous mutant embryos (0.02393 ± 0.001587) compared to control *Pdgfra*$^{+/+}$;*Pdgfrb*$^{+/+}$;*Wnt1-Cre*$^{+/Tg}$ embryos (0.03852 ± 0.004417, $p = 0.0390$; **Figure 4F**). Finally, the length of the stream entering PA4 was significantly different across the five genotypes (Welch's ANOVA test $p = 0.0012$), with *Pdgfra*$^{fl/fl}$;*Pdgfrb*$^{+/fl}$;*Wnt1-Cre*$^{+/Tg}$ embryos exhibiting significantly longer streams than those observed in every other genotype (**Figure 4F**).

Though we previously reported that *Pdgfrb*$^{fl/fl}$;*Wnt1-Cre*$^{+/Tg}$ embryos do not have obvious defects in NCC migration into the facial processes and pharyngeal arches (Fantauzzo and Soriano, 2016), we conducted a more detailed analysis here, analyzing the anterior-posterior heights and dorsal-ventral lengths of the NCC streams entering PA3 and PA4 of *Pdgfrb*$^{+/fl}$;*Wnt1-Cre*$^{+/Tg}$ and *Pdgfrb*$^{fl/fl}$;*Wnt1-Cre*$^{+/Tg}$ embryos at E10.5, when we observed the most significant changes in NCC stream size in the above allelic series of embryos. These analyses revealed no significant differences in the size or shape of these streams between control and single conditional knock-out embryos (**Figure 5**).

The above allelic series of E10.5 embryos was then scored for bifurcations in streams entering PA3 and PA4 and intermingling of the two streams. For a handful of embryos with a relatively high number of somite pairs (≥39), the stream entering PA3 was no longer visible and hence was not assayed for bifurcation or intermingling with the stream entering PA4. The stream entering PA3 was not bifurcated in any of the double-heterozygous mutant embryos ($n = 4$), but was found to be bifurcated in 33% of *Pdgfra*$^{+/fl}$;*Pdgfrb*$^{fl/fl}$;*Wnt1-Cre*$^{+/Tg}$ embryos ($n = 3$), 50% of *Pdgfra*$^{fl/fl}$;*Pdgfrb*$^{+/fl}$;*Wnt1-Cre*$^{+/Tg}$ embryos ($n = 2$), and 67% of double-homozygous mutant embryos ($n = 3$; **Table 3**). Bifurcation of the stream entering PA4 was observed in 40% of double-heterozygous mutant embryos ($n = 5$), 67% of *Pdgfra*$^{fl/fl}$;*Pdgfrb*$^{+/fl}$;*Wnt1-Cre*$^{+/Tg}$ embryos ($n = 3$) and was fully penetrant in *Pdgfra*$^{+/fl}$;*Pdgfrb*$^{fl/fl}$;*Wnt1-Cre*$^{+/Tg}$ embryos (100%; $n = 3$) and double-homozygous mutant embryos (100%; $n = 4$; **Table 3**). Finally, the streams entering PA3 and PA4 were intermingled in 75% of double-heterozygous mutant embryos ($n = 4$) and in all *Pdgfra*$^{+/fl}$;

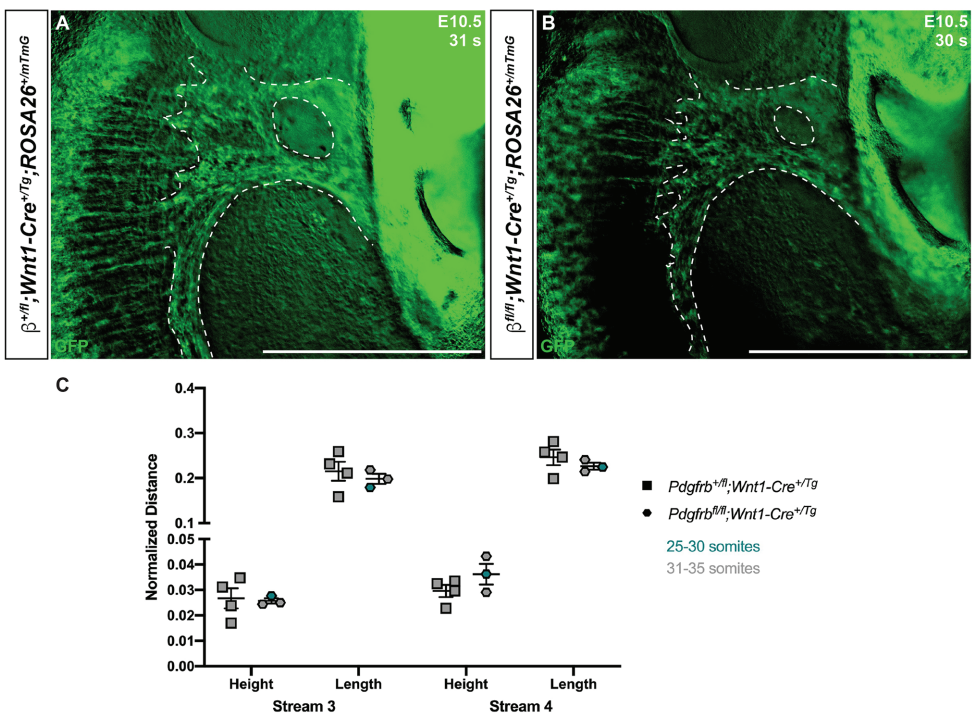

FIGURE 5 | Ablation of *Pdgfrb* in the NCC lineage does not affect cNCC streams entering PA3 and PA4 at E10.5. **(A,B)** Zoomed-in images of GFP expression in cNCC streams (outlined by dotted lines) entering PA3 and PA4. **(C)** Scatter dot plot depicting the normalized anterior-posterior heights and dorsal-ventral lengths of cNCC streams entering PA3 and PA4 across two genotypes at E10.5. Data are presented as mean ± SEM. Colors correspond to number of somite pairs in assayed embryos.

TABLE 3 | Bifurcation and intermingling of NCC streams entering PA3 and PA4 at E10.5.

Genotype	Bifurcated stream 3	Bifurcated stream 4	Intermingling of streams 3 and 4
$\alpha^{+/fl};\beta^{+/fl};W1C^{+/Tg}$	0/4	2/5	3/4
$\alpha^{+/fl};\beta^{fl/fl};W1C^{+/Tg}$	1/3	3/3	3/3
$\alpha^{fl/fl};\beta^{+/fl};W1C^{+/Tg}$	1/2	2/3	2/2
$\alpha^{fl/fl};\beta^{fl/fl};W1C^{+/Tg}$	2/3	4/4	3/3

Pdgfrb$^{fl/fl}$;*Wnt1-Cre*$^{+/Tg}$ embryos (100%; $n = 3$), *Pdgfra*$^{fl/fl}$;*Pdgfrb*$^{+/fl}$; *Wnt1-Cre*$^{+/Tg}$ embryos (100%; $n = 2$), and double-homozygous mutant embryos (100%; $n = 3$; **Table 3**). Taken together, the results at E10.5 indicate that combined decreases in PDGFRα and PDGFRβ signaling lead to longer cNCC streams with reduced GFP intensity along the dorsal-ventral axis entering PA3 and PA4, with increased incidences of stream bifurcations and intermingling.

Finally, to assess the extent of NCCs and their derivatives in the facial processes at E9.5 and E10.5, we quantified GFP expression in frontal views of the head in control *Pdgfra*$^{+/+}$;*Pdgfrb*$^{+/+}$;*Wnt1-Cre*$^{+/Tg}$ embryos and among embryos with the four experimental genotypes (**Figure 6**). At E9.5, there were noticeable decreases in GFP intensity in the facial processes of experimental embryos (**Figures 6B'–E'**) compared to control embryos (**Figure 6A'**), particularly in the frontonasal and MxPs. GFP fluorescence values were significantly decreased in *Pdgfra*$^{fl/fl}$;*Pdgfrb*$^{+/fl}$;*Wnt1-Cre*$^{+/Tg}$ embryos ($8.449 \times 10^8 \pm 7.256 \times 10^7$) compared to control *Pdgfra*$^{+/+}$;*Pdgfrb*$^{+/+}$;*Wnt1-Cre*$^{+/Tg}$ embryos ($2.079 \times 10^9 \pm 2.539 \times 10^8$, $p = 0.0317$) and double-heterozygous mutant embryos ($1.373 \times 10^9 \pm 1.283 \times 10^8$, $p = 0.0325$; **Figure 6F**). Moreover, while double-homozygous mutant embryos had higher GFP fluorescence values than *Pdgfra*$^{fl/fl}$;*Pdgfrb*$^{+/fl}$;*Wnt1-Cre*$^{+/Tg}$ embryos, GFP fluorescence was significantly decreased in double-homozygous mutant embryos ($1.088 \times 10^9 \pm 1.022 \times 10^8$) compared to control *Pdgfra*$^{+/+}$;*Pdgfrb*$^{+/+}$;*Wnt1-Cre*$^{+/Tg}$ embryos ($2.079 \times 10^9 \pm 2.539 \times 10^8$, $p = 0.0448$; **Figure 6F**). At E10.5, there was a marked decrease in GFP intensity in the facial processes of double-heterozygous mutant embryos (**Figure 6H'**) compared to control *Pdgfra*$^{+/+}$;*Pdgfrb*$^{+/+}$;*Wnt1-Cre*$^{+/Tg}$ embryos (**Figure 6G'**) and a further decrease in *Pdgfra*$^{+/fl}$;*Pdgfrb*$^{fl/fl}$;*Wnt1-Cre*$^{+/Tg}$ embryos (**Figure 6I'**), *Pdgfra*$^{fl/fl}$;*Pdgfrb*$^{+/fl}$;*Wnt1-Cre*$^{+/Tg}$ embryos (**Figure 6J'**), and double-homozygous mutant embryos (**Figure 6K'**). Not surprisingly, GFP fluorescence values increased with the number of somite pairs, as NCC progenitors proliferate and differentiate over time (**Figure 6L**). However, for embryos with 31–35 somite pairs, relative fluorescence units decreased as additional alleles were ablated, with *Pdgfra*$^{fl/fl}$; *Pdgfrb*$^{+/fl}$;*Wnt1-Cre*$^{+/Tg}$ and double-homozygous mutant embryos having the lowest, and essentially equal, GFP fluorescence values (**Figure 6L**). Collectively, our assessment of early facial phenotypes in the context of *Pdgfra* and *Pdgfrb* ablation demonstrates that signaling through these receptors contributes to several aspects of NCC activity, including stream size, stream shape and, ultimately, the extent of their derivatives in the facial prominences. Importantly, PDGFRα signaling appears to play a more predominant role in cNCC migration than PDGFRβ.

PDGFRβ Plays a More Dominant Role in Proliferation of the Facial Mesenchyme Than PDGFRα Past Mid-Gestation

We next examined levels of cell death among one control, *Pdgfra*$^{+/fl}$;*Pdgfrb*$^{+/fl}$;*Wnt1-Cre*$^{+/+}$, and the four experimental genotypes containing the *Wnt1-Cre* transgene *via* TUNEL. At E10.5, the percentage of TUNEL-positive cells was determined within the mesenchyme of the lateral and medial nasal processes, as well as the MxPs and MdPs. The percentage of TUNEL-positive cells was higher in the MNPs than the other locations at this timepoint for all genotypes (**Figure 7A**). Interestingly, in contrast to the other genotypes, no TUNEL-positive cells were found across any of the sections analyzed for *Pdgfra*$^{fl/fl}$;*Pdgfrb*$^{+/fl}$;*Wnt1-Cre*$^{+/Tg}$ embryos and double-homozygous mutant embryos in the lateral nasal processes (LNPs; **Figure 7A**). In the MNPs, both *Pdgfra*$^{+/fl}$;*Pdgfrb*$^{fl/fl}$; *Wnt1-Cre*$^{+/Tg}$ embryos (0.5328 ± 0.2316, $p = 0.0212$) and *Pdgfra*$^{fl/fl}$; *Pdgfrb*$^{+/fl}$;*Wnt1-Cre*$^{+/Tg}$ embryos (0.3792 ± 0.09148, $p = 0.0137$) had a significant decrease in apoptosis compared to control embryos (2.263 ± 0.5778). Further, there was a significant difference in the percentage of TUNEL-positive cells across all five genotypes at this location as assessed by a Welch's ANOVA test ($p = 0.0453$; **Figure 7A**). While the level of cell death did not vary significantly between the five genotypes within the MxPs and MdPs, *Pdgfra*$^{fl/fl}$;*Pdgfrb*$^{+/fl}$;*Wnt1-Cre*$^{+/Tg}$ embryos had the highest percentages of TUNEL-positive cells at these locations (**Figure 7A**). In the MdP, there was a trend for each of the experimental genotypes to have a higher percentage of TUNEL-positive cells when compared to control embryos (**Figure 7A**). At E13.5, the percentage of TUNEL-positive cells was determined within the mesenchyme of the NS and anterior (aPS), middle (mPS), and posterior secondary palatal shelves (pPS). The percentage of TUNEL-positive cells was higher in the NS than in the secondary palatal shelves for all genotypes, consistent with the relatively high level of TUNEL-positive cells in the MNPs 3 days earlier at E10.5. Two genotypes, *Pdgfra*$^{+/fl}$;*Pdgfrb*$^{fl/fl}$;*Wnt1-Cre*$^{+/Tg}$ embryos and *Pdgfra*$^{fl/fl}$;*Pdgfrb*$^{+/fl}$; *Wnt1-Cre*$^{+/Tg}$ embryos, had a non-statistically significant increase in the percentage of TUNEL-positive cells compared to the control genotype at this location (**Figure 7B**). While the level of cell death did not vary significantly between the five genotypes within the secondary palatal shelves, there was a trend for each of the experimental genotypes to have a lower percentage of TUNEL-positive cells in the aPS when compared to control embryos (**Figure 7B**). In the mPS, three genotypes, double-heterozygous mutant embryos, *Pdgfra*$^{+/fl}$;*Pdgfrb*$^{fl/fl}$;*Wnt1-Cre*$^{+/Tg}$ embryos, and *Pdgfra*$^{fl/fl}$;*Pdgfrb*$^{+/fl}$;*Wnt1-Cre*$^{+/Tg}$ embryos, had a non-statistically significant increase in the percentage of TUNEL-positive cells compared to the control genotype (**Figure 7B**). Similarly, in the pPS, three genotypes, double-heterozygous mutant embryos, *Pdgfra*$^{fl/fl}$;*Pdgfrb*$^{+/fl}$;*Wnt1-Cre*$^{+/Tg}$ embryos, and double-homozygous mutant embryos, had a non-statistically significant increase in the percentage of TUNEL-positive cells

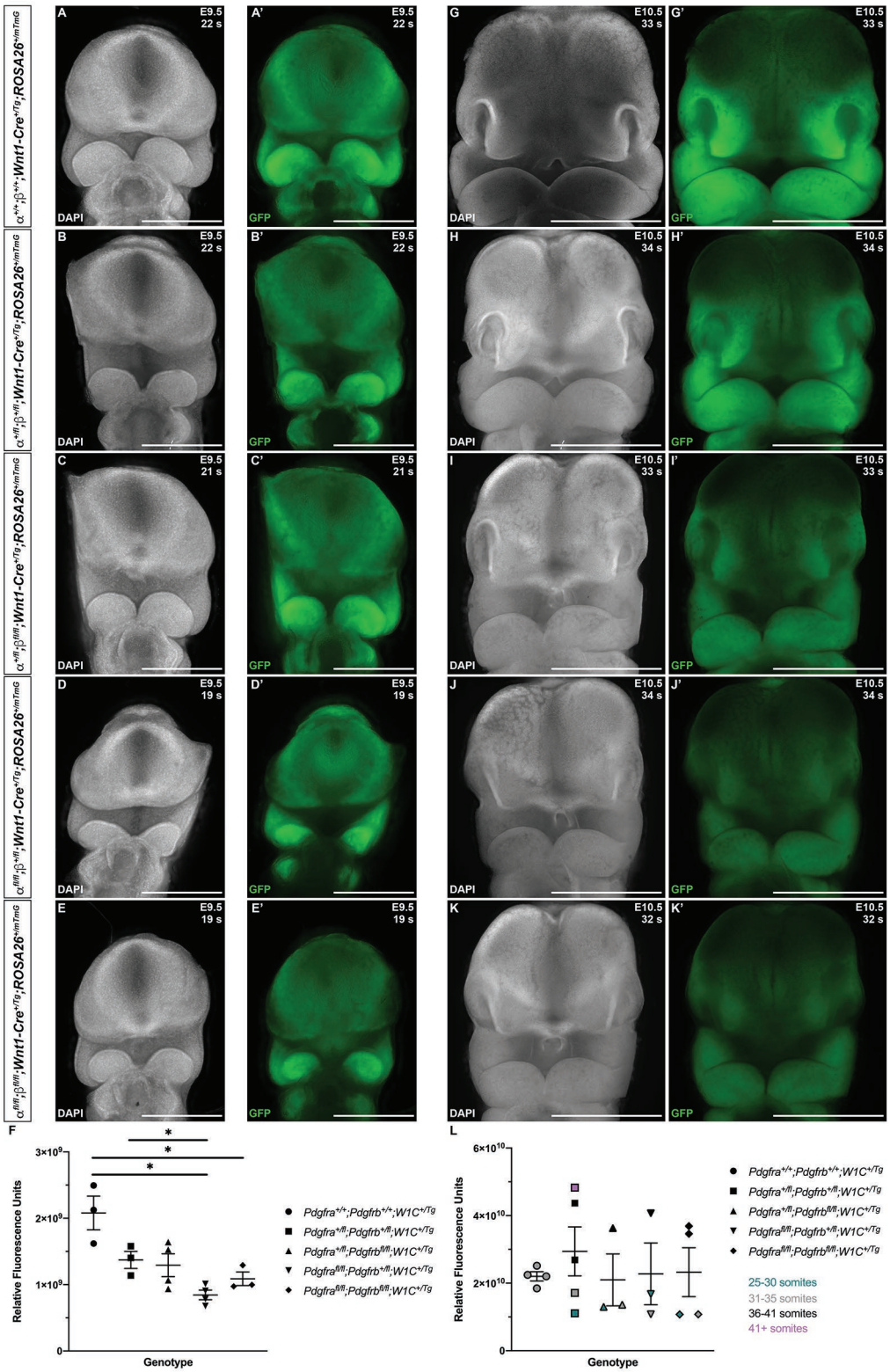

FIGURE 6 | Ablation of *Pdgfra* and *Pdgfrb* in the NCC lineage leads to decreased NCC derivatives in the facial prominences at mid-gestation. **(A–K')** Frontal, whole-mount fluorescence images of DAPI **(A–E,G–K)** and GFP **(A'–E',G'–K')** expression across five genotypes at E9.5 **(A–E')** and E10.5 **(G–K')**. **(F)** Scatter dot plot depicting GFP fluorescence intensity across five genotypes at E9.5. Data are presented as mean ± SEM. *$p < 0.05$. **(L)** Scatter dot plot depicting GFP fluorescence intensity across five genotypes at E10.5. Data are presented as mean ± SEM. Colors correspond to number of somite pairs in assayed embryos.

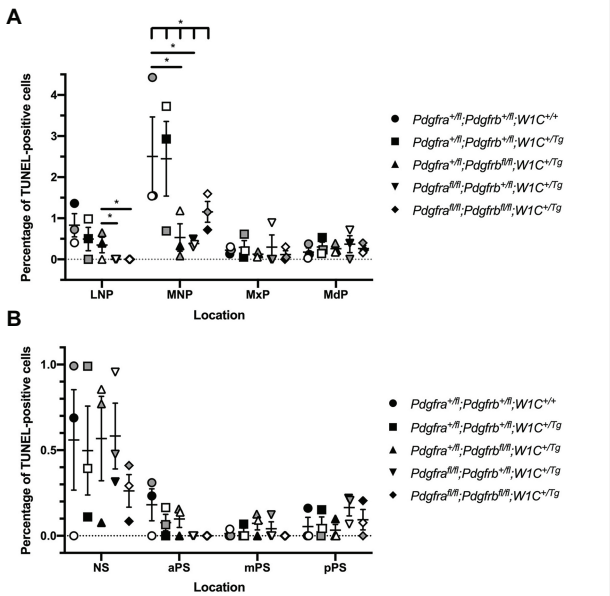

FIGURE 7 | Neither PDGFRα nor PDGFRβ signaling plays a critical role in cNCC-derived facial mesenchyme survival during mid-gestation. **(A)** Scatter dot plot depicting the average percentage of terminal deoxynucleotidyl transferase-mediated dUTP nick end labeling (TUNEL)-positive cells per embryo in the nasal processes and facial prominences across five genotypes at E10.5. Data are presented as mean ± SEM. $^*p < 0.05$. Shades correspond to independent experiments across three biological replicates. LNP, lateral nasal process; MNP, medial nasal process; MxP, maxillary prominence; and MdP, mandibular prominence. **(B)** Scatter dot plot depicting the average percentage of TUNEL-positive cells per embryo in the nasal septum (NS) and secondary palatal shelves across five genotypes at E13.5. Data are presented as mean ± SEM. Shades correspond to independent experiments across three biological replicates. NS, nasal septum; aPS, anterior secondary palatal shelves; mPS, middle secondary palatal shelves; and pPS, posterior secondary palatal shelves.

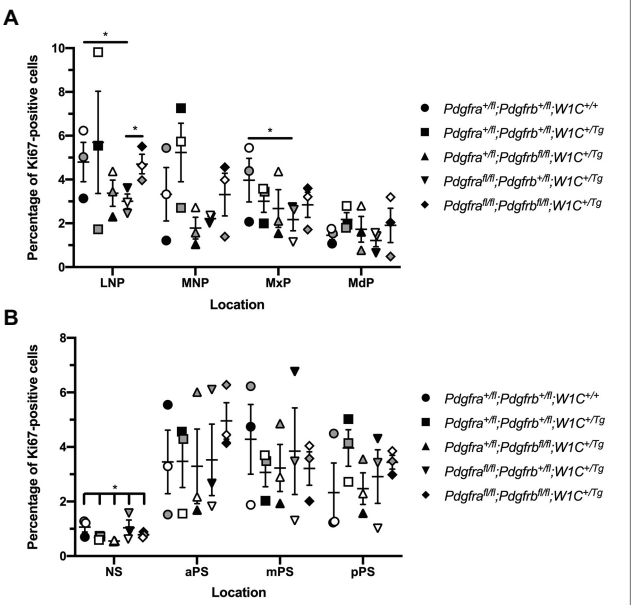

FIGURE 8 | PDGFRα plays a more dominant role in proliferation of the craniofacial mesenchyme at E10.5, while PDGFRβ has a more pronounced effect at E13.5. **(A)** Scatter dot plot depicting the average percentage of Ki67-positive cells per embryo in the nasal processes and facial prominences across five genotypes at E10.5. Data are presented as mean ± SEM. $^*p < 0.05$. Shades correspond to independent experiments across three biological replicates. LNP, lateral nasal process; MNP, medial nasal process; MxP, maxillary prominence; and MdP, mandibular prominence. **(B)** Scatter dot plot depicting the average percentage of Ki67-positive cells per embryo in the NS and secondary palatal shelves across five genotypes at E13.5. Data are presented as mean ± SEM. $^*p < 0.05$. Shades correspond to independent experiments across three biological replicates. NS, nasal septum; aPS, anterior secondary palatal shelves; mPS, middle secondary palatal shelves; and pPS, posterior secondary palatal shelves.

compared to the control genotype (**Figure 7B**). Taken together, the combined TUNEL assay results demonstrate that neither PDGFRα nor PDGFRβ signaling plays a critical role in cNCC-derived facial mesenchyme survival during mid-gestation.

We similarly examined levels of cell proliferation among one control, *Pdgfra*$^{+/fl}$;*Pdgfrb*$^{+/fl}$;*Wnt1-Cre*$^{+/+}$, and the four experimental genotypes containing the *Wnt1-Cre* transgene *via* Ki67 immunofluorescence analysis. At E10.5, the percentage of Ki67-positive cells was determined within the mesenchyme of the lateral and medial nasal processes, as well as the MxPs and MdPs. The percentage of Ki67-positive cells was highest in the LNPs and lowest in the MdPs for all genotypes (**Figure 8A**). *Pdgfra*$^{fl/fl}$;*Pdgfrb*$^{+/fl}$;*Wnt1-Cre*$^{+/Tg}$ embryos exhibited a significant decrease in cell proliferation in the LNPs (2.882 ± 0.5367) compared to control embryos (5.003 ± 0.7518, $p = 0.0450$) and double-homozygous mutant embryos (4.687 ± 0.4514, $p = 0.0368$), as well as a significant decrease in the MxPs (2.168 ± 0.5133) compared to control embryos (4.350 ± 0.7249, $p = 0.0494$; **Figure 8A**). Interestingly, the percentage of Ki67-positive cells was consistently lower in *Pdgfra*$^{+/fl}$;*Pdgfrb*$^{fl/fl}$;*Wnt1-Cre*$^{+/Tg}$ embryos and *Pdgfra*$^{fl/fl}$;*Pdgfrb*$^{+/fl}$;*Wnt1-Cre*$^{+/Tg}$ embryos than double-homozygous mutant embryos at all locations at this timepoint (**Figure 8A**). As above with the TUNEL analysis, at E13.5, the percentage of Ki67-positive cells was determined within the mesenchyme of the NS and aPS, mPS, and pPS. The percentage of Ki67-positive cells was consistently lower in the NS than the secondary palatal shelves (**Figure 8B**). Though there were no significant differences in cell proliferation in pair-wise comparisons between genotypes in the NS, there was a significant difference in the percentage of Ki67-positive cells across all five genotypes as assessed by a Welch's ANOVA test ($p = 0.0453$; **Figure 8B**). While the level of proliferation did not vary significantly between the five genotypes in the NS and along the anterior-posterior axis of the secondary palatal shelves, there were trends for each of the experimental genotypes to have a lower percentage of Ki67-positive cells in the NS and mPS when compared to these same locations in control embryos (**Figure 8B**). Intriguingly, *Pdgfra*$^{+/fl}$;*Pdgfrb*$^{fl/fl}$;*Wnt1-Cre*$^{+/Tg}$ embryos had a consistently lower percentage of Ki67-positive cells in the NS and aPS and mPS than *Pdgfra*$^{fl/fl}$;*Pdgfrb*$^{+/fl}$;*Wnt1-Cre*$^{+/Tg}$ embryos (**Figure 8B**). These findings indicate that both PDGFRα and PDGFRβ promote cell proliferation in the craniofacial mesenchyme, with PDGFRα

playing a more predominant role in E10.5 facial structures and PDGFRβ potentially having a more pronounced effect on cell proliferation at E13.5.

To confirm a role for PDGFRβ in promoting cell proliferation past mid-gestation, we determined the percentage of Ki67-positive cells within the mesenchyme of the NS and aPS of E13.5 *Pdgfrb*$^{+/fl}$;*Wnt1-Cre*$^{+/Tg}$ vs. *Pdgfrb*$^{fl/fl}$;*Wnt1-Cre*$^{+/Tg}$ embryos. The single conditional knock-out embryos exhibited a trend for decreased proliferation in the NS and a significant decrease in the percentage of Ki67-positive cells in the aPS (3.404 ± 0.5503) compared to heterozygous embryos (5.393 ± 0.3762, p = 0.0092; **Figure 9**).

We subsequently sought to determine the individual contribution of PDGFRα and PDGFRβ to proliferation of the craniofacial mesenchyme and to distinguish any potential proliferation defects from more wide-spread phenotypes observed upon ablation of *Pdgfra* or *Pdgfrb* in the NCC lineage. To do this, primary MEPM cells were dissected from E13.5 control (*Pdgfra*$^{+/fl}$;*Wnt1-Cre*$^{+/Tg}$ or *Pdgfrb*$^{+/fl}$;*Wnt1-Cre*$^{+/Tg}$) and conditional knock-out (*Pdgfra*$^{fl/fl}$;*Wnt1-Cre*$^{+/Tg}$ or *Pdgfrb*$^{fl/fl}$;*Wnt1-Cre*$^{+/Tg}$) littermate embryos for use in cell growth assays (**Figure 10A**). Primary MEPM cells are a faithful surrogate for embryonic facial mesenchyme, as wild-type cells express both PDGFRα and PDGFRβ as well as numerous additional *in vivo* palatal mesenchyme cell markers, and respond to stimulation with PDGF-AA, PDGF-BB, and PDGF-DD ligands (He and Soriano, 2013; Fantauzzo and Soriano, 2014, 2016, 2017; Vasudevan and Soriano, 2014; Vasudevan et al., 2015). Even after a single day in growth medium containing 10% FBS, control *Pdgfrb*$^{+/fl}$;*Wnt1-Cre*$^{+/Tg}$ cells [0.1077 ± 0.01233 arbitrary units (AUs); **Figure 10C**] had grown about half as much as control *Pdgfra*$^{+/fl}$;*Wnt1-Cre*$^{+/Tg}$ cells (0.2217 ± 0.07322 AU; **Figure 10B**). All cells grown in starvation medium containing 0.1% FBS, both control and conditional knock-out, immediately proliferated less than cells of the same genotypes grown in growth medium (**Figures 10B,C**). These trends continued after 5 days in culture, at which point significant differences were detected in all comparisons with the exception of *Pdgfrb*$^{fl/fl}$;*Wnt1-Cre*$^{+/Tg}$ cells, which did not proliferate significantly more in medium containing 10% FBS than in medium containing 0.1% FBS (**Figures 10B,C**). Importantly, conditional knock-out cells consistently fared worse than their control counterparts in both growth and starvation medium, though this difference was more pronounced in *Pdgfrb*$^{+/fl}$;*Wnt1-Cre*$^{+/Tg}$ vs. *Pdgfrb*$^{fl/fl}$;*Wnt1-Cre*$^{+/Tg}$ cells following 6 days in culture. At this time, control *Pdgfra*$^{+/fl}$;*Wnt1-Cre*$^{+/Tg}$ cells cultured in growth medium (0.8773 ± 0.08867 AU) had proliferated approximately 1.8 times the extent of *Pdgfra*$^{fl/fl}$;*Wnt1-Cre*$^{+/Tg}$ cells (0.4885 ± 0.03203 AU, p = 0.0357; **Figure 10B**), while control *Pdgfrb*$^{+/fl}$;*Wnt1-Cre*$^{+/Tg}$ cells (0.5897 ± 0.03588 AU) cultured in growth medium had an absorbance reading roughly 2.5 times that of *Pdgfrb*$^{fl/fl}$;*Wnt1-Cre*$^{+/Tg}$ cells (0.2394 ± 0.05482 AU, p = 0.0018; **Figure 10C**). Similarly, while there were no significant differences in absorbance readings between control *Pdgfra*$^{+/fl}$;*Wnt1-Cre*$^{+/Tg}$ and *Pdgfra*$^{fl/fl}$;*Wnt1-Cre*$^{+/Tg}$ cells cultured in starvation medium (**Figure 10B**), control *Pdgfrb*$^{+/fl}$;*Wnt1-Cre*$^{+/Tg}$ cells (0.2047 ± 0.009821 AU) cultured in starvation medium demonstrated a significant increase in absorbance reading over that of *Pdgfrb*$^{fl/fl}$;*Wnt1-Cre*$^{+/Tg}$ cells (0.1084 ± 0.01588 AU, p = 0.0022; **Figure 10C**). Taken together, these results confirm the Ki67 immunofluorescence findings and reveal that PDGFRβ plays a more dominant role in proliferation of the facial mesenchyme than PDGFRα past mid-gestation.

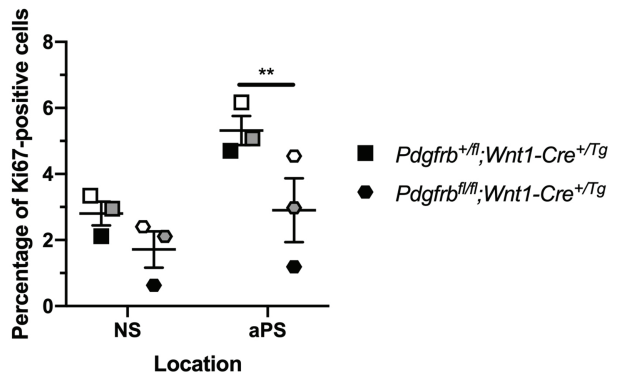

FIGURE 9 | Ablation of *Pdgfrb* in the NCC lineage leads to decreased proliferation in the anterior secondary palatal shelves (aPS) at E13.5. Scatter dot plot depicting the average percentage of Ki67-positive cells per embryo in the NS and aPS in *Pdgfrb*$^{+/fl}$;*Wnt1-Cre*$^{+/Tg}$ vs. *Pdgfrb*$^{fl/fl}$;*Wnt1-Cre*$^{+/Tg}$ embryos at E13.5. Data are presented as mean ± SEM. $^{**}p < 0.01$. Shades correspond to independent experiments across three biological replicates. NS, nasal septum; aPS, anterior secondary palatal shelves.

DISCUSSION

Here, we report the first detailed phenotypic characterization of mouse embryos in which both *Pdgfra* and *Pdgfrb* are ablated in the NCC lineage. Our results reveal that the two receptors genetically interact in this lineage during embryogenesis, as phenotypes observed in an allelic series of mutant embryos often worsened with the addition of conditional alleles. We characterized defects in craniofacial development at mid-gestation resulting from combined loss of *Pdgfra* and *Pdgfrb*, including incidences of facial clefting, blebbing, and hemorrhaging. These results confirm the phenotypes we observed from mid-to-late-gestation upon combining the constitutive *Pdgfra*^{PI3K} allele together with the conditional *Pdgfrb*^{fl} allele and the *Wnt1-Cre* driver (Fantauzzo and Soriano, 2016) and significantly extend those findings by exploring the cellular mechanisms through which these phenotypes arise. The defects observed here were shown to stem from aberrant cNCC migration, as well as reduced proliferation of the facial mesenchyme upon combined decreases in PDGFRα and PDGFRβ signaling. At present, however, our results cannot distinguish between synergistic effects of the two receptors on cNCC activity or whether the observed defects stem from non-redundant roles of PDGFRα and PDGFRβ in this lineage. Importantly, we found that PDGFRα plays a predominant role in cNCC migration while PDGFRβ primarily contributes to proliferation of the facial mesenchyme past mid-gestation.

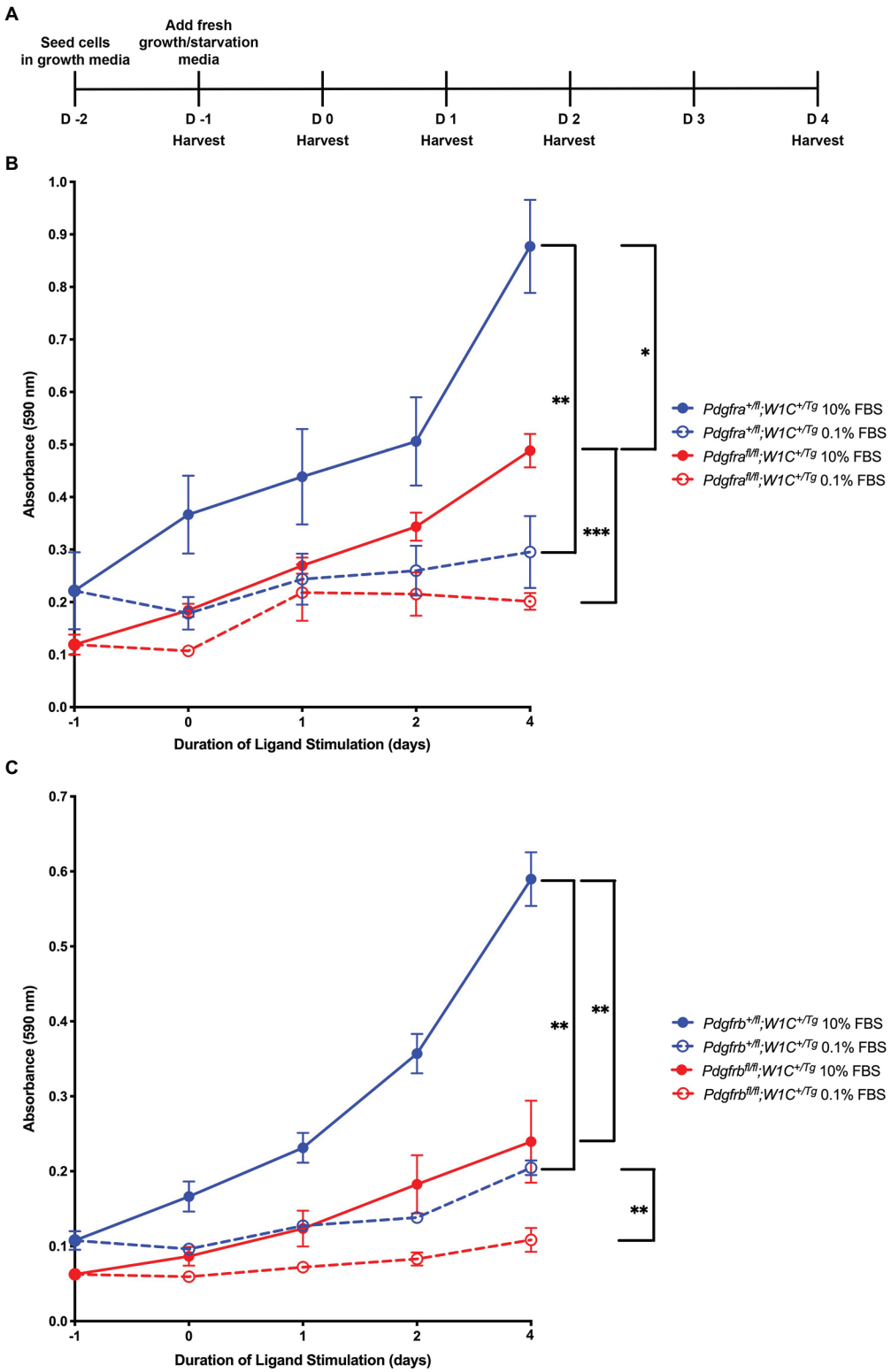

FIGURE 10 | PDGFRβ plays a more dominant role in proliferation of primary MEPM cells than PDGFRα. **(A)** Experimental design for cell growth assays. **(B)** Line graph depicting absorbance values at 590 nm in *Pdgfra*$^{+/fl}$;*Wnt1-Cre*$^{+/Tg}$ vs. *Pdgfra*$^{fl/fl}$;*Wnt1-Cre*$^{+/Tg}$ primary MEPM cells across conditions. Data are presented as mean ± SEM. *$p < 0.05$; **$p < 0.01$; ***$p < 0.001$. **(C)** Line graph depicting absorbance values at 590 nm in *Pdgfrb*$^{+/fl}$;*Wnt1-Cre*$^{+/Tg}$ vs. *Pdgfrb*$^{fl/fl}$;*Wnt1-Cre*$^{+/Tg}$ primary MEPM cells across conditions. Data are presented as mean ± SEM. **$p < 0.01$.

Our E13.5 gross morphology results further confirm that the *Pdgfra* conditional allele used in this study is hypomorphic, as facial blebbing and facial hemorrhaging were detected at increased incidences in embryos homozygous for this allele in the absence of the *Wnt1-Cre* transgene. While mice heterozygous for a *Pdgfra* null allele are viable (Soriano, 1997), $Pdgfra^{fl/-}$ embryos are not, exhibiting multiple phenotypes such as spina bifida and cleft palate (Tallquist and Soriano, 2003; McCarthy et al., 2016). Further, $Pdgfra^{fl/fl}$ mice in our own colony, which are maintained through homozygous intercrosses, generate small litters (average litter size of 4.2 pups at 5–10 days after birth compared to an average of 5.8 pups for wild-type 129S4 litters; $p = 0.0013$) and have shortened snouts with a pigment defect at the facial midline (data not shown). It has been hypothesized that these hypomorphic phenotypes arise due to the presence of a neomycin resistance cassette in the floxed allele that reduces expression of *Pdgfra* (Tallquist and Soriano, 2003). Hypomorphic phenotypes have not previously been attributed to the $Pdgfrb^{fl}$ allele, and $Pdgfrb^{fl/fl}$ mice in our colony, which are also maintained through homozygous intercrosses, give birth to litters of expected sizes (average litter size of 6.2 pups at 5–10 days after birth compared to an average of 5.8 pups for wild-type 129S4 litters; $p = 0.2998$).

It is useful to compare and contrast the defects observed in the allelic series of embryos analyzed here with single-homozygous mutant embryos. As mentioned above, a previous analysis found fewer NCCs in PA3–6 in E10.5 $Pdgfra^{fl/fl}$;$Wnt1\text{-}Cre^{+/Tg}$ embryos, with bifurcation of the streams entering these arches in a subset of embryos (He and Soriano, 2013). These results are consistent with the findings here, in which $Pdgfra^{fl/fl}$;$Pdgfrb^{+/fl}$;$Wnt1\text{-}Cre^{+/Tg}$ embryos exhibited cNCC streams with significantly altered sizes, reduced GFP intensity, and noticeable bifurcations compared to the other embryos analyzed. While it is tempting to speculate that these phenotypes stem from defective cNCC directional migration in this context, additional experiments will be required to test this hypothesis. Further, our Ki67 results at E10.5 demonstrated significantly decreased proliferation in the LNPs and MxPs of $Pdgfra^{fl/fl}$;$Pdgfrb^{+/fl}$;$Wnt1\text{-}Cre^{+/Tg}$ embryos vs. control embryos. This finding is consistent with observed decreases in proliferation in the frontonasal process of E9.5 $Pdgfra^{fl/fl}$;$Wnt1\text{-}Cre^{+/Tg}$ embryos as assessed by BrdU staining (He and Soriano, 2013) and in primary MEPM cells derived from $Pdgfra^{PI3K/PI3K}$ embryos in response to PDGF-AA ligand treatment (He and Soriano, 2013; Fantauzzo and Soriano, 2014), but contrasts with previously-observed decreases in proliferation in the MNPs of E11.5 $Pdgfra^{fl/fl}$;$Wnt1\text{-}Cre^{+/Tg}$ embryos (He and Soriano, 2013, 2015). Importantly, our findings are the first to demonstrate a role for PDGFRβ in regulating cNCC migration and proliferation in the developing mouse embryo. While $Pdgfrb^{fl/fl}$;$Wnt1\text{-}Cre^{+/Tg}$ embryos do not have cNCC migration defects, the size of cNCC streams entering PA1 and PA2 were significantly longer in $Pdgfra^{+/fl}$;$Pdgfrb^{fl/fl}$;$Wnt1\text{-}Cre^{+/Tg}$ embryos than double-heterozygous embryos, indicating that PDGFRβ signaling contributes to cNCC migration. However, signaling through this receptor appears to play a more prominent role in facial mesenchyme proliferation, even more so than signaling through PDGFRα. We detected a 37% decrease in cell proliferation in the aPS of E13.5 *Pdgfrb* conditional knock-out embryos compared to heterozygous littermates, which is greater than the decreases in proliferation detected in *Pdgfra* conditional knock-out embryos in the frontonasal process at E9.5 and the MNP at E11.5 (He and Soriano, 2013).

Interestingly, in several parameters examined here, including the lengths of cNCC streams entering the PAs and the percentage of Ki67-positive cells in the LNPs at E10.5, the phenotype of $Pdgfra^{fl/fl}$;$Pdgfrb^{+/fl}$;$Wnt1\text{-}Cre^{+/Tg}$ embryos was significantly more severe than that of double-homozygous mutant embryos. This result is contrary to our previous observations in which $Pdgfra^{PI3K/PI3K}$;$Pdgfrb^{+/fl}$;$Wnt1\text{-}Cre^{+/Tg}$ embryos did not exhibit facial clefting at E13.5, while this phenotype was fully penetrant in $Pdgfra^{PI3K/PI3K}$;$Pdgfrb^{fl/fl}$;$Wnt1\text{-}Cre^{+/Tg}$ embryos (Fantauzzo and Soriano, 2016). The most likely explanation for this finding is that reduced, but not absent, PDGFRβ signaling has a negative effect on cNCC activity and subsequent facial development in a context in which PDGFRα signaling is completely abolished, as observed here. Further studies will be required to determine the mechanism(s) by which this phenomenon occurs.

In *Xenopus*, *pdgfra* is expressed by pre-migratory and migratory cNCCs, while its ligand *pdgfa* is expressed in pre-migratory NCCs and the tissues surrounding migratory NCCs (Bahm et al., 2017). Functional studies revealed dual roles for PDGF-A-dependent PDGFRα signaling in NCC development. During early NCC migration, PI3K/Akt-mediated PDGFRα signaling cell autonomously upregulates N-cadherin to promote contact inhibition of locomotion and cell dispersion. Following initiation of the epithelial-to-mesenchymal transition, migrating NCCs chemotax toward PDGF-A ligand in the surrounding tissue, resulting in directional migration (Bahm et al., 2017). The ligand *pdgfb* is also expressed in tissues adjacent to migrating NCCs in *Xenopus* embryos (Giannetti et al., 2016) and knock-down of this ligand results in impaired cNCC migration and defective development of the craniofacial cartilages and cranial nerves in a subset of morpholino-injected embryos (Corsinovi et al., 2019). In zebrafish, *pdgfra* is similarly expressed by pre-migratory and migratory cNCCs, while its ligand *pdgfaa* is correspondingly expressed at early stages in the midbrain and later in the oral ectoderm (Eberhart et al., 2008). A hypomorphic zebrafish mutant of *pdgfra* exhibits palatal clefting and a shortened neurocrania due to defective cNCC migration (Eberhart et al., 2008; McCarthy et al., 2016). *Pdgfrb* is also expressed by migratory cNCCs in zebrafish, and the phenotypes observed in *pdgfra* mutants are exacerbated in double *pdgfra;pdgfrb* mutant fish in which cNCCs fail to properly condense in the maxillary domain (McCarthy et al., 2016). In contrast to a previous study in which cNCC migration was reportedly unperturbed upon combined ablation of *Pdgfra* and *Pdgfrb* in the murine NCC lineage (Richarte et al., 2007), our results confirm the findings in lower vertebrates that both receptors play a role in NCC migration and that aspects of the phenotype observed upon conditional ablation of *Pdgfra* in the NCC lineage are exacerbated in double-homozygous mutant embryos.

In summary, our findings provide insight into the distinct mechanisms by which PDGFRα and PDGFRβ signaling regulate cNCC activity and subsequent craniofacial development in a mammalian system. Future studies will seek to identify the

intracellular signaling molecules and gene expression responses that mediate the effects of these receptors on migration and proliferation.

DATA AVAILABILITY STATEMENT

The original contributions presented in the study are included in the article. Further inquiries can be directed to the corresponding author.

ETHICS STATEMENT

The animal study was reviewed and approved by The Institutional Animal Care and Use Committee of the University of Colorado Anschutz Medical Campus.

AUTHOR CONTRIBUTIONS

KF conceived and designed the study. JM, RL, and KF performed experimentation. JM and KF analyzed data. KF wrote the original draft of the manuscript, which was revised and edited in an iterative process with JM. All authors contributed to the article and approved the submitted version.

FUNDING

This work was supported by National Institutes of Health/National Institute of Dental and Craniofacial Research (NIH/NIDCR) grants R03DE025263, R01DE027689, and K02DE028572 (to KF).

ACKNOWLEDGMENTS

We are grateful to Damian Garno and Elliott Brooks for technical assistance. We thank members of the Fantauzzo laboratory for their helpful discussions and critical comments on the manuscript. The content of this manuscript previously appeared online in a preprint (Mo et al., 2020).

REFERENCES

Bahm, I., Barriga, E. H., Frolov, A., Theveneau, E., Frankel, P., and Mayor, R. (2017). PDGF controls contact inhibition of locomotion by regulating N-cadherin during neural crest migration. *Development* 144, 2456–2468. doi: 10.1242/dev.147926

Boström, H., Willetts, K., Pekny, M., Levéen, P., Lindahl, P., Hedstrand, H., et al. (1996). PDGF-A signaling is a critical event in lung alveolar myofibroblast development and alveogenesis. *Cell* 85, 863–873. doi: 10.1016/S0092-8674(00)81270-2

Bush, J. O., and Jiang, R. (2012). Palatogenesis: morphogenetic and molecular mechanisms of secondary palate development. *Development* 139, 231–243. doi: 10.1242/dev.067082

Bush, J. O., and Soriano, P. (2010). Ephrin-B1 forward signaling regulates craniofacial morphogenesis by controlling cell proliferation across Eph-ephrin boundaries. *Genes Dev.* 24, 2068–2080. doi: 10.1101/gad.1963210

Choi, S. J., Marazita, M. L., Hart, P. S., Sulima, P. P., Field, L. L., McHenry, T. G., et al. (2009). The PDGF-C regulatory region SNP rs28999109 decreases promoter transcriptional activity and is associated with CL/P. *Eur. J. Hum. Genet.* 17, 774–784. doi: 10.1038/ejhg.2008.245

Corsinovi, D., Giannetti, K., Cericola, A., Naef, V., and Ori, M. (2019). PDGF-B: the missing piece in the mosaic of PDGF family role in craniofacial development. *Dev. Dyn.* 248, 603–612. doi: 10.1002/dvdy.47

Danielian, P. S., Muccino, D., Rowitch, D. H., Michael, S. K., and McMahon, A. P. (1998). Modification of gene activity in mouse embryos in utero by a tamoxifen-inducible form of Cre recombinase. *Curr. Biol.* 8, 1323–1326. doi: 10.1016/S0960-9822(07)00562-3

Ding, H., Wu, X., Boström, H., Kim, I., Wong, N., Tsoi, B., et al. (2004). A specific requirement for PDGF-C in palate formation and PDGFR-alpha signaling. *Nat. Genet.* 36, 1111–1116. doi: 10.1038/ng1415

Ding, H., Wu, X., Kim, I., Tam, P. P., Koh, G. Y., and Nagy, A. (2000). The mouse Pdgfc gene: dynamic expression in embryonic tissues during organogenesis. *Mech. Dev.* 96, 209–213. doi: 10.1016/S0925-4773(00)00425-1

Eberhart, J. K., He, X., Swartz, M. E., Yan, Y. L., Song, H., Boling, T. C., et al. (2008). MicroRNA Mirn140 modulates Pdgf signaling during palatogenesis. *Nat. Genet.* 40, 290–298. doi: 10.1038/ng.82

Fantauzzo, K. A., and Soriano, P. (2014). PI3K-mediated PDGFRα signaling regulates survival and proliferation in skeletal development through p53-dependent intracellular pathways. *Genes Dev.* 28, 1005–1017. doi: 10.1101/gad.238709.114

Fantauzzo, K. A., and Soriano, P. (2016). PDGFRβ regulates craniofacial development through homodimers and functional heterodimers with PDGFRα. *Genes Dev.* 30, 2443–2458. doi: 10.1101/gad.288746.116

Fantauzzo, K. A., and Soriano, P. (2017). Generation of an immortalized mouse embryonic palatal mesenchyme cell line. *PLoS One* 12:e0179078. doi: 10.1371/journal.pone.0179078

Giannetti, K., Corsinovi, D., Rossino, C., Appolloni, I., Malatesta, P., and Ori, M. (2016). Platelet derived growth factor B gene expression in the *Xenopus laevis* developing central nervous system. *Int. J. Dev. Biol.* 60, 175–179. doi: 10.1387/ijdb.160045mo

Hamilton, T. G., Klinghoffer, R. A., Corrin, P. D., and Soriano, P. (2003). Evolutionary divergence of platelet-derived growth factor alpha receptor signaling mechanisms. *Mol. Cell. Biol.* 23, 4013–4025. doi: 10.1128/MCB.23.11.4013-4025.2003

He, F., and Soriano, P. (2013). A critical role for PDGFRα signaling in medial nasal process development. *PLoS Genet.* 9:e1003851. doi: 10.1371/journal.pgen.1003851

He, F., and Soriano, P. (2015). Sox10ERT2CreERT2 mice enable tracing of distinct neural crest cell populations. *Dev. Dyn.* 244, 1394–1403. doi: 10.1002/dvdy.24320

Heldin, C. H., and Westermark, B. (1999). Mechanism of action and in vivo role of platelet-derived growth factor. *Physiol. Rev.* 79, 1283–1316. doi: 10.1152/physrev.1999.79.4.1283

Johnston, J. J., Sanchez-Contreras, M. Y., Keppler-Noreuil, K. M., Sapp, J., Crenshaw, M., Finch, N. C. A., et al. (2015). A point mutation in PDGFRB causes autosomal-dominant penttinen syndrome. *Am. J. Hum. Genet.* 97, 465–474. doi: 10.1016/j.ajhg.2015.07.009

Klinghoffer, R. A., Hamilton, T. G., Hoch, R., and Soriano, P. (2002). An allelic series at the PDGFαR locus indicates unequal contributions of distinct signaling pathways during development. *Dev. Cell* 2, 103–113. doi: 10.1016/S1534-5807(01)00103-4

Levéen, P., Pekny, M., Gebre-Medhin, S., Swolin, B., Larsson, E., and Betsholtz, C. (1994). Mice deficient for PDGF B show renal, cardiovascular, and hematological abnormalities. *Genes Dev.* 8, 1875–1887. doi: 10.1101/gad.8.16.1875

Mayor, R., and Theveneau, E. (2013). The neural crest. *Development* 140, 2247–2251. doi: 10.1242/dev.091751

McCarthy, N., Liu, J. S., Richarte, A. M., Eskiocak, B., Lovely, C. B., Tallquist, M. D., et al. (2016). Pdgfra and Pdgfrb genetically interact during craniofacial development. *Dev. Dyn.* 245, 641–652. doi: 10.1002/dvdy.24403

Mo, J., Long, R., and Fantauzzo, K. A. (2020). *Pdgfra* and *Pdgfrb* genetically interact in the murine neural crest lineage to regulate migration and proliferation. bioRxiv [Preprint]. doi: 10.1101/2020.07.29.227306

Morrison-Graham, K., Schatteman, G. C., Bork, T., Bowen-Pope, D. F., and Weston, J. A. (1992). A PDGF receptor mutation in the mouse (Patch) perturbs the development of a non-neuronal subset of neural crest-derived cells. *Development* 115, 133–142.

Muzumdar, M. D., Tasic, B., Miyamichi, K., Li, N., and Luo, L. (2007). A global double-fluorescent cre reporter mouse. *Genesis* 45, 593–605. doi: 10.1002/dvg.20335

Orr-Urtreger, A., and Lonai, P. (1992). Platelet-derived growth factor-a and its receptor are expressed in separate, but adjacent cell layers of the mouse embryo. *Development* 115, 1045–1058.

Parker, S. E., Mai, C. T., Canfield, M. A., Rickard, R., Wang, Y., Meyer, R. E., et al. (2010). Updated national birth prevalence estimates for selected birth defects in the United States, 2004-2006. *Birth Defects Res. A. Clin. Mol. Teratol.* 88, 1008–1016. doi: 10.1002/bdra.20735

Rattanasopha, S., Tongkobpetch, S., Srichomthong, C., Siriwan, P., Suphapeetiporn, K., and Shotelersuk, V. (2012). PDGFRa mutations in humans with isolated cleft palate. *Eur. J. Hum. Genet.* 20, 1058–1062. doi: 10.1038/ejhg.2012.55

Richarte, A. M., Mead, H. B., and Tallquist, M. D. (2007). Cooperation between the PDGF receptors in cardiac neural crest cell migration. *Dev. Biol.* 306, 785–796. doi: 10.1016/j.ydbio.2007.04.023

Sandell, L. L., Kurosaka, H., and Trainor, P. A. (2012). Whole mount nuclear fluorescent imaging: convenient documentation of embryo morphology. *Genesis* 50, 844–850. doi: 10.1002/dvg.22344

Schmahl, J., Rizzolo, K., and Soriano, P. (2008). The PDGF signaling pathway controls multiple steroid-producing lineages. *Genes Dev.* 22, 3255–3267. doi: 10.1101/gad.1723908

Soriano, P. (1994). Abnormal kidney development and hematological disorders in PDGF beta-receptor mutant mice. *Genes Dev.* 8, 1888–1896. doi: 10.1101/gad.8.16.1888

Soriano, P. (1997). The PDGF alpha receptor is required for neural crest cell development and for normal patterning of the somites. *Development* 124, 2691–2700.

Takenouchi, T., Yamaguchi, Y., Tanikawa, A., Kosaki, R., Okano, H., and Kosaki, K. (2015). Novel overgrowth syndrome phenotype due to recurrent de novo PDGFRB mutation. *J. Pediatr.* 166, 483–486. doi: 10.1016/j.jpeds.2014.10.015

Tallquist, M. D., and Soriano, P. (2003). Cell autonomous requirement for PDGFRalpha in populations of cranial and cardiac neural crest cells. *Development* 130, 507–518. doi: 10.1242/dev.00241

Trainor, P. A. (2005). Specification of neural crest cell formation and migration in mouse embryos. *Semin. Cell Dev. Biol.* 16, 683–693. doi: 10.1016/j.semcdb.2005.06.007

Vasudevan, H. N., Mazot, P., He, F., and Soriano, P. (2015). Receptor tyrosine kinases modulate distinct transcriptional programs by differential usage of intracellular pathways. *elife* 4:e07186. doi: 10.7554/eLife.07186

Vasudevan, H. N. N., and Soriano, P. (2014). SRF regulates craniofacial development through selective recruitment of MRTF cofactors by PDGF signaling. *Dev. Cell* 31, 332–344. doi: 10.1016/j.devcel.2014.10.005

Conflict of Interest: The authors declare that the research was conducted in the absence of any commercial or financial relationships that could be construed as a potential conflict of interest.

frontiers in Physiology

REVIEW
published: 25 November 2020
doi: 10.3389/fphys.2020.586432

In vivo Neural Crest Cell Migration Is Controlled by "Mixotaxis"

Elias H. Barriga[1] and Eric Theveneau[2]**

[1] Mechanisms of Morphogenesis Lab, Instituto Gulbenkian de Ciência, Oeiras, Portugal, [2] Centre de Biologie du Développement (CBD), Centre de Biologie Intégrative (CBI), Université de Toulouse, CNRS, UPS, Toulouse, France

Directed cell migration is essential all along an individual's life, from embryogenesis to tissue repair and cancer metastasis. Thus, due to its biomedical relevance, directed cell migration is currently under intense research. Directed cell migration has been shown to be driven by an assortment of external biasing cues, ranging from gradients of soluble (chemotaxis) to bound (haptotaxis) molecules. In addition to molecular gradients, gradients of mechanical properties (duro/mechanotaxis), electric fields (electro/galvanotaxis) as well as iterative biases in the environment topology (ratchetaxis) have been shown to be able to direct cell migration. Since cells migrating *in vivo* are exposed to a challenging environment composed of a convolution of biochemical, biophysical, and topological cues, it is highly unlikely that cell migration would be guided by an individual type of "taxis." This is especially true since numerous molecular players involved in the cellular response to these biasing cues are often recycled, serving as sensor or transducer of both biochemical and biophysical signals. In this review, we confront literature on *Xenopus* cephalic neural crest cells with that of other cell types to discuss the relevance of the current categorization of cell guidance strategies. Furthermore, we emphasize that while studying individual biasing signals is informative, the hard truth is that cells migrate by performing a sort of "mixotaxis," where they integrate and coordinate multiple inputs through shared molecular effectors to ensure robustness of directed cell motion.

Keywords: directed cell migration, neural crest, morphogenesis, durotaxis, chemotaxis, galvanotaxis, electrotaxis, mixotaxis

OPEN ACCESS

Edited by:
Lisa Taneyhill, University of Maryland, College Park, United States

Reviewed by:
Shuyi Nie, Georgia Institute of Technology, United States
Anand Chandrasekhar, University of Missouri, United States

****Correspondence:***
Elias H. Barriga
ebarriga@igc.gulbenkian.pt
Eric Theveneau
eric.theveneau@univ-tlse3.fr

Specialty section:
This article was submitted to Craniofacial Biology and Dental Research, a section of the journal Frontiers in Physiology

Received: *23 July 2020*
Accepted: *03 November 2020*
Published: *25 November 2020*

Citation:
Barriga EH and Theveneau E (2020) In vivo Neural Crest Cell Migration Is Controlled by "Mixotaxis". Front. Physiol. 11:586432. doi: 10.3389/fphys.2020.586432

INTRODUCTION

Finding a solution to trigger directed cell migration is simple. An external signal that cells can interpret needs to be spatially organized. Then, cells can use that signal to generate a front–rear polarity allowing directional movement along that cue. Very much like drivers following road signs. Many inputs (e.g., chemical, mechanical, electrical, topological) can be shown to fulfill this function in controlled and simplified experiments (Zhao et al., 2006; Capuana et al., 2020; Zhu et al., 2020). However, living systems were not engineered by a designer to strictly follow a set of specifications in a logical manner that is then validated by external quality controls. Instead, *in vivo* migrating cells are often exposed to an overwhelming range of inputs which may at best appear to have no obvious hierarchy and at worst to be contradictory. Yet, the migratory response of cells to such convoluted environments is still logical. In addition, each polarity cue may not be as neatly organized as it would in an *in vitro* assay. Further, some cells may display a given migratory

behavior while their neighboring tissues do not. Hence, there may be cooperation, coordination and/or competition between directionally migrating cells and the activities of their neighbors. Furthermore, a given input may lead to different responses in different cell populations within the same time window indicating that the directional information is not carried by the signal itself but generated as a result of the interplay between cells and a given signal or set of signals (we discuss examples hereafter). This can be equated to how geneticists view the phenotype as a result of the interaction between a genotype and the local environment of an organism. Yet, for cells willing to undertake directed migration, it all comes down to two simple facts: (i) cells need to propel themselves and (ii) establish and sustain a front–rear polarity. This means that all inputs have to be somewhat integrated by a cell for a directional behavior to emerge. In groups of cells, intercellular communication may in addition lead to emerging properties such that what a cell collective does may differ from what a single cell would do in a similar context (Theveneau et al., 2010). Hence, unveiling the mechanisms that control directed cell migration in its full complexity could have countless impacts in our understanding of intricate morphogenetic events. In addition, a more integrative approach to directed cell migration would help designing effective ways to hinder cancer metastasis, improve wound healing or contribute to new methods for *ex vivo* organ patterning in the context of regenerative medicine. In this review, we used the Xenopus cephalic neural crest (NC) cells, an embryonic stem cell population that collectively and directionally migrates (Gouignard et al., 2018), as an example to discuss the complexity of the control of directed cell migration. We address first how motility is initiated in NC cells before discussing the strategies displayed by cells in order to bias their motion and perform directed cell migration. Drawing parallels between NC results and findings about directed cell migration in other cell types, we propose some working hypotheses for signal integration and the emergence of directional motion.

THE NEURAL CREST, EMT, AND THE ONSET OF CELL MOTION

NC are induced during mid to late gastrulation stages at the interface between the neural and non-neural ectoderm and between the epidermis and mesoderm (**Figure 1**). They later leave the dorsal neuroepithelium to collectively migrate throughout the developing embryo. Anterior NC cells make an outstanding contribution to the head morphology and sensory structures by providing cartilage and bones, meninges that surround the brain, smooth, and striated muscle cells and tendons as well as pigments cells among other structures (Dupin et al., 2006). In addition, NC cells cooperate with placodal cells to form the cephalic peripheral nervous system (Theveneau and Mayor, 2011). Cranial placodes are discrete thickenings of the ectoderm that produce some of the neurons that in turn form the cranial ganglia (Schlosser, 2014). The rest of the neurons and the glial cells are provided by the cephalic NC cells (Theveneau and Mayor, 2011). NC cells are an extremely powerful model to investigate cell migration. Their timing and pattern of migration has been documented in multiple species allowing comparative studies (Theveneau and Mayor, 2012). In chicken, mice and Xenopus embryos, NC cells can be manipulated *in vivo* and *ex vivo*, thanks to well-defined culture conditions. This has allowed researchers to perform in-depth cell and molecular biology studies. Whereas in genetically tractable species (e.g., zebrafish and mouse), transgenic lines have been generated for long-term observation and targeted molecular manipulation of these cells. In addition, the first part of NC cell migration occurs superficially, especially in cephalic regions, permitting direct observation of cell behavior by time-lapse cinematography in fish, chick or amphibians.

The first step toward directed motion is for cells to acquire motile capabilities. NC cells initiate migration by undergoing epithelial-mesenchymal transition (EMT). EMT leads to a qualitative and quantitative remodeling of adhesive properties, cytoskeleton dynamics and cell polarity such that cells have transient adhesions to one another, display faster membrane dynamics and go from apicobasal polarity associated with epithelial state to a front–rear polarity associated with motility. EMT is performed by a series of non-obligatory steps such that cells that initiate EMT do not systematically complete it (Yang et al., 2020) and is reversible (Pei et al., 2019). EMT in Xenopus NC cells is better described as a partial EMT with cells migrating at high cell density with frequent transient physical contacts via functional adherens junctions, as recently discussed (Gouignard et al., 2018).

Canonical EMT is controlled by an array of transcription factors whose expression is detected many hours before NC migration is initiated. In *Xenopus*, cephalic NC migration starts around stage 19–20 when the neural folds closure nears completion to form the neural tube. Nonetheless, the expression of key EMT transcriptional regulators such as Snail2 or Twist1 starts in NC cells at stages 12 and 14, respectively. One of the main targets of these factors is the cell–cell adhesion receptor E-cadherin (CDH-1) whose expression only starts to decrease in the NC at around stage 17.5 (Scarpa et al., 2015), suggesting that Snail2 and Twist1 may not be recruited to the E-cadherin promoter or that they may not even be active until stage 17.5. One way to control transcription factors' activity is to regulate their entry into the nucleus. Intriguingly, in mammalian cell lines, Twist has been shown to be imported to the nucleus when cells are exposed to stiff substrates (Wei et al., 2015; Fattet et al., 2020). In this situation, EphA2 is activated in a ligand-independent manner and leads to the phosphorylation of Twist via LYN kinase. This frees Twist from its cytoplasmic anchor G3BP2 and allows it to enter the nucleus. This is particularly interesting in the context of NC development because the onset of NC migration in Xenopus has been linked to the local increase of stiffness underneath the cephalic crest generated by the convergent extension movement of the mesoderm toward the midline of the embryo (Barriga et al., 2018). In addition, Twist expression is under the control of the Hif signaling pathway which also controls the expression of CXCR4, the receptor for the chemokine CXCL12/Stromal cell-derived factor 1 (Sdf1) (Barriga et al., 2013). Interestingly, in renal carcinoma cells, Hif1α and CXCR4 have been shown to take part in a feed forward

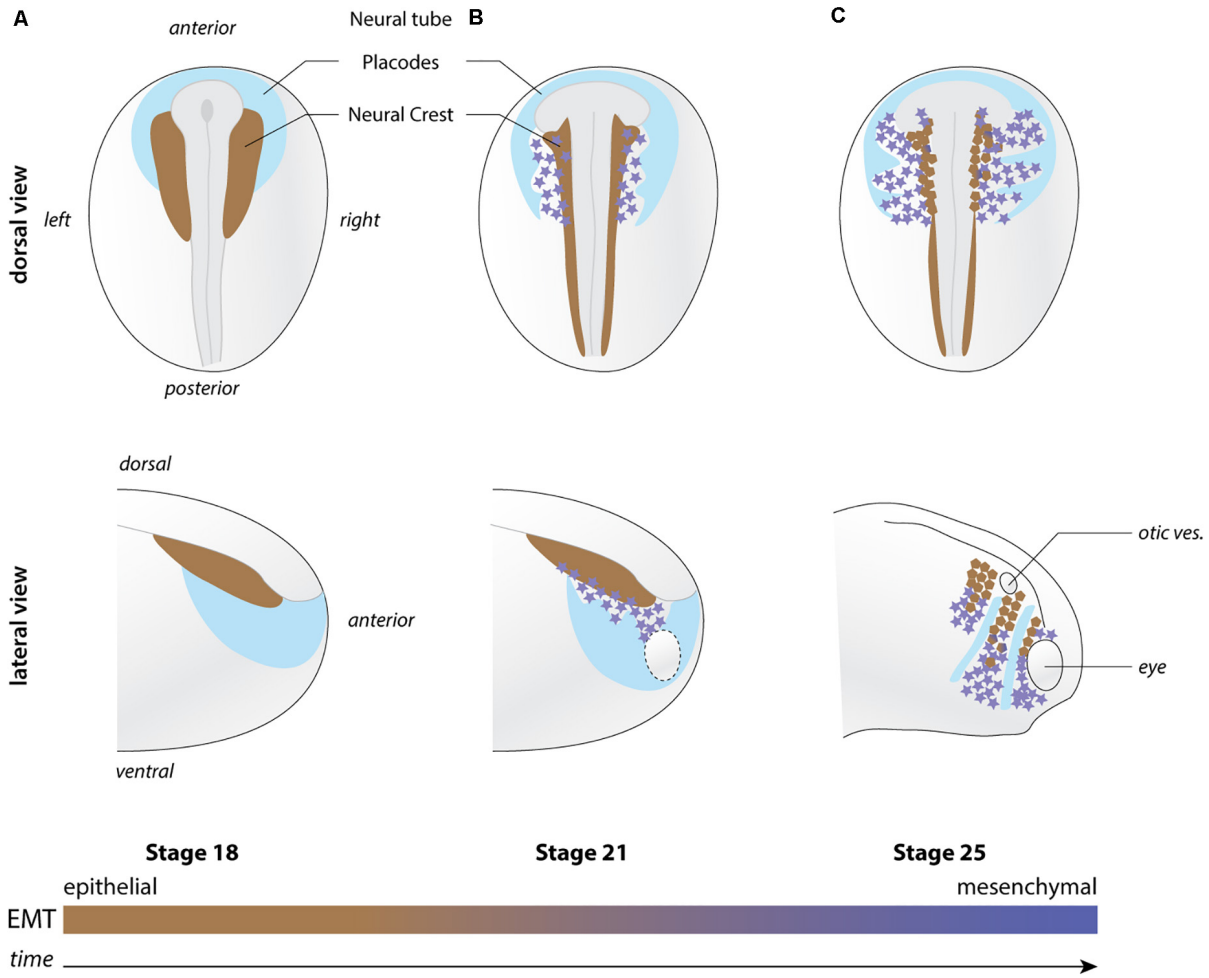

FIGURE 1 | Overview of neural crest migration. **(A–C)** Diagrams depicting the position of NC cells (shades of brown to magenta) with respect to the placodal region (light blue) at pre-migration (stage 18), early migration (stage 21), and late migration (stage 25). EMT is progressively implemented as NC migration proceeds. Brown NC cells are more epithelial while magenta star-shaped NC cells are more mesenchymal. Top and bottom rows shows lateral views and dorsal views, respectively. Orientations and structures are indicated on the figure. Ot. ves., otic vesicle.

loop for nuclear translocation such that, via a direct physical interaction between the two proteins, nuclear accumulation of CXCR4 favors entry of HIF-1α and HIF-1α then further promotes CXCR4 expression (Bao et al., 2019). Thus, one can propose a model in which Hif-1α primes NC cells for EMT and directional migration by regulating Twist and CXCR4 expressions until mesoderm stiffness reaches a threshold suitable for migration. Twist1 is not the main and certainly neither the only EMT-associated NC transcription factor, however, to date it is the most likely candidate to mediate a "rapid" response to environmental cues. Another example is that of Sox10, this transcription factor constantly shuttles between the nucleus and the cytoplasm and docks at the surface of mitochondria (Rehberg et al., 2002; Mou et al., 2009). However, experimental assessment of Sox10's function ties it to lineage decisions rather than NC migration in Xenopus (Aoki et al., 2003; Honore et al., 2003). Whether Sox10's nuclear localization is also mechanically controlled remains to be explored. In any case, controlling the emergence of cell motility does not explain directionality *per se*. Such cell intrinsic motility needs to be iteratively biased to sustain directed motion. The rest of this review is dedicated to the various cues that might bias NC directed motion.

CHEMOTAXIS

The directional migration of NC cells could be explained by chemotaxis, the ability of cells to follow gradients of soluble guidance cues (**Figure 2a**). As mentioned, NC and placodes cooperate to form the cephalic peripheral nervous system. Interestingly, NC and placodes interact early on during head morphogenesis and this interaction is crucial for directional migration of NC cells (Culbertson et al., 2011; Theveneau et al., 2013). Prior to the onset of NC migration, NC and placodes are located in adjacent domains of the lateral ectoderm. NC are on either side of the neural plate and the placodes are surrounding

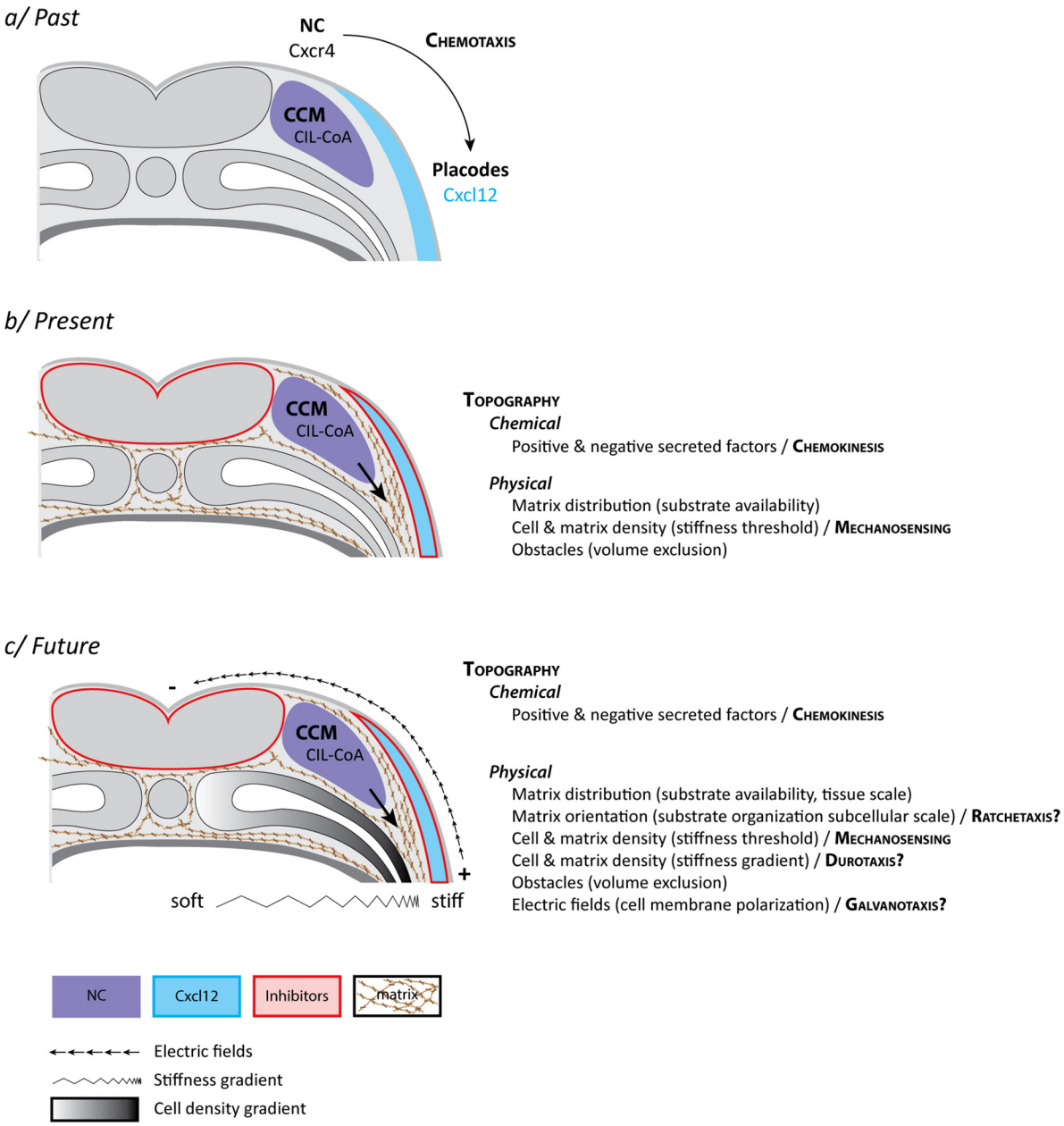

FIGURE 2 | Neural crest "mixotaxis." **(a)** The classical view of cephalic NC cell directed cell migration in *Xenopus laevis*. NC cells become motile via EMT and exhibit a collective behavior [collective cell migration (CCM)] due to a balance between dispersion (CIL) and mutual attraction (or co-attraction, CoA). Placodes, located in the lateral ectoderm, produce CXCL12, a well-known chemoattractant. NC cells express the main CXCL12 receptor, Cxcr4. NC are migrating toward latero-ventral territories due to CXCL12-dependent chemotaxis. **(b)** The current view of cephalic NC cell directed cell migration in *Xenopus laevis* in which CXCL12, by promoting cell-matrix adhesion, contributes to defining permissive areas for cell migration in the context of a biased distribution of topological features. These include chemical and physical cues and requires a minimal stiffness of the surrounding tissue for cell migration to proceed. The main difference with the classical view is that precise and biased spatial distribution of secreted molecules is dispensable. **(c)** A speculative view of what the actual control of cephalic NC cell directed cell migration in *Xenopus laevis* might look like with the inclusion of additional features such as a hypothetical graded distribution of stiffnesses (Durotaxis) and electric fields (Galvanotaxis) at tissue scale as well as iterative biases in topography at cellular and subcellular scales (Ratchetaxis). While most of these features can be experimentally disentangled under controlled *ex vivo* experiments, none of these cues relies on a specific set of molecular sensors and effectors but rather share downstream signal transduction machineries leading to cell adhesion and polarity. Therefore, *in vivo*, each input (e.g., chemical, mechanical, electrical) is likely to extensively feed into the others leading to the exciting idea that, in their native environment, NC cells may achieve directed migration by performing a sort of "mixotaxis." See main text for details.

the NC domains and the anterior neural plate, forming a horseshoe-shaped zone (**Figure 1**). Placodes secrete CXCL12 that promotes cell-matrix adhesion and motility via activation of Rac1 in NC cells (Theveneau et al., 2010, 2013; Bajanca et al., 2019). The presence of this chemokine stimulates migration such that NC move toward the CXCL12-producing placodes. When NC cells and placodes make a physical contact they exhibit contact-inhibition of locomotion (CIL), an active repolarization process upon cell–cell contact that leads to cells moving away from each other (Stramer and Mayor, 2017). However, placodes and NC cells do not have the same migratory capabilities. Placodes at this stage are epithelial, located in the deep layer of the ectoderm and are barely motile. NC cells being more active, they are systematically the ones filling local gaps between cells generated by the CIL response. This creates a bias that favors lateral migration of the crest cells toward the placode domain. Thus, once NC migration is initiated there is a progressive shift of the placodal cells laterally/ventrally that displaces the source of CXCL12. This has been proposed to generate a feed forward loop driving directed movement of both cell populations from medial to lateral (Theveneau et al., 2013; **Figure 1**). At first glance, this mechanism explains the directional movement of the NC cells and the progressive redistribution of placodes during head morphogenesis via a combination of CXCL12-dependent chemotaxis and heterotypic contact-inhibition between NC and placodes. So, what is missing?

There are several caveats. First, we infer lots of *in vivo* directional migratory behaviors and mechanisms (chemotaxis, haptotaxis, ratchetaxis, durotaxis) from *in vitro* data which in general show that cells have the ability to interpret and follow such signals. Nonetheless, clear demonstration of their actual implication in directed cell migration *in vivo* is tough, owing to the complex nature of native environments. Some of these directional cues are also not easy to distinguish from one another. In particular, it is difficult to assess whether cells undergo chemotaxis (soluble signal) vs. haptotaxis (bound signal) *in vivo*. For instance, CXCL12 and VEGFA, common examples of putative NC chemotactic cues (McLennan et al., 2010; Theveneau et al., 2010), are capable of binding to the extracellular matrix and we still do not understand whether their physiological relevance is linked to a soluble or a bound state. Also, graded distribution of a signal is not a proof that cells are detecting it or reading it. In the case of CXCL12 and VEGFA such unequivocal proof of graded distribution of the protein along migratory paths has not been obtained. Moreover, while CXCL12 is a powerful chemotactic factor for NC *in vitro* (Theveneau et al., 2010), its spatial distribution is dispensable *in vivo* as it primarily acts by promoting adhesion to the extracellular matrix rather than giving clear direction to the cells (Bajanca et al., 2019). This has been demonstrated by showing that *in vivo* directed NC migration can occur in the absence of CXCL12/CXCR4 signaling if Rac1 is homogenously and iteratively activated in NC cells to allow for cell-matrix adhesions to form (Bajanca et al., 2019). This suggests that CXCR4-CXCL12 may work as a chemokinetic factor (promoting motility via cell-matrix adhesion) rather than a chemotactic one (biasing directionality). If CXCR4-CXCL12 signaling does not provide a directional bias what are the mechanisms ensuring sustained directed motion and how does CXCR4-CXCL12 integrate with them?

DUROTAXIS

Durotaxis is the directed motion of cells according to local gradients of rigidity (stiffness) with cells moving from compliant to rather stiff regions of a given substrate (Lo et al., 2000). For example, in Xenopus, cell proliferation drives local changes in brain tissue stiffness, creating local gradient that are followed by axons of developing neurons (Thompson et al., 2019). Given that NC cells are able to sense differences in rigidity and that stiffness of the underlying mesoderm is a key factor for the initiation of NC migration (Barriga et al., 2018), one could also propose that there might be a gradient from dorsal to ventral promoting stiffness-dependent directional migration. The main driver of this observed increase of stiffness is the local accumulation of mesodermal cells underneath the NC domain (Barriga et al., 2018). In the trunk, the medio-dorsal mesoderm aggregates as somites and thus is denser than the ventro-lateral mesoderm (**Figure 2**). Therefore, if there is a cell density associated gradient of mesoderm stiffness it would be oriented ventro-dorsally which is opposite to the direction of trunk NC migration. In the head, where mesoderm does not form somites, such spatial distribution of cell density and stiffness has not been assessed so far. Though, published data suggest that the emergence of such a gradient is unlikely owing to the high degree of mechanical heterogeneities observed in that region (Barriga et al., 2018). Yet, even if true, such gradient of stiffness leading to durotaxis could not be seen as an absolute signal that would restrict any kind of cell movement in a dorsoventral manner. While cephalic NC cells are migrating ventralward, the surface ectoderm is moving dorsalward to accompany dorsal neural tube closure. In addition, myeloid cells (macrophages) are undergoing random migration from the cardiac region to survey the entire developing embryo (Agricola et al., 2016). Myeloid cells migrate as single cells, display extensive dispersion, and cross areas that NC cells are completely unable to use. Thus, during head morphogenesis, there are concomitant migration events (e.g., epidermis, neural crest, myeloid cells) that follow different directions despite sharing a common environment. This highlights the importance of considering the interaction between cells and the environment as the main driver of cell behavior rather than intrinsic cell motility.

Mechanosensing of the substrate requires functional cell-matrix adhesions. Thus, in NC cells, the putative distinction between durotaxis and chemotaxis/chemokinesis downstream of CXCR4 is further blurred by the fact that CXCL12 regulates cell-matrix adhesion (Bajanca et al., 2019). This does not mean that CXCR4 is involved in mechanosensing in NC cells. Instead, we could see CXCR4 signaling as priming cells to undergo mechanosensing by allowing them to functionally interact with the matrix. Interestingly, cell-matrix adhesion in cephalic NC cells also involves cadherins (Huang et al., 2016; Langhe et al., 2016). There is an indirect role such that contact-dependent cell polarity primes NC cells to respond to CXCR4 signaling

(Theveneau et al., 2010). But there is also a direct role of cadherins. During migration, inhibiting E-cadherin affects adhesion to fibronectin rather than cell–cell adhesion (Huang et al., 2016) and cadherin-11 actively contributes to the formation of focal adhesion (Langhe et al., 2016). This means that we should regard EMT as a way to coordinate the quantitative and qualitative changes in cell–cell and cell-matrix adhesions rather than as a mechanism for cell dispersion in which loss of cell–cell adhesion and motility would be regulated in parallel and as purely cell autonomous properties.

Cadherins take part in regulating cell-matrix adhesions (directly and indirectly) and cell-matrix adhesions are needed to sense substrate stiffness. In turns, when substrate stiffness reaches a threshold it promotes Twist nuclear entry which favors cadherin repression. One wonders about the molecular control of such intricate feedback loops. It could also mean that what has been labeled as CXCR4-dependent chemotaxis might be part of a global change of adhesive property taking place during EMT that prepares cells for efficient stiffness sensing. The existence of stiffness gradients around the cephalic NC cells is still highly speculative. But do cells need such spatially organized mechanical cue to promote directed movement? If so, how could we distinguish durotaxis from the so-called chemotaxis?

CONFINEMENT, TOPOLOGICAL BIASES, AND RATCHETAXIS

During EMT, cells pass from stable to transient cell–cell adhesions and this favors cell dispersion *in vitro*. This is further accentuated by CIL that biases cell's front–rear polarity such that cells move away from cell–cell contacts. However, *in vivo*, cephalic NC cells migrate at high cell density and do not undertake widespread dispersion despite EMT and CIL. The reason for this is that NC cells actively sense and follow each other via complement factor C3a signaling (Carmona-Fontaine et al., 2011) and are constrained by their surrounding tissues physically and chemically (Szabo et al., 2016). When NC cells initiate migration, there are several epithelial structures around them such as the neural plate/tube, the eye, the epidermis, and the cranial placodes. Placodes, as discussed above, are slowly displaced by NC cells such that they organize as discrete structures forming dorsoventral corridors restricting NC migration (**Figure 1**). This is reinforced by the fact that placodes are also the source of negative regulators of NC motility such as semaphorins rendering their vicinity non-permissive for migration (Yu and Moens, 2005; Bajanca et al., 2019). Interestingly, physical and chemical confinement together with intrinsic motility, CIL and mutual attraction are sufficient to drive directed NC migration even in absence of a stiffness gradient or a chemotactic cue (Szabo et al., 2016; Szabó et al., 2019).

Another putative level of signaling interplay in this context is related to the fact that CXCR4 can physically interact with C3aR, the receptor of C3a, the chemokine mediating NC cell gregarious behavior (Carmona-Fontaine et al., 2011). C3 signaling can enhance CXCR4 signaling and both receptors colocalize in lipid rafts (Honczarenko et al., 2005; Ratajczak et al., 2006; Wysoczynski et al., 2007). Interestingly, lipid rafts are mechanosensitive (Fuentes and Butler, 2012). Thus, stiffness of the mesoderm underlying cephalic NC cells may also modulate a putative C3aR/CXCR4 cooperative signaling by promoting lipid raft remodeling. C3a-dependent mutual attraction increases the likelihood of transient cell–cell contacts. These contacts are known to block Rac1 activity at the site of transient junctions but also to promote an overall increase of Rac1 level in the cells (Theveneau et al., 2010; Carmona-Fontaine et al., 2011). In addition, CXCR4 also promotes Rac1 activity and Rac1 is a key factor in protrusion and focal adhesion formation in cephalic NC cells (Theveneau et al., 2010). Thus, a lack of mutual attraction might also reduce the ability of NC cells to sense substrate stiffness (by lowering the ability to polarize and form cell-matrix adhesions) and might act a selection mechanism to prevent extensive migration of cells that are unable to properly interact with one another. A similar hypothesis could be drawn from the fact that N-cadherin-deficient cephalic NC cells disperse better *in vitro* but fail to polarize efficiently, do not migrate extensively *in vivo* and show signs of weaker cell-matrix adhesion (Kuriyama et al., 2014). This is even more relevant knowing that, in other cells, N-cadherin junctions can be regulated by the association of N-cadherin with lipid rafts and F-actin (Causeret et al., 2005). Thus, cross-regulating cell–cell interaction (N-cadherin and C3) and cell-matrix adhesion (Rac1, CXCR4) in a stiffness-dependent manner during collective cell migration may be a robust way to ensure that only functional cells can efficiently travel together to their final location.

Another level of integration could be mediated by proteases. Xenopus NC cells express Matrix Metalloproteinase MMP14 (a.k.a. MT1-MMP) (Tomlinson et al., 2009; Garmon et al., 2018). Interestingly, MMP14 can cleave Fibronectin (Shi and Sottile, 2011) the main substrate of cephalic NC migration but also inactivates CXCL12 by removing a few of its N-terminal aminoacid (McQuibban et al., 2001). This is even more interesting knowing that CXCL12 exhibit a high binding affinity for Fibronectin (Pelletier et al., 2000). Therefore, Xenopus cephalic NC cells could use MMP14 to remodel Fibronectin (e.g., organization, density), release CXCL12 from the matrix (haptotaxis vs. chemotaxis/chemokinesis) and inactivate CXCL12. This would further crosslink CXCR4-dependent cell-matrix adhesion with mechanosensing and blurs the lines between chemo and haptotaxis.

Xenopus cephalic NC cells are clearly exposed to a topologically biased environment at the onset of migration favoring ventralward migration. The medial part of the embryo with the neural plate/tube acting as an epithelial obstacle which releases several inhibitors of migration and a lower content in fibronectin than the lateral regions (Bajanca et al., 2019) is definitively an unfavorable territory for migration. However, it is unclear if *in vivo* cells experience repeated geometrical or mechanical anisotropy in environment organization known to generate ratchetaxis (Caballero et al., 2015). A more relaxed view of this concept relies on repeated topological anomalies (e.g., repetition of narrow and large spaces) that cells have to cross (Reversat et al., 2020). An important difference

between topological bias and confinement as discussed above and ratchetaxis or its declinations is the scale at which these mechanisms act. The aforementioned chemical/physical topological bias acts at tissue scale, defining broad domains that are unsuitable for migration, whereas ratchetaxis occurs as the single cell level or subcellular level biasing individual cell polarity and cytoskeleton dynamics. We currently do not have tools to investigate whether ratchetaxis and the likes are indeed physiologically relevant for Xenopus NC cell migration. A detailed analysis of extracellular matrix composition and organization over time as well as a clear quantification of the roughness index of the NC migratory environment would need to be performed with modern tools. Even if repeated topological biases at microscopic scale would be observed it is unclear how such biases would be implemented and maintained in 4D throughout head morphogenesis to sustain directed NC migration over time. In addition to MMP14 discussed above, MMP2, 3, 7, 9, 11, 13, 15, 16, 18, 20, 24, and 28, as well as multiple ADAMs, are expressed by cephalic NC cells or produced by the environment they cross during migration (see Christian et al., 2013, Table 1 in Gouignard et al., 2020 and references therein). Thus, in this context, the likelihood of relatively stable and iteratively distributed topological or mechanical cue (a requirement for ratchetaxis) along the dorsoventral path of cephalic NC migration appears quite low.

GALVANO/ELECTROTAXIS

Another mechanism that can generate directed cell motion is the detection of electric fields, known as galvanotaxis (or electrotaxis). Interestingly, in mammalian cell lines, lipid rafts were shown to take part in galvanotaxis (Lin et al., 2017) and electric fields also affect the GSK3β-dependent polarization of the Golgi apparatus (Cao et al., 2011) which helps organizing the non-centrosomal microtubule network, a key player in front–rear cell polarity (Meiring et al., 2020). GSK3β is required for cephalic NC migration in Xenopus (Gonzalez Malagon et al., 2018) and is a known regulator of Snail cytoplasmic-nuclear shuttle (Muqbil et al., 2014). Thus, by regulating C3aR/CXCR4 carrying lipid rafts and GSK3β, electric fields might be acting on multiple levels during Xenopus NC cell migration: EMT, front-rear polarity, cell–cell, and cell-matrix adhesions. The ability of trunk NC cells to undergo galvanotaxis was shown using quail, Xenopus and axolotl embryos trunk neural tube explants *in vitro*, which were sometimes cultured for days before fields were applied (Stump and Robinson, 1983; Cooper and Keller, 1984; Nuccitelli and Smart, 1989; Gruler and Nuccitelli, 1991; Nuccitelli et al., 1993). However, to our knowledge, electrotaxis has not been assessed in primary cephalic Xenopus NC cell culture. Some of the behaviors described in the literature appear to be somewhat artefactual with cells permanently elongated perpendicularly to the applied field. One of the reason may be the strengths of the applied electric fields used ranging from 100 to 600 mV/mm (Nuccitelli and Erickson, 1983; Cooper and Keller, 1984) which are 4–22 times higher than what has been measured *in vivo* in Xenopus (Hotary and Robinson, 1994). Indeed, from early in development, the Xenopus embryo has a transepithelial potential and electrical currents (Hotary and Robinson, 1994). An anteroposterior gradient is detected from the blastopore and applying electric fields to nullify it led to developmental defects such as failure of anterior neural tube closure and reduced head development. Noticeably, it led to expulsion of cells from the blastopore which might indicate that the anteriorward displacement of mesoderm is partially affected. Given that this movement is crucial to generate a stiff environment for cephalic NC cells to migrate (Barriga et al., 2018), one could propose that the observed head defects in embryos with nullified electric fields might be due to a partial failure of cephalic NC migration linked to improper mesoderm development. As for the other putative guiding mechanisms discussed, electric fields will not be a one-size-fit-all cue. While most cell types exposed to electric fields seem to migrate toward the cathode, some, such as macrophages, seem to prefer the anode (Sun et al., 2019). Also, as discussed for the other taxis, some of the cellular structures required for sensing and implementation of a polarity bias at the single cell level are not specific to electric fields as an input (e.g., lipid rafts, cell surface receptors).

CONCLUSION

All these interplays are mind blowing and place us, as experimentalists, in a chicken and egg situation. Hierarchy between signals and pathways is difficult to dissect because of the numerous cross-regulations taking place during migration itself. Exposure to chemokines is needed for cell-matrix adhesion. Cell-matrix adhesions are needed for motility and mechanosensing. Mechanosensing controls nuclear shuttling of transcription factors. These factors control expression of adhesion molecules and cytoskeleton components which in turn feedback into cell polarity, etc. Therefore, rather than being driven by competing guidance strategies, cephalic NC cells seem to iteratively use the molecular machinery of cell motility and adhesion to read the various signals at their disposal. This blurs the lines between the different kinds of taxis even if for most of them the initial cue is clearly identifiable (e.g., chemokine, rigidity, electric field). This may mean that an understanding of the complexity of an *in vivo* morphogenetic process such as NC cell migration requires a systems biology approach with contribution from multiple disciplines to integrate studies in which cues, genes or pathways are handled one at a time. We can think of it as studying the role that each individual LEGO piece plays in forming a bigger structure. Taking a single piece out is extremely powerful to gather information about it. However, at some point, one needs to try to fit all pieces together. The added difficulty is that in the regulation of *in vivo* cell migration each LEGO piece has melted and started to blend with several of its direct neighbors.

Our aim with this review is to raise awareness about artificial distinctions between supposedly different modes of cell guidance.

In that context, we (as a community of NC researchers) should always keep in mind that the signal we are looking at in a given project may actually influence other inputs. The reason for that is that NC cells are exposed to multiple signals and may have evolved to use them all at once, not one by one. That is already a fact based on published data but we probably underestimate it. Thus, we might need to systematically assess what knocking down one input does "outside" of its expected canonical function and with that in mind, design appropriate controls for our experimental approaches. We believe that the point we are making here invites the field to leave the current comfort zone and to address directed cell migration both in the context where it takes place and with the complexity it deserves.

AUTHOR CONTRIBUTIONS

EB and ET designed and wrote the review. Both authors contributed to the article and approved the submitted version.

FUNDING

Work in ET lab was supported by Fondation pour la Recherche Medicale (FRMAJE201224), the Midi-Pyrenees Regional Council (grant 13053025), and the CNRS and Universite Paul Sabatier. EB was supported by a La Caixa Junior Leader grant (94978) and by Calouste Gulbenkian Foundation I-411133.01.

REFERENCES

Agricola, Z. N., Jagpal, A. K., Allbee, A. W., Prewitt, A. R., Shifley, E. T., Rankin, S. A., et al. (2016). Identification of genes expressed in the migrating primitive myeloid lineage of Xenopus laevis. *Dev. Dyn.* 245, 47–55. doi: 10.1002/dvdy.24314

Aoki, Y., Saint-Germain, N., Gyda, M., Magner-Fink, E., Lee, Y. H., Credidio, C., et al. (2003). Sox10 regulates the development of neural crest-derived melanocytes in Xenopus. *Dev. Biol.* 259, 19–33. doi: 10.1016/s0012-1606(03)00161-1

Bajanca, F., Gouignard, N., Colle, C., Parsons, M., Mayor, R., and Theveneau, E. (2019). In vivo topology converts competition for cell-matrix adhesion into directional migration. *Nat. Commun.* 10:1518.

Bao, Y., Wang, Z., Liu, B., Lu, X., Xiong, Y., Shi, J., et al. (2019). A feed-forward loop between nuclear translocation of CXCR4 and HIF-1alpha promotes renal cell carcinoma metastasis. *Oncogene* 38, 881–895. doi: 10.1038/s41388-018-0452-4

Barriga, E. H., Franze, K., Charras, G., and Mayor, R. (2018). Tissue stiffening coordinates morphogenesis by triggering collective cell migration in vivo. *Nature* 554, 523–527. doi: 10.1038/nature25742

Barriga, E. H., Maxwell, P. H., Reyes, A. E., and Mayor, R. (2013). The hypoxia factor Hif-1alpha controls neural crest chemotaxis and epithelial to mesenchymal transition. *J. Cell Biol.* 201, 759–776. doi: 10.1083/jcb.201212100

Caballero, D., Comelles, J., Piel, M., Voituriez, R., and Riveline, D. (2015). Ratchetaxis: long-range directed cell migration by local cues. *Trends Cell Biol.* 25, 815–827. doi: 10.1016/j.tcb.2015.10.009

Cao, L., Pu, J., and Zhao, M. (2011). GSK-3beta is essential for physiological electric field-directed Golgi polarization and optimal electrotaxis. *Cell. Mol. Life Sci.* 68, 3081–3093. doi: 10.1007/s00018-010-0608-z

Capuana, L., Bostrom, A., and Etienne-Manneville, S. (2020). Multicellular scale front-to-rear polarity in collective migration. *Curr. Opin. Cell Biol.* 62, 114–122. doi: 10.1016/j.ceb.2019.10.001

Carmona-Fontaine, C., Theveneau, E., Tzekou, A., Tada, M., Woods, M., Page, K. M., et al. (2011). Complement fragment C3a controls mutual cell attraction during collective cell migration. *Dev. Cell* 21, 1026–1037. doi: 10.1016/j.devcel.2011.10.012

Causeret, M., Taulet, N., Comunale, F., Favard, C., and Gauthier-Rouviere, C. (2005). N-cadherin association with lipid rafts regulates its dynamic assembly at cell-cell junctions in C2C12 myoblasts. *Mol. Biol. Cell* 16, 2168–2180. doi: 10.1091/mbc.e04-09-0829

Christian, L., Bahudhanapati, H., and Wei, S. (2013). Extracellular metalloproteinases in neural crest development and craniofacial morphogenesis. *Crit. Rev. Biochem. Mol. Biol.* 48, 544–560. doi: 10.3109/10409238.2013.838203

Cooper, M. S., and Keller, R. E. (1984). Perpendicular orientation and directional migration of amphibian neural crest cells in dc electrical fields. *Proc. Natl. Acad. Sci. U.S.A.* 81, 160–164. doi: 10.1073/pnas.81.1.160

Culbertson, M. D., Lewis, Z. R., and Nechiporuk, A. V. (2011). Chondrogenic and gliogenic subpopulations of neural crest play distinct roles during the assembly of epibranchial ganglia. *PLoS One* 6:e24443. doi: 10.1371/journal.pone.0024443

Dupin, E., Creuzet, S., and Le Douarin, N. M. (2006). The contribution of the neural crest to the vertebrate body. *Adv. Exp. Med. Biol.* 589, 96–119. doi: 10.1007/978-0-387-46954-6_6

Fattet, L., Jung, H. Y., Matsumoto, M. W., Aubol, B. E., Kumar, A., Adams, J. A., et al. (2020). Matrix rigidity controls epithelial-mesenchymal plasticity and tumor metastasis via a mechanoresponsive EPHA2/LYN complex. *Dev. Cell* 54, 302–316.e7.

Fuentes, D. E., and Butler, P. J. (2012). Coordinated mechanosensitivity of membrane rafts and focal adhesions. *Cell. Mol. Bioeng.* 5, 143–154. doi: 10.1007/s12195-012-0225-z

Garmon, T., Wittling, M., and Nie, S. (2018). MMP14 regulates cranial neural crest epithelial-to-mesenchymal transition and migration. *Dev. Dyn.* 247, 1083–1092. doi: 10.1002/dvdy.24661

Gonzalez Malagon, S. G., Lopez Munoz, A. M., Doro, D., Bolger, T. G., Poon, E., Tucker, E. R., et al. (2018). Glycogen synthase kinase 3 controls migration of the neural crest lineage in mouse and Xenopus. *Nat. Commun.* 9:1126.

Gouignard, N., Andrieu, C., and Theveneau, E. (2018). Neural crest delamination and migration: looking forward to the next 150 years. *Genesis* 56:e23107. doi: 10.1002/dvg.23107

Gouignard, N., Theveneau, E., and Saint-Jeannet, J. P. (2020). Dynamic expression of MMP28 during cranial morphogenesis. *Philos. Trans. R. Soc. Lond. B Biol. Sci.* 375:20190559. doi: 10.1098/rstb.2019.0559

Gruler, H., and Nuccitelli, R. (1991). Neural crest cell galvanotaxis: new data and a novel approach to the analysis of both galvanotaxis and chemotaxis. *Cell Motil. Cytoskel.* 19, 121–133. doi: 10.1002/cm.970190207

Honczarenko, M., Ratajczak, M. Z., Nicholson-Weller, A., and Silberstein, L. E. (2005). Complement C3a enhances CXCL12 (SDF-1)-mediated chemotaxis of bone marrow hematopoietic cells independently of C3a receptor. *J. Immunol.* 175, 3698–3706. doi: 10.4049/jimmunol.175.6.3698

Honore, S. M., Aybar, M. J., and Mayor, R. (2003). Sox10 is required for the early development of the prospective neural crest in Xenopus embryos. *Dev. Biol.* 260, 79–96. doi: 10.1016/s0012-1606(03)00247-1

Hotary, K. B., and Robinson, K. R. (1994). Endogenous electrical currents and voltage gradients in Xenopus embryos and the consequences of their disruption. *Dev. Biol.* 166, 789–800. doi: 10.1006/dbio.1994.1357

Huang, C., Kratzer, M. C., Wedlich, D., and Kashef, J. (2016). E-cadherin is required for cranial neural crest migration in Xenopus laevis. *Dev. Biol.* 411, 159–171. doi: 10.1016/j.ydbio.2016.02.007

Kuriyama, S., Theveneau, E., Benedetto, A., Parsons, M., Tanaka, M., Charras, G., et al. (2014). In vivo collective cell migration requires an LPAR2-dependent increase in tissue fluidity. *J. Cell Biol.* 206, 113–127. doi: 10.1083/jcb.201402093

Langhe, R. P., Gudzenko, T., Bachmann, M., Becker, S. F., Gonnermann, C., Winter, C., et al. (2016). Cadherin-11 localizes to focal adhesions and promotes cell-substrate adhesion. *Nat. Commun.* 7:10909.

Lin, B. J., Tsao, S. H., Chen, A., Hu, S. K., Chao, L., and Chao, P. G. (2017). Lipid rafts sense and direct electric field-induced migration. *Proc. Natl. Acad. Sci. U.S.A.* 114, 8568–8573. doi: 10.1073/pnas.1702526114

Lo, C. M., Wang, H. B., Dembo, M., and Wang, Y. L. (2000). Cell movement is guided by the rigidity of the substrate. *Biophys. J.* 79, 144–152. doi: 10.1016/s0006-3495(00)76279-5

McLennan, R., Teddy, J. M., Kasemeier-Kulesa, J. C., Romine, M. H., and Kulesa, P. M. (2010). Vascular endothelial growth factor (VEGF) regulates cranial neural crest migration in vivo. *Dev. Biol.* 339, 114–125. doi: 10.1016/j.ydbio.2009.12.022

McQuibban, G. A., Butler, G. S., Gong, J. H., Bendall, L., Power, C., Clark-Lewis, I., et al. (2001). Matrix metalloproteinase activity inactivates the CXC chemokine stromal cell-derived factor-1. *J. Biol. Chem.* 276, 43503–43508. doi: 10.1074/jbc.m107736200

Meiring, J. C. M., Shneyer, B. I., and Akhmanova, A. (2020). Generation and regulation of microtubule network asymmetry to drive cell polarity. *Curr. Opin. Cell Biol.* 62, 86–95. doi: 10.1016/j.ceb.2019.10.004

Mou, Z., Tapper, A. R., and Gardner, P. D. (2009). The armadillo repeat-containing protein, ARMCX3, physically and functionally interacts with the developmental regulatory factor Sox10. *J. Biol. Chem.* 284, 13629–13640. doi: 10.1074/jbc.m901177200

Muqbil, I., Wu, J., Aboukameel, A., Mohammad, R. M., and Azmi, A. S. (2014). Snail nuclear transport: the gateways regulating epithelial-to-mesenchymal transition? *Semin. Cancer Biol.* 27, 39–45. doi: 10.1016/j.semcancer.2014.06.003

Nuccitelli, R., and Erickson, C. A. (1983). Embryonic cell motility can be guided by physiological electric fields. *Exp. Cell Res.* 147, 195–201. doi: 10.1016/0014-4827(83)90284-7

Nuccitelli, R., and Smart, T. (1989). Extracellular calcium levels strongly influence neural crest cell galvanotaxis. *Biol. Bull.* 176, 130–135. doi: 10.2307/1541662

Nuccitelli, R., Smart, T., and Ferguson, J. (1993). Protein kinases are required for embryonic neural crest cell galvanotaxis. *Cell Motil. Cytoskel.* 24, 54–66. doi: 10.1002/cm.970240107

Pei, D., Shu, X., Gassama-Diagne, A., and Thiery, J. P. (2019). Mesenchymal-epithelial transition in development and reprogramming. *Nat. Cell Biol.* 21, 44–53. doi: 10.1038/s41556-018-0195-z

Pelletier, A. J., van der Laan, L. J., Hildbrand, P., Siani, M. A., Thompson, D. A., Dawson, P. E., et al. (2000). Presentation of chemokine SDF-1 alpha by fibronectin mediates directed migration of T cells. *Blood* 96, 2682–2690. doi: 10.1182/blood.v96.8.2682.h8002682_2682_2690

Ratajczak, M. Z., Reca, R., Wysoczynski, M., Yan, J., and Ratajczak, J. (2006). Modulation of the SDF-1-CXCR4 axis by the third complement component (C3)–implications for trafficking of CXCR4+ stem cells. *Exp. Hematol.* 34, 986–995. doi: 10.1016/j.exphem.2006.03.015

Rehberg, S., Lischka, P., Glaser, G., Stamminger, T., Wegner, M., and Rosorius, O. (2002). Sox10 is an active nucleocytoplasmic shuttle protein, and shuttling is crucial for Sox10-mediated transactivation. *Mol. Cell. Biol.* 22, 5826–5834. doi: 10.1128/mcb.22.16.5826-5834.2002

Reversat, A., Gaertner, F., Merrin, J., Stopp, J., Tasciyan, S., Aguilera, J., et al. (2020). Cellular locomotion using environmental topography. *Nature* 582, 582–585. doi: 10.1038/s41586-020-2283-z

Scarpa, E., Szabo, A., Bibonne, A., Theveneau, E., Parsons, M., and Mayor, R. (2015). Cadherin switch during EMT in neural crest cells leads to contact inhibition of locomotion via repolarization of forces. *Dev. Cell* 34, 421–434. doi: 10.1016/j.devcel.2015.06.012

Schlosser, G. (2014). Development and evolution of vertebrate cranial placodes. *Dev. Biol.* 389, 82–97. doi: 10.1016/j.ydbio.2014.01.017

Shi, F., and Sottile, J. (2011). MT1-MMP regulates the turnover and endocytosis of extracellular matrix fibronectin. *J. Cell Sci.* 124, 4039–4050. doi: 10.1242/jcs.087858

Stramer, B., and Mayor, R. (2017). Mechanisms and in vivo functions of contact inhibition of locomotion. *Nat. Rev. Mol. Cell Biol.* 18, 43–55. doi: 10.1038/nrm.2016.118

Stump, R. F., and Robinson, K. R. (1983). Xenopus neural crest cell migration in an applied electrical field. *J. Cell Biol.* 97, 1226–1233. doi: 10.1083/jcb.97.4.1226

Sun, Y., Reid, B., Ferreira, F., Luxardi, G., Ma, L., Lokken, K. L., et al. (2019). Infection-generated electric field in gut epithelium drives bidirectional migration of macrophages. *PLoS Biol.* 17:e3000044. doi: 10.1371/journal.pbio.3000044

Szabo, A., Melchionda, M., Nastasi, G., Woods, M. L., Campo, S., Perris, R., et al. (2016). In vivo confinement promotes collective migration of neural crest cells. *J. Cell Biol.* 213, 543–555. doi: 10.1083/jcb.201602083

Szabó, A., Theveneau, E., Turan, M., and Mayor, R. (2019). Neural crest streaming as an emergent property of tissue interactions during morphogenesis. *PLoS Comput. Biol.* 15:e1007002. doi: 10.1371/journal.pcbi.1007002

Theveneau, E., Marchant, L., Kuriyama, S., Gull, M., Moepps, B., Parsons, M., et al. (2010). Collective chemotaxis requires contact-dependent cell polarity. *Dev. Cell* 19, 39–53. doi: 10.1016/j.devcel.2010.06.012

Theveneau, E., and Mayor, R. (2011). Collective cell migration of the cephalic neural crest: the art of integrating information. *Genesis* 49, 164–176. doi: 10.1002/dvg.20700

Theveneau, E., and Mayor, R. (2012). Neural crest delamination and migration: from epithelium-to-mesenchyme transition to collective cell migration. *Dev. Biol.* 366, 34–54. doi: 10.1016/j.ydbio.2011.12.041

Theveneau, E., Steventon, B., Scarpa, E., Garcia, S., Trepat, X., Streit, A., et al. (2013). Chase-and-run between adjacent cell populations promotes directional collective migration. *Nat. Cell Biol.* 15, 763–772. doi: 10.1038/ncb2772

Thompson, A. J., Pillai, E. K., Dimov, I. B., Foster, S. K., Holt, C. E., and Franze, K. (2019). Rapid changes in tissue mechanics regulate cell behaviour in the developing embryonic brain. *eLife* 8:e39356.

Tomlinson, M. L., Guan, P., Morris, R. J., Fidock, M. D., Rejzek, M., Garcia-Morales, C., et al. (2009). A chemical genomic approach identifies matrix metalloproteinases as playing an essential and specific role in Xenopus melanophore migration. *Chem. Biol.* 16, 93–104. doi: 10.1016/j.chembiol.2008.12.005

Wei, S. C., Fattet, L., Tsai, J. H., Guo, Y., Pai, V. H., Majeski, H. E., et al. (2015). Matrix stiffness drives epithelial-mesenchymal transition and tumour metastasis through a TWIST1-G3BP2 mechanotransduction pathway. *Nat. Cell Biol.* 17, 678–688. doi: 10.1038/ncb3157

Wysoczynski, M., Kucia, M., Ratajczak, J., and Ratajczak, M. Z. (2007). Cleavage fragments of the third complement component (C3) enhance stromal derived factor-1 (SDF-1)-mediated platelet production during reactive postbleeding thrombocytosis. *Leukemia* 21, 973–982. doi: 10.1038/sj.leu.2404629

Yang, J., Antin, P., Berx, G., Blanpain, C., Brabletz, T., Bronner, M., et al. (2020). Association, Guidelines and definitions for research on epithelial-mesenchymal transition. *Nat. Rev. Mol. Cell Biol.* 21, 341–352.

Yu, H. H., and Moens, C. B. (2005). Semaphorin signaling guides cranial neural crest cell migration in zebrafish. *Dev. Biol.* 280, 373–385. doi: 10.1016/j.ydbio.2005.01.029

Zhao, M., Song, B., Pu, J., Wada, T., Reid, B., Tai, G., et al. (2006). Electrical signals control wound healing through phosphatidylinositol-3-OH kinase-gamma and PTEN. *Nature* 442, 457–460. doi: 10.1038/nature04925

Zhu, K., Hum, N. R., Reid, B., Sun, Q., Loots, G. G., and Zhao, M. (2020). Electric fields at breast cancer and cancer cell collective galvanotaxis. *Sci. Rep.* 10:8712.

Conflict of Interest: The authors declare that the research was conducted in the absence of any commercial or financial relationships that could be construed as a potential conflict of interest.

frontiers in Physiology

MINI REVIEW
published: 26 November 2020
doi: 10.3389/fphys.2020.608812

Insights Into the Early Gene Regulatory Network Controlling Neural Crest and Placode Fate Choices at the Neural Border

Subham Seal[1,2] *and Anne H. Monsoro-Burq*[1,2,3]*

[1]*Université Paris-Saclay, CNRS UMR 3347, INSERM U1021, Orsay, France,* [2]*Institut Curie Research Division, PSL Research University, Orsay Cedex, France,* [3]*Institut Universitaire de France, Paris, France*

The neural crest (NC) cells and cranial placodes are two ectoderm-derived innovations in vertebrates that led to the acquisition of a complex head structure required for a predatory lifestyle. They both originate from the neural border (NB), a portion of the ectoderm located between the neural plate (NP), and the lateral non-neural ectoderm. The NC gives rise to a vast array of tissues and cell types such as peripheral neurons and glial cells, melanocytes, secretory cells, and cranial skeletal and connective cells. Together with cells derived from the cranial placodes, which contribute to sensory organs in the head, the NC also forms the cranial sensory ganglia. Multiple *in vivo* studies in different model systems have uncovered the signaling pathways and genetic factors that govern the positioning, development, and differentiation of these tissues. In this literature review, we give an overview of NC and placode development, focusing on the early gene regulatory network that controls the formation of the NB during early embryonic stages, and later dictates the choice between the NC and placode progenitor fates.

Keywords: neural border, neural crest, placodes, signaling, gene-regulatory-network, ectoderm patterning, fate decision

OPEN ACCESS

Edited by:
Patrick Blader,
FR3743 Centre de Biologie Intégrative (CBI), France

Reviewed by:
Chenbei Chang,
University of Alabama at Birmingham, United States
Sally Ann Moody,
George Washington University, United States

***Correspondence:**
Anne H. Monsoro-Burq
anne-helene.monsoro-burq@curie.fr

Specialty section:
This article was submitted to Embryonic and Developmental Physiology, a section of the journal Frontiers in Physiology

Received: *21 September 2020*
Accepted: *02 November 2020*
Published: *26 November 2020*

Citation:
Seal S and Monsoro-Burq AH (2020) Insights Into the Early Gene Regulatory Network Controlling Neural Crest and Placode Fate Choices at the Neural Border. Front. Physiol. 11:608812. doi: 10.3389/fphys.2020.608812

INTRODUCTION

The "New Head" hypothesis (Gans and Northcutt, 1983; Northcutt, 2005) suggests that the presence of a complex head is a significant evolutionary difference between vertebrates and other chordates. During evolution, the vertebrate head has appeared concomitantly with two unique tissues, which are not present (or present in rudimentary form) in earlier-derived organisms: the neural crest (NC) and the sensory placodes. These tissues are formed at the border of the neural fold on the dorsal side of the embryo: placode progenitors (PP) are present rostrally and NC precursors are located more posteriorly (**Figure 1A**). The NC cells are morphologically distinguishable at the late neurulation stage when they delaminate and migrate away from the edge of the neuroectoderm, towards the final locations where they differentiate (Shellard and Mayor, 2019; Alkobtawi and Monsoro-Burq, 2020; Thiery et al., 2020). In parallel, during neurulation, the pan-placodal ectoderm is subdivided into thickened epithelial areas defining each placode, which contribute to cranial sensory structures (Schlosser, 2008, 2010; Pieper et al., 2011; Grocott el al., 2012; Streit, 2018; Buzzi et al., 2019). Lineage tracing

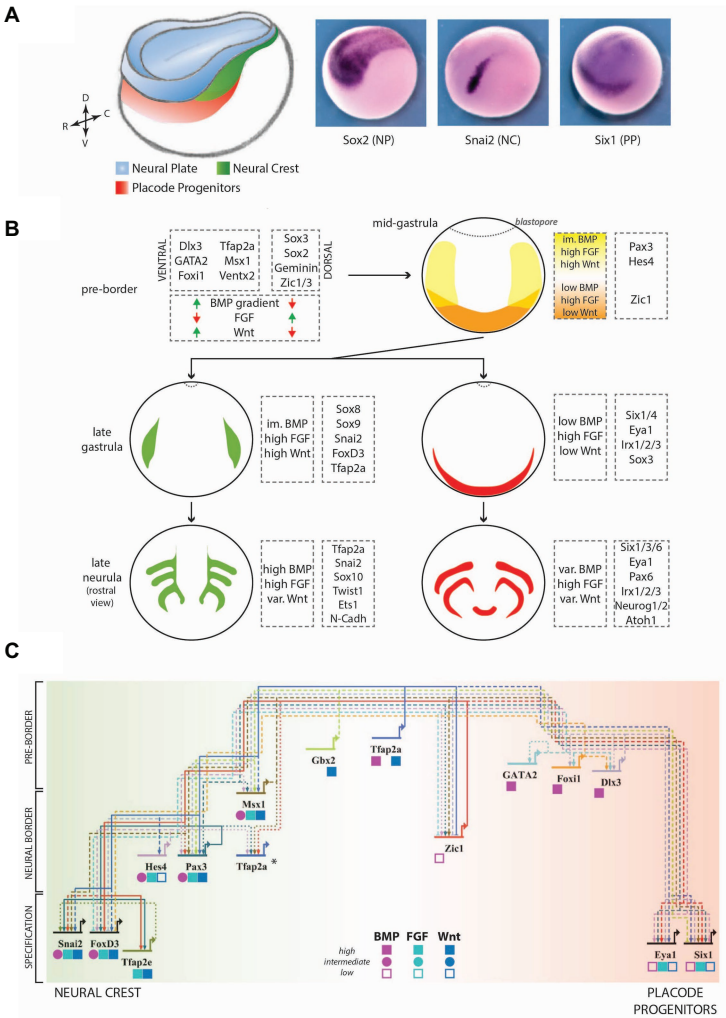

FIGURE 1 | A simplified view of the vertebrate gene regulatory network (GRN) controlling neural crest (NC) and placode induction. **(A)** Model of a *Xenopus* embryo at the mid-neurula stage, depicting the relative positions of the neural plate (NP, blue), the NC (green), and the placode progenitors (PP, red). These tissues express specific transcription factors (TFs), such as Sox2, Snai2, and Six1 respectively. DV, dorsoventral axis; RC, rostrocaudal axis. **(B)** The combined effects of signaling pathways and TFs lead to the development of different tissues in a temporally and spatially regulated manner. Here, the major genes involved at each stage have been indicated, along with the signaling levels of major secreted pathways (BMP, FGF, and WNT). Signaling pathways and genes have been selected according to their conserved functions in various vertebrate animal models and to the availability of detailed studies about their regulation and function in ectoderm patterning. At the mid-gastrula stage (pre-border stage), orange labels the anterior neural border (NB), and yellow depicts the posterior NB. At later stages, green and red depict the NC and the pre-placodal ectoderm respectively. im., intermediate; var., variable. **(C)** A synthetic view of the NB-development GRN in *Xenopus laevis*. Genes have been arranged from top to bottom according to the first stage during which their function is required. Genes positioned towards the left of the map favor the NC fate (green) while genes positioned towards the right of the map favor the PP fate (red). Gene-specific requirements of different signaling pathway activity have been depicted by shapes under the respective gene names (low, intermediate, and high). *Tfap2a has reiterated functions during the different stages, for which it interacts with different binding partners (de Croze et al., 2011; Rothstein and Simoes-Costa, 2020). Solid lines depict direct interactions, dashed lines depict epistasis interactions (either indirect or not proven to be direct) and dotted lines depict a feedback regulation. Arrows depict activation and bars depict repression. The GRN map has been constructed using the BioTapestry software (Longabaugh et al., 2005). Data from other model systems have not been included for the sake of simplicity, but the selected genes broadly display conserved functions in frog and chick. (For more detailed views of placode and NC GRNs, refer to Simoes-Costa and Bronner, 2015; Maharana and Schlosser, 2018; Prasad et al., 2019; Rogers and Nie, 2019; Thiery et al., 2020).

studies have detailed the respective contributions of the NC and the placodes (Noden, 1975; Keller, 1976; Le Douarin, 1980; D'Amico-Martel and Noden, 1983; Couly and Le Douarin, 1985, 1987; Eagleson and Harris, 1990; Garcia-Martinez and Schoenwolf, 1993; Eagleson et al., 1995; Kozlowski et al., 1997; Streit, 2002; Bhattacharya et al., 2004; Xu et al., 2008). Genetic screens conducted in multiple vertebrate species, in particular frog and chick embryos, have identified transcription factors (TFs) which uniquely demarcate NC and PP (Nieto et al., 1994; Ohto et al., 1999; LaBonne and Bronner-Fraser, 2000; Gamill and Bronner-Fraser, 2002; Plouhinec et al., 2014, 2017; Riddiford and Schlosser, 2016; Roellig et al., 2017). NC and PP originate from a common

ectodermal domain, located between the dorsal neural plate (NP; future brain and spinal cord) and the ventral non-neural ectoderm (future epidermis), named the "neural border" (NB, also called "neural plate border" elsewhere; Meulemans and Bronner-Fraser, 2004; Groves and LaBonne, 2014; Pla and Monsoro-Burq, 2018; Thiery et al., 2020). At gastrula stages, *pax3/7* genes (*pax3* paralog in *Xenopus* species, *pax7* paralog in chick, and *pax3/7* ancestor gene in lamprey) mark the lateral and posterior NB, but not it's rostral most portion, while *zic1* marks the anterior NB (**Figure 1**; **Table 1**). The formation, positioning, and henceforth specification of the NB into NC and PP are regulated by the coordinated activity of multiple signaling pathways (e.g., FGF, BMP, and WNT pathways) and specific TFs (e.g., *tfap2a/b/c*, *pax3/7*, *zic1*, and *hes4*; **Figure 1B**). At neurula stages, NC and PP are marked by unique gene sets (e.g., *snai2/foxD3* and *six1/eya1* respectively, **Table 1**).

Principally, the cephalic NC and the placodes form the head sense organs and peripheral nervous system. The cranial NC forms neurons, glial cells, melanocytes, secretory cells, osteocytes, and chondrocytes (Dupin et al., 2018; Etchevers et al., 2019; Alkobtawi and Monsoro-Burq, 2020). The pan-placodal ectoderm develops into non-neurogenic placodes (e.g., adenohypophysis, lens), and neurogenic placodes (epibranchial, otic, paratympanic, trigeminal, and olfactory). In addition, aquatic anamniote vertebrates possess lateral line placodes, which generate a lateral line system comprised of mechanosensory organs in the head and the trunk (Piotrowski and Baker, 2014; Schlosser, 2014; Singh and Groves, 2016; Buzzi et al., 2019). Additionally, by a coordinated migration and morphogenesis, NC, and placode cells form the cranial sensory ganglia (D'Amico-Martel and Noden, 1983; Forni et al., 2011). In humans, defective NC development leads to neurocristopathies, which represent one-third of all developmental diseases, such as cleft palate, Waardenburg syndrome, and Hirschsprung's disease (Vega-Lopez et al., 2018). Similarly, defects in placode development lead to diseases such as BOR/BO syndrome (Kochhar et al., 2007). In order to understand the development of these tissues and uncover the molecular basis of human pathologies, functional studies have been conducted using various vertebrate animal models. In this brief literature review, we focus on the regulation of the early stages of NB development, followed by its specification into NC and PP. We particularly emphasize the common and specific pathways and the gene regulatory network (GRN) controlling the balanced emergence of both cell types around the NP.

TABLE 1 | Important references.

	References	
	Xenopus	**Chick**
A. Gene		
Dlx3/5	Feledy et al., 1999; Luo et al., 2001; Pieper et al., 2012	Pera et al., 1999; McLarren et al., 2003; Khudyakov and Bronner-Fraser, 2009; Linker et al., 2009
Eya1/2	Pieper et al., 2012; Maharana and Schlosser, 2018	McLarren et al., 2003
Foxd3	Monsoro-Burq et al., 2003; Sato et al., 2005; Steventon et al., 2009; Maharana and Schlosser, 2018	Cheung et al., 2005; Khudyakov and Bronner-Fraser, 2009; Simoes-Costa et al., 2012
Foxi1/3	Matsuo-Takasaki et al., 2005; Pieper et al., 2012; Maharana and Schlosser, 2018	Khatri and Groves, 2013
Gata2/3	Pieper et al., 2012; Maharana and Schlosser, 2018	Sheng and Stern, 1999
Gbx2	Li et al., 2009; Steventon and Mayor, 2012	Steventon and Mayor, 2012
Hes4 (Hairy2b)	Nichane et al., 2008a,b; de Croze et al., 2011; Maharana and Schlosser, 2018	
Msx1	Suzuki et al., 1997; Tribulo et al., 2003; Monsoro-Burq et al., 2005	Streit and Stern, 1999; Khudyakov and Bronner-Fraser, 2009; Linker et al., 2009
Pax3/7	Monsoro-Burq et al., 2005; Sato et al., 2005; Hong and St-Jeannet, 2007; de Croze et al., 2011; Milet et al., 2013; Plouhinec et al., 2014; Maharana and Schlosser, 2018	Basch et al., 2006; Otto et al., 2006; Khudyakov and Bronner-Fraser, 2009; Linker et al., 2009; Stuhlmiller and Garcia-Castro, 2012; Vadasz et al., 2013; Simoes-Costa and Bronner, 2015
Six1	Pandur and Moody, 2000; Brugmann et al., 2004; Ahrens and Schlosser, 2005; Pieper et al., 2012; Maharana and Schlosser, 2018	McLarren et al., 2003; Christophorou et al., 2009
Snai2	Mancilla and Mayor, 1996; Monsoro-Burq et al., 2003, 2005; Steventon et al., 2009	Nieto et al., 1994; del Barrio and Nieto, 2002; Khudyakov and Bronner-Fraser, 2009
Tfap2a	Luo et al., 2002, 2003; de Croze et al., 2011; Maharana and Schlosser, 2018	Khudyakov and Bronner-Fraser, 2009; Rothstein and Simoes-Costa, 2020
Tfap2e	Hong et al., 2014	
Zic1	Mizuseki et al., 1998; Monsoro-Burq et al., 2005; Sato et al., 2005; Hong and St-Jeannet, 2007; Marchal et al., 2009; Milet et al., 2013; Plouhinec et al., 2014; Maharana and Schlosser, 2018	Khudyakov and Bronner-Fraser, 2009; Simoes-Costa and Bronner, 2015
B. Transcriptome analysis		
	Plouhinec et al., 2014; Riddiford and Schlosser, 2016; Plouhinec et al., 2017; Maharana and Schlosser, 2018	Khudyakov and Bronner-Fraser, 2009; Simoes-Costa et al., 2014; Simoes-Costa and Bronner, 2016; Hintze et al., 2017; Morrison et al., 2017; Roellig et al., 2017; Trevers et al., 2018

In this mini review article, we have gathered as many references as possible and apologize to the authors whose work could not be quoted. We add here a list of additional references for each of the genes described in the text and point to several relevant large-scale transcriptome screening. Studies using frog as a model are indicated in blue, studies using chick embryos in black; A: references describing NC and PP markers; and B: references of transcriptome analysis of NC and PP progenitors.

NEURAL CREST DEVELOPMENT, AN OVERVIEW

The neural crest is an exclusive feature of vertebrates, acquired about 500 million years ago during evolution (Sauka-Spengler et al., 2007). Since NC generates tissues typical of both ectodermal (ganglia) and mesodermal (mesenchyme, bone) origin, it has been referred to as the fourth embryonic germ layer (Hall, 2018). The NC develops from the NB positioned adjacent to the NP along the rostrocaudal axis during gastrulation and neurulation. Classically, the NC is subdivided into cranial and trunk areas, followed by further anatomical subdivisions (Alkobtawi and Monsoro-Burq, 2020). At the end of neurulation, upon neural tube closure, the NC cells start to migrate in multiple streams, delineating the main craniofacial domains and along the somites in the trunk (Theveneau and Mayor, 2012; Szabo and Mayor, 2018; Rocha et al., 2020). Upon reaching their target tissues, poorly understood genetic programs and interactions with the environment dictate NC differentiation into multiple cell types (Bronner and Le Douarin, 2012).

Before migration, NC cells follow a typical epithelial-to-mesenchymal transition (EMT), which involves the activation of specific TFs (EMT-TFs, e.g., Snail1/2, Twist1), a cadherin switch, and the fine-tuned dynamics of multiple cytoskeletal and cell-polarity proteins. This results in the loss of the polarized epithelial phenotype and acquisition of cell motility (Bahm et al., 2017; Morrison et al., 2017; Shellard and Mayor, 2019). In most species, NC migration involves "contact inhibition of locomotion" (CIL), the mechanism allowing cell dispersion *in vitro* and *in vivo*, as well as "co-attraction," a mechanism maintaining collective migration of cranial NC cells (Carmona-Fontaine et al., 2008; Wynn et al., 2013; Richardson et al., 2016; Li et al., 2019). In addition, cranial NC cells interact with placodal cells, some of which also delaminate. This helps orient the direction of migration of both cell types (Freter et al., 2013; Theveneau et al., 2013; Colombi et al., 2020). The cellular mechanisms of NC migration have been extensively reviewed elsewhere (Mayor and Theveneau, 2013; Shellard and Mayor, 2019; Alkobtawi and Monsoro-Burq, 2020; Giniunaite et al., 2020; Piacentino et al., 2020; Thiery et al., 2020).

Recent works have focused on premigratory NC induction and specification, starting at late gastrulation/NP stages, as denoted by the expression of early NC specifier genes (e.g., *snai2*, *foxd3*, *tfap2e*, *sox8*, and *sox9*). These earlier NC-specifiers in turn induce later NC specifiers such as *sox10*, *ets1*, and *twist1* during the second half of neurulation, when neural folds elevate and fuse dorsally (Alkobtawi and Monsoro-Burq, 2020). The NC specifiers collectively maintain their own expression by positive feedback stimulations (Lander et al., 2013).

PLACODE DEVELOPMENT, AN OVERVIEW

Placodes, the second key vertebrate innovation leading to the formation of specialized head structures, develop from the dorsal-rostral pan-placodal domain which also derives from the NB (**Figure 1A**). Post neurulation, some placodes undergo epithelial folding. Other placode cells are primed for neurogenesis and delaminate from the epithelium (Lassiter et al., 2014). However, unlike NC migration, placode migration does not seem to involve EMT: EMT markers are absent, and cells do not exhibit a mesenchymal morphology and migrate as neuronal cells through a breach in the basal lamina (Graham et al., 2007). During migration, placode cells interact with specific subpopulations of NC cells to form sensory ganglia.

The Six and Eya family of TFs are the major genes involved in early PP development. At late gastrula stages, Six1/4 and Eya1/2 are induced throughout the PP and are essential for its development (**Table 1**). These genes are also required at later stages for placode cell-proliferation and neurogenesis (Schlosser et al., 2008). Grown in isolation, PP continues expressing *six1*/*eya2*, but adopts a lens fate "by default," highlighting that additional regulators control the formation of the other placodes (Bailey et al., 2006). Although, genetic screens have identified a few genes functioning upstream/downstream of the Six/Eya complex, such as Znf462, Homer2, Hes2, Atoh1, the placode GRN remains incompletely understood (Christophorou et al., 2009; Riddiford and Schlosser, 2016; Hintze et al., 2017).

REGULATION OF NEURAL CREST AND PLACODE FATE SPECIFICATION

Neural crest and PP are specified at late gastrula and neurula stages, while the induction of the NB itself is concomitant to neural induction in dorsal ectoderm, at early gastrula stages (de Crozé et al., 2011). Both these processes are tightly regulated by the activity of signaling pathways and TFs, leading to a strict temporal developmental sequence, resulting in well-defined margins demarcating each tissue.

Secreted Signaling Pathways Broadly Pattern the Ectoderm

Levels of activity and cross-regulations between BMP, FGF, and WNT signaling pathways are particularly important for the induction of NC and PP, as they initiate spatial subdivisions of the dorsal ectoderm during gastrulation (Wilson and Hemmati-Brivanlou, 1995; Streit and Stern, 1999; Monsoro-Burq et al., 2003; Kudoh et al., 2004; Steventon et al., 2009; Stuhlmiller and Garcia-Castro, 2012; Yardley and Garcia-Castro, 2012; Schille and Schambony, 2017). Activity levels are influenced by the source of ligands and their antagonists. BMP ligands are secreted by the non-neural ectoderm and the ventral mesoderm, while the NP and the organizer produce BMP antagonists (e.g., Noggin, Chordin, Cerberus and Follistatin; Hawley et al., 1995; Wilson and Hemmati-Brivanlou, 1995; Fletcher and Harland, 2008; Patthey et al., 2008; Branney et al., 2009; Linker et al., 2009). This sets up a low-to-high gradient of BMP signaling from the dorsal midline towards the lateral zones. FGF ligands are produced by the paraxial mesoderm, while WNT ligands come from both the paraxial mesoderm and the non-neural ectoderm (Faure et al., 2002;

Monsoro-Burq et al., 2003; Steventon et al., 2009). Rostral to the NP, WNT antagonists limit WNT signaling (Pera and De Robertis, 2000; Wilson et al., 2001; Carmona-Fontaine et al., 2007). All these pathways are also modulated temporally as they are required at different levels at multiple stages of neural/NC/PP and epidermis specification. At the early gastrula stage, FGF signaling, along with BMP and WNT antagonists, promotes neural development while high BMP and WNT signaling lead to non-neural ectoderm development (Groves and LaBonne, 2014). Henceforth, FGF/BMP antagonists activate neural factors demarcating the dorsal ectoderm (e.g., *sox2/3*, *otx2*; Streit et al., 2000). BMP activity upregulates the expression of *tfap2a*, *foxi1*, *gata2/3*, and *dlx3/5* in the non-neural ectoderm (Nguyen et al., 1998; Luo et al., 2002; Tribulo et al., 2003; Matsuo-Takasaki et al., 2005; Esterberg and Fritz, 2009; Kwon et al., 2010; de Croze et al., 2011).

Between the neural and non-neural ectoderm, the lateral NB is characterized by high FGF, high WNT, and low to intermediate BMP activity, and uniquely marked by *pax3/7* with an overlapping expression of *tfap2a*, *msx1*, *zic1*, *gbx2*, and *hes4* (**Table 1**). In contrast, the anterior NB is subjected to high FGF/low BMP/low WNT levels (**Figure 1C**; Chang and Hemmati-Brivanlou, 1998; Piacentino and Bronner, 2018; Tambalo et al., 2020). The NB is progressively subdivided into NC, PP, dorsal neural tube, and non-neural ectoderm progenitors. Different relative levels of BMP and WNT activity control NC induction and fate maintenance (Steventon et al., 2009; Steventon and Mayor, 2012). It is not yet completely understood how the activity levels of these pathways change dynamically in time and space. One hypothesis is that morphogenesis during neurulation positions the NB close to distinct parts of the mesoderm over time: at mid/late gastrula stages, the dorsal-lateral marginal zone (immature paraxial and intermediate mesoderm precursors) is required for NC induction, while the intermediate mesoderm (pronephros progenitors) maintains NC identity at the early neurula stage. In frog and chick neurula embryos, premigratory NC progenitors exhibit increased BMP activity due to novel signaling modulators (Tribulo et al., 2003; Kwon et al., 2010; Piacentino and Bronner, 2018). Although it remains difficult to compare stages between different species, in zebrafish embryos, a low level of BMP signaling is essential for NC induction while it seems to inhibits PP formation (Nguyen et al., 1998).

Emerging functions of other signaling pathways also contribute to this complex patterning. Retinoic acid signaling contributes to NC induction and migration (Villanueva et al., 2002; Martinez-Morales et al., 2011). Notch signaling is required for *bmp4* and *snail2* expression, regulating NC induction and cell fates at the neural NB (Endo et al., 2002, 2003; Hernandez-Lagunas et al., 2011). AKT signaling is required for premigratory NC induction and maintenance (Sittewelle and Monsoro-Burq, 2018).

Transcription Factors Control Fate Decisions at the Neural Border

The integration of those multiple signals triggers the activation of specific TFs, which in turn bias NB cells towards a given fate (**Figure 1C**). Tfap2a and Gbx2, the earliest genes involved in NC induction, both activate *msx1*, *pax3*, and *hes4* (Li et al., 2009; de Croze et al., 2011). Tfap2a is required for both PP (*six1/eya1*) and NC (foxd3) fates (Luo et al., 2003; Kwon et al., 2010; Pieper et al., 2012; Maharana and Schlosser, 2018). In contrast, Gbx2 favors NC fate by inhibiting *six1* expression (Li et al., 2009). Gata2/3 and Foxi TFs (frog *foxi1a* and chick *foxi3*) promote the PP fate by directly activating *six1* expression and also upregulating *dlx3/5* expression (McLarren et al., 2003; Matsuo-Takasaki et al., 2005; Kwon et al., 2010; Sato et al., 2010; Pieper et al., 2012; Khatri et al., 2014; Hintze et al., 2017). Dlx3 (frog) and Dlx5 (chick) are necessary for PP formation through enhancer-mediated activation of *six1* (Sato et al., 2005, 2010). On the other hand, in mouse, chick, and zebrafish, Msx1 inhibits PP fate by repressing *six1* expression, thus promoting NC fate (Zhang et al., 1997; Phillips et al., 2006; Sato et al., 2010). Interestingly, a recent study in *Xenopus* suggests that Msx1 is required for *six1/eya1* expression, as Msx1 depletion slightly decreases *six1* expression, while its overexpression expands *six1/eya1* ectopically (Maharana and Schlosser, 2018). These seemingly contradictory results may be explained by distinct stage-specific requirements for each gene in different experimental settings. Accordingly, it is known that certain genes, like *tfap2a* and *msx1*, are also required for later NC developmental steps (de Croze et al., 2011; Rothstein and Simoes-Costa, 2020). Mechanistically, the Tfap2a protein dimerizes with either Tfap2c or Tfap2b, at NB and NC stage, respectively, to activate different sets of targets (Rothstein and Simoes-Costa, 2020).

The NB marker Pax3 and the more anteriorly localized Zic1 factor are necessary and sufficient for inducing NC and PP in "naive" ectoderm (Monsoro-Burq et al., 2005; Hong and Saint-Jeannet, 2007; Milet et al., 2013; Bae et al., 2014; Plouhinec et al., 2014). *In vivo* and in ectoderm explants, fate choice is controlled by their relative levels: high Pax3 promotes a hatching gland fate (frog-specific ectoderm cell type), high Zic1 promotes PP fate, while a combination of Pax3 and Zic1 promotes NC fate. Zic1 induces PP fate in a Dlx3-dependent manner while Pax3 strongly represses *six1/eya1* expression (Maharana and Schlosser, 2018). Pax3/Zic1 together lead to the direct expression of the NC specifiers *snai1*, *snai2*, and *foxd3* (Milet et al., 2013; Plouhinec et al., 2014; Simoes-Costa et al., 2014). Consequently *in vivo*, during gastrula NB stages, the PP forms in the Zic1-positive/Pax3-negative anterior NB portion, while NC forms in the region where Pax3 and Zic1 overlap. Interestingly, there is some overlap between *pax3/7*-negative and *six1/eya1*-positive areas, thus leading to an interesting conundrum: how are cells sorted in this overlap region? In chick, a few NB cells continue expressing combinations of fate-specific markers until neurula stages and ultimately get sorted into their final domains (Roellig et al., 2017). Future studies considering the temporal and morphogenetic differences in the neurulation between different species will further address this question.

Several recent transcriptomics screens have uncovered novel regulators of NC/PP fate choice (**Table 1**). For example, in *Xenopus*, *hes4* (*hairy2b*) and *znf703*, expressed broadly at the NB, are required for NC induction. Hes4 upregulates *foxd3*, maintains NC multipotency, and, through the activity of Notch/

Delta signaling triggering Id3, promotes NC differentiation (Nagatomo and Hashimoto, 2007; Nichane et al., 2008a,b; de Croze et al., 2011). Znf703, a target of Pax3 and Zic1, is required for NC specifiers expression (Hong and St-Jeannet, 2017; Janesick et al., 2019). In chick, Axud1, a target of WNT signaling, cooperates with NB specifiers Pax7 and Msx1 for NC induction (Simoes-Costa and Bronner, 2015), while Znf462 and Pdlim4 regulate *foxi3* and *dlx5* respectively, affecting PP development (Hintze et al., 2017). These studies highlight the urgent need for functional studies weaving those numerous novel regulators into the current scaffold of the NB-GRN.

DISCUSSION

Research in multiple model systems has highlighted essential elements of the GRN governing NB induction and NC/PP fate choice (a frog-specific simplified NB-GRN is shown in **Figure 1C**). Importantly, the functions of the key regulators are largely conserved across species (**Table 1**). However major questions remain unanswered. Genetic and transcriptome screens show that the NB-GRN is largely incomplete. Moreover, while complex epistasis relationships begin to be established, most direct regulations await a functional validation. Furthermore, complex feed-back and feed-forward mechanisms between signaling pathways and NB specifiers remain incompletely understood (Litsiou et al., 2005; Garnett et al., 2012). BMP signaling activates Tfap2a, Foxi1, and Gata3, which then regulate each other (McLarren et al., 2003; Ahrens and Schlosser, 2005; Litsiou et al., 2005; Kwon et al., 2010; Pieper et al., 2012; Khatri et al., 2014). Gata2 upregulates both BMP and WNT ligands (Sykes et al., 1998). The NB specifiers Pax3, Zic1, Msx1, Hes4, and Tfap2a regulate each other in a feed-forward loop and require additional WNT signaling (Monsoro-Burq et al., 2005; Sato et al., 2005; Maczkowiak et al., 2010; de Croze et al., 2011; Simoes-Costa and Bronner, 2015). Frog PP specifiers *six1/eya1* affect NB and NC specifiers expression (*pax3*, *foxd3*) as well as NB inducers (*tfap2a*, *msx1*, *dlx3*, *gata2*, *foxi1*; Maharana and Schlosser, 2018). As a whole, these complex cross-talk and feedback regulations stabilize fate choices.

Another debated question is how multipotency, a key characteristic of NC and placodes, is controlled during NB development (Baggiolini et al., 2015). Whether high (NC) or more limited (placodes), the diversity of NC/placode derivatives surpasses other cells' potential at a similar stage and promotes the formation of the New Head. While the molecular basis of placode multipotency remains unexplored, a first model has proposed that NC progenitors retained blastula-type multipotency (Buitrago-Delgado et al., 2015). However, this model is debated since single-cell transcriptomes have shown that the multipotency gene signature proposed by Buitrago-Delgado et al. was not specific to multipotent cells (Briggs et al., 2018). Rather, functional analysis of the vertebrate-specific genetic innovations Nanog/Oct4 (and their orthologs Ventx/Pou5) before or after gastrulation rather suggests that NC progenitors *de novo* activate pluripotency regulators after NB induction (Scerbo and Monsoro-Burq, 2020). This reinitiates multipotency and promotes the ectomesenchyme fate. From an evolutionary perspective, the cranial NB/NC-GRN requires Ventx/Nanog, Pou5/Oct4 and later NC specifier Ets1 to promote jawed structures formation in gnathostomes (Simoes-Costa and Bronner, 2016; Martik et al., 2019; Soldatov et al., 2019; Scerbo and Monsoro-Burq, 2020). Later on, NC specifiers' downregulation leads to the loss of pluripotency and the initiation of cell differentiation (Dottori et al., 2001; Sasai et al., 2001; Teng et al., 2008; Betancur et al., 2010; Mundell and Labosky, 2011; Dupin et al., 2018).

Despite their limitations, all these studies shed light on the two alternative models proposed for NB development. The "binary competence" model proposes that early in development, the competence to develop either NC or placodes is restricted to the NB and the non-neural ectoderm, respectively (Schlosser, 2008; Pieper et al., 2011, 2012). The "NB" model proposes, that early on, the multipotent NB generates both NC and PP, the relative positions of which are determined at later stages by distinct specifiers. Recent experiments suggest a combination of both models *in vivo*: at blastula to late-gastrula stages, the multipotent NB shows co-expression of markers of either fate and no spatial segregation of fate-biased cells (NB model), but as development proceeds, the capability to form either NC or PP would restrict to subzones of the border (binary competence; Roellig et al., 2017; Briggs et al., 2018; Maharana and Schlosser, 2018). When single-cell transcriptomics studies will explore these early stages with increased resolution in the near future, it will be interesting to re-evaluate how cell lineage choices are controlled at the NB. Altogether, the recent functional analyses of early ectoderm patterning have shed important novel information, increasing knowledge of the GRN acting to promote NC and/or PP for the benefit of future studies of human pathologies.

AUTHOR CONTRIBUTIONS

All authors listed have made a substantial, direct and intellectual contribution to the work, and approved it for publication.

FUNDING

The authors gratefully acknowledge financial support provided by the European Union's Horizon 2020 Research and Innovation Program under Marie Skłodowska-Curie (grant agreement No 860635, ITN NEUcrest); by Université Paris Saclay; by Centre National de la Recherche Scientifique (CNRS); by Agence Nationale pour la Recherche (ANR-15-CE13-0012-01-CRESTNETMETABO); and by Institut Universitaire de France.

ACKNOWLEDGMENTS

We are grateful to Dr. M. Alkobtawi for proofreading the manuscript and to all members of the AM-B team for their support.

REFERENCES

Ahrens, K., and Schlosser, G. (2005). Tissues and signals involved in the induction of placodal Six1 expression in *Xenopus laevis*. *Dev. Biol.* 288, 40–59. doi: 10.1016/j.ydbio.2005.07.022

Alkobtawi, M., and Monsoro-Burq, A. H. (2020). "Chapter 1: The neural crest, a vertebrate invention" in *Evolving neural crest cells. 1st Edn.* eds. B. F. Eames, D. M. Medeiros and I. Adameyko (Boca Raton: Imprint CRC Press), 5–66.

Bae, C. J., Park, B. Y., Lee, Y. H., Tobias, J. W., Hong, C. S., and Saint-Jeannet, J. P. (2014). Identification of Pax3 and Zic1 targets in the developing neural crest. *Dev. Biol.* 386, 473–483. doi: 10.1016/j.ydbio.2013.12.011

Baggiolini, A., Varum, S., Mateos, J. M., Bettosini, D., John, N., Bonalli, M., et al. (2015). Premigratory and migratory neural crest cells are multipotent in vivo. *Cell Stem Cell* 16, 314–322. doi: 10.1016/j.stem.2015.02.017

Bahm, I., Barriga, E. H., Frolov, A., Theveneau, E., Frankel, P., and Mayor, R. (2017). PDGF controls contact inhibition of locomotion by regulating N-cadherin during neural crest migration. *Development* 144, 2456–2468. doi: 10.1242/dev.147926

Bailey, A. P., Bhattacharyya, S., Bronner-Fraser, M., and Streit, A. (2006). Lens specification is the ground state of all sensory placodes, from which FGF promotes olfactory identity. *Dev. Cell* 11, 505–517. doi: 10.1016/j.devcel.2006.08.009

Basch, M. L., Bronner-Fraser, M., and García-Castro, M. I. (2006). Specification of the neural crest occurs during gastrulation and requires Pax7. *Nature* 441, 218–222. doi: 10.1038/nature04684

Betancur, P., Bronner-Fraser, M., and Sauka-Spengler, T. (2010). Assembling neural crest regulatory circuits into a gene regulatory network. *Annu. Rev. Cell Dev. Biol.* 26, 581–603. doi: 10.1146/annurev.cellbio.042308.113245

Bhattacharyya, S., Bailey, A. P., Bronner-Fraser, M., and Streit, A. (2004). Segregation of lens and olfactory precursors from a common territory: cell sorting and reciprocity of Dlx5 and Pax6 expression. *Dev. Biol.* 271, 403–414. doi: 10.1016/j.ydbio.2004.04.010

Branney, P. A., Faas, L., Steane, S. E., Pownall, M. E., and Isaacs, H. V. (2009). Characterisation of the fibroblast growth factor dependent transcriptome in early development. *PLoS One* 4:e4951. doi: 10.1371/journal.pone.0004951

Briggs, J. A., Weinreb, C., Wagner, D. E., Megason, S., Peshkin, L., Kirschner, M. W., et al. (2018). The dynamics of gene expression in vertebrate embryogenesis at single-cell resolution. *Science* 360:eaar5780. doi: 10.1126/science.aar5780

Bronner, M. E., and LeDouarin, N. M. (2012). Development and evolution of the neural crest: an overview. *Dev. Biol.* 366, 2–9. doi: 10.1016/j.ydbio.2011.12.042

Brugmann, S. A., Pandur, P. D., Kenyon, K. L., Pignoni, F., and Moody, S. A. (2004). Six1 promotes a placodal fate within the lateral neurogenic ectoderm by functioning as both a transcriptional activator and repressor. *Development* 131, 5871–5881. doi: 10.1242/dev.01516

Buitrago-Delgado, E., Nordin, K., Rao, A., Geary, L., and LaBonne, C. (2015). Shared regulatory programs suggest retention of blastula-stage potential in neural crest cells. *Science* 348, 1332–1335. doi: 10.1126/science.aaa3655

Buzzi, A. L., Hintze, M. S., and Streit, A. (2019). "Development of neurogenic placodes in vertebrates" in *eLS*. ed. J. Wiley (Chichester, UK: John Wiley & Sons, Ltd.), 1–14.

Carmona-Fontaine, C., Acuña, G., Ellwanger, K., Niehrs, C., and Mayor, R. (2007). Neural crests are actively precluded from the anterior neural fold by a novel inhibitory mechanism dependent on Dickkopf1 secreted by the prechordal mesoderm. *Dev. Biol.* 309, 208–221. doi: 10.1016/j.ydbio.2007.07.006

Carmona-Fontaine, C., Matthews, H. K., Kuriyama, S., Moreno, M., Dunn, G. A., Parsons, M., et al. (2008). Contact inhibition of locomotion in vivo controls neural crest directional migration. *Nature* 456, 957–961. doi: 10.1038/nature07441

Chang, C., and Hemmati-Brivanlou, A. (1998). Neural crest induction by Xwnt7B in *Xenopus*. *Dev. Biol.* 194, 129–134. doi: 10.1006/dbio.1997.8820

Cheung, M., Chaboissier, M. C., Mynett, A., Hirst, E., Schedl, A., and Briscoe, J. (2005). The transcriptional control of trunk neural crest induction, survival, and delamination. *Dev. Cell* 8, 179–192. doi: 10.1016/j.devcel.2004.12.010

Christophorou, N. A. D., Bailey, A. P., Hanson, S., and Streit, A. (2009). Activation of Six1 target genes is required for sensory placode formation. *Dev. Biol.* 336, 327–336. doi: 10.1016/j.ydbio.2009.09.025

Colombi, A., Scianna, M., Painter, K. J., and Preziosi, L. (2020). Modelling chase-and-run migration in heterogeneous populations. *J. Math. Biol.* 80, 423–456. doi: 10.1007/s00285-019-01421-9

Couly, G. F., and Le Douarin, N. M. (1985). Mapping of the early neural primordium in quail-chick chimeras. I. Developmental relationships between placodes, facial ectoderm, and prosencephalon. *Dev. Biol.* 110, 422–439. doi: 10.1016/0012-1606(85)90101-0

Couly, G. F., and Le Douarin, N. M. (1987). Mapping of the early neural primordium in quail-chick chimeras. II. The prosencephalic neural plate and neural folds: implications for the genesis of cephalic human congenital abnormalities. *Dev. Biol.* 120, 198–214. doi: 10.1016/0012-1606(87)90118-7

D'amico-Martel, A., and Noden, D. M. (1983). Contributions of placodal and neural crest cells to avian cranial peripheral ganglia. *Am. J. Anat.* 166, 445–468. doi: 10.1002/aja.1001660406

De Crozé, N., Maczkowiak, F., and Monsoro-Burq, A. H. (2011). Reiterative AP2a activity controls sequential steps in the neural crest gene regulatory network. *Proc. Natl. Acad. Sci. U. S. A.* 108, 155–160. doi: 10.1073/pnas.1010740107

del Barrio, M. G., and Nieto, M. A. (2002). Overexpression of Snail family members highlights their ability to promote chick neural crest formation. *Development* 129, 1583–1593.

Dottori, M., Gross, M. K., Labosky, P., and Goulding, M. (2001). The winged-helix transcription factor Foxd3 suppresses interneuron differentiation and promotes neural crest cell fate. *Development* 128, 4127–4138.

Dupin, E., Calloni, G. W., Coelho-Aguiar, J. M., and Le Douarin, N. M. (2018). The issue of the multipotency of the neural crest cells. *Dev. Biol.* 444, S47–S59. doi: 10.1016/j.ydbio.2018.03.024

Eagleson, G., Ferreiro, B., and Harris, W. A. (1995). Fate of the anterior neural ridge and the morphogenesis of the *Xenopus* forebrain. *J. Neurobiol.* 28, 146–158. doi: 10.1002/neu.480280203

Eagleson, G. W., and Harris, W. A. (1990). Mapping of the presumptive brain regions in the neural plate of *Xenopus laevis*. *J. Neurobiol.* 21, 427–440. doi: 10.1002/neu.480210305

Endo, Y., Osumi, N., and Wakamatsu, Y. (2002). Bimodal functions of Notch-mediated signaling are involved in neural crest formation during avian ectoderm development. *Development* 129, 863–873.

Endo, Y., Osumi, N., and Wakamatsu, Y. (2003). Deltex/Dtx mediates NOTCH signaling in regulation of Bmp4 expression in cranial neural crest formation during avian development. *Develop. Growth Differ.* 45, 241–248. doi: 10.1046/j.1524-4725.2003.693.x

Esterberg, R., and Fritz, A. (2009). dlx3b/4b are required for the formation of the preplacodal region and otic placode through local modulation of BMP activity. *Dev. Biol.* 325, 189–199. doi: 10.1016/j.ydbio.2008.10.017

Etchevers, H. C., Dupin, E., and Le Douarin, N. M. (2019). The diverse neural crest: from embryology to human pathology. *Dev.* 146:dev169821. doi: 10.1242/dev.169821

Faure, S., De Santa Barbara, P., Roberts, D. J., and Whitman, M. (2002). Endogenous patterns of BMP signaling during early chick development. *Dev. Biol.* 244, 44–65. doi: 10.1006/dbio.2002.0579

Feledy, J. A., Beanan, M. J., Sandoval, J. J., Goodrich, J. S., Lim, J. H., Matsuo-Takasaki, M., et al. (1999). Inhibitory patterning of the anterior neural plate in *Xenopus* by homeodomain factors D1x3 and Msx1. *Dev. Biol.* 212, 455–464. doi: 10.1006/dbio.1999.9374

Fletcher, R. B., and Harland, R. M. (2008). The role of FGF signaling in the establishment and maintenance of mesodermal gene expression in *Xenopus*. *Dev. Dyn.* 237, 1243–1254. doi: 10.1002/dvdy.21517

Forni, P. E., Taylor-Burds, C., Melvin, V. S., Williams, T., and Wray, S. (2011). Neural crest and ectodermal cells intermix in the nasal placode to give rise to GnRH-1 neurons, sensory neurons, and olfactory ensheathing cells. *J. Neurosci.* 31, 6915–6927. doi: 10.1523/JNEUROSCI.6087-10.2011

Freter, S., Fleenor, S. J., Freter, R., Liu, K. J., and Begbie, J. (2013). Cranial neural crest cells form corridors prefiguring sensory neuroblast migration. *Development* 140, 3595–3600. doi: 10.1242/dev.091033

Gammill, L. S., and Bronner-Fraser, M. (2002). Genomic analysis of neural crest induction. *Development* 129, 5731–5741. doi: 10.1242/dev.00175

Gans, C., and Northcutt, R. G. (1983). Neural crest and the origin of vertebrates: a new head. *Science* 220, 268–274. doi: 10.1126/science.220.4594.268

Garcia-Martinez, V., and Schoenwolf, G. C. (1993). Primitive-streak origin of the cardiovascular system in avian embryos. *Dev. Biol.* 159, 706–719. doi: 10.1006/dbio.1993.1276

Garnett, A. T., Square, T. A., and Medeiros, D. M. (2012). BMP, wnt and FGF signals are integrated through evolutionarily conserved enhancers to achieve robust expression of Pax3 and Zic genes at the zebrafish neural plate border. *Development* 139, 4220–4231. doi: 10.1242/dev.081497

Giniūnaitė, R., McLennan, R., McKinney, M. C., Baker, R. E., Kulesa, P. M., and Maini, P. K. (2020). An interdisciplinary approach to investigate collective cell migration in neural crest. *Dev. Dyn.* 249, 270–280. doi: 10.1002/dvdy.124

Graham, A., Blentic, A., Duque, S., and Begbie, J. (2007). Delamination of cells from neurogenic placodes does not involve an epithelial-to-mesenchymal transition. *Development* 134, 4141–4145. doi: 10.1242/dev.02886

Grocott, T., Tambalo, M., and Streit, A. (2012). The peripheral sensory nervous system in the vertebrate head: a gene regulatory perspective. *Dev. Biol.* 370, 3–23. doi: 10.1016/j.ydbio.2012.06.028

Groves, A. K., and LaBonne, C. (2014). Setting appropriate boundaries: fate, patterning and competence at the neural plate border. *Dev. Biol.* 389, 2–12. doi: 10.1016/j.ydbio.2013.11.027

Hall, B. K. (2018). Germ layers, the neural crest and emergent organization in development and evolution. *Genesis* 56:e23103. doi: 10.1002/dvg.23103

Hawley, S. H. B., Wünnenberg-Stapleton, K., Hashimoto, C., Laurent, M. N., Watabe, T., Blumberg, B. W., et al. (1995). Disruption of BMP signals in embryonic *Xenopus* ectoderm leads to direct neural induction. *Genes Dev.* 9, 2923–2935. doi: 10.1101/gad.9.23.2923

Hernandez-Lagunas, L., Powell, D. R., Law, J., Grant, K. A., and Artinger, K. B. (2011). Prdm1a and Olig4 act downstream of NOTCH signaling to regulate cell fate at the neural plate border. *Dev. Biol.* 356, 496–505. doi: 10.1016/j.ydbio.2011.06.005

Hintze, M., Prajapati, R. S., Tambalo, M., Christophorou, N. A. D., Anwar, M., Grocott, T., et al. (2017). Cell interactions, signals and transcriptional hierarchy governing placode progenitor induction. *Dev.* 144, 2810–2823. doi: 10.1242/dev.147942

Hong, C. S., Devotta, A., Lee, Y. H., Park, B. Y., and Saint-Jeannet, J. P. (2014). Transcription factor AP2 epsilon (Tfap2e) regulates neural crest specification in *Xenopus*. *Dev. Neurobiol.* 74, 894–906. doi: 10.1002/dneu.22173

Hong, C. S., and Saint-Jeannet, J. P. (2007). The activity of Pax3 and Zic1 regulates three distinct cell fates at the neural plate border. *Mol. Biol. Cell* 18, 2192–2202. doi: 10.1091/mbc.E06-11-1047

Hong, C. S., and Saint-Jeannet, J. P. (2017). Znf703, a novel target of Pax3 and Zic1, regulates hindbrain and neural crest development in *Xenopus*. *Genesis* 55:e23082. doi: 10.1002/dvg.23082

Janesick, A., Tang, W., Ampig, K., and Blumberg, B. (2019). Znf703 is a novel RA target in the neural plate border. *Sci. Rep.* 9:8275. doi: 10.1038/s41598-019-44722-1

Keller, R. E. (1976). Vital dye mapping of the gastrula and neurula of Xenopus laevis. II. Prospective areas and morphogenetic movements of the deep layer. *Dev. Biol.* 51, 118–137. doi: 10.1016/0012-1606(76)90127-5

Khatri, S. B., Edlund, R. K., and Groves, A. K. (2014). Foxi3 is necessary for the induction of the chick otic placode in response to FGF signaling. *Dev. Biol.* 391, 158–169. doi: 10.1016/j.ydbio.2014.04.014

Khatri, S. B., and Groves, A. K. (2013). Expression of the Foxi2 and Foxi3 transcription factors during development of chicken sensory placodes and pharyngeal arches. *Gene Expr. Patterns* 13, 38–42. doi: 10.1016/j.gep.2012.10.001

Khudyakov, J., and Bronner-Fraser, M. (2009). Comprehensive spatiotemporal analysis of early chick neural crest network genes. *Dev. Dyn.* 238, 716–723. doi: 10.1002/dvdy.21881

Kochhar, A., Fischer, S. M., Kimberling, W. J., and Smith, R. J. H. (2007). Branchio-oto-renal syndrome. *Am. J. Med. Genet* 143, 1671–1678. doi: 10.1002/ajmg.a.31561

Kozlowski, D. J., Murakami, T., Ho, R. K., and Weinberg, E. S. (1997). Regional cell movement and tissue patterning in the zebrafish embryo revealed by fate mapping with caged fluorescein. *Biochem. Cell Biol.* 75, 551–562. doi: 10.1139/o97-090

Kudoh, T., Concha, M. L., Houart, C., Dawid, I. B., and Wilson, S. W. (2004). Combinatorial Fgf and Bmp signalling patterns the gastrula ectoderm into prospective neural and epidermal domains. *Development* 131, 3581–3592. doi: 10.1242/dev.01227

Kwon, H. J., Bhat, N., Sweet, E. M., Cornell, R. A., and Riley, B. B. (2010). Identification of early requirements for preplacodal ectoderm and sensory organ development. *PLoS Genet.* 6:e1001133. doi: 10.1371/journal.pgen.1001133

Labonne, C., and Bronner-Fraser, M. (2000). Snail-related transcriptional repressors are required in *Xenopus* for both the induction of the neural crest and its subsequent migration. *Dev. Biol.* 221, 195–205. doi: 10.1006/dbio.2000.9609

Lander, R., Nasr, T., Ochoa, S. D., Nordin, K., Prasad, M. S., and Labonne, C. (2013). Interactions between Twist and other core epithelial-mesenchymal transition factors are controlled by GSK3-mediated phosphorylation. *Nat. Commun.* 4:1542. doi: 10.1038/ncomms2543

Lassiter, R. N. T., Stark, M. R., Zhao, T., and Zhou, C. J. (2014). Signaling mechanisms controlling cranial placode neurogenesis and delamination. *Dev. Biol.* 389, 39–49. doi: 10.1016/j.ydbio.2013.11.025

Le Douarin, N. M. (1980). The ontogeny of the neural crest in avian embryo chimaeras. *Nature* 286, 663–669. doi: 10.1038/286663a0

Li, B., Kuriyama, S., Moreno, M., and Mayor, R. (2009). The posteriorizing gene Gbx2 is a direct target of WNT signalling and the earliest factor in neural crest induction. *Development* 136, 3267–3278. doi: 10.1242/dev.036954

Li, Y., Vieceli, F. M., Gonzalez, W. G., Li, A., Tang, W., Lois, C., et al. (2019). In vivo quantitative imaging provides insights into trunk neural crest migration. *Cell Rep.* 26, 1489.e3–1500.e3. doi: 10.1016/j.celrep.2019.01.039

Linker, C., De Almeida, I., Papanayotou, C., Stower, M., Sabado, V., Ghorani, E., et al. (2009). Cell communication with the neural plate is required for induction of neural markers by BMP inhibition: evidence for homeogenetic induction and implications for *Xenopus* animal cap and chick explant assays. *Dev. Biol.* 327, 478–486. doi: 10.1016/j.ydbio.2008.12.034

Litsiou, A., Hanson, S., and Streit, A. (2005). A balance of FGF, BMP and WNT signaling positions the future placode territory in the head. *Development* 132, 4051–4062. doi: 10.1242/dev.01964

Longabaugh, W. J. R., Davidson, E. H., and Bolouri, H. (2005). Computational representation of developmental genetic regulatory networks. *Dev. Biol.* 283, 1–16. doi: 10.1016/j.ydbio.2005.04.023

Luo, T., Lee, Y. H., Saint-Jeannet, J. P., and Sargent, T. D. (2003). Induction of neural crest in *Xenopus* by transcription factor AP2α. *Proc. Natl. Acad. Sci. U. S. A.* 100, 532–537. doi: 10.1073/pnas.0237226100

Luo, T., Matsuo-Takasaki, M., and Sargent, T. D. (2001). Distinct roles for distal-less genes dlx3 and dlx5 in regulating ectodermal development in *Xenopus*. *Mol. Reprod. Dev.* 60, 331–337. doi: 10.1002/mrd.1095

Luo, T., Matsuo-Takasaki, M., Thomas, M. L., Weeks, D. L., and Sargent, T. D. (2002). Transcription factor AP-2 is an essential and direct regulator of epidermal development in *Xenopus*. *Dev. Biol.* 245, 136–144. doi: 10.1006/dbio.2002.0621

Maczkowiak, F., Matéos, S., Wang, E., Roche, D., Harland, R., and Monsoro-Burq, A. H. (2010). The Pax3 and Pax7 paralogs cooperate in neural and neural crest patterning using distinct molecular mechanisms, in *Xenopus laevis* embryos. *Dev. Biol.* 340, 381–396. doi: 10.1016/j.ydbio.2010.01.022

Maharana, S. K., and Schlosser, G. (2018). A gene regulatory network underlying the formation of pre-placodal ectoderm in *Xenopus laevis*. *BMC Biol.* 16:79. doi: 10.1186/s12915-018-0540-5

Mancilla, A., and Mayor, R. (1996). Neural crest formation in *Xenopus laevis*: mechanisms of Xslug induction. *Dev. Biol.* 177, 580–589. doi: 10.1006/dbio.1996.0187

Marchal, L., Luxardi, G., Thomé, V., and Kodjabachian, L. (2009). BMP inhibition initiates neural induction via FGF signaling and Zic genes. *Proc. Natl. Acad. Sci. U. S. A.* 106, 17437–17442. doi: 10.1073/pnas.0906352106

Martik, M. L., Gandhi, S., Uy, B. R., Gillis, J. A., Green, S. A., Simoes-Costa, M., et al. (2019). Evolution of the new head by gradual acquisition of neural crest regulatory circuits. *Nature* 574, 675–678. doi: 10.1038/s41586-019-1691-4

Martínez-Morales, P. L., del Corral, R. D., Olivera-Martínez, I., Quiroga, A. C., Das, R. M., Barbas, J. A., et al. (2011). FGF and retinoic acid activity gradients control the timing of neural crest cell emigration in the trunk. *J. Cell Biol.* 194, 489–503. doi: 10.1083/jcb.201011077

Matsuo-Takasaki, M., Matsumura, M., and Sasai, Y. (2005). An essential role of *Xenopus* Foxi1a for ventral specification of the cephalic ectoderm during gastrulation. *Development* 132, 3885–3894. doi: 10.1242/dev.01959

Mayor, R., and Theveneau, E. (2013). The neural crest. *Development* 140, 2247–2251. doi: 10.1242/dev.091751

McLarren, K. W., Litsiou, A., and Streit, A. (2003). Dlx5 positions the neural crest and preplacode region at the border of the neural plate. *Dev. Biol.* 259, 34–47. doi: 10.1016/S0012-1606(03)00177-5

Meulemans, D., and Bronner-Fraser, M. (2004). Gene-regulatory interactions in neural crest evolution and development. *Dev. Cell* 7, 291–299. doi: 10.1016/j.devcel.2004.08.007

Milet, C., Maczkowiak, F., Roche, D. D., and Monsoro-Burq, A. H. (2013). Pax3 and Zic1 drive induction and differentiation of multipotent, migratory, and functional neural crest in *Xenopus* embryos. *Proc. Natl. Acad. Sci.* 110, 5528–5533. doi: 10.1073/pnas.1219124110

Mizuseki, K., Kishi, M., Matsui, M., Nakanishi, S., and Sasai, Y. (1998). Xenopus Zic-related-1 and Sox-2, two factors induced by chordin, have distinct activities in the initiation of neural induction. *Development* 125, 579–587.

Monsoro-Burq, A. H., Fletcher, R. B., and Harland, R. M. (2003). Neural crest induction by paraxial mesoderm in *Xenopus* embryos requires FGF signals. *Development* 130, 3111–3124. doi: 10.1242/dev.00531

Monsoro-Burq, A. H., Wang, E., and Harland, R. (2005). Msx1 and Pax3 cooperate to mediate FGF8 and WNT signals during *Xenopus* neural crest induction. *Dev. Cell* 8, 167–178. doi: 10.1016/j.devcel.2004.12.017

Morrison, J. A., McLennan, R., Wolfe, L. A., Gogol, M. M., Meier, S., McKinney, M. C., et al. (2017). Single-cell transcriptome analysis of avian neural crest migration reveals signatures of invasion and molecular transitions. *eLife* 6:e28415. doi: 10.7554/eLife.28415

Mundell, N. A., and Labosky, P. A. (2011). Neural crest stem cell multipotency requires Foxd3 to maintain neural potential and repress mesenchymal fates. *J. Cell Sci.* 124, 641–652. doi: 10.1242/jcs.086983

Nagatomo, K. -I., and Hashimoto, C. (2007). *Xenopus* hairy2 functions in neural crest formation by maintaining cells in a mitotic and undifferentiated state. *Dev. Dyn.* 236, 1475–1483. doi: 10.1002/dvdy.21152

Nguyen, V. H., Schmid, B., Trout, J., Connors, S. A., Ekker, M., and Mullins, M. C. (1998). Ventral and lateral regions of the zebrafish gastrula, including the neural crest progenitors, are established by a Bmp2b/Swirl pathway of genes. *Dev. Biol.* 199, 93–110. doi: 10.1006/dbio.1998.8927

Nichane, M., de Crozé, N., Ren, X., Souopgui, J., Monsoro-Burq, A. H., and Bellefroid, E. J. (2008a). Hairy2-Id3 interactions play an essential role in *Xenopus* neural crest progenitor specification. *Dev. Biol.* 322, 355–367. doi: 10.1016/j.ydbio.2008.08.003

Nichane, M., Ren, X., Souopgui, J., and Bellefroid, E. J. (2008b). Hairy2 functions through both DNA-binding and non DNA-binding mechanisms at the neural plate border in *Xenopus*. *Dev. Biol.* 322, 368–380. doi: 10.1016/j.ydbio.2008.07.026

Nieto, M. A., Sargent, M. G., Wilkinson, D. G., and Cooke, J. (1994). Control of cell behavior during vertebrate development by Slug, a zinc finger gene. *Science* 264, 835–839. doi: 10.1126/science.7513443

Noden, D. M. (1975). An analysis of the migratory behavior of avian cephalic neural crest cells. *Dev. Biol.* 42, 106–130. doi: 10.1016/0012-1606(75)90318-8

Northcutt, R. G. (2005). The new head hypothesis revisited. *J. Exp. Zool. B Mol. Dev. Evol.* 304, 274–297. doi: 10.1002/jez.b.21063

Ohto, H., Kamada, S., Tago, K., Tominaga, S. -I., Ozaki, H., Sato, S., et al. (1999). Cooperation of six and Eya in activation of their target genes through nuclear translocation of Eya. *Mol. Cell. Biol.* 19, 6815–6824. doi: 10.1128/mcb.19.10.6815

Otto, A., Schmidt, C., and Patel, K. (2006). Pax3 and Pax7 expression and regulation in the avian embryo. *Anat. Embryol.* 211, 293–310. doi: 10.1007/s00429-006-0083-3

Pandur, P. D., and Moody, S. A. (2000). *Xenopus* Six1 gene is expressed in neurogenic cranial placodes and maintained in the differentiating lateral lines. *Mech. Dev.* 96, 253–257. doi: 10.1016/S0925-4773(00)00396-8

Patthey, C., Gunhaga, L., and Edlund, T. (2008). Early development of the central and peripheral nervous systems is coordinated by WNT and BMP signals. *PLoS One* 3:e1625. doi: 10.1371/journal.pone.0001625

Pera, E., Stein, S., and Kessel, M. (1999). Ectodermal patterning in the avian embryo: epidermis versus neural plate. *Development* 126, 63–73.

Pera, E. M., and De Robertis, E. M. (2000). A direct screen for secreted proteins in *Xenopus* embryos identifies distinct activities for the Wnt antagonists Crescent and Frzb-1. *Mech. Dev.* 96, 183–195. doi: 10.1016/S0925-4773(00)00394-4

Phillips, B. T., Kwon, H. J., Melton, C., Houghtaling, P., Fritz, A., and Riley, B. B. (2006). Zebrafish msxB, msxC and msxE function together to refine the neural-nonneural border and regulate cranial placodes and neural crest development. *Dev. Biol.* 294, 376–390. doi: 10.1016/j.ydbio.2006.03.001

Piacentino, M. L., and Bronner, M. E. (2018). Intracellular attenuation of BMP signaling via CKIP-1/Smurf1 is essential during neural crest induction. *PLoS Biol.* 16:e2004425. doi: 10.1371/journal.pbio.2004425

Piacentino, M. L., Li, Y., and Bronner, M. E. (2020). Epithelial-to-mesenchymal transition and different migration strategies as viewed from the neural crest. *Curr. Opin. Cell Biol.* 66, 43–50. doi: 10.1016/j.ceb.2020.05.001

Pieper, M., Ahrens, K., Rink, E., Peter, A., and Schlosser, G. (2012). Differential distribution of competence for panplacodal and neural crest induction to non-neural and neural ectoderm. *Development* 139, 1175–1187. doi: 10.1242/dev.074468

Pieper, M., Eagleson, G. W., Wosniok, W., and Schlosser, G. (2011). Origin and segregation of cranial placodes in *Xenopus laevis*. *Dev. Biol.* 360, 257–275. doi: 10.1016/j.ydbio.2011.09.024

Piotrowski, T., and Baker, C. V. H. (2014). The development of lateral line placodes: taking a broader view. *Dev. Biol.* 389, 68–81. doi: 10.1016/j.ydbio.2014.02.016

Pla, P., and Monsoro-Burq, A. H. (2018). The neural border: induction, specification and maturation of the territory that generates neural crest cells. *Dev. Biol.* 444, S36–S46. doi: 10.1016/j.ydbio.2018.05.018

Plouhinec, J. L., Medina-Ruiz, S., Borday, C., Bernard, E., Vert, J. P., Eisen, M. B., et al. (2017). A molecular atlas of the developing ectoderm defines neural, neural crest, placode, and nonneural progenitor identity in vertebrates. *PLoS Biol.* 15:e2004045. doi: 10.1371/journal.pbio.2004045

Plouhinec, J. L., Roche, D. D., Pegoraro, C., Figueiredo, A. L., Maczkowiak, F., Brunet, L. J., et al. (2014). Pax3 and Zic1 trigger the early neural crest gene regulatory network by the direct activation of multiple key neural crest specifiers. *Dev. Biol.* 386, 461–472. doi: 10.1016/j.ydbio.2013.12.010

Prasad, M. S., Charney, R. M., and García-Castro, M. I. (2019). Specification and formation of the neural crest: perspectives on lineage segregation. *Genesis* 57:e23276. doi: 10.1002/dvg.23276

Richardson, J., Gauert, A., Briones Montecinos, L., Fanlo, L., Alhashem, Z. M., Assar, R., et al. (2016). Leader cells define directionality of trunk, but not cranial, neural crest cell migration. *Cell Rep.* 15, 2076–2088. doi: 10.1016/j.celrep.2016.04.067

Riddiford, N., and Schlosser, G. (2016). Dissecting the pre-placodal transcriptome to reveal presumptive direct targets of Six1 and Eya1 in cranial placodes. *eLife* 5:e17666. doi: 10.7554/eLife.17666

Rocha, M., Singh, N., Ahsan, K., Beiriger, A., and Prince, V. E. (2020). Neural crest development: insights from the zebrafish. *Dev. Dyn.* 249, 88–111. doi: 10.1002/dvdy.122

Roellig, D., Tan-Cabugao, J., Esaian, S., and Bronner, M. E. (2017). Dynamic transcriptional signature and cell fate analysis reveals plasticity of individual neural plate border cells. *eLife* 6:e21620. doi: 10.7554/eLife.21620

Rogers, C. D., and Nie, S. (2019). Specifying neural crest cells: from chromatin to morphogens and factors in between. *Wiley Interdiscip. Rev. Dev. Biol.* 7:e322. doi: 10.1002/wdev.322

Rothstein, M., and Simoes-Costa, M. (2020). Heterodimerization of Tfap2 pioneer factors drives epigenomic remodeling during neural crest specification. *Genome Res.* 30, 35–48. doi: 10.1101/gr.249680.119

Sasai, N., Mizuseki, K., and Sasai, Y. (2001). Requirement of Foxd3-class signaling for neural crest determination in *Xenopus*. *Development* 128, 2525–2536.

Sato, S., Ikeda, K., Shioi, G., Ochi, H., Ogino, H., Yajima, H., et al. (2010). Conserved expression of mouse Six1 in the pre-placodal region (PPR) and identification of an enhancer for the rostral PPR. *Dev. Biol.* 344, 158–171. doi: 10.1016/j.ydbio.2010.04.029

Sato, T., Sasai, N., and Sasai, Y. (2005). Neural crest determination by co-activation of Pax3 and Zic1 genes in *Xenopus* ectoderm. *Development* 132, 2355–2363. doi: 10.1242/dev.01823

Sauka-Spengler, T., Meulemans, D., Jones, M., and Bronner-Fraser, M. (2007). Ancient evolutionary origin of the neural crest gene regulatory network. *Dev. Cell* 13, 405–420. doi: 10.1016/j.devcel.2007.08.005

Scerbo, P., and Monsoro-Burq, A. H. (2020). The vertebrate-specific VENTX/NANOG gene empowers neural crest with ectomesenchyme potential. *Sci. Adv.* 6:eaaz1469. doi: 10.1126/sciadv.aaz1469

Schille, C., and Schambony, A. (2017). Signaling pathways and tissue interactions in neural plate border formation. *Neurogenesis* 4:e1292783. doi: 10.1080/23262133.2017.1292783

Schlosser, G. (2008). Do vertebrate neural crest and cranial placodes have a common evolutionary origin? *BioEssays* 30, 659–672. doi: 10.1002/bies.20775

Schlosser, G. (2010). "Making senses development of vertebrate cranial placodes" in *International review of cell and molecular biology*. ed. K. Jeon (Elsevier), 129–234.

Schlosser, G. (2014). Early embryonic specification of vertebrate cranial placodes. *Wiley Interdiscip. Rev. Dev. Biol.* 3, 349–363. doi: 10.1002/wdev.142

Schlosser, G., Awtry, T., Brugmann, S. A., Jensen, E. D., Neilson, K., Ruan, G., et al. (2008). Eya1 and Six1 promote neurogenesis in the cranial placodes in a SoxB1-dependent fashion. *Dev. Biol.* 320, 199–214. doi: 10.1016/j.ydbio.2008.05.523

Shellard, A., and Mayor, R. (2019). Integrating chemical and mechanical signals in neural crest cell migration. *Curr. Opin. Genet. Dev.* 57, 16–24. doi: 10.1016/j.gde.2019.06.004

Sheng, G., and Stern, C. D. (1999). Gata2 and Gata3: novel markers for early embryonic polarity and for non-neural ectoderm in the chick embryo. *Mech. Dev.* 87, 213–216. doi: 10.1016/S0925-4773(99)00150-1

Simoes-Costa, M., and Bronner, M. E. (2015). Establishing neural crest identity: a gene regulatory recipe. *Development* 142, 242–257. doi: 10.1242/dev.105445

Simoes-Costa, M., and Bronner, M. E. (2016). Reprogramming of avian neural crest axial identity and cell fate. *Science* 352, 1570–1573. doi: 10.1126/science.aaf2729

Simões-Costa, M. S., McKeown, S. J., Tan-Cabugao, J., Sauka-Spengler, T., and Bronner, M. E. (2012). Dynamic and differential regulation of stem cell factor Foxd3 in the neural crest is encrypted in the genome. *PLoS Genet.* 8:e1003142. doi: 10.1371/journal.pgen.1003142

Simões-Costa, M., Tan-Cabugao, J., Antoshechkin, I., Sauka-Spengler, T., and Bronner, M. E. (2014). Transcriptome analysis reveals novel players in the cranial neural crest gene regulatory network. *Genome Res.* 24, 281–290. doi: 10.1101/gr.161182.113

Singh, S., and Groves, A. K. (2016). The molecular basis of craniofacial placode development. *Wiley Interdiscip. Rev. Dev. Biol.* 5, 363–376. doi: 10.1002/wdev.226

Sittewelle, M., and Monsoro-Burq, A. H. (2018). AKT signaling displays multifaceted functions in neural crest development. *Dev. Biol.* 444, S144–S155. doi: 10.1016/j.ydbio.2018.05.023

Soldatov, R., Kaucka, M., Kastriti, M. E., Petersen, J., Chontorotzea, T., Englmaier, L., et al. (2019). Spatiotemporal structure of cell fate decisions in murine neural crest. *Science* 364:eaas9536. doi: 10.1126/science.aas9536

Steventon, B., Araya, C., Linker, C., Kuriyama, S., and Mayor, R. (2009). Differential requirements of BMP and WNT signalling during gastrulation and neurulation define two steps in neural crest induction. *Development* 136, 771–779. doi: 10.1242/dev.029017

Steventon, B., and Mayor, R. (2012). Early neural crest induction requires an initial inhibition of WNT signals. *Dev. Biol.* 365, 196–207. doi: 10.1016/j.ydbio.2012.02.029

Streit, A. (2002). Extensive cell movements accompany formation of the otic placode. *Dev. Biol.* 249, 237–254. doi: 10.1006/dbio.2002.0739

Streit, A. (2018). Specification of sensory placode progenitors: signals and transcription factor networks. *Int. J. Dev. Biol.* 62, 191–201. doi: 10.1387/ijdb.170298as

Streit, A., Berliner, A. J., Papanayotou, C., Slrulnik, A., and Stern, C. D. (2000). Initiation of neural induction by FGF signalling before gastrulation. *Nature* 406, 74–78. doi: 10.1038/35017617

Streit, A., and Stern, C. D. (1999). Establishment and maintenance of the border of the neural plate in the chick: involvement of FGF and BMP activity. *Mech. Dev.* 82, 51–66. doi: 10.1016/S0925-4773(99)00013-1

Stuhlmiller, T. J., and García-Castro, M. I. (2012). Current perspectives of the signaling pathways directing neural crest induction. *Cell. Mol. Life Sci.* 69, 3715–3737. doi: 10.1007/s00018-012-0991-8

Suzuki, A., Ueno, N., and Hemmati-Brivanlou, A. (1997). *Xenopus* msx1 mediates epidermal induction and neural inhibition by BMP4. *Development* 124, 3037–3044.

Sykes, T. G., Rodaway, A. R. F., Walmsley, M. E., and Patient, R. K. (1998). Suppression of GATA factor activity causes axis duplication in *Xenopus*. *Development* 125, 4595–4605.

Szabó, A., and Mayor, R. (2018). Mechanisms of neural crest migration. *Annu. Rev. Genet.* 52, 43–63. doi: 10.1146/annurev-genet-120417-031559

Tambalo, M., Mitter, R., and Wilkinson, D. G. (2020). A single cell transcriptome atlas of the developing zebrafish hindbrain. *Development* 147:dev184143. doi: 10.1242/dev.184143

Teng, L., Mundel, N. A., Frist, A. Y., Wang, Q., and Labosky, P. A. (2008). Requirement for Foxd3 in the maintenance of neural crest progenitors. *Development* 135, 1615–1624. doi: 10.1242/dev.012179

Theveneau, E., and Mayor, R. (2012). Neural crest delamination and migration: from epithelium-to-mesenchyme transition to collective cell migration. *Dev. Biol.* 366, 34–54. doi: 10.1016/j.ydbio.2011.12.041

Theveneau, E., Steventon, B., Scarpa, E., Garcia, S., Trepat, X., Streit, A., et al. (2013). Chase-and-run between adjacent cell populations promotes directional collective migration. *Nat. Cell Biol.* 15, 763–772. doi: 10.1038/ncb2772

Thiery, A., Buzzi, A. L., and Streit, A. (2020). "Cell fate decisions during the development of the peripheral nervous system in the vertebrate head" in *Current topics in developmental biology*. ed. I. S. Peter (Cambridge, MA, United States: Academic Press, Elsevier) 127–167.

Trevers, K. E., Prajapati, R. S., Hintze, M., Stower, M. J., Strobl, A. C., Tambalo, M., et al. (2018). Neural induction by the node and placode induction by head mesoderm share an initial state resembling neural plate border and ES cells. *Proc. Natl. Acad. Sci. U. S. A.* 115, 355–360. doi: 10.1073/pnas.1719674115

Tribulo, C., Aybar, M. J., Nguyen, V. H., Mullins, M. C., and Mayor, R. (2003). Regulation of Msx genes by a Bmp gradient is essential for neural crest specification. *Development* 130, 6441–6452. doi: 10.1242/dev.00878

Vadasz, S., Marquez, J., Tulloch, M., Shylo, N. A., and García-Castro, M. I. (2013). Pax7 is regulated by cMyb during early neural crest development through a novel enhancer. *Development* 140, 3691–3702. doi: 10.1242/dev.088328

Vega-Lopez, G. A., Cerrizuela, S., Tribulo, C., and Aybar, M. J. (2018). Neurocristopathies: new insights 150 years after the neural crest discovery. *Dev. Biol.* 444, S110–S143. doi: 10.1016/j.ydbio.2018.05.013

Villanueva, S., Glavic, A., Ruiz, P., and Mayor, R. (2002). Posteriorization by FGF, WNT, and retinoic acid is required for neural crest induction. *Dev. Biol.* 241, 289–301. doi: 10.1006/dbio.2001.0485

Wilson, P. A., and Hemmati-Brivanlou, A. (1995). Induction of epidermis and inhibition of neural fate by Bmp-4. *Nature* 376, 331–333. doi: 10.1038/376331a0

Wilson, S. I., Rydström, A., Trimborn, T., Willert, K., Musse, R., Jessell, T. M., et al. (2001). The status of WNT signalling regulates neural and epidermal fates in the chick embryo. *Nature* 411, 325–330. doi: 10.1038/35077115

Wynn, M. L., Rupp, P., Trainor, P. A., Schnell, S., and Kulesa, P. M. (2013). Follow-the-leader cell migration requires biased cell-cell contact and local microenvironmental signals. *Phys. Biol.* 10:035003. doi: 10.1088/1478-3975/10/3/035003

Xu, H., Dude, C. M., and Baker, C. V. H. (2008). Fine-grained fate maps for the ophthalmic and maxillomandibular trigeminal placodes in the chick embryo. *Dev. Biol.* 317, 174–186. doi: 10.1016/j.ydbio.2008.02.012

Yardley, N., and García-Castro, M. I. (2012). FGF signaling transforms non-neural ectoderm into neural crest. *Dev. Biol.* 372, 166–177. doi: 10.1016/j.ydbio.2012.09.006

Zhang, J. M., Hoffmann, R., and Sieber-Blum, M. (1997). Mitogenic and anti-proliferative signals for neural crest cells and the neurogenic action of TGF-β1. *Dev. Dyn.* 208, 375–386. doi: 10.1002/(SICI)1097-0177(199703)208:3<375::AID-AJA8>3.0.CO;2-F

Conflict of Interest: The authors declare that the research was conducted in the absence of any commercial or financial relationships that could be construed as a potential conflict of interest.

frontiers in Physiology

REVIEW
published: 07 December 2020
doi: 10.3389/fphys.2020.608880

Building the Border: Development of the Chordate Neural Plate Border Region and Its Derivatives

Ankita Thawani[1] *and Andrew K. Groves*[1,2]*

[1]Department of Neuroscience, Baylor College of Medicine, Houston, TX, United States, [2]Department of Molecular and Human Genetics, Baylor College of Medicine, Houston, TX, United States

The paired cranial sensory organs and peripheral nervous system of vertebrates arise from a thin strip of cells immediately adjacent to the developing neural plate. The neural plate border region comprises progenitors for four key populations of cells: neural plate cells, neural crest cells, the cranial placodes, and epidermis. Putative homologues of these neural plate border derivatives can be found in protochordates such as amphioxus and tunicates. In this review, we summarize key signaling pathways and transcription factors that regulate the inductive and patterning events at the neural plate border region that give rise to the neural crest and placodal lineages. Gene regulatory networks driven by signals from WNT, fibroblast growth factor (FGF), and bone morphogenetic protein (BMP) signaling primarily dictate the formation of the crest and placodal lineages. We review these studies and discuss the potential of recent advances in spatio-temporal transcriptomic and epigenomic analyses that would allow a mechanistic understanding of how these signaling pathways and their downstream transcriptional cascades regulate the formation of the neural plate border region.

Keywords: neural crest, placodes, CNS - central nervous system, PNS, signaling / signaling pathways, transcription factor, embryo, development

OPEN ACCESS

Edited by:
Jean-Pierre Saint-Jeannet, New York University, United States

Reviewed by:
David W. McCauley, University of Oklahoma,United States
Gerhard Schlosser, National University of Ireland Galway, Ireland

***Correspondence:**
Andrew K. Groves
akgroves@bcm.edu

Specialty section:
This article was submitted to Embryonic and Developmental Physiology, a section of the journal Frontiers in Physiology

Received: *21 September 2020*
Accepted: *19 November 2020*
Published: *07 December 2020*

Citation:
Thawani A and Groves AK (2020) Building the Border: Development of the Chordate Neural Plate Border Region and Its Derivatives. Front. Physiol. 11:608880. doi: 10.3389/fphys.2020.608880

INTRODUCTION

The neural plate border is one of the most developmentally complex regions in the vertebrate embryo. During the gastrulation, the epiblast begins to display signs of patterning, with the medial portion adopting a neural identity and the lateral aspect adopting a non-neural (epidermal) identity. The neural plate border region arises between the future anterior neural plate and the future epidermis in response to a series of inductive signals. Cells that intermingle at the border of the neural plate give rise to four distinct cell lineages: (1) neural progenitors that form the anterior central nervous system (CNS), (2) neural crest cells that form the peripheral nervous system, pigment cells, and much of the bone and cartilage of the face, (3) the craniofacial placodes that form complex sensory organs such as the inner ear and the olfactory epithelium, and (4) the cranial epidermis (Grocott et al., 2012; Groves and LaBonne, 2014). The fascination

with this transient embryonic region is due not only to its biological significance but also to its relevance to human disease: genetic or environmental perturbations of this region collectively contribute to an enormous range of birth defects affecting the brain, skull, face, and sensory organs.

The differentiation of the neural plate border region is remarkable for several reasons. First, the four lineages generated at the border each give rise to a large number of very different cell types. Segregation of the border region into CNS neuroepithelial stem cells, neural crest cells, placodal progenitors, and epidermal stem cells requires that the four lineages become distinct from each other, while individually retaining the potential to generate a wide variety of fates within each lineage. Second, this process of segregation is extremely rapid – the events described in this review occur over a period of about 12 h in amniotes and even more rapidly in fish and amphibians, while throughout this time, the cells are dividing and changing position with respect to each other at the border. Third, the secreted inducing signals, such as BMPs, FGFs, and WNTs, that induce border region fates act over very short distances and for very short periods of time, yet somehow manage to co-operate to quickly segregate the four lineages to preclude any subsequent conversion of progenitors from one lineage into those of another. Fourth, recent studies from non-vertebrate chordates suggest that the first step in the evolution of neural crest and cranial placodes – two vertebrate novelties that appear to have arisen independently – may already have begun as the first chordates arose, and understanding the mechanisms underlying these early events may shed light on the mechanisms of border region development in vertebrates.

As gastrulation proceeds, the commitment of epiblast to one of the four border region lineages described above requires large-scale epigenetic and transcriptional changes. At present, we know almost nothing about how the chromatin of border region progenitors is rearranged and reconfigured to render some regions of the genome accessible in each lineage while simultaneously placing other regions permanently beyond use. At one extreme, the epigenome of primitive ectoderm or epiblast could gradually be transformed into multipotential cells of progressively more restricted fates, culminating in the four border lineages. At the other extreme, large scale chromatin remodeling of epiblast cells could assign them to one of these four lineages in a very short period without passing through a more multipotential intermediate. Recent advances in the ability to profile the transcriptomic and epigenetic states of individual cells mean that answering these questions may finally be experimentally tractable.

Here, we discuss the known molecular mechanisms of neural plate border differentiation, focusing on the role of morphogenetic signaling pathways and transcriptional regulators in refining boundaries between the derivatives of the neural plate border. A number of excellent reviews of the neural plate border region and its evolutionary origins have appeared in recent years, and so in addition to summarizing these mechanisms, we will also focus on a series of unresolved questions concerning the neural plate border and possible ways to address them in future.

DEVELOPMENT OF THE NEURAL PLATE BORDER AND THE FATES AND POTENTIALS OF BORDER PROGENITORS

The Temporal Sequence of Neural Plate Border Formation

The first evidence of division of embryonic epiblast into future neural and non-neural domains can be seen in many vertebrates prior to the onset of gastrulation. Early neural markers, such as *Otx2*, *Sox3*, *ERNI*, and *Geminin*, are expressed in dorsal ectoderm destined to give rise to the neural plate (Bally-Cuif et al., 1995; Rex et al., 1997; Kroll et al., 1998; Streit et al., 2000; Papanayotou et al., 2008). Some of these genes, sometimes referred to as "pre-neural" markers, can be induced by neural fate-inducing molecules, such as FGFs, or WNT and BMP antagonists (Streit et al., 2000; Wilson and Edlund, 2001; Albazerchi and Stern, 2007; Papanayotou et al., 2008; Rogers et al., 2011; Stern and Downs, 2012). Regions of the embryo where WNT and BMP signaling are not being actively inhibited begin to express the markers broadly considered as non-neural, such as members of the *Ap2*, *Dlx*, *Foxi*, *Gata2/3*, and *Msx* transcription factor gene families (Papalopulu and Kintner, 1993; Pera et al., 1999; Sheng and Stern, 1999; Luo et al., 2001; Knight et al., 2003; McLarren et al., 2003; Woda et al., 2003; Ohyama and Groves, 2004a; Brown et al., 2005; Matsuo-Takasaki et al., 2005; Phillips et al., 2006; Hans et al., 2007; Hoffman et al., 2007; Li and Cornell, 2007; Pieper et al., 2012; **Figure 1**).

As the early epiblast continues to receive signals from the organizer, additional genes considered to define neural tissue, such as *Sox2*, begin to express (Rex et al., 1997; Streit et al., 1997; Uchikawa et al., 2003). Simultaneously, expression of many non-neural genes becomes restricted to regions close to the developing neural plate (Feledy et al., 1999a; Streit, 2002; Woda et al., 2003; Khudyakov and Bronner-Fraser, 2009; Kwon et al., 2010; Pieper et al., 2012) under the influence of specific levels of BMP inhibition and FGF signaling. It is at this point that the earliest components of the neural crest gene regulatory network appear at the edge of the developing neural plate, such as *Pax* and *Zic* gene family members, *Msx1/2*, and *Ap2* (Monsoro-Burq et al., 2003; Basch et al., 2006; Hong and Saint-Jeannet, 2007; Khudyakov and Bronner-Fraser, 2009; Murdoch et al., 2010; Milet et al., 2013; Prasad et al., 2020), followed by later neural crest gene regulatory network-related members such as *Snail* and *Twist* family members, *Foxd3*, *Sox9*, and later, *Sox10* (reviewed in Prasad et al., 2012; Martik and Bronner, 2018; Hovland et al., 2020). BMP, FGF, and WNT signals derived from the future epidermis, neural plate, and mesoderm all participate in the positioning of these genes at the neural plate border (reviewed in Groves and LaBonne, 2014; Pla and Monsoro-Burq, 2018; Prasad et al., 2019; **Figure 1**). The source and timings of these signals varies in different vertebrate groups, but their function of inducing early neural plate border markers is generally conserved (reviewed in this Research Topic by York et al., 2020).

Shortly after the first evidence of neural crest formation, a band of ectoderm slightly lateral to the domain of neural crest

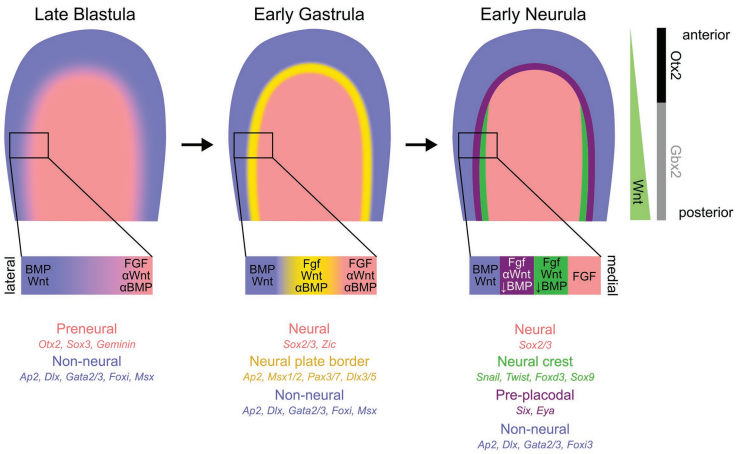

FIGURE 1 | Early ectodermal patterning at the anterior epiblast. Although the ectodermal patterning varies significantly across chordates, and even within amniotes, we illustrate, here, the key stages of ectodermal patterning most faithful to amniote development. The medial epiblast begins to exhibit molecular differences compared to the surrounding tissue, with the medial region expressing pre-neural/neural (salmon) markers and lateral (blue) region with predominantly non-neural/epidermal gene expression. At the initial stages of gastrulation, the transitional zone between the neural and non-neural ectoderm, called the neural plate border (yellow), becomes more defined. By the early stages of neurulation, two distinct spatially segregated populations of cells can be detected at the border region – pre-placodal ectoderm laterally (purple) and neural crest cell progenitors medially (green). Although much remains uncertain about the roles and timing of WNT, BMP, and FGF signaling pathways and associated gene-regulatory networks during the early ectodermal patterning, a general consensus of the signaling levels and classic spatially distinct markers are indicated below the epiblast cartoons. Additionally, the asymmetric WNT signaling along the anterior-posterior axis and, subsequently, key molecular expression differences are also presented on the right-most panel.

markers begins to express members of the Six and Eya families (Streit, 2002; Litsiou et al., 2005; Christophorou et al., 2009; Grocott et al., 2012). This region contains undifferentiated placodal progenitors and has been termed the pre-placodal region (Grocott et al., 2012; Groves and LaBonne, 2014; Patthey et al., 2014; Schlosser et al., 2014). Some genes that initially appear to be broadly expressed in non-neural ectoderm, such as *Foxi3* and *Gata3*, refine to the pre-placodal region (Streit, 2007; Khatri et al., 2014). In contrast, *Six* and *Eya* family genes appear *de novo* in the anterior neural plate border region, extending from approximately the first pair of somites to the most anterior regions of the neural plate (Mishima and Tomarev, 1998; Esteve and Bovolenta, 1999; Kobayashi et al., 2000; Pandur and Moody, 2000; McLarren et al., 2003; Bessarab et al., 2004; Brugmann et al., 2004; Ahrens and Schlosser, 2005; Litsiou et al., 2005; Ishihara et al., 2008; **Figure 1**). *Six* and *Eya* gene family members continue to be expressed in many placodal derivatives as they differentiate (Xu et al., 1999; Zhu et al., 2002; Zheng et al., 2003; Bessarab et al., 2004; Zhang et al., 2004; Zou et al., 2004, 2006; Purcell et al., 2005; Schlosser, 2007; Ahmed et al., 2012a,b), but genes specific to sub-populations of placodes subsequently appear in this region in response to local inducing signals – for example, *Pax2/8* genes in the otic and epibranchial placode region, *Pax3* in the ophthalmic trigeminal ganglion, and *Pax6* in the future lens and olfactory placodes (Baker et al., 1999; Groves and Bronner-Fraser, 2000; Bhattacharyya et al., 2004; Ohyama and Groves, 2004b).

Rostro-Caudal Patterning of the Neural Plate Border Region

Neural crest cells originating from the neural folds, delaminate during the neural tube closure, and migrate into the head and trunk to generate various skeletal and sensory structures along the anterior-posterior axis: (1) skeletal mesenchyme of the face, (2) parasympathetic ganglia and glia, (3) sympathetic ganglia and glia, (4) enteric nervous system and glia, (5) glial cells and sensory neurons of the head and dorsal root ganglia, and (6) pigment cells (Begbie, 2013). Similarly, the pre-placodal domain gives rise to multiple patches of thickened epithelium that invaginate or migrate short distances to form distinct mature derivatives from anterior to posterior end of the cranial region: (1) adenohypophysis (pituitary gland), (2) olfactory neurons, (3) lens, (4) trigeminal ganglion (cranial ganglion V), (5) inner ear, (6) epibranchial ganglia (cranial ganglia VII, IX, and X), and (7) the anterior and posterior lateral line (absent in amniotes; **Figure 2**; Begbie, 2013; Singh and Groves, 2016). The vertebrate cranial placodes differentiate into many cell types: sensory neurons, secondary sensory receptor cells, and secretory cells, as well as their associated supporting cells. Migrating cranial neural crest cells have a close relationship with placodal development, despite that the crest cells migrate much large distances from the neural folds compared to the placodes that thicken, invaginate, and migrate short distances. The neural crest cells populate placode-derived sensory ganglia with glial cells (see, for example, Sandell et al., 2014).

Molecular asymmetries emerge along the rostro-caudal axis during gastrulation as the ectoderm receives progressively more posteriorizing neural induction signals. *Otx2* and *Gbx2* are expressed in the anterior and posterior epiblast, respectively, and this pattern is maintained by mutual repression as the neural plate is induced and patterned, ultimately delineating the boundary between midbrain and hindbrain (**Figure 1**; reviewed in Wurst and Bally-Cuif, 2001). Slightly later, additional

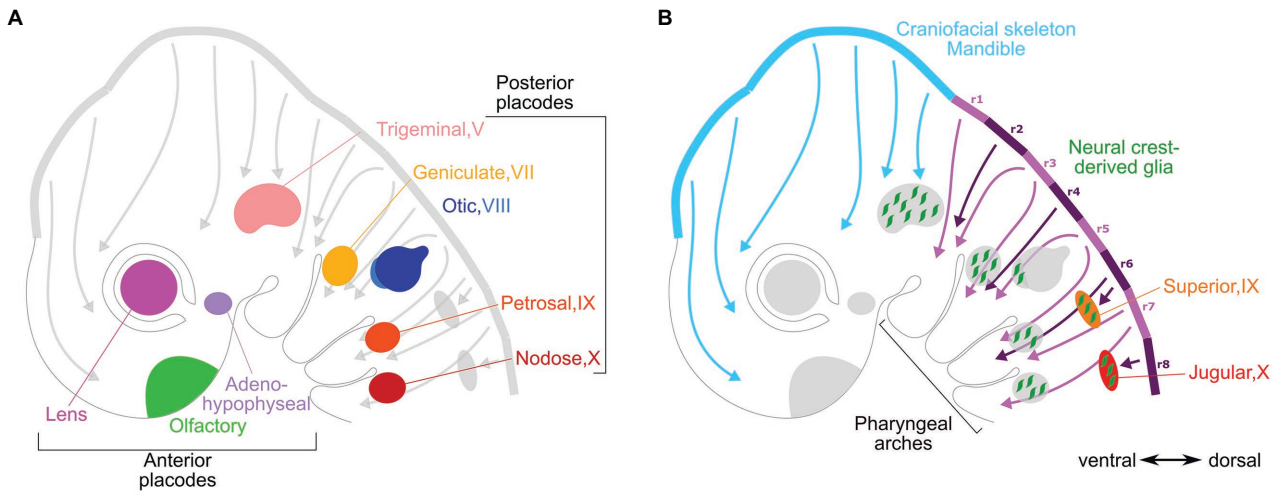

FIGURE 2 | Vertebrate placodal and neural crest derivatives. Diagrams of an approximately 10-day old mouse embryo show **(A)** cranial placodal derivatives and **(B)** cranial neural crest derivatives. The arrows from dorsal to ventral sides of the embryo represent paths of the neural crest migration from the dorsal neural folds that would begin during neurulation around day 8. In both panels, the roman numerals represent the cranial nerves that the sensory ganglia are associated with: the posterior placodal-derived ganglia in **(A)** and neural crest-derived proximal ganglia in **(B)**. In panel **(B)** the rhombomeres are indicated in purple (numbered r1–r8) and midbrain and diencephalon in light blue.

transcription factors, such as members of the Pax, Six, and Irx families, are also expressed in mutually exclusive domains along the rostral-caudal axis of the neural plate (reviewed in Gómez-Skarmeta et al., 2003). For example, Pax6 is expressed in an anterior domain of the future forebrain, whereas Pax2 is in the future midbrain, while Six1 and Irx3 sub-divide the forebrain into anterior and posterior compartments. Interestingly, some of these anterior-posterior patterning events also occur in the pre-placodal region, with Otx2 and Gbx2 being expressed in register with their domains in the neural plate, and being required for aspects of trigeminal and otic placode development, respectively (Steventon et al., 2012). Several *Pax* genes are expressed along the anterior-posterior axis in a spatially distinct pattern with *Pax6*, *Pax3*, and *Pax2/8* contributing to patterning the placodal derivatives, and also labeling them at later stages of development (Groves and Bronner-Fraser, 2000; Saint-Jeannet and Moody, 2014).

In contrast to more anterior neural patterning genes, Hox genes are not expressed in pre-placodal ectoderm and are restricted to the neural plate posterior to rhombomere 1 of the hindbrain but not to pre-placodal ectoderm. As neural crest cells migrate out of the hindbrain to populate the branchial arches, they maintain some parts of the combinatorial Hox code, but not others – for example, crest cells invading the first branchial arch express no Hox genes at all, whereas crest cells invading the second arch maintain expression of *Hoxa2* and *Hoxb2*, but not *Hoxb1* (reviewed in Parker et al., 2018). It is known that the environment into which crest cells migrate can modulate Hox gene expression (Trainor and Krumlauf, 2000a,b), but the environmental signals and transcriptional regulators that exclude Hox genes from the adjacent pre-placodal ectoderm are unknown. As progress continues to be made in understanding how signals that regulate Hox genes interact with the neural crest gene regulatory network (Parker et al., 2018), it will be of interest to understand how mechanisms that exclude Hox genes from placodal precursors arose during the evolution of neural crest and placodes in basal chordate lineages.

Why do the most anterior regions of the neural plate not generate neural crest? The olfactory placode is derived from the anterior neural fold (Couly and Le Douarin, 1985) which contains multipotent progenitors able to form epidermis, the olfactory placode and the olfactory bulb, and forebrain (Bhattacharyya and Bronner, 2013; Torres-Paz et al., 2020), but not neural crest cells. However, the anterior neural fold has transient competence to generate at least some neural crest, as grafting the chick anterior neural fold to the rostral hindbrain produces migratory neural crest. These cells also give rise to some epidermis, just as they do in their normal location (Ezin et al., 2014). The environmental signals that specifically promote placodal differentiation and repress the neural crest program in the anterior region of the neural plate border are currently unknown, although it is clear that WNT, BMP, and retinoic acid signals that affect the gross anterior-posterior pattern of the neural plate (for example, Kiecker and Niehrs, 2001) can also regulate neural crest production (Villanueva et al., 2002). For instance, knockdown of the WNT antagonist genes *Dkk* and some *Tcf/Lef* members in the anterior epiblast results in crest cell induction at the anterior neural fold (Carmona-Fontaine et al., 2007; Mašek et al., 2016).

Unresolved Issues Concerning Lineage Segregation at the Neural Plate Border

In the previous section, we described the main gene markers whose appearance defines the neural plate, neural crest,

pre-placodal region, and future epidermis. It should be emphasized, however, that the expression of many genes in the border region early stage is not uniform, with some sets of genes previously assigned as markers of a particular lineage being expressed more laterally in the border region than other markers of the same lineage. Moreover, the appearance of these markers by themselves tells us little about how and when the four neural plate border lineages segregate from each other. This is due to a paucity of fate mapping or lineage tracing data of cells at the neural plate border, and specifically an inability to correlate early marker expression with fate. For example, *Zic* and *Pax3/7* genes are considered some of the earliest markers to define the neural crest gene regulatory network (reviewed in Pla and Monsoro-Burq, 2018), yet there have been very few lineage tracing studies of these early Zic+; Pax3/7+ border progenitor cells, and the few that have been done using Cre-Lox lineage tracing suggest these cells may also contribute to placodes such as the olfactory and otic placodes (Freyer and Morrow, 2010; Murdoch et al., 2012). There is thus a clear and unmet need for genetic lineage tracing approaches to map the fate of cells expressing markers of different border region populations as well as their spatial segregation from their earliest times of expression. Moreover, only a few studies have attempted to map multiple markers for the four border lineages at early stages to test the extent to which these markers initially overlap before segregating into distinct territories (Roellig et al., 2017), although the advent of faithful multi-color mRNA visualization technologies such as RNAscope (Wang et al., 2012), Hybridization Chain Reaction (Choi et al., 2016; Roellig et al., 2017), and *in vivo* transcriptomic techniques, such as MERFISH (Chen et al., 2015), is beginning to make the simultaneous visualization of border genes more tractable.

Although these points may seem only of academic interest, they have clear implications for understanding the mechanisms of how the four border lineages segregate from each other. For example, Schlosser et al. have proposed a "binary competence" model based on grafting experiments and evolutionary considerations in which neural ectoderm exclusively is competent to form neural crest, but only non-neural ectoderm is competent to develop into placodes (Ahrens and Schlosser, 2005; Schlosser, 2008; Pieper et al., 2012). However, another school of thought of a multipotent "preborder state" proposes the induced ectoderm expresses a common set of markers during the first few hours of development and then opt a lineage specific differentiation path based on the signals received thereafter (Hintze et al., 2017; Trevers et al., 2017). The ability to label and follow the descendants of cells expressing, for example, *Zic*, *Msx*, or *FoxI* family genes, or to map the fates of *FoxD3* or *TFAP2A*-expressing cells may resolve whether the descendant cells activating expression of these genes are restricted to neural crest, placodes, or to multiple derivatives.

Another possible way of determining if a particular gene marks one of the four border lineages exclusively from early times is to perform loss-of-function studies to see if loss of a gene or gene family results in exclusive loss of a particular border lineage. In practice, however, such experiments are confounded by a number of considerations. First, some loss-of-function approaches in vertebrate embryos, such as antisense morpholinos, reduce but do not abolish gene function – thus, there are many studies reporting a *reduction* in neural crest or placode markers but not a complete loss (Woda et al., 2003; Lillevali et al., 2006; Robledo and Lufkin, 2006; Hoffman et al., 2007; Li and Cornell, 2007; Esterberg and Fritz, 2009; reviewed in Barriga et al., 2015), and there may be qualitative differences in the requirement for genes between different vertebrate groups (Barriga et al., 2015). Second, it is known that the development of a given border lineage can be regulated by its neighbors in an adjacent border derivative – for example, *Zic1* can regulate the formation of placodes in a non-cell autonomous fashion by regulating the production of retinoic acid in the neural plate (Hong and Saint-Jeannet, 2007; Jaurena et al., 2015). Despite these potential confounding factors, there are examples where loss of a single gene leads to loss of at least some derivatives specific to one of the four main border derivatives. In one such example, *Foxi3* mutant mice, deletion of the Foxi3 transcription factor leads to a complete loss of the otic placode and other posterior placodal derivatives but not anterior placodes such as the lens or olfactory epithelium (Birol et al., 2016).

The Developmental Potential of Neural Crest Cells – Pluripotential or "Partly Pluripotential"?

Out of the four multipotential lineages that arise at the neural plate border, the neural crest is particularly striking for the diversity of derivatives it produces. This is especially true in the head, where in addition to neurons, glia, and pigment cells, neural crest gives rise to a wide range of skeletal and cartilaginous structures and specialized derivatives such as corneal endothelium more typically associated with mesoderm. These long-standing observations, together with more recent data suggesting that markers associated with neural crest specification may appear much earlier in development than previously thought (Basch et al., 2006; Betters et al., 2018; Prasad et al., 2019, 2020) have led to a renewed interest in the origin of neural crest cells and their developmental potential. Work in *Xenopus* and mice has recently shown that a number of genes previously thought to be definitive neural crest markers are actually expressed in the early amphibian blastula or mouse embryonic stem cells, and conversely, some genes typically associated with pluripotency in amphibians and mammals were expressed in the developing neural crest (Liu and Labosky, 2008; Lin et al., 2014; Buitrago-Delgado et al., 2015). Moreover, knockdown or over-expression of dominant negative versions of neural crest transcriptional effectors, such as *Snail* or *Sox5*, depleted pluripotency-associated genes in the amphibian blastula and reduced their competence to form mesoderm. Induction of a neural crest or neural plate border state by over-expression of transcription factors also extended the competence of animal cap cell descendants to form mesoderm and endoderm. Neural plate border tissue could also be induced to form endoderm

in response to high concentrations of activin (Buitrago-Delgado et al., 2015). This developmental potential is regulated in part by FGF/MAPK signaling, and a transition to PI3K/Akt signaling, together with a replacement of SoxB effectors with SoxE effectors appears to drive the transition to a more developmentally restricted state (Buitrago-Delgado et al., 2018; Geary and LaBonne, 2018).

These results suggest several intriguing possibilities regarding the potential of neural crest cells and the origin of this potential. One possibility is that the neural crest is the remnants of some blastula/epiblast stem cells that were retained during gastrulation, coming to reside at the neural plate border where they could subsequently be induced to migrate and form neural crest derivatives, while still transiently possessing the competence to express mesodermal or even endodermal genes. In this model, these "set aside" cells would retain some or all aspects of the pluripotency gene regulatory network associated with the anamniote blastula or amniote epiblast. Alternatively, cells at the neural plate border could be induced to regain or recapitulate some or all aspects of the pluripotency circuit. It is certainly possible to induce the neural crest cell state *de novo* by recombining ectoderm and intermediate neural plate (Dickinson et al., 1995), treating intermediate neural plate with inducing factors (Liem et al., 1995; Garcia-Castro et al., 2002), or treating embryonic stems cells with neural- or neural crest-inducing factors (Rada-Iglesias et al., 2011; Leung et al., 2016; Gomez et al., 2019a,b; Kobayashi et al., 2020). However, technical difficulties in directly following the expression of pluripotency factors in cells as they transition from the blastula/epiblast toward neural induction and the formation of the neural plate border has made it hard to distinguish between the *persistence* of pluripotent circuits in neural crest vs. the *recapitulation* of these circuits. A recent single cell analysis of *Xenopus* embryos (Briggs et al., 2018) identified eight pluripotency genes expressed in neural crest cells (*foxd3*, *c-myc*, *id3*, *tfap2*, *ventx2*, *ets1*, *snai1*, and *oct25*) but was unable to find a unique cell cluster expressing all eight genes simultaneously, nor evidence that the eight factors were persisting from earlier precursors. Rather, this single cell analysis suggested that neural crest proceeds through a "classical" neural crest induction pathway, with neural crest arising from neuroectodermal progenitors (Briggs et al., 2018). Moreover, another recent study suggested that the amphibian *Nanog* pluripotency gene homologue, *Ventx2*, is expressed broadly in an ectodermal domain that encompasses *Pax3*- and *Zic1*-expressing crest precursors (Scerbo and Monsoro-Burq, 2020). While *Ventx2* is clearly necessary and in some cases, sufficient for expression of neural crest genes, its major role seems to be in the formation of ectomesenchymal derivatives of the neural crest (Scerbo and Monsoro-Burq, 2020), suggesting that any pluripotency or increased multipotency of crest cells by *Ventx2* may be occur secondarily to neural crest induction.

Finally, in addition to simply examining markers of pluripotency, the past 10 years have witnessed enormous progress in defining the transcriptional and epigenetic characteristics of the pluripotent state in mammals and proposing *functional* assays of varying stringency to demonstrate pluripotency *in vitro* or *in vivo* (De Los Angeles et al., 2015; The International Stem Cell Initiative, 2018). The advent of single cell technologies to analyze gene expression, chromatin accessibility, and histone modifications means that it is now feasible to compare the epigenetic and transcriptional states of stem cells as they transition toward a neural crest cell fate. This will resolve the question of which gene regulatory networks governing pluripotency are present in pre-migratory and migratory neural crest cells, and even neural crest-like peripheral glia stem cells (Adameyko et al., 2009; Dyachuk et al., 2014).

HOW INDUCTIVE SIGNALS AND TRANSCRIPTIONAL EFFECTORS FORM DISTINCT, PATTERNED LINEAGES AT THE NEURAL PLATE BORDER

Quality, Quantity, and Duration – Orchestrating Inducing Signals to Form the Neural Plate Border

Studies over the last 40 years have identified secreted signals – FGFs, WNTs, and BMPs that induce and pattern embryonic ectoderm to form the nervous system in a concentration-dependent manner. It is well-established that non-neural genes are induced in embryonic ectoderm by BMP and WNT signaling, whereas WNT and BMP antagonists from the organizer and FGF signaling promote early neural markers (Wilson and Edlund, 2001; Rogers et al., 2009) and subsequently pattern the neural plate along its anterior-posterior axis as FGF and WNT signaling are continuously modulated (reviewed in Stern, 2002; Levine and Brivanlou, 2007). Similar approaches have been used more recently to understand how the same limited set of signals are re-deployed to regulate the narrowing of the border at the edge of the neural plate and further patterning and formation of pre-migratory neural crest and the pre-placodal region (reviewed in Groves and LaBonne, 2014), and we summarize these briefly below.

Pre-placodal induction is regulated by the same signals used to induce the neural plate, although the location and timing of these signals are different from earlier stages when neural induction is initiated. FGFs, such as *Fgf8* and *Fgf4*, are expressed in cranial mesoderm underlying the neural plate border region, and removal or ectopic grafting of this mesoderm can modulate induction of pre-placodal marker genes such as members of the *Six* and *Eya* families (Ahrens and Schlosser, 2005; Litsiou et al., 2005). The role of FGFs in this cranial mesoderm was shown by gain- and loss-of-function approaches: FGF8 is sufficient to induce at least some pre-placodal genes, such as *Eya2*, in competent ectoderm, while inhibition of FGF signaling in chick and *Xenopus* can downregulate *Six* and *Eya* gene expression (Brugmann et al., 2004; Ahrens and Schlosser, 2005; Litsiou et al., 2005). WNT and BMP family members are expressed in non-neural ectoderm lateral and posterior to the pre-placodal region (*Wnt8c* and *Wnt6*: Garcia-Castro et al., 2002; Schubert et al., 2002; Kil et al., 2005; Litsiou et al., 2005;

Jayasena et al., 2008; BMP4 and 7: Fainsod et al., 1994; Streit et al., 1998; Faure et al., 2002), and several antagonists of both BMPs and WNTs, such as *Cerberus* and *DAN*, are expressed in mesoderm beneath the pre-placodal region (Rodriguez Esteban et al., 1999; Ogita et al., 2001; Chapman et al., 2004; **Figure 1**). This suggests that downregulation or inhibition of both BMP and WNT signaling may promote pre-placodal gene expression at the neural plate border, and this was again shown by gain- and loss-of-function approaches: WNT activation reduces expression of *Six* and *Eya* genes, whereas WNT inhibition expands the expression domain of these genes (Brugmann et al., 2004; Litsiou et al., 2005). Similarly, BMPs can block expression of pre-placodal genes, whereas BMP inhibition expands the expression of pre-placodal genes (Ahrens and Schlosser, 2005; Litsiou et al., 2005; Kwon et al., 2010).

As discussed above, some genes considered to be neural crest markers are expressed in pluripotent tissue in amphibians and mammals, and some early crest markers, such as *Pax7*, are expressed in epiblast prior to formation of the definitive neural plate (Basch et al., 2006; Betters et al., 2018; Prasad et al., 2019, 2020). Nevertheless, neural crest induction has classically been considered to occur as a result of interactions between the neural plate and non-neural ectoderm (reviewed in Sauka-Spengler and Bronner-Fraser, 2008; Milet and Monsoro-Burq, 2012; Prasad et al., 2012; Begbie, 2013). FGFs, BMPs, and WNTs have been implicated in crest induction, with FGF and WNT signaling acting at early stages (Mayor et al., 1997; LaBonne and Bronner-Fraser, 1998; Villanueva et al., 2002; Monsoro-Burq et al., 2003, 2005; Stuhlmiller and Garcia-Castro, 2012), and crest induction being maintained and further promoted by WNTs from the neural folds and BMPs in the dorsal neural folds and surrounding epidermis (Garcia-Castro et al., 2002; Steventon et al., 2009; **Figure 1**).

Incomplete Picture of the Interplay Between the Inductive Signaling Pathways

It has been difficult to untangle how FGF, BMP, and WNT signals are interpreted to yield very different fates at the neural plate border. Cells at the developing border region receiving these signals are within a few cell diameters of each other, and so explaining border differentiation by simple spatial gradients of these three signals cannot easily explain how such very different lineages develop in close proximity. Most of the studies described above have tended to focus on one particular neural plate border derivative and a handful of the respective lineage-specific markers without considering the effects of their experimental manipulations on other border lineages. It has also proven difficult to visualize the levels of BMP, FGF, or WNT signaling at the neural plate border in real time to observe how different cells at the border respond to these signals dynamically. Recently, Warmflash et al. have made use of simplified *in vitro* systems in which human embryonic stem cells are allowed to self-organize on micro-patterned surfaces to generate different embryonic derivatives (Warmflash et al., 2014; Deglincerti et al., 2016; reviewed in Heemskerk and Warmflash, 2016). This approach allows fine control of the level and duration of inducing signals and the patterned structures can be examined at different times to determine the timing of differentiation. This approach has recently been used to investigate patterning of the neural plate border (Britton et al., 2019). Here, the authors carefully varied the strength and duration of WNT and BMP signals to devise a protocol that used an initial phase of SMAD2/3 inhibition to simulate the differentiation of ectoderm by Nodal antagonists, followed by exposure to BMP4 and a subsequent exposure to WNT inhibitors to curtail the endogenous WNT signals arising in the micro-patterned cultures. The combined effect of this protocol produced a central zone of neural tissue (expressing Sox2, Pax6, and N-cadherin), surrounded by a ring of neural crest tissue (expressing Sox9 and Pax3), a ring of pre-placodal tissue (expressing Six1), and an outer layer of non-neural ectoderm (expressing AP2α, Gata3, and E-cadherin; Britton et al., 2019). These remarkable results showed the importance of precisely controlling the level and duration of BMP and WNT signaling in neural crest and placode formation but also emphasize the utility in allowing progenitor cells to achieve this differentiation through self-organization; for instance, increased WNT ligand concentration or delayed WNT inhibition in the induced ectoderm favors the neural crest fate over the pre-placodal domain. The ability to rapidly modify embryonic stem cell lines using CRISPR means that it will be possible to over-express or inactivate individual genes in this system in a temporally and spatially controlled manner, and also to use cells expressing reporters for FGF, BMP, and WNT signaling to visualize the cell-cell interactions as the neural plate border derivatives self-organize. Although undoubtedly simplified, such self-organizing *in vitro* systems are likely to generate new hypotheses for border formation that can be tested in embryos.

Transcriptional Cross-Activation and Cross-Repression as a Mechanism for Self-Organizing Fates at the Neural Plate Border

Visualizing the formation of the neural plate border with immunostaining or *in situ* hybridization for markers of the different border derivatives shows that the boundaries between cells differentiating into different derivatives are initially very imprecise and then sharpen into clear domains (reviewed in Streit, 2007; Groves and LaBonne, 2014; Pla and Monsoro-Burq, 2018). As described above, this same process of self-organization and refinement has recently been demonstrated in micropatterned cultures of embryonic stem cells (Britton et al., 2019). Although the local cell-cell interactions that lead to this refinement are currently still poorly understood, a large body of work has suggested that transcription factor interactions within a given cell can lead to selection of one fate over another. Broadly speaking, two mechanisms underlie this transcriptional refinement: Transcription factors specific to a given lineage mutually promote each other's transcription, while transcription factors specific to different lineages tend to mutually repress each other in the same cell (reviewed in

Grocott et al., 2012; Groves and LaBonne, 2014). We summarize some of these interactions below.

Over-expression and knockdown studies in different species have demonstrated cross-repressive interactions between transcription factors expressed in early non-neural ectoderm and transcription factors expressed in the definitive neural plate. For example, over-expression of *Dlx*, *Gata*, *Msx*, *Foxi*, and *Ap2* factors repress neural markers such as *Sox2*, whereas knockdown of the same genes expand the neural plate at the expense of non-neural ectoderm (Feledy et al., 1999b; Luo et al., 2001; McLarren et al., 2003; Tribulo et al., 2003; Woda et al., 2003; Matsuo-Takasaki et al., 2005; Linker et al., 2009; Kwon et al., 2010; de Crozé et al., 2011; Pieper et al., 2012). Conversely, positive autoregulatory interactions between non-neural genes can sharpen the boundary between neural and non-neural domains (Kwon et al., 2010; Pieper et al., 2012). For example, *Ap2c*, *Foxi1*, and *Gata2* positively regulate one another's expression in the zebrafish border region once they have been induced by BMP signaling (Kwon et al., 2010; Pieper et al., 2012; Bhat et al., 2013). As the pre-placodal region begins to differentiate, similar cross-repressive and autoregulatory interactions within this region and with adjacent non-neural ectoderm appear to refine its boundaries. For example, *Dlx* family member expression can upregulate expression of both *Six* and *Eya* pre-placodal genes and knockdown of the same *Dlx* genes can repress pre-placodal gene expression (Solomon and Fritz, 2002; McLarren et al., 2003; Kaji and Artinger, 2004; Esterberg and Fritz, 2009; Pieper et al., 2012). *Foxi3* and *Dlx5* can activate each other in chick ectoderm, and a similar positive relationship has been demonstrated between *Foxi3* and *Six1* (Khatri et al., 2014). In amphibians, Iroquois (Irx) transcription factors are expressed in the pre-placodal region immediately before *Six* and *Eya* genes and can positively regulate their expression (Gomez-Skarmeta et al., 1998; Goriely et al., 1999; Glavic et al., 2002, 2004; Khudyakov and Bronner-Fraser, 2009). Neural crest progenitors also appear to become distinct from other border derivatives by the same kinds of transcriptional dynamics. As crest cells appear at the neural plate border region, early components of the neural crest gene regulatory network, such as *Pax3* or *Pax7*, are expressed at the future neural plate border over-lapping with genes such as *Dlx5/6*, *Gata2/3*, *Foxi1/3*, *Msx1/2*, *Zic1*, *Gbx2*, and *Ap2* (Basch et al., 2006; Khudyakov and Bronner-Fraser, 2009; Murdoch et al., 2010, 2012; Grocott et al., 2012; Milet et al., 2013). Some of these genes, such as *Msx1/2*, *Zic1*, and *Foxd3*, will eventually localize with *Pax3* or *Pax7* to the neural folds where neural crest forms (Hong and Saint-Jeannet, 2005; Betancur et al., 2010) and some of these changes are driven by repression – for example, the pre-placodal gene *Six1* can repress the neural crest factors *Msx1* and *Foxd3*, whereas *Pax7* and *Msx1* repress *Six1* (Sato et al., 2010); and downregulation of *Axud1*, a WNT-responsive gene upstream of *Foxd3* neural crest program can upregulate Six/Eya expression (Simões-Costa et al., 2015).

It is important to note that the majority of these studies characterizing cross-repressive and autoregulatory interactions at the neural plate border have used over-expression of transcription factors or knockdown or dominant-negative inhibition of transcription factor function (for example, Maharana and Schlosser, 2018). There is a need for lineage tracing to directly visualize the conversion of one cell type into another as the neural plate border lineages segregate. For example, lineage tracing of Six1-expressing progenitors with Cre mice could be used to demonstrate repression of Six1 by Msx1 or Foxd3 in nascent neural crest cells – in this example, a suitably sensitive Six1-Cre line might label some pre-migratory or migratory neural crest derivatives. Similarly, the use of single cell RNA-seq technology to interrogate the border region might be able to identify intermediate cells expressing genes of two or more ectodermal derivatives as the four domains segregate from each other.

EVOLUTION OF THE NEURAL PLATE BORDER IN CHORDATES AND THE "NEW" VERTEBRATE HEAD

As animals diverged from a purely filter-feeding aquatic lifestyle to develop more complex predation behavior, the anterior head began to develop jaws (in gnathostomes) and the anterior sensory organs became more complex. This generation of a "new head" in vertebrates was a consequence of the emergence of migratory neural crest cells and invaginating placodes from the neural plate border region (Gans and Northcutt, 1983; Northcutt and Gans, 1983; reviewed in Patthey et al., 2014; Schlosser et al., 2014). It is now well-accepted that the gene regulatory networks and inductive signals that induce and pattern the vertebrate CNS are conserved to a large degree in cephalochordates (amphioxus) and urochordates (tunicates and appendicularians; reviewed in Holland, 2009). The presence of a clearly patterned anterior CNS in non-vertebrate chordates raised the controversial question of whether any cells resembling neural crest or placodal derivatives could be found in these close vertebrate relatives. It is now becoming clear from work over the past two decades that these vertebrate innovations likely began to emerge in rudimentary forms in non-vertebrate chordates, and that at least some elements of the gene regulatory networks and the secreted signals that activate them at the vertebrate neural plate border can be seen in sister chordates groups. We first describe evidence for neural crest- and placode-like elements in urochordates and cephalochordates and then summarize recent work that suggests a conserved molecular and genetic basis for their formation with vertebrates.

Evidence for Neural Crest and Placodal Rudiments in Non-vertebrate Chordates

Though urochordates and cephalochordates do not possess a complex head and numerous paired sensory organs like most vertebrates, several putative precursors of placodal and neural crest derivatives can be found (Gans and Northcutt, 1983). The presence of crest- and placode-like derivatives in amphioxus has been recently reviewed in depth by Schlosser (2017).

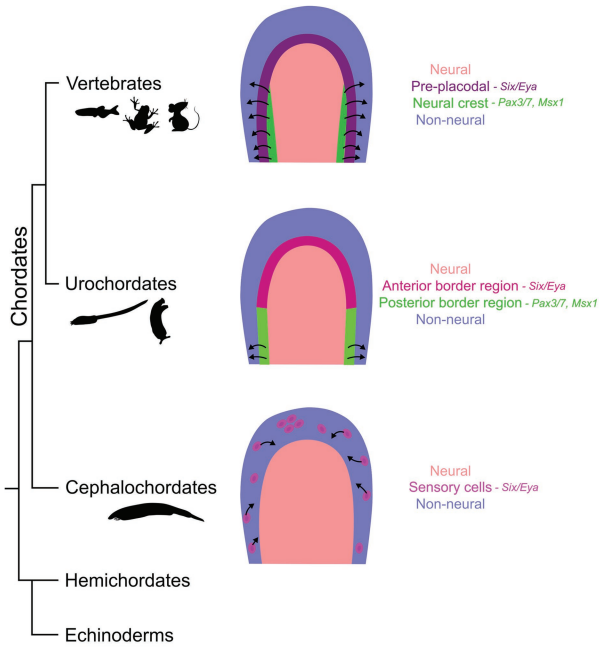

FIGURE 3 | Evolution of the neural plate border in chordates. The diagrams compare the neural plate border (neural – salmon; non-neural – blue) derivatives between different taxa within the phylum Chordata. The vertebrate neural plate border gives rise to two distinct cell populations – the placodes (purple) that thicken and invaginate in the anterior embryo and the neural crest cells (green) that migrate along the entire length of the embryo except for the anterior neural fold (black arrows show migratory properties). However, this feature is an evolutionary novelty in vertebrates. The embryos from the sister clade, urochordates, have a molecularly distinct border region with several gene markers common with the vertebrates (magenta and light green); however, the crest-like migratory cell populations (light green) are relatively limited, such as the bipolar tail neurons. Cephalochordates, the phylogenetic neighbors considered less evolved to tunicate-vertebrate group, have some migratory epidermal sensory cells (pink) with similar molecular signatures to the vertebrate placodes; however, these are largely scattered individual cells that delaminate from the ectoderm much lateral to the neural/non-neural boundary.

Although amphioxus does not possess clear organized cranial sensory organs, several scattered primary and secondary sensory cells, with chemo- and/or mechanosensory roles, are spread along the anterior-posterior axis of the animal that delaminate from the non-neural ectoderm and migrate (**Figure 3**). Just behind the oral opening, Hatschek's pit, a structure containing both exocrine and endocrine cells, has been proposed to be a homologue of adenohypophyseal and olfactory placodes. Some gonadotropin releasing hormone (GnRH)-expressing neurons can be observed in the CNS of amphioxus (for example, Castro et al., 2003), although the presence of GnRH reactivity in Hatschek's pit is less certain (Castro et al., 2006). However, this organ is not derived in its entirety from the ectoderm, like the vertebrate adenohypophysis is. It is also not connected to the CNS like neurosecretory cells, thus offering key compelling arguments against this homology, as elaborated in the review by Schlosser (2017). Finally, small collections of ciliated cells, the corpuscles of de Quatrefages have been observed in anterior regions of amphioxus (Baatrup, 1982). Though hypothesized to be mechanoreceptive, the function of these cells is still uncertain (Schlosser, 2017). Although the cephalochordates do possess pigment cells and sensory neurons (Holland and Holland, 2001; Holland, 2009), migratory cells arising at the neural plate border or in the neural tube have not been observed. Rather, the peripheral sensory neurons of amphioxus arise in the ciliated epidermis, shed their cilia, and delaminate and migrate dorsally toward the neural tube before re-inserting into epidermis and sending projections in the CNS (Kaltenbach et al., 2009).

Urochordates are considered the closest extant taxa to vertebrates. The tunicate *Ciona* has become a popular non-vertebrate model system to study nervous system evolution. In its embryonic (or larval) form, *Ciona* shares many similarities with vertebrate embryonic development. Until recently, few obvious signs of neural crest-like derivatives could be observed in *Ciona* larvae. In 2012, Levine et al. reported the presence of pigmented cells in the larval CNS of *Ciona* (Abitua et al., 2012). Although these cells underwent an epithelial-mesenchymal transition, they remained in the larval neural tube. However, they could be induced to become migratory by the misexpression of the *Twist* gene that regulates migratory behavior in vertebrate neural crest (reviewed in Kuriyama and Mayor, 2008). This suggests that elements regulating two aspects of neural crest behavior – epithelial-mesenchymal transition and melanocytic differentiation – may have arisen in *Ciona* before the co-option of genes allowing those cells to become migratory. More recently, analysis of the embryonic origins of bipolar tail neurons in *Ciona* revealed that their progenitors originate in the posterior lateral neural plate ectoderm, delaminate and migrate to the middle of the larval tail, ultimately sending one process to the tip of the tail and the other to the hatchling brain (Stolfi et al., 2015; Horie et al., 2018; **Figure 3**). Although these migrating cells expressed some genes observed in migratory neuroblasts, such as orthologues of *Neurog* and *Isl* family members (Stolfi et al., 2015), they did not express genes typically associated with migratory neural crest. This suggests that the migratory bipolar tail neuron progenitors may represent an intermediate evolutionary phase between a neuroepithelial cell and the *bona fide* crest cells of vertebrates.

Ciona also has a number of cell types that can be considered homologous to anterior placodal derivatives. For example, the *Ciona* larva contains GnRH-expressing neurons that persist beyond metamorphosis (Abitua et al., 2015) and may be considered homologous to neurons derived from the olfactory or adenohypophyseal placodes of vertebrates, although evidence for expression of additional markers of these placodes in *Ciona* would provide a more solid foundation for such homology. They also contain neurons in their adhesive palps that arise from the edge of the larval neural plate (Wagner et al., 2014; Horie et al., 2018) that have been proposed to act as both chemo- and mechanosensors. In addition, cells resembling mechanosensory hair cells have been observed lining the atrial siphon of mature tunicates, where they have been proposed to help detect water flow (Manni et al., 2004;

Burighel et al., 2010). The progenitors for these placode-like derivatives can be traced back to the ectoderm lateral to the neural plate (the neural plate border) of the gastrula that also express elements of the pre-placodal gene regulatory network (see below).

Conservation of Inductive Signals and Molecular Elements of Crest and Placode Gene Regulatory Networks in Non-vertebrate Chordates

Several inductive signals that pattern the anterior epiblast and the border region that arises from the interaction of neural and non-neural ectoderm are also conserved across chordates. Similar to vertebrates, cephalochordates, and many other bilaterian taxa, employ BMP signaling to defining neural vs. non-neural identity with high BMP2/4 signaling activating epidermal fate genes, and regions of low BMP signaling, promoted by BMP antagonists (like chordin) forming a central neural ectoderm (Yu et al., 2007, 2008; Benito-Gutiérrez and Arendt, 2009; Niehrs, 2010). Similar to vertebrates, upregulation or exogenous exposure to BMP signaling in amphioxus favors the epidermal fate (Yu et al., 2008). BMP/Chordin interactions are involved in neural plate patterning in tunicates too, however, the effect of BMP over-expression is limited as early neural markers are still detected (Darras and Nishida, 2001; Lemaire et al., 2008). Protochordates also exhibit regional neural and non-neural transcription factor expression domains, neural/dorsal (SoxB and Zic), and non-neural/ventral (Dlx3/5, AP2, and Msx1) ectoderm (Sharman et al., 1999; Meulemans and Bronner-Fraser, 2004; Yu et al., 2008), molecular expression boundaries that narrow with time. In amphioxus, the lateral neural plate also expresses Pax3/7 and Snail, markers associated with neural plate border and neural crest cell development in vertebrates (Yu et al., 2008). Though, Six/Eya expression has not been observed in the amphioxus lateral neural plate or the adjacent non-neural ectoderm, Six1/2 expression has been observed in the Hatschek's pit (possible analog to the vertebrate adenohypophysis) and epidermal sensory cell patches in late neurula stages (Kozmik et al., 2007).

Though the ascidian embryos differ from the vertebrates and amphioxus, since the cells divide and select a fate based on their lineage instead of a field of equipotent cells exposed to diffusing morphogenetic cues, the row of cells at the dorsal-most non-neural ectoderm in the *Ciona* gastrula has been shown to express *Six1/2*, *Pax3/7*, and *Msxb* (Horie et al., 2018), some of the definitive markers for the vertebrate neural plate border ectoderm (reviewed in Schlosser et al., 2014; Thiery et al., 2020). Through lineage tracing experiments and cellular fate maps of *Ciona*, we know that the *Six1* and *Foxg* cells contribute to the sensory organs like the palp adhesive organs and the oral siphon primordium (Mazet et al., 2005; Liu and Satou, 2019), whereas *Msxb* domain contributes to the bipolar tail neurons (Horie et al., 2018). *FoxG1* transcription factor labels olfactory, optic, and otic placode in vertebrates (Hebert and McConnell, 2000; Duggan et al., 2008; Ermakova et al., 2019). It has been suggested that the neural plate border of the *Ciona* embryo is compartmentalized into anterior and posterior domains with *Six1* and *Msxb* expression, comparable to vertebrate pre-placodal and neural crest progenitors, respectively. In fact, these domains can be transformed into each other in misexpression experiments (Horie et al., 2018). Additionally, another ascidian sensory patch called the atrial siphon primordium expresses *HrPax-258* (Wada et al., 1998), a homologue of the vertebrate *Pax2/5/8* gene family expressed in the otic-epibranchial placodal domain (Groves and Bronner-Fraser, 2000; Saint-Jeannet and Moody, 2014). Early neural crest cell markers like Pax3/7 are also expressed in cephalochordates and urochordates; however, many other classic neural crest cell markers like FoxD and Twist are largely absent from the ectoderm. Twist over-expression in the cephalic melanocyte lineage in *Ciona* enables those cells to migrate in a manner reminiscent of ectomesenchyme derivatives of neural crest cells (Abitua et al., 2012). In amphioxus, a defined and continuous Six/Eya-positive pan-placodal domain is absent around the neural plate compared to the other chordates. However, some Six/Eya-expressing patches can be found at later stages of development as scattered sensory cells and the Hatschek's pit (Kozmik et al., 2007; Schlosser et al., 2014; Schlosser, 2017). Broad *AmphiMsx* expression is observed in the lateral ectoderm of the late gastrula; however, the expression becomes confined to the neural tube over time only to reappear at the presumptive location of the corpuscles of de Quatrefages at the larval stages; evidence for the lineage of these *AmphiMsx* patches is lacking (Sharman et al., 1999). Furthermore, use of an *AmphiFoxD* (homologue of vertebrate *FoxD*) enhancer to drive a GFP reporter in chick embryos shows the labeled cells localize to the neural tube, somites, and notochord but not the migrating neural crest cells, indicating that the amphioxus enhancer lacks the cis-regulatory elements for expression in migrating crest cells (Yu et al., 2008). The expression of these border region genes indicates protochordates possess the ability to segregate neural and non-neural ectoderm, with the tunicate-vertebrate clade gaining a defined border domain that gives rise to sensory cells. Despite the molecular and patterning similarities, these protochordate cells are not *bona fide* neural crest cells and placodes since they lack the capacity for invagination or long-range migration or the ability to generate various cell types of the ectomesenchyme, as seen in the vertebrate head.

Both neural crest cells and placodes arose around the same time during evolution, generate some similar cell types (sensory neurons), and a portion of these cells possess migratory properties. Furthermore, as described above, these cells in the invertebrate chordate lateral non-neural ectoderm or the neural ectoderm express transcription factors homologous to the neural crest progenitors and pre-placodal domain. This raises the question of whether basal chordates or early vertebrates possessed a hybrid neural border cell population, a common ancestral cell type to neural crest and pre-placodal progenitors (reviewed in Schlosser, 2008).

Probing an Ancient Border With Modern Tools

The invertebrate chordates do not have placodes or neural crest cells similar to the vertebrate taxa; however, scattered cells and patches that possess comparable molecular characteristics and sometimes migratory properties of ectodermal patterning during late gastrulation/early neurulation can be used to track the origins of the gene regulatory networks that gave rise to the neural plate border of vertebrates. Comparative studies across the evolutionary spectrum can also shed light on the role of signaling pathways and transcription factors for cell type-specific development. For example, single cell RNA- and ATAC-sequencing of mammalian hair cells and the ciliated primary sensory cells of the ascidians could compare the transcriptomic and epigenomic regulation of fate specification in the two taxa.

Another unaddressed question that has been debated for several decades is whether neural crest cells and the pre-placodal domain share a common evolutionary origin. The two cell populations form adjacent to each other at the neural plate border during early epiblast development, the cells possess migratory properties, they migrate along the same "corridors" during neurulation (Steventon et al., 2014), and the two lineages share some resultant cell fates like sensory neurons. Fine signaling pathway or transcription factor misexpressing easily transforms one cell type to another as demonstrated, for example, in tunicate embryos in Horie et al. (2018) and *in vitro* ectodermal patterning by Britton et al. (2019). A detailed review by Schlosser (2008), however, argues against this, since the neural crest cells are specified and migrate from the neural plate border before the placodes, and many cell fates are exclusive to each of the lineages – only neural crest cells make bone and cartilage, while only placodes form specialized mechano- or chemoreceptive sensory cells. Also, the defining gene regulatory networks of placodes (Six/Eya) and neural crest cells (Pax3/Msx/FoxD) are quite different. For further evidence for the interplay of these gene regulatory networks, we need a comprehensive comparison of active, repressed, and accessible genome loci across the two neural plate border lineages during late gastrulation and early neurulation stages. Single cell transcriptomics studies in *Ciona* show that misexpression of anterior lateral plate border genes (like *Foxc*) in the posterior counterpart (*Pax3/7*) result in transformation to the anterior fate along with a significant number of cells with a hybrid anterior-posterior lateral plate border transcriptome (Horie et al., 2018), supporting the theory of a multipotent intermediate cell population at the border that gives rise to crest-like and placode-like cells.

The question remains as to what mechanisms localized the proto-neural plate border gene regulatory network to the edge of the neural plate during evolution. How did transcription factors that define border populations such as *Six/Eya/Pax* genes gain regulatory elements regulated by WNT/BMP/FGF signaling that allowed their expression in a domain separate from neural and non-neural ectoderm? Many such questions remain to be explored in the field of early ectodermal patterning in chordates and with the emergence of novel tools to probe gene expression and regulation at the single cell level, we can continue to piece together the mystery of neural plate border induction, specification, and lineage commitment.

CONCLUSION: TOWARD A MULTI-OMICS INVESTIGATION OF THE NEURAL PLATE BORDER REGION

Many questions in the field of neural plate border development remain to be addressed. How do cells segregate from pluripotential epiblast cells to one of four lineages; each remaining multipotent but nonetheless distinct and restricted in their fates from the other lineages? What is the precise combination of WNT/BMP/FGF signaling that gives rise to each of the four ectodermal cell fates, and what is the downstream signaling cascade for each lineage? Do the neural crest progenitors and pre-placodal ectoderm arise from a common pool of cells at the border region in a hybrid stage, or do they come from the neural and non-neural ectoderm respectively? Is the chromatin conformation of the border irreversible at early developmental stages when the first neural crest cell or pre-placodal marker expression is observed, or does it remain plastic? Do neural crest cells retain some or all aspects of pluripotency? How similar are the cell types that originate in the non-neural ectoderm adjacent to the neural plate in protochordates to those in vertebrates that generate sensory patches and organs? To address these questions, we need to follow the transcriptomic and epigenomic states of cells at the neural plate border in the medial-lateral as well as anterior-posterior axes.

Embryonic cellular maps are difficult to construct due to the rapidly changing nature of embryonic tissue, unlike the atlases of adult organs. Histochemical methods can only reveal spatial expression of certain known genes and proteins in the organism, with further limitations pertaining to lack of cross-species utility of those tools. Introduction of single cell sequencing techniques in the last decade has finally made it possible to observe a more holistic picture of a developing cell and its state at a particular point in embryonic time. Single-cell level transcriptomic, epigenomic, and other sequencing techniques provide the necessary apparatuses to capture the dynamic state of the developing embryo to track lineages, observe fate specification, and study the multipotency of the differentiating cells. Several recent studies present a comprehensive atlas of different cell types of the developing mouse embryos pre-gastrulation (Mohammed et al., 2017; Cheng et al., 2019) and from gastrulation to organogenesis (Pijuan-Sala et al., 2019). Statistical clustering of single cells can be used to discover previously unidentified or non-distinct cell populations as well as observe detailed similarities and differences in the transcriptional states of known cell types. Molecular maps of cell lineage induction and specification can be gathered by profiling the tissue of interest from multiple ages simultaneously, which can further help to understand the gene regulatory networks involved. For example, Pijuan-Sala et al. (2019) show the origins of endodermal lineages in the mouse embryo during gastrulation and identify a population of early myeloid

progenitors that can contribute to microglia. A similar analysis in tunicate embryos permitted virtual lineage tracing of the nervous system. This transcriptomic study revealed molecular similarities between the vertebrate telencephalon and the anterior domain of the tunicate embryo (palp sensory cells and anterior sensory vesicle) supporting the idea that protochordate ectodermal gene regulatory modules must have evolved to expand the vertebrate forebrain (Cao et al., 2019). It will be possible to compare the transcriptomic profile of bipolar tail neurons, atrial siphon primordium, oral siphon primordium, and palp organs with vertebrate transcriptomes of crest and placode derivatives to comprehensively explore the parallels between vertebrate and protochordate neural plate border ectoderm development.

As a complement to single cell RNA sequencing, multi-color imaging methods like RNAscope or *in situ* Hybridization Chain Reaction can be used to record and validate spatial expression of key genetic variations observed in cell clustering (Choi et al., 2016; Lignell et al., 2017). The neural plate border region of the chordates is only a few cells thick and techniques like Slide-seq and MERFISH may be able to give higher resolution spatial information of the cellular transcriptome during border development (Chen et al., 2015; Rodriques et al., 2019). While the former method transfers single cell thick tissue sections onto a single cell RNA sequencing grid (Rodriques et al., 2019), the latter method probes the same tissue sections for thousands of RNA transcripts by using a robust multichannel ISH technique (Chen et al., 2015); both methods provide a spatial context to the transcriptomic profiles. Depending on the cellular resolution of these techniques, they may be useful for parsing out the cellular identities at the neural plate border region where the four ectodermal lineages are intermingled over just a few cell diameters. For instance, although WNT, BMP, and FGF signaling are important for neural crest progenitors and pre-placodal domain patterning, far less is known of the fine-tuned signaling levels and subsequent cascade of downstream molecules that specify these cell fates. Single cell RNA sequencing techniques can elaborate upon the levels of signaling and expression of respective downstream effectors to delve deeper into the signaling pathway interactions at the neural plate border. Advances in transgenic animal models, CRISPR technology, and high-resolution live imaging of fluorescent reporter of cell signaling can help us visualize signaling spatiotemporally. For example, we can evaluate whether an intermediate cell fate that can give rise to both neural crest cells and placodes exists in the developing epiblast, thereby testing the "binary competence model" of ectodermal patterning (Patthey et al., 2014; Schlosser et al., 2014).

Ideally, we would want to interrogate the expression levels and cell state of every cell in an embryo at a chosen state of development and be able to track each individual cell through time and space. However, sequencing technologies are often not a comprehensive picture of the cell states with anywhere between 16 and 62% coverage of the cells at the early embryonic development stages observed with each individual cell identified with only a couple of thousand transcripts (Tam and Ho, 2020). Although it is enough to cluster the single cells identified, the studies may give an incomplete picture of the transitional states due to insufficient sequencing depth. With the realistic limitations of the technology, integrating databases across published studies can help us trace the lineage of cell clusters along the developmental timeline (Tam and Ho, 2020). Alternatively, higher sensitivity but lower throughput techniques, such as MATQ-seq and SMARTer-seq, can detect a higher number of genes per cell and are useful for a deeper transcriptomic analysis of single cells (Sheng et al., 2017; Verboom et al., 2019). For example, a recent study uses SMART-seq2 to understand the fate programs of neural crest cells with over 7,000 genes detected per cell for a finer understanding of the transcriptomic decisions made by pre-migratory/migratory crest cells as they proceed toward sensory, glial, or mesenchymal fates (Soldatov et al., 2019).

Several key transcription factors like *FoxD3*, *Foxi3*, *Pax3/7*, and *Zic* have been implicated in broader patterning of the ectoderm around the neural plate border (reviewed in Pla and Monsoro-Burq, 2018). Techniques like ChIP-seq and CUT&RUN can identify the genomic loci bound by a transcription factor of interest, or which genomic loci are "primed" by particular histone modifications (Skene and Henikoff, 2017; Kaya-Okur et al., 2019). Comparison of the transcriptomic and epigenomic data from the neural plate, neural crest, and pre-placodal domain cells can identify "active" transcription loci (SCENIC; Aibar et al., 2017). In addition to the transcriptomic status of the cells at the developing neural plate border region, it remains to be addressed when the cells are fully committed to a lineage. Epigenomic sequencing analysis, such as ATAC-seq, can identify accessible genomic loci available for transcriptional activity. Single cell ATAC-seq is now feasible, and it is now possible to combine scRNA-seq and ATAC-seq in a single cell (for example, Cao et al., 2018; Rosenberg et al., 2018; Reyes et al., 2019). Using this data, we can identify relevant enhancers for lineage specific transcription factors and evaluate plasticity of the cells, whether trans-differentiation is feasible from one ectodermal path to another. For example, combining single cell RNA-seq, ATAC-seq, and ChIP-seq data, Lukoseviciute et al. (2018) identified a bimodal function for *FoxD3*, a key transcription factor that is important for neural crest specification and differentiation. Their data show that FoxD3 binds to cis-regulatory elements for neural crest specifier genes as an activator, and at later stages, represses mesenchymal and migratory programs to prevent premature differentiation (Lukoseviciute et al., 2018). Yet another transcription factor, AP2 (or TFAP2) has been shown to play a dual role in activating neural crest induction genes (*Pax*, *Zic*, and *Msx*) and, at a later stage of development, neural crest specification genes (*FoxD* and *Sox10*). Combining multiple sequencing efforts to collate single cell RNA-seq, ATAC-seq, and AP2 CUT&RUN data shows that this transcription factor performs these two distinct roles based on its dimerization partner (Rothstein and Simoes-Costa, 2020). The ability to interrogate the gene expression, histones, nucleosome availability, and more recently, genome occupancy is finally shedding light on the role of such key transcription factors and signaling cascades for ectodermal patterning to generate and specify distinct lineages.

AUTHOR CONTRIBUTIONS

AT and AG wrote and edited the manuscript together. Both the authors contributed to the article and approved the submitted version.

FUNDING

The authors are funded by NIH (RO1 DC013072) to AG.

ACKNOWLEDGMENTS

We thank our colleagues in the neural crest and placode field for many interesting discussions over the years that spurred ideas in this review, and we apologize for omission of many articles from the review for reasons of space. We also thank Alyssa Crowder from Groves lab for proofreading the article.

REFERENCES

Abitua, P. B., Gainous, T. B., Kaczmarczyk, A. N., Winchell, C. J., Hudson, C., Kamata, K., et al. (2015). The pre-vertebrate origins of neurogenic placodes. *Nature* 524, 462–465. doi: 10.1038/nature14657

Abitua, P. B., Wagner, E., Navarrete, I. A., and Levine, M. (2012). Identification of a rudimentary neural crest in a non-vertebrate chordate. *Nature* 492, 104–107. doi: 10.1038/nature11589

Adameyko, I., Lallemend, F., Aquino, J. B., Pereira, J. A., Topilko, P., Müller, T., et al. (2009). Schwann cell precursors from nerve innervation are a cellular origin of melanocytes in skin. *Cell* 139, 366–379. doi: 10.1016/j.cell.2009.07.049

Ahmed, M., Wong, E. Y., Sun, J., Xu, J., Wang, F., and Xu, P. X. (2012a). Eya1-Six1 interaction is sufficient to induce hair cell fate in the cochlea by activating Atoh1 expression in cooperation with Sox2. *Dev. Cell* 22, 377–390. doi: 10.1016/j.devcel.2011.12.006

Ahmed, M., Xu, J., and Xu, P. X. (2012b). EYA1 and SIX1 drive the neuronal developmental program in cooperation with the SWI/SNF chromatin-remodeling complex and SOX2 in the mammalian inner ear. *Development* 139, 1965–1977. doi: 10.1242/dev.071670

Ahrens, K., and Schlosser, G. (2005). Tissues and signals involved in the induction of placodal Six1 expression in *Xenopus laevis*. *Dev. Biol.* 288, 40–59. doi: 10.1016/j.ydbio.2005.07.022

Aibar, S., González-Blas, C. B., Moerman, T., Huynh-Thu, V. A., Imrichova, H., Hulselmans, G., et al. (2017). SCENIC: single-cell regulatory network inference and clustering. *Nat. Methods* 14, 1083–1086. doi: 10.1038/nmeth.4463

Albazerchi, A., and Stern, C. D. (2007). A role for the hypoblast (AVE) in the initiation of neural induction, independent of its ability to position the primitive streak. *Dev. Biol.* 301, 489–503. doi: 10.1016/j.ydbio.2006.08.057

Baatrup, E. (1982). On the structure of the Corpuscles of de Quatrefages (*Branchiostoma lanceolatum* (P)). *Acta Zool.* 63, 39–44. doi: 10.1111/j.1463-6395.1982.tb00757.x

Baker, C. V., Stark, M. R., Marcelle, C., and Bronner-Fraser, M. (1999). Competence, specification and induction of Pax-3 in the trigeminal placode. *Development* 126, 147–156.

Bally-Cuif, L., Gulisano, M., Broccoli, V., and Boncinelli, E. (1995). c-otx2 is expressed in two different phases of gastrulation and is sensitive to retinoic acid treatment in chick embryo. *Mech. Dev.* 49, 49–63. doi: 10.1016/0925-4773(94)00301-3

Barriga, E. H., Trainor, P. A., Bronner, M., and Mayor, R. (2015). Animal models for studying neural crest development: is the mouse different? *Development* 142, 1555–1560. doi: 10.1242/dev.121590

Basch, M. L., Bronner-Fraser, M., and García-Castro, M. I. (2006). Specification of the neural crest occurs during gastrulation and requires Pax7. *Nature* 441, 218–222. doi: 10.1038/nature04684

Begbie, J. (2013). "Induction and patterning of neural crest and ectodermal placodes and their derivatives" in *Patterning and cell type specification in the developing CNS and PNS*. eds. J. L. R. Rubenstein and R. P. Amsterdam (Oxford, UK: Elsevier Inc).

Benito-Gutiérrez, È., and Arendt, D. (2009). CNS evolution: new insight from the mud. *Curr. Biol.* 19, 640–642. doi: 10.1016/j.cub.2009.06.020

Bessarab, D. A., Chong, S. -W., and Korzh, V. (2004). Expression of zebrafish six1 during sensory organ development and myogenesis. *Dev. Dyn.* 230, 781–786. doi: 10.1002/dvdy.20093

Betancur, P., Bronner-Fraser, M., and Sauka-Spengler, T. (2010). Assembling neural crest regulatory circuits into a gene regulatory network. *Annu. Rev. Cell Dev. Biol.* 26, 581–603. doi: 10.1146/annurev.cellbio.042308.113245

Betters, E., Charney, R. M., and Garcia-Castro, M. I. (2018). Early specification and development of rabbit neural crest cells. *Dev. Biol.* 444, S181–S192. doi: 10.1016/j.ydbio.2018.06.012

Bhat, N., Kwon, H. J., and Riley, B. B. (2013). A gene network that coordinates preplacodal competence and neural crest specification in zebrafish. *Dev. Biol.* 373, 107–117. doi: 10.1016/j.ydbio.2012.10.012

Bhattacharyya, S., Bailey, A. P., Bronner-Fraser, M., and Streit, A. (2004). Segregation of lens and olfactory precursors from a common territory: cell sorting and reciprocity of Dlx5 and Pax6 expression. *Dev. Biol.* 271, 403–414. doi: 10.1016/j.ydbio.2004.04.010

Bhattacharyya, S., and Bronner, M. E. (2013). Clonal analyses in the anterior pre-placodal region: implications for the early lineage bias of placodal progenitors. *Int. J. Dev. Biol.* 757, 753–757. doi: 10.1387/ijdb.130155mb

Birol, O., Ohyama, T., Edlund, R. K., Drakou, K., Georgiades, P., and Groves, A. K. (2016). The mouse Foxi3 transcription factor is necessary for the development of posterior placodes. *Dev. Biol.* 409, 139–151. doi: 10.1016/j.ydbio.2015.09.022

Briggs, J. A., Weinreb, C., Wagner, D. E., Megason, S., Peshkin, L., Kirschner, M. W., et al. (2018). The dynamics of gene expression in vertebrate embryogenesis at single-cell resolution. *Science* 360:eaar5780. doi: 10.1126/science.aar5780

Britton, G., Heemskerk, I., Hodge, R., Qutub, A. A., and Warmflash, A. (2019). A novel self-organizing embryonic stem cell system reveals signaling logic underlying the patterning of human ectoderm. *Development* 146:dev179093. doi: 10.1242/dev.179093

Brown, S. T., Wang, J., and Groves, A. K. (2005). Dlx gene expression during chick inner ear development. *J. Comp. Neurol.* 483, 48–65. doi: 10.1002/cne.20418

Brugmann, S. A., Pandur, P. D., Kenyon, K. L., Pignoni, F., and Moody, S. A. (2004). Six1 promotes a placodal fate within the lateral neurogenic ectoderm by functioning as both a transcriptional activator and repressor. *Development* 131, 5871–5881. doi: 10.1242/dev.01516

Buitrago-Delgado, E., Nordin, K., Rao, A., Geary, L., and LaBonne, C. (2015). Shared regulatory programs suggest retention of blastula-stage potential in neural crest cells. *Science* 348, 1332–1335. doi: 10.1126/science.aaa3655

Buitrago-Delgado, E., Schock, E. N., Nordin, K., and LaBonne, C. (2018). A transition from SoxB1 to SoxE transcription factors is essential for progression from pluripotent blastula cells to neural crest cells. *Dev. Biol.* 444, 50–61. doi: 10.1016/j.ydbio.2018.08.008

Burighel, P., Caicci, F., and Manni, L. (2010). Hair cells in non-vertebrate models: lower chordates and molluscs. *Hear. Res.* 273, 14–24. doi: 10.1016/j.heares.2010.03.087

Cao, J., Cusanovich, D. A., Ramani, V., Aghamirzaie, D., Pliner, H. A., Hill, A. J., et al. (2018). Joint profiling of chromatin accessibility and gene expression in thousands of single cells. *Science* 1385, 1380–1385. doi: 10.1126/science.aau0730(2018)

Cao, C., Lemaire, L. A., Wang, W., Yoon, P. H., Choi, Y. A., Parsons, L. R., et al. (2019). Comprehensive single-cell transcriptome lineages of a proto-vertebrate. *Nature* 571, 349–354. doi: 10.1038/s41586-019-1385-y

Carmona-Fontaine, C., Acuna, G., Ellwanger, K., Niehrs, C., and Mayor, R. (2007). Neural crests are actively precluded from the anterior neural fold by a novel inhibitory mechanism dependent on Dickkopf1 secreted by the prechordal mesoderm. *Dev. Biol.* 309, 208–221. doi: 10.1016/j.ydbio.2007.07.006

Castro, A., Manso, M. J., and Anadón, R. (2003). Distribution of neuropeptide Y immunoreactivity in the central and peripheral nervous systems of amphioxus (*Branchiostoma lanceolatum* Pallas). *J. Comp. Neurol.* 461, 350–361. doi: 10.1002/cne.10694

Castro, L. F. C., Rasmussen, S. L. K., Holland, P. W. H., Holland, N. D., and Holland, L. Z. (2006). A Gbx homeobox gene in amphioxus: insights into ancestry of the ANTP class and evolution of the midbrain/hindbrain boundary. *Dev. Biol.* 295, 40–51. doi: 10.1016/j.ydbio.2006.03.003

Chapman, S. C., Brown, R., Lees, L., Schoenwolf, G. C., and Lumsden, A. (2004). Expression analysis of chick Wnt and frizzled genes and selected inhibitors in early chick patterning. *Dev. Dyn.* 229, 668–676. doi: 10.1002/dvdy.10491

Chen, K. H., Boettiger, A. N., Moffitt, J. R., Wang, S., and Zhuang, X. (2015). RNA imaging. Spatially resolved, highly multiplexed RNA profiling in single cells. *Science* 348, 1360–1363. doi: 10.1126/science.aaa6090

Cheng, S., Pei, Y., He, L., Peng, G., Reinius, B., Tam, P. P. L., et al. (2019). Single-cell RNA-Seq reveals cellular heterogeneity of pluripotency transition and X chromosome dynamics during early mouse development. *Cell Rep.* 26, 2593.e3–2607.e3. doi: 10.1016/j.celrep.2019.02.031

Choi, H. M. T., Calvert, C. R., Husain, N., Huss, D., Barsi, J. C., Deverman, B. E., et al. (2016). Mapping a multiplexed zoo of mRNA expression. *Development* 143, 3632–3637. doi: 10.1242/dev.140137

Christophorou, N. A. D. D., Bailey, A. P., Hanson, S., and Streit, A. (2009). Activation of Six1 target genes is required for sensory placode formation. *Dev. Biol.* 336, 327–336. doi: 10.1016/j.ydbio.2009.09.025

Couly, G. F., and Le Douarin, N. M. (1985). Mapping of the early neural primordium in quail-chick chimeras. I. Developmental relationships between placodes, facial ectoderm, and prosencephalon. *Dev. Biol.* 110, 422–439. doi: 10.1016/0012-1606(85)90101-0

Darras, S., and Nishida, H. (2001). The BMP/CHORDIN antagonism controls sensory pigment cell specification and differentiation in the ascidian embryo. *Dev. Biol.* 236, 271–288. doi: 10.1006/dbio.2001.0339

de Crozé, N., Maczkowiak, F., and Monsoro-Burq, A. H. (2011). Reiterative AP2a activity controls sequential steps in the neural crest gene regulatory network. *Proc. Natl. Acad. Sci. U. S. A.* 108, 155–160. doi: 10.1073/pnas.1010740107

De Los Angeles, A., Ferrari, F., Xi, R., Fujiwara, Y., Benvenisty, N., Deng, H., et al. (2015). Hallmarks of pluripotency. *Nature* 525, 469–478. doi: 10.1038/nature15515

Deglincerti, A., Etoc, F., Ozair, M. Z., and Brivanlou, A. H. (2016). Self-organization of spatial patterning in human embryonic stem cells. *Curr. Top. Dev. Biol.* 116, 99–113. doi: 10.1016/bs.ctdb.2015.11.010

Dickinson, M. E., Selleck, M. A., McMahon, A. P., and Bronner-Fraser, M. (1995). Dorsalization of the neural tube by the non-neural ectoderm. *Development* 121, 2099–2106.

Duggan, C. D., DeMaria, S., Baudhuin, A., Stafford, D., and Ngai, J. (2008). Foxg1 is required for development of the vertebrate olfactory system. *J. Neurosci.* 28, 5229–5239. doi: 10.1523/JNEUROSCI.1134-08.2008

Dyachuk, V., Furlan, A., Shahidi, M. K., Giovenco, M., Kaukua, N., Konstantinidou, C., et al. (2014). Parasympathetic neurons originate from nerve-associated peripheral glial progenitors. *Science* 345, 82–87. doi: 10.1126/science.1253281

Ermakova, G. V., Kucheryavyy, A. V., Zaraisky, A. G., and Bayramov, A. V. (2019). The expression of FoxG1 in the early development of the European river lamprey *Lampetra fluviatilis* demonstrates significant heterochrony with that in other vertebrates. *Gene Expr. Patterns* 34:119073. doi: 10.1016/j.gep.2019.119073

Esterberg, R., and Fritz, A. (2009). dlx3b/4b are required for the formation of the preplacodal region and otic placode through local modulation of BMP activity. *Dev. Biol.* 325, 189–199. doi: 10.1016/j.ydbio.2008.10.017

Esteve, P., and Bovolenta, P. (1999). cSix4, a member of the six gene family of transcription factors, is expressed during placode and somite development. *Mech. Dev.* 85, 161–165. doi: 10.1016/S0925-4773(99)00079-9

Ezin, M., Barembaum, M., and Bronner, M. E. (2014). Stage-dependent plasticity of the anterior neural folds to form neural crest. *Differentiation* 88, 42–50. doi: 10.1016/j.diff.2014.09.003

Fainsod, A., Steinbeisser, H., and De Robertis, E. M. (1994). On the function of BMP-4 in patterning the marginal zone of the *Xenopus* embryo. *EMBO J.* 13, 5015–5025. doi: 10.1002/j.1460-2075.1994.tb06830.x

Faure, S., Barbara, P. D. S., Roberts, D. J., and Whitman, M. (2002). Endogenous patterns of BMP signaling during early chick development. *Dev. Biol.* 65, 44–65. doi: 10.1006/dbio.2002.0579

Feledy, J. A., Beanan, M. J., Sandoval, J. J., Goodrich, J. S., Lim, J. H., Matsuo-Takasaki, M., et al. (1999a). Inhibitory patterning of the anterior neural plate in *Xenopus* by homeodomain factors Dlx3 and Msx1. *Dev. Biol.* 212, 455–464. doi: 10.1006/dbio.1999.9374

Feledy, J. A., Morasso, M. I., Jang, S. I., and Sargent, T. D. (1999b). Transcriptional activation by the homeodomain protein distal-less 3. *Nucleic Acids Res.* 27, 764–770. doi: 10.1093/nar/27.3.764

Freyer, L., and Morrow, B. E. (2010). Canonical Wnt signaling modulates Tbx1, Eya1, and Six1 expression, restricting neurogenesis in the otic vesicle. *Dev. Dyn.* 239, 1708–1722. doi: 10.1002/dvdy.22308

Gans, C., and Northcutt, R. G. (1983). Neural crest and the origin of vertebrates: a new head. *Science* 220, 268–273. doi: 10.1126/science.220.4594.268

Garcia-Castro, M. I., Marcelle, C., and Bronner-Fraser, M. (2002). Ectodermal Wnt function as a neural crest inducer. *Science* 297, 848–851. doi: 10.1126/science.1070824

Geary, L., and LaBonne, C. (2018). FGF mediated mapk and pi3k/akt signals make distinct contributions to pluripotency and the establishment of neural crest. *eLife* 7:e33845. doi: 10.7554/eLife.33845

Glavic, A., Gomez-Skarmeta, J. L., and Mayor, R. (2002). The homeoprotein Xiro1 is required for midbrain-hindbrain boundary formation. *Development* 129, 1609–1621.

Glavic, A., Maris Honore, S., Gloria Feijoo, C., Bastidas, F., Allende, M. L., and Mayor, R. (2004). Role of BMP signaling and the homeoprotein Iroquois in the specification of the cranial placodal field. *Dev. Biol.* 272, 89–8103. doi: 10.1016/j.ydbio.2004.04.020

Gomez, G. A., Prasad, M. S., Sandhu, N., Shelar, P. B., Leung, A. W., and García-Castro, M. I. (2019a). Human neural crest induction by temporal modulation of WNT activation. *Dev. Biol.* 449, 99–106. doi: 10.1016/j.ydbio.2019.02.015

Gomez, G. A., Prasad, M. S., Wong, M., Charney, R. M., Shelar, P. B., Sandhu, N., et al. (2019b). WNT/β-catenin modulates the axial identity of embryonic stem cell-derived human neural crest. *Development* 146:dev175604. doi: 10.1242/dev.175604

Gómez-Skarmeta, J. L., Campuzano, S., and Modolell, J. (2003). Half a century of neural prepatterning: the story of a few bristles and many genes. *Nat. Rev. Neurosci.* 4, 587–598. doi: 10.1038/nrn1142

Gomez-Skarmeta, J. L., Glavic, A., de la Calle-Mustienes, E., Modolell, J., and Mayor, R. (1998). Xiro, a *Xenopus* homolog of the *Drosophila Iroquois* complex genes, controls development at the neural plate. *EMBO J.* 17, 181–190. doi: 10.1093/emboj/17.1.181

Goriely, A., Diez del Corral, R., and Storey, K. G. (1999). c-Irx2 expression reveals an early subdivision of the neural plate in the chick embryo. *Mech. Dev.* 87, 203–206. doi: 10.1016/S0925-4773(99)00149-5

Grocott, T., Tambalo, M., and Streit, A. (2012). The peripheral sensory nervous system in the vertebrate head: a gene regulatory perspective. *Dev. Biol.* 370, 3–23. doi: 10.1016/j.ydbio.2012.06.028

Groves, A. K., and Bronner-Fraser, M. (2000). Competence, specification and commitment in otic placode induction. *Development* 127, 3489–3499.

Groves, A. K., and LaBonne, C. (2014). Setting appropriate boundaries: fate, patterning and competence at the neural plate border. *Dev. Biol.* 389, 2–12. doi: 10.1016/j.ydbio.2013.11.027

Hans, S., Christison, J., Liu, D., and Westerfield, M. (2007). Fgf-dependent otic induction requires competence provided by Foxi1 and Dlx3b. *BMC Dev. Biol.* 7:5. doi: 10.1186/1471-213X-7-5

Hebert, J. M., and McConnell, S. K. (2000). Targeting of cre to the Foxg1 (BF-1) locus mediates loxP recombination in the telencephalon and other developing head structures. *Dev. Biol.* 222, 296–306. doi: 10.1006/dbio.2000.9732

Heemskerk, I., and Warmflash, A. (2016). Pluripotent stem cells as a model for embryonic patterning: from signaling dynamics to spatial organization in a dish. *Dev. Dyn.* 245, 976–990. doi: 10.1002/dvdy.24432

Hintze, M., Prajapati, R. S., Tambalo, M., Christophorou, N. A. D., Anwar, M., Grocott, T., et al. (2017). Cell interactions, signals and transcriptional hierarchy governing placode progenitor induction. *Development* 144, 2810–2823. doi: 10.1242/dev.147942

Hoffman, T. L., Javier, A. L., Campeau, S. A., Knight, R. D., and Schilling, T. F. (2007). Tfap2 transcription factors in zebrafish neural crest development and ectodermal evolution. *J. Exp. Zool. B Mol. Dev. Evol.* 308, 679–691. doi: 10.1002/jez.b.21189

Holland, L. Z. (2009). Chordate roots of the vertebrate nervous system: expanding the molecular toolkit. *Nat. Rev. Neurosci.* 10, 736–746. doi: 10.1038/nrn2703

Holland, L. Z., and Holland, N. D. (2001). Evolution of neural crest and placodes: amphioxus as a model for the ancestral vertebrate? *J. Anat.* 199, 85–98. doi: 10.1046/j.1469-7580.199.parts1-2.8.x

Hong, C. S., and Saint-Jeannet, J. P. (2005). Sox proteins and neural crest development. *Semin. Cell Dev. Biol.* 16, 694–703. doi: 10.1016/j.semcdb.2005.06.005

Hong, C. S., and Saint-Jeannet, J. P. (2007). The activity of Pax3 and Zic1 regulates three distinct cell fates at the neural plate border. *Mol. Biol. Cell* 18, 2192–2202. doi: 10.1091/mbc.E06-11-1047

Horie, R., Hazbun, A., Chen, K., Cao, C., Levine, M., and Horie, T. (2018). Shared evolutionary origin of vertebrate neural crest and cranial placodes. *Nature* 560, 228–232. doi: 10.1038/s41586-018-0385-7

Hovland, A. S., Rothstein, M., and Simoes-Costa, M. (2020). Network architecture and regulatory logic in neural crest development. *Wiley Interdiscip. Rev. Syst. Biol. Med.* 12, 1–15. doi: 10.1002/wsbm.1468

Ishihara, T., Sato, S., Ikeda, K., Yajima, H., and Kawakami, K. (2008). Multiple evolutionarily conserved enhancers control expression of Eya1. *Dev. Dyn.* 237, 3142–3156. doi: 10.1002/dvdy.21716

Jaurena, M. B., Juraver-Geslin, H., Devotta, A., and Saint-Jeannet, J. P. (2015). Zic1 controls placode progenitor formation non-cell autonomously by regulating retinoic acid production and transport. *Nat. Commun.* 6, 1–10. doi: 10.1038/ncomms8476

Jayasena, C. S., Ohyama, T., Segil, N., and Groves, A. K. (2008). Notch signaling augments the canonical Wnt pathway to specify the size of the otic placode. *Development* 135, 2251–2261. doi: 10.1242/dev.017905

Kaji, T., and Artinger, K. B. (2004). dlx3b and dlx4b function in the development of Rohon-Beard sensory neurons and trigeminal placode in the zebrafish neurula. *Dev. Biol.* 276, 523–540. doi: 10.1016/j.ydbio.2004.09.020

Kaltenbach, S. L., Yu, J. -K., and Holland, N. D. (2009). The origin and migration of the earliest-developing sensory neurons in the peripheral nervous system of amphioxus. *Evol. Dev.* 11, 142–151. doi: 10.1111/j.1525-142X.2009.00315.x

Kaya-Okur, H. S., Wu, S. J., Codomo, C. A., Pledger, E. S., Bryson, T. D., Henikoff, J. G., et al. (2019). CUT&tag for efficient epigenomic profiling of small samples and single cells. *Nat. Commun.* 10:1930. doi: 10.1038/s41467-019-09982-5

Khatri, S. B., Edlund, R. K., and Groves, A. K. (2014). Foxi3 is necessary for the induction of the chick otic placode in response to FGF signaling. *Dev. Biol.* 391, 158–169. doi: 10.1016/j.ydbio.2014.04.014

Khudyakov, J., and Bronner-Fraser, M. (2009). Comprehensive spatiotemporal analysis of early chick neural crest network genes. *Dev. Dyn.* 238, 716–723. doi: 10.1002/dvdy.21881

Kiecker, C., and Niehrs, C. (2001). A morphogen gradient of Wnt/beta-catenin signalling regulates anteroposterior neural patterning in *Xenopus*. *Development* 128, 4189–4201.

Kil, S. H., Streit, A., Brown, S. T., Agrawal, N., Collazo, A., Zile, M. H., et al. (2005). Distinct roles for hindbrain and paraxial mesoderm in the induction and patterning of the inner ear revealed by a study of vitamin-A-deficient quail. *Dev. Biol.* 285, 252–271. doi: 10.1016/j.ydbio.2005.05.044

Knight, R. D., Nair, S., Nelson, S. S., Afshar, A., Javidan, Y., Geisler, R., et al. (2003). Lockjaw encodes a zebrafish tfap2a required for early neural crest development. *Development* 130, 5755–5768. doi: 10.1242/dev.00575

Kobayashi, G. S., Musso, C. M., Moreira, D. d. P., Pontillo-Guimarães, G., Hsia, G. S. P., Caires-Júnior, L. C., et al. (2020). Recapitulation of neural crest specification and EMT via induction from neural plate border-like cells. *Stem Cell Rep.* 15, 776–788. doi: 10.1016/j.stemcr.2020.07.023

Kobayashi, M., Osanai, H., Kawakami, K., and Yamamoto, M. (2000). Expression of three zebrafish Six4 genes in the cranial sensory placodes and the developing somites. *Mech. Dev.* 98, 151–155. doi: 10.1016/S0925-4773(00)00451-2

Kozmik, Z., Holland, N. D., Kreslova, J., Oliveri, D., Schubert, M., Jonasova, K., et al. (2007). Pax-Six-Eya-Dach network during amphioxus development: conservation in vitro but context specificity in vivo. *Dev. Biol.* 306, 143–159. doi: 10.1016/j.ydbio.2007.03.009

Kroll, K. L., Salic, A. N., Evans, L. M., and Kirschner, M. W. (1998). Geminin, a neuralizing molecule that demarcates the future neural plate at the onset of gastrulation. *Development* 125, 3247–3258.

Kuriyama, S., and Mayor, R. (2008). Molecular analysis of neural crest migration. *Philos. Trans. R. Soc. B Biol. Sci.* 363, 1349–1362. doi: 10.1098/rstb.2007.2252

Kwon, H. J., Bhat, N., Sweet, E. M., Cornell, R. A., and Riley, B. B. (2010). Identification of early requirements for preplacodal ectoderm and sensory organ development. *PLoS Genet.* 6:e1001133. doi: 10.1371/journal.pgen.1001133

LaBonne, C., and Bronner-Fraser, M. (1998). Neural crest induction in *Xenopus*: evidence for a two-signal model. *Development* 125, 2403–2414.

Lemaire, P., Smith, W. C., and Nishida, H. (2008). Ascidians and the plasticity of the chordate developmental program. *Curr. Biol.* 18, 620–631. doi: 10.1016/j.cub.2008.05.039

Leung, A. W., Murdoch, B., Salem, A. F., Prasad, M. S., Gomez, G. A., and García-Castro, M. I. (2016). WNT/β-catenin signaling mediates human neural crest induction via a pre-neural border intermediate. *Development* 143, 398–410. doi: 10.1242/dev.130849

Levine, A. J., and Brivanlou, A. H. (2007). Proposal of a model of mammalian neural induction. *Dev. Biol.* 308, 247–256. doi: 10.1016/j.ydbio.2007.05.036

Li, W., and Cornell, R. A. (2007). Redundant activities of Tfap2a and Tfap2c are required for neural crest induction and development of other non-neural ectoderm derivatives in zebrafish embryos. *Dev. Biol.* 304, 338–354. doi: 10.1016/j.ydbio.2006.12.042

Liem, K. F., Tremml, G., Roelink, H., and Jessell, T. M. (1995). Dorsal differentiation of neural plate cells induced by BMP-mediated signals from epidermal ectoderm. *Cell* 82, 969–979. doi: 10.1016/0092-8674(95)90276-7

Lignell, A., Kerosuo, L., Streichan, S. J., Cai, L., and Bronner, M. E. (2017). Identification of a neural crest stem cell niche by Spatial Genomic Analysis. *Nat. Commun.* 8:1830. doi: 10.1038/s41467-017-01561-w

Lillevali, K., Haugas, M., Matilainen, T., Pussinen, C., Karis, A., and Salminen, M. (2006). Gata3 is required for early morphogenesis and Fgf10 expression during otic development. *Mech. Dev.* 123, 415–429. doi: 10.1016/j.mod.2006.04.007

Lin, Y., Li, X. Y., Willis, A. L., Liu, C., Chen, G., and Weiss, S. J. (2014). Snail1-dependent control of embryonic stem cell pluripotency and lineage commitment. *Nat. Commun.* 5:3070. doi: 10.1038/ncomms4070

Linker, C., De Almeida, I., Papanayotou, C., Stower, M., Sabado, V., Ghorani, E., et al. (2009). Cell communication with the neural plate is required for induction of neural markers by BMP inhibition: evidence for homeogenetic induction and implications for *Xenopus* animal cap and chick explant assays. *Dev. Biol.* 327, 478–486. doi: 10.1016/j.ydbio.2008.12.034

Litsiou, A., Hanson, S., and Streit, A. (2005). A balance of FGF, BMP and WNT signalling positions the future placode territory in the head. *Development* 132, 4051–4062. doi: 10.1242/dev.01964

Liu, Y., and Labosky, P. A. (2008). Regulation of embryonic stem cell self-renewal and pluripotency by foxd3. *Stem Cells* 26, 2475–2484. doi: 10.1634/stemcells.2008-0269

Liu, B., and Satou, Y. (2019). Foxg specifies sensory neurons in the anterior neural plate border of the ascidian embryo. *Nat. Commun.* 10, 1–3. doi: 10.1038/s41467-019-12839-6

Lukoseviciute, M., Gavriouchkina, D., Williams, R. M., Hochgreb-Hagele, T., Senanayake, U., Chong-Morrison, V., et al. (2018). From pioneer to repressor: bimodal foxd3 activity dynamically remodels neural crest regulatory landscape in vivo. *Dev. Cell* 47, 608.e6–628.e6. doi: 10.1016/j.devcel.2018.11.009

Luo, T., Matsuo-Takasaki, M., Lim, J. H., and Sargent, T. D. (2001). Differential regulation of Dlx gene expression by a BMP morphogenetic gradient. *Int. J. Dev. Biol.* 45, 681–684.

Maharana, S. K., and Schlosser, G. (2018). A gene regulatory network underlying the formation of pre-placodal ectoderm in *Xenopus laevis*. *BMC Biol.* 16:79. doi: 10.1186/s12915-018-0540-5

Manni, L., Caicci, Ã. F., Gasparini, F., Zaniolo, G., and Burighel, P. (2004). Hair cells in ascidians and the evolution of lateral line placodes. *Evol. Dev.* 6, 379–381. doi: 10.1111/j.1525-142X.2004.04046.x

Martik, M. L., and Bronner, M. E. (2018). Regulatory logic underlying diversification of the neural crest. *Trends Genet.* 33, 715–727. doi: 10.1016/j.tig.2017.07.015

Mašek, J., Machoň, O., Kořínek, V., Taketo, M. M., and Kozmik, Z. (2016). Tcf7l1 protects the anterior neural fold from adopting the neural crest fate. *Development* 143, 2206–2216. doi: 10.1242/dev.132357

Matsuo-Takasaki, M., Matsumura, M., and Sasai, Y. (2005). An essential role of *Xenopus* foxi1a for ventral specification of the cephalic ectoderm during gastrulation. *Development* 132, 3885–3894. doi: 10.1242/dev.01959

Mayor, R., Guerrero, N., and Martinez, C. (1997). Role of FGF and noggin in neural crest induction. *Dev. Biol.* 189, 1–12. doi: 10.1006/dbio.1997.8634

Mazet, F., Hutt, J. A., Milloz, J., Millard, J., Graham, A., and Shimeld, S. M. (2005). Molecular evidence from *Ciona intestinalis* for the evolutionary origin of vertebrate sensory placodes. *Dev. Biol.* 282, 494–508. doi: 10.1016/j.ydbio.2005.02.021

McLarren, K. W., Litsiou, A., and Streit, A. (2003). DLX5 positions the neural crest and preplacode region at the border of the neural plate. *Dev. Biol.* 259, 34–47. doi: 10.1016/S0012-1606(03)00177-5

Meulemans, D., and Bronner-Fraser, M. (2004). Gene-regulatory interactions in neural crest evolution and development. *Dev. Cell* 7, 291–299. doi: 10.1016/j.devcel.2004.08.007

Milet, C., Maczkowiak, F., Roche, D. D., and Monsoro-Burq, A. H. (2013). Pax3 and Zic1 drive induction and differentiation of multipotent, migratory, and functional neural crest in *Xenopus* embryos. *Proc. Natl. Acad. Sci. U. S. A.* 110, 5528–5533. doi: 10.1073/pnas.1219124110

Milet, C., and Monsoro-Burq, A. H. (2012). Neural crest induction at the neural plate border in vertebrates. *Dev. Biol.* 366, 22–33. doi: 10.1016/j.ydbio.2012.01.013

Mishima, N., and Tomarev, S. (1998). Chicken eyes absent 2 gene: isolation and expression pattern during development. *Int. J. Dev. Biol.* 42, 1109–1115.

Mohammed, H., Hernando-Herraez, I., Savino, A., Scialdone, A., Macaulay, I., Mulas, C., et al. (2017). Single-cell landscape of transcriptional heterogeneity and cell fate decisions during mouse early gastrulation. *Cell Rep.* 20, 1215–1228. doi: 10.1016/j.celrep.2017.07.009

Monsoro-Burq, A. -H. H., Fletcher, R. B., and Harland, R. M. (2003). Neural crest induction by paraxial mesoderm in *Xenopus* embryos requires FGF signals. *Development* 130, 3111–3124. doi: 10.1242/dev.00531

Monsoro-Burq, A. -H. H., Wang, E., and Harland, R. (2005). Msx1 and Pax3 cooperate to mediate FGF8 and WNT signals during *Xenopus* neural crest induction. *Dev. Cell* 8, 167–178. doi: 10.1016/j.devcel.2004.12.017

Murdoch, B., DelConte, C., and Garcia-Castro, M. I. (2010). Embryonic Pax7-expressing progenitors contribute multiple cell types to the postnatal olfactory epithelium. *J. Neurosci.* 30, 9523–9532. doi: 10.1523/JNEUROSCI.0867-10.2010

Murdoch, B., DelConte, C., and Garcia-Castro, M. I. (2012). Pax7 lineage contributions to the mammalian neural crest. *PLoS One* 7:e41089. doi: 10.1371/journal.pone.0041089

Niehrs, C. (2010). On growth and form: a Cartesian coordinate system of Wnt and BMP signaling specifies bilaterian body axes. *Development* 137, 845–857. doi: 10.1242/dev.039651

Northcutt, R. G., and Gans, C. (1983). The genesis of neural crest and epidermal placodes: a reinterpretation of vertebrate origins. *Q. Rev. Biol.* 58, 1–28. doi: 10.1086/413055

Ogita, J., Isogai, E., Sudo, H., Sakiyama, S., Nakagawara, A., and Koseki, H. (2001). Expression of the Dan gene during chicken embryonic development. *Mech. Dev.* 109, 363–365. doi: 10.1016/s0925-4773(01)00522-6

Ohyama, T., and Groves, A. K. (2004a). Expression of mouse Foxi class genes in early craniofacial development. *Dev. Dyn.* 231, 640–646. doi: 10.1002/dvdy.20160

Ohyama, T., and Groves, A. K. (2004b). Generation of Pax2-Cre mice by modification of a Pax2 bacterial artificial chromosome. *Genesis* 38, 195–199. doi: 10.1002/gene.20017

Pandur, P. D., and Moody, S. A. (2000). *Xenopus* Six1 gene is expressed in neurogenic cranial placodes and maintained in the differentiating lateral lines. *Mech. Dev.* 96, 253–257. doi: 10.1016/S0925-4773(00)00396-8

Papalopulu, N., and Kintner, C. (1993). *Xenopus* distal-less related homeobox genes are expressed in the developing forebrain and are induced by planar signals. *Development* 117, 961–975.

Papanayotou, C., Mey, A., Birot, A. -M., Saka, Y., Boast, S., Smith, J. C., et al. (2008). A mechanism regulating the onset of Sox2 expression in the embryonic neural plate. *PLoS Biol.* 6:e2. doi: 10.1371/journal.pbio.0060002

Parker, H. J., Pushel, I., and Krumlauf, R. (2018). Coupling the roles of Hox genes to regulatory networks patterning cranial neural crest. *Dev. Biol.* 444, S67–S78. doi: 10.1016/j.ydbio.2018.03.016

Patthey, C., Schlosser, G., and Shimeld, S. M. (2014). The evolutionary history of vertebrate cranial placodes—I: cell type evolution. *Dev. Biol.* 389, 82–97. doi: 10.1016/j.ydbio.2014.01.017

Pera, E., Stein, S., and Kessel, M. (1999). Ectodermal patterning in the avian embryo: epidermis versus neural plate. *Development* 126, 63–73.

Phillips, B. T., Kwon, H. -J. J., Melton, C., Houghtaling, P., Fritz, A., and Riley, B. B. (2006). Zebrafish msxB, msxC and msxE function together to refine the neural-nonneural border and regulate cranial placodes and neural crest development. *Dev. Biol.* 294, 376–390. doi: 10.1016/j.ydbio.2006.03.001

Pieper, M., Ahrens, K., Rink, E., Peter, A., and Schlosser, G. (2012). Differential distribution of competence for panplacodal and neural crest induction to non-neural and neural ectoderm. *Development* 139, 1175–1187. doi: 10.1242/dev.074468

Pijuan-Sala, B., Griffiths, J. A., Guibentif, C., Hiscock, T. W., Jawaid, W., Calero-Nieto, F. J., et al. (2019). A single-cell molecular map of mouse gastrulation and early organogenesis. *Nature* 566, 490–495. doi: 10.1038/s41586-019-0933-9

Pla, P., and Monsoro-Burq, A. H. (2018). The neural border: induction, specification and maturation of the territory that generates neural crest cells. *Dev. Biol.* 444, S36–S46. doi: 10.1016/j.ydbio.2018.05.018

Prasad, M. S., Charney, R. M., and García-Castro, M. I. (2019). Specification and formation of the neural crest: perspectives on lineage segregation. *Genesis* 57, 1–21. doi: 10.1002/dvg.23276

Prasad, M. S., Sauka-Spengler, T., and LaBonne, C. (2012). Induction of the neural crest state: control of stem cell attributes by gene regulatory, post-transcriptional and epigenetic interactions. *Dev. Biol.* 366, 10–21. doi: 10.1016/j.ydbio.2012.03.014

Prasad, M. S., Uribe-Querol, E., Marquez, J., Vadasz, S., Yardley, N., Shelar, P. B., et al. (2020). Blastula stage specification of avian neural crest. *Dev. Biol.* 458, 64–74. doi: 10.1016/j.ydbio.2019.10.007

Purcell, P., Oliver, G., Mardon, G., Donner, A. L., and Maas, R. L. (2005). Pax6-dependence of Six3, Eya1 and Dach1 expression during lens and nasal placode induction. *Gene Expr. Patterns* 6, 110–118. doi: 10.1016/j.modgep.2005.04.010

Rada-Iglesias, A., Bajpai, R., Swigut, T., Brugmann, S. A., Flynn, R. A., and Wysocka, J. (2011). A unique chromatin signature uncovers early developmental enhancers in humans. *Nature* 470, 279–283. doi: 10.1038/nature09692

Rex, M., Orme, A., Uwanogho, D., Tointon, K., Wigmore, P. M., Sharpe, P. T., et al. (1997). Dynamic expression of chicken Sox2 and Sox3 genes in ectoderm induced to form neural tissue. *Dev. Dyn.* 209, 323–332. doi: 10.1002/(SICI)1097-0177(199707)209:3<323::AID-AJA7>3.0.CO;2-K

Reyes, M., Billman, K., Hacohen, N., and Blainey, P. C. (2019). Simultaneous profiling of gene expression and chromatin accessibility in single cells. *Adv. Biosyst.* 3:1900065. doi: 10.1002/adbi.201900065

Robledo, R. F., and Lufkin, T. (2006). Dlx5 and Dlx6 homeobox genes are required for specification of the mammalian vestibular apparatus. *Genesis* 44, 425–437. doi: 10.1002/dvg.20233

Rodriguez Esteban, C., Capdevila, J., Economides, A. N., Pascual, J., Ortiz, A., and Izpisua Belmonte, J. C. (1999). The novel Cer-like protein Caronte mediates the establishment of embryonic left-right asymmetry. *Nature* 401, 243–251. doi: 10.1038/45738

Rodriques, S. G., Stickels, R. R., Goeva, A., Martin, C. A., Murray, E., Vanderburg, C. R., et al. (2019). Slide-seq: a scalable technology for measuring genome-wide expression at high spatial resolution. *Science* 363, 1463–1467. doi: 10.1126/science.aaw1219

Roellig, D., Tan-Cabugao, J., Esaian, S., and Bronner, M. E. (2017). Dynamic transcriptional signature and cell fate analysis reveals plasticity of individual neural plate border cells. *eLife* 6, 1–24. doi: 10.7554/eLife.21620

Rogers, C. D., Ferzli, G. S., and Casey, E. S. (2011). The response of early neural genes to FGF signaling or inhibition of BMP indicate the absence of a conserved neural induction module. *BMC Dev. Biol.* 11:74. doi: 10.1186/1471-213X-11-74

Rogers, C. D., Moody, S. A., and Casey, E. S. (2009). Neural induction and factors that stabilize a neural fate. *Birth Defects Res. C Embryo Today* 87, 249–262. doi: 10.1002/bdrc.20157

Rosenberg, A. B., Roco, C. M., Muscat, R. A., Kuchina, A., Sample, P., Yao, Z., et al. (2018). Single-cell profiling of the developing mouse brain and spinal cord with split-pool barcoding. *Science* 360, 176–182. doi: 10.1126/science.aam8999

Rothstein, M., and Simoes-Costa, M. (2020). Heterodimerization of TFAP2 pioneer factors drives epigenomic remodeling during neural crest specification. *Genome Res.* 30, 35–48. doi: 10.1101/gr.249680.119

Saint-Jeannet, J. P., and Moody, S. A. (2014). Establishing the pre-placodal region and breaking it into placodes with distinct identities. *Dev. Biol.* 389, 13–27. doi: 10.1016/j.ydbio.2014.02.011

Sandell, L. L., Butler Tjaden, N. E., Barlow, A. J., and Trainor, P. A. (2014). Cochleovestibular nerve development is integrated with migratory neural crest cells. *Dev. Biol.* 385, 200–210. doi: 10.1016/j.ydbio.2013.11.009

Sato, S., Ikeda, K., Shioi, G., Ochi, H., Ogino, H., Yajima, H., et al. (2010). Conserved expression of mouse Six1 in the pre-placodal region (PPR) and identification of an enhancer for the rostral PPR. *Dev. Biol.* 344, 158–171. doi: 10.1016/j.ydbio.2010.04.029

Sauka-Spengler, T., and Bronner-Fraser, M. (2008). A gene regulatory network orchestrates neural crest formation. *Nat. Rev. Mol. Cell Biol.* 9, 557–568. doi: 10.1038/nrm2428

Scerbo, P., and Monsoro-Burq, A. H. (2020). The vertebrate-specific VENTX/NANOG gene empowers neural crest with ectomesenchyme potential. *Sci. Adv.* 6:eaaz1469. doi: 10.1126/sciadv.aaz1469

Schlosser, G. (2007). How old genes make a new head: redeployment of Six and Eya genes during the evolution of vertebrate cranial placodes. *Integr. Comp. Biol.* 47, 343–359. doi: 10.1093/icb/icm031

Schlosser, G. (2008). Do vertebrate neural crest and cranial placodes have a common evolutionary origin? *BioEssays* 30, 659–672. doi: 10.1002/bies.20775

Schlosser, G. (2017). From so simple a beginning—what amphioxus can teach us about placode evolution. *Int. J. Dev. Biol.* 61, 633–648. doi: 10.1387/ijdb.170127gs

Schlosser, G., Patthey, C., and Shimeld, S. M. (2014). The evolutionary history of vertebrate cranial placodes II. Evolution of ectodermal patterning. *Dev. Biol.* 389, 98–119. doi: 10.1016/j.ydbio.2014.01.019

Schubert, F. R., Mootoosamy, R. C., Walters, E. H., Graham, A., Tumiotto, L., Munsterberg, A. E., et al. (2002). Wnt6 marks sites of epithelial transformations in the chick embryo. *Mech. Dev.* 114, 143–148. doi: 10.1016/S0925-4773(02)00039-4

Sharman, A. C., Shimeld, S. M., and Holland, P. W. H. (1999). An amphioxus Msx gene expressed predominantly in the dorsal neural tube. *Dev. Genes Evol.* 209, 260–263. doi: 10.1007/s004270050251

Sheng, K., Cao, W., Niu, Y., Deng, Q., and Zong, C. (2017). Effective detection of variation in single-cell transcriptomes using MATQ-seq. *Nat. Methods* 14, 267–270. doi: 10.1038/nmeth.4145

Sheng, G., and Stern, C. D. (1999). Gata2 and Gata3: novel markers for early embryonic polarity and for non-neural ectoderm in the chick embryo. *Mech. Dev.* 87, 213–216. doi: 10.1016/S0925-4773(99)00150-1

Simões-Costa, M., Stone, M., and Bronner, M. E. (2015). Axud1 integrates Wnt signaling and transcriptional inputs to drive neural crest formation. *Dev. Cell* 34, 544–554. doi: 10.1016/j.devcel.2015.06.024

Singh, S., and Groves, A. K. (2016). The molecular basis of craniofacial placode development. *Wiley Interdiscip. Rev. Dev. Biol.* 5, 363–376. doi: 10.1002/wdev.226

Skene, P. J., and Henikoff, S. (2017). An efficient targeted nuclease strategy for high-resolution mapping of DNA binding sites. *eLife* 6, 1–35. doi: 10.7554/eLife.21856

Soldatov, R., Kaucka, M., Kastriti, M. E., Petersen, J., Chontorotzea, T., Englmaier, L., et al. (2019). Spatiotemporal structure of cell fate decisions in murine neural crest. *Science* 364:eaas9536. doi: 10.1126/science.aas9536

Solomon, K. S., and Fritz, A. (2002). Concerted action of two dlx paralogs in sensory placode formation. *Development* 129, 3127–3136.

Stern, C. D. (2002). Induction and initial patterning of the nervous system—the chick embryo enters the scene. *Curr. Opin. Genet. Dev.* 12, 447–451. doi: 10.1016/S0959-437X(02)00324-6

Stern, C. D., and Downs, K. M. (2012). The hypoblast (visceral endoderm): an evo-devo perspective. *Development* 139, 1059–1069. doi: 10.1242/dev.070730

Steventon, B., Araya, C., Linker, C., Kuriyama, S., and Mayor, R. (2009). Differential requirements of BMP and Wnt signalling during gastrulation and neurulation define two steps in neural crest induction. *Development* 136, 771–779. doi: 10.1242/dev.029017

Steventon, B., Mayor, R., and Streit, A. (2012). Mutual repression between Gbx2 and Otx2 in sensory placodes reveals a general mechanism for ectodermal patterning. *Dev. Biol.* 367, 55–65. doi: 10.1016/j.ydbio.2012.04.025

Steventon, B., Mayor, R., and Streit, A. (2014). Neural crest and placode interaction during the development of the cranial sensory system. *Dev. Biol.* 389, 28–38. doi: 10.1016/j.ydbio.2014.01.021

Stolfi, A., Ryan, K., Meinertzhagen, I. A., and Christiaen, L. (2015). Migratory neuronal progenitors arise from the neural plate borders in tunicates. *Nature* 527, 371–374. doi: 10.1038/nature15758

Streit, A. (2002). Extensive cell movements accompany formation of the otic placode. *Dev. Biol.* 249, 237–254. doi: 10.1006/dbio.2002.0739

Streit, A. (2007). The preplacodal region: an ectodermal domain with multipotential progenitors that contribute to sense organs and cranial sensory ganglia. *Int. J. Dev. Biol.* 51, 447–461. doi: 10.1387/ijdb.072327as

Streit, A., Berliner, A. J., Papanayotou, C., Slrulnik, A., Stern, C. D., Sirulnik, A., et al. (2000). Initiation of neural induction by FGF signalling before gastrulation. *Nature* 406, 74–78. doi: 10.1038/35017617

Streit, A., Lee, K. J., Woo, I., Roberts, C., Jessell, T. M., and Stern, C. D. (1998). Chordin regulates primitive streak development and the stability of induced neural cells, but is not sufficient for neural induction in the chick embryo. *Development* 125, 507–519.

Streit, A., Sockanathan, S., Perez, L., Rex, M., Scotting, P. J., Sharpe, P. T., et al. (1997). Preventing the loss of competence for neural induction: HGF/SF, L5 and Sox-2. *Development* 124, 1191–1202.

Stuhlmiller, T. J., and Garcia-Castro, M. I. (2012). Current perspectives of the signaling pathways directing neural crest induction. *Cell. Mol. Life Sci.* 69, 3715–3737. doi: 10.1007/s00018-012-0991-8

Tam, P. P. L., and Ho, J. W. K. (2020). Cellular diversity and lineage trajectory: insights from mouse single cell transcriptomes. *Development* 147, 1–7. doi: 10.1242/dev.179788

The International Stem Cell Initiative., Allison, T. F., Andrews, P. W., Avior, Y., Barbaric, I., Benvenisty, N., Bock, C., et al. (2018). Assessment of established techniques to determine developmental and malignant potential of human pluripotent stem cells. *Nat. Commun.* 9:1925. doi: 10.1038/s41467-018-04011-3

Thiery, A., Buzzi, A. L., and Streit, A. (2020). Cell fate decisions during the development of the peripheral nervous system in the vertebrate head. *Curr. Top. Dev. Biol.* 139, 127–167. doi: 10.1016/bs.ctdb.2020.04.002

Torres-Paz, J., Tine, E. M., and Whitlock, K. E. (2020). Dissecting the neural divide: a continuous neurectoderm gives rise to both the olfactory placode and olfactory bulb. *Int. J. Dev. Biol.* doi: 10.1387/ijdb.200097kw [Epub ahead of print]

Trainor, P. A., and Krumlauf, R. (2000a). Patterning the cranial neural crest: hindbrain segmentation and Hox gene plasticity. *Nat. Rev. Neurosci.* 1, 116–124. doi: 10.1038/35039056

Trainor, P. A., and Krumlauf, R. (2000b). Plasticity in mouse neural crest cells reveals a new patterning role for cranial mesoderm. *Nat. Cell Biol.* 2, 96–102. doi: 10.1038/35000051

Trevers, K. E., Prajapati, R. S., Hintze, M., Stower, M. J., Strobl, A. C., Tambalo, M., et al. (2017). Neural induction by the node and placode induction by head mesoderm share an initial state resembling neural plate border and ES cells. *Proc. Natl. Acad. Sci. U. S. A.* 115, 355–360. doi: 10.1073/pnas.1719674115

Tribulo, C., Aybar, M. J., Nguyen, V. H., Mullins, M. C., Mayor, R., Tríbulo, C., et al. (2003). Regulation of Msx genes by a bmp gradient is essential for neural crest specification. *Development* 130, 6441–6452. doi: 10.1242/dev.00878

Uchikawa, M., Ishida, Y., Takemoto, T., Kamachi, Y., and Kondoh, H. (2003). Functional analysis of chicken Sox2 enhancers highlights an array of diverse regulatory elements that are conserved in mammals. *Dev. Cell* 4, 509–519. doi: 10.1016/s1534-5807(03)00088-1

Verboom, K., Everaert, C., Bolduc, N., Livak, K. J., Yigit, N., Rombaut, D., et al. (2019). SMARTer single cell total RNA sequencing. *Nucleic Acids Res.* 47:e93. doi: 10.1093/nar/gkz535

Villanueva, S., Glavic, A., Ruiz, P., and Mayor, R. (2002). Posteriorization by FGF, Wnt, and retinoic acid is required for neural crest induction. *Dev. Biol.* 241, 289–301. doi: 10.1006/dbio.2001.0485

Wada, H., Saiga, H., Satoh, N., and Holland, P. W. H. (1998). Tripartite organization of the ancestral chordate brain and the antiquity of placodes: insights from ascidian Pax-2/5/8, Hox and Otx genes. *Development* 125, 1113–1122.

Wagner, E., Stolfi, A., Choi, Y. G., and Levine, M. (2014). Islet is a key determinant of ascidian palp morphogenesis. *Development* 141, 3084–3092. doi: 10.1242/dev.110684

Wang, F., Flanagan, J., Su, N., Wang, L. -C., Bui, S., Nielson, A., et al. (2012). RNAscope: a novel in situ RNA analysis platform for formalin-fixed, paraffin-embedded tissues. *J. Mol. Diagn.* 14, 22–29. doi: 10.1016/j.jmoldx.2011.08.002

Warmflash, A., Sorre, B., Etoc, F., Siggia, E. D., and Brivanlou, A. H. (2014). A method to recapitulate early embryonic spatial patterning in human embryonic stem cells. *Nat. Methods* 11, 847–854. doi: 10.1038/nMeth.3016

Wilson, S. I., and Edlund, T. (2001). Neural induction: toward a unifying mechanism. *Nat. Neurosci.* 4, 1161–1168. doi: 10.1038/nn747

Woda, J. M., Pastagia, J., Mercola, M., and Artinger, K. B. (2003). Dlx proteins position the neural plate border and determine adjacent cell fates. *Development* 130, 331–342. doi: 10.1242/dev.00212

Wurst, W., and Bally-Cuif, L. (2001). Neural plate patterning: upstream and downstream of the isthmic organizer. *Nat. Rev. Neurosci.* 2, 99–108. doi: 10.1038/35053516

Xu, P. X., Adams, J., Peters, H., Brown, M. C., Heaney, S., and Maas, R. (1999). Eya1-deficient mice lack ears and kidneys and show abnormal apoptosis of organ primordia. *Nat. Genet.* 23, 113–117. doi: 10.1038/12722

York, J. R., Yuan, T., and McCauley, D. W. (2020). Evolutionary and developmental associations of neural crest and placodes in the vertebrate head: insights from jawless vertebrates. *Front. Physiol.* 11:986. doi: 10.3389/fphys.2020.00986

Yu, J. -K., Meulemans, D., McKeown, S. J., and Bronner-Fraser, M. (2008). Insights from the amphioxus genome on the origin of vertebrate neural crest. *Genome Res.* 18, 1127–1132. doi: 10.1101/gr.076208.108

Yu, J. -K., Satou, Y., Holland, N. D., Shin-I, T., Kohara, Y., Satoh, N., et al. (2007). Axial patterning in cephalochordates and the evolution of the organizer. *Nature* 445, 613–617. doi: 10.1038/nature05472

Zhang, Y., Knosp, B. M., Maconochie, M., Friedman, R. A., and Smith, R. J. H. (2004). A comparative study of Eya1 and Eya4 protein function and its implication in branchio-oto-renal syndrome and DFNA10. *J. Assoc. Res. Otolaryngol.* 5, 295–304. doi: 10.1007/s10162-004-4044-3

Zheng, W., Huang, L., Wei, Z. -B., Silvius, D., Tang, B., and Xu, P. -X. (2003). The role of Six1 in mammalian auditory system development. *Development* 130, 3989–4000. doi: 10.1242/dev.00628

Zhu, C. C., Dyer, M. A., Uchikawa, M., Kondoh, H., Lagutin, O. V., and Oliver, G. (2002). Six3-mediated auto repression and eye development requires its interaction with members of the Groucho-related family of co-repressors. *Development* 129, 2835–2849.

Zou, D., Silvius, D., Davenport, J., Grifone, R., Maire, P., and Xu, P. X. (2006). Patterning of the third pharyngeal pouch into thymus/parathyroid by Six and Eya1. *Dev. Biol.* 293, 499–512. doi: 10.1016/j.ydbio.2005.12.015

Zou, D., Silvius, D., Fritzsch, B., and Xu, P. X. (2004). Eya1 and Six1 are essential for early steps of sensory neurogenesis in mammalian cranial placodes. *Development* 131, 5561–5572. doi: 10.1242/dev.01437

Conflict of Interest: The authors declare that the research was conducted in the absence of any commercial or financial relationships that could be construed as a potential conflict of interest.

frontiers in Physiology

REVIEW
published: 08 December 2020
doi: 10.3389/fphys.2020.606889

Sorting Sox: Diverse Roles for Sox Transcription Factors During Neural Crest and Craniofacial Development

Elizabeth N. Schock[1] *and Carole LaBonne*[1,2]*

[1] Department of Molecular Biosciences, Northwestern University, Evanston, IL, United States, [2] NSF-Simons Center for Quantitative Biology, Northwestern University, Evanston, IL, United States

Sox transcription factors play many diverse roles during development, including regulating stem cell states, directing differentiation, and influencing the local chromatin landscape. Of the twenty vertebrate Sox factors, several play critical roles in the development the neural crest, a key vertebrate innovation, and the subsequent formation of neural crest-derived structures, including the craniofacial complex. Herein, we review the specific roles for individual Sox factors during neural crest cell formation and discuss how some factors may have been essential for the evolution of the neural crest. Additionally, we describe how Sox factors direct neural crest cell differentiation into diverse lineages such as melanocytes, glia, and cartilage and detail their involvement in the development of specific craniofacial structures. Finally, we highlight several SOXopathies associated with craniofacial phenotypes.

Keywords: neural crest, craniofacial development, SoxB1, SoxE, stem cells

OPEN ACCESS

Edited by:
Jean-Pierre Saint-Jeannet, New York University, United States

Reviewed by:
Martin Chi Hang Cheung, The University of Hong Kong, Hong Kong
Elisabeth Sock, University of Erlangen–Nuremberg, Germany

***Correspondence:**
Carole LaBonne
clabonne@northwestern.edu

Specialty section:
This article was submitted to Craniofacial Biology and Dental Research, a section of the journal Frontiers in Physiology

Received: *15 September 2020*
Accepted: *09 November 2020*
Published: *08 December 2020*

Citation:
Schock EN and LaBonne C (2020) Sorting Sox: Diverse Roles for Sox Transcription Factors During Neural Crest and Craniofacial Development. Front. Physiol. 11:606889. doi: 10.3389/fphys.2020.606889

INTRODUCTION

Since the hallmark discovery of the *SRY* gene, the master regulator of male sex determination (Gubbay et al., 1990; Lovell-Badge, 2010), twenty mammalian SRY-related HMG box containing (SOX) transcription factors have been identified. A significant number of important developmental functions have been described for Sox transcription factors. These range from maintaining stem cell states to promoting differentiation (reviewed in Kamachi and Kondoh, 2013). The growing number of developmental disorders associated with mutations in *SOX* genes underscores the importance of these factors during development (Angelozzi and Lefebvre, 2019). In this review we focus on the Sox factors that have roles in the formation of the neural crest as well as those important for the development of cell types within and components of the craniofacial complex. Finally, we highlight the "SOXopathies" that are associated with a variety of craniofacial phenotypes.

SOX TRANSCRIPTION FACTOR FAMILIES

The twenty mammalian Sox factors are divided into nine subfamilies (A, B1, B2-H) based mainly upon the homology of a 79 amino acid DNA binding region termed the High Mobility Group (HMG) domain (**Figure 1A**; Bowles et al., 2000). Duplication events, slow divergence, and co-option of functional elements are hypothesized to have driven Sox family evolution (Bowles et al., 2000). Consistent with this, members of the same subfamily often having overlapping expression patterns and various degrees of functional redundancy (**Figure 1B**; Heenan et al., 2016). SOX factors bind DNA at

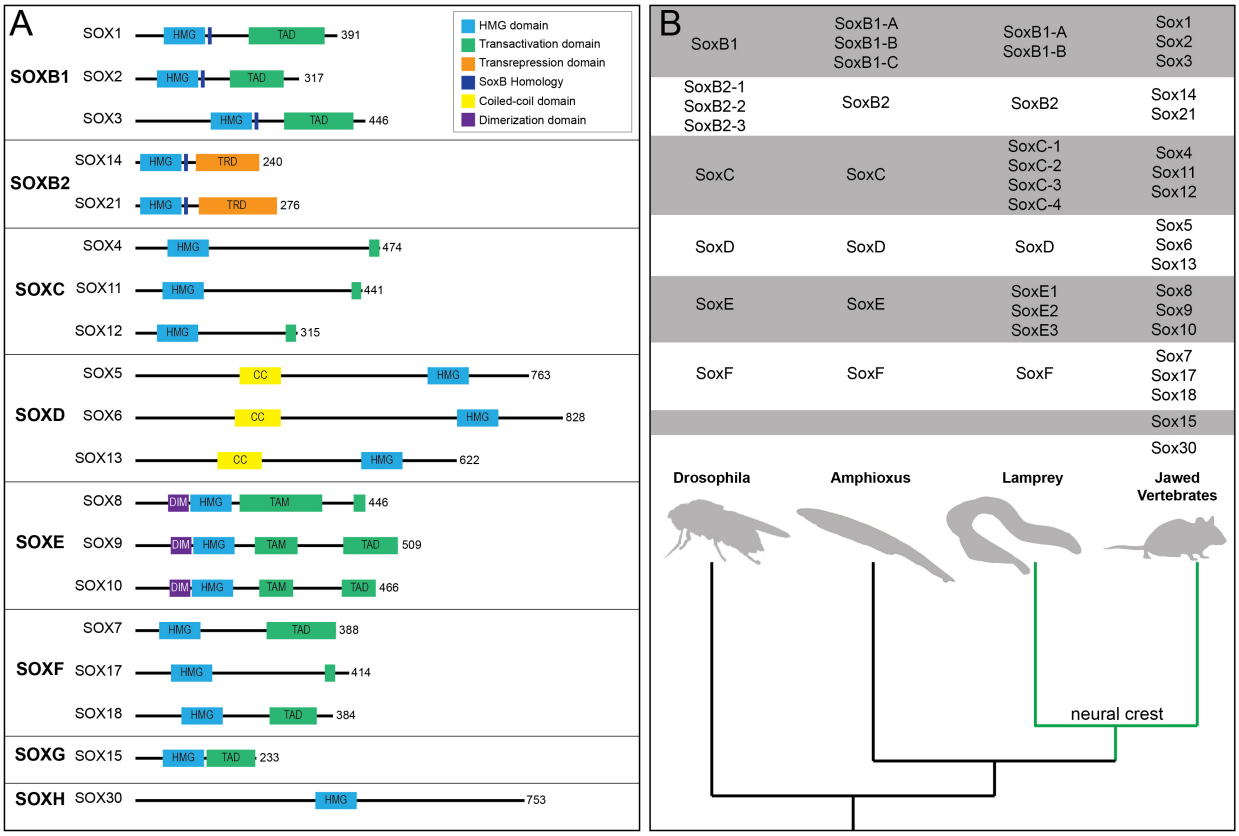

FIGURE 1 | Sox transcription factor subfamiles and their functional domains. **(A)** Diagram of human SOX proteins grouped by subfamily. Major protein functional domains are depicted as colored boxes: High-mobility group (HMG) domain (light blue), transactivation domain (TAD; green), transrepression domain (TRD; orange), SoxB homology domain (dark blue), coiled-coil (CC) domain (yellow), and dimerization (DIM) domain (purple). **(B)** Phylogenetic tree depicting Sox subfamily members across key organisms. The emergence of the neural crest (green) in vertebrates coincided with duplication events among various Sox subfamilies, most notably SoxC and SoxE.

C[A/T]TTG[T/A][T/A] sequences or similar motifs. Notably, the HMG domain binds DNA at the minor groove causing the DNA to bend. This facilitates local chromatin modifications and can increase DNA accessibility for partner factor binding (Hou et al., 2017). Furthermore, some SOX factors (SOX2 and SOX9) have been shown to engage at regions of condensed chromatin and are considered pioneer factors (Adam et al., 2015; Soufi et al., 2015; Julian et al., 2017). SOX2, through the HMG domain, recognizes a degenerate Sox motif on nucleosomal DNA (Soufi et al., 2015). At these degenerate sites less DNA bending occurs which facilitates SOX2 binding on the minor groove of nucleosomal DNA (Soufi et al., 2015). At some of these sites, binding may, in part, be facilitated or stabilized by chromatin-associated proteins such as poly(ADP-ribose) polymerase-1 (PARP-1) (Liu and Kraus, 2017). The extent to which SOX9's pioneer activity mechanistically mimics that of SOX2 is not known and is an area ripe for future investigation. In order to activate gene expression, SOX factors generally require cooperation with a partner factor (reviewed in Kondoh and Kamachi, 2010). Examples of this include SOX10-MITF pairing during melanocyte specification, SOX2-OCT3/4 pairing in embryonic stem cells, and SOX2-BRN2 pairing in neural progenitors (Ambrosetti et al., 1997; Jiao et al., 2004; Tanaka et al., 2004; Takahashi and Yamanaka, 2006). Sox factors, other than the SoxB2 subfamily, were initially characterized as transcriptional activators, however, it has since been shown that many Sox factors can function as either activators or repressors in a context-dependent manner (reviewed in Chew and Gallo, 2009).

Within a Sox subfamily, the structural domains of the proteins outside of the HMG domain are similar, but not identical. These domains include coiled-coiled, dimerization, and transactivation/transrepression domains (**Figure 1A**). SoxD factors harbor a coiled-coil domain that mediates homo- or hetero-dimerization with other SoxD factors, stabilizing binding to adjacent HMG sites on DNA (Lefebvre et al., 1998). SoxE factors possess a 40 amino acid dimerization (DIM) domain upstream of the HMG domain (Peirano and Wegner, 2000). Their dimerization (homo- or hetero-) is DNA dependent and reliant upon the presence of a palindromic DNA binding sequence (Peirano and Wegner, 2000; Peirano et al., 2000; Schlierf et al., 2002; Huang et al., 2015). While SOXE factors can form heterodimers, they do not appear to dimerize with non-SoxE proteins (Huang et al., 2015; Hou et al., 2017). SoxE factors additionally possess both a C-terminal transactivation

domain (TAD) and a second transactivation domain in the middle of the protein (TAM, or K2 domain) (Schreiner et al., 2007). Recent work suggests that these two domains synergize, resulting in a SOXE factor bipartite transactivation mechanism (Haseeb and Lefebvre, 2019). The members of other Sox subfamilies possess a single transactivation/repression domain. Interestingly, Sox transcriptional activity can depend upon whether the transcriptional partner is an activator or repressor (Kamachi and Kondoh, 2013). For example, SOX2-OCT3/4 synergistically activate *Fgfr4* expression and the SOX9-SOX5/6 complex activates *Col2a1* during chondrogenesis (Ambrosetti et al., 1997; Liu and Lefebvre, 2015). In contrast, SOX9-GLI2/3 represses *Col10a1* in non-hypertrophic chondrocytes (Leung et al., 2011). SOX proteins also associate with non-DNA binding cofactors, such as Groucho co-repressors. SOX2-GRG5 represses neural differentiation markers and SOX9-GRG4 represses *Dct* expression during melanocyte development (Lee et al., 2012; Liu et al., 2014). These findings highlight the importance of cellular context and partner protein/cofactor availability for Sox function.

Sox factors have diverse roles during development and typically members of the same subfamily have similar or redundant functions. The contributions of SoxB1 factors to maintaining pluripotency have been intensely studied (reviewed in Abdelalim et al., 2014), and SOX2 is one of the four Yamanaka factors able to reprogram somatic cells to a pluripotent state (Takahashi and Yamanaka, 2006). Interestingly, other subfamilies of Sox factors are capable of replacing SoxB1 function either during the reprogramming process or in stem cells. SOX15 and SOX18 can substitute for SOX2 during the reprogramming process, but are less efficient (Nakagawa et al., 2008). While SOX17 is not an effective substitute for SOX2, a reengineered SOX17 (SOX17 E122K) reprograms cells with high efficiency (Jauch et al., 2011). Likewise, the reprogramming efficiency of SOX18 increases when it is reengineered to have an analogous point mutation within the HMG domain and the C-terminal of the protein is swapped for the SOX17 C-terminal (Aksoy et al., 2013). The point mutation within the SOX18 HMG domain alone was not sufficient for reprogramming nor was swapping the C-terminal for that of SOX2 (Aksoy et al., 2013). With respect to regulating a stem cell state in embryos, morpholino mediated knockdown of Sox2 and Sox3 in *Xenopus* leads to a loss of pluripotency and this can be partially rescued by expression of *SoxE* factors (Buitrago-Delgado et al., 2018). Together these data suggest that while specific subfamilies of Sox factors may be optimized for particular developmental roles, other Sox subfamilies may be able to serve as a substitute, albeit less efficiently. This paradigm is particularly interesting in the context of the neural crest and the retention of embryonic potential in those cells (discussed below; Buitrago-Delgado et al., 2015).

ROLES FOR SOX FACTORS DURING NEURAL CREST FORMATION

The neural crest is a vertebrate specific population of cells that contribute significantly to the vertebrate body plan, including much of the craniofacial complex. In addition to giving rise to the bone and cartilage of the face, the neural crest also give rise to melanocytes, the majority of the peripheral nervous system, and contribute directly to facial structures such as the tongue, teeth, and palate (Chai et al., 2000; Haldin and LaBonne, 2010; Bronner and LeDouarin, 2012; Prasad et al., 2012). Embryonically, neural crest cells (and cranial placodes) arise at the neural plate border which lies between the neural plate and non-neural ectoderm. Gradients of BMP, FGF, and WNT signaling have all been implicated in the establishment of these three regions. The initial formation of the neural plate border occurs in cells with intermediate levels of BMP signaling and high WNT signaling. A unique signature of transcription factors (*pax3/7*, *zic1/2*, *msx1*, *myc*) define the neural plate border region and these factors subsequently activate the neural crest gene regulatory network (GRN), which includes several Sox factors (Simoes-Costa and Bronner, 2015). *Sox2*, *sox3*, *sox8*, *sox9*, *sox11*, and *sox15* are expressed within the neural plate border (**Figure 2**; Spokony et al., 2002; Wakamatsu et al., 2004; O'Donnell et al., 2006; Roellig et al., 2017). *SOX2* expressing cells within the neural plate border can contribute to both the neural crest and the non-neural ectoderm, and modulating levels of *SOX2* can impact the balance between neural and neural crest domains (Roellig et al., 2017). The observed expression of *sox8* and *sox9* correlates with the formation of definitive neural crest cells within the neural plate border.

Sox Subfamily Function During Neural Crest Formation

Sox transcription factors play important roles in controlling the developmental potential of the neural crest progenitor population as well as in their subsequent lineage decisions. Members of the *SoxC*, *SoxG*, *SoxD*, and *SoxE* families are expressed in the pre-migratory neural crest and functional roles for most of these factors have been reported (**Figure 2**). By contrast, *SoxB1* factors are expressed in the neural plate and pre-placodal ectoderm and can inhibit neural crest formation (Wakamatsu et al., 2004; Roellig et al., 2017; Buitrago-Delgado et al., 2018). *SoxC* factors (*sox4/11/12*) are expressed in the neural crest and the neural plate of *Xenopus* and lamprey (*Petromyzon marinus*) embryos and seem to have evolutionarily conserved functions. Loss of function experiments for SoxC factors resulted in failed neural crest formation in both species (Uy et al., 2015). *SoxC* factors are also expressed in migrating neural crest, but a requirement for these factors during migration or subsequent lineage diversification has yet to be described (Cizelsky et al., 2013; Uy et al., 2015). Similarly, the SoxG family member, *Sox15*, is expressed in the pre-migratory neural crest, but a role for Sox15 in neural crest development has yet to be reported. Interestingly, *Sox15* is expressed in mouse embryonic stem cells and, like SOXB1 proteins, can associate with OCT3/4 (Maruyama et al., 2005). While *Sox15*-null mice are viable, it is possible that SOX15 function is redundant to that of SOXB1 factors in ES cells. As neural crest cells retain stem-cell like potential, it would be interesting to investigate if SOX15 plays a role in controlling the developmental potential of these cells (Buitrago-Delgado et al., 2015).

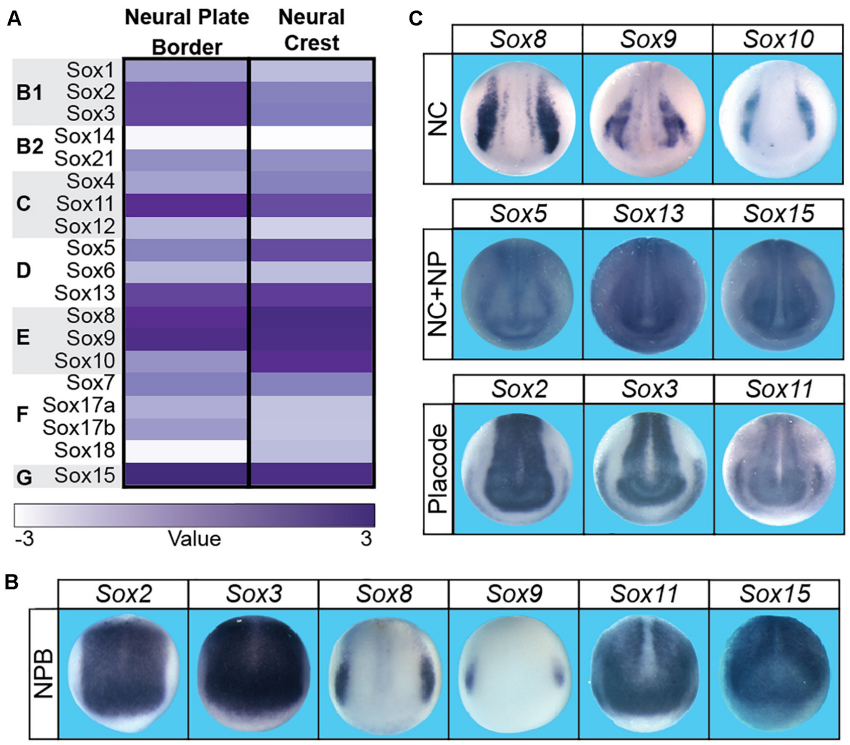

FIGURE 2 | There were boxes subdividing the three sections **(A–C)** in the submitted figure. These boxes are not present in this proof. *Sox* factor expression during neural plate border and neural crest formation in *Xenopus laevis*. **(A)** Heatmap of *Sox* gene expression in neural plate border and neural crest cells in *Xenopus laevis*. High levels of expression are associated with a dark purple while low levels are depicted as white. **(B)** *In situ* hybridizations in early neurula *Xenopus laevis* embryos for *sox2*, *sox3*, *sox8*, *sox9*, *sox11,* and *sox15*. Each of these factors has neural plate border expression (domain most clearly defined by *sox8* expression). **(C)** *In situ* hybridizations in late neurula *Xenopus laevis* embryos for *sox f*actors expressed in the neural crest (*sox8*, *sox9*, *sox10*), neural crest + neural plate (*sox5*, *sox13, sox15),* and neural plate + placodes (*sox2, sox3, sox11*).

Of the three SoxD family members, *Sox5* and *Sox13* are expressed in the forming neural crest; however, only a role for SOX5 has been reported in these cells. *SOX5* is expressed in the pre-migratory neural crest in both chick and *Xenopus* embryos. Loss of function experiments demonstrated that Sox5 is necessary for neural crest, placode, and neural plate border formation. Interestingly, increasing Sox5 levels phenocopies these effects (Nordin and LaBonne, 2014), suggesting that maintaining the correct level of *sox5* expression is key to proper neural crest formation. Sox5 can serve as an effector of BMP signaling in the ectoderm (and in other biological contexts). Through its central coiled-coil domain, Sox5 physically interacts with BMP R-Smad complexes and promotes activation of BMP target genes (Nordin and LaBonne, 2014). Since BMP signaling is essential for neural plate border/neural crest formation, Sox5 likely aids in activation of BMP targets in neural plate border/neural crest cells. Expression of *sox5* persists as neural crest cells migrate, and overexpression of *sox5* results in both a delay in migration and an increase in the total number of neural crest cells (Perez-Alcala et al., 2004; Nordin and LaBonne, 2014). Whether this increase is at the expense of other cell types in the ectoderm remains to be determined.

The evolutionary emergence of the neural crest correlated with the duplication, diversification, and neofunctionalization of a single ancestral *SoxE* gene (Tai et al., 2016). Where it has been examined, vertebrates possess two/three *SoxE* paralogs (Tai et al., 2016). SoxE factors have been shown to be required for neural crest formation across multiple species (Spokony et al., 2002; Honore et al., 2003; Hong and Saint-Jeannet, 2005; Taylor and LaBonne, 2005; O'Donnell et al., 2006; Buitrago-Delgado et al., 2018). Interestingly, the temporal order of *SoxE* gene expression within the neural crest differs across species. In *Xenopus*, *sox8* is expressed first followed by *sox9* then *sox10* (O'Donnell et al., 2006; Buitrago-Delgado et al., 2018). In chick and mouse, *Sox9* is the first SoxE factor to be expressed within the neural crest followed by *Sox10* then *Sox8* (Cheung and Briscoe, 2003). In zebrafish, *sox9a* and *sox9b* expression precedes that of *sox10* in the neural crest while *sox8* is not expressed in these cells (Dutton et al., 2001; Li et al., 2002; Yan et al., 2005). The varied timing of *Sox* expression is consistent with a high degree of functional redundancy among these factors. In the agnathan, *Petromyzon marinus, SoxE1* and *SoxE2* are expressed in the neural folds and migrating neural crest while *SoxE3*, the ortholog to *Sox9* in gnathostomes, lacks early embryonic expression (McCauley and Bronner-Fraser, 2006). The differences in order of expression and function between agnathan and gnathostome SoxE factors may suggest independent divergence from the ancestral *SoxE* (Lakiza et al., 2011).

Evidence across multiple organisms suggests that while SoxE factors are required for neural crest formation, the individual factors may be functionally redundant. Loss of function studies in *Xenopus* demonstrated that *sox8, sox9,* and *sox10* are necessary for neural crest formation and proper migration (Spokony et al., 2002; Honore et al., 2003; Taylor and LaBonne, 2005; O'Donnell et al., 2006). The neural crest can be rescued in Sox8 morphants by any of the SoxE factors suggesting there is functional redundancy between the SoxE factors (Taylor and LaBonne, 2005; O'Donnell et al., 2006). By contrast, murine SoxE mutants do not have obvious early neural crest defects. *Sox8* null mice are viable with no obvious morphological defects suggesting that during mammalian development the other SoxE factors are able to compensate for loss of *Sox8* (Sock et al., 2001). Additionally, the neural crest in $Sox9^{fl/fl;}$ *Wnt1Cre* embryos migrates normally to the craniofacial complex; this suggests that neural crest formation is not altered in these conditional mutants; however, increased apoptosis has been observed in the trunk neural crest of $Sox9^{-/-}$ mice (Cheung et al., 2005). The $Sox9^{fl/fl;}$ *Wnt1Cre* mice do, however, have major craniofacial defects, as discussed below (Mori-Akiyama et al., 2003). In $Sox10^{lacZ}/Sox10^{lacZ}$ mice and *Sox10* hypomorphs, neural crest formation and migration is not altered (Britsch et al., 2001; Schreiner et al., 2007). Again, this suggests that the other SoxE factors can compensate for the loss of a single SoxE factor during neural crest formation. In contrast, during neural crest cell differentiation, each SoxE factor may have unique functions. This is evidenced by $Sox10^{Sox8ki/Sox8ki}$ embryos, where *Sox8* has been inserted into the *Sox10* locus. These mice still have severe enteric nervous system defects and lack melanocytes which phenotypically parallel a loss of *Sox10* (Kellerer et al., 2006).

Post-translational Modifications of SOX Proteins in the Neural Crest

SOX proteins undergo a number of post-translational modifications, including: acetylation, methylation, phosphorylation, SUMOylation, and ubiquitination (Williams et al., 2019). Several of these modifications have been shown to impact neural crest development (Huang et al., 2000; Taylor and LaBonne, 2005, 2007; Sakai et al., 2006; Lee et al., 2012; Liu et al., 2013). Phosphorylation of SOX9 at serine 64 and serine 211, conserved residues in amniotes, by PKA increased SOX9 DNA-binding affinity at a *Col2a1* enhancer element and promoted reporter activation (Huang et al., 2000). Furthermore, phosphorylation of the analogous serine residues in chick is required for delamination of trunk neural crest cells (Liu et al., 2013). Delamination is mediated through SOX9-SNAI2 interaction, and phosphorylation of SOX9 is required for this pairing. Additionally, SOX9 serine 64 and serine 181 phosphorylation (in chick) promotes SOX9 SUMOylation (Liu et al., 2013). SOX9 SUMOylation is not required for trunk delamination, but SUMOylation state impacts neural crest cell formation (Taylor and LaBonne, 2005; Liu et al., 2013). Blocking Sox9 SUMOylation promotes neural crest formation whereas constitutively SUMOylated Sox9 represses neural crest formation (Taylor and LaBonne, 2005). Sox9 inhibition of the neural crest state is mediated through SUMO-dependent recruitment of the Groucho family protein Grg4, which is a transcriptional co-repressor (Lee et al., 2012). The SUMOylation state of Sox9 also influences inner ear development. A constitutively SUMOylated form of Sox9 promotes otic vesicle formation whereas a form of Sox9 that cannot be SUMOylated inhibits ear formation, but promotes ectopic melanocytes (Taylor and LaBonne, 2005).

Likewise, SOX10 is SUMOylated at three conserved lysine residues (Taylor and LaBonne, 2005; Girard and Goossens, 2006). SUMOylation state of SOX10 does not impact nuclear localization or the ability of SOX10 to bind DNA; however, it inhibits the transcriptional activation of target genes such as *MITF* (Girard and Goossens, 2006). Furthermore, it was demonstrated that SUMOylation interferes with the ability of SOX10 to synergize with PAX3 to activate *MITF* gene expression. This was also true for SOX10 and ERG2 and their target *GJB1* in Schwann cells (Girard and Goossens, 2006). Whether this relationship between SOX10 SUMOylation state and transcriptional activation is true for all target genes is yet to be determined. It is likely, however, that this relationship is more complex and context dependent as observed with other transcription factors (Long et al., 2004; Taylor and LaBonne, 2005; Rosonina et al., 2017). Finally, SoxE factors also have putative acetylation and methylation sites (Williams et al., 2019); however, functional roles for these modifications during neural crest development remains largely unknown. One study demonstrated that Sox9 is acetylated by Tip60; however, the acetylation state did not impact the ability of Sox9 to activate *Col2a1* expression (Hattori et al., 2008). Whether Sox9 acetylation state affects transcription of other target genes or if other Sox9 post-translational modifications regulate *Col2a1* expression are questions that remain to be answered.

SOX Transcriptional Targets in the Neural Crest

The functional relationship between SoxE factors and other transcription factors essential for neural crest formation has been examined in several systems. Studies in *Xenopus h*ave shown that Snail1 promotes *sox10* expression and knockdown of *sox9* leads to reduced *twist*, *snail1* and *pax3* expression in the neural crest, whereas *sox9* or *sox10* gain-of-function expands the domains of *foxD*3, *snail2*, and *sox10* expression at the neural plate border (Spokony et al., 2002; Honore et al., 2003; Buitrago-Delgado et al., 2018). In chick, overexpression of *SOX9* is not sufficient to induce *PAX3/7,* but can induce *SNAI2, FOXD3,* and *SOX10* (Cheung and Briscoe, 2003). Additionally, a *SOX10* enhancer element has been identified in chick which requires ETS1, SOX9, and/or cMYB activity to drive reporter expression (Betancur et al., 2010). While such candidate-driven functional studies have provided some insights into the functions of SoxE factors within the neural crest gene regulatory network, a more comprehensive understanding of Sox targets in the neural crest remains lacking. Moreover, as SOX factors require DNA-binding partners for efficient regulation of target genes, it is also essential to identify

and study the SOXE partners that play roles in the development and evolution of the neural crest.

SoxE Factors and the Retention of Embryonic Potential in the Neural Crest

Evolutionarily, the emergence of the neural crest coincided with duplication and diversification of an ancestral *SoxE* gene (**Figure 1B**; Tai et al., 2016). The significance of SoxE function to neural crest evolution is interesting to contemplate given the central role these factors play in the establishment of the neural crest stem cell state. As SoxB1 factors are essential regulators of pluripotency in blastula cells, it is possible that this role was handed off to SoxE factors in the neural crest. Consistent with this, recent work has shown that SoxE function can at least partially replace SoxB1 factors in maintaining the pluripotency of blastula stem cells, although SoxB1 factors are unable to replace SoxE factor function in the neural crest (Buitrago-Delgado et al., 2018). These data suggest that SoxE factors can engage in the pluripotency gene regulatory network, maintaining expression of key targets in the absence of SoxB1 factors, even in a cellular context in which they are normally not expressed. Whether this is a unique feature of SoxE factors or if other Sox subfamilies can function in a similar context remains to be seen; however, other Sox factors can substitute for SoxB1 factors during cell reprogramming (Nakagawa et al., 2008; Jauch et al., 2011). Interestingly, SOX17 sits at the top of the specification hierarchy for human primordial germ cells (Irie et al., 2015). Other pluripotency genes, such as *NANOG* and *OCT4*, but not *SOX2*, are also expressed in human primordial germ cells downstream of *SOX17* (Tan and Tee, 2019). Thus, the SoxB1 to SoxE hand-off in the neural crest may serve as a paradigm for transitioning molecular regulatory circuitry from one Sox subfamily to another to maintain a stem cell-like state.

Why might a transition from SoxB1 to SoxE function have been important for the evolutionary emergence of neural crest stem cells? By the end of gastrulation SoxB1 factors cease to direct pluripotency and instead are expressed in, and essential to, the formation of the neuronal progenitor pool, and continue to play prominent roles in neural lineages later in development (Rex et al., 1997; Graham et al., 2003; Ellis et al., 2004; Schlosser et al., 2008). Once SoxB1 factors have transitioned to controlling the neuronal progenitor state, SoxE factors may take over the regulation of targets essential to maintaining developmental potential in the neural crest. Furthermore, the inability of SoxB1 factors to replace SoxE factor function in the neural crest implies this switch was necessary for the emergence of the neural crest and its derivatives (Buitrago-Delgado et al., 2018). Mechanistically, it is possible that SoxB1 factors are unable to correctly regulate some SoxE target genes unique to neural crest. Furthermore, this switch in Sox factor deployment may also have facilitated the subsequent lineage diversification of neural crest cells to non-neural cell types including cartilage, melanocytes, and glia, which require SoxE function for their formation (Bi et al., 1999; Britsch et al., 2001; Aoki et al., 2003). Understanding this transition, as well as why SoxE factors play essential roles in directing the development of only a subset of neural crest lineages, will require a more complete understanding of SoxE targets and partners in both neural crest stem cells and their derivatives.

SOX FACTORS AND DEVELOPMENT OF THE CRANIOFACIAL COMPLEX

An excellent context in which to investigate the roles and regulation of Sox factors in neural crest lineage diversification is the craniofacial complex, a compilation of multiple structures that together create both the form and function of the face. While development of many of these structures occur simultaneously, the molecular mechanisms that govern their development are unique. The neural crest contributes to a significant portion of the craniofacial complex, giving rise to chondrocytes, melanocytes, a majority of the peripheral nervous system, and contributing to the mesenchymal component of structures such as the tooth and palate (Chai et al., 2000; Bronner and LeDouarin, 2012). Several Sox factors are expressed throughout the facial ectoderm and mesenchyme (**Table 1**), many of which play essential roles in the development of specific craniofacial structures. Other Sox factors, while expressed during craniofacial development, have yet to be functionally characterized. SoxE functions within neural crest-derived cell types of the face are of particular evolutionary significance. The basal chordate amphioxus possesses a single SoxE gene and lacks neural crest cells, yet has an oral skeleton (Jandzik et al., 2015). Interestingly, expression of amphioxus SoxE within the chick neural tube is sufficient to induce neural crest formation. These amphioxus SoxE expressing cells later expressed markers for DRG lineages, including those cells positioned dorsolaterally that would typically become melanocytes (Tai et al., 2016). These data suggest that co-option of SoxE to proto neural crest-like cells may have occurred prior to genome duplication, but required the aquisition of new *cis*-regulatory sequences (Jandzik et al., 2015; Tai et al., 2016). It further suggests that duplication and divergence of the SoxE family was necessary for neural crest lineage diversification and the subsequent elaboration of the vertebrate head.

Neural Crest Derivatives

Sox Factors and Craniofacial Bone and Cartilage

The craniofacial skeleton serves as the framework for the face. The bones of the craniofacial complex differ from long bones, such as those of the arms, legs, or ribs, in two main ways. First, a majority of anterior craniofacial bones are derived from the neural crest while long bones are derived from the mesoderm (Noden and Trainor, 2005). Second, long bones form through a process called endochondral ossification, whereas the flat bones of the face and the bones of the skull form through intramembranous ossification (Berendsen and Olsen, 2015). The small subset of endochondral facial bones included the malleus, incus, and nasal capsule (Mori-Akiyama et al., 2003). These and the facial cartilages (such as Meckel's) form through a chondrogenic mechanism that requires Sox transcription factors.

SOX9 serves as the central transcriptional regulator for chondrogenesis (Bell et al., 1997; Bi et al., 1999). In vertebrates,

TABLE 1 | *Sox* gene expression in various craniofacial structures in mouse embryos.

Sox Family	Gene	Cartilage	Palate	Teeth	Tongue
B1	Sox1	n.e.	n.e.	n.e.	Muscle
	Sox2	n.e.	Epithelium	Epithelium	Epi + Mus
	Sox3	n.e.	n.e.	n.e.	n.e.
B2	Sox14	n.e.	n.e.	Epithelium	n.e.
	Sox21	n.e.	n.e.	Epithelium	Epi + Mes + Mus
C	Sox4	Yes (broadly Mes)	Mesenchyme	Epi + Mes	Epi + Mes + Mus
	Sox11	n.e.	Epi + Mes	Epi + Mes	Epi + Mes + Mus
	Sox12	n.e.	Epi + Mes	Epi + Mes	Epi + Mes + Mus
D	Sox5	Yes	Mesenchyme	Mesenchyme	Epi + Mes
	Sox6	Yes	Epi + Mes	Epi + Mes	Epi + Mes + Mus
	Sox13	n.e.	Epi + Mes	Epi + Mes	Mes
E	Sox8	n.e.	Mesenchyme	Epi + Mes	Mes + Mus
	Sox9	Yes	Mesenchyme	Epi + Mes	Epi + Mes + Mus
	Sox10	n.e.	n.e.	n.e.	Mes + Mus
F	Sox7	n.e.	n.e.	n.e.	n.e.
	Sox17	n.e.	n.e.	Epithelium	n.e.
	Sox18	n.e.	n.e.	n.e.	n.e.
G	Sox15	n/a	n/a	n/a	n/a

More detailed expression patterns for factors can be found in: (Kawasaki et al., 2015; Watanabe et al., 2016; Ishikawa et al., 2018). Epithelial (Epi), Mesenchymal (Mes), Muscle (Mus), Not expressed (n.e).

Sox9 is expressed in the neural crest-derived facial mesenchyme (Wright et al., 1995; Healy et al., 1996; Spokony et al., 2002). Heterozygous *Sox9* knock-out mice display cleft secondary palate, domed skull, and a short snout (Akiyama et al., 2002). Conditional deletion of *Sox9* in the neural crest (*Sox9*$^{fl/fl}$*;Wnt1-Cre*) results in complete loss of facial cartilages and endochondral derived bones (Mori-Akiyama et al., 2003). Likewise, in *Xenopus*, Sox9 morphants display gross morphological defects in their craniofacial chondrogenic elements, including complete loss of Meckel's cartilage (Spokony et al., 2002). In the absence of *Sox9*, the prechondrogenic mesenchymal condensation fails to form and *Col2a1*, a direct target of SOX9, fails to be expressed (Lefebvre et al., 1997; Mori-Akiyama et al., 2003). The cells that should have become chondrocytes begin to express osteoblast markers (such as *Runx2*), indicating that SOX9 not only functions to promote chondrogenesis, but also inhibits osteoblast formation (Mori-Akiyama et al., 2003). Additionally, SOX9 is required for the expression of *Sox5* and *Sox6* during chondrogenesis (Akiyama et al., 2002). *Sox5*$^{-/-}$ and *Sox6*$^{-/-}$ mutants experience early postnatal lethality, but do not have major defects in chondrogenic elements. Interestingly, while *Sox5*$^{-/-}$ mice display minor defects in the craniofacial cartilage; *Sox6*$^{-/-}$ mutants do not. In contrast, *Sox5*$^{-/-}$;*Sox6*$^{-/-}$ double mutants die at e16.5 and fail to form cartilages. While these mutants still express *Sox9* and *Col2a1* in prechondrogenic regions, cells fail to differentiate into chondrocytes (Smits et al., 2001). These data indicate that SoxD factors have both unique roles and redundant roles during chondrogenesis. Analysis of DNA occupancy by SOX9 and SOX5/6 in chondrogenic cells indicates shared binding at enhancers and suggests that SOX5/6 act cooperatively with SOX9 to promote gene activation (Liu and Lefebvre, 2015). Indeed, the triple combination of SOX9-SOX5-SOX6 can promote chondrogenesis in mesenchymal stem cell without the addition of growth factors, such as TGFβ3 (Raftery et al., 2020).

Sox Factors and Melanocytes

The pigment of the skin, hair, and choroid layer of the eye is produced by melanocytes. These cells are derived from the neural crest and localize to the vascular uvea of the eye, the basal layer of the epidermis, or hair follicles (Hirobe, 1984; Holbrook et al., 1989; Sitiwin et al., 2019). Sox10 plays a central role in the gene regulatory network (GRN) controlling melanocyte development (**Figure 3**), although Sox5, Sox9, and Sox18 may also play minor roles in melanogenesis (reviewed in Harris et al., 2010). *Sox10,* first expressed in the neural crest cells prior to migration, persists in the neural crest cells that become melanocytes (Aoki et al., 2003). Studies with mouse *Dom* mutants, which possess a frameshift mutation in *Sox10* (Herbarth et al., 1998), demonstrate that *Sox10* is required for melanocyte development. Dom mutants lack expression of *Dct/Trp2*, an early melanocyte marker (Southard-Smith et al., 1998). Supporting these findings, *Sox10*$^{LacZ/+}$ heterozygous mice have fewer melanocytes and *colorless* zebrafish mutants (premature stop codon in *sox10*) have reduced melanocytes, iridoblasts, and xanthoblasts (Kelsh and Eisen, 2000; Britsch et al., 2001; Dutton et al., 2001). Overexpression of *sox10* in *Xenopus* embryos results in a massive expansion of melanocyte precursor cells and is sufficient to induce the expression of melanocyte marker *dct/trp2* in naïve ectoderm (Aoki et al., 2003). Likewise, expression of *sox9* produces supernumerary melanocytes in *Xenopus* embryos (Taylor and LaBonne, 2005).

In the GRN controlling melanocyte development Sox10 has been shown to directly activate *Mitf*, *Dct/Trp2*, *Tyr*, and *Tyrp1* (Bondurand et al., 2000; Potterf et al., 2000; Jiao et al., 2004; Murisier et al., 2006, 2007). SOX10 acts synergistically with PAX3

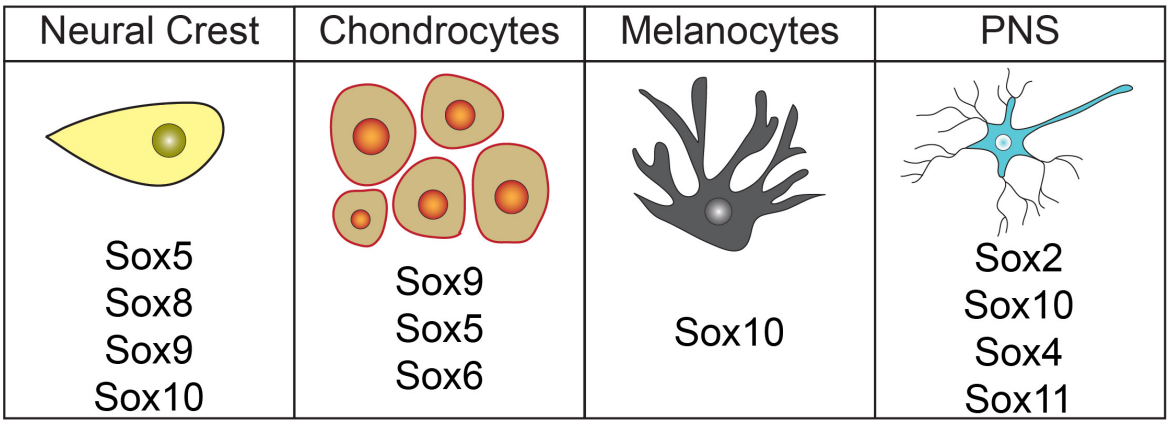

FIGURE 3 | Sox factors involved in neural crest formation and lineage diversification. Diagram highlighting Sox factors known to have roles in neural crest cell, chondrocyte, melanocyte, and peripheral nervous system development.

to activate *MITF* expression (Bondurand et al., 2000; Potterf et al., 2000). Subsequently, MITF becomes a transcriptional partner for SOX10 and together they promote *DCT/TRP2* expression (Jiao et al., 2004; Ludwig et al., 2004). In the absence of *Sox10*, MITF alone is unable to direct formation of pigmented cells (Hou et al., 2006). Additionally, BRG1, a key member of the chromatin remodeling SWI/SNF complex, regulates proximal and distal promotor accessibility of melanocyte-specific SOX10 target genes. SOX10 directly interacts with BRG1, possibly recruiting BRG1 to these sites (Marathe et al., 2017). Global analysis of SOX10 binding sites in an immortalized melanocyte cell line further indicates that SOX10 binds to target sites as either a monomer or homodimer and most of these sites were found at distal regulatory regions. Interestingly, target genes are both up and downregulated in $Sox10^{LacZ/+}$ cells providing further evidence that SOX10 can have both activator and repressor functions (Fufa et al., 2015). Validating and integrating these targets into the existing melanocyte GRN will greatly advance our understanding of melanocyte formation and disease etiology for Waardenburg Syndrome.

SOX10 activity during melanocyte formation is regulated in several ways. First, SOX5 can bind to Sox10 target regions within promotors of melanocyte genes and recruit the transcriptional corepressors HDAC1 and CtBP2 (Stolt et al., 2008). Although it has not been demonstrate that competition for binding sites occurs *in vivo*, $Sox5^{-/-}$, $Sox10^{+/lacZ}$ double mutant embryos display a less severe melanocyte phenotype than $Sox10^{+/lacZ}$ single mutant embryos, consistent with a role for SOX5 as a recruiter of corepressors (Stolt et al., 2008). Post-translational modification of SOX10 may also regulate its function during melanocyte formation. SOX10 can be SUMOylated at three lysine residues and this modification represses transcriptional activation of the *MITF* promotor *in vitro* (Taylor and LaBonne, 2005; Girard and Goossens, 2006).

In addition to regulating melanocyte formation during embryonic development, Sox factors are also integrally involved in postnatal melanocyte maintenance and progression of melanoma. A population of melanocyte stem cells resides at the base of hair follicle cells and contributes to the pigmentation of each hair shaft. *Sox10* is expressed in these stem cells and gain and loss of *Sox10* function both lead to a reduction in this cell population and the presence of white/gray hairs, consistent with disruptions in melanocyte stem cell function (Harris et al., 2013). Additionally, *Sox10* is expressed in the differentiated melanocytes of hair follicles and is required for retention of melanocytes (Harris et al., 2013). *SOX9* is expressed in postnatal melanocytes and can induce expression of SOX10 melanocyte target genes in B16 melanoma cells. Additionally, increased expression of *SOX9* leads to enhanced melanin production (Passeron et al., 2007). Together these findings suggest a SOX9 function in adult melanocytes that parallels that of SOX10 during embryonic development. Finally, both *SOX9* and *SOX10* have roles in the etiology of melanoma. While a detailed description of their functions in this context is beyond the scope of this review, we highlight that these SoxE factors may have antagonistic roles in melanoma cells (Shakhova et al., 2015). Sox functions in various cancers has recently been reviewed (Grimm et al., 2019).

Sox Factors and the Peripheral Nervous System

Neural crest cells also give rise to much of the peripheral nervous system (PNS), including the cephalic ganglia, dorsal root ganglia (DRG), Rohon-Beard cell, satellite cells, and Schwann cells (D'Amico-Martel and Noden, 1983; LeDouarin and Kalcheim, 1999). *Sox2, Sox4*, *Sox5*, *Sox10*, and *Sox11* are each expressed in various neural crest-derived PNS cells (Britsch et al., 2001; Perez-Alcala et al., 2004; Aquino et al., 2006). While functions for *Sox2*, *Sox4*, and *Sox10* have been described, only expression data for *Sox5* and *Sox11* has been reported (**Figure 3**). Schwann cell precursors, satellite glia, myelinating/non-myelinating cells, peripheral glia, and NC-derived cells within trigeminal ganglion express *Sox5* (Perez-Alcala et al., 2004; Morales et al., 2007). *Sox11* is expressed in several PNS cell types including DRG, cranial ganglia, and sympathetic ganglia (Hargrave et al., 1997; Kuhlbrodt et al., 1998a; Sock et al., 2004). Expression in these regions was noted to decrease over time and was very weak by e15.5 of mouse embryogenesis, suggesting that Sox11 may

function in fate determination or early stages of differentiation (Hargrave et al., 1997; Kuhlbrodt et al., 1998a; Sock et al., 2004). Another SoxC subfamily member, Sox4, may possibly have an opposing role in PNS development and act as a negative regulator of Schwann cell myelination. Sox4 overexpression in Schwann cells leads to delayed myelination and hypomyelination. Interestingly, *Sox4* expression is elevated in mouse models of demyelinating neuropathies (Bartesaghi et al., 2015). These Sox11 and Sox4 findings provide evidence that members of the same Sox subfamily can play divergent roles.

Sox2, which is critical for maintaining stem-cell attributes in central nervous system progenitors, also functions in a subset of PNS cells (Wakamatsu et al., 2004; Le et al., 2005; Pevny and Placzek, 2005; Aquino et al., 2006; Adameyko et al., 2012). *Sox2* is expressed in neuroglial progenitors cells, but is downregulated upon differentiation (Aquino et al., 2006). *In ovo* electroporation of *SOX2* in chick embryos results in increased proliferation of DRG cells, but blocks neuroglial progenitor differentiation to both neural and glial fates (Wakamatsu et al., 2004) while knockdown/knockout of Sox2 in the DRG neural progenitors reduces the number of DRG neurons (Cimadamore et al., 2011). Together, these data indicate that SOX2 is an essential regulator of sensory neurogenesis. In addition, SOX2, is expressed in immature Schwann cells where it suppresses expression of genes associated with Schwann cell myelination and blocks myelination, an indicator of Schwann cell differentiation and maturation (Le et al., 2005; Roberts et al., 2017; Wust et al., 2020). It is thus clear that Sox2 plays critical roles in both the developing PNS and CNS.

Importantly, the SoxE factor, *Sox10,* is also a critical regulator of glial cell development. *Sox10* is expressed in Schwann cell precursors and sensory ganglia, and is required for the specification of all glia within the PNS (Kuhlbrodt et al., 1998b; Southard-Smith et al., 1998; Britsch et al., 2001). In the absence of *Sox10* (*Sox10^{lacZ}*/*Sox10^{lacZ}* or *colorless*) cranial ganglia, enteric ganglia, and DRG numbers are reduced or display aberrant cell morphology (Kelsh and Eisen, 2000; Britsch et al., 2001; Dutton et al., 2001) and Schwann cell precursors are absent in both mutants (Kelsh and Eisen, 2000; Britsch et al., 2001; Dutton et al., 2001). These phenotypes are reminiscent of loss of neuregulin/ErbB signaling, which promotes the differentiation of neural crest into glia (Britsch et al., 2001; Britsch, 2007). *ErbB3* expression is decreased in *Sox10^{lacZ}*/*Sox10^{lacZ}* mutants and, subsequently, migration and survival of progenitor cells is compromised (Britsch et al., 2001). In addition to regulating expression of *ErbB3*, *in vitro* studies have demonstrated that SOX10 synergies with OCT6 (POU3F1) and BRN2 (POU3F2) to activate *EGR2* (*KROX-20*), which is essential for myelination of Schwann cells (Kuhlbrodt et al., 1998b; Le et al., 2005). SOX10 then partners with EGR2 to activate others myelin genes (LeBlanc et al., 2007). Indeed, SOX10 and EGR2 are sufficient to reprogram skin fibroblasts into Schwann cells, emphasizing the importance of both of these factors for Schwann cell development (Mazzara et al., 2017). Regulation of Sox10 in Schwann cells has been linked with eEF1A1 which, upon acetylation, removes SOX10 from the nucleus. In Schwann cells, this activity is blocked by HDAC1/2, Sox10 co-factors essential for myelination, which deacetylate eEF1A1 causing it to return to the cytoplasm and preventing nuclear export of Sox10 (Duman et al., 2020). Finally, one of the essential functions of Sox10 is to direct the neuroglial progenitor cells of the DRG toward the glial lineage. Mechanistically this is attributed to Sox10 biasing neuroglia progenitor cells toward the glial lineage (vs. sensory neurons) by promoting the ubiquitination and subsequent degradation of transcription factor Neurog2 through upregulation of Fbxo9 (Liu et al., 2020).

Craniofacial Structures

Palatogenesis

Cleft lip/palate is one of the most common birth defects, and numerous genes have been associated with this congenital malformation (Dixon et al., 2011). Mammalian palatogenesis begins with proliferation of the neural crest-derived cells within the palatal shelves, which leads to vertical outgrowth. The palatal shelves then elevate, sitting horizontal above the tongue, and the epithelium of the two shelves fuse. The epithelial seam formed at the midline is then removed to create a confluent mesenchyme (Bush and Jiang, 2012). A defect in any of these steps can result in a cleft secondary palate. Of the Sox transcription factors, only *SOX11* has been associated with a patient presenting with cleft palate (Khan et al., 2018). Nevertheless, several Sox mutant mice (*Sox11$^{-/-}$*, *Sox9$^{fl/fl}$;Wnt1-Cre*, *Sox2^{HYP}*, *Sox5$^{-/-}$*) develop cleft palates (Smits et al., 2001; Mori-Akiyama et al., 2003; Sock et al., 2004; Langer et al., 2014). During e12.5-e14.5 of murine palatogenesis, expression of *Sox2*, *Sox4*, *Sox5*, *Sox6*, *Sox8*, *Sox9*, *Sox11*, *Sox12*, *Sox13*, and *Sox21* can be detected via *in situ* hybridization (**Table 1**; Watanabe et al., 2016). *Sox2* is expressed in the epithelium; *Sox4/5/8/9* are expressed in the mesenchyme, while *Sox6/11/12/13* are expressed in both the palatal mesenchyme and epithelium (Watanabe et al., 2016). Of note, both *Sox2* and *Sox11* are expressed in the palatal epithelial seam at e14.5. While it is unclear if/how Sox factors regulate palatogenesis, the spatio/temporal expression patterns make it tempting to speculate that several factors play roles in this process.

Odontogenesis

Tooth development begins as the oral epithelium thickens and the underlying neural crest-derived mesenchyme condenses around the invaginating placode. The placode continues to elongate (bud stage) and then branch (bell stage). Subsequently, cells begin to differentiate into ameleoblasts and odontoblasts (bell stage) and terminally differentiate/mineralize just prior to root formation and eruption (Thesleff, 2014). Several Sox factors are expressed throughout odontogenesis (see Kawasaki et al., 2015 for detailed expression analysis); however, functional roles for most factors have not been described (**Table 1**). *Sox2* is expressed in the oral epithelium beginning at tooth initiation and continues to be expressed through cap stages in the lingual bud epithelium (Juuri et al., 2012; Kawasaki et al., 2015). Conditional deletion of *Sox2* from the oral epithelium (*Sox2$^{fl/fl}$;Shh:GFP-Cre*) results in only minor defects in the second and third molars; however, recombination of *Shh:GFP-Cre* was mosaic and some SOX2 protein still detectable (Juuri et al., 2013).

In contrast, conditional deletion of *Sox2* from both the oral and dental epithelium (*Sox2*$^{fl/fl}$*;Pitx2-Cre*) produces abnormally shaped molars and underdeveloped incisors that regressed until undetectable at P0 (Sun et al., 2016). The regression of the incisors is consistent with a role for SOX2 in dental epithelial stem cells (DESCs). Lineage tracing experiments have revealed that Sox2 + DESCs reside in the labial cervical loop and contribute to all epithelial lineages in the mouse incisor (Juuri et al., 2012). Ablation of *Sox2* prior to incisor injury dramatically decreases the ability of the incisor to regrow (Sun et al., 2016). These mutants also display reduced proliferation in labial cervical loops, suggesting that SOX2 regulates DESC proliferation (Sun et al., 2016). In addition to murine DESCs, Sox2 defines an analogous stem cell population in cartilaginous fish, which regenerate teeth successionally, suggesting that SOX2 function in DESCs is evolutionarily conserved (Martin et al., 2016).

Salivary Gland Development

Three pairs of salivary glands, the sublingual (SL), the submandibular (SMG), and the parotid (PG), reside inside the oral cavity and together secrete up to a quart of saliva daily (Knosp et al., 2012). Embryonically, these structures begin as placodes within the oral epithelium and then subsequently undergo elongation and branching morphogenesis (Affolter et al., 2003). *Sox9*, *Sox10*, and *Sox2* are all expressed during salivary gland development (Lombaert et al., 2013; Chatzeli et al., 2017; Emmerson et al., 2017). *Sox9* is expressed in the oral epithelium that gives rise to the SMG, SL, and PG. Sox9^{+} epithelial cells serve as the progenitor cells for the entire epithelial component of these salivary glands (Chatzeli et al., 2017). As SMG/SL/PG development progresses *Sox9* becomes restricted to the distal progenitor cells of the bud. Conditional deletion of *Sox9* within the oral epithelium (*Sox9*$^{fl/fl}$*;K14-Cre*) results in arrested SMG, SL, and PG development at the bud stage (Chatzeli et al., 2017). In the conditional mutants, these cells fail to become specified; however, the proximal progenitors (*Sox9*$^{-}$) are specified normally (Chatzeli et al., 2017). In the absence of distal progenitor cells, branching morphogenesis fails to occur. Embryonic expression of *Sox9* ceases during lumen formation, but *Sox9* becomes expressed again in the adult and contributes to regulation of the stem/progenitor cell properties of a subpopulation of salivary gland cells (Chatzeli et al., 2017; Tanaka et al., 2019). *Sox10* is expressed in the distal progenitor cells of the bud and is also an acinar (mucin producing cells) progenitor marker (Lombaert et al., 2013). *Sox10* lies downstream of Sox9, Sox2, Kit, and FGF signaling in these cells (Lombaert et al., 2013; Chatzeli et al., 2017; Emmerson et al., 2017). While a specific function for Sox10 within the distal/acinar progenitor cells has not been determined, it is known to be essential for branching and acinar formation of other glands (Chen et al., 2014). *Sox2* is expressed in both duct and acinar progenitor cells but is only required for acinar cell formation. Sox2 promotes the expression of acinar-specific genes, including *Sox10*, and promotes survival of acinar progenitor cells through both maintaining proliferation and preventing apoptosis. Interestingly, parasympathetic nerves are required to maintain the Sox2 + progenitor cells, and thus are necessary for acinar cell formation (Emmerson et al., 2017).

SOXOPATHIES WITH ASSOCIATED CRANIOFACIAL PHENOTYPES

Given the importance of Sox factors to the formation of the vertebrate craniofacial complex, it is perhaps unsurprising that a number of human syndromes presenting with craniofacial defects are linked to mutations in *SOX* genes (**Table 2**).

Campomelic Dysplasia

One of the most dramatic of these SOXopathies is Campomelic dysplasia (CD) which is caused by mutations in *SOX9* (Foster et al., 1994; Wagner et al., 1994). Individuals with CD typically die shortly after birth and display an undermineralized skeleton and dramatic bowing of the lower limbs. Within the craniofacial complex, common CD phenotypes include cleft palate, micrognathia, a small skull, and mid-facial hypoplasia (Csukasi et al., 2019). Most CD cases are caused by a *de novo* mutation within a *SOX9* allele (autosomal dominant). While the exact mutations within the *SOX9* gene varies among CD patients, there is evidence for both haploinsufficiency and dominant negative protein function underlying the observed phenotypes (Foster et al., 1994; Csukasi et al., 2019), and in mice, loss of one allele of *Sox9* phenocopies CD (Bi et al., 2001). Cell culture studies have shown that both *SOX9* haploinsufficiency and dominant negative forms of SOX9 (nonsense mutations in the C-terminal transactivation domain) fail to robustly activate *Col2a1* gene expression indicating that the chondrogenic program is not being fully initiated in cases of CD (Csukasi et al., 2019). Notably, although it is dysmorphic, a majority of the skeleton still forms in CD patients and animal models. Perhaps most SOX9 target genes are still activated despite loss of one functional allele. Alternately, SOX5 and SOX6 have partial functional redundant functions to SOX9 during chondrogenesis and may be able to compensate.

Waardenburg Syndrome

Waardenburg syndrome (WS) is a neurocristopathy characterized by pigment abnormalities in the hair, skin, and eyes, hearing loss, and craniofacial alterations such as hypertelorism, dystopia cantorum, nasal hypoplasia, and harelip (Banerjee, 1986; Dourmishev et al., 1999; Pingault et al., 2010; Wildhardt et al., 2013; Chen et al., 2015). There are four different subtypes of WS, two of which are associated with mutations in *SOX10,* type 2 and type 4 (Pingault et al., 1998; Southard-Smith et al., 1999; Bondurand et al., 2007). Individuals with type 2 present with additional neurological defects while those with type 4 also have Hirschsprung's disease (Bondurand et al., 2007). Over 40 different *SOX10* mutations have been reported across WS patients. Many mutations are truncating, causing the *SOX10* transcript to undergo nonsense-mediated RNA decay resulting in a phenotype driven by haploinsufficiency (Inoue et al., 2004). A few variants have also been reported that alter the *SOX10* stop codon and extend the protein (Pingault et al., 2010). For these variants, there is *in vitro* evidence that these elongated proteins

TABLE 2 | SOXopathies with craniofacial phenotypes.

Syndrome	Associated Craniofacial Phenotypes	Gene	Mutations (gene and protein)	Associated structural domain	References
Campomelic dysplasia	cleft palate, micrognathia, small skull, mid-facial hypoplasia	*SOX9*	198_228del; 66_75del	DIM domain	Csukasi et al., 2019
			C228A; A76E	DIM domain	Kwok et al., 1995
			G258A; W86X	DIM domain	Meyer et al., 1997
			C324T; P108L	HMG domain	McDowall et al., 1999
			T334C; P112L	HMG domain	Sock et al., 2003
			C351G; Q117X	HMG domain	
			C356T; A119V	HMG domain	
			T429C; W143R	HMG domain	
			G444T; E148X	HMG domain	
			G456C; R152P	HMG domain	
			C495T; H165Y	HMG domain	
			C510G; P170R	HMG domain	
			C543A; S181X	HMG domain	
			C585T; Q195X		
			246fs		
			261fs		
			831_ 840del; E277SfsTer1		
			286fs		
			C957G; Y319X		
			329fs		
			1071_ 1113del; Q357fsTer11		
			357fs	PQA rich domain	
			1103_1104insA; 368fs	PQA rich domain	
			C1125T; Q375X	PQA rich domain	
			C1173T; Q391X		
			C1180T; R394X		
			G1200T; E400X		
			C1234T; Q412X	Transactivation domain	
			C1320G; Y440X	Transactivation domain	
			1519ins4; 507fs	Transactivation domain	
Coffin-Siris syndrome	cleft palate, frontal bossing, wide mouth with prominent lips, deep set eyes, broad nasal bridge, thick and high arched eyebrows, grooved/shortened philtrum	*SOX11*	C87A; C29X		Khan et al., 2018
			G150C; K50N		Tsurusaki et al., 2014
			T178C; S60P	HMG domain	
			C305T; A102V	HMG domain	
			A347G; Y116C	HMG domain	
			C359A; P120H		
			1148dupG; G384RfsTer14		
		SOX4	C198A; F66L		Zawerton et al., 2019
			G334C; A112P		
			T176G; I59S		
			G315T; K105N		
Lamb-Shaffer syndrome	micrognathia, prominent chin, thinned upper lip, broad/full nasal tip, epicanthus	*SOX5*	R18X		Zawerton et al., 2020
			G518A; W173X		
			C622T; Q208X	Coiled-coil domain	
			C637T; R213X	Coiled-coil domain	
			C703T; R235C	Coiled-coil domain	
			E246fs	Coiled-coil domain	
			747_748del; R250TfsTer36	Coiled-coil domain	
			C820T; Q274X	Coiled-coil domain	
			P302S		
			T928A; C310S		
			G354X		

(Continued)

TABLE 2 | Continued

Syndrome	Associated Craniofacial Phenotypes	Gene	Mutations (gene and protein)	Associated structural domain	References
			R471X	Coiled-coil domain	
			1465dup; L489PfsTer3	Coiled-coil domain	
			C1477T; R493X	Coiled-coil domain	
			T499fs		
			C1613G; R538X		
			A1678G; M560V	HMG domain	
			A1681C; N561H	HMG domain	
			C1711T; R571W	HMG domain	
			G1712T; R571L	HMG domain	
			G1782A; W594X	HMG domain	
			G1786G; A596P	HMG domain	
			A597fs	HMG domain	
			A1814G; Y605C	HMG domain	
			R611G	HMG domain	
			A1868G; Y623C	HMG domain	
			C1895A; T632N		
			C2078T; S693L		
Hypotrichosis-lymphedema-telangiectasia syndrome	thick lips; microcephaly, periorbital swelling; broad nasal tip	*SOX18*	T283A; W95R	HMG domain	Valenzuela et al., 2018
			G310C; A104P	HMG domain	
			C481T; G161X	HMG domain	
			492_505dup; E169GfsTer14	Transactivation domain	
			C541T; Q181X	Transactivation domain	
			G712T; G238X	Transactivation domain	
			C720A; C240X	Transactivation domain	
Waardenburg syndrome		*SOX10*	50_73del; S17CfsTer7		Chan et al., 2003
			112_131del; G38QfsTer21		Harris et al., 2010
			126_127delinsCT; R43X		Iso et al., 2008
			169delG; E57SfsTer52	DIM domain	Morin et al., 2008
			C249A; Y83X	DIM domain	Pingault et al., 1998
			328_329del; A110LfsTer23	HMG domain	Pingault et al., 2002
			S135T	HMG domain	Pingault et al., 2010
			C470T; A157V	HMG domain	Sanchez-Mejias et al., 2010
			477_482dup; L160_R161dup	HMG domain	Sham et al., 2001
			506delC; P169RfsTer117	HMG domain	Shimotake et al., 2007
			C519G; Y173X	HMG domain	Southard-Smith et al., 1999
			G565T; E189X		Toki et al., 2003
			Y207X		
			644_648del; R215PfsTer64		
			C702T; Q234X		
			C750T; Q250X		
			C754A; S251X		
			780delG; R261AfsTer25	Transactivation domain	
			778delG	Transactivation domain	
			795delG	Transactivation domain	
			811delA; I271SfsTer15	Transactivation domain	
			Y313X		
			1047dupT; V350CfsTer52		
			1077_1078del; E359DfsTer42		
			C1116T; Q372X		
			C1129A; S376X		
			C1131T; Q377X		
			1195_1196del; Q399VfsTer2	Transactivation domain	
			1400del12	Transactivation domain	
			T1401A; X467K	Transactivation domain	

have dominant negative effects (Inoue et al., 1999; Sham et al., 2001; Chan et al., 2003). During normal embryonic development, SOX10 is essential for neural crest stem cell formation and then subsequently for formation of specific derivatives, including melanocytes and enteric ganglia neurons (Southard-Smith et al., 1998; Britsch et al., 2001; Dutton et al., 2001). SOX10 also promotes survival and proliferation of Schwann cells (Britsch et al., 2001). In addition to *SOX10*, mutations in *PAX3*, *MITF*, *SNAI2*, *EDN3*, and *EDNRB* have all been identified as causative genetic insults for Waardenburg syndrome (Pingault et al., 2010). Together with SOX10, these genes are components of the gene regulatory networks controlling melanocyte (*PAX3*, *MITF*, *SNAI2*) or PNS (*EDN3, EDNRB*) development (Bondurand et al., 2007). Thus, WS patients with mutations in different genes can present with the same disease etiology due to disruptions in a shared gene regulatory network.

Lamb-Shaffer Syndrome

Lamb-Shaffer syndrome (LAMSHF) is classified as a neurodevelopmental disorder with common phenotypes including: developmental delays, intellectual disability, and language/motor deficits (Lamb et al., 2012). Patients also have a signature set of craniofacial features: micrognathia, prominent chin, thinned upper lip, broad/full nasal tip, and epicanthus (Zawerton et al., 2020). Mutations in *SOX5*, a member of the SoxD family, have been linked with LAMSHF. The observed skeletal defects such as micrognathia, broad/full nasal tip, and prominent chin are consistent with SOX5 having a role in chondrogenesis. *Sox5* is strongly expressed in Meckel's cartilage in mice (Ishikawa et al., 2018), which could explain the presentation of micrognathia, specifically. The general lack of severity of these craniofacial phenotypes is most likely due to individuals possessing other functional SOXD alleles, which is supported by $Sox5^{-/-}$ having only minor skeletal defects (Smits et al., 2001). *In vitro* studies suggest that haploinsufficiency, rather than a dominant negative effect associated with SOX5 variants, are most likely causative of LAMSHF. Furthermore, SOX5 variants with nonsense mutations or missense mutations within the HMG were localized cytoplasmically, unable to bind DNA, and failed to activate gene expression. While molecular studies demonstrated that some SOX5 variants could still activate target gene expression and other variants could not, the study could not identify any genotype-phenotype correlation among LAMSHF patients (Zawerton et al., 2020).

Coffin-Siris Syndrome

Another syndrome that has been associated with mutations in *SOX* genes, specifically Sox C family members is Coffin-Siris syndrome (CSS). Individuals with CSS have fifth fingers with clinodactyly, nail hypoplasia, microcephaly, and intellectual disabilities. Craniofacial features include cleft palate, frontal bossing, wide mouth with prominent lips, deep set eyes, broad nasal bridge, thick and high arched eyebrows, and a grooved/shortened philtrum (Tsurusaki et al., 2014; Hempel et al., 2016; Khan et al., 2018; Okamoto et al., 2018). Most patients with CSS (55–70%) have mutations in genes that encode for subunits of the BAF complex (Tsurusaki et al., 2014). Of the remaining cases, mutations in *SOX11* have been identified as causal for several unrelated patients (Tsurusaki et al., 2014; Hempel et al., 2016; Khan et al., 2018; Okamoto et al., 2018). Most of the identified mutations in *SOX11* lie within the HMG domain and result in decreased transcription of SOX11 target genes *in vitro* (Tsurusaki et al., 2014; Hempel et al., 2016). One variant has a mutation outside of this domain that is predicted to produce a truncated, non-functional protein (Khan et al., 2018). Additionally, there have been four cases of CSS where heterozygous mutations in *SOX4* have been identified. Like SOX11, these mutations were within the HMG domain and variant proteins were unable to bind DNA and activate target gene expression (Zawerton et al., 2019). Little is known about the roles of SoxC factors in the context of craniofacial development. *Sox4* and *Sox11* are broadly expressed in the neural crest-derived facial mesenchyme, and *Sox11* is, interestingly, expressed in the palatal epithelial seam (Watanabe et al., 2016). Whether Sox11 is functionally important for the removal of the epithelial seam is unknown, but this could explain occurrences of cleft palate in some CSS patients. In other cellular contexts, *Sox4* and *Sox11* promote proliferation (Gadi et al., 2013; Dai et al., 2017), thus it is possible that they may be regulating proliferation to some extent within the facial mesenchyme. Misregulation of proliferation could lead to phenotypes such as broad nasal bridge, shortened philtrum, and prominent lips. In the future, it would be interesting to use animal models to study the effects of single or combined loss of *Sox4* and *Sox11* on craniofacial development.

Hypotrichosis-Lymphedema-Telangiectasia Syndrome

Lastly, mutations in *Sox18* have been identified in patients with a rare condition called Hypotrichosis-lymphedema-telangiectasia syndrome (HLTS) (Irrthum et al., 2003). As the name suggests, the predominating features of these patients are sparse hair, tissue swelling due to malfunctioning lymphatic system, and presence of dilated vessels skin surface. While most case studies do not report a craniofacial phenotype with HLTS (either no phenotype or not assessed), a few patients have mild craniofacial defects that include: thick lips, microcephaly, periorbital swelling, and broad nasal tip (Bastaki et al., 2016; Valenzuela et al., 2018; Wangberg et al., 2018). Unlike the other syndromes associated with mutations in *SOX* genes, HLTS is associated with both autosomal dominant and autosomal recessive modes of inheritance (Irrthum et al., 2003; Wangberg et al., 2018). The autosomal dominant mode of inheritance is typically associated with nonsense mutations in the SOX18 transactivation domain while the autosomal recessive form is marked by missense mutations within the HMG domain (Valenzuela et al., 2018). Expression data in mice indicates that *Sox18* primarily localizes to sites of vascularization within the developing murine craniofacial complex (Ishikawa et al., 2018). Given this expression, it is unclear how loss of *Sox18* could result in phenotypes such as microcephaly or broad nasal tip. Clearly, further study into the

molecular mechanisms underlying this syndrome, specifically those associated with the craniofacial defects, is necessary.

CONCLUSION AND PERSPECTIVES

The emergence of neural crest drove the evolution of vertebrates including the elaboration of an intricate craniofacial complex. While Sox transcription factors are heavily utilized during invertebrate development, new roles have evolved for many of these factors within vertebrate cell types and structures, aided by duplication events. SoxE factors are initially required for the formation of neural crest stem cells, analogous to the role that SoxB1 factors play in blastula (inner cell mass) stem cells. Subsequently, SoxE factors are essential for the diversification of neural crest cells into a subset of non-neural lineages including cartilage, melanocytes and glia. By contrast SoxB1 factors transition to maintaining a neural progenitor state, and some SoxB1 partner pairings, including POU factors, are maintained between blastula stem cells and neural progenitor cells. Conserved SoxB1 roles within these cell populations could have necessitated the deployment of a different Sox subfamily, SoxE, in neural crest progenitors and derivatives. Evolutionarily, SoxE factor duplications at the base of the vertebrates may have helped drive neural crest lineage diversification and the development of the vertebrate craniofacial complex. Understanding the role of Sox proteins in the emergence of specialized cell types and complex forms in vertebrates will require a fuller understanding of the shared and unique functions of different Sox factors and families, and the mechanisms regulating those functions. This includes defining their transcriptional targets in different cellular contexts. Such studies should also prove to be of high clinical significance given the many congenital defects associated with Sox mutations. In particular, the plethora of craniofacial phenotypes associated with SOXopathies underscores the critical roles these factors play in the development and evolution of the vertebrate craniofacial complex.

It has been 30 years since the discovery of the SRY gene yet we are continuously learning more about the roles and regulation of this important family of transcription factors. Within the context of the neural crest and craniofacial complex, there are several outstanding questions that are ripe for study. Sox9 has been shown to have pioneer activity in hair follicle stem cells (Adam et al., 2015); however, it is unknown whether this function extends to the neural crest. One intriguing possibility is that Sox9 and other SoxE factors, through pioneer activity, set the stage in the chromatin landscape of neural crest progenitors for the subsequent adoption of specific lineage states. Recent data has shown that the chromatin of vagal neural crest is biased toward specific lineages prior to the onset of migration (Ling and Sauka-Spengler, 2019). It will be important to determine if such biases also exist in cranial neural crest and if different SoxE factors play roles in establishing these predispositions. In addition, there is evidence for direct interaction of Sox factors with epigenetic factors, such as HDACs, to regulate cell fate decisions (Duman et al., 2020). To date, studies of Sox partners/co-factors have predominately focused on other transcription factors. It is essential, however, to broaden our understanding of Sox interacting factors to include epigenetic modifiers, and to determine how these interactions shape the chromatin landscape within the neural crest and its derivatives. Finally, global histone acetylation in the neural crest differs from that of differentiated cells and actually more closely resembles that of blastula stem cells (Rao and LaBonne, 2018). To what degree are these similar epigenetic signatures mediated by Sox factors? Does switching regulation from SoxB1 in blastula stem cells to SoxE factors in neural crest stem cells lead to maintained chromatin architecture at Sox targets within the pluripotency GRN? As more large-scale sequencing experiments are conducted, and with the growing power of single cell approaches, such questions are likely to be answered in the near future.

AUTHOR CONTRIBUTIONS

ES wrote the manuscript. CL edited the manuscript. Both authors contributed to the article and approved the submitted version.

FUNDING

The authors acknowledge funding support from the NIH (1F32DE029113-ES and R01GM116538-CL), the National Science Foundation (1764421), and Simons Foundation (SFARI 597491-RWC).

REFERENCES

Abdelalim, E. M., Emara, M. M., and Kolatkar, P. R. (2014). The SOX transcription factors as key players in pluripotent stem cells. *Stem Cells Dev.* 23, 2687–2699. doi: 10.1089/scd.2014.0297

Adam, R. C., Yang, H., Rockowitz, S., Larsen, S. B., Nikolova, M., Oristian, D. S., et al. (2015). Pioneer factors govern super-enhancer dynamics in stem cell plasticity and lineage choice. *Nature* 521, 366–370. doi: 10.1038/nature14289

Adameyko, I., Lallemend, F., Furlan, A., Zinin, N., Aranda, S., Kitambi, S. S., et al. (2012). Sox2 and Mitf cross-regulatory interactions consolidate progenitor and melanocyte lineages in the cranial neural crest. *Development* 139, 397–410. doi: 10.1242/dev.065581

Affolter, M., Bellusci, S., Itoh, N., Shilo, B., Thiery, J. P., and Werb, Z. (2003). Tube or not tube: remodeling epithelial tissues by branching morphogenesis. *Dev. Cell* 4, 11–18.

Akiyama, H., Chaboissier, M. C., Martin, J. F., Schedl, A., and de Crombrugghe, B. (2002). The transcription factor Sox9 has essential roles in successive steps of the chondrocyte differentiation pathway and is required for expression of Sox5 and Sox6. *Genes Dev.* 16, 2813–2828. doi: 10.1101/gad.1017802

Aksoy, I., Jauch, R., Eras, V., Chng, W. B., Chen, J., Divakar, U., et al. (2013). Sox transcription factors require selective interactions with Oct4 and specific transactivation functions to mediate reprogramming. *Stem Cells* 31, 2632–2646. doi: 10.1002/stem.1522

Ambrosetti, D. C., Basilico, C., and Dailey, L. (1997). Synergistic activation of the fibroblast growth factor 4 enhancer by Sox2 and Oct-3 depends on protein-protein interactions facilitated by a specific spatial arrangement of factor binding sites. *Mol. Cell. Biol.* 17, 6321–6329. doi: 10.1128/mcb.17.11.6321

Angelozzi, M., and Lefebvre, V. (2019). SOXopathies: growing family of developmental disorders due to SOX mutations. *Trends Genet. TIG* 35, 658–671. doi: 10.1016/j.tig.2019.06.003

Aoki, Y., Saint-Germain, N., Gyda, M., Magner-Fink, E., Lee, Y. H., Credidio, C., et al. (2003). Sox10 regulates the development of neural crest-derived melanocytes in *Xenopus*. *Dev. Biol.* 259, 19–33. doi: 10.1016/s0012-1606(03)00161-1

Aquino, J. B., Hjerling-Leffler, J., Koltzenburg, M., Edlund, T., Villar, M. J., and Ernfors, P. (2006). In vitro and in vivo differentiation of boundary cap neural crest stem cells into mature Schwann cells. *Exp. Neurol.* 198, 438–449. doi: 10.1016/j.expneurol.2005.12.015

Banerjee, A. K. (1986). Waardenburg's syndrome associated with ostium secundum atrial septal defect. *J. R. Soc. Med.* 79, 677–678.

Bartesaghi, L., Arnaud Gouttenoire, E., Prunotto, A., Medard, J. J., Bergmann, S., and Chrast, R. (2015). Sox4 participates in the modulation of Schwann cell myelination. *Eur. J. Neurosci.* 42, 1788–1796. doi: 10.1111/ejn.12929

Bastaki, F., Mohamed, M., Nair, P., Saif, F., Tawfiq, N., Al-Ali, M. T., et al. (2016). A novel SOX18 mutation uncovered in Jordanian patient with hypotrichosis-lymphedema-telangiectasia syndrome by whole exome sequencing. *Mol. Cell. Probes* 30, 18–21. doi: 10.1016/j.mcp.2015.11.005

Bell, D. M., Leung, K. K., Wheatley, S. C., Ng, L. J., Zhou, S., Ling, K. W., et al. (1997). SOX9 directly regulates the type-II collagen gene. *Nat. Genet.* 16, 174–178. doi: 10.1038/ng0697-174

Berendsen, A. D., and Olsen, B. R. (2015). Bone development. *Bone* 80, 14–18. doi: 10.1016/j.bone.2015.04.035

Betancur, P., Bronner-Fraser, M., and Sauka-Spengler, T. (2010). Genomic code for Sox10 activation reveals a key regulatory enhancer for cranial neural crest. *Proc. Natl. Acad. Sci. U.S.A.* 107, 3570–3575. doi: 10.1073/pnas.0906596107

Bi, W., Deng, J. M., Zhang, Z., Behringer, R. R., and de Crombrugghe, B. (1999). Sox9 is required for cartilage formation. *Nat. Genet.* 22, 85–89. doi: 10.1038/8792

Bi, W., Huang, W., Whitworth, D. J., Deng, J. M., Zhang, Z., Behringer, R. R., et al. (2001). Haploinsufficiency of Sox9 results in defective cartilage primordia and premature skeletal mineralization. *Proc. Natl. Acad. Sci. U.S.A.* 98, 6698–6703. doi: 10.1073/pnas.111092198

Bondurand, N., Dastot-Le Moal, F., Stanchina, L., Collot, N., Baral, V., Marlin, S., et al. (2007). Deletions at the SOX10 gene locus cause Waardenburg syndrome types 2 and 4. *Am. J. Hum. Genet.* 81, 1169–1185. doi: 10.1086/522090

Bondurand, N., Pingault, V., Goerich, D. E., Lemort, N., Sock, E., Le Caignec, C., et al. (2000). Interaction among SOX10, PAX3 and MITF, three genes altered in Waardenburg syndrome. *Hum. Mol. Genet.* 9, 1907–1917. doi: 10.1093/hmg/9.13.1907

Bowles, J., Schepers, G., and Koopman, P. (2000). Phylogeny of the SOX family of developmental transcription factors based on sequence and structural indicators. *Dev. Biol.* 227, 239–255. doi: 10.1006/dbio.2000.9883

Britsch, S. (2007). The neuregulin-I/ErbB signaling system in development and disease. *Adv. Anat. Embryol. Cell Biol.* 190, 1–65. doi: 10.1007/978-3-540-37107-6_1

Britsch, S., Goerich, D. E., Riethmacher, D., Peirano, R. I., Rossner, M., Nave, K. A., et al. (2001). The transcription factor Sox10 is a key regulator of peripheral glial development. *Genes Dev.* 15, 66–78. doi: 10.1101/gad.186601

Bronner, M. E., and LeDouarin, N. M. (2012). Development and evolution of the neural crest: an overview. *Dev. Biol.* 366, 2–9. doi: 10.1016/j.ydbio.2011.12.042

Buitrago-Delgado, E., Nordin, K., Rao, A., Geary, L., and LaBonne, C. (2015). NEURODEVELOPMENT. Shared regulatory programs suggest retention of blastula-stage potential in neural crest cells. *Science* 348, 1332–1335. doi: 10.1126/science.aaa3655

Buitrago-Delgado, E., Schock, E. N., Nordin, K., and LaBonne, C. (2018). A transition from SoxB1 to SoxE transcription factors is essential for progression from pluripotent blastula cells to neural crest cells. *Dev. Biol.* 444, 50–61. doi: 10.1016/j.ydbio.2018.08.008

Bush, J. O., and Jiang, R. (2012). Palatogenesis: morphogenetic and molecular mechanisms of secondary palate development. *Development* 139, 231–243. doi: 10.1242/dev.067082

Chai, Y., Jiang, X., Ito, Y., Bringas, P. Jr., Han, J., Rowitch, D. H., et al. (2000). Fate of the mammalian cranial neural crest during tooth and mandibular morphogenesis. *Development* 127, 1671–1679.

Chan, K. K., Wong, C. K., Lui, V. C., Tam, P. K., and Sham, M. H. (2003). Analysis of SOX10 mutations identified in Waardenburg-Hirschsprung patients: differential effects on target gene regulation. *J. Cell. Biochem.* 90, 573–585. doi: 10.1002/jcb.10656

Chatzeli, L., Gaete, M., and Tucker, A. S. (2017). Fgf10 and Sox9 are essential for the establishment of distal progenitor cells during mouse salivary gland development. *Development* 144, 2294–2305. doi: 10.1242/dev.146019

Chen, K., Zong, L., Zhan, Y., Wu, X., Liu, M., and Jiang, H. (2015). Genetic counseling for a three-generation Chinese family with Waardenburg syndrome type II associated with a rare SOX10 mutation. *Int. J. Pediatr. Otorhinolaryngol.* 79, 745–748. doi: 10.1016/j.ijporl.2015.03.006

Chen, Z., Huang, J., Liu, Y., Dattilo, L. K., Huh, S. H., Ornitz, D., et al. (2014). FGF signaling activates a Sox9-Sox10 pathway for the formation and branching morphogenesis of mouse ocular glands. *Development* 141, 2691–2701. doi: 10.1242/dev.108944

Cheung, M., and Briscoe, J. (2003). Neural crest development is regulated by the transcription factor Sox9. *Development* 130, 5681–5693. doi: 10.1242/dev.00808

Cheung, M., Chaboissier, M. C., Mynett, A., Hirst, E., Schedl, A., and Briscoe, J. (2005). The transcriptional control of trunk neural crest induction, survival, and delamination. *Dev. Cell* 8, 179–192. doi: 10.1016/j.devcel.2004.12.010

Chew, L. J., and Gallo, V. (2009). The Yin and Yang of Sox proteins: activation and repression in development and disease. *J. Neurosci. Res.* 87, 3277–3287. doi: 10.1002/jnr.22128

Cimadamore, F., Fishwick, K., Giusto, E., Gnedeva, K., Cattarossi, G., Miller, A., et al. (2011). Human ESC-derived neural crest model reveals a key role for SOX2 in sensory neurogenesis. *Cell Stem Cell* 8, 538–551. doi: 10.1016/j.stem.2011.03.011

Cizelsky, W., Hempel, A., Metzig, M., Tao, S., Hollemann, T., Kuhl, M., et al. (2013). sox4 and sox11 function during Xenopus laevis eye development. *PLoS One* 8:e69372. doi: 10.1371/journal.pone.0069372

Csukasi, F., Duran, I., Zhang, W., Martin, J. H., Barad, M., Bamshad, M., et al. (2019). Dominant-negative SOX9 mutations in campomelic dysplasia. *Hum. Mutat.* 40, 2344–2352. doi: 10.1002/humu.23888

Dai, W., Xu, X., Li, S., Ma, J., Shi, Q., Guo, S., et al. (2017). SOX4 promotes proliferative signals by regulating glycolysis through AKT activation in melanoma cells. *J. Invest. Dermatol.* 137, 2407–2416. doi: 10.1016/j.jid.2017.06.026

D'Amico-Martel, A., and Noden, D. M. (1983). Contributions of placodal and neural crest cells to avian cranial peripheral ganglia. *Am. J. Anat.* 166, 445–468. doi: 10.1002/aja.1001660406

Dixon, M. J., Marazita, M. L., Beaty, T. H., and Murray, J. C. (2011). Cleft lip and palate: understanding genetic and environmental influences. *Nat. Rev. Genet.* 12, 167–178. doi: 10.1038/nrg2933

Dourmishev, A. L., Dourmishev, L. A., Schwartz, R. A., and Janniger, C. K. (1999). Waardenburg syndrome. *Int. J. Dermatol.* 38, 656–663.

Duman, M., Vaquie, A., Nocera, G., Heller, M., Stumpe, M., Siva Sankar, D., et al. (2020). EEF1A1 deacetylation enables transcriptional activation of remyelination. *Nat. Commun.* 11:3420.

Dutton, K. A., Pauliny, A., Lopes, S. S., Elworthy, S., Carney, T. J., Rauch, J., et al. (2001). Zebrafish colourless encodes sox10 and specifies non-ectomesenchymal neural crest fates. *Development* 128, 4113–4125.

Ellis, P., Fagan, B. M., Magness, S. T., Hutton, S., Taranova, O., Hayashi, S., et al. (2004). SOX2, a persistent marker for multipotential neural stem cells derived from embryonic stem cells, the embryo or the adult. *Dev. Neurosci.* 26, 148–165. doi: 10.1159/000082134

Emmerson, E., May, A. J., Nathan, S., Cruz-Pacheco, N., Lizama, C. O., Maliskova, L., et al. (2017). SOX2 regulates acinar cell development in the salivary gland. *eLife* 6:e26620.

Foster, J. W., Dominguez-Steglich, M. A., Guioli, S., Kwok, C., Weller, P. A., Stevanovic, M., et al. (1994). Campomelic dysplasia and autosomal sex reversal caused by mutations in an SRY-related gene. *Nature* 372, 525–530. doi: 10.1038/372525a0

Fufa, T. D., Harris, M. L., Watkins-Chow, D. E., Levy, D., Gorkin, D. U., Gildea, D. E., et al. (2015). Genomic analysis reveals distinct mechanisms and

functional classes of SOX10-regulated genes in melanocytes. *Hum. Mol. Genet.* 24, 5433–5450. doi: 10.1093/hmg/ddv267

Gadi, J., Jung, S. H., Lee, M. J., Jami, A., Ruthala, K., Kim, K. M., et al. (2013). The transcription factor protein Sox11 enhances early osteoblast differentiation by facilitating proliferation and the survival of mesenchymal and osteoblast progenitors. *J. Biol. Chem.* 288, 25400–25413. doi: 10.1074/jbc.m112.413377

Girard, M., and Goossens, M. (2006). Sumoylation of the SOX10 transcription factor regulates its transcriptional activity. *FEBS Lett.* 580, 1635–1641. doi: 10.1016/j.febslet.2006.02.011

Graham, V., Khudyakov, J., Ellis, P., and Pevny, L. (2003). SOX2 functions to maintain neural progenitor identity. *Neuron* 39, 749–765. doi: 10.1016/s0896-6273(03)00497-5

Grimm, D., Bauer, J., Wise, P., Kruger, M., Simonsen, U., Wehland, M., et al. (2019). The role of SOX family members in solid tumours and metastasis. *Semin. Cancer Biol.* [Epub ahead of print].

Gubbay, J., Collignon, J., Koopman, P., Capel, B., Economou, A., Munsterberg, A., et al. (1990). A gene mapping to the sex-determining region of the mouse Y chromosome is a member of a novel family of embryonically expressed genes. *Nature* 346, 245–250. doi: 10.1038/346245a0

Haldin, C. E., and LaBonne, C. (2010). SoxE factors as multifunctional neural crest regulatory factors. *Int. J. Biochem. Cell Biol.* 42, 441–444. doi: 10.1016/j.biocel.2009.11.014

Hargrave, M., Wright, E., Kun, J., Emery, J., Cooper, L., and Koopman, P. (1997). Expression of the Sox11 gene in mouse embryos suggests roles in neuronal maturation and epithelio-mesenchymal induction. *Dev. Dyn.* 210, 79–86. doi: 10.1002/(sici)1097-0177(199710)210:2<79::aid-aja1>3.0.co;2-6

Harris, M. L., Baxter, L. L., Loftus, S. K., and Pavan, W. J. (2010). Sox proteins in melanocyte development and melanoma. *Pigment Cell Melanoma Res.* 23, 496–513. doi: 10.1111/j.1755-148x.2010.00711.x

Harris, M. L., Buac, K., Shakhova, O., Hakami, R. M., Wegner, M., Sommer, L., et al. (2013). A dual role for SOX10 in the maintenance of the postnatal melanocyte lineage and the differentiation of melanocyte stem cell progenitors. *PLoS Genet.* 9:e1003644. doi: 10.1371/journal.pgen.1003644

Haseeb, A., and Lefebvre, V. (2019). The SOXE transcription factors-SOX8, SOX9 and SOX10-share a bi-partite transactivation mechanism. *Nucleic Acids Res.* 47, 6917–6931. doi: 10.1093/nar/gkz523

Hattori, T., Coustry, F., Stephens, S., Eberspaecher, H., Takigawa, M., Yasuda, H., et al. (2008). Transcriptional regulation of chondrogenesis by coactivator Tip60 via chromatin association with Sox9 and Sox5. *Nucleic Acids Res.* 36, 3011–3024. doi: 10.1093/nar/gkn150

Healy, C., Uwanogho, D., and Sharpe, P. T. (1996). Expression of the chicken Sox9 gene marks the onset of cartilage differentiation. *Ann. N. Y. Acad. Sci.* 785, 261–262. doi: 10.1111/j.1749-6632.1996.tb56278.x

Heenan, P., Zondag, L., and Wilson, M. J. (2016). Evolution of the Sox gene family within the chordate phylum. *Gene* 575, 385–392. doi: 10.1016/j.gene.2015.09.013

Hempel, A., Pagnamenta, A. T., Blyth, M., Mansour, S., McConnell, V., Kou, I., et al. (2016). Deletions and de novo mutations of SOX11 are associated with a neurodevelopmental disorder with features of Coffin-Siris syndrome. *J. Med. Genet.* 53, 152–162. doi: 10.1136/jmedgenet-2015-103393

Herbarth, B., Pingault, V., Bondurand, N., Kuhlbrodt, K., Hermans-Borgmeyer, I., Puliti, A., et al. (1998). Mutation of the Sry-related Sox10 gene in Dominant megacolon, a mouse model for human Hirschsprung disease. *Proc. Natl. Acad. Sci. U.S.A.* 95, 5161–5165. doi: 10.1073/pnas.95.9.5161

Hirobe, T. (1984). Histochemical survey of the distribution of the epidermal melanoblasts and melanocytes in the mouse during fetal and postnatal periods. *Anat. Rec.* 208, 589–594. doi: 10.1002/ar.1092080414

Holbrook, K. A., Underwood, R. A., Vogel, A. M., Gown, A. M., and Kimball, H. (1989). The appearance, density and distribution of melanocytes in human embryonic and fetal skin revealed by the anti-melanoma monoclonal antibody, HMB-45. *Anat. Embryol.* 180, 443–455. doi: 10.1007/bf00305119

Hong, C. S., and Saint-Jeannet, J. P. (2005). Sox proteins and neural crest development. *Semin. Cell Dev. Biol.* 16, 694–703. doi: 10.1016/j.semcdb.2005.06.005

Honore, S. M., Aybar, M. J., and Mayor, R. (2003). Sox10 is required for the early development of the prospective neural crest in *Xenopus embryos*. *Dev. Biol.* 260, 79–96. doi: 10.1016/s0012-1606(03)00247-1

Hou, L., Arnheiter, H., and Pavan, W. J. (2006). Interspecies difference in the regulation of melanocyte development by SOX10 and MITF. *Proc. Natl. Acad. Sci. U.S.A.* 103, 9081–9085. doi: 10.1073/pnas.0603114103

Hou, L., Srivastava, Y., and Jauch, R. (2017). Molecular basis for the genome engagement by Sox proteins. *Semin. Cell Dev. Biol.* 63, 2–12. doi: 10.1016/j.semcdb.2016.08.005

Huang, W., Zhou, X., Lefebvre, V., and de Crombrugghe, B. (2000). Phosphorylation of SOX9 by cyclic AMP-dependent protein kinase A enhances SOX9's ability to transactivate a Col2a1 chondrocyte-specific enhancer. *Mol. Cell. Biol.* 20, 4149–4158. doi: 10.1128/mcb.20.11.4149-4158.2000

Huang, Y. H., Jankowski, A., Cheah, K. S., Prabhakar, S., and Jauch, R. (2015). SOXE transcription factors form selective dimers on non-compact DNA motifs through multifaceted interactions between dimerization and high-mobility group domains. *Sci. Rep.* 5:10398.

Inoue, K., Khajavi, M., Ohyama, T., Hirabayashi, S., Wilson, J., Reggin, J. D., et al. (2004). Molecular mechanism for distinct neurological phenotypes conveyed by allelic truncating mutations. *Nat. Genet.* 36, 361–369. doi: 10.1038/ng1322

Inoue, K., Tanabe, Y., and Lupski, J. R. (1999). Myelin deficiencies in both the central and the peripheral nervous systems associated with a SOX10 mutation. *Ann. Neurol.* 46, 313–318. doi: 10.1002/1531-8249(199909)46:3<313::aid-ana6>3.0.co;2-7

Irie, N., Weinberger, L., Tang, W. W., Kobayashi, T., Viukov, S., Manor, Y. S., et al. (2015). SOX17 is a critical specifier of human primordial germ cell fate. *Cell* 160, 253–268. doi: 10.1016/j.cell.2014.12.013

Irrthum, A., Devriendt, K., Chitayat, D., Matthijs, G., Glade, C., Steijlen, P. M., et al. (2003). Mutations in the transcription factor gene SOX18 underlie recessive and dominant forms of hypotrichosis-lymphedema-telangiectasia. *Am. J. Hum. Genet.* 72, 1470–1478. doi: 10.1086/375614

Ishikawa, R., Kawasaki, M., Kawasaki, K., Yamada, A., Trakanant, S., Meguro, F., et al. (2018). Sox genes show spatiotemporal expression during murine tongue and eyelid development. *Int. J. Dent.* 2018:1601363.

Iso, M., Fukami, M., Horikawa, R., Azuma, N., Kawashiro, N., and Ogata, T. (2008). *SOX10* mutation in Waardenburg syndrome type II. *Am. J. Med. Genet. A* 146A, 2162–2163. doi: 10.1002/ajmg.a.32403

Jandzik, D., Garnett, A. T., Square, T. A., Cattell, M. V., Yu, J. K., and Medeiros, D. M. (2015). Evolution of the new vertebrate head by co-option of an ancient chordate skeletal tissue. *Nature* 518, 534–537. doi: 10.1038/nature14000

Jauch, R., Aksoy, I., Hutchins, A. P., Ng, C. K., Tian, X. F., Chen, J., et al. (2011). Conversion of Sox17 into a pluripotency reprogramming factor by reengineering its association with Oct4 on DNA. *Stem Cells* 29, 940–951. doi: 10.1002/stem.639

Jiao, Z., Mollaaghababa, R., Pavan, W. J., Antonellis, A., Green, E. D., and Hornyak, T. J. (2004). Direct interaction of Sox10 with the promoter of murine Dopachrome Tautomerase (Dct) and synergistic activation of Dct expression with Mitf. *Pigment. Cell Res.* 17, 352–362. doi: 10.1111/j.1600-0749.2004.00154.x

Julian, L. M., McDonald, A. C., and Stanford, W. L. (2017). Direct reprogramming with SOX factors: masters of cell fate. *Curr. Opin. Genet. Dev.* 46, 24–36. doi: 10.1016/j.gde.2017.06.005

Juuri, E., Jussila, M., Seidel, K., Holmes, S., Wu, P., Richman, J., et al. (2013). Sox2 marks epithelial competence to generate teeth in mammals and reptiles. *Development* 140, 1424–1432. doi: 10.1242/dev.089599

Juuri, E., Saito, K., Ahtiainen, L., Seidel, K., Tummers, M., Hochedlinger, K., et al. (2012). Sox2+ stem cells contribute to all epithelial lineages of the tooth via Sfrp5+ progenitors. *Dev. Cell* 23, 317–328. doi: 10.1016/j.devcel.2012.05.012

Kamachi, Y., and Kondoh, H. (2013). Sox proteins: regulators of cell fate specification and differentiation. *Development* 140, 4129–4144. doi: 10.1242/dev.091793

Kawasaki, K., Kawasaki, M., Watanabe, M., Idrus, E., Nagai, T., Oommen, S., et al. (2015). Expression of Sox genes in tooth development. *Int. J. Dev. Biol.* 59, 471–478. doi: 10.1387/ijdb.150192ao

Kellerer, S., Schreiner, S., Stolt, C. C., Scholz, S., Bosl, M. R., and Wegner, M. (2006). Replacement of the Sox10 transcription factor by Sox8 reveals incomplete functional equivalence. *Development* 133, 2875–2886. doi: 10.1242/dev.02477

Kelsh, R. N., and Eisen, J. S. (2000). The zebrafish colourless gene regulates development of non-ectomesenchymal neural crest derivatives. *Development* 127, 515–525.

Khan, U., Study, D., Baker, E., and Clayton-Smith, J. (2018). Observation of cleft palate in an individual with SOX11 mutation: indication of a role for SOX11 in human palatogenesis. *Cleft. Palate. Craniofac. J.* 55, 456–461. doi: 10.1177/1055665617739312

Knosp, W. M., Knox, S. M., and Hoffman, M. P. (2012). Salivary gland organogenesis. Wiley interdisciplinary reviews. *Dev. Biol.* 1, 69–82. doi: 10.1002/wdev.4

Kondoh, H., and Kamachi, Y. (2010). SOX-partner code for cell specification: regulatory target selection and underlying molecular mechanisms. *Int. J. Biochem. Cell Biol.* 42, 391–399. doi: 10.1016/j.biocel.2009.09.003

Kuhlbrodt, K., Herbarth, B., Sock, E., Enderich, J., Hermans-Borgmeyer, I., and Wegner, M. (1998a). Cooperative function of POU proteins and SOX proteins in glial cells. *J. Biol. Chem.* 273, 16050–16057. doi: 10.1074/jbc.273.26.16050

Kuhlbrodt, K., Herbarth, B., Sock, E., Hermans-Borgmeyer, I., and Wegner, M. (1998b). Sox10, a novel transcriptional modulator in glial cells. *J. Neurosci.* 18, 237–250. doi: 10.1523/jneurosci.18-01-00237.1998

Kwok, C., Weller, P. A., Guioli, S., Foster, J. W., Mansour, S., Zuffardi, O., et al. (1995). Mutations in SOX9, the gene responsible for Campomelic dysplasia and autosomal sex reversal. *Am. J. Hum. Genet.* 57, 1028–1036.

Lakiza, O., Miller, S., Bunce, A., Lee, E. M., and McCauley, D. W. (2011). SoxE gene duplication and development of the lamprey branchial skeleton: insights into development and evolution of the neural crest. *Dev. Biol.* 359, 149–161. doi: 10.1016/j.ydbio.2011.08.012

Lamb, A. N., Rosenfeld, J. A., Neill, N. J., Talkowski, M. E., Blumenthal, I., Girirajan, S., et al. (2012). Haploinsufficiency of SOX5 at 12p12.1 is associated with developmental delays with prominent language delay, behavior problems, and mild dysmorphic features. *Hum. Mutation* 33, 728–740. doi: 10.1002/humu.22037

Langer, L., Sulik, K., and Pevny, L. (2014). Cleft Palate in a Mouse Model of SOX2 Haploinsufficiency. *Cleft. Palate. Craniofac. J.* 51, 110–114. doi: 10.1597/12-260

Le, N., Nagarajan, R., Wang, J. Y., Araki, T., Schmidt, R. E., and Milbrandt, J. (2005). Analysis of congenital hypomyelinating Egr2Lo/Lo nerves identifies Sox2 as an inhibitor of Schwann cell differentiation and myelination. *Proc. Natl. Acad. Sci. U.S.A.* 102, 2596–2601. doi: 10.1073/pnas.0407836102

LeBlanc, S. E., Ward, R. M., and Svaren, J. (2007). Neuropathy-associated Egr2 mutants disrupt cooperative activation of myelin protein zero by Egr2 and Sox10. *Mol. Cell. Biol.* 27, 3521–3529. doi: 10.1128/mcb.01689-06

LeDouarin, N. M., and Kalcheim, C. (1999). *The Neural Crest*, 2nd Edn. Cambridge, MA: Cambridge University Press.

Lee, P. C., Taylor-Jaffe, K. M., Nordin, K. M., Prasad, M. S., Lander, R. M., and LaBonne, C. (2012). SUMOylated SoxE factors recruit Grg4 and function as transcriptional repressors in the neural crest. *J. Cell Biol.* 198, 799–813. doi: 10.1083/jcb.201204161

Lefebvre, V., Huang, W., Harley, V. R., Goodfellow, P. N., and de Crombrugghe, B. (1997). SOX9 is a potent activator of the chondrocyte-specific enhancer of the pro alpha1(II) collagen gene. *Mol. Cell. Biol.* 17, 2336–2346. doi: 10.1128/mcb.17.4.2336

Lefebvre, V., Li, P., and de Crombrugghe, B. (1998). A new long form of Sox5 (L-Sox5), Sox6 and Sox9 are coexpressed in chondrogenesis and cooperatively activate the type II collagen gene. *EMBO J.* 17, 5718–5733. doi: 10.1093/emboj/17.19.5718

Leung, V. Y., Gao, B., Leung, K. K., Melhado, I. G., Wynn, S. L., Au, T. Y., et al. (2011). SOX9 governs differentiation stage-specific gene expression in growth plate chondrocytes via direct concomitant transactivation and repression. *PLoS Genet.* 7:e1002356. doi: 10.1371/journal.pgen.1002356

Li, M., Zhao, C., Wang, Y., Zhao, Z., and Meng, A. (2002). Zebrafish sox9b is an early neural crest marker. *Dev. Genes Evol.* 212, 203–206. doi: 10.1007/s00427-002-0235-2

Ling, I. T. C., and Sauka-Spengler, T. (2019). Early chromatin shaping predetermines multipotent vagal neural crest into neural, neuronal and mesenchymal lineages. *Nat. Cell Biol.* 21, 1504-1517. doi: 10.1038/s41556-019-0428-9

Liu, C. F., and Lefebvre, V. (2015). The transcription factors SOX9 and SOX5/SOX6 cooperate genome-wide through super-enhancers to drive chondrogenesis. *Nucleic Acids Res.* 43, 8183–8203. doi: 10.1093/nar/gkv688

Liu, J. A., Tai, A., Hong, J., Cheung, M. P. L., Sham, M. H., Cheah, K. S. E., et al. (2020). Fbxo9 functions downstream of Sox10 to determine neuron-glial fate choice in the dorsal root ganglia through Neurog2 destabilization. *Proc. Natl. Acad. Sci. U.S.A.* 117, 4199–4210. doi: 10.1073/pnas.1916164117

Liu, J. A., Wu, M. H., Yan, C. H., Chau, B. K., So, H., Ng, A., et al. (2013). Phosphorylation of Sox9 is required for neural crest delamination and is regulated downstream of BMP and canonical Wnt signaling. *Proc. Natl. Acad. Sci. U.S.A.* 110, 2882–2887. doi: 10.1073/pnas.1211747110

Liu, Y. R., Laghari, Z. A., Novoa, C. A., Hughes, J., Webster, J. R., Goodwin, P. E., et al. (2014). Sox2 acts as a transcriptional repressor in neural stem cells. *BMC Neurosci.* 15:95. doi: 10.1186/1471-2202-15-95

Liu, Z., and Kraus, W. L. (2017). Catalytic-independent functions of PARP-1 determine Sox2 pioneer activity at intractable genomic loci. *Mol. Cell.* 65, e589.

Lombaert, I. M., Abrams, S. R., Li, L., Eswarakumar, V. P., Sethi, A. J., Witt, R. L., et al. (2013). Combined KIT and FGFR2b signaling regulates epithelial progenitor expansion during organogenesis. *Stem Cell Rep.* 1, 604–619. doi: 10.1016/j.stemcr.2013.10.013

Long, J., Wang, G., He, D., and Liu, F. (2004). Repression of Smad4 transcriptional activity by SUMO modification. *Biochem. J.* 379, 23–29. doi: 10.1042/bj20031867

Lovell-Badge, R. (2010). The early history of the Sox genes. *Int. J. Biochem. Cell Biol.* 42, 378–380. doi: 10.1016/j.biocel.2009.12.003

Ludwig, A., Rehberg, S., and Wegner, M. (2004). Melanocyte-specific expression of dopachrome tautomerase is dependent on synergistic gene activation by the Sox10 and Mitf transcription factors. *FEBS Lett.* 556, 236–244. doi: 10.1016/s0014-5793(03)01446-7

Marathe, H. G., Watkins-Chow, D. E., Weider, M., Hoffmann, A., Mehta, G., Trivedi, A., et al. (2017). BRG1 interacts with SOX10 to establish the melanocyte lineage and to promote differentiation. *Nucleic Acids Res.* 45, 6442–6458. doi: 10.1093/nar/gkx259

Martin, K. J., Rasch, L. J., Cooper, R. L., Metscher, B. D., Johanson, Z., and Fraser, G. J. (2016). Sox2+ progenitors in sharks link taste development with the evolution of regenerative teeth from denticles. *Proc. Natl. Acad. Sci. U.S.A.* 113, 14769–14774. doi: 10.1073/pnas.1612354113

Maruyama, M., Ichisaka, T., Nakagawa, M., and Yamanaka, S. (2005). Differential roles for Sox15 and Sox2 in transcriptional control in mouse embryonic stem cells. *J. Biol. Chem.* 280, 24371–24379. doi: 10.1074/jbc.m501423200

Mazzara, P. G., Massimino, L., Pellegatta, M., Ronchi, G., Ricca, A., Iannielli, A., et al. (2017). Two factor-based reprogramming of rodent and human fibroblasts into Schwann cells. *Nat. Commun.* 8:14088.

McCauley, D. W., and Bronner-Fraser, M. (2006). Importance of SoxE in neural crest development and the evolution of the pharynx. *Nature* 441, 750–752. doi: 10.1038/nature04691

McDowall, S., Argentaro, A., Ranganathan, S., Weller, P., Mertin, S., Mansour, S., et al. (1999). Functional and structural studies of wild type SOX9 and mutations causing campomelic dysplasia. *J. Biol. Chem.* 274, 24023–24030. doi: 10.1074/jbc.274.34.24023

Meyer, J., Sudbeck, P., Held, M., Wagner, T., Schmitz, M. L., Bricarelli, F. D., et al. (1997). Mutational analysis of the *SOX9* gene in campomelic dysplasia and autosomal sex reversal: lack of genotype/phenotype correlations. *Hum. Mol. Genet.* 6, 91–98. doi: 10.1093/hmg/6.1.91

Morales, A. V., Perez-Alcala, S., and Barbas, J. A. (2007). Dynamic Sox5 protein expression during cranial ganglia development. *Dev. Dyn.* 236, 2702–2707. doi: 10.1002/dvdy.21282

Mori-Akiyama, Y., Akiyama, H., Rowitch, D. H., and de Crombrugghe, B. (2003). Sox9 is required for determination of the chondrogenic cell lineage in the cranial neural crest. *Proc. Natl. Acad. Sci. U.S.A.* 100, 9360–9365. doi: 10.1073/pnas.1631288100

Morin, M., Vinuela, A., Rivera, T., Villamar, M., Moreno-Pelayo, M. A., Moreno, F., et al. (2008). A de novo missense mutation in the gene encoding the SOX10 transcription factor in a Spanish sporadic case of Waardenburg syndrome type IV. *Am. J. Med. Genet. A* 146A, 1032–1037. doi: 10.1002/ajmg.a.32181

Murisier, F., Guichard, S., and Beermann, F. (2006). A conserved transcriptional enhancer that specifies Tyrp1 expression to melanocytes. *Dev. Biol.* 298, 644–655. doi: 10.1016/j.ydbio.2006.05.011

Murisier, F., Guichard, S., and Beermann, F. (2007). The tyrosinase enhancer is activated by Sox10 and Mitf in mouse melanocytes. *Pigment. Cell Res.* 20, 173–184. doi: 10.1111/j.1600-0749.2007.00368.x

Nakagawa, M., Koyanagi, M., Tanabe, K., Takahashi, K., Ichisaka, T., Aoi, T., et al. (2008). Generation of induced pluripotent stem cells without Myc from mouse and human fibroblasts. *Nat. Biotechnol.* 26, 101–106. doi: 10.1038/nbt1374

Noden, D. M., and Trainor, P. A. (2005). Relations and interactions between cranial mesoderm and neural crest populations. *J. Anat.* 207, 575–601. doi: 10.1111/j.1469-7580.2005.00473.x

Nordin, K., and LaBonne, C. (2014). Sox5 Is a DNA-binding cofactor for BMP R-Smads that directs target specificity during patterning of the early ectoderm. *Dev. Cell.* 31, 374–382. doi: 10.1016/j.devcel.2014.10.003

O'Donnell, M., Hong, C. S., Huang, X., Delnicki, R. J., and Saint-Jeannet, J. P. (2006). Functional analysis of Sox8 during neural crest development in *Xenopus*. *Development* 133, 3817–3826. doi: 10.1242/dev.02558

Okamoto, N., Ehara, E., Tsurusaki, Y., Miyake, N., and Matsumoto, N. (2018). Coffin-Siris syndrome and cardiac anomaly with a novel SOX11 mutation. *Congenit. Anom.* 58, 105–107. doi: 10.1111/cga.12242

Passeron, T., Valencia, J. C., Bertolotto, C., Hoashi, T., Le Pape, E., Takahashi, K., et al. (2007). SOX9 is a key player in ultraviolet B-induced melanocyte differentiation and pigmentation. *Proc. Natl. Acad. Sci. U.S.A.* 104, 13984–13989. doi: 10.1073/pnas.0705117104

Peirano, R. I., Goerich, D. E., Riethmacher, D., and Wegner, M. (2000). Protein zero gene expression is regulated by the glial transcription factor Sox10. *Mol. Cell. Biol.* 20, 3198–3209. doi: 10.1128/MCB.20.9.3198-3209.2000

Peirano, R. I., and Wegner, M. (2000). The glial transcription factor Sox10 binds to DNA both as monomer and dimer with different functional consequences. *Nucleic Acids Res.* 28, 3047–3055. doi: 10.1093/nar/28.16.3047

Perez-Alcala, S., Nieto, M. A., and Barbas, J. A. (2004). LSox5 regulates RhoB expression in the neural tube and promotes generation of the neural crest. *Development* 131, 4455–4465. doi: 10.1242/dev.01329

Pevny, L., and Placzek, M. (2005). SOX genes and neural progenitor identity. *Curr. Opin. Neurobiol.* 15, 7–13. doi: 10.1016/j.conb.2005.01.016

Pingault, V., Bondurand, N., Kuhlbrodt, K., Goerich, D. E., Prehu, M. O., Puliti, A., et al. (1998). SOX10 mutations in patients with Waardenburg-Hirschsprung disease. *Nat. Genet.* 18, 171–173. doi: 10.1038/ng0298-171

Pingault, V., Girard, M., Bondurand, N., Dorkins, H., Van Maldergem, L., Mowat, D., et al. (2002). *SOX10* mutations in chronic intestinal pseudo-obstruction suggest a complex physiopathological mechanism. *Hum. Genet.* 111, 198–206. doi: 10.1007/s00439-002-0765-8

Pingault, V., Ente, D., Dastot-Le Moal, F., Goossens, M., Marlin, S., and Bondurand, N. (2010). Review and update of mutations causing Waardenburg syndrome. *Hum. Mutat.* 31, 391–406. doi: 10.1002/humu.21211

Potterf, S. B., Furumura, M., Dunn, K. J., Arnheiter, H., and Pavan, W. J. (2000). Transcription factor hierarchy in Waardenburg syndrome: regulation of MITF expression by SOX10 and PAX3. *Hum. Genet.* 107, 1–6. doi: 10.1007/s004390000328

Prasad, M. S., Sauka-Spengler, T., and LaBonne, C. (2012). Induction of the neural crest state: control of stem cell attributes by gene regulatory, post-transcriptional and epigenetic interactions. *Dev. Biol.* 366, 10–21. doi: 10.1016/j.ydbio.2012.03.014

Raftery, R. M., Gonzalez Vazquez, A. G., Chen, G., and O'Brien, F. J. (2020). Activation of the SOX-5, SOX-6, and SOX-9 trio of transcription factors using a gene-activated scaffold stimulates mesenchymal stromal cell chondrogenesis and inhibits endochondral ossification. *Adv. Healthc. Mater.* 9:e1901827. doi: 10.1002/adhm.201901827

Rao, A., and LaBonne, C. (2018). Histone deacetylase activity has an essential role in establishing and maintaining the vertebrate neural crest. *Development* 145:dev163386. doi: 10.1242/dev.163386

Rex, M., Orme, A., Uwanogho, D., Tointon, K., Wigmore, P. M., Sharpe, P. T., et al. (1997). Dynamic expression of chicken Sox2 and Sox3 genes in ectoderm induced to form neural tissue. *Dev. Dyn.* 209, 323–332. doi: 10.1002/(SICI)1097-0177(199707)209:3<323::AID-AJA7>3.0.CO;2-K

Roberts, S. L., Dun, X. P., Doddrell, R. D. S., Mindos, T., Drake, L. K., Onaitis, M. W., et al. (2017). Sox2 expression in Schwann cells inhibits myelination in vivo and induces influx of macrophages to the nerve. *Development* 144, 3114–3125. doi: 10.1242/dev.150656

Roellig, D., Tan-Cabugao, J., Esaian, S., and Bronner, M. E. (2017). Dynamic transcriptional signature and cell fate analysis reveals plasticity of individual neural plate border cells. *eLife* 6:e21620. doi: 10.7554/eLife.21620.032

Rosonina, E., Akhter, A., Dou, Y., Babu, J., and Sri Theivakadadcham, V. S. (2017). Regulation of transcription factors by sumoylation. *Transcription* 8, 220–231. doi: 10.1080/21541264.2017.1311829

Sakai, D., Suzuki, T., Osumi, N., and Wakamatsu, Y. (2006). Cooperative action of Sox9, Snail2 and PKA signaling in early neural crest development. *Development* 133, 1323–1333. doi: 10.1242/dev.02297

Sanchez-Mejias, A., Watanabe, Y., R, M. F., López-Alonso, M., Antinolo, G., Bondurand, N., Borrego, S., et al. (2010). Involvement of *SOX10* in the pathogenesis of Hirschsprung disease: report of a truncating mutation in an isolated patient. *J. Mol. Med.* 88, 507–514. doi: 10.1007/s00109-010-0592-7

Schlierf, B., Ludwig, A., Klenovsek, K., and Wegner, M. (2002). Cooperative binding of Sox10 to DNA: requirements and consequences. *Nucleic Acids Res.* 30, 5509–5516. doi: 10.1093/nar/gkf690

Schlosser, G., Awtry, T., Brugmann, S. A., Jensen, E. D., Neilson, K., Ruan, G., et al. (2008). Eya1 and Six1 promote neurogenesis in the cranial placodes in a SoxB1-dependent fashion. *Dev. Biol.* 320, 199–214. doi: 10.1016/j.ydbio.2008.05.523

Schreiner, S., Cossais, F., Fischer, K., Scholz, S., Bosl, M. R., Holtmann, B., et al. (2007). Hypomorphic Sox10 alleles reveal novel protein functions and unravel developmental differences in glial lineages. *Development* 134, 3271–3281. doi: 10.1242/dev.003350

Shakhova, O., Cheng, P., Mishra, P. J., Zingg, D., Schaefer, S. M., Debbache, J., et al. (2015). Antagonistic cross-regulation between Sox9 and Sox10 controls an anti-tumorigenic program in melanoma. *PLoS Genet.* 11:e1004877. doi: 10.1371/journal.pgen.1004877

Sham, M. H., Lui, V. C., Chen, B. L., Fu, M., and Tam, P. K. (2001). Novel mutations of SOX10 suggest a dominant negative role in Waardenburg-Shah syndrome. *J. Med. Genet.* 38:E30. doi: 10.1136/jmg.38.9.e30

Shimotake, T., Tanaka, S.-C, Fukui, R., Makino, S., and Maruyama, R. (2007). Neuroglial disorders of central and peripheral nervous systems in a patient with Hirschsprung's disease carrying allelic SOX10 truncating mutation. *J. Pediatr. Surg.* 42, 725–731. doi: 10.1016/j.jpedsurg.2006.12.003

Simoes-Costa, M., and Bronner, M. E. (2015). Establishing neural crest identity: a gene regulatory recipe. *Development* 142, 242–257. doi: 10.1242/dev.105445

Sitiwin, E., Madigan, M. C., Gratton, E., Cherepanoff, S., Conway, R. M., Whan, R., et al. (2019). Shedding light on melanins within in situ human eye melanocytes using 2-photon microscopy profiling techniques. *Sci. Rep.* 9:18585. doi: 10.1038/s41598-019-54871-y

Smits, P., Li, P., Mandel, J., Zhang, Z., Deng, J. M., Behringer, R. R., et al. (2001). The transcription factors L-Sox5 and Sox6 are essential for cartilage formation. *Dev. Cell* 1, 277–290. doi: 10.1016/S1534-5807(01)00003-X

Sock, E., Pagon, R. A., Keymolen, K., Lissens, W., Wegner, M., and Scherer, G. (2003). Loss of DNA-dependent dimerization of the transcription factor SOX9 as a cause for campomelic dysplasia. *Hum. Mol. Genet.* 12, 1439–1447. doi: 10.1093/hmg/ddg158

Sock, E., Rettig, S. D., Enderich, J., Bosl, M. R., Tamm, E. R., and Wegner, M. (2004). Gene targeting reveals a widespread role for the high-mobility-group transcription factor Sox11 in tissue remodeling. *Mol. Cell. Biol.* 24, 6635–6644. doi: 10.1128/MCB.24.15.6635-6644.2004

Sock, E., Schmidt, K., Hermanns-Borgmeyer, I., Bosl, M. R., and Wegner, M. (2001). Idiopathic weight reduction in mice deficient in the high-mobility-group transcription factor Sox8. *Mol. Cell. Biol.* 21, 6951–6959. doi: 10.1128/MCB.21.20.6951-6959.2001

Soufi, A., Garcia, M. F., Jaroszewicz, A., Osman, N., Pellegrini, M., and Zaret, K. S. (2015). Pioneer transcription factors target partial DNA motifs on nucleosomes to initiate reprogramming. *Cell* 161, 555–568. doi: 10.1016/j.cell.2015.03.017

Southard-Smith, E. M., Angrist, M., Ellison, J. S., Agarwala, R., Baxevanis, A. D., Chakravarti, A., et al. (1999). The Sox10(Dom) mouse: modeling the genetic variation of Waardenburg-Shah (WS4) syndrome. *Genome Res.* 9, 215–225.

Southard-Smith, E. M., Kos, L., and Pavan, W. J. (1998). Sox10 mutation disrupts neural crest development in Dom Hirschsprung mouse model. *Nat. Genet.* 18, 60–64. doi: 10.1038/ng0198-60

Spokony, R. F., Aoki, Y., Saint-Germain, N., Magner-Fink, E., and Saint-Jeannet, J. P. (2002). The transcription factor Sox9 is required for cranial neural crest development in *Xenopus*. *Development* 129, 421–432.

Stolt, C. C., Lommes, P., Hillgartner, S., and Wegner, M. (2008). The transcription factor Sox5 modulates Sox10 function during melanocyte development. *Nucleic Acids Res.* 36, 5427–5440. doi: 10.1093/nar/gkn527

Sun, Z., Yu, W., Sanz Navarro, M., Sweat, M., Eliason, S., Sharp, T., et al. (2016). Sox2 and Lef-1 interact with Pitx2 to regulate incisor development and stem cell renewal. *Development* 143, 4115–4126. doi: 10.1242/dev.138883

Tai, A., Cheung, M., Huang, Y. H., Jauch, R., Bronner, M. E., and Cheah, K. S. (2016). SOXE neofunctionalization and elaboration of the neural crest during chordate evolution. *Sci. Rep.* 6:34964. doi: 10.1038/srep34964

Takahashi, K., and Yamanaka, S. (2006). Induction of pluripotent stem cells from mouse embryonic and adult fibroblast cultures by defined factors. *Cell* 126, 663–676. doi: 10.1016/j.cell.2006.07.024

Tan, H., and Tee, W. W. (2019). Committing the primordial germ cell: an updated molecular perspective. *Wiley Interdiscip. Rev. Syst. Biol. Med.* 11"e1436. doi: 10.1002/wsbm.1436

Tanaka, J., Mabuchi, Y., Hata, K., Yasuhara, R., Takamatsu, K., Kujiraoka, S., et al. (2019). Sox9 regulates the luminal stem/progenitor cell properties of salivary glands. *Exp. Cell Res.* 382:111449. doi: 10.1016/j.yexcr.2019.05.030

Tanaka, S., Kamachi, Y., Tanouchi, A., Hamada, H., Jing, N., and Kondoh, H. (2004). Interplay of SOX and POU factors in regulation of the Nestin gene in neural primordial cells. *Mol. Cell. Biol.* 24, 8834–8846. doi: 10.1128/MCB.24.20.8834-8846.2004

Taylor, K. M., and LaBonne, C. (2005). SoxE factors function equivalently during neural crest and inner ear development and their activity is regulated by SUMOylation. *Dev. Cell* 9, 593–603. doi: 10.1016/j.devcel.2005.09.016

Taylor, K. M., and LaBonne, C. (2007). Modulating the activity of neural crest regulatory factors. *Curr. Opin. Genet. Dev.* 17, 326–331. doi: 10.1016/j.gde.2007.05.012

Thesleff, I. (2014). Current understanding of the process of tooth formation: transfer from the laboratory to the clinic. *Aust. Dent. J.* 59(Suppl. 1), 48–54. doi: 10.1111/adj.12102

Toki, F., Suzuki, N., Inoue, K., Suzuki, M., Hirakata, K., Nagai, K., et al. (2003). Intestinal aganglionosis associated with the Waardenburg syndrome: report of two cases and review of the literature. *Pediatr. Surg. Int.* 19, 725–728. doi: 10.1007/s00383-003-1057-7

Tsurusaki, Y., Koshimizu, E., Ohashi, H., Phadke, S., Kou, I., Shiina, M., et al. (2014). De novo SOX11 mutations cause Coffin-Siris syndrome. *Nat. Commun.* 5:4011. doi: 10.1038/ncomms5011

Uy, B. R., Simoes-Costa, M., Koo, D. E., Sauka-Spengler, T., and Bronner, M. E. (2015). Evolutionarily conserved role for SoxC genes in neural crest specification and neuronal differentiation. *Dev. Biol.* 397, 282–292. doi: 10.1016/j.ydbio.2014.09.022

Valenzuela, I., Fernandez-Alvarez, P., Plaja, A., Ariceta, G., Sabate-Rotes, A., Garcia-Arumi, E., et al. (2018). Further delineation of the SOX18-related hypotrichosis, lymphedema, telangiectasia syndrome (HTLS). *Eur. J. Med. Genet.* 61, 269–272. doi: 10.1016/j.ejmg.2018.01.001

Wagner, T., Wirth, J., Meyer, J., Zabel, B., Held, M., Zimmer, J., et al. (1994). Autosomal sex reversal and campomelic dysplasia are caused by mutations in and around the SRY-related gene SOX9. *Cell* 79, 1111–1120. doi: 10.1016/0092-8674(94)90041-8

Wakamatsu, Y., Endo, Y., Osumi, N., and Weston, J. A. (2004). Multiple roles of Sox2, an HMG-box transcription factor in avian neural crest development. *Dev. Dyn.* 229, 74–86. doi: 10.1002/dvdy.10498

Wangberg, H., Wigby, K., and Jones, M. C. (2018). A novel autosomal dominant mutation in SOX18 resulting in a fatal case of hypotrichosis-lymphedema-telangiectasia syndrome. *Am. J. Med. Genet. A* 176, 2824–2828. doi: 10.1002/ajmg.a.40532

Watanabe, M., Kawasaki, K., Kawasaki, M., Portaveetus, T., Oommen, S., Blackburn, J., et al. (2016). Spatio-temporal expression of Sox genes in murine palatogenesis. *Gene Exp. Patterns GEP* 21, 111–118. doi: 10.1016/j.gep.2016.05.002

Wildhardt, G., Zirn, B., Graul-Neumann, L. M., Wechtenbruch, J., Suckfull, M., Buske, A., et al. (2013). Spectrum of novel mutations found in Waardenburg syndrome types 1 and 2: implications for molecular genetic diagnostics. *BMJ Open* 3:e001917. doi: 10.1136/bmjopen-2012-001917

Williams, C. A. C., Soufi, A., and Pollard, S. M. (2019). Post-translational modification of SOX family proteins: key biochemical targets in cancer?. *Semin. Cancer Biol.* [Epub ahead of print]. doi: 10.1016/j.semcancer.2019.09.009

Wright, E., Hargrave, M. R., Christiansen, J., Cooper, L., Kun, J., Evans, T., et al. (1995). The Sry-related gene Sox9 is expressed during chondrogenesis in mouse embryos. *Nat. Genet.* 9, 15–20. doi: 10.1038/ng0195-15

Wust, H. M., Wegener, A., Frob, F., Hartwig, A. C., Wegwitz, F., Kari, V., et al. (2020). Egr2-guided histone H2B monoubiquitination is required for peripheral nervous system myelination. *Nucleic Acids Res.* 48, 8959–8976. doi: 10.1093/nar/gkaa606

Yan, Y. L., Willoughby, J., Liu, D., Crump, J. G., Wilson, C., Miller, C. T., et al. (2005). A pair of Sox: distinct and overlapping functions of zebrafish sox9 co-orthologs in craniofacial and pectoral fin development. *Development* 132, 1069–1083. doi: 10.1242/dev.01674

Zawerton, A., Mignot, C., Sigafoos, A., Blackburn, P. R., Haseeb, A., McWalter, K., et al. (2020). Widening of the genetic and clinical spectrum of Lamb-Shaffer syndrome, a neurodevelopmental disorder due to SOX5 haploinsufficiency. *Genet. Med.* 22, 524–537. doi: 10.1038/s41436-019-0657-0

Zawerton, A., Yao, B., Yeager, J. P., Pippucci, T., Haseeb, A., Smith, J. D., et al. (2019). De novo SOX4 variants cause a neurodevelopmental disease associated with mild *Dysmorphism*. *Am. J. Hum. Genet.* 104, 246–259. doi: 10.1016/j.ajhg.2018.12.014

Conflict of Interest: The authors declare that the research was conducted in the absence of any commercial or financial relationships that could be construed as a potential conflict of interest.

frontiers in Physiology

REVIEW
published: 11 December 2020
doi: 10.3389/fphys.2020.610970

Why Does the Face Predict the Brain? Neural Crest Induction, Craniofacial Morphogenesis, and Neural Circuit Development

Anthony-Samuel LaMantia[1,2]*

[1]Laboratory of Developmental Disorders and Genetics and Center for Neurobiology Research, Fralin Biomedical Research Institute, Department of Pediatrics, Virginia Tech-Carilion School of Medicine, Virginia Tech, Roanoke, VA, United States, [2]Department of Biological Sciences, Virginia Tech, Blacksburg, VA, United States

Mesenchephalic and rhombencephalic neural crest cells generate the craniofacial skeleton, special sensory organs, and subsets of cranial sensory receptor neurons. They do so while preserving the anterior-posterior (A-P) identity of their neural tube origins. This organizational principle is paralleled by central nervous system circuits that receive and process information from facial structures whose A-P identity is in register with that in the brain. Prior to morphogenesis of the face and its circuits, however, neural crest cells act as "inductive ambassadors" from distinct regions of the neural tube to induce differentiation of target craniofacial domains and establish an initial interface between the brain and face. At every site of bilateral, non-axial secondary induction, neural crest constitutes all or some of the mesenchymal compartment for non-axial mesenchymal/epithelial (M/E) interactions. Thus, for epithelial domains in the craniofacial primordia, aortic arches, limbs, the spinal cord, and the forebrain (Fb), neural crest-derived mesenchymal cells establish local sources of inductive signaling molecules that drive morphogenesis and cellular differentiation. This common mechanism for building brains, faces, limbs, and hearts, A-P axis specified, neural crest-mediated M/E induction, coordinates differentiation of distal structures, peripheral neurons that provide their sensory or autonomic innervation in some cases, and central neural circuits that regulate their behavioral functions. The essential role of this neural crest-mediated mechanism identifies it as a prime target for pathogenesis in a broad range of neurodevelopmental disorders. Thus, the face and the brain "predict" one another, and this mutual developmental relationship provides a key target for disruption by developmental pathology.

Keywords: neural crest, placodes, olfactory, sensory pathways, inductive signaling, 22q11 deletion syndrome

OPEN ACCESS

Edited by:
Lisa Taneyhill, University of Maryland, College Park, United States

Reviewed by:
Kristin Artinger, University of Colorado Denver, United States
Pierfrancesco Pagella, University of Zurich, Switzerland

***Correspondence:**
Anthony-Samuel LaMantia
anthonysl@vtc.vt.edu

Specialty section:
This article was submitted to Embryonic and Developmental Physiology, a section of the journal Frontiers in Physiology

Received: *28 September 2020*
Accepted: *24 November 2020*
Published: *11 December 2020*

Citation:
LaMantia A-S (2020) Why Does the Face Predict the Brain? Neural Crest Induction, Craniofacial Morphogenesis, and Neural Circuit Development. Front. Physiol. 11:610970. doi: 10.3389/fphys.2020.610970

INTRODUCTION

Nearly 60 years ago, Demyer et al. (1964) published a description of a series of cases with varying degrees of craniofacial malformations: from near cyclopia in still born fetuses to two patients, described in detail, with mild, but detectable, craniofacial anomalies. Based upon limited clinical observations, they argued that the degree of craniofacial malformation in these

individuals correlated with brain dysmorphology and dysfunction. This apparent relationship led them to conclude, in a memorable – if not fully appreciated – title that "The Face Predicts the Brain." The subtitle of their paper was prescient: "Diagnostic Significance of Median Facial Anomalies for Holoprosencephaly (Arhinencephaly)." The mechanistic significance of this relationship, including the consequences for the olfactory periphery (the nose) and its forebrain (Fb) targets [the olfactory bulbs (OBs) and other basal Fb nuclei], as well as additional peripheral sensory, brainstem, cerebral cortical, or basal Fb structures and circuits, however, was unclear at the time. Subsequent studies from the late 1980s onward give cell biological and molecular definition to the 1964 provocative idea of DeMyer et al. The face does indeed predict the brain. The central role of the neural crest in this predictive relationship is the subject of this review.

If the face predicts the brain, it is essential to define the nature of the prediction. This relationship reflects the central role of interactions between the craniofacial primordia, cranial placodes, and the rhombencephalic and mesencephalic neural crests, which provides a "mirror" representation of the axial organization of the neural tube to distal sites of secondary induction and differentiation: the facial skeleton and cartilage, key sensory structures, like the nose, eyes, ears, and cranial ganglia, and their targets in the central nervous system. Parallel neural crest-mediated interactions influence the aortic arches that become the great vessels of the heart, and this mechanism also influences limb bud patterning and differentiation (**Figure 1A**). This "mirror" representation of the early developing brain casts its reflection by localizing cardinal signaling molecules: retinoic acid (RA; Richman, 1992; Morriss-Kay, 1993; Rawson and LaMantia, 2006; Williams and Bohnsack, 2019), Fgfs (Tucker et al., 1999; Nie et al., 2006b; Szabo-Rogers et al., 2008; Stanier and Pauws, 2012), Shh (Hardcastle et al., 1999; Nasrallah and Golden, 2001; Smith et al., 2014; Okuhara et al., 2019), Bmps, other Tgfβ family members and their antagonists (Greene and Pisano, 2005; Nie et al., 2006a; Matsui and Klingensmith, 2014; Graf et al., 2016; Young et al., 2017), and Wnts (Alexander et al., 2014; Ji et al., 2019). Thus, it may well be that DeMyer reversed the valence of their prediction: the face may *reflect* the brain, but the brain, *via* the neural crest, *predicts* the face.

The distribution of the neural crest in the midgestation embryo includes several discrete accumulations of mesenchymal cells at bilaterally symmetrical locations (**Figures 1B,C, 2**). The neural crest-derived mesenchyme at some of these sites will contribute to special sensory organs: the frontonasal masses [olfactory epithelium (OE) and nose], the eyes (cornea, scleral, and choroidal cells), and the otic placodes (middle ear bones and epithelia); others will generate cranial skeletal elements, teeth, and cartilage (Jiang et al., 2002; Lwigale et al., 2004; Tucker and Sharpe, 2004; Balmer and LaMantia, 2005; Creuzet et al., 2005; Yoshida et al., 2008; Edlund et al., 2015; Williams and Bohnsack, 2015; Dash and Trainor, 2020). Each of these mesenchymal neural crest populations derives from a distinct anterior to posterior (A-P) location in the mesencephalic, rhombencephalic, vagal/cardiac, or trunk neural crest (**Figure 1B**). The somewhat surprising inclusion of the limb bud in this list of sites of early neural crest mesenchymal accumulation in the early limb bud prior to morphogenesis has been commented on in classical embryological studies (Erickson, 1985; Grim and Christ, 1993) and suggested – sometimes without comment – by additional work using molecular and genetic methods (Noakes and Bennett, 1987; Shen et al., 1997; Barlow et al., 2002; Akiyama et al., 2005; Olaopa et al., 2011; Wade et al., 2012). Our work using transgenic reporters and molecular markers for neural crest have reinforced the likely presence of neural crest in the limb bud mesenchyme (Maynard et al., 2002; Bhasin et al., 2003; Meechan et al., 2006; Rawson et al., 2010) prior to the ingression of nerves and

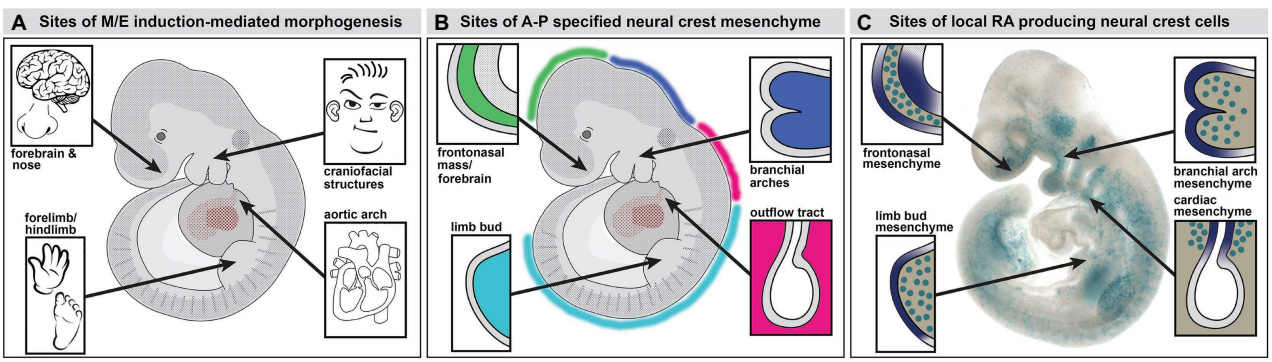

FIGURE 1 | Neural crest mediated mesenchymal/epithelial (M/E) induction prefigures nasal/forebrain (Fb), craniofacial, heart, and limb morphogenesis. **(A)** A summary of the sites of non-axial M/E induction and their morphogenetic endpoints. The arrows point to the embryonic regions illustrated in panel B. **(B)** A summary of the relationship between anterior-posterior (A-P) regionally specified neural crest and the sites of M/E induction that establish the nose and Fb, the face, the heart, and the limbs. At each site, a primarily neural crest-derived population of A-P specified mesenchymal cells is opposed to the adjacent surface ectoderm, which is also axially specified. **(C)** Subsets of neural crest-derived mesenchymal cells, labeled with a knock-in reporter transgene (βgeo6; LaMantia et al., 2000; Bhasin et al., 2003) at each of the sites of M/E induction produce the morphogenetic signaling molecule retinoic acid (RA). These cells drive locally patterned expression of several target genes in placodal domains (purple shading) immediately adjacent to the RA-producing mesenchymal cells.

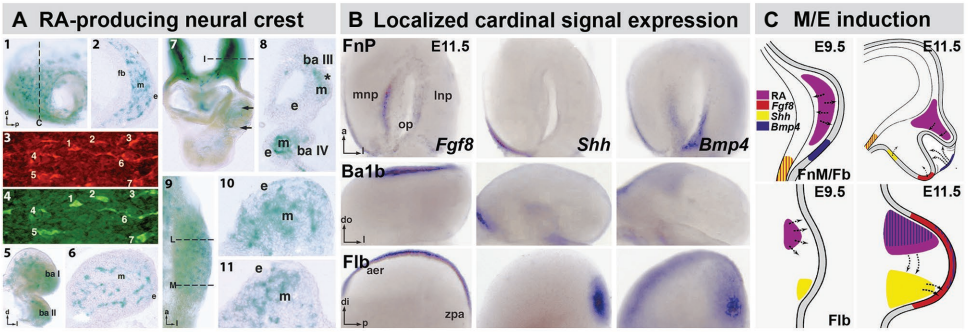

FIGURE 2 | The distribution of RA producing neural crest at sites of M/E induction and its relationship to epithelia and mesenchymal sources of additional cardinal inductive signals. **(A)** Subsets of frontonasal (panels 1, 2), branchial arch (panels 5, 6), aortic arch (panels 7, 8), and forelimb bud (Flb; panels 9–11) are labeled by the βgeo6 reporter. These cells are coincident with Raldh2-expressing cells in the frontonasal mesenchyme (FnM; panels 3, 4) as well as other sites of non-axial M/E interaction. The dotted lines in panels 1, 7, and 9 indicate the approximate plane of the sections shown in panels 2, 8, 10, and 11, respectively. **(B)** *In situ* hybridization identifies local expression of cardinal inductive/morphogenetic signals *Fgf8*, *Shh*, and *Bmp4* in epithelial as well as mesenchymal domains in the frontonasal process (FnP), mandibular arch (Ba1b), and Flb. *Fgf8* and *Shh* are limited to epithelial domains in the medial nasal process (mnp) while *Bmp4* is enhanced in the lateral nasal process epithelium. *Fgf8* is found in a limited dorsal-lateral epithelial domain in Ba1b, *Shh* in a medial domain, and *Bmp4* in a dorsal medial location. In the Flb, these three cardinal signals define the apical ectodermal ridge (aer) and zone of polarizing activity (zpa), two embryologically defined signaling regions that drive limb morphogenesis and patterning (REFS). **(C)** Schematic summary of the localization and signaling interactions (arrows) of local mesenchymal and epithelial sources of RA, Fgf8, Shh, and Bmp4 in the frontonasal mass/Fb (top) and Flb (bottom) during the initial establishment of these sites of non-axial neural crest-mediated M/E induction (Embryonic day E9.5 in the mouse) and as signaling and morphogenesis moves forward (E11.5). The direction of the arrows was determined using *in vitro* mesenchymal/epithelial co-cultures or isolated explants of the epithelium or mesenchyme alone (LaMantia et al., 2000; Bhasin et al., 2003).

vascular cells (Le Douarin et al., 1991; Jessen and Mirsky, 2005). Thus, subsets of neural crest cells that migrate to distinct peripheral sites of morphogenesis, including the facial primorida, bring with them a record of A-P neural tube position and presumably share aspects of molecular identity with neural progenitor cells that remain behind. These include expression and activity of *Hox* genes and related factors within distinct A-P domains.

The fates of these distal mesenchymal neural crest cells will ultimately include skeletogenic progenitors, sensory and autonomic neurons, Schwann cells, melanocytes, and in some cases vascular cells (Thomas and Erickson, 2008; Nitzan et al., 2013; Trost et al., 2013; Petersen and Adameyko, 2017). Nevertheless, during an earlier epoch of development, after migration but before terminal differentiation, they serve a distinct function. These mesenchymal neural crest cells localize sources of inductive signals directly, or *via* interactions with adjacent ectoderm (**Figure 2**) to drive morphogenesis and differentiation (LaMantia et al., 1993, 2000; Neubuser et al., 1997; Bhasin et al., 2003; Thesleff, 2003). These local sites of mesenchymal/epithelial (M/E) induction generate essential, bilaterally symmetric peripheral structures in all vertebrates that facilitate the organism's interactions with its environment, as well as circuits in the central nervous system that animate these structures.

Many "cardinal" morphogenetic signals, including Shh, Bmps, and Fgfs, are expressed in epithelial domains at sites where mesenchymal neural crest accumulates in the head as well as heart and limbs (**Figure 2**). Their expression relies on localization of the neural crest and its capacity to secrete signaling molecules, particularly RA (Bhasin et al., 2003). Thus, the brain, *via* neural crest specified along the A-P axis of the neural tube, drives the development of facial structures, including the nose and jaws, and the neural crest from more posterior regions of the neural tube performs a similar function for the great vessels of the heart or for patterning and morphogenesis in the limbs (**Figure 2**). With the benefit of nearly 60 years of subsequent embryological, cell biological, molecular, and genetic observations, one can confidently revise and extend the conclusion of DeMyer et al. that "the face predicts the brain": *the brain builds the face – and other non-axial bilaterally symmetric structures along the A-P axis*. This morphogenetic relationship between the brain, neural crest, and the periphery has another essential consequence: developmental coordination that integrates sensory and/or motor functions of biomechanical specializations that execute essential behaviors. Accordingly, this mechanism is a likely target for central nervous system dysfunction and related peripheral dysmorphology in multiple neurodevelopmental disorders.

COORDINATED DIFFERENTIATION OF A SENSORY PATHWAY BY NEURAL CREST: OLFACTORY DEVELOPMENT

If the brain does indeed build the face and other target sites, what are the likely purposes of this construction effort? Data from my laboratory over several decades suggests that an essential purpose of brain-constructed facial primordia is to coordinate the development of peripheral sensory sites with that of their central nervous system targets. Our work on initial specification and subsequent differentiation of the primary olfactory pathway provided initial support for this hypothesis (LaMantia et al., 1993, 2000; Anchan et al., 1997). The inspiration

for this hypothesis came from classical embryological experiments that demonstrated the inductive capacity of the entire olfactory placode (op), presumably both ectodermal and mesenchymal components, to induce a supernumerary limb when transplanted beneath the flank ectoderm (Balinsky, 1956). In addition, extirpation and transplantation experiments suggested that the olfactory op exerted significant inductive influence on its primary target, the anterior Fb in both the frog and the mouse (Graziadei et al., 1978; Stout and Graziadei, 1980; Graziadei and Monti-Graziadei, 1992). Finally, observations in hamster embryos suggested that RA teratogenesis at a limited period of early Fb development – after the neural crest has arrived in the anterior cranial region – results in a loss of both the OE and the OB (Shenefelt, 1972). Thus, based upon tissue-tissue interactions and the apparent involvement of a key morphogenetic signal, it seemed possible that early induction played a role in olfactory pathway development.

We first asked whether there was inductive signaling *via* RA that normally prefigures the establishment of the anlagen of the OE and the OB, and whether this signaling influences the initial projection of olfactory sensory afferents to their OB targets (LaMantia et al., 1993). The coordinated effects of frontonasal mesenchyme (FnM) signaling, *via* production of RA by the mesenchyme only, establish domains of RA-mediated gene expression in the cranial surface ectoderm and ventral Fb neuroectoderm. These domains are sites of the earliest neurogenesis in the cranial periphery and the Fb (**Figure 3**). They will eventually differentiate as the OE in the periphery and the OB in the Fb. Finally, the cranial mesenchyme apparently constrains the initial growth of olfactory receptor neuron (ORN) axons to the presumptive OB as well as the morphogenesis of the bulb itself (Whitesides and LaMantia, 1996; Tucker et al., 2006). These inductive events are critically dependent on the migration of primarily mesencephalic neural crest cells into the most anterior aspect of the embryo as the anterior neural tube closes (Serbedzija et al., 1992; Osumi-Yamashita et al., 1994). These cells constitute the FnM interposed between the anterior surface ectoderm and the ventral neuroepithelium of the nascent prosencephalic vesicle.

Substantial attention has been given to the fates of neural crest cells that constitute the frontonasal as well as the branchial arch and lateral cranial mesenchyme (Noden, 1988; Gross and Hanken, 2008; Weston and Thiery, 2015). Ultimately, subsets of these cells will become progenitors for facial and pharyngeal bones and cartilage including those of the nose. Others will contribute to the cranial sensory ganglia (D'Amico-Martel and Noden, 1983; Freyer et al., 2011; Karpinski et al., 2016; Thiery et al., 2020). Still, others will constitute populations of melanocytes or vascular cells (Miller et al., 2017; Vandamme and Berx, 2019). Prior to acquiring those fates, however, subsets of these cells serve transient but distinct developmental functions: they provide molecular signals to adjacent tissues to elicit focally patterned gene expression and drive local cellular differentiation. This role for neural crest has been established for initial patterning and differentiation of cranial musculature and vasculature from mesodermal progenitors (Hill et al., 2015; Ziermann et al., 2018). Similar neural crest-mediated signaling mechanisms, prior to fate restriction and differentiation of these cells, also coordinate cranial peripheral and central nervous system development.

Focal-inductive signaling mediated by cranial neural crest prefigures and likely drives specification of peripheral and central "olfactory" progenitors for distinct neuronal fates. The neural crest cells of the FnM fulfill this role in at least three ways (**Figure 3**): first, they provide signals that pattern additional signaling centers in adjacent epithelia that then drive neuronal as well as skeletal differentiation (Bhasin et al., 2003; Marcucio et al., 2005). Second, they signal directly to neural progenitors to modulate division, migration, or fate in the OE as well as Fb precursors that generate OB interneurons (LaMantia et al., 1993; Anchan et al., 1997; Whitesides et al., 1998; Tucker et al., 2006, 2008). Third, they provide molecular guidance cues to growing ORN axons (Whitesides and LaMantia, 1996; LaMantia et al., 2000; Rawson et al., 2010).

Our data indicates that only a subset of FnM neural crest cells produce RA, based upon *in vitro* transcriptional "indicator" assays with a monolayer of heterologous cells substituting for endogenous target epithelia (Whitesides et al., 1998; LaMantia et al., 2000; Bhasin et al., 2003). Moreover, *in vivo*, the activation of a similar RA signaling reporter in subsets of presumed RA-responsive cells or expression of RA-responsive genes in the OE and Fb (**Figure 3**) indicates that the neural crest-derived FnM provides a local source of RA to drive expression of downstream genes in cranial ectodermal and neural tube domains that eventually generate OE and OB neurons (LaMantia et al., 1993, 2000; Whitesides et al., 1998; Rawson and LaMantia, 2007). The RA signaling capacity of neural crest mesenchymal cells in the frontonasal processes and other sites of non-axial M/E apposition reflects local expression and activity of RA synthetic enzymes, including Raldh2 and Raldh3 (Berggren et al., 1999; Haselbeck et al., 1999; Niederreither et al., 1999, 2002, 2003; Mic et al., 2000; Suzuki et al., 2000; Mey et al., 2001). RA synthesis and activity can be further influenced by expression of retinoid binding proteins and differential expression and activity of RA receptors and binding proteins in adjacent neural crest or target epithelial cells (Perez-Castro et al., 1989; Maden et al., 1991; Ruberte et al., 1991; Gustafson et al., 1993; Lohnes et al., 1994; Whitesides et al., 1998). The expression of many of these molecules persists throughout through adulthood and may influence ongoing ORN genesis and differentiation in the adult OE and OB (Whitesides et al., 1998; Thompson Haskell et al., 2002; Haskell and LaMantia, 2005; Hagglund et al., 2006; Peluso et al., 2012; Paschaki et al., 2013; Micucci et al., 2014; Login et al., 2015).

A WATCH ON THE "RHINE": RHINENCEPHALIC MUTANTS, M/E INDUCTION, AND OLFACTORY DEVELOPMENT

Genetic analysis reinforced the essential contribution of M/E interactions between neural crest and additional local epithelial

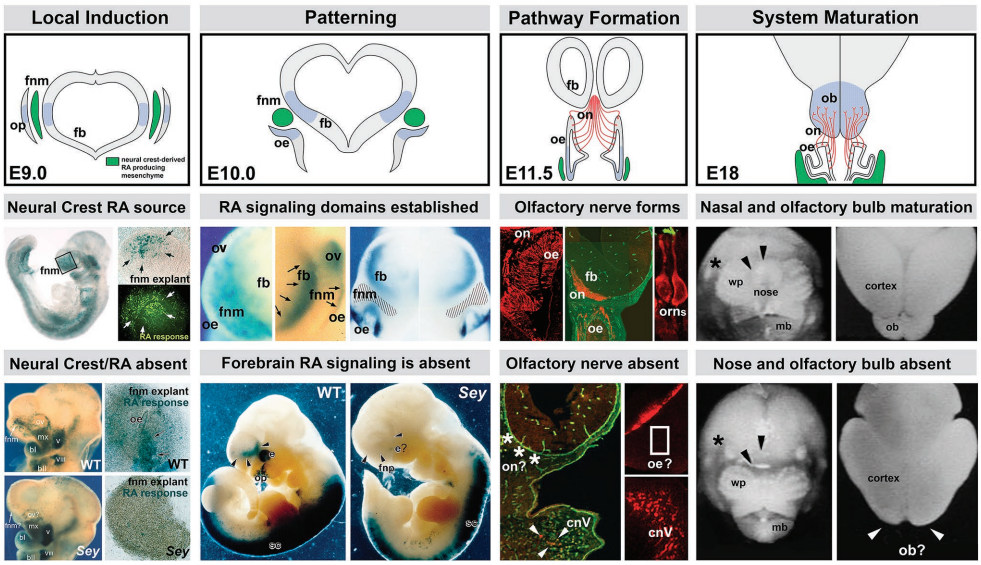

FIGURE 3 | The sequence of neural crest-mediated M/E induction and its consequences for local patterning, neuronal differentiation, and initial establishment of the axon growth and targeting from the olfactory placode. The ***top panels*** show the stepwise initial development of the olfactory placode (op; blue shading), olfactory epithelium (OE; blue shading), and olfactory receptor neurons (ORNs) and their axons that constitute the nascent olfactory nerve (ON; red). A sub-population of mesencephalic/diencephalic neural crest cells in the FnM (green) produce RA and establish domains of RA-mediated gene expression (blue shading) in the Fb as well as the olfactory periphery. This Fb domain will generate the olfactory bulb (OB), the target of the axons from the OE *via* the ON. The ***middle panels*** summarize the inductive, patterning, sensory neuron differentiation and axon outgrowth, peripheral and brain morphogenetic events diagramed in the **top panels**. The ***bottom panels*** show the disruption of neural crest-mediated M/E interaction in the *Pax6*$^{Sey/Sey}$ mutant and its consequences for each subsequent step of initial olfactory pathway formation (**top panel** adapted from LaMantia et al., 1993; **middle** and **bottom panels** adapted from LaMantia et al., 1993, 2000; Anchan et al., 1997; Balmer and LaMantia, 2004; Tucker et al., 2010).

or mesenchymal cells in the initial assembly of the primary olfactory pathway from nose to brain. We selected four fully or partially arhinencephalic mutants in which initial olfactory pathway morphogenesis is disrupted: the *Pax6* "*Small Eye*" mutation (Hill et al., 1991) in which both the OE and OB fail to form (Grindley et al., 1995; Anchan et al., 1997; Jimenez et al., 2000); The *Gli3 Extra Toes*^{J} mutation (Schimmang et al., 1992; Hui and Joyner, 1993) where the OE differentiates, but olfactory axons fail to enter the Fb in which the OB is absent (Sullivan et al., 1995; LaMantia, 1999; Balmer and LaMantia, 2004; Taroc et al., 2020); the *Shh* null mutant (Chiang et al., 1996; Ishibashi and McMahon, 2002; Hayhurst and McConnell, 2003), which is a model for the most extreme cases of holoprosencephaly or arhinencephaly – the clinical dysmorphologies that initially inspired DeMyer et al. to conclude that "the face predicts the brain" – and the *Fgf8*^{Neo} hypomorphic mutant in which ORN neurogenesis and OB morphogenesis is disrupted (Meyers et al., 1998; Kawauchi et al., 2005; Tucker et al., 2010). In each case, frontonasal and Fb M/E interactions are compromised with morphogenetic as well as cellular consequences for olfactory pathway development.

In the *Pax6*$^{-/-}$ mutant, the OB and OE are absent, and the anterior snout, maxilla, and mandible are either absent or dysmorphic (Grindley et al., 1995; Anchan et al., 1997; Enwright and Grainger, 2000). In this mutant, RA signaling is abolished in domains that generate the OE and OB due to the failure of the RA-producing neural crest to migrate into the frontonasal region. The absence of the neural crest derived mesenchymal cells, and the failure of placodal and ventral Fb RA-mediated M/E signaling prefigures the morphogenetic failure of both the OE and the OB (**Figure 3**). The residual mesenchyme from *Pax6*$^{Sey/Sey}$ cannot support olfactory neuron differentiation in WT pre-placodal ectoderm (LaMantia et al., 2000). Nevertheless, the capacity for RA responsiveness in both the cranial ectoderm and Fb neuroectoderm remains; however pharmacological activation of this responsiveness by exogenous RA fails to elicit recognizable differentiation of olfactory structures or their constituent neurons (Anchan et al., 1997).

The three additional mutants – *Gli3*, *Shh*, and *Fgf8* – provide further support for a primary role of M/E interactions that engage neural crest and adjacent epithelia in olfactory pathway development. In *Gli3*^{XtJ} homozygotes, the Fb neuroepithelium is refractory to RA signaling despite local production of RA by neural crest-derived frontonasal mesenchymal cells and the OB does not form (LaMantia, 1999). Axons from differentiated ORNs grow into the apparently normally patterned FnM; however, they mostly fail to enter the undifferentiated Fb, with the exception of a few misrouted axon fascicles that manage to fenestrate the Fb basal lamina (Whitesides and LaMantia, 1996; Balmer and LaMantia, 2004). *Shh*$^{-/-}$ mutants have a fused proboscis, and a single fused OE in which ORNs differentiate. This OE appears to be primarily "lateral" in its identity, surrounded by FnM that is also "lateral" based upon restricted expression of neural crest-associated markers,

including Pax7 (Mansouri et al., 1996; Monsoro-Burq, 2015). In the *Shh*$^{-/-}$ mutant, as in *Gli3*$^{-/-}$, where RA signaling (LaMantia, 1999; Maynard et al., 2013) as well as Shh signaling (Tole et al., 2000; Stamataki et al., 2005) is disrupted, ORN axons grow toward, but fail to enter, the dysmorphic Fb (Balmer and LaMantia, 2004).

Finally, in *Fgf8*$^{Neo/Neo}$ mutants, the expression levels of one of the inductive targets of the RA-producing FnM, *Fgf8* (see **Figure 2**), are substantially diminished (Meyers et al., 1998). ORN frequency in these mutants is diminished and their distribution altered due to disrupted proliferative capacities and neurogenic potential of distinct ORN precursor classes (Tucker et al., 2010). These changes parallel the disruption of OB differentiation in the dysmorphic Fb of *Fgf8*$^{Neo/Neo}$ mutants (Meyers et al., 1998; Kawauchi et al., 2005). These observations suggest that in the absence of downstream signaling molecules like Fgf8, whose local sources in the cranial ectoderm or Fb are patterned and maintained by neural crest-derived mesenchymal RA-producing cells (Bhasin et al., 2003), morphogenesis and assembly of the olfactory pathway fails. Thus, observations in WT and mutant embryos define the central role of neural crest in local M/E interactions, especially those mediated by RA signals provided by neural crest mesenchymal cells, for the coordination of morphogenesis and subsequent connectivity of the olfactory system during early stages of Fb development.

OTHER CRANIAL NEURAL CREST CELLS AND OTHER CRANIAL NERVES

The role of the neural crest in the patterning or differentiation in other placodal derivatives that establish additional cranial sensory specializations is less clear. In contrast to early "inductive" events that specify cranial sensory pre-placodal ectoderm (Jacobson, 1963; Maier et al., 2014; Moody and LaMantia, 2015; Thiery et al., 2020), the subsequent interactions between each of the placodes, once specified, and neural crest cells – aside from those that influence differentiation of the embryonic OE – are less well understood. Embryological experiments suggest that the neural crest is not essential for the initial placode induction (Begbie et al., 1999; Haworth et al., 2004). Thus, the initial specification of the preplacodal ectoderm that will generate neural progenitors for the olfactory, trigeminal, and epibranchial/sensory placodes, as well as the lens and otic placode, relies upon planar signals and transcriptional effectors within the cranial ectoderm, as well as extrinsic signals from the lateral head mesoderm and prechordal mesendoderm (Hintze et al., 2017), and this process is coincident with the specification of the neural crest at the neural plate border zone (Rogers et al., 2012; Saint-Jeannet and Moody, 2014).

In contrast, post-migratory neural crest cells have distinct intermediate functions as well as terminal fates during initial morphogenesis of the eye, ear, and cranial ganglia. In the developing eye, neural crest-derived mesenchymal cells establish a local source of Tgfβ ligands that suppresses lens fate in presumptive lens epithelium, a placodal derivative (Grocott et al., 2012). In addition, RA-mediated signaling between the optic cup epithelium (neural tube-derived) and the neural crest-derived mesenchyme surrounding the eye is essential for ocular morphogenesis (Creuzet et al., 2005; Matt et al., 2005; Bailey et al., 2006). Less is known about the role of neural crest in signaling during otic placode differentiation. Neural crest cells contribute to the middle ear as well as generating glial cells that ensheathe axons from the acoustic/spiral ganglion (Chapman, 2011; Thompson and Tucker, 2013; Ritter and Martin, 2019). There is also some evidence that neural crest cells contribute to the inner ear (Freyer et al., 2011). Signaling *via* RA and Fgf8 from partly defined sources contributes to A-P patterning of the otic placode ectoderm, which is presumably the source of sensory neurogenic precursors, as well as the periotic mesenchyme which generates middle ear bones and epithelia (Frenz et al., 2010; Bok et al., 2011; Nakajima, 2015). The otic placode epithelium, presomitic, somatic mesoderm, and periotic mesenchyme have been suggested as RA sources during initial otic vesicle patterning; however, the contribution of neural crest to periotic mesenchyme has not been considered in the context of signaling prior to differentiation. Thus, the role of neural crest derived M/E interactions in the eye and ear, vs. the nose, remains uncertain.

We have begun to assess interactions between neural crest and placodal cells underlying development of cranial somatosensory ganglia. The dual origin of cranial ganglion sensory neurons, as well as their divergent fates – primarily mechanoreceptive for placode descendants, nociceptive for those from the neural crest (D'Amico-Martel and Noden, 1983) – is well established, and our analyses in the mouse (Karpinski et al., 2016; Maynard et al., 2020a; Motahari et al., 2020) confirmed and extended earlier studies. Using transcriptional lineage tracing, we identified diversity within the neural crest population (**Figure 4**). Neural crest-associated progenitors in all cranial ganglia include a population derived from a *Wnt1* expressing domain in the dorsal/alar hindbrain (McMahon et al., 1992; Chai et al., 2000), and a population apparently not derived from this region that nevertheless expresses established neural crest markers including Foxd3 and Sox10. The proportions of these populations, placode-derived cells and each of the two molecularly distinct neural crest cell classes, are statistically similar in most cranial ganglia (Karpinski et al., 2016). In contrast, placode-derived populations predominate in the "special sense" organs – the OE and the inner ear. There is some uncertainty, however, over the contribution of the neural crest to initial populations of OE progenitors and early generated ORNs (Forni et al., 2011; Karpinski et al., 2016). It is also possible that at later fetal stages and in the adult OE, neural crest-derived progenitors can generate ORNs (Katoh et al., 2011; Suzuki et al., 2013). For auditory peripheral receptors and relay neurons, there is some evidence that subsets of sensory receptors (outer and inner hair cells) in the inner ear, as well as sensory relay neurons in the spiral ganglion (Cranial Nerve ganglion VIII; **Figure 4**), are derived from neural crest progenitors (Freyer et al., 2011).

Nevertheless, the four cranial ganglia responsible for the somatosensory regulation of orofacial sensory-motor integration:

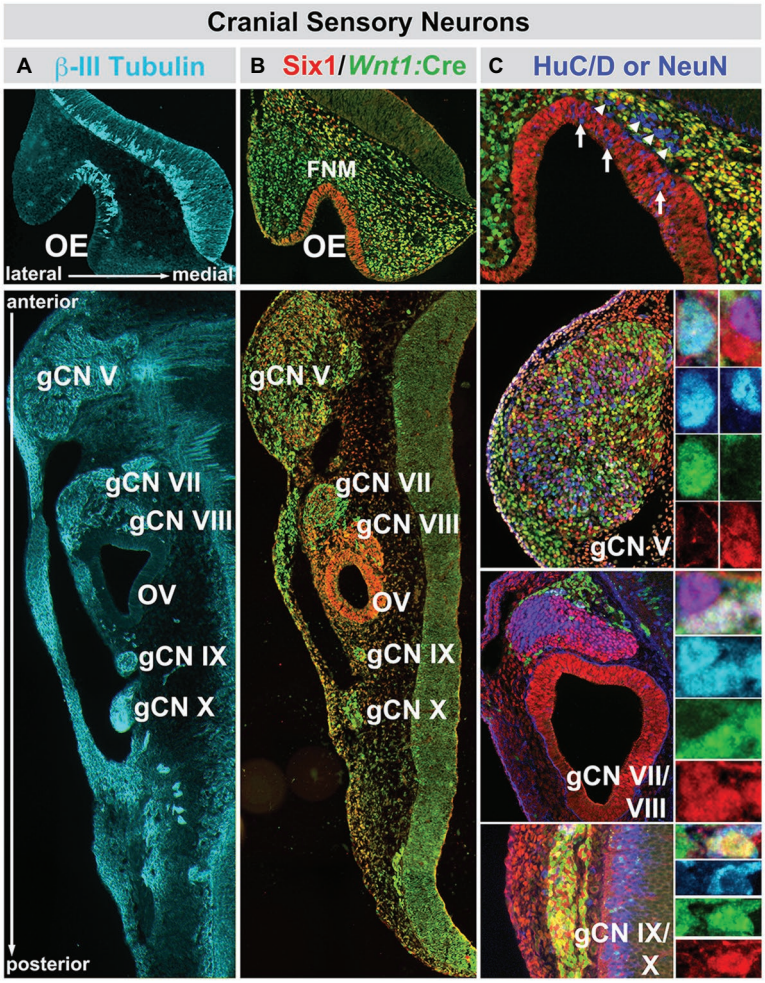

FIGURE 4 | The relationship between nascent cranial sensory neurons, ectodermal placode, and neural crest-derived neural progenitors and neuroblasts in the cranial sensory ganglia at midgestation (E10.5) in the mouse. **(A)** The neuronal microtubule protein βIII-tubulin is expressed in newly generated ORNs (OE, top panel) as well as cranial sensory neurons in the trigeminal (gCN V), facial (gCN VII), spiral (gCN VIII), glossopharyngeal (gCN IX), and vagal (gCN X) cranial nerve ganglia and their axons that extend toward central (OE, gCNV, VII, VIII, IX, and X) as well as peripheral (gCNV, VII, VIII, IX, and X) targets. **(B)** Six1 (red), a marker of placode-associated cells and *Wnt1:Cre* recombination-mediated expression of a conditional GFP reporter allele (green), shows the relationship between placode-associated cells and neural crest-derived cells in the OE, FnM and cranial ganglia. Cells in the OE are labeled exclusively by Six1. Cells in the FnM are uniformly labeled by the *Wnt1:Cre* reporter, but a subset of them in the lateral nasal process also expresses Six1. Each of the cranial nerve ganglia, except for gCN VIII, is composed of primarily Six1-expressing placode-derived cells. The mesenchyme between the cranial nerve ganglia and the hindbrain at this stage of development has cells that express Six1 as well as the *Wnt1:Cre* reporter, as is the case for the cranial epithelium in the periphery. **(C)** Relationship between Six1-expressing, Wnt1:Cre reporter-expressing, and HuC/D-expressing cells in the OE and cranial nerve ganglia. In the OE, HuC/D-expressing newly generated neurons (blue) are scattered through the epithelium and have downregulated Six1 (arrows). In addition, there is a population of HuC/D expressing neurons (arrowheads) in the FnM that have also downregulated Six1 and are not labeled by the *Wnt1:Cre* reporter. These cells are most likely the GnRH-expressing neurons that migrate from the OE to enter the ventral Fb along newly extending ORN axons at this stage of development. In gCN V, gCN VII, and gCN IX/X, HuC/D-expressing neurons are coincident with cells labeled by Six1, the *Wnt1:Cre* reporter, or both (adapted from Karpinski et al., 2016).

trigeminal (CNgV), facial (CNgVII), glossopharyngeal (CNgIX), and vagal (CNgX) are mosaics of substantial populations of placode-and neural crest-derived cells that condense with the cranial mesenchyme sometime after the anterior neural tube closes in most vertebrate embryos. Thus, for all cranial sensory neurons or the sensory organs in which they are found, neural crest-derived cells accumulate, interact with cranial ectodermal placodal cells, and either induce supporting structures or special sensory neurons or coalesce to form cranial ganglia after the translocation of placodal cells into the cranial mesenchyme. This confluence of neural crest and cranial ectoderm indicates that at the earliest stages of development, the fates of cells that will constitute the face and those that will comprise neural circuits in the peripheral and central nervous system that innervate the face (Cordes, 2001) are closely related. Parallel work in the spinal cord and its musculoskeletal or visceral targets suggests that coordination between early neural tube and peripheral patterning is essential for establishing appropriate

neural circuits to control limb and visceral targets (Philippidou and Dasen, 2013). Thus, like the development of the spinal cord and limb, the hindbrain and the face may reflect a singular developmental program that coordinates peripheral structures and the neural circuits that control these structures.

BEYOND THE FACE? A GENETIC DISORDER WITH FACE, LIMB, HEART, AND FB ANOMALIES

The coincidence of so-called minor physical anomalies – mild to severe malformations of craniofacial structures, including ears, eyes, and noses and the limbs – as well as increased coincidence of cardiovascular malformations in a number of clinically diagnosed behavioral syndromes like schizophrenia and autism or multiple genetic neurodevelopmental disorders (Tripi et al., 2008; Compton et al., 2011; Delice et al., 2016; Myers et al., 2017), led to an additional test of our central hypothesis: the coordinated regulation of neural crest-mediated M/E interaction may be central to optimal morphogenesis at each of the sites of non-axial induction, including limbs, face, heart, and Fb. Accordingly, this mechanism may be uniformly disrupted in disorders that include minor physical anomalies, cardiovascular malformations, and Fb developmental disruption – reflected in complex behavioral deficits that define clinically diagnosed neurodevelopmental disorders like schizophrenia and autistic spectrum disorder as well as several genetic neurodevelopmental syndromes.

We selected the microdeletion disorder 22q11.2 Deletion Syndrome (22q11DS), also known as DiGeorge or Velocardiofacial syndrome, to evaluate our hypothesis. 22q11DS is a global developmental disorder whose phenotypic spectrum includes highly penetrant cardiovascular malformations, as well as craniofacial anomalies, mild limb and digit anomalies, and a high frequency of behavioral difficulties that resemble clinically diagnosed neurodevelopmental disorders, including schizophrenia, autistic spectrum disorder, and attention deficit disorder, accompanied by altered brain morphology and function (Schneider et al., 2014; McDonald-McGinn et al., 2015; Rogdaki et al., 2020). 22q11DS, as the name suggests, is not caused by a single loss-of-function mutation but deletion of a limited number of genes: minimally 32 in humans (Morrow et al., 2018) and their subsequent approximately 50% diminished expression (Meechan et al., 2006; Maynard et al., 2008, 2013, 2020a). There is a high level of conservation of these genes, as a colinear set, across multiple vertebrates, including the mouse, in which 28 of the 32 minimally critically deleted genes are found adjacent to one another on murine Chromosome 16 (Meechan et al., 2015). There is remarkable homology of the colinear set of 22q11-deleted genes in multiple species, and their cellular, developmental, and homeostatic functions in a broad range of cells, tissues, and organs appear to be similar in most vertebrates – and even some invertebrates – analyzed thus far (Meechan et al., 2015; Motahari et al., 2019). A key aspect of 22q11 gene function across these species may be the apparent relationship to neural crest, and non-axial M/E signaling at midgestation, and its consequences for subsequent morphogenesis and neural circuit development.

LOCATION, LOCATION, LOCATION: RESTRICTED EXPRESSION AND ACTIVITY OF 22q11 GENES AT M/E SITES

The first question we asked was whether one, two, or a few of the genes deleted in 22q11DS were expressed at sites of non-axial M/E interaction where 22q11DS phenotypes will eventually arise: limb buds, cardiac-related/pharyngeal arches, craniofacial pharyngeal arches, and the cranial or FnM (Maynard et al., 2002, 2003). Rather than a few 22q11 deleted genes, we found that 21/28 are expressed selectively at these sites based upon qPCR analysis in micro-dissected samples of each M/E inductive site as well as whole mount *in situ* or immunolabeling (**Figure 5**). None of the 22q11 genes is known to selectively alter neural crest specification or migration (Motahari et al., 2019). Instead, many of these genes, including several candidates for specific 22q11DS phenotypes, seem to modulate either local patterning, differentiation, or signaling. Complete loss of function mutations of some of these genes lead to substantial dysmorphology at several sites of non-axial M/E induction (Scambler, 2010; Paronett et al., 2015; Motahari et al., 2019), while heterozygous deletion, usually in the context of broader 22q11 gene deletion, leads to variable dysmorphology or dysfunction in a variety of organ systems.

Two additional observations reinforce the conclusion that 22q11 genes, as a group, contribute to the local regulation of M/E interactions at sites of non-axial induction. First, disrupted signaling, particularly *via* RA, Fgfs, Bmps, or Wnts – all implicated in non-axial M/E signaling and morphogenesis – can recapitulate, at least partially, some of the phenotypes associated with 22q11DS (Frank et al., 2002; Bachiller et al., 2003; Vermot et al., 2003; Aggarwal et al., 2006; Huh and Ornitz, 2010; Guo et al., 2011). Several of these signaling pathways are sensitive to 22q11 gene dosage, based upon dysmorphic phenotypes or altered patterns and levels of gene expression in mouse models. There are genetic interactions between diminished dosage of 22q11 genes, particularly *Tbx1*, a 22q11 gene for cardiovascular and pharyngeal arch phenotypes, and the RA, Shh, Fgf, and Bmp signaling pathways (Garg et al., 2001; Ryckebusch et al., 2010; Maynard et al., 2013). Our data suggests that interactions between the 22q11 genes, RA and Shh signaling, are enhanced by full 22q11 deletion compared to that seen in $Tbx1^{+/-}$ mutants. Together, these observations suggest reciprocal local regulation for 22q11 gene dosage and cardinal signaling pathways at sites of non-axial accumulation of neural crest mesenchymal cells, neural crest-mediated M/E inductive interactions, and downstream morphogenetic mechanisms.

22q11DS has been classified as a neural crest disorder or "neurocristopathy" based upon the coincidence of cardiovascular and craniofacial phenotypes (Walker and Trainor, 2006; Vega-Lopez et al., 2018). The available evidence, however, indicates that, at least for the cardiovascular malformations, the differentiation capacity of the neural crest is not substantially targeted by 22q11

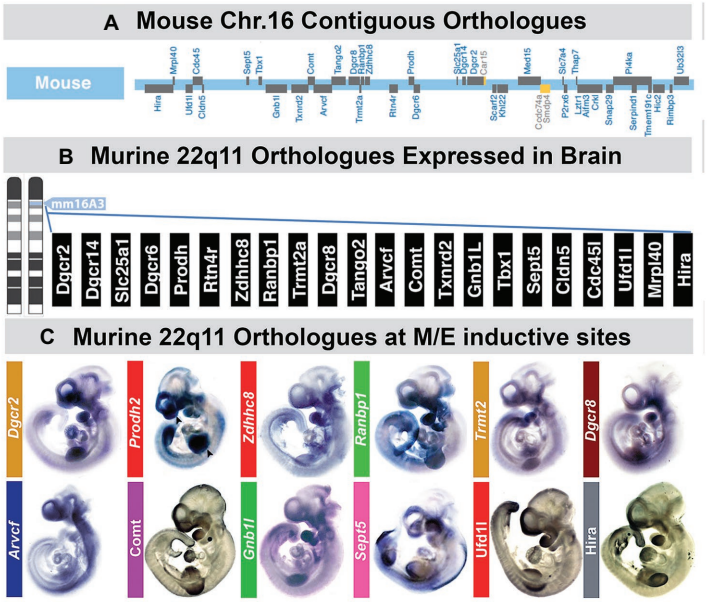

FIGURE 5 | A large subset of mouse orthologues of the genes on human Chr. 22 deleted in DiGeorge/22q11 Deletion syndrome (22q11DS) are expressed in the developing or adult brain as well as sites of neural crest-mediated M/E induction at midgestation. **(A)** The location on mouse chromosome 16 of 28/32 orthologues of the genes in the minimal critical deleted region of human chromosome 22 whose heterozygous deletion causes 22q11DS. **(B)** PCR, *in situ* hybridization, immunoblotting, and immunlocalization identify expression of 22 of the 28 murine 22q11 orthologues in the developing and adult mouse brain. **(C)** Multiple 22q11 orthologues are expressed uniformly at sites of neural crest-mediated M/E induction as well as in the nascent central nervous system in the midgestation mouse embryo (E10.5). The purple-blue label shows *in situ* hybridization labeling of mRNA for several 22q11 genes at these sites, and the brown label shows the localization of proteins encoded by three of the deleted genes (panel **A, B**, adapted from Meechan et al., 2015; panel **C** adapted from Motahari et al., 2019).

deletion or heterozygous loss of function of *Tbx1*, a 22q11 gene considered a candidate for the cardiovascular phenotype whose expression and activity is limited to the pharyngeal mesoderm and endoderm (Kelly et al., 2004; Arnold et al., 2006; Aggarwal et al., 2010). Instead, 22q11DS phenotypes may result from altered neural crest-mediated interactions with mesodermal or endodermal targets that express *Tbx1*. Our evidence suggest that a significant portion of the 22q11DS phenotypic spectrum reflects the coordinated expression of multiple 22q11 genes and their dosage-sensitive influence on neural crest-mediated M/E induction beyond that of *Tbx1* (Maynard et al., 2013, 2020a; Karpinski et al., 2014; Motahari et al., 2020). These 22q11 genes have reciprocal regulatory interactions with cardinal inductive signaling pathways critical for optimal M/E induction at each of the phenotypic sites. When these interactions are disrupted by diminished dosage of multiple 22q11 genes, altered M/E induction results in a sequence of pathogenic changes that contribute to the phenotypic spectrum associated with 22q11DS.

OTHER FACES, OTHER BRAINS: AN UNMAPPED MONOGENIC DISORDER WITH FACE, LIMB, AND BEHAVIORAL PHENOTYPES

The relationship between 22q11 genes and cardinal signaling pathways at sites of M/E interaction and pathogenesis of 22q11DS phenotypes suggests that mutations of additional genes that influence early neural crest-mediated M/E induction may result in craniofacial and brain anomalies in additional human genetic developmental disorders. To evaluate this possibility, we identified an apparently monogenic, homozygous autosomal recessive, human genetic disorder in a consanguineous pedigree (Manzini et al., 2010). Affected individuals had craniofacial and limb dysmorphology as well as Fb-related behavioral disruption. We mapped and identified the mutated gene and then assessed the timing and localization of expression of this gene during development in both human and mouse (**Figure 6**).

The proband for this study was an affected male with craniofacial and limb morphological/skeletal anomalies, dysarthria, developmental delay, and intellectual/cognitive impairment. Unaffected siblings had none of these phenotypes (**Figure 6**). In addition to these "core" morphological and behavioral features, this disorder was accompanied by spasticity, and some evidence of neurological degenerative change over the lifespan. The causal mutation for this disorder in the Omani pedigree was a novel variant of the *SPG20* gene (**Figure 6**) that encodes a protein called Spartin. Mutations in *SPG20* had been previously linked to Troyer Syndrome, a Hereditary Spastic Paraplegia variant identified in Amish pedigrees in which craniofacial phenotypes were not reported (Patel et al., 2002). Spartin is a microtubule interaction/intracellular trafficking-related protein thought to be involved in a range of cellular functions including microtubule dynamics, cytokinesis, endosome

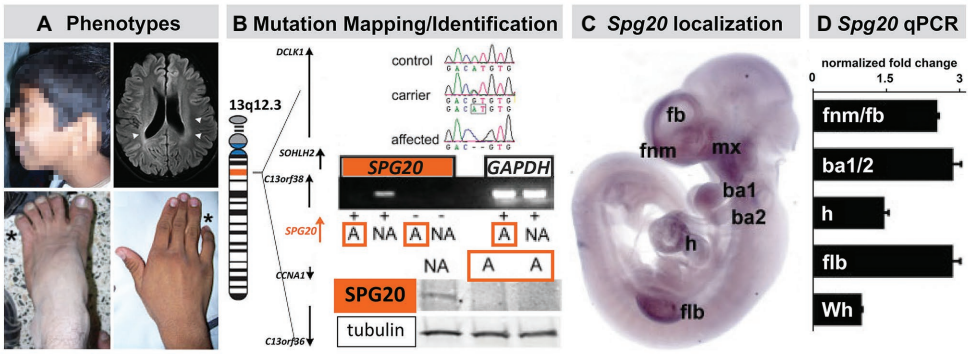

FIGURE 6 | The mutant gene in a rare monogenic disorder characterized clinically by craniofacial, limb, and Fb anomalies is initially expressed focally and maximally at sites of neural crest-mediated M/E induction. **(A)** Craniofacial, brain, hand (forelimb), and foot (hindlimb) anomalies in a 19-year-old male. This individual also had developmental delay, poor academic performance, and poor language skills from an early age. **(B)** Mapping and confirming the causal mutant gene for this Mendelian, monogenic disorder. The mutant gene SPG20, is a microtubule-interacting trafficking molecule involved in multiple signaling and metabolic cellular processes. The mutation in this Omani pedigree is a novel *SPG20* two base pair deletion mutation that results in undetectable expression of *SPG20* in fibroblasts from affected individuals in the pedigree, as well as undectectable Spartin protein expression. **(C)** Localization of *Spg20*, the murine orthologue of *SPG20* by *in situ* hybridization in an E10.5 mouse embryo, shows focal, selective expression at sites of neural crest-mediated M/E induction, including FnM and Fb, the maxillary process (mx), and as well as the nascent mandibular process (ba1), the hyoid process (ba2), the heart (h), and Flb. **(D)** qPCR in microdissected frontonasal mass/Fb, branchial arches, h and Flb confirms enhanced expression of *Spg20* at these M/E inductive sites. These expression levels, especially for the fnm/fb, ba1/2, and flb, are substantially elevated above the expression level detected in the whole E10.5 embryo (wh; adapted from Manzini et al., 2010).

trafficking, mitochondrial integrity, and signaling *via* EGF and Bmps (Bakowska et al., 2007; Renvoise et al., 2010, 2012; Nahm et al., 2013). The question that emerged was whether the craniofacial morphological anomalies, overbite, hypertelorism, expanded philtrum, low set, enlarged pinnae, and the hand and foot skeletal anomalies, might reflect early morphogenetic disruption due to altered M/E interaction vs. subsequent consequences of neurodegenerative mechanisms underlying progressive spasticity.

An apparent answer to this question emerged from a quantitative expression analysis in human brain and a parallel analysis in the mouse brain as well as the early mouse embryo (**Figure 6**). We found that *SPG20* is expressed at varying levels in distinct regions of the adult human brain and at a comparatively higher level in the fetal human brain. While this does not discount functional significance for Spartin function in the mature human brain, it indicates that its expression is neither ubiquitous nor robust. Instead, it suggests a role for Spartin in neural development. We replicated these observations in parallel regions of the mouse brain at parallel ages; however, in the mouse, we were also able to compare *Spg20* expression levels in distinct brain regions with those in the early embryo. We found that *Spg20* is maximally expressed in the whole mouse embryo at midgestation – E10 – at relative levels far greater than any reached in the postnatal developing or mature brain (Manzini et al., 2010). We then assessed regional localization in midgestation embryos in two ways: whole embryo *in situ* hybridization to assess spatial localization and qPCR in microdissected limb buds, branchial arches, hearts, and frontonasal mass/Fb: sites of M/E interaction that share mechanistic and morphogenetic properties (**Figure 6**). We found selective spatial expression of *Spg20* in the mesenchyme and epithelium of the limb buds, aortic and branchial arches, frontonasal mass (most likely the mesenchyme interposed between the Fb neuroepithelium and surface ectoderm), and Fb. There was limited expression in the hindbrain and no label above background in the spinal cord. qPCR analysis showed that the expression levels of *Spg20* were highest in microdissected samples of limb buds, branchial arches, and frontonasal mass/Fb from E10.5 embryos.

Thus, there is a maximal expression of a novel gene at sites of neural crest M/E induction, and mutation of this gene results in craniofacial and limb morphogenetic disruption, as well as developmental delay and cognitive deficits, presumably due to altered brain development. Thus, consistent with the assertion that "The Face Predicts the Brain," a combination of facial and brain phenotypes in this monogenic disorder predicted the pattern and schedule of expression and perhaps the activity of a single gene. These data suggest that Spartin may contribute to early non-axial morphogenetic mechanisms that depend upon coordinated neural crest-mediated M/E induction, including craniofacial, limb, and early Fb development.

PUTTING IT TOGETHER: FACE, BRAIN, AND BEHAVIOR

The predictive relationship between the face and the brain, extended to the limbs and the heart, provides a foundation to consider how development of neural circuits that organize distinct behaviors and peripheral structures that execute these behaviors might be coordinated. Such coordination may be facilitated by the ambassadorial signaling capacity of the A-P specified neural crest from distinct regions of the neural tube where related circuits will differentiate. The relationship

between A-P patterning of the hindbrain, the hindbrain neural crest, the craniofacial primordia, and the cranial nerves has been assessed in the context of A-P signaling and transcriptional regulation including that *via* Hox genes and other regulators of early axial patterning (Wilkinson, 1993; Parker and Krumlauf, 2020) or for their role in coordinating the differentiation of intrinsic brainstem neural circuits (Gavalas et al., 2003; Narita and Rijli, 2009; Di Bonito and Studer, 2017). Less attention has been paid to the integration of parallel development of craniofacial structures, cranial sensory and motor nerves, and neural circuits that coordinate essential oro-facial motor behaviors. We, therefore, sought to define a distinct behavior whose neural control and biomechanical execution might be facilitated by coordinated development of the face and brain *via* neural crest-mediated signaling.

The coordination of cranial sensory placode differentiation and that of brain targets, best exemplified by the development of the olfactory pathway, suggests the integrated development for neural circuits that relay and represent cranial "special" sensory information in one direction: from the periphery to the central nervous system. This information is further integrated by Fb "association" circuits to generate complex representations and behaviors from multi-modal sensory input (Sosulski et al., 2011; Uchida et al., 2014). In contrast, we sought to identify a behavior for which sensory inputs and motor function were more closely aligned and more precisely associated with peripheral craniofacial structures, independent, at least initially (Muscatelli and Bouret, 2018), of additional integration in Fb association circuits. One essential behavior emerged as a likely candidate: suckling, feeding, and swallowing (S/F/S; LaMantia et al., 2016; Maynard et al., 2020b). This fundamental, innate behavior shared across all mammals relies upon sequential sensory inputs and motor commands from cranial sensory and motor nerves in an approximate A-P order (**Figure 7**). This integrated sensory motor information subsequently activates distinct craniofacial structures to execute the biomechanical operations that permit optimal S/F/S from birth onward. Thus, S/F/S may represent a behavior whose neural and biomechanical bases reflect the predictive relationship between the face and the brain – or the brain and the face.

To evaluate this relationship, we once again began with the genetics of human developmental disorders and their consequences for morphological and behavioral disruption. The incidence of S/F/S difficulties from birth through early childhood – collectively referred to as pediatric dysphagia – is significantly elevated in genetic developmental syndromes as well as children with clinically diagnosed behavioral neurodevelopmental disorders (Berlin et al., 2011; Kleinert, 2017; Robertson et al., 2017; Bianco and Rota, 2018; Maynard et al., 2020b; Nordstrom et al., 2020), including infants and toddlers with 22q11DS (Eicher et al., 2000). Craniofacial and brain anomalies characterize all of these developmental disorders, including 22q11DS. If S/F/S is the result of coordinated neural and craniofacial development *via* neural crest-dependent signaling, genetic lesions that underlie developmental disorders should disrupt this process. This would indicate a predictive relationship between the face and brain in optimal circumstances and pathologic consequences when that relationship is disrupted in clinically or genetically diagnosed developmental disorders.

SWALLOW HARD: DOES THE FACE PREDICT THE BRAIN AND BEHAVIOR FOR S/F/S?

To assess whether distinct behavioral capacities reflect the predictive relationship between the face and the brain, we asked whether disrupted coordination of craniofacial and neural circuit differentiation in the *LgDel* mouse model of 22q11DS (Merscher et al., 2001; Meechan et al., 2015) might result in divergent S/F/S capacity that parallels dysphagia in infants and toddlers with 22q11DS. S/F/S is disrupted in *LgDel* mouse pups. We found changes in milk ingestion, transit, and distribution in *LgDel* pups. These pups have acute nasopharyngeal, as well as lung aspiration, naso-sinus/lung accumulation of milk protein accompanied by inflammation or infection in register with lymphocyte infiltration of these anomalous protein aggregates and diminished growth based on reduced rate of weight gain over the first 30 postnatal days (Karpinski et al., 2014; Yitsege et al., 2020). These disruptions parallel key features of pediatric dysphagia, including that in infants and toddlers with 22q11DS. Additional observations identify partially penetrant morphological changes in the *LgDel* mandible and midline craniofacial bones (Karpinski et al., 2014; Welby et al., 2020). The sizes, gene expression profiles, and differentiation of subsets of cranial sensory and motor neurons are disrupted in *LgDel* pups (Karpinski et al., 2014; Wang et al., 2020). Finally, altered hypoglossal motor neuron activity, including divergent dysregulation of protruder and retractor tongue muscles, is seen in *LgDel* pups (Wang et al., 2017, 2020), prefiguring craniofacial anomalies as well as disruption of tongue movement and feeding-related behaviors seen in adult *LgDel* mice (Welby et al., 2020).

It seemed possible that these disruptions of integrated craniofacial biomechanical morphogenesis, operation, and cranial sensory and motor control might be prefigured by disruption of an early developmental "program" that coordinates craniofacial and neural morphogenesis and differentiation to ensure optimal S/F/S at birth. To address this question, we first focused on potential changes in A-P hindbrain patterning that would have parallel consequences for establishing identity and signaling capacity for hindbrain cranial neural crest as well as cranial ectoderm and hindbrain neural progenitors. We reasoned that early disruption of a developmental program that coordinates face and brain development for optimal S/F/S might begin with aberrant specification of neural crest as well as neural tube progenitors of cranial/oropharyngeal skeletal elements and cranial nerve circuits (**Figure 7**).

We found an apparent RA-mediated "posteriorization" of anterior rhombomeres, altered expression of additional rhombomere-specific genes, and apparent increased RA signaling in posterior rhombomeres by E9.5 in the hindbrain of *LgDel* embryos (Karpinski et al., 2014; Motahari et al., 2020; Yitsege et al., 2020). This early disruption of hindbrain A-P

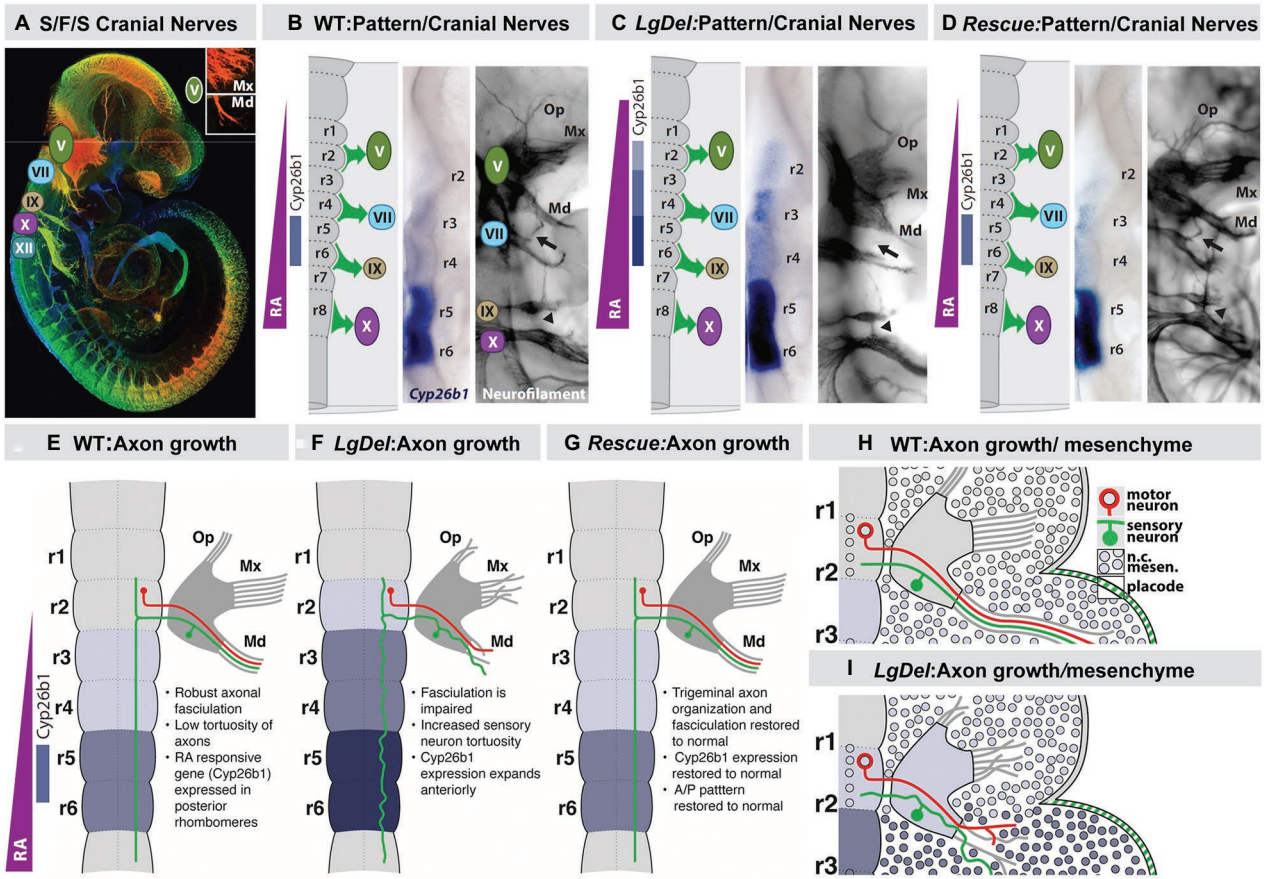

FIGURE 7 | Early disruption of hindbrain patterning alters anterior cranial nerve differentiation, prefiguring anomalous oropharyngeal sensory/motor function that likely contributes to suckling, feeding, and swallowing (S/F/S) difficulties in early post-natal *LgDel* mouse pups who carry a heterozygous deletion of the 28 murine orthologues of the genes deleted in 22q11DS. **(A)** The five cranial nerves that contribute to sensory/motor control of S/F/S have begun to differentiate by E10.5 in the mouse. In this preparation, they have been immunolabeled in the whole by the early marker for neuron and axons, βIII-tubulin, and visualized in a high-resolution confocal image in which embryo volume/depth is color coded, with warm colors representing structures close to the viewer and cooler colors representing those deeper in the embryo. The inset shows the multiple small axon fascicles that characterize the maxillary branch (Mx) of the trigeminal nerve (V) and the single fascicle of axons that forms as the mandibular branch in typically developing WT embryos. **(B)** The A-P array of S/F/S contributing cranial nerves is prefigured in E9.5 embryos by a gradient of RA-signaling that distinguishes posterior (r5,6) from anterior (r2,3) rhombomeres in the developing hindbrain. This posterior RA-dependent patterning, as well as opposing anterior signaling *via* Fgfs and Wnts, specifies the precursors of the cranial sensory neurons and hindbrain motor neurons that then differentiate as the cranial nerves within 24 h. **(C)** In *LgDel* E9.5 embryos, the gradient of RA signaling is enhanced in and shifted beyond posterior rhombomeres; it now elicits RA-regulated gene expression in anterior rhombomeres. Within a day, anterior cranial nerves, V (trigeminal) and VII (facial) are dysmorphic. The multiple axon fascicles normally seen in the Mx of V are diminished, the mandibular branch is similarly hypotrophic, and the facial nerve (VII) lacks its nascent anterior branch (arrow). In addition, the posterior cranial nerves IX (glossopharyngeal) and X (vagus) have either small axonal anastomoses (arrowhead) or in extreme cases are fused. **(D)** When RA signaling levels are diminished genetically by heterozygous deletion of the RA synthetic gene *Raldh2* in *LgDel* embryos ("Rescue"), the pattern of RA-dependent gene expression in the anterior rhombomeres returns to that seen in the WT. In parallel, initial differentiation of the nascent trigeminal and facial nerve is restored to the WT state. The ophthalamic (Op), Mx, and mandibular branches of the trigeminal nerve (V) extend toward their targets as in the WT with similar degrees of fasciculation. The facial nerve branches appropriately (arrow). The fusion of the posterior cranial nerves IX and X persists, most likely because this reflects the disrupted differentiation of cardiovascular targets due to Tbx1 heterozygous deletion, independent of hindbrain RA-dependent A-P patterning. **(E–H)** Schematics of the relationship between RA-dependent hindbrain patterning and the growth and trajectory of individual trigeminal motor and sensory axons in the WT embryo. Individual trigeminal motor axons, as well as primarily placodal derived trigeminal sensory axons, respond differently as they interact with neural crest derived mesenchymal substrates in the periphery whose A-P identity has been presumably altered by enhanced RA signaling in the anterior rhombomeres.

patterning was accompanied by a 22q11 deletion-specific changes in position and initial axon outgrowth of the trigeminal nerve (CN V) in *LgDel* embryos (Karpinski et al., 2014; Maynard et al., 2020a; Motahari et al., 2020; Yitsege et al., 2020). We did not see these changes of initial CN V morphology and axon growth in $Tbx1^{+/-}$ embryos where posterior cranial nerve disruptions have been reported previously (Vitelli et al., 2002; Calmont et al., 2011, 2018). In contrast, they were enhanced in $Ranbp1^{-/-}$ embryos (Paronett et al., 2015) in which the mutant gene, *Ranbp1*, is typically expressed in premigratory neural crest and at sites of M/E induction (Maynard et al., 2002, 2003). Thus, in $Ranbp1^{-/-}$ embryos,

the posterior shift of rhombomere patterning, based upon ectopic RA-regulated gene expression, is far more prominent than that in *LgDel*, as is disruption of CN V differentiation (Motahari et al., 2020).

We confirmed the RA-dependence of this hindbrain patterning change in *LgDel* and its relationship to initial cranial nerve dysmorphology *via* genetic rescue of the anomalous RA-dependent shift in patterning. We diminished RA signaling by approximately 20% (Maynard et al., 2013) using a heterozygous null allele of the rate limiting RA synthetic enzyme *Raldh2* (Zhao et al., 1996; Niederreither et al., 1999). In these compound, *LgDel*:*Raldh2*$^{+/-}$ embryos at E9.5, hindbrain patterning, and RA-dependent gene expression, detected by *in situ* hybridization (**Figure 7**) approximates the WT pattern (**Figure 7**), as does CN V differentiation and appropriately directed axon growth (Karpinski et al., 2014; Motahari et al., 2020). To confirm this impression based upon *in situ* hybridization, we performed qPCR for Cyp26b1 message, as well as that of three other RA-regulated genes: *Gli1*, *Rarα* and *Hoxa2*, in microdissected E9.5 hindbrains from E9.5 WT, *LgDel*, and *LgDel:Raldh2*$^{+/-}$ embryos. The mRNA levels for all four genes are significantly elevated above WT in the *LgDel* hindbrain and return to WT levels in the *LgDel:Raldh2*$^{+/-}$ hindbrain (Karpinski et al., 2014). Thus, the return of RA regulated gene expression toward WT A-P patterns and WT expression levels in *LgDel* hindbrain at E9.5 prefigures CN V differentiation in *LgDel* that is also indistinguishable from the WT by E10.5.

The RA sources that lead to altered hindbrain patterning in *LgDel* embryos remain uncertain. There is evidence that graded, as well as focal RA, signaling, activated by RA synthesized in the anterior somites as well as in the neural tube, leads to the typical RA-mediated pattern of posterior vs. anterior gene expression in the hindbrain, as well as in the differentiating cervical and lumbar spinal cord (Colbert et al., 1993; McCaffery and Drager, 1994; Maden et al., 1998; Gavalas and Krumlauf, 2000). It is uncertain whether the posteriorized pattern of gene expression in *LgDel* reflects enhanced RA production from these established sources or a shift in RA-synthetic capacity of hindbrain neural crest, migrating into the mesenchyme adjacent to anterior rhombomeres. Subsets of these neural crest mesenchymal cells produce RA (see **Figure 2**) once they reach the branchial arches (Bhasin et al., 2003), and they may do so ectopically to alter A-P patterning in the *LgDel* hindbrain.

These initial disruptions of hindbrain patterning, craniofacial, and cranial nerve development are accompanied by divergent differentiation of neural crest-derived cranial sensory neurons and the additional sensory and motor neurons, derived from the trigeminal placode and hindbrain neuroepithelium, respectively, with which they interact. Cell biological and lineage analysis, as well as transcriptomic comparison of WT and *LgDel* trigeminal ganglia (CNgV), indicates that the proportions of neural crest-derived and placode-derived sensory neurons in *LgDel* CNgV are altered, with placode cells and related transcripts predominating (Karpinski et al., unpublished; Maynard et al., 2020a). These changes are matched by altered mRNA transcript levels of multiple neural crest and placode-associated genes in the embryonic trigeminal ganglion (Maynard et al., 2020a), including regulators of placode (*Six1*) and neural crest-associated transcription factors (*Sox10*, *Foxd3*, *Cited4*). The proportional change of placodal vs. neural crest-derived CNgV sensory neurons reflects altered local cell-cell interactions as the ganglion coalesces that prefigure premature asymmetric neurogenic divisions by neural crest-derived CNgV progenitors (Karpinski et al., unpublished). These changes are paralleled by disrupted initial growth of CN V sensory and motor axons (Motahari et al., 2020). Aberrant axons at this early stage originate primarily in placode-derived sensory neurons or hindbrain-derived motor neurons; however, they interact extensively with anomalously patterned, transcriptionally divergent *LgDel* neural crest (**Figure 7**), both within CNgV and in their maxillary and mandibular targets composed largely of neural crest-derived mesenchymal cells (Motahari et al., 2020).

This early divergence of the developmental program coordinating the craniofacial periphery, cranial nerves, and hindbrain essential for optimal S/F/S prefigure dysfunction and cellular changes in cranial motor and sensory neurons in nursing *LgDel* pups. Levels of expression of genes associated with neural crest-derived nociceptive neurons in CNgV are altered in *LgDel* P8 pups (Karpinski et al., unpublished). Cranial motor neurons essential for S/F/S are also compromised in *LgDel* pups. Intrinsic excitable properties, firing rates, and effectiveness of excitatory vs. inhibitory inputs onto hypoglossal and laryngeal motor neurons are compromised in *LgDel* pups (Wang et al., 2017, 2020). These changes differ for hypoglossal motor neurons that project to protruder vs. retractor muscles of the tongue, and there are selective changes in dendritic architecture for these two target muscle-defined neuron classes (Wang et al., 2020). Additional analyses indicate similar physiological changes in laryngeal motor neurons (Caudill et al., unpublished). Finally, we found that the physiological changes in hypoglossal motor neurons are accompanied by cytological changes in distribution, morphology, and apparent neurotransmitter content of GABAergic presumed inhibitory synapses (Popratiloff et al., unpublished). Thus, multiple neuronal types, sensory neurons derived from the neural crest, as well as placode-derived sensory and hindbrain-generated motor neurons that project to oropharyngeal targets whose development relies upon the neural crest, are compromised by 22q11 deletion-dependent altered patterning of hindbrain neural crest and neural tube cells essential for morphogenetic interactions that underlie craniofacial and neuronal differentiation for optimal S/F/S.

MANY FACES (AND BRAINS) IN THE CROWD

DeMyer et al. described the face's capacity to "predict" the brain in the context of craniofacial and neurodevelopmental pathology; however, it is unlikely that this relationship serves primarily as a target for morphogenetic and behavioral pathology (LaMantia, 1999; Fish, 2016; Maynard et al., 2020b).

Instead, the predictive relationship between the face and the brain may reflect adaptive flexibility that matches craniofacial specializations for sensation, as well as facial and oropharyngeal movement in individuals, as well as across vertebrate species where the cranial sensory and musculoskeletal interface for distinct environments – aquatic, terrestrial, and arboreal modes of sensory detection, breathing, food ingestion, and facial expression must be optimized for maximal adaptive advantage (Kuratani et al., 2013; Fish, 2019; York et al., 2020). This requirement for adaptive flexibility to match the face and the brain with environment and niche may be solved by deploying neural crest cells, in varying quantities with modest changes in molecular identities and genetic control networks (Depew et al., 2005; Yu, 2010; Moody and LaMantia, 2015). Once in place, similarly modest variations of neural crest/placode M/E interaction, signaling pathways, and downstream transcriptional regulation (Cotney et al., 2013; Graf et al., 2016; Dubey et al., 2018; Williams and Bohnsack, 2019; Dash and Trainor, 2020) could result in species-specific distinctions in register with demands of adaptation and selection. Such flexibility in individuals or species for neural crest as inductive ambassadors would yield substantial adaptive capacity. Accordingly, distinctions between craniofacial structures and related neural circuits in fish, frogs, birds, and mammals may reflect quantitatively modified M/E interactions that coordinate the face and the brain rather than divergent, novel mechanisms for each of these species to "put on" an adaptive face and build the neural circuits to control it effectively.

MIRROR IMAGES: DOES THE FACE PREDICT THE BRAIN OR THE BRAIN PREDICT THE FACE?

The sum of the evidence on coordination of craniofacial and neural development suggests that the provocative proposal of DeMyer et al. can easily be rephrased in mirror image: *the brain predicts the face*. This reflection is due primarily to the critical role played by subsets of mesenchymal neural crest cells, derived from distinct regions of the neural tube, in inducing local patterned expression of key signaling molecules and downstream effectors *via* M/E interaction to drive craniofacial and central neural circuit differentiation. Indeed, this predictive relationship between the development of neural circuits and their peripheral targets due to neural crest-mediated M/E induction is likely to constrain differentiation of the spinal cord, dorsal root ganglia, and limbs (Philippidou and Dasen, 2013), morphogenesis of the developing heart and development of its autonomic and central innervation (Vegh et al., 2016), auditory sensory differentiation and brainstem auditory circuits (Frank and Goodrich, 2018), sensory and motor circuits for cranial somatosensation (Erzurumlu et al., 2010; Kitazawa and Rijli, 2018),

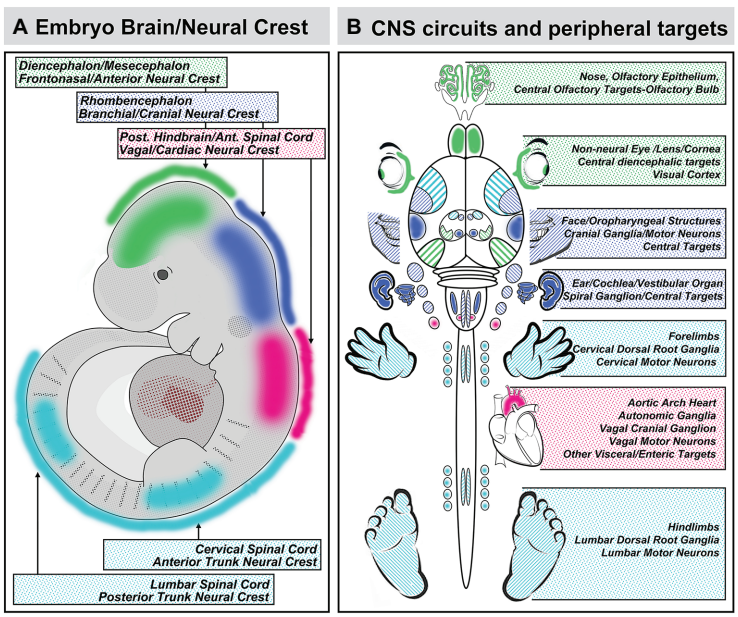

FIGURE 8 | Coordination of A-P identity in the nascent central nervous system and peripheral sites of neural crest-mediated M/E induction prefigures coordinated differentiation of peripheral sensory organs, the heart and viscera, and the limbs as well as neural circuits that control each structure in the peripheral and central nervous system. **(A)** A summary of the A-P locations in the neural tube that generate neural crest and the brain regions they reflect. **(B)** The potential relationship between peripheral structures, sensory organs, and sensory ganglia induced or patterned by non-axial neural crest-mediated M/E interactions and the central neural circuits that control the function of these structures. It is unclear whether the coordination of peripheral induction *via* the neural crest in the A-P axis and corresponding regions of the neural tube has a direct influence on the regional differentiation of anterior Fb regions that process relevant information, with the exception of the OB. The locations of the relevant regions of the cerebral cortex that receive thalamic (diencephalic) inputs from relay nucleic for vision (eye), audition (ear), and somatosensation (sensory cranial ganglia) are indicated for completeness.

ocular differentiation and visual relay circuits (Petros et al., 2008; Fuhrmann, 2010), in addition to the primary olfactory pathway as well as S/F/S oropharynageal structures and circuits (**Figure 8**). In each instance, coordination of central neural circuit differentiation and peripheral target morphogenesis is at least constrained or at most controlled by the initial A-P identities of the neural crest cells that depart the neural tube and the neural progenitors with the same A-P identities that remain.

There is, however, an important transformation of the fundamental mechanisms for coordinated craniofacial and neural circuit development implied by the mirror image of dictum of DeMyer et al. If the brain predicts the face rather than the face predicting the brain, the fundamental pathogenic divergence in genetic or clinically diagnosed disorders that include behavioral and craniofacial disruption as key features may actually occur at the very earliest stages of *brain* development: when neural crest as well as neural stem cells in the nascent neural plate and tube begin to acquire appropriate positional identities and developmental capacities. This event precedes coalescence of the neural crest in the differentiating neural tube and its departure for M/E inductive sites (Huang and Saint-Jeannet, 2004; Sauka-Spengler and Bronner-Fraser, 2008; Stuhlmiller and Garcia-Castro, 2012). It relies upon an extensive gene and signaling network that provides a substantial set of targets for mutation, as well as environmental disruption. Thus, when the presumptive brain – neural stem cells in the neural plate and tube – is disrupted, neither the brain and the neural circuits it comprises, nor the face and the sensory specializations it will help build acquire typical, optimal states of differentiation. In this hall of mirrors, the brain does indeed predict the face before the face predicts the brain.

AUTHOR CONTRIBUTIONS

The sole author conceived, wrote, edited, and illustrated the manuscript.

FUNDING

This work has been funded by the National Institutes of Health, Eunice Kennedy Shriver National Institute of Child Health and Human Development grants HD083157 and HD083157, as well as the Simons Foundation Autism Research Initiative 342005. Past funding sources, dating back to the early 1990s have included the Sloan Foundation, the March of Dimes, the National Down syndrome Society, NARSAD, the National Institute of Mental Health and the National Institute for Deafness and Communication Disorders.

ACKNOWLEDGMENTS

Melissa Colbert and Elwood Linney joined me for the initial work on retinoid signaling, beginning in the early 1990s. Their collaborative generosity was invaluable. The members of my lab have inspired this work over 30 years, especially John Whitesides, Ray Anchan, Gloria Haskell, Eric Tucker, and Tom Maynard. I thank Michael Fox and Tom Maynard for helpful comments on the manuscript. The work in my laboratory has been supported by the NIMH, NICHD, NIDCD, The Sloan Foundation, The National Down Syndrome Society, NARSAD, The March of Dimes, and The Simons Foundation Autism Research Initiative (SFARI).

REFERENCES

Aggarwal, V. S., Carpenter, C., Freyer, L., Liao, J., Petti, M., and Morrow, B. E. (2010). Mesodermal Tbx1 is required for patterning the proximal mandible in mice. *Dev. Biol.* 344, 669–681. doi: 10.1016/j.ydbio.2010.05.496

Aggarwal, V. S., Liao, J., Bondarev, A., Schimmang, T., Lewandoski, M., Locker, J., et al. (2006). Dissection of Tbx1 and Fgf interactions in mouse models of 22q11DS suggests functional redundancy. *Hum. Mol. Genet.* 15, 3219–3228. doi: 10.1093/hmg/ddl399

Akiyama, H., Kim, J. E., Nakashima, K., Balmes, G., Iwai, N., Deng, J. M., et al. (2005). Osteo-chondroprogenitor cells are derived from Sox9 expressing precursors. *Proc. Natl. Acad. Sci. U. S. A.* 102, 14665–14670. doi: 10.1073/pnas.0504750102

Alexander, C., Piloto, S., Le Pabic, P., and Schilling, T. F. (2014). Wnt signaling interacts with bmp and edn1 to regulate dorsal-ventral patterning and growth of the craniofacial skeleton. *PLoS Genet.* 10:e1004479. doi: 10.1371/journal.pgen.1004479

Anchan, R. M., Drake, D. P., Haines, C. F., Gerwe, E. A., and LaMantia, A. S. (1997). Disruption of local retinoid-mediated gene expression accompanies abnormal development in the mammalian olfactory pathway. *J. Comp. Neurol.* 379, 171–184.

Arnold, J. S., Werling, U., Braunstein, E. M., Liao, J., Nowotschin, S., Edelmann, W., et al. (2006). Inactivation of Tbx1 in the pharyngeal endoderm results in 22q11DS malformations. *Development* 133, 977–987. doi: 10.1242/dev.02264

Bachiller, D., Klingensmith, J., Shneyder, N., Tran, U., Anderson, R., Rossant, J., et al. (2003). The role of chordin/bmp signals in mammalian pharyngeal development and DiGeorge syndrome. *Development* 130, 3567–3578. doi: 10.1242/dev.00581

Bailey, A. P., Bhattacharyya, S., Bronner-Fraser, M., and Streit, A. (2006). Lens specification is the ground state of all sensory placodes, from which FGF promotes olfactory identity. *Dev. Cell* 11, 505–517. doi: 10.1016/j.devcel.2006.08.009

Bakowska, J. C., Jupille, H., Fatheddin, P., Puertollano, R., and Blackstone, C. (2007). Troyer syndrome protein spartin is mono-ubiquitinated and functions in EGF receptor trafficking. *Mol. Biol. Cell* 18, 1683–1692. doi: 10.1091/mbc.e06-09-0833

Balinsky, B. I. (1956). A new theory of limb induction. *Proc. Natl. Acad. Sci. U. S. A.* 42, 781–785. doi: 10.1073/pnas.42.10.781

Balmer, C. W., and LaMantia, A. S. (2004). Loss of Gli3 and Shh function disrupts olfactory axon trajectories. *J. Comp. Neurol.* 472, 292–307. doi: 10.1002/cne.20053

Balmer, C. W., and LaMantia, A. S. (2005). Noses and neurons: induction, morphogenesis, and neuronal differentiation in the peripheral olfactory pathway. *Dev. Dyn.* 234, 464–481. doi: 10.1002/dvdy.20582

Barlow, G. M., Lyons, G. E., Richardson, J. A., Sarnat, H. B., and Korenberg, J. R. (2002). DSCAM: an endogenous promoter drives expression in the developing CNS and neural crest. *Biochem. Biophys. Res. Commun.* 299, 1–6. doi: 10.1016/s0006-291x(02)02548-2

Begbie, J., Brunet, J. F., Rubenstein, J. L., and Graham, A. (1999). Induction of the epibranchial placodes. *Development* 126, 895–902.

Berggren, K., McCaffery, P., Drager, U., and Forehand, C. J. (1999). Differential distribution of retinoic acid synthesis in the chicken embryo as determined by immunolocalization of the retinoic acid synthetic enzyme, RALDH-2. *Dev. Biol.* 210, 288–304. doi: 10.1006/dbio.1999.9286

Berlin, K. S., Lobato, D. J., Pinkos, B., Cerezo, C. S., and LeLeiko, N. S. (2011). Patterns of medical and developmental comorbidities among children presenting with feeding problems: a latent class analysis. *J. Dev. Behav. Pediatr.* 32, 41–47. doi: 10.1097/DBP.0b013e318203e06d

Bhasin, N., Maynard, T. M., Gallagher, P. A., and LaMantia, A. S. (2003). Mesenchymal/epithelial regulation of retinoic acid signaling in the olfactory placode. *Dev. Biol.* 261, 82–98. doi: 10.1016/s0012-1606(03)00295-1

Bianco, E., and Rota, D. (2018). Oral findings in Rett syndrome: an update and review of the literature. *Dent. Med. Probl.* 55, 441–445. doi: 10.17219/dmp/99203

Bok, J., Raft, S., Kong, K. A., Koo, S. K., Drager, U. C., and Wu, D. K. (2011). Transient retinoic acid signaling confers anterior-posterior polarity to the inner ear. *Proc. Natl. Acad. Sci. U. S. A.* 108, 161–166. doi: 10.1073/pnas.1010547108

Calmont, A., Anderson, N., Suntharalingham, J. P., Ang, R., Tinker, A., and Scambler, P. J. (2018). Defective vagal innervation in murine Tbx1 mutant hearts. *J. Cardiovasc. Dev. Dis.* 5:49. doi: 10.3390/jcdd5040049

Calmont, A., Thapar, N., Scambler, P. J., and Burns, A. J. (2011). Absence of the vagus nerve in the stomach of Tbx1−/− mutant mice. *Neurogastroenterol. Motil.* 23, 125–130. doi: 10.1111/j.1365-2982.2010.01615.x

Chai, Y., Jiang, X., Ito, Y., Bringas, P. Jr., Han, J., Rowitch, D. H., et al. (2000). Fate of the mammalian cranial neural crest during tooth and mandibular morphogenesis. *Development* 127, 1671–1679.

Chapman, S. C. (2011). Can you hear me now? Understanding vertebrate middle ear development. *Front. Biosci.* 16, 1675–1692. doi: 10.2741/3813

Chiang, C., Litingtung, Y., Lee, E., Young, K. E., Corden, J. L., Westphal, H., et al. (1996). Cyclopia and defective axial patterning in mice lacking sonic hedgehog gene function. *Nature* 383, 407–413. doi: 10.1038/383407a0

Colbert, M. C., Linney, E., and LaMantia, A. S. (1993). Local sources of retinoic acid coincide with retinoid-mediated transgene activity during embryonic development. *Proc. Natl. Acad. Sci. U. S. A.* 90, 6572–6576. doi: 10.1073/pnas.90.14.6572

Compton, M. T., Chan, R. C., Walker, E. F., and Buckley, P. F. (2011). Minor physical anomalies: potentially informative vestiges of fetal developmental disruptions in schizophrenia. *Int. J. Dev. Neurosci.* 29, 245–250. doi: 10.1016/j.ijdevneu.2010.10.006

Cordes, S. P. (2001). Molecular genetics of cranial nerve development in mouse. *Nat. Rev. Neurosci.* 2, 611–623. doi: 10.1038/35090039

Cotney, J., Leng, J., Yin, J., Reilly, S. K., DeMare, L. E., Emera, D., et al. (2013). The evolution of lineage-specific regulatory activities in the human embryonic limb. *Cell* 154, 185–196. doi: 10.1016/j.cell.2013.05.056

Creuzet, S., Vincent, C., and Couly, G. (2005). Neural crest derivatives in ocular and periocular structures. *Int. J. Dev. Biol.* 49, 161–171. doi: 10.1387/ijdb.041937sc

D'Amico-Martel, A., and Noden, D. M. (1983). Contributions of placodal and neural crest cells to avian cranial peripheral ganglia. *Am. J. Anat.* 166, 445–468. doi: 10.1002/aja.1001660406

Dash, S., and Trainor, P. A. (2020). The development, patterning and evolution of neural crest cell differentiation into cartilage and bone. *Bone* 137:115409. doi: 10.1016/j.bone.2020.115409

Delice, M., Gurbuz, O., Oflezer, C., Kurt, E., and Mandali, G. (2016). Palate size and shape in schizophrenia. *Psychiatry Res.* 244, 273–278. doi: 10.1016/j.psychres.2016.05.035

Demyer, W., Zeman, W., and Palmer, C. G. (1964). The face predicts the brain: diagnostic significance of median facial anomalies for holoprosencephaly (arhinencephaly). *Pediatrics* 34, 256–263.

Depew, M. J., Simpson, C. A., Morasso, M., and Rubenstein, J. L. (2005). Reassessing the dlx code: the genetic regulation of branchial arch skeletal pattern and development. *J. Anat.* 207, 501–561. doi: 10.1111/j.1469-7580.2005.00487.x

Di Bonito, M., and Studer, M. (2017). Cellular and molecular underpinnings of neuronal assembly in the central auditory system during mouse development. *Front. Neural Circuits* 11:18. doi: 10.3389/fncir.2017.00018

Dubey, A., Rose, R. E., Jones, D. R., and Saint-Jeannet, J. P. (2018). Generating retinoic acid gradients by local degradation during craniofacial development: one cell's cue is another cell's poison. *Genesis* 56:e23091. doi: 10.1002/dvg.23091

Edlund, R. K., Birol, O., and Groves, A. K. (2015). The role of foxi family transcription factors in the development of the ear and jaw. *Curr. Top. Dev. Biol.* 111, 461–495. doi: 10.1016/bs.ctdb.2014.11.014

Eicher, P. S., McDonald-Mcginn, D. M., Fox, C. A., Driscoll, D. A., Emanuel, B. S., and Zackai, E. H. (2000). Dysphagia in children with a 22q11.2 deletion: unusual pattern found on modified barium swallow. *J. Pediatr.* 137, 158–164. doi: 10.1067/mpd.2000.105356

Enwright, J. F. 3rd, and Grainger, R. M. (2000). Altered retinoid signaling in the heads of small eye mouse embryos. *Dev. Biol.* 221, 10–22. doi: 10.1006/dbio.2000.9652

Erickson, C. A. (1985)., Control of neural crest cell dispersion in the trunk of the avian embryo. *Dev. Biol.* 111, 138–157. doi: 10.1016/0012-1606(85)90442-7

Erzurumlu, R. S., Murakami, Y., and Rijli, F. M. (2010). Mapping the face in the somatosensory brainstem. *Nat. Rev. Neurosci.* 11, 252–263. doi: 10.1038/nrn2804

Fish, J. L. (2016). Developmental mechanisms underlying variation in craniofacial disease and evolution. *Dev. Biol.* 415, 188–197. doi: 10.1016/j.ydbio.2015.12.019

Fish, J. L. (2019). Evolvability of the vertebrate craniofacial skeleton. *Semin. Cell Dev. Biol.* 91, 13–22. doi: 10.1016/j.semcdb.2017.12.004

Forni, P. E., Taylor-Burds, C., Melvin, V. S., Williams, T., and Wray, S. (2011). Neural crest and ectodermal cells intermix in the nasal placode to give rise to GnRH-1 neurons, sensory neurons, and olfactory ensheathing cells. *J. Neurosci.* 31, 6915–6927. doi: 10.1523/JNEUROSCI.6087-10.2011

Frank, D. U., Fotheringham, L. K., Brewer, J. A., Muglia, L. J., Tristani-Firouzi, M., Capecchi, M. R., et al. (2002). An Fgf8 mouse mutant phenocopies human 22q11 deletion syndrome. *Development* 129, 4591–4603.

Frank, M. M., and Goodrich, L. V. (2018). Talking back: development of the olivocochlear efferent system. *Wiley Interdiscip. Rev. Dev. Biol.* 7:e324. doi: 10.1002/wdev.324

Frenz, D. A., Liu, W., Cvekl, A., Xie, Q., Wassef, L., Quadro, L., et al. (2010). Retinoid signaling in inner ear development: a "goldilocks" phenomenon. *Am. J. Med. Genet. A* 152A, 2947–2961. doi: 10.1002/ajmg.a.33670

Freyer, L., Aggarwal, V., and Morrow, B. E. (2011). Dual embryonic origin of the mammalian otic vesicle forming the inner ear. *Development* 138, 5403–5414. doi: 10.1242/dev.069849

Fuhrmann, S. (2010). Eye morphogenesis and patterning of the optic vesicle. *Curr. Top. Dev. Biol.* 93, 61–84. doi: 10.1016/B978-0-12-385044-7.00003-5

Garg, V., Yamagishi, C., Hu, T., Kathiriya, I. S., Yamagishi, H., and Srivastava, D. (2001). Tbx1, a DiGeorge syndrome candidate gene, is regulated by sonic hedgehog during pharyngeal arch development. *Dev. Biol.* 235, 62–73. doi: 10.1006/dbio.2001.0283

Gavalas, A., and Krumlauf, R. (2000). Retinoid signalling and hindbrain patterning. *Curr. Opin. Genet. Dev.* 10, 380–386. doi: 10.1016/s0959-437x(00)00100-3

Gavalas, A., Ruhrberg, C., Livet, J., Henderson, C. E., and Krumlauf, R. (2003). Neuronal defects in the hindbrain of Hoxa1, Hoxb1 and Hoxb2 mutants reflect regulatory interactions among these Hox genes. *Development* 130, 5663–5679. doi: 10.1242/dev.00802

Graf, D., Malik, Z., Hayano, S., and Mishina, Y. (2016). Common mechanisms in development and disease: BMP signaling in craniofacial development. *Cytokine Growth Factor Rev.* 27, 129–139. doi: 10.1016/j.cytogfr.2015.11.004

Graziadei, P. P., Levine, R. R., and Graziadei, G. A. (1978). Regeneration of olfactory axons and synapse formation in the forebrain after bulbectomy in neonatal mice. *Proc. Natl. Acad. Sci. U. S. A.* 75, 5230–5234. doi: 10.1073/pnas.75.10.5230

Graziadei, P. P., and Monti-Graziadei, A. G. (1992). The influence of the olfactory placode on the development of the telencephalon in *Xenopus laevis*. *Neuroscience* 46, 617–629. doi: 10.1016/0306-4522(92)90149-v

Greene, R. M., and Pisano, M. M. (2005). Recent advances in understanding transforming growth factor beta regulation of orofacial development. *Hum. Exp. Toxicol.* 24, 1–12. doi: 10.1191/0960327105ht492oa

Grim, M., and Christ, B. (1993). Neural crest cell migration into the limb bud of avian embryos. *Prog. Clin. Biol. Res.* 383A, 391–402.

Grindley, J. C., Davidson, D. R., and Hill, R. E. (1995). The role of Pax-6 in eye and nasal development. *Development* 121, 1433–1442.

Grocott, T., Tambalo, M., and Streit, A. (2012). The peripheral sensory nervous system in the vertebrate head: a gene regulatory perspective. *Dev. Biol.* 370, 3–23. doi: 10.1016/j.ydbio.2012.06.028

Gross, J. B., and Hanken, J. (2008). Review of fate-mapping studies of osteogenic cranial neural crest in vertebrates. *Dev. Biol.* 317, 389–400. doi: 10.1016/j.ydbio.2008.02.046

Guo, C., Sun, Y., Zhou, B., Adam, R. M., Li, X., Pu, W. T., et al. (2011). A Tbx1-Six1/Eya1-Fgf8 genetic pathway controls mammalian cardiovascular and craniofacial morphogenesis. *J. Clin. Invest.* 121, 1585–1595. doi: 10.1172/JCI44630

Gustafson, A. L., Dencker, L., and Eriksson, U. (1993). Non-overlapping expression of CRBP I and CRABP I during pattern formation of limbs and craniofacial structures in the early mouse embryo. *Development* 117, 451–460.

Hagglund, M., Berghard, A., Strotmann, J., and Bohm, S. (2006). Retinoic acid receptor-dependent survival of olfactory sensory neurons in postnatal and adult mice. *J. Neurosci.* 26, 3281–3291. doi: 10.1523/JNEUROSCI.4955-05.2006

Hardcastle, Z., Hui, C. C., and Sharpe, P. T. (1999). The Shh signalling pathway in early tooth development. *Cell. Mol. Biol.* 45, 567–578.

Haselbeck, R. J., Hoffmann, I., and Duester, G. (1999). Distinct functions for Aldh1 and Raldh2 in the control of ligand production for embryonic retinoid signaling pathways. *Dev. Genet.* 25, 353–364. doi: 10.1002/(SICI)1520-6408(1999)25:4<353::AID-DVG9>3.0.CO;2-G

Haskell, G. T., and LaMantia, A. S. (2005). Retinoic acid signaling identifies a distinct precursor population in the developing and adult forebrain. *J. Neurosci.* 25, 7636–7647. doi: 10.1523/JNEUROSCI.0485-05.2005

Haworth, K. E., Healy, C., Morgan, P., and Sharpe, P. T. (2004). Regionalisation of early head ectoderm is regulated by endoderm and prepatterns the orofacial epithelium. *Development* 131, 4797–4806. doi: 10.1242/dev.01337

Hayhurst, M., and McConnell, S. K. (2003). Mouse models of holoprosencephaly. *Curr. Opin. Neurol.* 16, 135–141. doi: 10.1097/01.wco.0000063761.15877.40

Hill, R. E., Favor, J., Hogan, B. L., Ton, C. C., Saunders, G. F., Hanson, I. M., et al. (1991). Mouse small eye results from mutations in a paired-like homeobox-containing gene. *Nature* 354, 522–525. doi: 10.1038/354522a0

Hill, C., Jacobs, B., Kennedy, L., Rohde, S., Zhou, B., Baldwin, S., et al. (2015). Cranial neural crest deletion of VEGFa causes cleft palate with aberrant vascular and bone development. *Cell Tissue Res.* 361, 711–722. doi: 10.1007/s00441-015-2150-7

Hintze, M., Prajapati, R. S., Tambalo, M., Christophorou, N. A. D., Anwar, M., Grocott, T., et al. (2017). Cell interactions, signals and transcriptional hierarchy governing placode progenitor induction. *Development* 144, 2810–2823. doi: 10.1242/dev.147942

Huang, X., and Saint-Jeannet, J. P. (2004). Induction of the neural crest and the opportunities of life on the edge. *Dev. Biol.* 275, 1–11. doi: 10.1016/j.ydbio.2004.07.033

Huh, S. H., and Ornitz, D. M. (2010). Beta-catenin deficiency causes DiGeorge syndrome-like phenotypes through regulation of Tbx1. *Development* 137, 1137–1147. doi: 10.1242/dev.045534

Hui, C. C., and Joyner, A. L. (1993). A mouse model of greig cephalopolysyndactyly syndrome: the extra-toesJ mutation contains an intragenic deletion of the Gli3 gene. *Nat. Genet.* 3, 241–246. doi: 10.1038/ng0393-241

Ishibashi, M., and McMahon, A. P. (2002). A sonic hedgehog-dependent signaling relay regulates growth of diencephalic and mesencephalic primordia in the early mouse embryo. *Development* 129, 4807–4819.

Jacobson, A. G. (1963). The determination and positioning of the nose, lens and ear. I. Interactions within the ectoderm, and between the ectoderm and underlying tissues. *J. Exp. Zool.* 154, 273–283. doi: 10.1002/jez.1401540303

Jessen, K. R., and Mirsky, R. (2005). The origin and development of glial cells in peripheral nerves. *Nat. Rev. Neurosci.* 6, 671–682. doi: 10.1038/nrn1746

Ji, Y., Hao, H., Reynolds, K., McMahon, M., and Zhou, C. J. (2019). Wnt signaling in neural crest ontogenesis and oncogenesis. *Cell* 8:1173. doi: 10.3390/cells8101173

Jiang, X., Iseki, S., Maxson, R. E., Sucov, H. M., and Morriss-Kay, G. M. (2002). Tissue origins and interactions in the mammalian skull vault. *Dev. Biol.* 241, 106–116. doi: 10.1006/dbio.2001.0487

Jimenez, D., Garcia, C., de Castro, F., Chedotal, A., Sotelo, C., de Carlos, J. A., et al. (2000). Evidence for intrinsic development of olfactory structures in Pax-6 mutant mice. *J. Comp. Neurol.* 428, 511–526.

Karpinski, B. A., Bryan, C. A., Paronett, E. M., Baker, J. L., Fernandez, A., Horvath, A., et al. (2016). A cellular and molecular mosaic establishes growth and differentiation states for cranial sensory neurons. *Dev. Biol.* 415, 228–241. doi: 10.1016/j.ydbio.2016.03.015

Karpinski, B. A., Maynard, T. M., Fralish, M. S., Nuwayhid, S., Zohn, I. E., Moody, S. A., et al. (2014). Dysphagia and disrupted cranial nerve development in a mouse model of DiGeorge (22q11) deletion syndrome. *Dis. Model. Mech.* 7, 245–257. doi: 10.1242/dmm.012484

Katoh, H., Shibata, S., Fukuda, K., Sato, M., Satoh, E., Nagoshi, N., et al. (2011). The dual origin of the peripheral olfactory system: placode and neural crest. *Mol. Brain* 4:34. doi: 10.1186/1756-6606-4-34

Kawauchi, S., Shou, J., Santos, R., Hebert, J. M., McConnell, S. K., Mason, I., et al. (2005). Fgf8 expression defines a morphogenetic center required for olfactory neurogenesis and nasal cavity development in the mouse. *Development* 132, 5211–5223. doi: 10.1242/dev.02143

Kelly, R. G., Jerome-Majewska, L. A., and Papaioannou, V. E. (2004). The del22q11.2 candidate gene Tbx1 regulates branchiomeric myogenesis. *Hum. Mol. Genet.* 13, 2829–2840. doi: 10.1093/hmg/ddh304

Kitazawa, T., and Rijli, F. M. (2018). Barrelette map formation in the prenatal mouse brainstem. *Curr. Opin. Neurobiol.* 53, 210–219. doi: 10.1016/j.conb.2018.09.008

Kleinert, J. O. (2017). Pediatric feeding disorders and severe developmental disabilities. *Semin. Speech Lang.* 38, 116–125. doi: 10.1055/s-0037-1599109

Kuratani, S., Adachi, N., Wada, N., Oisi, Y., and Sugahara, F. (2013). Developmental and evolutionary significance of the mandibular arch and prechordal/premandibular cranium in vertebrates: revising the heterotopy scenario of gnathostome jaw evolution. *J. Anat.* 222, 41–55. doi: 10.1111/j.1469-7580.2012.01505.x

LaMantia, A. S. (1999). Forebrain induction, retinoic acid, and vulnerability to schizophrenia: insights from molecular and genetic analysis in developing mice. *Biol. Psychiatry* 46, 19–30. doi: 10.1016/s0006-3223(99)00002-5

LaMantia, A. S., Bhasin, N., Rhodes, K., and Heemskerk, J. (2000). Mesenchymal/epithelial induction mediates olfactory pathway formation. *Neuron* 28, 411–425. doi: 10.1016/s0896-6273(00)00121-5

LaMantia, A. S., Colbert, M. C., and Linney, E. (1993). Retinoic acid induction and regional differentiation prefigure olfactory pathway formation in the mammalian forebrain. *Neuron* 10, 1035–1048. doi: 10.1016/0896-6273(93)90052-s

LaMantia, A. S., Moody, S. A., Maynard, T. M., Karpinski, B. A., Zohn, I. E., Mendelowitz, D., et al. (2016). Hard to swallow: developmental biological insights into pediatric dysphagia. *Dev. Biol.* 409, 329–342. doi: 10.1016/j.ydbio.2015.09.024

Le Douarin, N., Dulac, C., Dupin, E., and Cameron-Curry, P. (1991). Glial cell lineages in the neural crest. *Glia* 4, 175–184. doi: 10.1002/glia.440040209

Login, H., Haglin, S., Berghard, A., and Bohm, S. (2015). The stimulus-dependent gradient of Cyp26B1+ olfactory sensory neurons is necessary for the functional integrity of the olfactory sensory map. *J. Neurosci.* 35, 13807–13818. doi: 10.1523/JNEUROSCI.2247-15.2015

Lohnes, D., Mark, M., Mendelsohn, C., Dolle, P., Dierich, A., Gorry, P., et al. (1994). Function of the retinoic acid receptors (RARs) during development (I). Craniofacial and skeletal abnormalities in RAR double mutants. *Development* 120, 2723–2748.

Lwigale, P. Y., Conrad, G. W., and Bronner-Fraser, M. (2004). Graded potential of neural crest to form cornea, sensory neurons and cartilage along the rostrocaudal axis. *Development* 131, 1979–1991. doi: 10.1242/dev.01106

Maden, M., Hunt, P., Eriksson, U., Kuroiwa, A., Krumlauf, R., and Summerbell, D. (1991). Retinoic acid-binding protein, rhombomeres and the neural crest. *Development* 111, 35–43.

Maden, M., Sonneveld, E., van der Saag, P. T., and Gale, E. (1998). The distribution of endogenous retinoic acid in the chick embryo: implications for developmental mechanisms. *Development* 125, 4133–4144.

Maier, E. C., Saxena, A., Alsina, B., Bronner, M. E., and Whitfield, T. T. (2014). Sensational placodes: neurogenesis in the otic and olfactory systems. *Dev. Biol.* 389, 50–67. doi: 10.1016/j.ydbio.2014.01.023

Mansouri, A., Stoykova, A., Torres, M., and Gruss, P. (1996). Dysgenesis of cephalic neural crest derivatives in Pax7−/− mutant mice. *Development* 122, 831–838.

Manzini, M. C., Rajab, A., Maynard, T. M., Mochida, G. H., Tan, W. H., Nasir, R., et al. (2010). Developmental and degenerative features in a complicated spastic paraplegia. *Ann. Neurol.* 67, 516–525. doi: 10.1002/ana.21923

Marcucio, R. S., Cordero, D. R., Hu, D., and Helms, J. A. (2005). Molecular interactions coordinating the development of the forebrain and face. *Dev. Biol.* 284, 48–61. doi: 10.1016/j.ydbio.2005.04.030

Matsui, M., and Klingensmith, J. (2014). Multiple tissue-specific requirements for the BMP antagonist noggin in development of the mammalian craniofacial skeleton. *Dev. Biol.* 392, 168–181. doi: 10.1016/j.ydbio.2014.06.006

Matt, N., Dupe, V., Garnier, J. M., Dennefeld, C., Chambon, P., Mark, M., et al. (2005). Retinoic acid-dependent eye morphogenesis is orchestrated by neural crest cells. *Development* 132, 4789–4800. doi: 10.1242/dev.02031

Maynard, T. M., Gopalakrishna, D., Meechan, D. W., Paronett, E. M., Newbern, J. M., and LaMantia, A. S. (2013). 22q11 gene dosage establishes an adaptive range for sonic hedgehog and retinoic acid signaling during early development. *Hum. Mol. Genet.* 22, 300–312. doi: 10.1093/hmg/dds429

Maynard, T. M., Haskell, G. T., Bhasin, N., Lee, J. M., Gassman, A. A., Lieberman, J. A., et al. (2002). RanBP1, a velocardiofacial/DiGeorge syndrome candidate gene, is expressed at sites of mesenchymal/epithelial induction. *Mech. Dev.* 111, 177–180. doi: 10.1016/s0925-4773(01)00616-5

Maynard, T. M., Haskell, G. T., Peters, A. Z., Sikich, L., Lieberman, J. A., and LaMantia, A. S. (2003). A comprehensive analysis of 22q11 gene expression

in the developing and adult brain. *Proc. Natl. Acad. Sci. U. S. A.* 100, 14433–14438. doi: 10.1073/pnas.2235651100

Maynard, T. M., Horvath, A., Bernot, J. P., Karpinski, B. A., Tavares, A. L. P., Shah, A., et al. (2020a). Transcriptional dysregulation in developing trigeminal sensory neurons in the LgDel mouse model of DiGeorge 22q11.2 deletion syndrome. *Hum. Mol. Genet.* 29, 1002–1017. doi: 10.1093/hmg/ddaa024

Maynard, T. M., Meechan, D. W., Dudevoir, M. L., Gopalakrishna, D., Peters, A. Z., Heindel, C. C., et al. (2008). Mitochondrial localization and function of a subset of 22q11 deletion syndrome candidate genes. *Mol. Cell. Neurosci.* 39, 439–451. doi: 10.1016/j.mcn.2008.07.027

Maynard, T. M., Zohn, I. E., Moody, S. A., and LaMantia, A. S. (2020b). Suckling, feeding, and swallowing: behaviors, circuits, and targets for neurodevelopmental pathology. *Annu. Rev. Neurosci.* 43, 315–336. doi: 10.1146/annurev-neuro-100419-100636

McCaffery, P., and Drager, U. C. (1994). Hot spots of retinoic acid synthesis in the developing spinal cord. *Proc. Natl. Acad. Sci. U. S. A.* 91, 7194–7197. doi: 10.1073/pnas.91.15.7194

McDonald-McGinn, D. M., Sullivan, K. E., Marino, B., Philip, N., Swillen, A., Vorstman, J. A., et al. (2015). 22q11.2 deletion syndrome. *Nat. Rev. Dis. Primers* 1:15071. doi: 10.1038/nrdp.2015.71

McMahon, A. P., Joyner, A. L., Bradley, A., and McMahon, J. A. (1992). The midbrain-hindbrain phenotype of Wnt-1-/Wnt-1-mice results from stepwise deletion of engrailed-expressing cells by 9.5 days postcoitum. *Cell* 69, 581–595. doi: 10.1016/0092-8674(92)90222-x

Meechan, D. W., Maynard, T. M., Tucker, E. S., Fernandez, A., Karpinski, B. A., Rothblat, L. A., et al. (2015). Modeling a model: mouse genetics, 22q11.2 deletion syndrome, and disorders of cortical circuit development. *Prog. Neurobiol.* 130, 1–28. doi: 10.1016/j.pneurobio.2015.03.004

Meechan, D. W., Maynard, T. M., Wu, Y., Gopalakrishna, D., Lieberman, J. A., and LaMantia, A. S. (2006). Gene dosage in the developing and adult brain in a mouse model of 22q11 deletion syndrome. *Mol. Cell. Neurosci.* 33, 412–428. doi: 10.1016/j.mcn.2006.09.001

Merscher, S., Funke, B., Epstein, J. A., Heyer, J., Puech, A., Lu, M. M., et al. (2001). TBX1 is responsible for cardiovascular defects in velo-cardio-facial/DiGeorge syndrome. *Cell* 104, 619–629. doi: 10.1016/s0092-8674(01)00247-1

Mey, J., McCaffery, P., and Klemeit, M. (2001). Sources and sink of retinoic acid in the embryonic chick retina: distribution of aldehyde dehydrogenase activities, CRABP-I, and sites of retinoic acid inactivation. *Brain Res. Dev. Brain Res.* 127, 135–148. doi: 10.1016/s0165-3806(01)00127-4

Meyers, E. N., Lewandoski, M., and Martin, G. R. (1998). An Fgf8 mutant allelic series generated by Cre-and Flp-mediated recombination. *Nat. Genet.* 18, 136–141. doi: 10.1038/ng0298-136

Mic, F. A., Molotkov, A., Fan, X., Cuenca, A. E., and Duester, G. (2000). RALDH3, a retinaldehyde dehydrogenase that generates retinoic acid, is expressed in the ventral retina, otic vesicle and olfactory pit during mouse development. *Mech. Dev.* 97, 227–230. doi: 10.1016/s0925-4773(00)00434-2

Micucci, J. A., Layman, W. S., Hurd, E. A., Sperry, E. D., Frank, S. F., Durham, M. A., et al. (2014). CHD7 and retinoic acid signaling cooperate to regulate neural stem cell and inner ear development in mouse models of CHARGE syndrome. *Hum. Mol. Genet.* 23, 434–448. doi: 10.1093/hmg/ddt435

Miller, S. R., Perera, S. N., and Baker, C. V. (2017). Constitutively active Notch1 converts cranial neural crest-derived frontonasal mesenchyme to perivascular cells in vivo. *Biol. Open* 6, 317–325. doi: 10.1242/bio.023887

Monsoro-Burq, A. H. (2015). PAX transcription factors in neural crest development. *Semin. Cell Dev. Biol.* 44, 87–96. doi: 10.1016/j.semcdb.2015.09.015

Moody, S. A., and LaMantia, A. S. (2015). Transcriptional regulation of cranial sensory placode development. *Curr. Top. Dev. Biol.* 111, 301–350. doi: 10.1016/bs.ctdb.2014.11.009

Morriss-Kay, G. (1993). Retinoic acid and craniofacial development: molecules and morphogenesis. *BioEssays* 15, 9–15. doi: 10.1002/bies.950150103

Morrow, B. E., McDonald-McGinn, D. M., Emanuel, B. S., Vermeesch, J. R., and Scambler, P. J. (2018). Molecular genetics of 22q11.2 deletion syndrome. *Am. J. Med. Genet. A* 176, 2070–2081. doi: 10.1002/ajmg.a.40504

Motahari, Z., Maynard, T. M., Popratiloff, A., Moody, S. A., and LaMantia, A. S. (2020). Aberrant early growth of individual trigeminal sensory and motor axons in a series of mouse genetic models of 22q11.2 deletion syndrome. *Hum. Mol. Genet.* 29, 3081–3093. doi: 10.1093/hmg/ddaa199

Motahari, Z., Moody, S. A., Maynard, T. M., and LaMantia, A. S. (2019). In the line-up: deleted genes associated with DiGeorge/22q11.2 deletion syndrome: are they all suspects? *J. Neurodev. Disord.* 11:7. doi: 10.1186/s11689-019-9267-z

Muscatelli, F., and Bouret, S. G. (2018). Wired for eating: how is an active feeding circuitry established in the postnatal brain? *Curr. Opin. Neurobiol.* 52, 165–171. doi: 10.1016/j.conb.2018.07.003

Myers, L., Anderlid, B. M., Nordgren, A., Willfors, C., Kuja-Halkola, R., Tammimies, K., et al. (2017). Minor physical anomalies in neurodevelopmental disorders: a twin study. *Child Adolesc. Psychiatry Ment. Health* 11:57. doi: 10.1186/s13034-017-0195-y

Nahm, M., Lee, M. J., Parkinson, W., Lee, M., Kim, H., Kim, Y. J., et al. (2013). Spartin regulates synaptic growth and neuronal survival by inhibiting BMP-mediated microtubule stabilization. *Neuron* 77, 680–695. doi: 10.1016/j.neuron.2012.12.015

Nakajima, Y. (2015). Signaling regulating inner ear development: cell fate determination, patterning, morphogenesis, and defects. *Congenit. Anom.* 55, 17–25. doi: 10.1111/cga.12072

Narita, Y., and Rijli, F. M. (2009). Hox genes in neural patterning and circuit formation in the mouse hindbrain. *Curr. Top. Dev. Biol.* 88, 139–167. doi: 10.1016/S0070-2153(09)88005-8

Nasrallah, I., and Golden, J. A. (2001). Brain, eye, and face defects as a result of ectopic localization of sonic hedgehog protein in the developing rostral neural tube. *Teratology* 64, 107–113. doi: 10.1002/tera.1052

Neubuser, A., Peters, H., Balling, R., and Martin, G. R. (1997). Antagonistic interactions between FGF and BMP signaling pathways: a mechanism for positioning the sites of tooth formation. *Cell* 90, 247–255. doi: 10.1016/s0092-8674(00)80333-5

Nie, X., Luukko, K., and Kettunen, P. (2006a). BMP signalling in craniofacial development. *Int. J. Dev. Biol.* 50, 511–521. doi: 10.1387/ijdb.052101xn

Nie, X., Luukko, K., and Kettunen, P. (2006b). FGF signalling in craniofacial development and developmental disorders. *Oral Dis.* 12, 102–111. doi: 10.1111/j.1601-0825.2005.01176.x

Niederreither, K., Fraulob, V., Garnier, J. M., Chambon, P., and Dolle, P. (2002). Differential expression of retinoic acid-synthesizing (RALDH) enzymes during fetal development and organ differentiation in the mouse. *Mech. Dev.* 110, 165–171. doi: 10.1016/s0925-4773(01)00561-5

Niederreither, K., Subbarayan, V., Dolle, P., and Chambon, P. (1999). Embryonic retinoic acid synthesis is essential for early mouse post-implantation development. *Nat. Genet.* 21, 444–448. doi: 10.1038/7788

Niederreither, K., Vermot, J., Le Roux, I., Schuhbaur, B., Chambon, P., and Dolle, P. (2003). The regional pattern of retinoic acid synthesis by RALDH2 is essential for the development of posterior pharyngeal arches and the enteric nervous system. *Development* 130, 2525–2534. doi: 10.1242/dev.00463

Nitzan, E., Pfaltzgraff, E. R., Labosky, P. A., and Kalcheim, C. (2013). Neural crest and Schwann cell progenitor-derived melanocytes are two spatially segregated populations similarly regulated by Foxd3. *Proc. Natl. Acad. Sci. U. S. A.* 110, 12709–12714. doi: 10.1073/pnas.1306287110

Noakes, P. G., and Bennett, M. R. (1987). Growth of axons into developing muscles of the chick forelimb is preceded by cells that stain with Schwann cell antibodies. *J. Comp. Neurol.* 259, 330–347. doi: 10.1002/cne.902590303

Noden, D. M. (1988). Interactions and fates of avian craniofacial mesenchyme. *Development* 103(Suppl), 121–140.

Nordstrom, M., Retterstol, K., Hope, S., and Kolset, S. O. (2020). Nutritional challenges in children and adolescents with down syndrome. *Lancet Child Adolesc. Health* 4, 455–464. doi: 10.1016/S2352-4642(19)30400-6

Okuhara, S., Birjandi, A. A., Adel Al-Lami, H., Sagai, T., Amano, T., Shiroishi, T., et al. (2019). Temporospatial sonic hedgehog signalling is essential for neural crest-dependent patterning of the intrinsic tongue musculature. *Development* 146:dev180075. doi: 10.1242/dev.180075

Olaopa, M., Zhou, H. M., Snider, P., Wang, J., Schwartz, R. J., Moon, A. M., et al. (2011). Pax3 is essential for normal cardiac neural crest morphogenesis but is not required during migration nor outflow tract septation. *Dev. Biol.* 356, 308–322. doi: 10.1016/j.ydbio.2011.05.583

Osumi-Yamashita, N., Ninomiya, Y., Doi, H., and Eto, K. (1994). The contribution of both forebrain and midbrain crest cells to the mesenchyme in the frontonasal mass of mouse embryos. *Dev. Biol.* 164, 409–419. doi: 10.1006/dbio.1994.1211

Parker, H. J., and Krumlauf, R. (2020). A Hox gene regulatory network for hindbrain segmentation. *Curr. Top. Dev. Biol.* 139, 169–203. doi: 10.1016/bs.ctdb.2020.03.001

Paronett, E. M., Meechan, D. W., Karpinski, B. A., LaMantia, A. S., and Maynard, T. M. (2015). Ranbp1, deleted in DiGeorge/22q11.2 deletion syndrome, is a microcephaly gene that selectively disrupts layer 2/3 cortical projection neuron generation. *Cereb. Cortex* 25, 3977–3993. doi: 10.1093/cercor/bhu285

Paschaki, M., Cammas, L., Muta, Y., Matsuoka, Y., Mak, S. S., Rataj-Baniowska, M., et al. (2013). Retinoic acid regulates olfactory progenitor cell fate and differentiation. *Neural Dev.* 8:13. doi: 10.1186/1749-8104-8-13

Patel, H., Cross, H., Proukakis, C., Hershberger, R., Bork, P., Ciccarelli, F. D., et al. (2002). SPG20 is mutated in Troyer syndrome, an hereditary spastic paraplegia. *Nat. Genet.* 31, 347–348. doi: 10.1038/ng937

Peluso, C. E., Jang, W., Drager, U. C., and Schwob, J. E. (2012). Differential expression of components of the retinoic acid signaling pathway in the adult mouse olfactory epithelium. *J. Comp. Neurol.* 520, 3707–3726. doi: 10.1002/cne.23124

Perez-Castro, A. V., Toth-Rogler, L. E., Wei, L. N., and Nguyen-Huu, M. C. (1989). Spatial and temporal pattern of expression of the cellular retinoic acid-binding protein and the cellular retinol-binding protein during mouse embryogenesis. *Proc. Natl. Acad. Sci. U. S. A.* 86, 8813–8817. doi: 10.1073/pnas.86.22.8813

Petersen, J., and Adameyko, I. (2017). Nerve-associated neural crest: peripheral glial cells generate multiple fates in the body. *Curr. Opin. Genet. Dev.* 45, 10–14. doi: 10.1016/j.gde.2017.02.006

Petros, T. J., Rebsam, A., and Mason, C. A. (2008). Retinal axon growth at the optic chiasm: to cross or not to cross. *Annu. Rev. Neurosci.* 31, 295–315. doi: 10.1146/annurev.neuro.31.060407.125609

Philippidou, P., and Dasen, J. S. (2013). Hox genes: choreographers in neural development, architects of circuit organization. *Neuron* 80, 12–34. doi: 10.1016/j.neuron.2013.09.020

Rawson, N. E., and LaMantia, A. S. (2006). Once and again: retinoic acid signaling in the developing and regenerating olfactory pathway. *J. Neurobiol.* 66, 653–676. doi: 10.1002/neu.20236

Rawson, N. E., and LaMantia, A. S. (2007). A speculative essay on retinoic acid regulation of neural stem cells in the developing and aging olfactory system. *Exp. Gerontol.* 42, 46–53. doi: 10.1016/j.exger.2006.05.021

Rawson, N. E., Lischka, F. W., Yee, K. K., Peters, A. Z., Tucker, E. S., Meechan, D. W., et al. (2010). Specific mesenchymal/epithelial induction of olfactory receptor, vomeronasal, and gonadotropin-releasing hormone (GnRH) neurons. *Dev. Dyn.* 239, 1723–1738. doi: 10.1002/dvdy.22315

Renvoise, B., Parker, R. L., Yang, D., Bakowska, J. C., Hurley, J. H., and Blackstone, C. (2010). SPG20 protein spartin is recruited to midbodies by ESCRT-III protein Ist1 and participates in cytokinesis. *Mol. Biol. Cell* 21, 3293–3303. doi: 10.1091/mbc.E09-10-0879

Renvoise, B., Stadler, J., Singh, R., Bakowska, J. C., and Blackstone, C. (2012). Spg20−/− mice reveal multimodal functions for Troyer syndrome protein spartin in lipid droplet maintenance, cytokinesis and BMP signaling. *Hum. Mol. Genet.* 21, 3604–3618. doi: 10.1093/hmg/dds191

Richman, J. M. (1992). The role of retinoids in normal and abnormal embryonic craniofacial morphogenesis. *Crit. Rev. Oral Biol. Med.* 4, 93–109. doi: 10.1177/10454411920040010701

Ritter, K. E., and Martin, D. M. (2019). Neural crest contributions to the ear: implications for congenital hearing disorders. *Hear. Res.* 376, 22–32. doi: 10.1016/j.heares.2018.11.005

Robertson, J., Chadwick, D., Baines, S., Emerson, E., and Hatton, C. (2017). Prevalence of dysphagia in people with intellectual disability: a systematic review. *Intellect. Dev. Disabil.* 55, 377–391. doi: 10.1352/1934-9556-55.6.377

Rogdaki, M., Gudbrandsen, M., McCutcheon, R. A., Blackmore, C. E., Brugger, S., Ecker, C., et al. (2020). Magnitude and heterogeneity of brain structural abnormalities in 22q11.2 deletion syndrome: a meta-analysis. *Mol. Psychiatry* 25, 1704–1717. doi: 10.1038/s41380-019-0638-3

Rogers, C. D., Jayasena, C. S., Nie, S., and Bronner, M. E. (2012). Neural crest specification: tissues, signals, and transcription factors. *Wiley Interdiscip. Rev. Dev. Biol.* 1, 52–68. doi: 10.1002/wdev.8

Ruberte, E., Dolle, P., Chambon, P., and Morriss-Kay, G. (1991). Retinoic acid receptors and cellular retinoid binding proteins. II. Their differential pattern of transcription during early morphogenesis in mouse embryos. *Development* 111, 45–60.

Ryckebusch, L., Bertrand, N., Mesbah, K., Bajolle, F., Niederreither, K., Kelly, R. G., et al. (2010). Decreased levels of embryonic retinoic acid synthesis accelerate recovery from arterial growth delay in a mouse model of DiGeorge syndrome. *Circ. Res.* 106, 686–694. doi: 10.1161/CIRCRESAHA.109.205732

Saint-Jeannet, J. P., and Moody, S. A. (2014). Establishing the pre-placodal region and breaking it into placodes with distinct identities. *Dev. Biol.* 389, 13–27. doi: 10.1016/j.ydbio.2014.02.011

Sauka-Spengler, T., and Bronner-Fraser, M. (2008). A gene regulatory network orchestrates neural crest formation. *Nat. Rev. Mol. Cell Biol.* 9, 557–568. doi: 10.1038/nrm2428

Scambler, P. J. (2010). 22q11 deletion syndrome: a role for TBX1 in pharyngeal and cardiovascular development. *Pediatr. Cardiol.* 31, 378–390. doi: 10.1007/s00246-009-9613-0

Schimmang, T., Lemaistre, M., Vortkamp, A., and Ruther, U. (1992). Expression of the zinc finger gene Gli3 is affected in the morphogenetic mouse mutant extra-toes (Xt). *Development* 116, 799–804.

Schneider, M., Debbane, M., Bassett, A. S., Chow, E. W., Fung, W. L., van den Bree, M., et al. (2014). Psychiatric disorders from childhood to adulthood in 22q11.2 deletion syndrome: results from the international consortium on brain and behavior in 22q11.2 deletion syndrome. *Am. J. Psychiatry* 171, 627–639. doi: 10.1176/appi.ajp.2013.13070864

Serbedzija, G. N., Bronner-Fraser, M., and Fraser, S. E. (1992). Vital dye analysis of cranial neural crest cell migration in the mouse embryo. *Development* 116, 297–307.

Shen, H., Wilke, T., Ashique, A. M., Narvey, M., Zerucha, T., Savino, E., et al. (1997). Chicken transcription factor AP-2: cloning, expression and its role in outgrowth of facial prominences and limb buds. *Dev. Biol.* 188, 248–266. doi: 10.1006/dbio.1997.8617

Shenefelt, R. E. (1972). Morphogenesis of malformations in hamsters caused by retinoic acid: relation to dose and stage at treatment. *Teratology* 5, 103–118. doi: 10.1002/tera.1420050115

Smith, S. M., Garic, A., Berres, M. E., and Flentke, G. R. (2014). Genomic factors that shape craniofacial outcome and neural crest vulnerability in FASD. *Front. Genet.* 5:224. doi: 10.3389/fgene.2014.00224

Sosulski, D. L., Bloom, M. L., Cutforth, T., Axel, R., and Datta, S. R. (2011). Distinct representations of olfactory information in different cortical centres. *Nature* 472, 213–216. doi: 10.1038/nature09868

Stamataki, D., Ulloa, F., Tsoni, S. V., Mynett, A., and Briscoe, J. (2005). A gradient of Gli activity mediates graded sonic hedgehog signaling in the neural tube. *Genes Dev.* 19, 626–641. doi: 10.1101/gad.325905

Stanier, P., and Pauws, E. (2012). Development of the lip and palate: FGF signalling. *Front. Oral Biol.* 16, 71–80. doi: 10.1159/000337618

Stout, R. P., and Graziadei, P. P. (1980). Influence of the olfactory placode on the development of the brain in *Xenopus laevis* (Daudin). I. Axonal growth and connections of the transplanted olfactory placode. *Neuroscience* 5, 2175–2186. doi: 10.1016/0306-4522(80)90134-7

Stuhlmiller, T. J., and Garcia-Castro, M. I. (2012). Current perspectives of the signaling pathways directing neural crest induction. *Cell. Mol. Life Sci.* 69, 3715–3737. doi: 10.1007/s00018-012-0991-8

Sullivan, S. L., Bohm, S., Ressler, K. J., Horowitz, L. F., and Buck, L. B. (1995). Target-independent pattern specification in the olfactory epithelium. *Neuron* 15, 779–789. doi: 10.1016/0896-6273(95)90170-1

Suzuki, R., Shintani, T., Sakuta, H., Kato, A., Ohkawara, T., Osumi, N., et al. (2000). Identification of RALDH-3, a novel retinaldehyde dehydrogenase, expressed in the ventral region of the retina. *Mech. Dev.* 98, 37–50. doi: 10.1016/s0925-4773(00)00450-0

Suzuki, J., Yoshizaki, K., Kobayashi, T., and Osumi, N. (2013). Neural crest-derived horizontal basal cells as tissue stem cells in the adult olfactory epithelium. *Neurosci. Res.* 75, 112–120. doi: 10.1016/j.neures.2012

Szabo-Rogers, H. L., Geetha-Loganathan, P., Nimmagadda, S., Fu, K. K., and Richman, J. M. (2008). FGF signals from the nasal pit are necessary for normal facial morphogenesis. *Dev. Biol.* 318, 289–302. doi: 10.1016/j.ydbio.2008.03.027

Taroc, E. Z. M., Naik, A. S., Lin, J. M., Peterson, N. B., Keefe, D. L. Jr., Genis, E., et al. (2020). Gli3 regulates vomeronasal neurogenesis, olfactory ensheathing cell formation, and GnRH-1 neuronal migration. *J. Neurosci.* 40, 311–326. doi: 10.1523/JNEUROSCI.1977-19.2019

Thesleff, I. (2003). Epithelial-mesenchymal signalling regulating tooth morphogenesis. *J. Cell Sci.* 116, 1647–1648. doi: 10.1242/jcs.00410

Thiery, A., Buzzi, A. L., and Streit, A. (2020). Cell fate decisions during the development of the peripheral nervous system in the vertebrate head. *Curr. Top. Dev. Biol.* 139, 127–167. doi: 10.1016/bs.ctdb.2020.04.002

Thomas, A. J., and Erickson, C. A. (2008). The making of a melanocyte: the specification of melanoblasts from the neural crest. *Pigment Cell Melanoma Res.* 21, 598–610. doi: 10.1111/j.1755-148X.2008.00506.x

Thompson Haskell, G., Maynard, T. M., Shatzmiller, R. A., and Lamantia, A. S. (2002). Retinoic acid signaling at sites of plasticity in the mature central nervous system. *J. Comp. Neurol.* 452, 228–241. doi: 10.1002/cne.10369

Thompson, H., and Tucker, A. S. (2013). Dual origin of the epithelium of the mammalian middle ear. *Science* 339, 1453–1456. doi: 10.1126/science.1232862

Tole, S., Ragsdale, C. W., and Grove, E. A. (2000). Dorsoventral patterning of the telencephalon is disrupted in the mouse mutant extra-toes(J). *Dev. Biol.* 217, 254–265. doi: 10.1006/dbio.1999.9509

Tripi, G., Roux, S., Canziani, T., Bonnet Brilhault, F., Barthelemy, C., and Canziani, F. (2008). Minor physical anomalies in children with autism spectrum disorder. *Early Hum. Dev.* 84, 217–223. doi: 10.1016/j.earlhumdev.2007.04.005

Trost, A., Schroedl, F., Lange, S., Rivera, F. J., Tempfer, H., Korntner, S., et al. (2013). Neural crest origin of retinal and choroidal pericytes. *Invest. Ophthalmol. Vis. Sci.* 54, 7910–7921. doi: 10.1167/iovs.13-12946

Tucker, E. S., Lehtinen, M. K., Maynard, T., Zirlinger, M., Dulac, C., Rawson, N., et al. (2010). Proliferative and transcriptional identity of distinct classes of neural precursors in the mammalian olfactory epithelium. *Development* 137, 2471–2481. doi: 10.1242/dev.049718

Tucker, E. S., Polleux, F., and LaMantia, A. S. (2006). Position and time specify the migration of a pioneering population of olfactory bulb interneurons. *Dev. Biol.* 297, 387–401. doi: 10.1016/j.ydbio.2006.05.009

Tucker, E. S., Segall, S., Gopalakrishna, D., Wu, Y., Vernon, M., Polleux, F., et al. (2008). Molecular specification and patterning of progenitor cells in the lateral and medial ganglionic eminences. *J. Neurosci.* 28, 9504–9518. doi: 10.1523/JNEUROSCI.2341-08.2008

Tucker, A., and Sharpe, P. (2004). The cutting-edge of mammalian development; how the embryo makes teeth. *Nat. Rev. Genet.* 5, 499–508. doi: 10.1038/nrg1380

Tucker, A. S., Yamada, G., Grigoriou, M., Pachnis, V., and Sharpe, P. T. (1999). Fgf-8 determines rostral-caudal polarity in the first branchial arch. *Development* 126, 51–61.

Uchida, N., Poo, C., and Haddad, R. (2014). Coding and transformations in the olfactory system. *Annu. Rev. Neurosci.* 37, 363–385. doi: 10.1146/annurev-neuro-071013-013941

Vandamme, N., and Berx, G. (2019). From neural crest cells to melanocytes: cellular plasticity during development and beyond. *Cell. Mol. Life Sci.* 76, 1919–1934. doi: 10.1007/s00018-019-03049-w

Vega-Lopez, G. A., Cerrizuela, S., Tribulo, C., and Aybar, M. J. (2018). Neurocristopathies: new insights 150 years after the neural crest discovery. *Dev. Biol.* 444 (Suppl. 1), S110–S143. doi: 10.1016/j.ydbio.2018.05.013

Vegh, A. M. D., Duim, S. N., Smits, A. M., Poelmann, R. E., Ten Harkel, A. D. J., DeRuiter, M. C., et al. (2016). Part and parcel of the cardiac autonomic nerve system: unravelling its cellular building blocks during development. *J. Cardiovasc. Dev. Dis.* 3:28. doi: 10.3390/jcdd3030028

Vermot, J., Niederreither, K., Garnier, J. M., Chambon, P., and Dolle, P. (2003). Decreased embryonic retinoic acid synthesis results in a DiGeorge syndrome phenotype in newborn mice. *Proc. Natl. Acad. Sci. U. S. A.* 100, 1763–1768. doi: 10.1073/pnas.0437920100

Vitelli, F., Morishima, M., Taddei, I., Lindsay, E. A., and Baldini, A. (2002). Tbx1 mutation causes multiple cardiovascular defects and disrupts neural crest and cranial nerve migratory pathways. *Hum. Mol. Genet.* 11, 915–922. doi: 10.1093/hmg/11.8.915

Wade, C., Brinas, I., Welfare, M., Wicking, C., and Farlie, P. G. (2012). Twist2 contributes to termination of limb bud outgrowth and patterning through direct regulation of Grem1. *Dev. Biol.* 370, 145–153. doi: 10.1016/j.ydbio.2012.07.025

Walker, M. B., and Trainor, P. A. (2006). Craniofacial malformations: intrinsic vs extrinsic neural crest cell defects in Treacher Collins and 22q11 deletion syndromes. *Clin. Genet.* 69, 471–479. doi: 10.1111/j.0009-9163.2006.00615.x

Wang, X., Bryan, C., LaMantia, A. S., and Mendelowitz, D. (2017). Altered neurobiological function of brainstem hypoglossal neurons in DiGeorge/22q11.2 deletion syndrome. *Neuroscience* 359, 1–7. doi: 10.1016/j.neuroscience.2017.06.057

Wang, X., Popratiloff, A., Motahari, Z., LaMantia, A. S., and Mendelowitz, D. (2020). Disrupted coordination of hypoglossal motor control in a mouse model of pediatric dysphagia in DiGeorge/22q11.2 deletion syndrome. *eNeuro* 7:ENEURO.0520-19.2020. doi: 10.1523/ENEURO.0520-19.2020

Welby, L., Caudill, H., Yitsege, G., Hamad, A., Bunyak, F., Zohn, I. E., et al. (2020). Persistent feeding and swallowing deficits in a mouse model of 22q11.2 deletion syndrome. *Front. Neurol.* 11:4. doi: 10.3389/fneur.2020.00004

Weston, J. A., and Thiery, J. P. (2015). Pentimento: neural crest and the origin of mesectoderm. *Dev. Biol.* 401, 37–61. doi: 10.1016/j.ydbio.2014.12.035

Whitesides, J. G. 3rd, and LaMantia, A. S. (1996). Differential adhesion and the initial assembly of the mammalian olfactory nerve. *J. Comp. Neurol.* 373, 240–254. doi: 10.1002/(SICI)1096-9861(19960916)373:2<240::AID-CNE7>3.0.CO;2-3

Whitesides, J., Hall, M., Anchan, R., and LaMantia, A. S. (1998). Retinoid signaling distinguishes a subpopulation of olfactory receptor neurons in the developing and adult mouse. *J. Comp. Neurol.* 394, 445–461.

Wilkinson, D. G. (1993). Molecular mechanisms of segmental patterning in the vertebrate hindbrain. *Perspect. Dev. Neurobiol.* 1, 117–125.

Williams, A. L., and Bohnsack, B. L. (2015). Neural crest derivatives in ocular development: discerning the eye of the storm. *Birth Defects Res. C Embryo Today* 105, 87–95. doi: 10.1002/bdrc.21095

Williams, A. L., and Bohnsack, B. L. (2019). What's retinoic acid got to do with it? Retinoic acid regulation of the neural crest in craniofacial and ocular development. *Genesis* 57:e23308. doi: 10.1002/dvg.23308

Yitsege, G., Stokes, B. A., Sabatino, J. A., Sugrue, K. F., Banyai, G., Paronett, E. M., et al. (2020). Variations in maternal vitamin a intake modifies phenotypes in a mouse model of 22q11.2 deletion syndrome. *Birth Defects Res.* 112, 1194–1208. doi: 10.1002/bdr2.1709

York, J. R., Yuan, T., and McCauley, D. W. (2020). Evolutionary and developmental associations of neural crest and placodes in the vertebrate head: insights from jawless vertebrates. *Front. Physiol.* 11:986. doi: 10.3389/fphys.2020.00986

Yoshida, T., Vivatbutsiri, P., Morriss-Kay, G., Saga, Y., and Iseki, S. (2008). Cell lineage in mammalian craniofacial mesenchyme. *Mech. Dev.* 125, 797–808. doi: 10.1016/j.mod.2008.06.007

Young, J. J., Kjolby, R. A. S., Wu, G., Wong, D., Hsu, S. W., and Harland, R. M. (2017). Noggin is required for first pharyngeal arch differentiation in the frog *Xenopus tropicalis*. *Dev. Biol.* 426, 245–254. doi: 10.1016/j.ydbio.2016.06.034

Yu, J. K. (2010). The evolutionary origin of the vertebrate neural crest and its developmental gene regulatory network—insights from amphioxus. *Zoology* 113, 1–9. doi: 10.1016/j.zool.2009.06.001

Zhao, D., McCaffery, P., Ivins, K. J., Neve, R. L., Hogan, P., Chin, W. W., et al. (1996). Molecular identification of a major retinoic-acid-synthesizing enzyme, a retinaldehyde-specific dehydrogenase. *Eur. J. Biochem.* 240, 15–22. doi: 10.1111/j.1432-1033.1996.0015h.x

Ziermann, J. M., Diogo, R., and Noden, D. M. (2018). Neural crest and the patterning of vertebrate craniofacial muscles. *Genesis* 56:e23097. doi: 10.1002/dvg.23097

Conflict of Interest: The author declares that the research was conducted in the absence of any commercial or financial relationships that could be construed as a potential conflict of interest.

frontiers in Physiology

ORIGINAL RESEARCH
published: 11 January 2021
doi: 10.3389/fphys.2020.612230

Hoxb3 Regulates *Jag1* Expression in Pharyngeal Epithelium and Affects Interaction With Neural Crest Cells

*Haoran Zhang[1], Junjie Xie[1], Karl Kam Hei So[1], Ka Kui Tong[1], Jearn Jang Sae-Pang[1], Li Wang[1], Sze Lan Tsang[1], Wood Yee Chan[2], Elaine Yee Man Wong[1] and Mai Har Sham[1,2]**

[1] School of Biomedical Sciences, LKS Faculty of Medicine, The University of Hong Kong, Pokfulam, Hong Kong, [2] School of Biomedical Sciences, The Chinese University of Hong Kong, Shatin, Hong Kong

Craniofacial morphogenesis depends on proper migration of neural crest cells and their interactions with placodes and other cell types. *Hox* genes provide positional information and are important in patterning the neural crest and pharyngeal arches (PAs) for coordinated formation of craniofacial structures. *Hox* genes are expressed in the surface ectoderm and epibranchial placodes, their roles in the pharyngeal epithelium and their downstream targets in regulating PA morphogenesis have not been established. We altered the *Hox* code in the pharyngeal region of the *Hoxb3*$^{Tg/+}$ mutant, in which *Hoxb3* is driven to ectopically expressed in *Hoxb2* domain in the second pharyngeal arch (PA2). In the transgenic mutant, ectopic *Hoxb3* expression was restricted to the surface ectoderm, including the proximal epibranchial placodal region and the distal pharyngeal epithelium. The *Hoxb3*$^{Tg/+}$ mutants displayed hypoplasia of PA2, multiple neural crest-derived facial skeletal and nerve defects. Interestingly, we found that in the *Hoxb3*$^{Tg/+}$ mutant, expression of the Notch ligand *Jag1* was specifically up-regulated in the ectodermal pharyngeal epithelial cells of PA2. By molecular experiments, we demonstrated that Hoxb3 could bind to an upstream genomic site S2 and directly regulate *Jag1* expression. In the *Hoxb3*$^{Tg/+}$ mutant, elevated expression of *Jag1* in the pharyngeal epithelium led to abnormal cellular interaction and deficiency of neural crest cells migrating into PA2. In summary, we showed that *Hoxb3* regulates Jag1 expression and proposed a model of pharyngeal epithelium and neural crest interaction during pharyngeal arch development.

Keywords: *Hoxb3*, *JAG1*, pharyngeal arch, epibranchial placodes, pharyngeal epithelium, cranial neural crest, craniofacial development

OPEN ACCESS

Edited by:
Jean-Pierre Saint-Jeannet, New York University, United States

Reviewed by:
Heather C. Etchevers, INSERM U1251 Centre de Génétique Médicale de Marseille (MMG), France
Juhee Jeong, New York University, United States

***Correspondence:**
Mai Har Sham
mhsham@cuhk.edu.hk

Specialty section:
This article was submitted to Craniofacial Biology and Dental Research, a section of the journal Frontiers in Physiology

Received: *30 September 2020*
Accepted: *09 December 2020*
Published: *11 January 2021*

Citation:
Zhang H, Xie J, So KKH, Tong KK, Sae-Pang JJ, Wang L, Tsang SL, Chan WY, Wong EYM and Sham MH (2021) Hoxb3 Regulates Jag1 Expression in Pharyngeal Epithelium and Affects Interaction With Neural Crest Cells. Front. Physiol. 11:612230. doi: 10.3389/fphys.2020.612230

INTRODUCTION

An important phase of mammalian craniofacial development is the formation of the transient pharyngeal arch (PA) structures. These PAs are comprised of an outer surface ectoderm, an inner covering of endoderm, a mesenchymal core, and the cranial neural crest-derived ectomesenchyme. The coordinated development of the different embryonic components give rise to the pharynx, the jaw, the ear and the face. Dysregulation of PA development can lead to many human congenital craniofacial malformations.

The cranial neural crest cells which delaminate from the dorsal region of hindbrain rhombomeres have important structural roles in craniofacial morphogenesis. Neural crest cells originating from different anteroposterior levels of the hindbrain rhombomeres are marked by combinations of *Hox* genes which specify their identity. Molecular analysis have shown that regulation of *Hox* expression in the hindbrain rhombomeres and in the neural crest could be independently controlled by separate *cis*-acting regulatory elements and *trans*-acting factors (Frasch et al., 1995; Nonchev et al., 1996; Maconochie et al., 1999; Trainor and Krumlauf, 2000). The neural crest cells arising from distinct rhombomere locations are not pre-patterned, but remain plastic, and can respond to signals in the environment they migrate to Trainor and Krumlauf (2000) and Le Douarin et al. (2004). In the PAs, neural crest cells respond to signals from the pharyngeal surface ectoderm and the endoderm in determining their cell fate (Graham et al., 2005). The neural crest cells give rise to cranial ganglia and nerves, muscle and facial bones and cartilages (Frisdal and Trainor, 2014). Defective migration, survival, proliferation, or differentiation of the cranial neural crest cells lead to multiple craniofacial abnormalities (Santagati and Rijli, 2003; Minoux and Rijli, 2010). More importantly, PAs can be formed and their antero-posterior and proximo-distal axes maintained in the absence of neural crest cells, indicating the important roles of pharyngeal epithelium and other cell types during PA development (Veitch et al., 1999; Gavalas et al., 2001; Trainor and Krumlauf, 2001).

The ectodermal pharyngeal epithelium covering the proximal and distal regions of the PAs are developmentally distinct. In the proximal PA region, epibranchial placodal cells not only give rise to neurogenic cranial ganglia, but also non-neuronal epithelial cells which play essential roles in pharyngeal segmentation (Zhang et al., 2017). The invagination of the proximal non-neuronal placode-derived epithelium and the outgrowth of the pharyngeal endoderm form the segmental plates, the contact points of the epithelial layers give rise to the pharyngeal clefts and pouches (Graham and Smith, 2001; Graham, 2003; Kulesa et al., 2010). Defective pharyngeal segmentation as displayed in the *Sox3* (Rizzoti and Lovell-Badge, 2007) and *Eya1* mutants (Xu et al., 2002; Zhang et al., 2017) would lead to abnormal PA development. Around the pharyngeal clefts, the non-neuronal epibranchial placodal epithelial cells express various signaling factors including Notch and Fgfs that are required for PA morphogenesis (Trokovic et al., 2005; Wang et al., 2020). The roles of the ectodermal pharyngeal epithelium in interacting with neural crest and other cell types in the developing PAs are not well understood.

Notch signaling factors are required for cranial ganglia neurogenesis and craniofacial morphogenesis (Wakeham et al., 1997; Jayasena et al., 2008; Lassiter et al., 2010; Lassiter et al., 2014). Mutations of the Notch ligand *JAG1* caused Alagille syndrome with craniofacial defects in human patients (Li et al., 1997; Kamath et al., 2003). *Jag1b* mutation in zebrafish led to mis-patterning of pharyngeal arch derived skeletons (Barske et al., 2016), while *Jag2* mutant mice displayed cleft palate (Vieira et al., 2005; Casey et al., 2006). Neural crest-specific knockout of *Jag1* or *Notch2* resulted in middle ear bone malformation (Humphreys et al., 2012; Teng et al., 2017). Knockout of *Rbpj*, a transcriptional cofactor of Notch, in neural crest cells led to shortened mandible formation (Mead and Yutzey, 2012). Deletion of Notch signaling target *Hey1* led to deformed pharyngeal arch arteries (Fujita et al., 2016). Interestingly, in *Presenilin1/2* null mutant mice which deficient in γ-secretase, the PA2 was absent (Donoviel et al., 1999). The $Maml1^{-/-};Maml3^{-/-}$ mutant embryos also displayed hypoplastic or even no PA2, indicating that morphogenesis of PA2 is particularly sensitive to Notch signaling activity (Oyama et al., 2011). The underlying cellular and molecular mechanisms for Notch signaling functions in the development of PAs remain elusive. In our previous studies, we showed that Notch1 intracellular domain (N1-ICD) was required in the epibranchial placodal epithelium in the proximal PAs to control cell fate commitment of neuronal and non-neuronal epibranchial placodal cells (Zhang et al., 2017). Moreover, Notch receptor signaling controlled rostral-caudal patterning of the non-neuronal placodal epithelial cells around the pharyngeal clefts, indicating important roles of Notch signaling in epithelial cell fate commitment and differentiation (Wang et al., 2020).

Combinatorial expression of *Hox* genes in hindbrain rhombomeres, neural crest and pharyngeal surface ectoderm are known to convey positional information in the PAs (Trainor and Krumlauf, 2001; Santagati and Rijli, 2003). Loss-of-function mouse mutant analyses have shown that *Hox* genes of the first three paralogous groups are required for the development of neural crest derivatives in the pharyngeal region. Mutations of *Hoxa* genes would lead to neural crest defects and malformation of craniofacial structures. Inactivation of *Hoxa2* resulted in homeotic transformation of PA2 components into PA1 (Rijli et al., 1993). *Hoxa1* mutation led to deletion of rhombomere 5 and severe reduction of r4, the mutant displayed hypoplasia of PA2 as a result of neural crest deficiency (Chisaka et al., 1992). *Hoxa3* mutants showed deformed neural crest derivatives of PA3 including the hyoid and thyroid cartilage (Chojnowski et al., 2016) and endoderm defects (Su et al., 2001; Kameda et al., 2004). Mutations of *Hoxb* genes led to neurogenic phenotypes. For instance, although double knockout of *Hoxa1* and *Hoxb1* in mice exacerbated the phenotypes of *Hoxa1* mutant and resulted in hypoplasia of PA2 and malformation of middle ear bones (Gavalas et al., 1998), *Hoxb1* mutant embryos did not exhibit any defects in neural crest-derived tissues of PA2, but displayed abnormal neuronal identity in hindbrain r4 (Goddard et al., 1996; Studer et al., 1996). *Hoxb2* mutant mice displayed retracted lower lip and mild craniofacial features (Barrow and Capecchi, 1996), *Hoxb3* null mutant had no craniofacial abnormalities (Manley and Capecchi, 1998). The specific functions of *Hox* genes in the different cell types of the developing PA are not entirely known.

Insights on the roles of *Hox* genes in cranial neural crest development have also been obtained by gain-of-function analysis. Cranial neural crest cells rostral to rhombomere 2 do not express *Hox* genes, and only *Hox*-free neural crest cells are capable of generating facial skeletal components (Couly et al., 1998; Le Douarin et al., 2004). Gain-of-function experiments by electroporation of *Hoxa2* into the *Hox*-free neural crest domain of chick embryos led to absence of lower jaw and frontonasal

structures; defective formation of PA1 derived skeletal structures were also observed in ectopic *Hoxa3* and *Hoxb4* expression experiments (Creuzet et al., 2002). Heterotopic transplantation experiments with fragments of neural folds have demonstrated that *Hox*-positive neural crest cells from the posterior region are incapable to replace *Hox*-free neural crest cells. These studies suggest that cross-talks among *Hox* genes, neural crest cells and extrinsic signals in the pharyngeal region, including ectodermal and endodermal derived factors, are required for the formation neural crest derived structures (Couly et al., 2002; Creuzet et al., 2002; Le Douarin et al., 2004; Minoux and Rijli, 2010).

We have previously generated a gain-of-function *Hoxb3* transgenic mutant $Hoxb3^{Tg}$ and shown that *Hoxb3* could transcriptionally suppress *Hoxb1* in the hindbrain and maintain anterior-posterior identity of rhombomere 4 and 5 (Wong et al., 2011). Using the *Hoxb2-r4* enhancer element (Maconochie et al., 1997; Szeto et al., 2009), we ectopically expressed *Hoxb3* to *Hoxb2* domains, including hindbrain rhombomere 4 and PA2 in $Hoxb3^{Tg/+}$, and examined the effect of altering the expression of *Hox* code in PA development. Although *Hoxb3* or *Hoxb2* null mutants had no or mild craniofacial defects, the $Hoxb3^{Tg/+}$ transgenic mutants displayed multiple neural crest-derived abnormalities. We found that ectopic expression of *Hoxb3* was restricted to the pharyngeal epithelium in the $Hoxb3^{Tg/+}$ mutant, allowing the study of interaction between pharyngeal epithelium and migrating neural crest cells. Interestingly, *Jag1* was ectopically expressed in the ectodermal epithelium of PA2, in cells which co-expressed *Hoxb3*. We showed that *Hoxb3* could transcriptionally regulate *Jag1* expression during PA development. Migration of neural crest cells into the PAs was affected, leading to neural crest deficiency and craniofacial defects at later stages. Our results suggest that *Hoxb3* positively regulates the expression of *Jag1* in the pharyngeal epithelial cells and affects the colonization and maintenance of neural crest cells in the developing PAs.

MATERIALS AND METHODS

Experimental Animals

The mouse lines used in this study include $Hoxb3^{Tg/+}$ [$Hoxb3^{Tg2}$ in Wong et al. (2011)], *B2-Cre* [*Hoxb2-r4-Cre* in Szeto et al. (2009)], *Wnt1-Cre* (Chai et al., 2000), and *Z/EG* (Novak et al., 2000). The $Hoxb3^{Tg/+}$ transgenic mice were maintained in FVB genetic background, other mouse lines were maintained in C57BL/6N background. All animals were housed at the Center for Comparative Medicine Research at the University of Hong Kong. The animal experiments were approved by the University of Hong Kong Committee on the Use of Live Animals for Teaching and Research (CULATR No. 4357–17 and 4588–18).

Riboprobe Labeling

Plasmids with target cDNA sequence including *Hoxa2* (Nonchev et al., 1996), *Hoxb2* (nucleotide 41–1114 of mRNA), *Hoxb3* (Wilkinson et al., 1989), *Jag1* (Jones et al., 2000) were cloned, linearized (restriction enzymes used were summarized in **Table 1**) and purified. RNA probes were prepared using 1 μg of purified DNA for reverse transcription and digoxigenin (DIG) labeling (Roche, 11277073910), synthesized RNA probe was precipitated in ethanol, dissolved in DEPC-treated water, and stored at -80°C.

Whole-Mount RNA *in situ* Hybridization

Embryos were harvested, fixed in 4% paraformaldehyde (PFA) at 4°C overnight, dehydrated in a series of methanol/PBST (Phosphate-buffered saline with 0.1% Tween-20) solutions and stored in absolute methanol at -20°C. Before *in situ* hybridization, samples were rehydrated with gradients of PBST series, treated with 1 μg/ml proteinase K, then post-fixed in 4% PFA, 0.2% glutaraldehyde in PBS. Embryos were then incubated with hybridization mix (50% formamide, 1.3x SSC, 50 μm EDTA, 50 μg/ml, 0.2% Tween20, 0.5% CHAPS, and 100 μg/ml heparin) at 65°C for 2 h, then incubated with the DIG-labeled RNA probe in hybridization mix at 65°C overnight. After hybridization, samples were washed with hybridization mix in maleic acid buffer with Tween-20 (MABT), blocked with 10% blocking reagent (Roche, 11096176001) and 20% heat-inactivated horse serum, and then incubated in 1:2000 alkaline phosphatase conjugated anti-DIG antibody (Roche, 11093274910) in the same blocking buffer at 4°C. After washing with MABT for 24 h, embryos were immersed in BM purple (Roche, 11442074001) for color development. Reaction was stopped by washing with PBST and post-fixed in 4% PFA.

Immunostaining and Antibodies

For whole mount immunostaining, E10.5 mouse embryos were harvested and fixed in 4% PFA for 1.5 h, followed by inactivation of endogenous peroxidase in 0.05% peroxide in PBS at 4°C overnight. Embryos were then blocked in PBS-TS (10% heat inactivated serum, 1% Triton X-100 in PBS) for 3 h at 4°C, incubated with 2H3 anti-neurofilament primary antibody (1:100, Developmental Studies Hybridoma Bank) at 4°C for 3 days. Embryos were then incubated with peroxidase-conjugated rabbit anti-mouse secondary antibody (1:200, Dako) and subjected to 4-chloro-1-napthol (Sigma) color development. The reaction was stopped by washes of 30% ethanol.

For section immunostaining, 10 μm thick cryo-sectioned samples were blocked with 10% heat-inactivated horse serum in PBS for 1 h. The sections were then incubated with primary antibodies including GFP [1:500, Rockland Immunochemicals, 600-101-215), Pax8 (1:500, Proteintech, 10336-1-AP), and Jag1 (1:300, Developmental Studies Hybridoma Bank, TS1.15H)] and E-cadherin (1:500, Cell signaling, 24E10) at 4°C overnight. After three washes of PBS, Alexa Fluor 488- or 594-conjugated secondary antibodies (1:500, Life technologies) were applied. DAPI (Sigma-Aldrich, D9542) was used as a counterstain for the nucleus. Sections were washed with PBS then mounted with mounting medium (Vectashield, Vector Laboratories).

Scanning Electron Microscopy

Embryos were fixed in 2.5% glutaraldehyde for 4 h and then in 1% osmium tetroxide for 1 h, dehydrated in graded ethanol and critical-point dried with transition fluid liquid carbon dioxide in a Ladd critical point dryer. Gold-palladium-coated specimens

TABLE 1 | Enzymes used for riboprobe labeling.

Antisense Probe	Restriction enzyme for anti-sense probe	RNA polymerase for RNA transcription	References
Hoxa2	*Eco*RI	T7	Nonchev et al., 1996
Hoxb2	*Bam*HI	T3	This study
Hoxb3	*Bam*HI	T3	Wilkinson et al., 1989
Jag1	*Eco*RI	T3	Jones et al., 2000

were examined with a JEOL JSM-6301FE scanning electron microscope operated at 5 KV.

Skeletal Preparations

Newborn mice were fixed in 95% ethanol overnight. After skin removal, the whole-mount skeletons were incubated in 0.015% Alcian Blue and 0.005% Alizarin Red stain diluted in 5% acetic acid in 70% ethanol for 1 week (Mcleod, 1980). The preparations were cleared in 20% glycerol, 1% potassium hydroxide, and then transferred to 50% glycerol/ethanol for photography.

Bioinformatics Analysis of Hoxb3 Binding Sites

The matrix of Hoxb3 binding sequence (PH0058.1) was obtained from the JASPAR database. Hoxb3 binding motif was scanned along 100 kb upstream of *Jag1* locus using Find Individual Motif Occurrences v5.0.5 (FIMO) with $p < 0.0005$ as cutoff. The genomic loci were further analyzed for sequence conservation among human, chicken, lizard and Xenopus with PhyloP score higher than 1. Genomic regions were further aligned with open chromatin regions in developing mouse embryo (E11.5) ATAC-seq data with following accession code: ENCSR150RMQ (facial prominence), ENCSR273UFV (forebrain), ENCSR382RUC (midbrain), ENCSR012YAB (hindbrain), and ENCSR282YTE (neural tube).

P19 Cell Culture

P19 mouse embryonal carcinoma cells were cultured on gelatin-coated (0.1%) tissue culture dishes in Dulbecco's Modified Eagle Medium (DMEM) medium (Gibco) supplemented with 10% FBS. Retinoic acid (RA) treatment (10^{-8} M) of P19 cells for activation of hindbrain *Hox* genes expression were performed as previously described (Okada et al., 2004; Wong et al., 2011). Using 10^{-8} M RA, expression of anterior *Hox* genes including Hoxb3 would be activated endogenously.

Quantitative Real-Time PCR

Total RNA samples were extracted according to TRIzol manufacturer's protocol from RA treated and control P19 cells. cDNA samples were generated from total extracted RNA using Superscript III (ThermoFisher) and polymerase chain reaction (PCR) performed with SYBR Green Premix Ex Taq II (TaKaRa) using the StepOnePlus Real-Time PCR system. Primers for *Hoxb3*: forward: 5′-GCAGA AAGCC ACCTA CTACG-3′, reverse: 5′-CCATT GAGCT CCTTG CTCTT-3′; for *Jag1*: forward: 5′-AACAC AGGGA TTGCC CACTT-3′, reverse: 5′-TGTTG CAATC AGGAC CCATC-3′; for Gapdh: forward: 5′-TTCAC CACCA TGGAG AAGGC-3′; reverse: 5′-GGCAT GGACT GTGGT CATGA-3′. Relative expression of *Hoxb3* and *Jag1* were normalized with *Gapdh* expression. All the experiments were performed in triplicates.

Chromatin Immunoprecipitation Assay

Chromatin immunoprecipitation (ChIP) assay (Hu and Rosenblum, 2005) was performed with the following modifications. For RA-treated P19 cells, 1×10^6 cells were harvested for each assay. For *in vivo* ChIP, 4 litters of E9.5 wildtype whole embryos were harvested in PBS, fixed in 1% formaldehyde for 20 min at 25°C, and then disintegrated with RIPA buffer. The cross-linked material was sonicated to 200–1,000 bp fragments (Vibracell sonicator; seven times for 10 s at 40% output), anti-Hoxb3 antibody (Santa Cruz, C-20, and sc-17169) or normal rabbit IgG were then used to pull down the chromatin. PCR amplifications were performed using the following primers: for S1: forward: 5′-AGTCA TCGTC TGCTG CCTTT-3′, reverse: 5′-GCAAC GAATT CATTC AGCAA-3′; for S2: forward: 5′-TTTTA GCCCC TGCTT GCTTA-3′, reverse: 5′-TTGGA GAACA GCCCT CATTT-3′; for S3: forward: 5′-CCTAA CCCCT TTCCC ATCAT-3′, reverse: 5′-TTCTT GTTTG GGCTT GCTCT-3′; for B3ARE: forward: 5′-GTAGG TGTGT GGGCA GAGGT-3′, and reverse: 5′-CTGAG TGGAG GATGG GTTGT-3′. The experiments were performed with 3 biological replicates and 3 technical replicates.

In vitro and *ex vivo* Luciferase Activity Assays

For the *in vitro* transactivation experiments, *pCIG-Hoxb3* cDNA (Yau et al., 2002) or *pCIG* control expression vector was co-electroporated with Firefly and Renilla luciferase reporters into human embryonic kidney cells 293T. The luciferase reporter constructs were *pGL3-Jag1-S2* which contained a 400 bp fragment (*Jag1* genomic DNA, mm10 chr2: 136979005-136979405) on the *Jag1* locus with the Hoxb3 binding site S2 CTGTAATTAACT, or *pGL3-Jag1-mS2* which contained a mutated Hoxb3 binding site mS2 CTGGCCGGCACT, or *pGL3* control luciferase vector. After 24 h, the cells were processed for luciferase assay as previously described (Dessaud et al., 2007; Wong et al., 2011). Briefly, cells were homogenized in lysis buffer on ice, Firefly and Renilla luciferase activities were measured with the Dual Luciferase Reporter Assay System (Promega).

For the *ex vivo* luciferase activity assay, *pCIG-Hoxb3* cDNA or *pCIG* control vector, together with *pGL3-Jag1-S2, pGL3-Jag1-mS2,* or control luciferase reporter construct, and Renilla luciferase reporter, were electroporated into the hindbrain region of E9.0 mouse embryos. After cultured for 24 h, the pharyngeal portion (**Figure 4D**) of the embryos were homogenized in

lysis buffer on ice, Firefly and Renilla luciferase activities were measured as above.

All the experiments were performed with 3 biological replicates and 3 technical replicates.

Statistical Test

Statistical comparison of two groups was performed by Student's *t*-test, where n number represented biological replicates using the same experimental condition. Error bars indicated standard error of the mean (SEM).

RESULTS

Expression of *Hox* Genes in Pharyngeal Ectoderm and Epibranchial Placodal Cells

The expression of *Hox* genes in the developing PAs have been well characterized. However, the expression and function of *Hox* genes in the pharyngeal surface ectoderm and the epibranchial placodal epithelium of the pharyngeal arches are not well understood. We showed that *Hoxa2* and *Hoxb2* were both expressed in PA2, PA3 and posterior PAs, and *Hoxb3* was expressed in PA3 and posterior PAs at E9.5 (**Figures 1A,C,E**). Interestingly, coronal sections at the level of proximal pharyngeal arches (refer to **Figure 1N**) of embryos hybridized with *Hoxa2* and *Hoxb2* probes revealed differential expression of these two genes in PA2. *Hoxa2* was expressed strongly in the neural crest derived ectomesenchyme but hardly detectable in the epibranchial placodal epithelium covering PA2 (**Figures 1B,B'**), although it was expressed in placodal epithelium and neural crest cells of posterior PAs. On the contrary, *Hoxb2* was distinctly expressed in the epibranchial placodal epithelium of PA2 and posterior PAs (**Figure 1D**), while expressed at lower levels in the neural crest cells of these PAs (**Figure 1D**). *Hoxb3* was strongly expressed in the pharyngeal surface ectoderm (**Figure 1E**), epibranchial placodal epithelium and neural crest cells of PA3 and posterior PAs (**Figure 1F**).

We have previously demonstrated that in the developing PAs, the proximal pharyngeal epithelium was derived from the posterior placodal area and overlap with the epibranchial placodal cells (**Figure 1I**, red dotted line; Zhang et al., 2017; Wang et al., 2020), while the distal PAs were enveloped by pharyngeal ectodermal epithelium. Therefore, the proximal and distal pharyngeal epithelium were composed of developmentally distinct epithelial cells. The *Hox* genes delineate the antero-posterior identity of the pharyngeal arches, including the neural crest cells delaminated from specific hindbrain rhombomeres. Neural crest cells in PA2 expressed *Hoxa2* and *Hoxb2*, while those in PA3 and posterior PAs expressed *Hoxb3* in addition to *Hoxa2* and *Hoxb2*. However, for the pharyngeal epithelium, we showed that *Hoxb2* marked PA2 (**Figures 1D,I**) and *Hoxb3* marked PA3 (**Figures 1F,I**). The distinct expression patterns of *Hox* genes in both the proximal and distal pharyngeal epithelium of specific PAs suggest a role of these genes in maintaining the functions of epibranchial placodal cells in the proximal regions.

Ectopic Expression of *Hoxb3* in PA2 of *Hoxb3$^{Tg/+}$* Transgenic Mutants

To investigate the role of the combinatorial *Hox* code in PA development as well as to understand the potential interactions between placodal cells and underlying neural crest cells, we investigated the *Hoxb3$^{Tg/+}$* gain-of-function transgenic mutant generated with the *Hoxb2-r4* enhancer (Wong et al., 2011). The *Hoxb2-r4* enhancer could direct reporter gene expression in hindbrain rhombomere 4 and PA2 (Maconochie et al., 1997; Ferretti et al., 2000). We analyzed the enhancer activity in the pharyngeal epithelium using the *B2-Cre* [*Hoxb2-r4-Cre*; (Szeto et al., 2009)] mouse line. Wholemount *B2-Cre;Z/EG* embryos showed expression of the GFP reporter in the pharyngeal region at E8.5 (**Figure 1J**), and in PA2 at E9.5 (**Figure 1L**). By immunostaining with Pax8, one of the earliest markers of the posterior placodal area (Schlosser and Ahrens, 2004; Washausen and Knabe, 2017), on coronal sections of E8.5 embryo, we showed that GFP + cells also expressed Pax8 (**Figures 1K,K'**), confirming the enhancer activity in the placodal epithelial cells. Coronal sections of E9.5 embryos showed *B2-Cre* activity in the proximal placodal epithelium and pharyngeal ectodermal region from second to posterior arches, as well as the neural crest cells in PA2 and PA3 (**Figures 1L,M**).

In the *Hoxb3$^{Tg/+}$* mutant, driven by the *Hoxb2-r4* enhancer element, ectopic *Hoxb3* was expressed not only in the entire proximal and distal PA2, but also in posterior region of PA1 (**Figures 1G,H**). Coronal sections of *Hoxb3$^{Tg/+}$* embryos showed that ectopic expression of *Hoxb3* was restricted to the pharyngeal epithelium of posterior PA1 and PA2 (**Figure 1H**), no expression could be observed in the neural crest cells of PA2. Therefore, in the *Hoxb3$^{Tg/+}$* mutant, we have ectopically expressed *Hoxb3* specifically in the pharyngeal epithelium of PA2 and posterior PA1, providing a gain-of-function genetic condition for analysis of epithelial cell function during PA development.

Ectopic Expression of *Jag1* in PA2 Epithelium of *Hoxb3$^{Tg/+}$* Mutant

To investigate the consequences of ectopic expression of *Hoxb3* in pharyngeal arch patterning, we examined the expression of genes in the distal PAs including *dHAND* which marked the medial regions (**Figure 2A**), *Gsc* which marked the ventral aspects (**Figure 2C**), and *Dlx5* which marked the lateral regions (**Figure 2E**) of PA1 and PA2 in E10.5 embryos. However, the regional specific expression patterns of *dHAND, Gsc,* and *Dlx3* were not changed in the *Hoxb3$^{Tg/+}$* mutants (**Figures 2B,D,F**), indicating the patterning of distal PAs remained unaffected with the ectopic expression of *Hoxb3*.

As Notch signaling has been shown to be critical for the development of epibranchial placodal epithelium and proximal PAs (Zhang et al., 2017; Wang et al., 2020), we examined *Jag1* which was expressed in the proximal pharyngeal epithelium of developing PAs and restricted to the pharyngeal clefts and pouches as the segmental plates were formed at E9.5 (**Figures 2G,I,K**). Interestingly, we found that the expression of *Jag1* was ectopically activated in the entire pharyngeal ectodermal region of PA2 and posterior PA1 in the *Hoxb3$^{Tg/+}$* mutants at

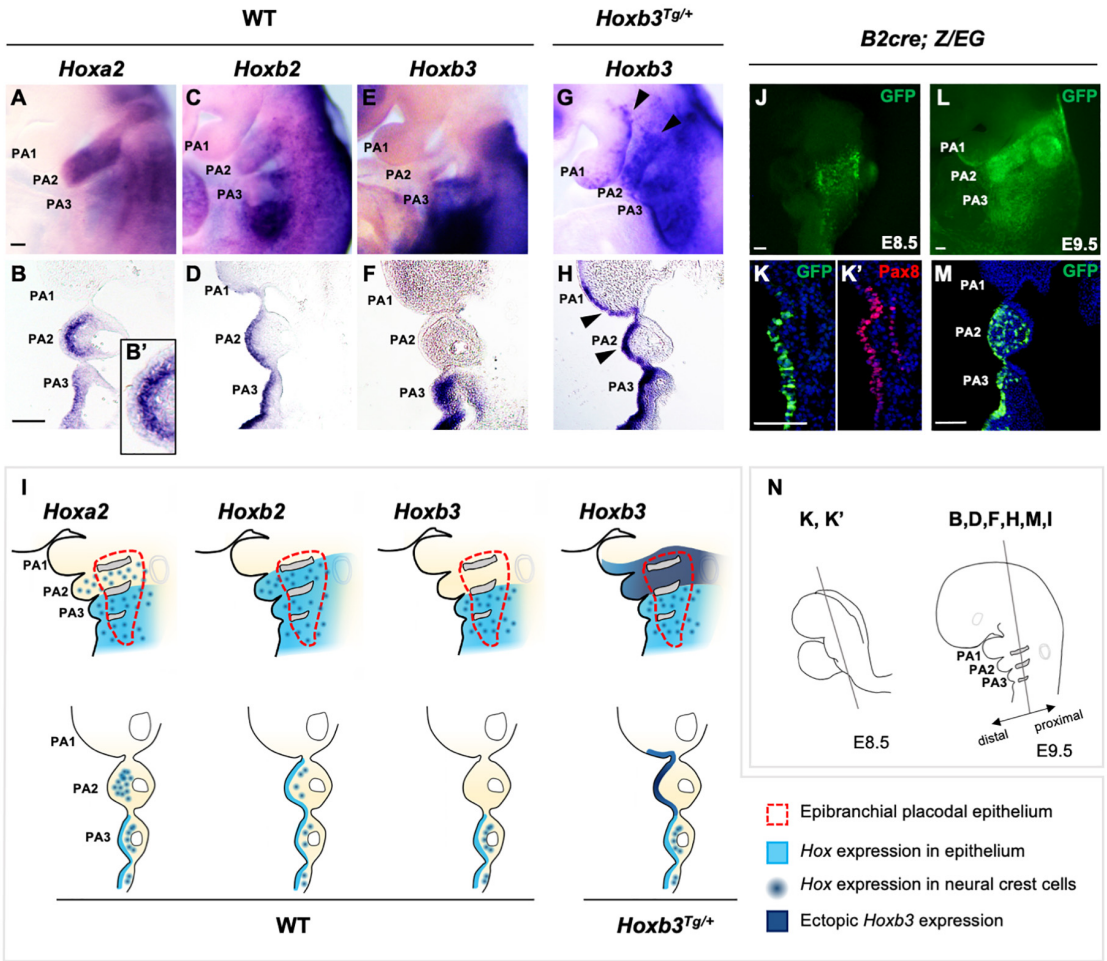

FIGURE 1 | Expression of *Hox* genes in pharyngeal arches of wildtype and $Hoxb3^{Tg/+}$ embryos. **(A–H)** Wholemount *in situ* hybridization and coronal sections showing expression of *Hoxa2, Hoxb2,* and *Hoxb3* in wildtype and mutant E9.5 embryos ($n = 3$). An enlarged image in **(B')** showing the absence of *Hoxa2* expression in the epithelium covering PA2. Arrowheads in **(G,H)** indicate ectopic expression of *Hoxb3* in the pharyngeal epithelium of PA1 and PA2. **(I)** Schematic summary of *Hox* gene expression in the pharyngeal ectoderm, epibranchial placodal region, and neural crest cells of E9.5 wildtype and $Hoxb3^{Tg/+}$ embryos. **(J,K)** Wholemount GFP autofluorescence **(J)** and co-immunostaining of GFP **(K)** and Pax8 **(K')** in coronal section of E8.5 *B2-Cre;Z/EG* embryos ($n = 3$). **(L,M)** Wholemount GFP autofluorescence **(L)** and immunostaining of GFP in coronal section **(M)** of E9.5 *B2-Cre; Z/EG* embryos ($n = 3$). **(N)** Schematic diagram illustrating the plane of embryo sections for the indicated panels in this figure. PA1, PA2, and PA3 indicate the 1st, 2nd, and 3rd pharyngeal arches. Scale bars: 100 μm.

E9.5 (**Figures 2H,J**). The expression of *Jag1* in the epibranchial placodal epithelium of PA1 and PA2 as shown in coronal section of $Hoxb3^{Tg/+}$ mutant (**Figure 2J**) was remarkably similar to the ectopic *Hoxb3* expression domains (**Figure 1H**). By immunostaining we could detect Jag1 protein in the pharyngeal epithelium of PA2 of $Hoxb3^{Tg/+}$ mutant (**Figure 2L**), suggesting that ectopic expression of *Hoxb3* in the pharyngeal epithelium in PA2 could activate Jag1 protein expression in PA2.

We have previously shown that over-expression of the Notch receptor protein N1-ICD in the epibranchial placodal epithelium would lead to misexpression of Fgf ligands and cell fate changes (Wang et al., 2020). Therefore, we examined the expression of *Fgf3* and *Fgf8*, which marked placodal epithelial cells flanking the pharyngeal clefts (**Figures 2M,O**). However, we found that ectopic expression of the Notch ligand *Jag1* did not cause changes of *Fgf3* or *Fgf8* expression in $Hoxb3^{Tg/+}$ mutants (**Figures 2N,P**), suggesting that the pharyngeal epithelial cell fates were not affected.

Malformations of Neural Crest Derived Structures in the $Hoxb3^{Tg}$ Mutants

We first examined the phenotypes of the $Hoxb3^{Tg}$ mutant PAs by scanning electron microscopy. Although the pharyngeal arch phenotypes of the mutant were mild, it was evident that the PA2 was smaller in $Hoxb3^{Tg/+}$ and significantly reduced in size in the $Hoxb3^{Tg/Tg}$ at E10.5 (**Figures 3A–C**). To investigate the neural components in the pharyngeal region, wholemount immunohistochemistry was performed using 2H3 anti-neurofilament antibody. In the $Hoxb3^{Tg/+}$ mutants, the vestibulocochlear nerve (VIIIn), the superficial petrosal nerve (spn), and the chorda tympanic nerve (ct) were

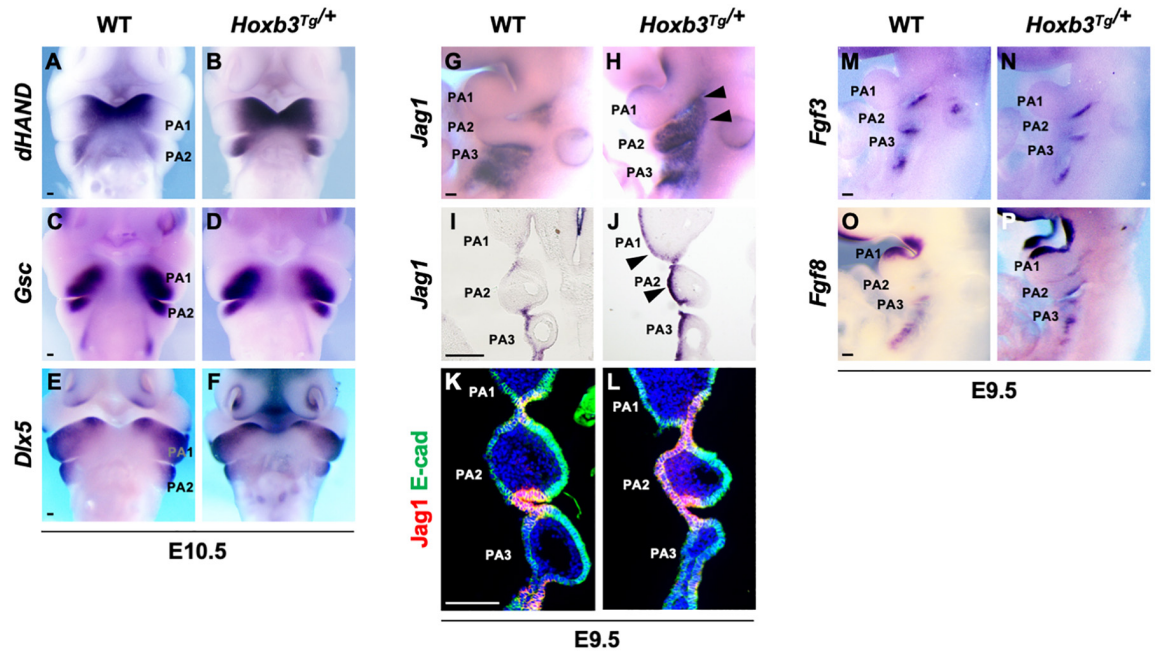

FIGURE 2 | Pharyngeal arch patterning and ectopic expression of Jag1 in the *Hoxb3*$^{Tg/+}$ mutants. **(A–F)** Wholemount *in situ* hybridization showing expression of *dHAND*, *Gsc,* and *Dlx5* in wildtype and *Hoxb3*$^{Tg/+}$ embryos at E10.5 ($n > 3$). **(G,H)** Wholemount *in situ* hybridization of *Jag1* showing ectopic expression in PA1 and PA2 (arrowheads) of E9.5 *Hoxb3*$^{Tg/+}$ embryos ($n = 4$). **(I,J)** Coronal sections of embryos subjected to wholemount *in situ* hybridization of *Jag1* showing ectopic expression in the ectodermal epithelium of PA1 and PA2 (arrowheads) in *Hoxb3*$^{Tg/+}$ embryos ($n = 3$). **(K,L)** Immunostaining for Jag1 (red) and E-cadherin (green) on coronal sections of E9.5 wildtype and *Hoxb3*$^{Tg/+}$ embryos ($n = 5$). **(M–P)** Wholemount *in situ* hybridization of *Fgf3* and *Fgf8* on E9.5 wildtype and *Hoxb3*$^{Tg/+}$ embryos ($n > 3$). PA1, PA2, and PA3 indicate the 1st, 2nd, and 3rd pharyngeal arches. Scale bars: 100 μm.

absent (**Figures 3D,E,G,H**). In the *Hoxb3*$^{Tg/Tg}$ mutants, there was abnormal fusion between the trigeminal ganglion (V) and the facial acoustic ganglia (VII; **Figures 3F,I**).

To examine the phenotypes of neural crest derived skeletal components, neonates were examined by skeletal staining. Among the PA1 derived structures, the mandible was reduced in length and poorly ossified and the coronoid process was absent in both *Hoxb3*$^{Tg/+}$ and *Hoxb3*$^{Tg/Tg}$ mutants. The condylar process was present in the *Hoxb3*$^{Tg/+}$ embryos, but missing in the *Hoxb3*$^{Tg/Tg}$ embryos (**Figures 3J–L**). The maxillary arch derived squamous bone was slightly affected with a duplication found in the retrotympanic process in the *Hoxb3*$^{Tg/+}$ embryos (**Figures 3M,N**). The squamous bone was more severely affected in the *Hoxb3*$^{Tg/Tg}$ mutants (**Figure 3O**). Among the PA1 derived middle ear structures, the malleus and incus were hypoplastic in the *Hoxb3*$^{Tg/+}$ embryos (**Figures 3P,Q**), and absent in the *Hoxb3*$^{Tg/Tg}$ mutants (**Figure 3R**). The otic capsule and tympanic ring were hypoplastic in the *Hoxb3*$^{Tg/Tg}$ mutants (**Figure 3R**). For the PA2 derived skeletal elements, the styloid process was slightly truncated in *Hoxb3*$^{Tg/+}$, while both the stapes and styloid process were severely reduced in the *Hoxb3*$^{Tg/Tg}$ mutants (**Figures 3Q,R**). The hyoid cartilage appeared normal in *Hoxb3*$^{Tg/+}$, the morphology of the greater horn of the hyoid cartilage was mildly affected in the *Hoxb3*$^{Tg/Tg}$ mutants (**Figures 3S–U**). Taken together, we showed that the development of both PA1 and PA2 neural crest derived skeletal structures were affected in the *Hoxb3*^{Tg} transgenic mutants.

Deficient Neural Crest Cell Migration Into PA2 of *Hoxb3*^{Tg} Mutant

We hypothesized that the hypoplastic PA2 and abnormal neural crest derived structures in the *Hoxb3*^{Tg} mutants could be due to neural crest cell deficiencies. By using the *Wnt1-cre;Z/EG* mice as neural crest cell lineage marker, we generated compound mutants and traced the migrating neural crest cells at E9.0 and E9.5. We observed consistently fewer neural crest cells migrating to PA2 of the *Hoxb3*$^{Tg/+}$, and significantly few cells entering PA2 of the *Hoxb3*$^{Tg/Tg}$ mutants at E9.0 and E9.5 (**Figures 3V–AA**). Therefore, the multiple neural and skeletal phenotypes observed in the mutant pharyngeal regions were likely due to insufficient neural crest cells populating PA2.

Hoxb3 Activates the Expression of Jag1 by Direct Binding to Specific Genomic Sites

To investigate the possibility that *Hoxb3* may directly activate *Jag1* expression by binding to genomic regulatory elements, we performed bioinformatics analyses to identify possible Hoxb3 binding sites around the *Jag1* gene. Using the consensus Hoxb3 binding matrix from JASPAR database, we searched the conserved regions within 100 kb upstream of Jag1 among six vertebrate species including mouse, human, chicken, lizard, Xenopus, and zebrafish. Furthermore, by comparing the open chromatin regions upstream of *Jag1* from several E11.5 mouse

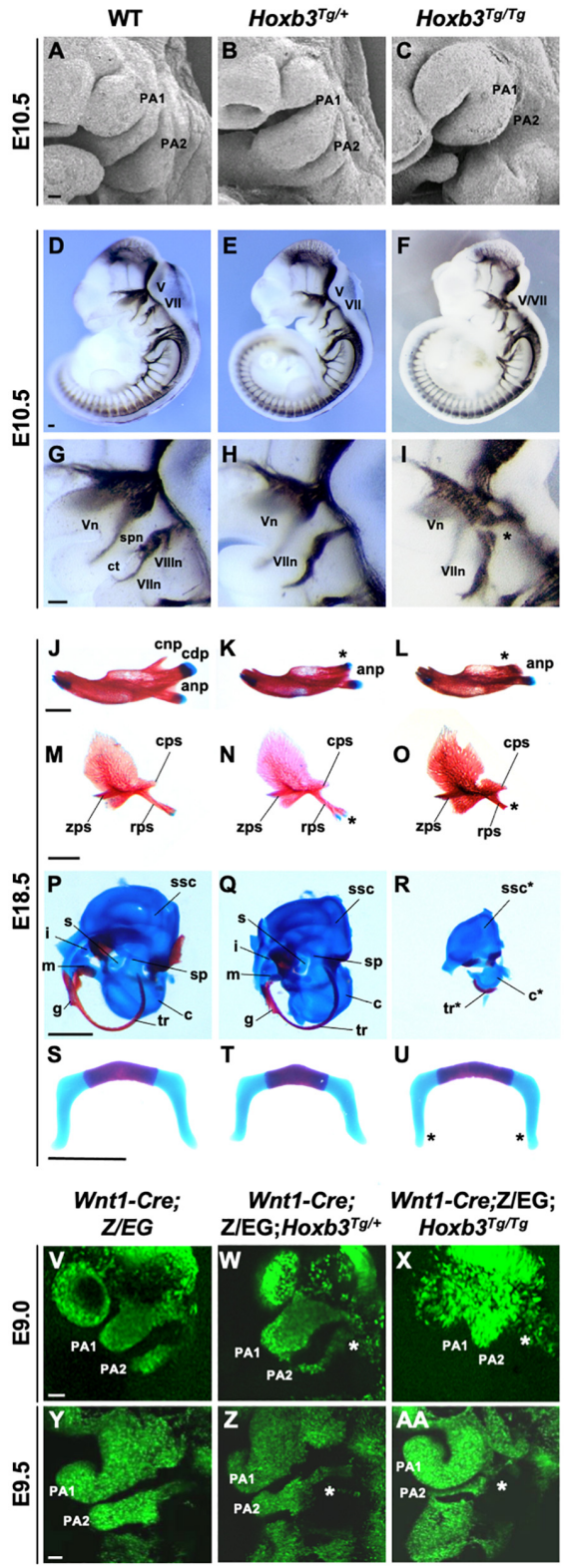

FIGURE 3 | Hypoplastic PA2 and defective neural crest development in *Hoxb3*^{Tg} mutants. **(A–C)** Scanning electron microscopy of E10.5 wildtype, *Hoxb3*$^{Tg/+}$ and *Hoxb3*$^{Tg/Tg}$ embryos (n = 3). **(D–I)** Neurofilament antibody *(Continued)*

FIGURE 3 | Continued
(2H3) staining showing cranial nerve defects in wildtype and *Hoxb3*^{Tg} mutants at E10.5 (n > 3). **(G–I)** are enlargements of pharyngeal regions showing abnormal facial nerve branching in *Hoxb3*$^{Tg/+}$ and nerve fusion in *Hoxb3*$^{Tg/Tg}$ (indicated with asterisk). V/Vn, trigeminal nerve; VII/VIIn, facial nerve; VIIIn, vestibuloaoustic nerve; spn, superficial petrosal nerve; and ct, chorda tympani nerve. **(J–R)** Skeletal preparations showing defective PA1 and PA2 neural crest cell derived structures in the *Hoxb3*^{Tg} mutants (n > 5). **(J–L)** Skeletal preparations showing defective mandibles of *Hoxb3*^{Tg} mutants. Absence of condylar process indicated with asterisks. **(M–O)** Defective squamous bones in *Hoxb3*^{Tg} mutants. Abnormal retrotympanic process indicated with asterisks. anp, angular process, cdp and cnp, condylar and coronoid processes of mandible; cps, caudal process of squamous; rps, retrotympanic process of squamous; zps, zygomatic process of squamous; and g, gonial. **(P–R)** Defective middle ear bones, inner ear otic capsules and associated elements in *Hoxb3*^{Tg} mutants. c, cochlea; i, incus; m, malleus; s, stapes; sp, styloid process; ssc, semi-circular canals; and tr, tympanic ring. **(S–U)** Skeletal preparations showing mild defects in the hyoid cartilage of *Hoxb3*$^{Tg/Tg}$ mutants. *indicates the greater horn. **(V–AA)** Wholemount GFP autofluorescence of *Wnt1-Cre;Z/EG;Hoxb3*^{Tg} compound mutant embryos showing abnormal distribution of GFP-positive neural crest cells (asterisks) to PA2 in E9.0 and E9.5 *Hoxb3*$^{Tg/+}$ and *Hoxb3*$^{Tg/Tg}$ embryos. PA1 and PA2 indicate the 1st and 2nd pharyngeal arches (n > 3). Scale bars: A-I and V-AA, 100 μm; J-U, 1,000 μm.

tissues, we identified three potential regulatory sites, named S1, S2, and S3. The S1 and S2 sites were located upstream of *Jag1* gene (mm10 chr2:137190579-137190732; chr2:137153318-137153475), the S3 site was in the intron between Exon2 and Exon3 of *Jag1* (mm10 chr2:137110522-137110680; **Figure 4A**).

To test whether Hoxb3 can directly bind to the three identified binding sites around *Jag1* gene, we performed *in vitro* and *in vivo* chromatin immunoprecipitation assays using P19 cells and mouse embryos. We treated P19 cells with RA to activate the endogenous expression of *Hoxb3*. The Quantitative real-time PCR (qRT-PCR) results showed that the expression of *Hoxb3* and *Jag1* were significantly increased after RA treatment (**Figure 4B**). Chromatin fragments from RA treated P19 cells were immunoprecipitated with a Hoxb3 antibody (**Supplementary Figure 1**). Several sets of primers were used to detect potential binding to the S1, S2, and S3 sites. A known Hoxb3 binding site, B3ARE in the auto-regulatory element (Yau et al., 2002; Wong et al., 2011), was used as a positive control. The qRT-PCR results of ChIP assays showed that Hoxb3 antibody could immunoprecipitate the B3ARE and S2 sites but not S1 or S3 sites. We further performed *in vivo* ChIP assays using wildtype E9.5 embryos. The entire embryos were lysed and the chromatin fragments were immunoprecipitated with IgG and Hoxb3 antibodies. The PCR results showed that endogenous Hoxb3 protein could form complex with chromatin fragments containing the S2 binding site (**Figure 4B**). To further investigate whether Hoxb3 could positively regulate the expression of *Jag1* through binding to the S2 site, we performed luciferase assay on human embryonic kidney cells 293T. Luciferase activity was significantly increased in the presence of Hoxb3, but no activation could be observed when Jag-S2 site was mutated (**Figure 4C**). To further investigate whether Hoxb3 could positively regulate the expression of *Jag1* through binding to the S2 site, we performed

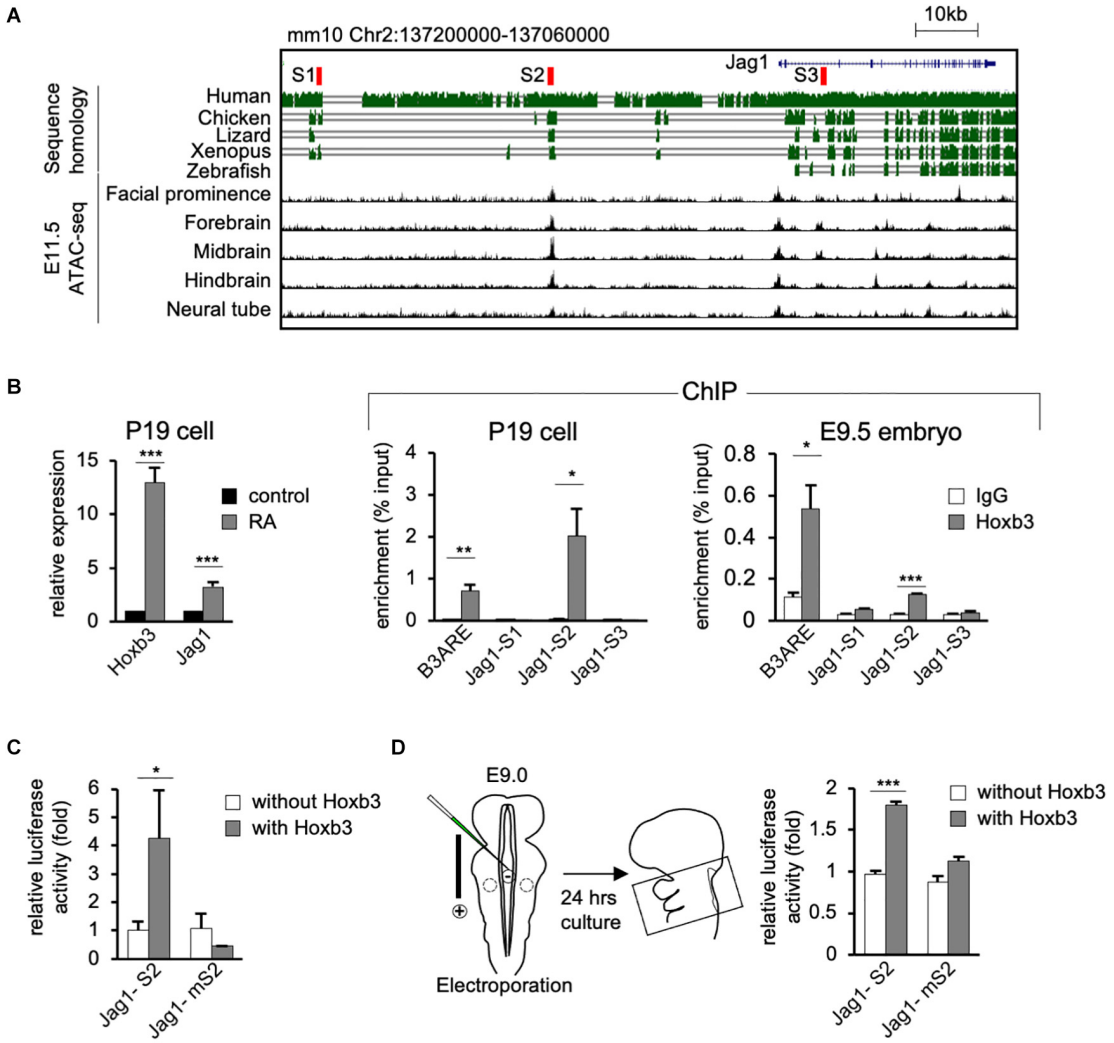

FIGURE 4 | Hoxb3 regulates Jag1 expression by binding to *cis*-regulatory region S2. **(A)** Genome browser tracks showing mouse *Jag1* locus including 100 Kb upstream genomic region. Alignment of genomic regions of human, chicken, lizard and xenopus revealed conserved regions and identification of potential Hoxb3 binding regions S1, S2, and S3 (highlighted in red). ATAC-seq tracks from ENCODE database of multiple E11.5 mouse embryo tissues showed an open chromatin region (S2) 40 kb upstream of *Jag1* transcription start site. **(B)** *In vitro* and *in vivo* chromatin immunoprecipitation (ChIP) analyses using RA treated P19 cells and mouse embryos. qRT-PCR analysis of P19 cells showed elevated expression of *Hoxb3* and *Jag1* after RA treatment. ChIP qRT-PCR analysis showed that Hoxb3 could bind to S2 site of *Jag1*, but not S1 or S3 sites. Hoxb3 could also bind to the B3ARE site, an autoregulatory element which served as a positive control. ChIP qRT-PCR analysis using E9.5 embryos also showed that Hoxb3 could bind to the S2 site and the positive control B3ARE site. **(C)** *In vitro* luciferase reporter assay using 293T cells. Expression of *Hoxb3* could activate luciferase activity when co-transfected with *Jag1-S2* reporter, the activity was much lower when co-transfected with *Jag1-mS2* reporter containing mutated S2 site. **(D)** *Ex vivo* luciferase reporter assay using E9.0 mouse embryos. Co-electroporation of *Hoxb3* expression vector with *Jag1-S2* or *Jag1-mS2* luciferase reporter showed that *Hoxb3* could elevate luciferase activity via the normal S2 site. Data in **(B–D)** are shown as mean ± SE (n = 3 biological replicates). $^{*}P < 0.05$, $^{**}P < 0.01$, and $^{***}P < 0.001$.

mouse *ex vivo* electroporation experiment (**Figure 4D**). Co-expression of the luciferase reporter containing S2 binding site of *Jag1* (Jag1-S2) and *Hoxb3* expression vector, luciferase activity could be detected in the embryo lysates. Without Hoxb3, luciferase activity was significantly reduced. However, with the S2 site mutated in the *Jag1* luciferase reporter (Jag1-mS2), electroporation of Hoxb3 expression vector could not increase the luciferase activity.

In conclusion, by molecular studies we demonstrated that endogenous Hoxb3 protein could directly activate the expression of *Jag1* through specific binding to the S2 regulatory site. This study revealed a novel regulatory mechanism for *Jag1* gene expression. During normal development, cell type-specific expression of *Jag1* could be regulated by *Hoxb3*.

DISCUSSION

The roles of *Hox* genes in providing positional information in axial development have long been established. In the pharyngeal region, combinatorial *Hox* expression defines the positional identify of the hindbrain rhombomeres and associated neural

crest cells. It has been suggested that the surface ectoderm also expresses combinatorial *Hox* genes, presenting segmentally patterned "ectomeres" where the ectodermal epithelium is regionally specified and associated with the *Hox*-patterned pharyngeal arches (Couly and Le Douarin, 1990; Hunt et al., 1991). However, the antero-posterior segmental specific functions of the ectodermal pharyngeal epithelium in the PAs remain elusive. The pharyngeal epithelium is important for providing environment cues for cranial neural crest cell homing, survival and differentiation. Our gain-of-function $Hoxb3^{Tg}$ mutant analysis here suggests that the cross-talk of *Hox* genes with molecular signaling in the pharyngeal epithelium is required for interaction and maintenance of neural crest cells during PA development.

Expression of *Hox* Genes and Neural Crest Defects in $Hoxb3^{Tg}$ Mutant PAs

In the $Hoxb3^{Tg}$ mutant, we have previously shown that hindbrain neurogenesis defect was observed as a result of the loss of *Hoxb1* expression in hindbrain r4 (Wong et al., 2011). However, here we found that the generation, delamination and migration of r4-derived neural crest was not affected, except that the population of neural crest cells entering the mutant PA2 were reduced (**Figures 3W,X,Z,AA**). The expression patterns of *Hoxa1, Hoxa2,* and *Hoxb1* in the PAs were not changed in the $Hoxb3^{Tg/+}$ mutant (**Supplementary Figure 2**). Therefore, in the $Hoxb3^{Tg/+}$ mutant, normal combinatorial *Hox* genes were expressed in the neural crest cells. The dorso-ventral patterning of PAs also remained unaffected in the mutant (**Figures 3A–F**). The specific changes in the $Hoxb3^{Tg/+}$ mutant were with the surface ectoderm, the entire proximal-distal pharyngeal epithelium of PA2 and posterior PA1 were the only cells expressing *Hoxb3* ectopically. Although PA1 is normally a *Hox*-free zone, and the enhancer activity of the *Hoxb2-r4* element used to drive ectopic gene expression is expected to cover PA2 only (**Figures 1L,M**), as a result of transgene insertion activity, ectopic *Hoxb3* expression was unexpectedly also found in PA1 epithelium. The ectopic expression patterns of *Hoxb3* would explain that neural crest structures derived from both PA1 and PA2 were affected in the $Hoxb3^{Tg}$ mutants. The malformations could be a direct effect of ectopic *Hoxb3* expression in the ectodermal pharyngeal epithelium, or through other signaling molecules including *Jag1* as discussed below.

In the heterozygous $Hoxb3^{Tg/+}$ transgenic mutant, the PA phenotypes were mild, but the hypoplasia of PA2 and craniofacial malformations were more evident in the homozygous $Hoxb3^{Tg/Tg}$ with a higher dosage of the transgene. The fusion of the trigeminal and facioacoustic ganglia observed in $Hoxb3^{Tg/Tg}$ suggests that there might be mixing or mis-routing of neural crest cells. As visualized by *Wnt1-Cre;Z/EG* lineage tracing experiments, in E9.0 $Hoxb3^{Tg/Tg}$ mutant embryo the neural crest cells appeared aggregated around the proximal PA1 and PA2 region (**Figure 3X**). As many of the neural crest cells did not reach PA2, a deficiency of neural crest cells would explain the pharyngeal skeletal phenotype in the $Hoxb3^{Tg}$ mutants.

Hoxb3 Directly Regulates *Jag1* Expression

To address how ectopic *Hoxb3* expression in the pharyngeal epithelium could affect interaction with neural crest cells, we examined the Notch signaling ligand *Jag1* and found that *Hoxb3* could directly regulate *Jag1* expression. *Jag1* is required for craniofacial morphogenesis and other developmental processes (Xue et al., 1999; Humphreys et al., 2012), but the spatial-temporal regulation of *Jag1* expression during development is unclear. By bioinformatics analyses, we identified several Hoxb3 binding sites in the highly conserved genomic regions around *Jag1* gene. Using *in vivo* ChIP assays and *in vitro*/*ex vivo* luciferase reporter assays, we demonstrated that Hoxb3 could directly bind to the S2 site and *trans*-activate gene expression. From ENCODE databases, many other transcription factors binding sites could be identified around S2, indicating that this 40 Kb upstream genomic region could be a *cis*-regulatory enhancer element for activating *Jag1* expression. In the $Hoxb3^{Tg}$ gain-of-function mutant, we showed that *Jag1* expression could be

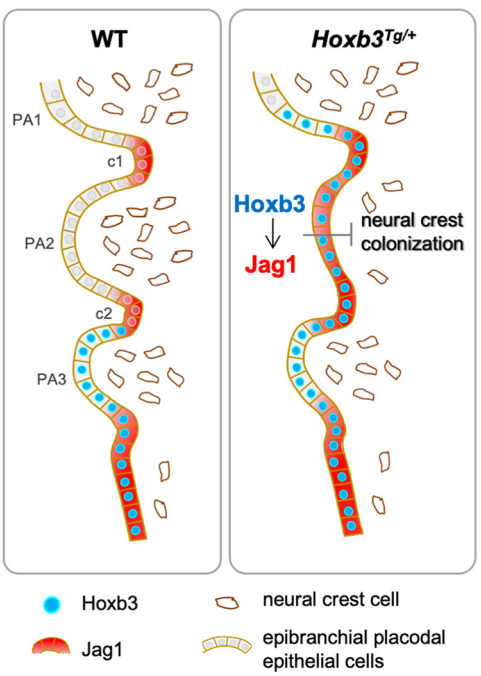

FIGURE 5 | Hoxb3 regulate Jag1 expression and affect pharyngeal epithelium and neural crest interactions. Schematic diagram showing expression of *Hoxb3* and *Jag1* in epibranchial placodal epithelial cells of wildtype and $Hoxb3^{Tg}$ mutant. In wildtype embryos, *Jag1* expression is restricted to the pharyngeal clefts which function as boundaries for neural crest migration into the pharyngeal arches. In the $Hoxb3^{Tg}$ mutant, ectopic *Hoxb3* expressed in the epibranchial placodal epithelium of PA2 could activate *Jag1* expression directly. Elevated *Jag1* expression is incompatible with neural crest migration into the pharyngeal arch. As a result, deficiency of neural crest colonization into PA2 led to abnormal development of multiple neural crest derivatives in the pharyngeal region of the $Hoxb3^{Tg}$ mutant. PA1, PA2, and PA3 indicate the 1st, 2nd, and 3rd pharyngeal arches; c1 and c2 indicate the 1st and 2nd pharyngeal clefts.

specifically activated by ectopic *Hoxb3* expression in the pharyngeal epithelium of PA1 and PA2 (**Figure 2J**). It is possible that during normal craniofacial development, *Hoxb3* is also required to maintain *Jag1* expression in the posterior pharyngeal arches and clefts to coordinate with the pharyngeal segmentation process.

The expression of *Jag1* has been reported to be activated by other *Hox3* genes. In hemogenic endothelium, overexpression of *Hoxa3* could activate the expression of *Jag1* (Sanghez et al., 2017). In HEL and K563 cells, overexpression of *Hoxd3* also led to elevated *Jag1* expression. Moreover, the expression level of *Jag1* was dependent on transfected *Hoxd3* expression (Taniguchi et al., 2001). These studies confirmed that the *Hox3* genes could regulate *Jag1* expression and Notch signaling in broader developmental contexts.

The Role of *Jag1* in PA Development

Recent studies of the proximal PA and epibranchial placode suggest that pharyngeal segments are gateways for neural crest cell migration into the PAs. Entering between the pharyngeal clefts, the neural crest cells populate the PAs distally, where subsequent morphogenetic events take place. For example, *Sox3* knockout mice with defective epibranchial placodal cells in the proximal pharyngeal epithelium displayed mis-migration of neural crest cells into the PAs and resulted in cranial skeletal defects (Rizzoti and Lovell-Badge, 2007). On the other hand, in the *Eya1* mutant which failed to maintain the epibranchial placodal cells, defective neural crest-derived maxilla and mandible were observed (Xu et al., 1999; Zhang et al., 2017). Importantly, both *Sox3* and *Eya1* are not expressed in neural crest but in the epibranchial placodal cells, indicating a non-cell autonomous role of epibranchial placodal epithelium in controlling the migration of neural crest cells to the PAs. In the $Hoxb3^{Tg/+}$ mutants described in this study, ectopic expression of *Hoxb3* and *Jag1* were found only in the pharyngeal epithelium, the neural crest-derived skeletal defects could be the consequence of misexpression of *Hoxb3* in the epibranchial placodal cells in the proximal PA.

We have previously shown that *Jag1* is initially broadly expressed in the proximal pharyngeal region in the epibranchial placodal cells at early stage (E8.5), but its expression is down-regulated in PA epithelium and became restricted to the pharyngeal clefts at around E9.5 (Zhang et al., 2017). While the functional role of *Jag1* in pharyngeal segmentation is not known, it appears that *Jag1* expressing regions serve as boundaries for neural crest cell migration. In the $Hoxb3^{Tg/+}$ mutant, persisted expression of *Jag1* in the proximal pharyngeal epithelium of PA2 could inhibit the colonization of neural crest cells into the arch (**Figure 5**), leading to the craniofacial abnormalities. Our genetic study has revealed the importance of the pharyngeal epithelial cells in interacting with cranial neural crest for proper craniofacial development.

DATA AVAILABILITY STATEMENT

The original contributions presented in the study are included in the article/**Supplementary Material**, further inquiries can be directed to the corresponding author.

ETHICS STATEMENT

The animal study was reviewed and approved by The University of Hong Kong Committee on the Use of Live Animals for Teaching and Research (CULATR Nos. 4357–17 and 4588–18).

AUTHOR CONTRIBUTIONS

HZ, EW, and MS conceived the study, designed the experiments, and wrote the manuscript. HZ, JX, KS, KT, JS-P, LW, EW, and WC conducted the experiments. ST, JS-P, EW, and HZ managed the experimental animals. JX, KS, KT, and MS reviewed and revised the manuscript and edited the figures. All authors participated in data analysis and revisions of the manuscript. MS obtained resources and funding for the study.

FUNDING

This work was supported by a research grant from the Hong Kong Research Grant Council (RGC GRF 777411) to MS.

ACKNOWLEDGMENTS

We thank Kathryn S.E. Cheah and Urban Lendahl for helpful discussions.

SUPPLEMENTARY MATERIAL

The Supplementary Material for this article can be found online at: https://www.frontiersin.org/articles/10.3389/fphys.2020.612230/full#supplementary-material

REFERENCES

Barrow, J. R., and Capecchi, M. R. (1996). Targeted disruption of the Hoxb-2 locus in mice interferes with expression of Hoxb-1 and Hoxb-4. *Development* 122, 3817–3828.

Barske, L., Askary, A., Zuniga, E., Balczerski, B., Bump, P., Nichols, J. T., et al. (2016). Competition between Jagged-Notch and Endothelin1 Signaling Selectively Restricts Cartilage Formation in the Zebrafish Upper Face. *PLoS Genet* 12:e1005967. doi: 10.1371/journal.pgen.1005967

Casey, L. M., Lan, Y., Cho, E. S., Maltby, K. M., Gridley, T., and Jiang, R. (2006). Jag2-Notch1 signaling regulates oral epithelial differentiation and palate development. *Dev. Dyn.* 235, 1830–1844. doi: 10.1002/dvdy.20821

Chai, Y., Jiang, X., Ito, Y., Bringas, P. Jr., Han, J., Rowitch, D. H., et al. (2000). Fate of the mammalian cranial neural crest during tooth and mandibular morphogenesis. *Development* 127, 1671–1679.

Chisaka, O., Musci, T. S., and Capecchi, M. R. (1992). Developmental defects of the ear, cranial nerves and hindbrain resulting from targeted disruption of the mouse homeobox gene Hox-# 150; 1.6. *Nature* 355, 516–520.

Chojnowski, J. L., Trau, H. A., Masuda, K., and Manley, N. R. (2016). Temporal and spatial requirements for Hoxa3 in mouse embryonic development. *Dev. Biol.* 415, 33–45. doi: 10.1016/j.ydbio.2016.05.010

Couly, G., and Le Douarin, N. (1990). Head morphogenesis in embryonic avian chimeras: evidence for a segmental pattern in the ectoderm corresponding to the neuromeres. *Development* 108, 543–558.

Couly, G., Creuzet, S., Bennaceur, S., Vincent, C., and Le Douarin, N. M. (2002). Interactions between Hox-negative cephalic neural crest cells and the foregut endoderm in patterning the facial skeleton in the vertebrate head. *Development* 129, 1061–1073.

Couly, G., Grapin-Botton, A., Coltey, P., Ruhin, B., and Le Douarin, N. M. (1998). Determination of the identity of the derivatives of the cephalic neural crest: incompatibility between Hox gene expression and lower jaw development. *Development* 125, 3445–3459.

Creuzet, S., Couly, G., Vincent, C., and Le Douarin, N. M. (2002). Negative effect of Hox gene expression on the development of the neural crest-derived facial skeleton. *Development* 129, 4301–4313.

Dessaud, E., Yang, L. L., Hill, K., Cox, B., Ulloa, F., Ribeiro, A., et al. (2007). Interpretation of the sonic hedgehog morphogen gradient by a temporal adaptation mechanism. *Nature* 450, 717–720. doi: 10.1038/nature06347

Donoviel, D. B., Hadjantonakis, A.-K., Ikeda, M., Zheng, H., Hyslop, P. S. G., and Bernstein, A. (1999). Mice lacking both presenilin genes exhibitearlyembryonic patterningdefects. *Genes Dev.* 13, 2801–2810. doi: 10.1101/gad.13.21.2801

Ferretti, E., Marshall, H., Popperl, H., Maconochie, M., Krumlauf, R., and Blasi, F. (2000). Segmental expression of Hoxb2 in r4 requires two separate sites that integrate cooperative interactions between Prep1. Pbx and Hox proteins. *Development* 127, 155–166.

Frasch, M., Chen, X., and Lufkin, T. (1995). Evolutionary-conserved enhancers direct region-specific expression of the murine Hoxa-1 and Hoxa-2 loci in both mice and Drosophila. *Development* 121, 957–974.

Frisdal, A., and Trainor, P. (2014). Development and evolution of the pharyngeal apparatus. *Wiley Interdiscip. Rev. Dev. Biol.* 3, 403–418. doi: 10.1002/wdev.147

Fujita, M., Sakabe, M., Ioka, T., Watanabe, Y., Kinugasa-Katayama, Y., Tsuchihashi, T., et al. (2016). Pharyngeal arch artery defects and lethal malformations of the aortic arch and its branches in mice deficient for the Hrt1/Hey1 transcription factor. *Mech. Dev.* 139, 65–73. doi: 10.1016/j.mod.2015.11.002

Gavalas, A., Studer, M., Lumsden, A., Rijli, F. M., Krumlauf, R., and Chambon, P. (1998). Hoxa1 and Hoxb1 synergize in patterning the hindbrain, cranial nerves and second pharyngeal arch. *Development* 125, 1123–1136.

Gavalas, A., Trainor, P., Ariza-Mcnaughton, L., and Krumlauf, R. (2001). Synergy between Hoxa1 and Hoxb1: the relationship between arch patterning and the generation of cranial neural crest. *Development* 128, 3017–3027.

Goddard, J. M., Rossel, M., Manley, N. R., and Capecchi, M. R. (1996). Mice with targeted disruption of Hoxb-1 fail to form the motor nucleus of the VIIth nerve. *Development* 122, 3217–3228.

Graham, A. (2003). Development of the pharyngeal arches. *Am. J. Med. Genet. A* 119A, 251–256. doi: 10.1002/ajmg.a.10980

Graham, A., and Smith, A. (2001). Patterning the pharyngeal arches. *Bioessays* 23, 54–61. doi: 10.1002/1521-1878(200101)23:1<54::AID-BIES1007<3.0.CO;2-5

Graham, A., Okabe, M., and Quinlan, R. (2005). The role of the endoderm in the development and evolution of the pharyngeal arches. *J. Anat.* 207, 479–487. doi: 10.1111/j.1469-7580.2005.00472.x

Hu, M. C., and Rosenblum, N. D. (2005). Smad1, β-catenin and Tcf4 associate in a molecular complex with the Myc promoter in dysplastic renal tissue and cooperate to control Myc transcription. *Development* 132, 215–225. doi: 10.1242/dev.01573

Humphreys, R., Zheng, W., Prince, L. S., Qu, X., Brown, C., Loomes, K., et al. (2012). Cranial neural crest ablation of Jagged1 recapitulates the craniofacial phenotype of Alagille syndrome patients. *Hum. Mol. Genet.* 21, 1374–1383. doi: 10.1093/hmg/ddr575

Hunt, P., Whiting, J., Muchamore, I., Marshall, H., and Krumlauf, R. (1991). Homeobox genes and models for patterning the hindbrain and branchial arches. *Dev. Suppl.* 1, 187–196.

Jayasena, C. S., Ohyama, T., Segil, N., and Groves, A. K. (2008). Notch signaling augments the canonical Wnt pathway to specify the size of the otic placode. *Development* 135, 2251–2261. doi: 10.1242/dev.017905

Jones, E. A., Clement-Jones, M., and Wilson, D. I. (2000). JAGGED1 expression in human embryos: correlation with the Alagille syndrome phenotype. *J. Med. Genet.* 37, 658–662. doi: 10.1136/jmg.37.9.658

Kamath, B., Bason, L., Piccoli, D., Krantz, I., and Spinner, N. (2003). Consequences of JAG1 mutations. *J. Med. Genet.* 40, 891–895. doi: 10.1136/jmg.40.12.891

Kameda, Y., Arai, Y., Nishimaki, T., and Chisaka, O. (2004). The role of Hoxa3 gene in parathyroid gland organogenesis of the mouse. *J. Histochem. Cytochem.* 52, 641–651. doi: 10.1177/002215540405200508

Kulesa, P. M., Bailey, C. M., Kasemeier-Kulesa, J. C., and Mclennan, R. (2010). Cranial neural crest migration: new rules for an old road. *Dev. Biol.* 344, 543–554. doi: 10.1016/j.ydbio.2010.04.010

Lassiter, R. N., Ball, M. K., Adams, J. S., Wright, B. T., and Stark, M. R. (2010). Sensory neuron differentiation is regulated by notch signaling in the trigeminal placode. *Dev. Biol.* 344, 836–848. doi: 10.1016/j.ydbio.2010.05.514

Lassiter, R. N., Stark, M. R., Zhao, T., and Zhou, C. J. (2014). Signaling mechanisms controlling cranial placode neurogenesis and delamination. *Dev. Biol.* 389, 39–49. doi: 10.1016/j.ydbio.2013.11.025

Le Douarin, N. M., Creuzet, S., Couly, G., and Dupin, E. (2004). Neural crest cell plasticity and its limits. *Development* 131, 4637–4650. doi: 10.1242/dev.01350

Li, L., Krantz, I. D., Deng, Y., Genin, A., Banta, A. B., Collins, C. C., et al. (1997). Alagille syndrome is caused by mutations in human Jagged1, which encodes a ligand for Notch1. *Nat. Genet.* 16, 243–251. doi: 10.1038/ng0797-243

Maconochie, M., Krishnamurthy, R., Nonchev, S., Meier, P., Manzanares, M., Mitchell, P. J., et al. (1999). Regulation of Hoxa2 in cranial neural crest cells involves members of the AP-2 family. *Development* 126, 1483–1494.

Maconochie, M., Nonchev, S., Studer, M., Chan, S.-K., Pöpperl, H., Sham, M. H., et al. (1997). Cross-regulation in the mouse HoxB complex: the expression of Hoxb2 in rhombomere 4 is regulated by Hoxb1. *Genes Dev.* 11, 1885–1895. doi: 10.1101/gad.11.14.1885

Manley, N. R., and Capecchi, M. R. (1998). Hox group 3 paralogs regulate the development and migration of the thymus, thyroid, and parathyroid glands. *Dev. Biol.* 195, 1–15. doi: 10.1006/dbio.1997.8827

Mcleod, M. J. (1980). Differential staining of cartilage and bone in whole mouse fetuses by alcian blue and alizarin red S. *Teratology* 22, 299–301. doi: 10.1002/tera.1420220306

Mead, T. J., and Yutzey, K. E. (2012). Notch pathway regulation of neural crest cell development in vivo. *Dev. Dyn.* 241, 376–389. doi: 10.1002/dvdy.23717

Minoux, M., and Rijli, F. M. (2010). Molecular mechanisms of cranial neural crest cell migration and patterning in craniofacial development. *Development* 137, 2605–2621. doi: 10.1242/dev.040048

Nonchev, S., Vesque, C., Maconochie, M., Seitanidou, T., Arizamcnaughton, L., Frain, M., et al. (1996). Segmental expression of Hoxa-2 in the hindbrain is directly regulated by Krox-20. *Development* 122, 543–554.

Novak, A., Guo, C., Yang, W., Nagy, A., and Lobe, C. G. (2000). Z/EG, a double reporter mouse line that expresses enhanced green fluorescent protein upon Cre−mediated excision. *Genesis* 28, 147–155. doi: 10.1002/1526-968x(200011/12)28:3/4<147::aid-gene90>3.0.co;2-g

Okada, Y., Shimazaki, T., Sobue, G., and Okano, H. (2004). Retinoic-acid-concentration-dependent acquisition of neural cell identity during *in vitro* differentiation of mouse embryonic stem cells. *Dev. Biol.* 275, 124–142. doi: 10.1016/j.ydbio.2004.07.038

Oyama, T., Harigaya, K., Sasaki, N., Okamura, Y., Kokubo, H., Saga, Y., et al. (2011). Mastermind-like 1 (MamL1) and mastermind-like 3 (MamL3) are essential for Notch signaling in vivo. *Development* 138, 5235–5246. doi: 10.1242/dev.062802

Rijli, F. M., Mark, M., Lakkaraju, S., Dierich, A., Dolle, P., and Chambon, P. (1993). A homeotic transformation is generated in the rostral branchial region of the head by disruption of Hoxa-2, which acts as a selector gene. *Cell* 75, 1333–1349. doi: 10.1016/0092-8674(93)90620-6

Rizzoti, K., and Lovell-Badge, R. (2007). SOX3 activity during pharyngeal segmentation is required for craniofacial morphogenesis. *Development* 134, 3437–3448. doi: 10.1242/dev.007906

Sanghez, V., Luzzi, A., Clarke, D., Kee, D., Rux, D., Osawa, M., et al. (2017). Notch activation is required for downregulation of HoxA3-dependent endothelial

cell phenotype during blood formation. *PLoS One* 12:e0186818. doi: 10.1371/journal.pone.0186818

Santagati, F., and Rijli, F. M. (2003). Cranial neural crest and the building of the vertebrate head. *Nat. Rev. Neurosci.* 4, 806–818. doi: 10.1038/nrn1221

Schlosser, G., and Ahrens, K. (2004). Molecular anatomy of placode development in Xenopus laevis. *Dev. Biol.* 271, 439–466. doi: 10.1016/j.ydbio.2004.04.013

Studer, M., Lumsden, A., Ariza-Mcnaughton, L., Bradley, A., and Krumlauf, R. (1996). Altered segmental identity and abnormal migration of motor neurons in mice lacking Hoxb-1. *Nature* 384, 630–634. doi: 10.1038/384630a0

Su, D., Ellis, S., Napier, A., Lee, K., and Manley, N. R. (2001). Hoxa3 and pax1 regulate epithelial cell death and proliferation during thymus and parathyroid organogenesis. *Dev. Biol.* 236, 316–329. doi: 10.1006/dbio.2001.0342

Szeto, I. Y., Leung, K. K., Sham, M. H., and Cheah, K. S. (2009). Utility of HoxB2 enhancer-mediated Cre activity for functional studies in the developing inner ear. *Genesis* 47, 361–365. doi: 10.1002/dvg.20507

Taniguchi, Y., Sato, M., Tanaka, O., Sekiguchi, M., Inoko, H., and Kimura, M. (2001). *"HOXD3 regulates expression of JAGGED1, a ligand for Notch receptors", in: Nucleic acids symposium series*. Oxford: Oxford University Press, 43–44.

Teng, C. S., Yen, H. Y., Barske, L., Smith, B., Llamas, J., Segil, N., et al. (2017). Requirement for Jagged1-Notch2 signaling in patterning the bones of the mouse and human middle ear. *Sci. Rep.* 7:2497. doi: 10.1038/s41598-017-02574-7

Trainor, P., and Krumlauf, R. (2000). Plasticity in mouse neural crest cells reveals a new patterning role for cranial mesoderm. *Nat. Cell Biol.* 2, 96–102. doi: 10.1038/35000051

Trainor, P., and Krumlauf, R. (2001). Hox genes, neural crest cells and branchial arch patterning. *Curr. Opin. Cell Biol.* 13, 698–705. doi: 10.1016/s0955-0674(00)00273-8

Trokovic, N., Trokovic, R., and Partanen, J. (2005). Fibroblast growth factor signalling and regional specification of the pharyngeal ectoderm. *Int. J. Dev. Biol.* 49, 797–805. doi: 10.1387/ijdb.051976nt

Veitch, E., Begbie, J., Schilling, T. F., Smith, M. M., and Graham, A. (1999). Pharyngeal arch patterning in the absence of neural crest. *Curr. Biol.* 9, 1481–1484. doi: 10.1016/s0960-9822(00)80118-9

Vieira, A. R., Avila, J. R., Daack-Hirsch, S., Dragan, E., Felix, T. M., Rahimov, F., et al. (2005). Medical sequencing of candidate genes for nonsyndromic cleft lip and palate. *PLoS Genet* 1:e64. doi: 10.1371/journal.pgen.0010064

Wakeham, A., Correia, K., Samper, E., Brown, S., Aguilera, R., Nakano, T., et al. (1997). Conservation of the Notch signalling pathway in mammalian neurogenesis. *Development* 124, 1139–1148.

Wang, L., Xie, J., Zhang, H., Tsang, L. H., Tsang, S. L., Braune, E. B., et al. (2020). Notch signalling regulates epibranchial placode patterning and segregation. *Development* 147:dev183665. doi: 10.1242/dev.183665

Washausen, S., and Knabe, W. (2017). Pax2/Pax8-defined subdomains and the occurrence of apoptosis in the posterior placodal area of mice. *Brain Struct. Funct.* 222, 2671–2695. doi: 10.1007/s00429-016-1364-0

Wilkinson, D. G., Bhatt, S., Cook, M., Boncinelli, E., and Krumlauf, R. (1989). Segmental expression of Hox-2 homoeobox-containing genes in the developing mouse hindbrain. *Nature* 341, 405–409. doi: 10.1038/341405a0

Wong, E. Y., Wang, X. A., Mak, S. S., Sae-Pang, J. J., Ling, K. W., Fritzsch, B., et al. (2011). Hoxb3 negatively regulates Hoxb1 expression in mouse hindbrain patterning. *Dev. Biol.* 352, 382–392. doi: 10.1016/j.ydbio.2011.02.003

Xu, P.-X., Adams, J., Peters, H., Brown, M. C., Heaney, S., and Maas, R. (1999). Eya1-deficient mice lack ears and kidneys and show abnormal apoptosis of organ primordia. *Nat. Genet.* 23, 113–117. doi: 10.1038/12722

Xu, P.-X., Zheng, W., Laclef, C., Maire, P., Maas, R. L., Peters, H., et al. (2002). Eya1 is required for the morphogenesis of mammalian thymus, parathyroid and thyroid. *Development* 129, 3033–3044.

Xue, Y., Gao, X., Lindsell, C. E., Norton, C. R., Chang, B., Hicks, C., et al. (1999). Embryonic lethality and vascular defects in mice lacking the Notch ligand Jagged1. *Hum. Mol. Genet.* 8, 723–730. doi: 10.1093/hmg/8.5.723

Yau, T. O., Kwan, C. T., Jakt, L. M., Stallwood, N., Cordes, S., and Sham, M. H. (2002). Auto/cross-regulation of Hoxb3 expression in posterior hindbrain and spinal cord. *Dev. Biol.* 252, 287–300. doi: 10.1006/dbio.2002.0849

Zhang, H., Wang, L., Wong, E. Y. M., Tsang, S. L., Xu, P. X., Lendahl, U., et al. (2017). An Eya1-Notch axis specifies bipotential epibranchial differentiation in mammalian craniofacial morphogenesis. *Elife* 6:e30126. doi: 10.7554/eLife.30126

Conflict of Interest: The authors declare that the research was conducted in the absence of any commercial or financial relationships that could be construed as a potential conflict of interest.

frontiers in Physiology

BRIEF RESEARCH REPORT
published: 03 February 2021
doi: 10.3389/fphys.2021.624037

Transcriptomic Identification of Draxin-Responsive Targets During Cranial Neural Crest EMT

*Erica J. Hutchins, Michael L. Piacentino and Marianne E. Bronner**

Division of Biology and Biological Engineering, California Institute of Technology, Pasadena, CA, United States

Canonical Wnt signaling plays an essential role in proper craniofacial morphogenesis, at least partially due to regulation of various aspects of cranial neural crest development. In an effort to gain insight into the etiology of craniofacial abnormalities resulting from Wnt signaling and/or cranial neural crest dysfunction, we sought to identify Wnt-responsive targets during chick cranial neural crest development. To this end, we leveraged overexpression of a canonical Wnt antagonist, Draxin, in conjunction with RNA-sequencing of cranial neural crest cells that have just activated their epithelial–mesenchymal transition (EMT) program. Through differential expression analysis, gene list functional annotation, hybridization chain reaction (HCR), and quantitative reverse transcription polymerase chain reaction (RT-qPCR), we validated a novel downstream target of canonical Wnt signaling in cranial neural crest – *RHOB* – and identified possible signaling pathway crosstalk underlying cranial neural crest migration. The results reveal novel putative targets of canonical Wnt signaling during cranial neural crest EMT and highlight important intersections across signaling pathways involved in craniofacial development.

Keywords: Draxin, Wnt, neural crest, EMT, craniofacial development

OPEN ACCESS

Edited by:
Jean-Pierre Saint-Jeannet, New York University, United States

Reviewed by:
Sergei Sokol, Icahn School of Medicine at Mount Sinai, United States
Jean-Loup Duband, INSERM U955 Institut Mondor de Recherche Biomédicale (IMRB), France

***Correspondence:**
Marianne E. Bronner
mbronner@caltech.edu

Specialty section:
This article was submitted to Craniofacial Biology and Dental Research, a section of the journal Frontiers in Physiology

Received: *30 October 2020*
Accepted: *07 January 2021*
Published: *03 February 2021*

Citation:
Hutchins EJ, Piacentino ML and Bronner ME (2021) Transcriptomic Identification of Draxin-Responsive Targets During Cranial Neural Crest EMT. Front. Physiol. 12:624037. doi: 10.3389/fphys.2021.624037

INTRODUCTION

The neural crest is a multipotent stem cell population in the vertebrate embryo that undergoes coordinated induction, specification, and epithelial–mesenchymal transition (EMT) events to migrate and ultimately differentiate into a wide range of cell types. The migratory pathways and derivatives formed by the neural crest are regionalized according to their axial level of origin, such that cells from a given axial level give rise to a characteristic array of progeny and follow distinct pathways from those arising at other axial levels (Gandhi and Bronner, 2018). The most anterior "cranial" neural crest population underlies much of the development of the face (Cordero et al., 2011), and is the only neural crest population *in vivo* with the ability to differentiate into facial skeleton, contributing to the upper and lower jaw, and bones of the neck (Noden, 1975; Le Douarin, 1982; Simoes-Costa and Bronner, 2015). Importantly, perturbation of various stages of cranial neural crest development results in a myriad of craniofacial malformations (Vega-Lopez et al., 2018).

Many facets of cranial neural crest development are regulated by Wnt signaling (Wu et al., 2003; Yanfeng et al., 2003; Steventon et al., 2009; Milet and Monsoro-Burq, 2012; Simoes-Costa et al., 2015; Rabadán et al., 2016; Hutchins and Bronner, 2018, 2019; Gandhi et al., 2020). Furthermore,

Wnt signaling is critical for normal facial patterning; mutations in Wnt pathway components or dysregulation of canonical Wnt signaling output result in defects in craniofacial morphogenesis (Huelsken et al., 2000; Chiquet et al., 2008; Reid et al., 2011; He and Chen, 2012; Kurosaka et al., 2014). Thus, identification of canonical Wnt targets during cranial neural crest development would greatly enhance understanding the etiology of craniofacial abnormalities resulting from Wnt signaling or cranial neural crest dysfunction.

Here, we took advantage of a canonical Wnt signaling inhibitor, Draxin, to identify Wnt-responsive targets during chick cranial neural crest development. As Draxin overexpression impedes cranial neural crest EMT in a β-catenin-dependent mechanism (Hutchins and Bronner, 2018, 2019), here we utilize Draxin overexpression together with RNA-sequencing (RNA-seq) on sorted populations of cranial neural crest cells to identify novel downstream targets of canonical Wnt signaling during cranial neural crest EMT.

MATERIALS AND METHODS

Embryo Electroporation and Expression Constructs

Electroporations were performed at Hamburger-Hamilton stage HH4 (Hamburger and Hamilton, 1951), using commercially available fertile chicken (*Gallus gallus*) eggs (Sunstate Ranch, Sylmar, CA, United States), as previously described (Hutchins and Bronner, 2018). The cranial neural crest-specific enhancer NC1.1m3:GFP (Simoes-Costa et al., 2012), Draxin overexpression (Hutchins and Bronner, 2018), BRE::GFP BMP reporter (Le Dreau et al., 2012), NC1-Δ90βcat canonical Wnt signaling activation (Hutchins and Bronner, 2018), and control expression (Betancur et al., 2010b) constructs were described previously.

Tissue Dissociation and FACS

Following electroporation, embryos were incubated at 37°C until HH9+. We then dissected embryonic heads anterior to the otic vesicle in Ringer's solution, washed tissue with sterile PBS (Corning cellgro #21-031-CV), then incubated tissue in Accumax (Innovative Cell Technologies, Inc. #AM-105) at 37°C for 15 min, with trituration every 5 min. Following dissociation, cells were washed with Hanks' Balanced Salt Solution (Thermo Fisher Scientific #88284), filtered through a 20 μM nylon net mesh filter (Millipore Product #NY2004700), and resuspended in Hanks' supplemented with 0.25% bovine serum albumin and 5% RQ1 DNase (Promega #M6101). GFP + cells were then collected using fluorescence activated cell sorting (FACS) at the Caltech Flow Cytometry Cell Sorting Facility.

Library Preparation and Sequencing

We used 1500 GFP+ cranial neural crest cells per replicate to prepare libraries. cDNA libraries were prepared using the Takara Bio SMART-Seq v4 Ultra Low Input cDNA kit, according to manufacturer instructions. RNA-Seq was performed at the Caltech Millard and Muriel Jacobs Genetics and Genomics Laboratory at 35 million reads on two biological replicates for both the control cranial and Draxin overexpression cranial neural crest cells. Sequencing libraries were built according to Illumina Standard Protocols and SR50 sequencing was performed in a HiSeq Illumina machine by the Caltech Millard and Muriel Jacobs Genetics and Genomics Laboratory. Sequence reads were aligned to the *G. gallus* genome (*galgal6*) with Bowtie2 (Langmead and Salzberg, 2012), transcript counts were calculated with HTSeq-Count (Anders et al., 2015), and differential expression analysis was performed with DESeq2 (Love et al., 2014). Gene lists were analyzed for functional annotation using PANTHER (Mi et al., 2019) and DAVID (Huang da et al., 2009a,b).

Hybridization Chain Reaction

Embryos to be processed for hybridization chain reaction (HCR) were fixed in 4% paraformaldehyde 1 h at room temperature, then dehydrated in graded methanol washes and stored at least one overnight at −20°C. HCR was performed as previously described (Gandhi et al., 2020), with custom probes designed and ordered through Molecular Technologies.

Image Acquisition and Analysis

Confocal images were acquired with an upright Zeiss LSM 880 at the Caltech Biological Imaging Facility. Images were minimally processed for brightness/contrast and pseudocolored using Fiji (Schindelin et al., 2012) and Adobe Photoshop 2020. Relative fluorescence intensity was determined in Fiji. For each whole mount image, the line tool was used to draw an ROI surrounding the area of neural crest indicated by positive HCR fluorescence for neural crest marker *TFAP2*β. Integrated density measurements were quantified for ROIs on the control electroporated (left) and experimental electroporated (right) sides from the same embryo. Relative fluorescence intensity was then calculated by dividing the integrated density measurements for the experimental versus the control side of the same embryo. Statistical analyses were performed using Prism (8; GraphPad Software). P values are defined in the text, and significance was established with $P < 0.05$. P values were calculated for embryos using one-tailed paired t-tests with integrated density measurements for control versus experimental sides, and for qRT-PCR using two-tailed one sample t-tests for $\Delta\Delta C_T$ values.

Quantitative Reverse Transcription PCR (RT-qPCR)

RNA was extracted from sorted cells (Draxin overexpression) and dissected HH9+ embryonic half heads (NC1-Δ90βcat canonical Wnt signaling activation) using the RNAqueous-Micro Total RNA Isolation Kit (Invitrogen), according to manufacturer instructions. Following RNA isolation in elution buffer, cDNA was reverse transcribed using the SuperScriptIII First-Strand Synthesis System (Invitrogen) with oligo-dT priming. Quantitative PCR (qPCR) was performed using gene-specific primers with FastStart Universal SYBR Green Master Mix with Rox (Roche) and cDNA (diluted 1:10) on a

QuantStudio 3 Real-Time PCR System (Applied Biosystems) in triplicate. We determined ΔC_T with normalization against 18S ribosomal RNA (ΔC_T = Target C_T − 18S C_T) for *Draxin*, *SNAI2*, and *RHOB* for samples, then calculated $\Delta\Delta C_T$ values ($\Delta\Delta C_T$ = Average Control ΔC_T − Perturbation ΔC_T) for each target and replicate. The gene-specific primers used for qPCR were: Draxin-F 5′-CTACGCTGTTATGCCAAATTCC; Draxin-R 5′-GAATGATCCCTGCTCTCCATT; SNAI2-F 5′-GCA ACAAGACCTATTCCACTTTC; SNAI2-R 5′-GTACTTG CAGCTGAACGATTTC; RHOB-F 5′-CGTGATCCTCATGT GCTTCT; RHOB-R 5′-TGCGCAGGTCTTTCTTGT; 18S-F 5′-CCATGATTAAGAGGGACGGC; 18S-R 5′-TGGCAAA TGCTTTCGCTTT.

RESULTS

Identification of Draxin-Responsive Genes in Migrating Cranial Neural Crest

We have previously shown that the secreted protein Draxin functions as a potent inhibitor of cranial neural crest cell migration during EMT (**Figure 1A**; Hutchins and Bronner, 2018, 2019). Its effects on neural crest are elicited extracellularly via β-catenin-dependent Wnt signaling inhibition, precisely at the early stages of cranial neural crest EMT at HH9+ (Hutchins and Bronner, 2018). To parse the cranial-specific targets of Draxin underlying its effect on neural crest EMT and uncover potential novel targets of canonical Wnt signaling, we performed RNA-sequencing (RNA-seq) on sorted chick cranial neural crest cells, with and without Draxin-mediated Wnt inhibition. To this end, we co-electroporated the FoxD3 NC1.1m3 enhancer, which drives GFP expression specifically in the cranial neural crest population (Simoes-Costa et al., 2012), with either a Draxin overexpression construct containing an internal ribosomal entry site (IRES) driving H2B-RFP (Hutchins and Bronner, 2018) or the same construct without the Draxin coding region as a control (**Figure 1B**). Embryos were subsequently developed to the onset of cranial neural crest EMT (HH9+), by which point Draxin-mediated effects on EMT are evident (**Figure 1C**; Hutchins and Bronner, 2018, 2019), to identify EMT-related genes sensitive to canonical Wnt inhibition. From heads dissected anterior to the otic vesicle, we isolated 1500 GFP+ cranial neural crest cells per replicate by FACS, then performed cDNA library preparation and sequencing (**Figure 1D**).

Differential expression analysis initially revealed 284 differentially expressed genes with ≥1.8 fold change and FDR < 0.01. For subsequent functional analysis, we filtered the gene lists to exclude lowly expressed genes (average normalized count values < 1000), resulting in a filtered list of 134 differentially expressed genes (36 downregulated, 98 upregulated) (**Figure 2A**). Using PANTHER analysis (Mi et al., 2019) to probe molecular functions of these gene targets, we observed enrichment of factors highly associated with transcriptional regulation, enzymatic reactions (including kinases) and secreted proteins indicative of targets associated with intracellular signaling pathways, and structural molecules (such as cytoskeletal and extracellular matrix proteins) indicative of cell migration-associated targets (**Figure 2B**). Among the most highly changed genes, we found significant enrichment of *Draxin*, as expected due to its experimental overexpression. Interestingly, we also detected significant downregulation of the Notch pathway effector *HES5* (and related genes), and *BMP4* (as well as its downstream target *MSX1*) (**Figures 2C,D**), suggesting potential signaling pathway crosstalk between Draxin, canonical Wnt signaling, and other pathways with critical roles in neural crest development. Given that Draxin has been shown to intersect with additional signaling pathways in other contexts (Ahmed et al., 2011; Hossain et al., 2013; Meli et al., 2015), further studies are needed to parse direct and indirect effects relevant to craniofacial morphogenesis and neural crest EMT.

Biological Pathway Analysis of Draxin-Responsive Genes in Cranial Neural Crest

To better understand the molecular processes in which Draxin, and by extension canonical Wnt signaling, function during cranial neural crest EMT, we performed functional annotation for the dataset using the Database for Annotation, Visualization and Integrated Discovery (DAVID) (Huang da et al., 2009a,b). Consistent with established roles of canonical Wnt signaling and Draxin-mediated inhibition during cranial neural crest EMT, we observed enrichment of genes associated with transcriptional regulation, cell adhesion, and lipid synthesis, which we have recently shown is important for cell signaling during cranial neural crest EMT (Piacentino et al., 2020). In addition, we found numerous genes associated with bone/cartilage formation (e.g., *CYTL1*, *ILK*, *NOV*), a critical function of cranial neural crest, and genes involved in ribosome biogenesis (e.g., *NOP56*, *PES1*, *NOC2L*), which has implications for craniofacial development (Ross and Zarbalis, 2014) (**Figure 3A**).

Among the targets associated with transcriptional regulation, we detected significant downregulation of *SNAI2*, which has been shown to be a direct target of canonical Wnt signaling, and subsequently Draxin (LaBonne and Bronner-Fraser, 1998; Monsoro-Burq et al., 2005; Wu et al., 2005; Hutchins and Bronner, 2018) (**Figure 3B**). In addition, we observed significant downregulation of genes that mediate cell adhesion and EMT (**Figure 3C**), including *RHOB*, shown to be required for neural crest delamination in the trunk (Liu and Jessell, 1998), and *EPCAM*, which has been shown to participate in cancer cell EMT (Wang et al., 2018). We also observed significant correlations for disease-associated genes, including those involved in craniofacial (**Figure 3D**) and nervous system dysfunction (**Figure 3E**). This was expected given the role of the cranial neural crest in craniofacial development, and established roles for Draxin in nervous system development (Islam et al., 2009; Tawarayama et al., 2018).

Functional Validation of a Novel Immediate Early Canonical Wnt Target

To validate Draxin-responsive targets from our dataset, we performed quantitative HCR on embryos bilaterally electroporated with the Draxin overexpression construct on

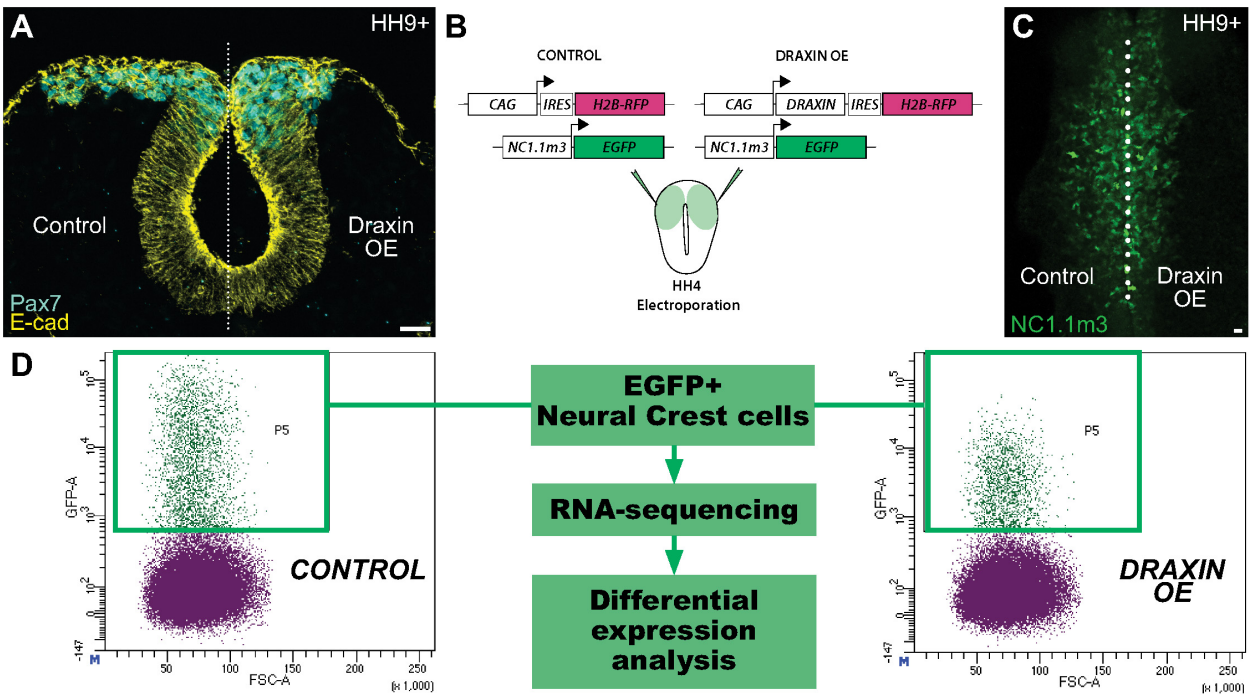

FIGURE 1 | Experimental design for identification of Draxin-responsive targets in cranial neural crest EMT. **(A)** Cross-section through embryo electroporated with a Draxin overexpression construct on the right side of the embryo. Immunostaining for E-cadherin (E-cad) and the neural crest marker Pax7 at HH9+ highlights the deleterious effects of Draxin overexpression on cranial neural crest EMT and migration away from the midline (dotted line), compared to the contralateral control side. **(B–D)** Experimental design to isolate cranial neural crest cells with or without Draxin overexpression. Gastrula stage chick embryos were co-electroporated with a neural crest-specific enhancer driving EGFP expression in cranial neural crest cells (NC1.1m3) and either a Draxin overexpression or control construct **(B)**. NC1.1m3 enhancer expression revealed EGFP + cranial neural crest cells were responsive to Draxin overexpression and exhibited EMT defects **(C)**. Fluorescence activated cell sorting (FACS) was used to isolate EGFP+ cranial neural crest cells with and without Draxin overexpression that were subsequently processed for RNA-sequencing and differential expression analysis **(D)**. Scale bar, 20 μm. HH, Hamburger-Hamilton stage; OE, overexpression; IRES, internal ribosomal entry site.

the right side of embryos and the control construct on the left side (as in **Figure 1B**). To establish the area of neural crest migration from which to measure target fluorescence intensities, we visualized expression of *TFAP2*β, a neural crest marker and non-target of Draxin. We focused on early HH9 + embryos, corresponding to the beginning of cranial neural crest EMT and initial stages of migration, in order to probe immediate early gene changes. As a result, modest defects were evident in the distance cranial neural crest cells migrated away from the midline (**Figures 4A–D**), consistent with a Draxin overexpression phenotype, albeit to a lesser extent than later stage HH9+ embryos in which migration has progressed more laterally (**Figures 1A,C**; Hutchins and Bronner, 2018, 2019). We measured *SNAI2* and *RHOB* fluorescence intensities for Draxin overexpression versus control sides of individual embryos, and found significant downregulation of gene expression (**Figure 4E**; 78.0 ± 2.8% of the control side for *SNAI2* and 81.0 ± 5.5% of the control side for *RHOB*; $P \leq 0.01$, one-tailed paired *t*-test), consistent with predicted trends based on our transcriptomic analyses. This is consistent with our previously published work indicating that Draxin acts upstream of Snail2 protein expression (Hutchins and Bronner, 2018). We further validated the effects of Draxin overexpression on *SNAI2* and *RHOB* using quantitative reverse transcription PCR (RT-qPCR) with sorted cells collected alongside sequenced cells from **Figure 1**; consistent with the HCR data (**Figures 4A–E**), we detected significant downregulation of both *SNAI2* and *RHOB* with Draxin overexpression (**Figure 4F**).

Given that *RHOB* has been previously shown to be a BMP-responsive target (Liu and Jessell, 1998) and insensitive to Wnt signaling (Taneyhill and Bronner-Fraser, 2005) in trunk neural crest, we next sought to determine whether the reduction in *RHOB* we observed in cranial neural crest was due to direct effects from Wnt signaling, or indirect effects through downregulation of BMP. We have previously shown that canonical Wnt signaling is active in cranial neural crest at the onset of EMT using a fluorescent reporter (Hutchins and Bronner, 2018), while BMP signaling is active in the presumptive cranial neural crest at earlier stages during their induction (Piacentino and Bronner, 2018); here we employed a similar approach to investigate the timing of BMP signaling activation in cranial neural crest at the onset of EMT. Electroporation of a fluorescent BMP reporter (BRE::GFP) revealed a lack of active BMP signaling in cranial neural crest cells that have undergone EMT and commenced migration at HH9+ (**Supplementary Figure 1**). Thus, it is unlikely that the reduction in *RHOB* we observed was due to suppressive effects on BMP signaling by Draxin. To more fully examine whether *RHOB* downregulation was due to direct effects from Wnt signaling, we performed RT-qPCR on embryos with

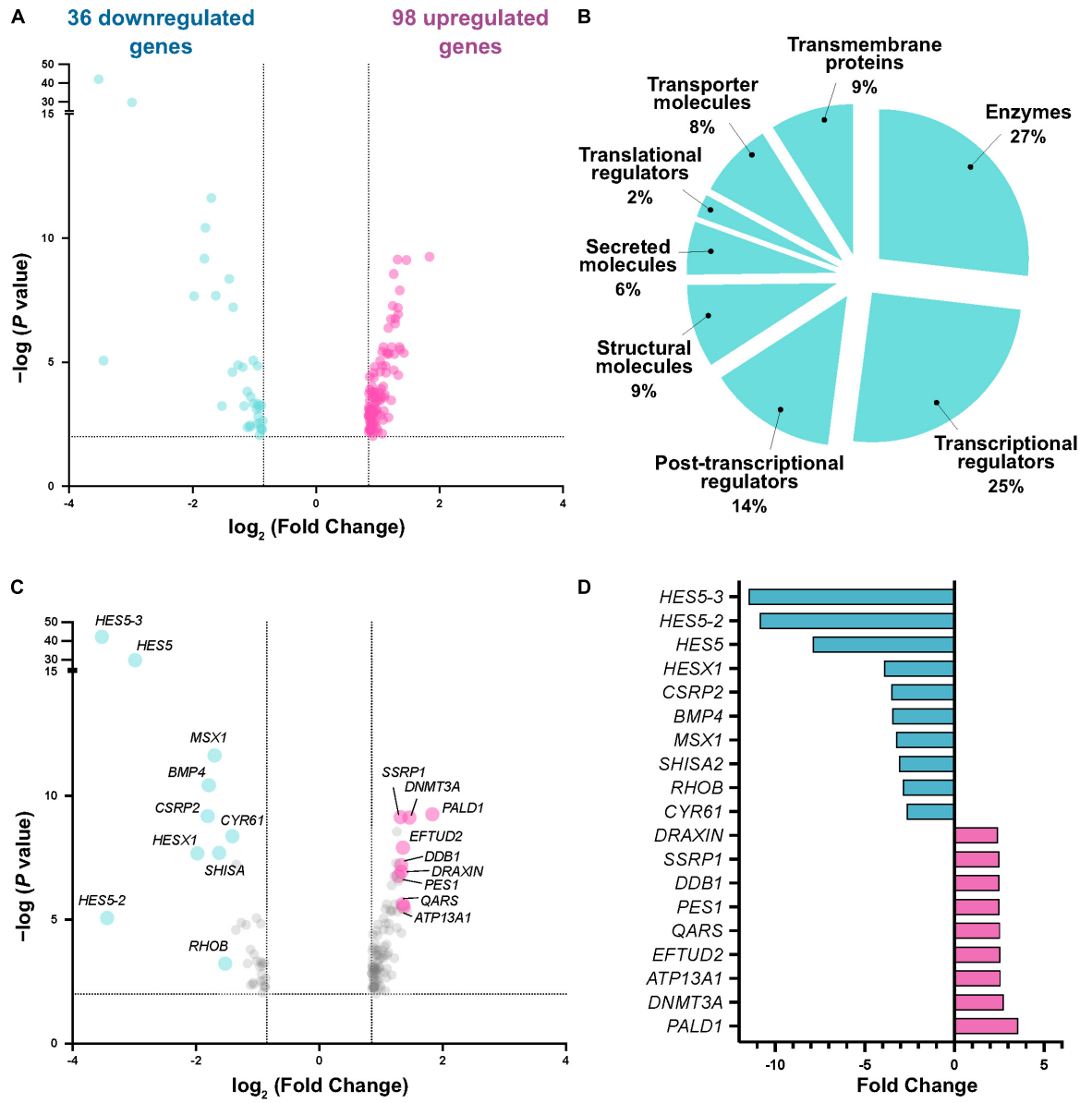

FIGURE 2 | Transcriptome analysis reveals differentially expressed genes responsive to Draxin-mediated canonical Wnt inhibition. **(A)** Volcano plot following differential expression analysis and filtering. Dotted lines indicate significance and fold change cutoffs for downstream analysis. **(B)** Molecular functions for the 134 differentially expressed genes. **(C,D)** Most enriched and depleted genes in cranial neural crest with Draxin overexpression.

and without canonical Wnt signaling activation during cranial neural crest EMT. Here, we specifically activated canonical Wnt signaling in specified cranial neural crest by driving expression of a stabilized form of β-catenin under the control of a neural crest-specific enhancer (NC1-Δ90βcat). Importantly, we observed upregulation of *SNAI2*, an established direct target of canonical Wnt signaling (LaBonne and Bronner-Fraser, 1998; Monsoro-Burq et al., 2005; Wu et al., 2005), as well as upregulation of *RHOB*, suggesting a direct link with Wnt signaling. Interestingly, we also observed concomitant downregulation of endogenous *DRAXIN*, suggesting the possibility of a negative feedback loop with respect to *DRAXIN* expression (**Figure 4G**).

Taken together, our data identify a novel target of Draxin and canonical Wnt signaling during cranial neural crest EMT (*RHOB*), and suggest that *Draxin* downregulation, and subsequent activation of Wnt signaling, is essential for crosstalk and feedback of signaling pathways that alter cranial neural crest transcriptional activation, and ultimately EMT.

DISCUSSION

Using transcriptome profiling of Draxin-responsive targets, we identified likely gene targets of canonical Wnt signaling

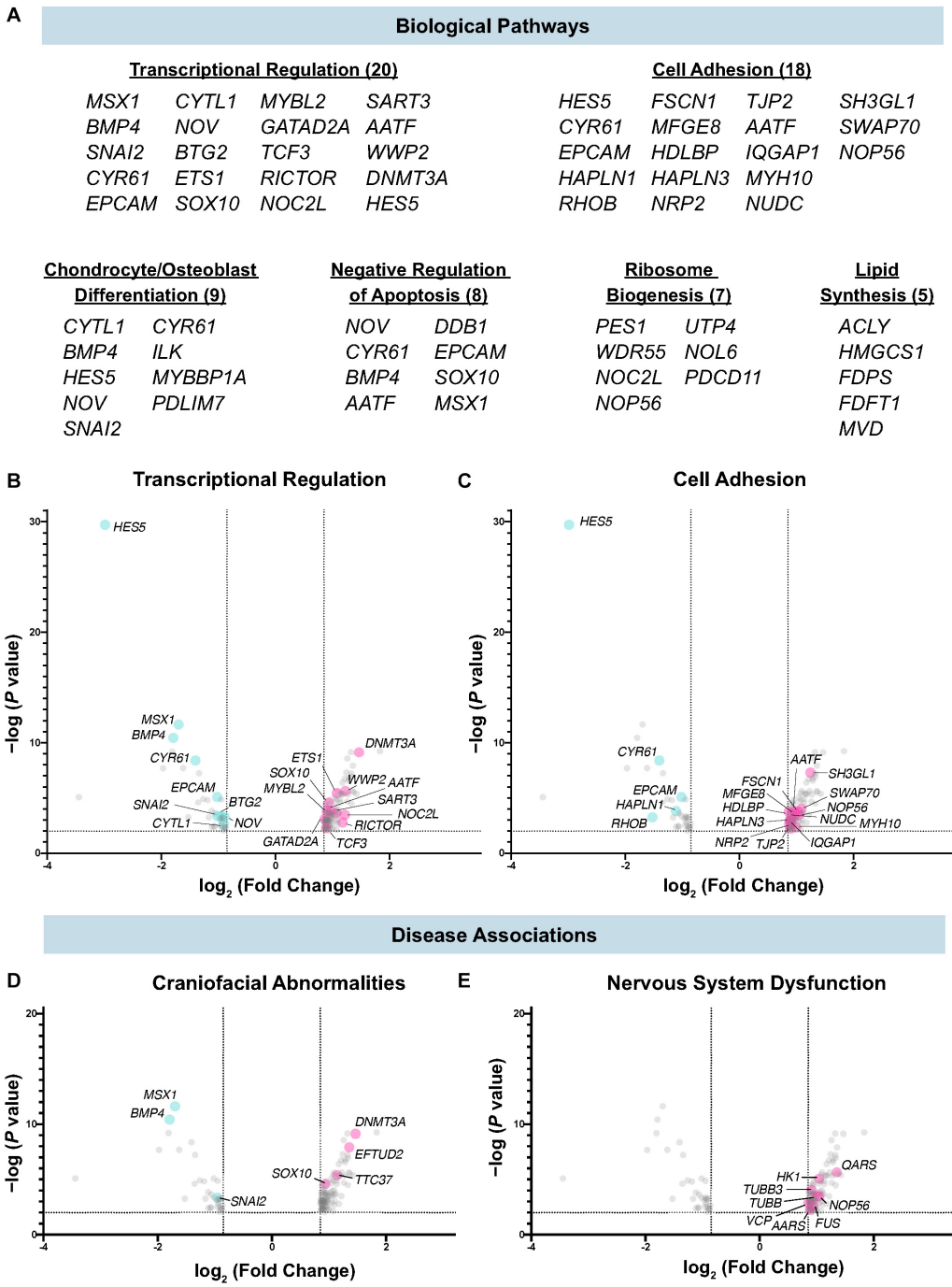

FIGURE 3 | Biological pathways and diseases associated with Draxin-responsive transcriptome dataset. **(A–C)** Biological pathway analysis identified enrichment of targets associated with transcriptional regulation, cell adhesion, chondrocyte/osteoblast differentiation, negative regulation of apoptosis, ribosome biogenesis, and lipid synthesis. **(D,E)** Functional annotation identified genes highly correlated with craniofacial abnormalities and nervous system dysfunction.

during cranial neural crest EMT. Consistent with our previously published work examining protein expression (Hutchins and Bronner, 2018), we verified transcript downregulation of canonical Wnt target *SNAI2* in response to Draxin overexpression. Furthermore, we also identified and validated a novel target – *RHOB*. RhoB is BMP-responsive in trunk neural crest and is necessary for delamination (Liu and Jessell, 1998); its misexpression has been associated with defects in laminin organization within the basement membrane (Perez-Alcala et al., 2004). Interestingly, we have previously demonstrated that Draxin, via regulation of canonical Wnt signaling, also is involved in regulating laminin organization and

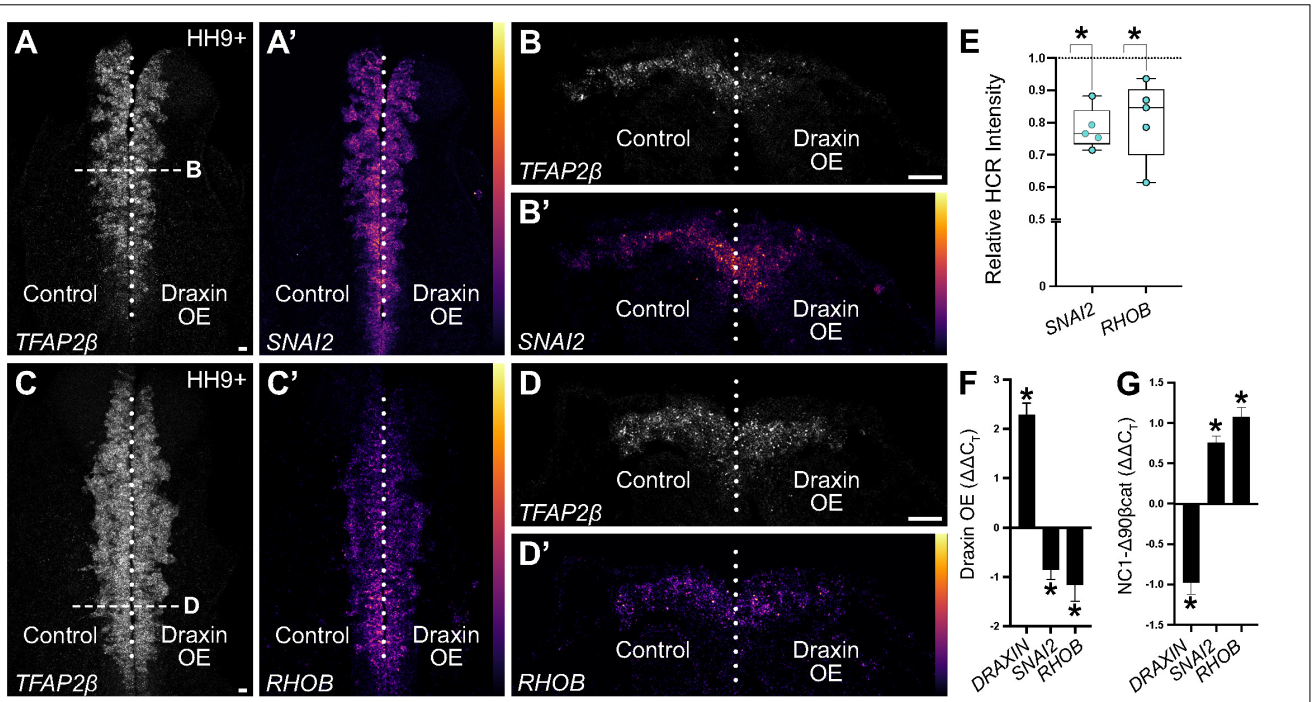

FIGURE 4 | Hybridization chain reaction (HCR) validation of identified neural crest EMT genes. **(A–D)** Representative images of quantitative HCR for neural crest marker *TFAP2β* and targets *SNAI2* and *RHOB* in embryos bilaterally electroporated with a control (left) or Draxin overexpression (right) construct. *SNAI2* and *RHOB* are pseudocolored based on fluorescence intensities as indicated by color scale in panels **(A′–D′)**. **(E)** Integrated density measurements revealed significant downregulation of *SNAI2* and *RHOB* (78.0 ± 2.8% of the control side for *SNAI2* and 81.0 ± 5.5% of the control side for *RHOB*; $P \leq 0.01$, one-tailed paired *t*-test) with Draxin overexpression. Scale bar, 20 μm. **(F)** $\Delta\Delta C_T$ values from quantitative reverse transcription PCR (RT-qPCR) for *DRAXIN*, *SNAI2*, and *RHOB* (normalized against *18S*, comparing control versus overexpression cells) from HH9+ sorted cranial neural crest cells co-electroporated with NC1.1m3 fluorescent GFP reporter with or without Draxin overexpression (DraxinOE). As expected, *DRAXIN* was significantly upregulated whereas *SNAI2* and *RHOB* were significantly downregulated in DraxinOE cranial neural crest cells. *$P < 0.05$, two-tailed one sample *t*-test. **(G)** $\Delta\Delta C_T$ values from quantitative reverse transcription PCR (RT-qPCR) for *DRAXIN*, *SNAI2*, and *RHOB* (normalized against *18S*, comparing control versus Wnt-activated cells) from dissected HH9+ cranial tissue from embryos co-electroporated with NC1.1m3 fluorescent RFP reporter with or without stabilized β-catenin expression (NC1-Δ90βcat). In contrast to Wnt inhibition via DraxinOE **(F)**, *SNAI2* and *RHOB* were significantly upregulated with Wnt activation via NC1-Δ90βcat, whereas *DRAXIN* was significantly downregulated. *$P \leq 0.02$, two-tailed one sample *t*-test.

remodeling of the basement membrane during cranial neural crest development (Hutchins and Bronner, 2019). Furthermore, we also observed downregulation of the BMP ligand *BMP4*, suggesting that BMP signaling may act downstream of Wnt signaling during or immediately after cranial neural crest EMT. In trunk, it has been shown that neural crest delamination is regulated by BMP, and that canonical Wnt signaling is controlled by BMP signaling through BMP-responsive expression of the *Wnt1* ligand (Burstyn-Cohen et al., 2004). This is particularly interesting in light of our observations from a GFP reporter construct that BMP signaling is inactive in cranial neural crest at the onset of EMT (**Supplementary Figure 1**). Interestingly, Draxin has also been shown to inhibit neural crest migration in the trunk (Su et al., 2009; Zhang et al., 2017). Thus, whether *RHOB* expression is differentially regulated based on axial level (i.e., in response to BMP signaling in trunk neural crest versus in response to Wnt signaling in cranial neural crest) or based on signaling pathway crosstalk (which may also be dependent on axial level) remains to be explored.

In searching our datasets for neural crest-specific factors, we also noted modest upregulation of *SOX10* and *ETS1*, genes associated with neural crest EMT (Tahtakran and Selleck, 2003; Theveneau et al., 2007; Simoes-Costa and Bronner, 2015), which seemed contradictory to the antagonistic role of Draxin in modulating cranial neural crest EMT. *ETS1* expression is restricted to the cranial population of neural crest and is itself activated via cMYB (Betancur et al., 2010a); together with Sox9, Ets1 and cMYB function as activating gene regulatory inputs into a *SOX10E2* enhancer (Betancur et al., 2010b), regulating *SOX10* expression in cranial neural crest. Interestingly, in other contexts, canonical Wnt signaling has been shown to trigger degradation of cMYB protein (Kanei-Ishii et al., 2004); given that *Draxin* is endogenously expressed at HH9, it is possible that its normal inhibitory effects on canonical Wnt signaling may be necessary to reduce degradation of cMYB to activate endogenous levels of *ETS1* and *SOX10*, which initiate expression prior to the onset of EMT. Thus, we postulate here that during early cranial neural crest migration, excess cMYB protein is stabilized via exogenous Draxin-mediated inhibition of canonical Wnt signaling; as a result, this may trigger upregulation of *ETS1* and *SOX10* gene expression. However, despite upregulation of factors positively associated with EMT, downregulation of *SNAI2* alone is sufficient to

impede cranial neural crest migration (Nieto et al., 1994; Hutchins and Bronner, 2019).

Taken together, our data identify novel targets of canonical Wnt signaling during cranial neural crest EMT, and highlight potential avenues of intersection for signaling pathways involved in craniofacial development. The results raise the intriguing possibility that the sequence and magnitude of signaling and gene expression crosstalk during cranial neural crest development may help precisely regulate craniofacial morphogenesis.

DATA AVAILABILITY STATEMENT

The datasets presented in this study can be found in online repositories. The names of the repository/repositories and accession number(s) can be found below: https://www.ncbi.nlm.nih.gov/bioproject/PRJNA673315.

ETHICS STATEMENT

Ethical review and approval was not required for the animal study because our study uses chicken embryos at E1-2. These are not considered vertebrate embryos until E10, and thus we do not require ethics committee approvals or protocols, as they are not considered vertebrates at the stages we work.

AUTHOR CONTRIBUTIONS

EH, MP, and MB conceived the project and conducted the experimental design and data interpretation. EH and MP performed the cell dissociations, library preparations, and RNA-seq analyses. EH performed the functional annotation, hybridization chain reaction experiments, imaging, quantitation, and statistical analyses. EH and MB wrote the manuscript with editing by MP. All authors contributed to the article and approved the submitted version.

FUNDING

This work was supported by the National Institutes of Health (R01DE027538 and R01DE027568 to MB, K99DE028592 to EH, and K99DE029240 to MP).

ACKNOWLEDGMENTS

We thank A. Collazo and G. Spigolon for imaging assistance at the Caltech Biological Imaging Facility; P. Cannon and R. Diamond of the Caltech Flow Cytometry Cell Sorting Facility for cell sorting assistance; I. Antoshechkin of the Caltech Millard and Muriel Jacobs Genetics and Genomics Laboratory for sequencing of our RNA-seq libraries; and M. Martik and S. Gandhi for assistance with data processing.

SUPPLEMENTARY MATERIAL

The Supplementary Material for this article can be found online at: https://www.frontiersin.org/articles/10.3389/fphys.2021.624037/full#supplementary-material

Supplementary Figure 1 | BMP-sensitive reporter expression is absent from delaminating and migratory cranial neural crest during EMT. **(A)** Schematic of cross section of cranial region at HH9+ examined in panel **(B)**. Locations of premigratory (pNC) and migratory crest cells (mNC) are indicated. **(B)** Following electroporation of a BMP fluorescent reporter construct (BRE:GFP), cross sections stained for a neural crest marker (Snail2, magenta) and membrane label (WGA, white) revealed BMP reporter activity (green) in pNC (white dotted line), but not in delaminating or mNC (yellow dotted line). WGA, wheat germ agglutinin; pNC, premigratory neural crest; mNC, migratory neural crest. Scale bar, 10 μm.

REFERENCES

Ahmed, G., Shinmyo, Y., Ohta, K., Islam, S. M., Hossain, M., Naser, I. B., et al. (2011). Draxin inhibits axonal outgrowth through the netrin receptor DCC. *J. Neurosci.* 31, 14018–14023. doi: 10.1523/JNEUROSCI.0943-11.2011

Anders, S., Pyl, P. T., and Huber, W. (2015). HTSeq–a Python framework to work with high-throughput sequencing data. *Bioinformatics* 31, 166–169. doi: 10.1093/bioinformatics/btu638

Betancur, P., Bronner-Fraser, M., and Sauka-Spengler, T. (2010a). Assembling neural crest regulatory circuits into a gene regulatory network. *Annu. Rev. Cell Dev. Biol.* 26, 581–603. doi: 10.1146/annurev.cellbio.042308.113245

Betancur, P., Bronner-Fraser, M., and Sauka-Spengler, T. (2010b). Genomic code for Sox10 activation reveals a key regulatory enhancer for cranial neural crest. *Proc. Natl. Acad. Sci. U.S.A.* 107, 3570–3575. doi: 10.1073/pnas.0906596107

Burstyn-Cohen, T., Stanleigh, J., Sela-Donenfeld, D., and Kalcheim, C. (2004). Canonical Wnt activity regulates trunk neural crest delamination linking BMP/noggin signaling with G1/S transition. *Development* 131, 5327–5339. doi: 10.1242/dev.01424

Chiquet, B. T., Blanton, S. H., Burt, A., Ma, D., Stal, S., Mulliken, J. B., et al. (2008). Variation in WNT genes is associated with non-syndromic cleft lip with or without cleft palate. *Hum. Mol. Genet.* 17, 2212–2218. doi: 10.1093/hmg/ddn121

Cordero, D. R., Brugmann, S., Chu, Y., Bajpai, R., Jame, M., and Helms, J. A. (2011). Cranial neural crest cells on the move: their roles in craniofacial development. *Am. J. Med. Genet. A* 155A, 270–279. doi: 10.1002/ajmg.a.33702

Gandhi, S., and Bronner, M. E. (2018). Insights into neural crest development from studies of avian embryos. *Int. J. Dev. Biol.* 62, 183–194. doi: 10.1387/ijdb.180038sg

Gandhi, S., Hutchins, E. J., Maruszko, K., Park, J. H., Thomson, M., and Bronner, M. E. (2020). Bimodal function of chromatin remodeler Hmga1 in neural crest induction and Wnt-dependent emigration. *Elife* 9:e57779. doi: 10.7554/eLife.57779

Hamburger, V., and Hamilton, H. L. (1951). A series of normal stages in the development of the chick embryo. *J. Morphol.* 88, 49–92.

He, F., and Chen, Y. (2012). Wnt signaling in lip and palate development. *Front. Oral Biol.* 16:81–90. doi: 10.1159/000337619

Hossain, M., Ahmed, G., Naser, I. B., Shinmyo, Y., Ito, A., Riyadh, M. A., et al. (2013). The combinatorial guidance activities of draxin and Tsukushi are essential for forebrain commissure formation. *Dev. Biol.* 374, 58–70. doi: 10.1016/j.ydbio.2012.11.029

Huang da, W., Sherman, B. T., and Lempicki, R. A. (2009a). Systematic and integrative analysis of large gene lists using DAVID bioinformatics resources. *Nat. Protoc.* 4, 44–57. doi: 10.1038/nprot.2008.211

Huang da, W., Sherman, B. T., Zheng, X., Yang, J., Imamichi, T., Stephens, R., et al. (2009b). Extracting biological meaning from large gene lists with DAVID.

Curr. Protoc. Bioinformatics Chapter 13:Unit 13.11. doi: 10.1002/0471250953.bi1311s27

Huelsken, J., Vogel, R., Brinkmann, V., Erdmann, B., Birchmeier, C., and Birchmeier, W. (2000). Requirement for beta-catenin in anterior-posterior axis formation in mice. *J. Cell Biol.* 148, 567–578. doi: 10.1083/jcb.148.3.567

Hutchins, E. J., and Bronner, M. E. (2018). Draxin acts as a molecular rheostat of canonical Wnt signaling to control cranial neural crest EMT. *J. Cell Biol.* 217, 3683–3697. doi: 10.1083/jcb.201709149

Hutchins, E. J., and Bronner, M. E. (2019). Draxin alters laminin organization during basement membrane remodeling to control cranial neural crest EMT. *Dev. Biol.* 446, 151–158. doi: 10.1016/j.ydbio.2018.12.021

Islam, S. M., Shinmyo, Y., Okafuji, T., Su, Y., Naser, I. B., Ahmed, G., et al. (2009). Draxin, a repulsive guidance protein for spinal cord and forebrain commissures. *Science* 323, 388–393. doi: 10.1126/science.1165187

Kanei-Ishii, C., Ninomiya-Tsuji, J., Tanikawa, J., Nomura, T., Ishitani, T., Kishida, S., et al. (2004). Wnt-1 signal induces phosphorylation and degradation of c-Myb protein via TAK1, HIPK2, and NLK. *Genes Dev.* 18, 816–829. doi: 10.1101/gad.1170604

Kurosaka, H., Iulianella, A., Williams, T., and Trainor, P. A. (2014). Disrupting hedgehog and WNT signaling interactions promotes cleft lip pathogenesis. *J. Clin. Invest.* 124, 1660–1671. doi: 10.1172/JCI72688

LaBonne, C., and Bronner-Fraser, M. (1998). Neural crest induction in *Xenopus*: evidence for a two-signal model. *Development* 125, 2403–2414.

Langmead, B., and Salzberg, S. L. (2012). Fast gapped-read alignment with Bowtie 2. *Nat. Methods* 9, 357–359. doi: 10.1038/nmeth.1923

Le Douarin, N. (1982). *The Neural Crest*. Cambridge: Cambridge University Press.

Le Dreau, G., Garcia-Campmany, L., Rabadan, M. A., Ferronha, T., Tozer, S., Briscoe, J., et al. (2012). Canonical BMP7 activity is required for the generation of discrete neuronal populations in the dorsal spinal cord. *Development* 139, 259–268. doi: 10.1242/dev.074948

Liu, J. P., and Jessell, T. M. (1998). A role for rhoB in the delamination of neural crest cells from the dorsal neural tube. *Development* 125, 5055–5067.

Love, M. I., Huber, W., and Anders, S. (2014). Moderated estimation of fold change and dispersion for RNA-seq data with DESeq2. *Genome Biol.* 15:550. doi: 10.1186/s13059-014-0550-8

Meli, R., Weisova, P., and Propst, F. (2015). Repulsive axon guidance by Draxin is mediated by protein Kinase B (Akt), glycogen synthase kinase-3beta (GSK-3beta) and microtubule-associated protein 1B. *PLoS One* 10:e0119524. doi: 10.1371/journal.pone.0119524

Mi, H., Muruganujan, A., Ebert, D., Huang, X., and Thomas, P. D. (2019). PANTHER version 14: more genomes, a new PANTHER GO-slim and improvements in enrichment analysis tools. *Nucleic Acids Res.* 47, D419–D426. doi: 10.1093/nar/gky1038

Milet, C., and Monsoro-Burq, A. H. (2012). Neural crest induction at the neural plate border in vertebrates. *Dev. Biol.* 366, 22–33. doi: 10.1016/j.ydbio.2012.01.013

Monsoro-Burq, A. H., Wang, E., and Harland, R. (2005). Msx1 and Pax3 cooperate to mediate FGF8 and WNT signals during Xenopus neural crest induction. *Dev. Cell* 8, 167–178. doi: 10.1016/j.devcel.2004.12.017

Nieto, M. A., Sargent, M. G., Wilkinson, D. G., and Cooke, J. (1994). Control of cell behavior during vertebrate development by Slug, a zinc finger gene. *Science* 264, 835–839.

Noden, D. M. (1975). An analysis of migratory behavior of avian cephalic neural crest cells. *Dev. Biol.* 42, 106–130.

Perez-Alcala, S., Nieto, M. A., and Barbas, J. A. (2004). LSox5 regulates RhoB expression in the neural tube and promotes generation of the neural crest. *Development* 131, 4455–4465. doi: 10.1242/dev.01329

Piacentino, M. L., and Bronner, M. E. (2018). Intracellular attenuation of BMP signaling via CKIP-1/Smurf1 is essential during neural crest induction. *PLoS Biol.* 16:e2004425. doi: 10.1371/journal.pbio.2004425

Piacentino, M. L., Hutchins, E. J., Andrews, C. J., and Bronner, M. E. (2020). Temporal changes in plasma membrane lipid content induce endocytosis to regulate developmental epithelial-to-mesenchymal transition. *bioRxiv* [Preprint]. doi: 10.1101/2020.10.18.344523

Rabadán, M. A., Herrera, A., Fanlo, L., Usieto, S., Carmona-Fontaine, C., Barriga, E. H., et al. (2016). Delamination of neural crest cells requires transient and reversible Wnt inhibition mediated by Dact1/2. *Development* 143, 2194–2205. doi: 10.1242/dev.134981

Reid, B. S., Yang, H., Melvin, V. S., Taketo, M. M., and Williams, T. (2011). Ectodermal Wnt/beta-catenin signaling shapes the mouse face. *Dev. Biol.* 349, 261–269. doi: 10.1016/j.ydbio.2010.11.012

Ross, A. P., and Zarbalis, K. S. (2014). The emerging roles of ribosome biogenesis in craniofacial development. *Front. Physiol.* 5:26. doi: 10.3389/fphys.2014.00026

Schindelin, J., Arganda-Carreras, I., Frise, E., Kaynig, V., Longair, M., Pietzsch, T., et al. (2012). Fiji: an open-source platform for biological-image analysis. *Nat. Methods* 9, 676–682. doi: 10.1038/nmeth.2019

Simoes-Costa, M. S., McKeown, S. J., Tan-Cabugao, J., Sauka-Spengler, T., and Bronner, M. E. (2012). Dynamic and differential regulation of stem cell factor FoxD3 in the neural crest is Encrypted in the genome. *PLoS Genet.* 8:e1003142. doi: 10.1371/journal.pgen.1003142

Simoes-Costa, M., and Bronner, M. E. (2015). Establishing neural crest identity: a gene regulatory recipe. *Development* 142, 242–257. doi: 10.1242/dev.105445

Simoes-Costa, M., Stone, M., and Bronner, M. E. (2015). Axud1 Integrates Wnt signaling and transcriptional inputs to drive neural crest formation. *Dev. Cell* 34, 544–554. doi: 10.1016/j.devcel.2015.06.024

Steventon, B., Araya, C., Linker, C., Kuriyama, S., and Mayor, R. (2009). Differential requirements of BMP and Wnt signalling during gastrulation and neurulation define two steps in neural crest induction. *Development* 136, 771–779. doi: 10.1242/dev.029017

Su, Y., Naser, I. B., Islam, S. M., Zhang, S., Ahmed, G., Chen, S., et al. (2009). Draxin, an axon guidance protein, affects chick trunk neural crest migration. *Dev. Growth Differ.* 51, 787–796. doi: 10.1111/j.1440-169X.2009.01137.x

Tahtakran, S. A., and Selleck, M. A. (2003). Ets-1 expression is associated with cranial neural crest migration and vasculogenesis in the chick embryo. *Gene Expr. Patterns* 3, 455–458.

Taneyhill, L. A., and Bronner-Fraser, M. (2005). Dynamic alterations in gene expression after Wnt-mediated induction of avian neural crest. *Mol. Biol. Cell* 16, 5283–5293. doi: 10.1091/mbc.e05-03-0210

Tawarayama, H., Yamada, H., Amin, R., Morita-Fujimura, Y., Cooper, H. M., Shinmyo, Y., et al. (2018). Draxin regulates hippocampal neurogenesis in the postnatal dentate gyrus by inhibiting DCC-induced apoptosis. *Sci. Rep.* 8:840. doi: 10.1038/s41598-018-19346-6

Theveneau, E., Duband, J. L., and Altabef, M. (2007). Ets-1 confers cranial features on neural crest delamination. *PLoS One* 2:e1142. doi: 10.1371/journal.pone.0001142

Vega-Lopez, G. A., Cerrizuela, S., Tribulo, C., and Aybar, M. J. (2018). Neurocristopathies: new insights 150 years after the neural crest discovery. *Dev. Biol.* 444, S110–S143. doi: 10.1016/j.ydbio.2018.05.013

Wang, M. H., Sun, R., Zhou, X. M., Zhang, M. Y., Lu, J. B., Yang, Y., et al. (2018). Epithelial cell adhesion molecule overexpression regulates epithelial-mesenchymal transition, stemness and metastasis of nasopharyngeal carcinoma cells via the PTEN/AKT/mTOR pathway. *Cell Death Dis.* 9:2. doi: 10.1038/s41419-017-0013-8

Wu, J., Saint-Jeannet, J. P., and Klein, P. S. (2003). Wnt-frizzled signaling in neural crest formation. *Trends Neurosci.* 26, 40–45.

Wu, J., Yang, J., and Klein, P. S. (2005). Neural crest induction by the canonical Wnt pathway can be dissociated from anterior-posterior neural patterning in *Xenopus*. *Dev. Biol.* 279, 220–232. doi: 10.1016/j.ydbio.2004.12.016

Yanfeng, W., Saint-Jeannet, J. P., and Klein, P. S. (2003). Wnt-frizzled signaling in the induction and differentiation of the neural crest. *Bioessays* 25, 317–325. doi: 10.1002/bies.10255

Zhang, S., Su, Y., Gao, J., Zhang, C., and Tanaka, H. (2017). A potential inhibitory function of draxin in regulating mouse trunk neural crest migration. *In Vitro Cell. Dev. Biol. Anim.* 53, 43–53. doi: 10.1007/s11626-016-0079-0

Conflict of Interest: The authors declare that the research was conducted in the absence of any commercial or financial relationships that could be construed as a potential conflict of interest.

frontiers in Physiology

ORIGINAL RESEARCH
published: 26 February 2021
doi: 10.3389/fphys.2021.626080

Olfactory Rod Cells: A Rare Cell Type in the Larval Zebrafish Olfactory Epithelium With a Large Actin-Rich Apical Projection

King Yee Cheung[1†], Suresh J. Jesuthasan[2,3†], Sarah Baxendale[1†], Nicholas J. van Hateren[1†], Mar Marzo[1†], Christopher J. Hill[1†] and Tanya T. Whitfield[1*†]*

[1] Department of Biomedical Science, Bateson Centre and Neuroscience Institute, University of Sheffield, Sheffield, United Kingdom, [2] Lee Kong Chian School of Medicine, Nanyang Technological University, Singapore, Singapore, [3] Institute of Molecular and Cell Biology, Singapore, Singapore

We report the presence of a rare cell type, the olfactory rod cell, in the developing zebrafish olfactory epithelium. These cells each bear a single actin-rich rod-like apical projection extending 5–10 μm from the epithelial surface. Live imaging with a ubiquitous Lifeact-RFP label indicates that the olfactory rods can oscillate. Olfactory rods arise within a few hours of the olfactory pit opening, increase in numbers and size during larval stages, and can develop in the absence of olfactory cilia. Olfactory rod cells differ in morphology from the known classes of olfactory sensory neuron, but express reporters driven by neuronal promoters. A sub-population of olfactory rod cells expresses a Lifeact-mRFPruby transgene driven by the *sox10* promoter. Mosaic expression of this transgene reveals that olfactory rod cells have rounded cell bodies located apically in the olfactory epithelium and have no detectable axon. We offer speculation on the possible function of these cells in the Discussion.

Keywords: olfactory rod cell, olfactory placode, olfactory epithelium, actin, actin-rich projection, Lifeact, zebrafish

OPEN ACCESS

Edited by:
Patrick Blader, FR3743 Centre de Biologie Intégrative (CBI), France

Reviewed by:
Erika Calvo-Ochoa, Hope College, United States
Thomas Schilling, University of California, Irvine, United States

***Correspondence:**
Tanya T. Whitfield
t.whitfield@sheffield.ac.uk
Suresh J. Jesuthasan
sureshjj@imcb.a-star.edu.sg;
sureshj@ntu.edu.sg

†ORCID:
King Yee Cheung
orcid.org/0000-0002-1098-4926
Suresh J. Jesuthasan
orcid.org/0000-0002-5733-6555
Sarah Baxendale
orcid.org/0000-0002-6760-9457
Nicholas J. van Hateren
orcid.org/0000-0002-0011-9947
Mar Marzo
orcid.org/0000-0003-1591-0309
Christopher J. Hill
orcid.org/0000-0002-6914-4411
Tanya T. Whitfield
orcid.org/0000-0003-1575-1504

Specialty section:
This article was submitted to Craniofacial Biology and Dental Research, a section of the journal Frontiers in Physiology

Received: *04 November 2020*
Accepted: *25 January 2021*
Published: *26 February 2021*

Citation:
Cheung KY, Jesuthasan SJ, Baxendale S, van Hateren NJ, Marzo M, Hill CJ and Whitfield TT (2021) Olfactory Rod Cells: A Rare Cell Type in the Larval Zebrafish Olfactory Epithelium With a Large Actin-Rich Apical Projection. Front. Physiol. 12:626080. doi: 10.3389/fphys.2021.626080

INTRODUCTION

The vertebrate olfactory epithelium (OE) is a multimodal sensor. The functions of this epithelium, which derives from paired cranial neurogenic placodes (Whitlock and Westerfield, 2000), are mediated by a diverse set of cells. Two broad classes of sensory receptor—ciliated and microvillous—have been identified in the OE on the basis of morphology, receptor expression, and projection pattern (reviewed in Elsaesser and Paysan, 2007). Olfactory sensory neurons (OSNs), which express G-protein-coupled odorant receptors (ORs) and give rise to the sense of smell, are bipolar neurons that extend a dendrite to the apical surface of the OE and an axon to the olfactory bulb (OB; reviewed in Axel, 1995). Other sensory cells, some of which have no detectable axon, are also present. In mammals, these include microvillous cells that express TrpM channels and other taste components (Hansen and Finger, 2008; Lin et al., 2008; Genovese and Tizzano, 2018); such solitary chemosensory cells (SCCs) also exist in alligators (Hansen, 2007). A subset of OSNs can act as mechanosensors (Grosmaitre et al., 2007; Brinkmann and Schild, 2016; Iwata et al., 2017). Thus, the wide range of cell types in the OE allows for the detection of mechanical and other chemical stimuli in addition to sensing odours.

This variety of receptors is seen not only in terrestrial (air-breathing) animals, but also in aquatic vertebrates. In zebrafish, five classes of OSN have been identified. Each occupies a stereotyped

position within the pseudostratified OE, with the dendrite bearing a distinct and characteristic specialisation projecting into the environment (Hansen and Zeiske, 1998; Hansen and Zielinski, 2005; Sato et al., 2005; reviewed in Maier et al., 2014). Ciliated neurons, which express olfactory marker protein (OMP) and OR genes, have a cell body that lies deep within the OE, an axon that projects to dorsal and medial regions of the OB, and a slender dendrite extending to the surface of the olfactory pit. Here, the dendritic knob bears a cluster of primary cilia that project into the olfactory cavity (Hansen and Zeiske, 1998; Hansen and Zielinski, 2005; Sato et al., 2005). Microvillous OSNs, characterised by the expression of TrpC2 and vomeronasal (VR)-type pheromone receptors, have cell bodies that lie in the intermediary layer of the OE, an axon that projects to the lateral part of the OB, and a dendrite bearing a tuft of short, actin-rich microvilli (Hansen and Zeiske, 1998; Hansen and Zielinski, 2005; Sato et al., 2005). Crypt neurons, less abundant than ciliated or microvillous OSNs, have rounded cell bodies that sit apically in the OE, with both cilia and microvilli extending from a crypt within the cell body (Hansen and Zeiske, 1998; Hansen and Zielinski, 2005; Parisi et al., 2014; Biechl et al., 2016; Bettini et al., 2017; Sepahi et al., 2019). Kappe neurons lie in the superficial layers of the adult zebrafish OE and are named for their apical actin-rich cap, presumed to be microvilli (Ahuja et al., 2014). Pear-shaped neurons are also positioned superficially in the adult OE and have short apical dendrites, but express some markers in common with ciliated neurons (Wakisaka et al., 2017). Aside from these OSNs, it is not known what other sensory cell types exist.

The OE is directly exposed to the environment, and is thus continually subject to damage and infection. Numerous mechanisms enable efficient sampling of stimuli while maintaining tissue integrity and defence. These functions are provided by non-sensory cells in the OE, which include basal (stem) cells that replenish the OSNs, sustentacular (support) cells, and goblet cells, which produce mucus containing anti-microbial peptides (Hansen and Zeiske, 1993, 1998; Byrd and Brunjes, 1995; Demirler et al., 2019; reviewed in Olivares and Schmachtenberg, 2019). Multiciliated cells, located around the rim of the olfactory pit in fish, each bear multiple long motile cilia. These have a characteristic 9+2 axoneme and beat at around 24 Hz, resulting in an asymmetric flow that draws water and odorants into the olfactory cavity and flushes them out again (Reiten et al., 2017). Additional cell types with critical functions, such as immune cells, also populate the OE (Sepahi et al., 2019; Kraus et al., 2020).

We report here the existence of a rare cell type, the olfactory rod cell, in the OE of larval zebrafish. Olfactory rod cells are characterised by a single actin-rich apical projection, and were initially observed in whole-mount phalloidin stains, which we use routinely to visualise the actin-rich stereociliary bundles on sensory hair cells of the inner ear and lateral line. It was unclear what these olfactory cells were, as they did not resemble previously described OSNs. The morphology of the olfactory rod matches descriptions of similar structures in the OE of several other fish species (Bannister, 1965; Schulte, 1972; Breipohl et al., 1973; Ichikawa and Ueda, 1977; Yamamoto and Ueda, 1978; Rhein et al., 1981; Hernádi, 1993; Datta and Bandopadhyay, 1997), many of which were previously dismissed either as senescent forms of OSNs or as fixation artefacts (Muller and Marc, 1984; Moran et al., 1992). Using a variety of transgenic lines and imaging techniques, including live imaging, we show that zebrafish olfactory rod cells are present in living fish and can be detected from early stages of larval development.

MATERIALS AND METHODS

Zebrafish Husbandry

Zebrafish strains used in this study were wild type (AB strain—ZFIN), *ift88*^{tz288b} (Tsujikawa and Malicki, 2004), *sox10*^{m618} (Dutton et al., 2001), *Tg(actb2:Lifeact-RFP)*^{e115} (Behrndt et al., 2012), *Tg*(*actb2:Lifeact-GFP)*^{e114} (Behrndt et al., 2012), *Tg(Xla.Tubb:jGCaMP7f)*^{sq214} (Chia et al., 2019), *Tg(elavl3:GCaMP6f)*^{jf1} (Dunn et al., 2016), *Tg(elavl3:H2B-GCaMP6s)*^{jf5} (Dunn et al., 2016), *Tg(pou4f3:GAP-GFP)*^{s356t} (Xiao et al., 2005) and *Tg(sox10:Lifeact-mRFPruby)*^{sh630} (this study). Homozygous *sox10*$^{-/-}$ mutant larvae were identified by their lack of body pigmentation at 5 days post-fertilisation (dpf). Adult zebrafish were kept in a 10 h dark/14 h light cycle at 28.5°C and spawned by pair-mating or marbling (Aleström et al., 2019). Eggs were collected and staged according to standard protocols (Kimmel et al., 1995; Nüsslein-Volhard and Dahm, 2002), and raised in E3 medium (5 mM NaCl, 0.17 mM KCl, 0.33 mM $CaCl_2$, 0.33 mM $MgSO_4$, with 0.0001% methylene blue at early stages) at 28.5°C. For controlling the developmental rate to obtain embryos at stages 34–46 h post-fertilisation (hpf), embryos were incubated at 25°C or 34°C in accordance with Kimmel's formula, $_{H_T=h\div(0.055T-0.57)}$ (Kimmel et al., 1995). For live imaging, zebrafish were anaesthetised with 0.5 mM tricaine mesylate in E3.

Generation of the *Tg(sox10:Lifeact-mRFPruby)* Transgenic Line

The *-4725sox10:Lifeact-mRFPruby* construct was generated using the Gateway Tol2 kit (Kawakami, 2007; Kwan et al., 2007). The p5E *-4725sox10* promoter (Dutton et al., 2008; Rodrigues et al., 2012), pME-*Lifeact-mRFPruby* (Riedl et al., 2008), and p3E polyA sequences were cloned into pDestTol2pA3 through an LR Clonase reaction. The 12.1 kb final plasmid was sequenced and injected into the AB strain. Injected embryos were grown to adulthood and crossed to AB. Transgenic progeny from one founder male were selected based on mRFPruby expression in the inner ear and grown to adulthood to generate a stable line. Embryos with bright fluorescence, presumed to be homozygous for the transgene, were chosen for imaging.

Immunohistochemistry and Phalloidin Staining

Zebrafish embryos and larvae were fixed in 4% paraformaldehyde (PFA) in phosphate-buffered saline (PBS) for 2 h at room temperature or overnight at 4°C. Zebrafish were washed three or

more times with PBS, and permeabilised by incubation in PBS-Triton X-100 (0.2% Triton for 36–48 hpf embryos, 1% Triton for later stages) for several hours at 4°C until staining.

To visualise F-actin, zebrafish were stained with either Alexa Fluor 488 phalloidin (Cell Signaling Technology; 1:150), Alexa Fluor 568 (Invitrogen ThermoFisher; 1:50), or Alexa Fluor 647 phalloidin (Invitrogen ThermoFisher; 1:50) in PBS overnight at 4°C. After staining, zebrafish were washed four times in PBS over two or more hours before imaging.

For antibody staining, after fixing and washing, zebrafish were washed a further three times in PBS-0.2% Triton and incubated in blocking solution (10% sheep serum in PBS-0.2% Triton) for 60 min at room temperature. The primary antibody was mouse IgG1 anti-acetylated α-tubulin antibody (Sigma-Aldrich; 1:100). Staining was carried out in blocking solution containing 1% dimethyl sulfoxide (DMSO; Sigma-Aldrich) overnight at 4°C. Zebrafish were washed three times in PBS-0.2% Triton, and a further four times over two or more hours. The secondary antibody was Alexa 647-conjugated goat anti-mouse IgG1 (Invitrogen ThermoFisher; 1:200). For double stains with phalloidin, Alexa Fluor 488 phalloidin (1:150) and DMSO (1%) were added together with the secondary antibody in blocking solution overnight at 4°C. Zebrafish were then washed four times in PBS-0.2% Triton and stored at 4°C until imaging. Controls with no primary antibody yielded no staining (not shown).

Neomycin Treatment

For neomycin treatment, a concentration of 500 μM was chosen, as it was an effective concentration used by Harris et al. (2003) for minimum lateral line hair cell survival, as measured by DASPEI staining. A 5 mM solution was made by adding neomycin trisulfate salt hydrate (Sigma-Aldrich) to MilliQ water and used at a 1:10 dilution in E3 fish medium. *Tg(pou4f3:GFP)* transgenic zebrafish were treated for 60 min at 28.5°C. An equivalent volume of MilliQ water in E3 was used for the control group. Zebrafish were washed three times in fresh E3 and left at 28.5°C for 2 h. GFP signal was screened using widefield fluorescence microscopy to analyse hair cell damage. Zebrafish were fixed and stained with Alexa Fluor 647 phalloidin as above.

Fluorescence Imaging

For confocal imaging, fixed zebrafish embryos and larvae were mounted in 1.5% low melting point (LMP) agarose in PBS, and live zebrafish were mounted in 1.5% LMP agarose in E3 in WillCo glass-bottomed dishes (mounted in frontal view for 36–48 hpf, dorsal view for later stages). Zebrafish were imaged on a Zeiss LSM880 Airyscan confocal microscope equipped with a Plan-Apochromat 20 × /0.8 M27 air objective, LD LCI Plan-Apochromat 40 × /1.2 Imm Korr DIC M27 water immersion objective, or Plan-Apochromat 63 × /1.4 oil DIC M27 objective. Images were acquired in Airyscan SR mode, Airyscan Fast scan mode with SR sampling, or Airyscan Fast scan mode with Opt sampling. Zebrafish were also imaged on a Zeiss LSM 800 attached to an upright microscope with a W Plan-Apochromat 40 × /1.0 DIC M27 or 63 × /1.0 M27 water dipping objective. The laser lines used were 488, 561, and 633 nm. Widefield imaging was performed on a Zeiss Axio Zoom.V16 fluorescence stereo zoom microscope equipped with a Zeiss 60N-C 1" 1.0 × C-mount and AxioCam MRm camera. For light-sheet imaging, live zebrafish larvae were mounted in 0.9% LMP agarose in E3 and imaged on a Zeiss Z1 Light-sheet microscope, with 4% tricaine in E3 in the sample chamber. Imaging was performed with a W Plan-Apochromat 20 × objective using brightfield illumination and the 561 nm laser line.

Scanning Electron Microscopy

For scanning electron microscopy, *ift88* homozygous mutant and phenotypically wild-type sibling larvae at 4 dpf were fixed overnight in 2.5% glutaraldehyde/0.1M sodium cacodylate buffer. Samples were washed in buffer, post-fixed in 2% aqueous osmium tetroxide for 1 h, washed in buffer again and then dehydrated through a graded ethanol series (50, 75, 95, 100%) before being dried in a mixture of 50% hexamethyldisilazane (HMDS) in 100% ethanol. Final drying was in 100% HMDS. After removal of the final HMDS wash, samples were left to dry in a fume hood overnight. Samples were mounted onto a pin stub using a Leit-C sticky tab and Leit-C mounting putty, gold-coated using an Edwards S150B sputter coater, and examined in a Tescan Vega3 LMU Scanning Electron Microscope at an operating voltage of 15 kV and imaged using a secondary electron detector.

Image Processing, Quantification, and Statistical Analyses

Zeiss LSM880 Airyscan confocal images were subjected to Airyscan processing on Zen Black 2.3 software (Zeiss) using "Auto" Airyscan processing parameters. Further processing was performed on Fiji (Schindelin et al., 2012). 3D rendering was performed using the 3D Viewer plugin (Schmid et al., 2010) on Fiji. Olfactory rod projection lengths were measured in 3D from confocal images using Fiji, and calculated in Microsoft Excel using the PyT method (based on the Pythagorean theorem) from Dummer et al. (2016). All quantifications were exported into GraphPad Prism 8, which was then used for performing statistical analyses and making graphs.

Statistical analyses were carried out in GraphPad Prism 8. Datasets were considered normally distributed if they passed at least one of four normality tests (Anderson-Darling, D'Agostino & Pearson, Shapiro-Wilk, and Kolmogorov-Smirnov tests). Statistical tests used are stated in the figure legends. Bars on graphs indicate mean ± standard error of the mean (S.E.M.), unless stated otherwise. *P* values are indicated as follows: $P > 0.05$ (not significant, ns), $P < 0.05$ (*), $P < 0.01$ (**), $P < 0.001$ (***), $P < 0.0001$ (****).

For mapping spatial distributions of olfactory rod cells within the olfactory pit, 2D maximum intensity projection images were imported into the Desmos Graphing Calculator (desmos.com). The positions and sizes of the images were adjusted to align the rims of olfactory pits with an ellipse to fit the shape of the rim, defined by $\frac{(x-35)^2}{5}+\frac{(y-33)^2}{10}=7.6^2$. The positions of the base of each olfactory rod, relative to the ellipse, were plotted as coordinates onto the graph. The resulting graphs were exported as .png image files.

Figures were prepared using Adobe Photoshop and Affinity Designer.

RESULTS

Actin-Rich Rod-Like Apical Projections, Distinct From OSN Microvilli and Cilia, Are Present in the Olfactory Epithelium of Larval and Juvenile Zebrafish

Staining of the wild-type larval and juvenile zebrafish OE with fluorescently conjugated phalloidin, which binds to F-actin, reveals the presence of several actin-rich rod-like projections ("olfactory rods") in each olfactory pit (**Figures 1A–B′**). These projections differ in number, distribution, size and morphology from any of the described apical projections of zebrafish OSNs. The projections extend from below the apical surface of the OE and project about 5–10 μm above it, tapering to a point. This is an order of magnitude longer than OSN microvilli, which are typically 0.5–0.8 μm in length (Hansen and Zeiske, 1998). Olfactory rods are shorter than the surrounding phalloidin-negative olfactory cilia (**Figures 1C–D′**), and do not label with an anti-acetylated α-tubulin antibody (**Figures 1C–C‴**). Olfactory rods are not evenly distributed across the OE, but are mostly clustered posterolaterally in each olfactory pit, although there is variation between individuals (**Figure 1E**). At low magnification, the olfactory rods appear similar to the actin-rich stereociliary bundle of mechanosensory hair cells of the inner ear and lateral line. However, higher magnification images reveal that

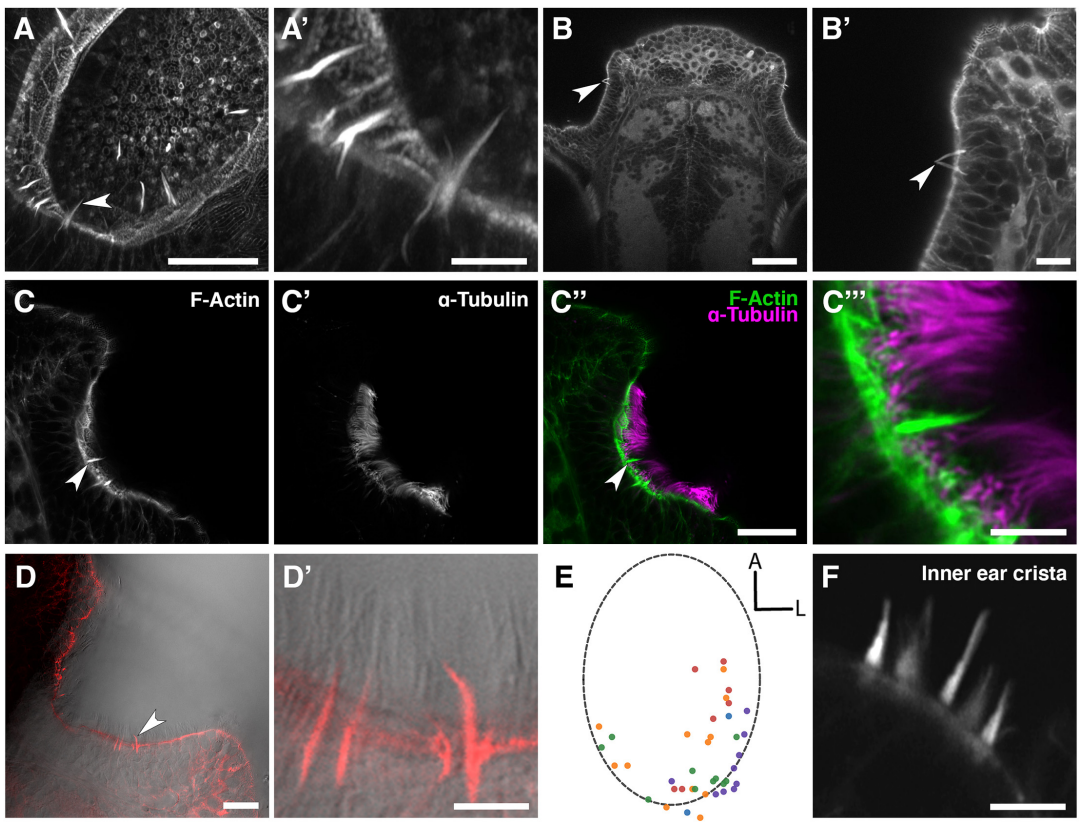

FIGURE 1 | Phalloidin staining reveals the presence of actin-rich rod-like projections, distinct from OSN microvilli and cilia, in the zebrafish larval and juvenile olfactory epithelium. **(A)** Maximum intensity projection of an Airyscan confocal image of phalloidin stain in an olfactory pit of a 5 dpf wild-type larva; anterior to the top right, lateral to the bottom right. Arrowhead marks one example olfactory rod. Scale bar = 20 μm. **(A′)** Enlargement of olfactory rods in panel **(A)**. Scale bar = 5 μm. **(B)** Dorsal view low power image of phalloidin stain in the head of an 18 dpf (5 mm) wild-type juvenile zebrafish; anterior to the top. Arrowhead marks the position of two olfactory rods in an olfactory pit. Scale bar = 50 μm. **(B′)** Enlargement of OE in panel **(B)**. Arrowhead marks two olfactory rods. Scale bar = 10 μm. **(C–C″)** Airyscan confocal image of Alexa-phalloidin signal **(C)**, acetylated α-tubulin immunohistochemistry signal **(C′)**, and merged signals **(C″)** in an olfactory pit of a 4 dpf wild-type larva; anterior to the top, lateral to the right. Arrowhead marks one example olfactory rod. Scale bar = 20 μm. **(C‴)** Enlargement of olfactory rod in panel **(C″)**. Scale bar = 5 μm. **(D)** Differential interference contrast (DIC) image and phalloidin stain (red) in an olfactory pit of a 5 dpf wild-type larva; anterior to the top, lateral to the right. Arrowhead marks one example olfactory rod. Scale bar = 20 μm. **(D′)** Enlargement of olfactory rods in panel **(D)**. Surrounding olfactory cilia are visible and unlabelled by Alexa-phalloidin. Scale bar = 5 μm. **(E)** A map of the positions of olfactory rod cell projection bases in olfactory pits of 4 dpf wild-type larvae (*N* of olfactory pits = 5), based on 2D maximum intensity projections of confocal images of phalloidin stains; anterior "A" to the top, lateral "L" to the right. One dot represents one olfactory rod. Different coloured dots represent olfactory rods from different larvae. **(F)** Airyscan confocal image of phalloidin stain in an inner ear crista of a 5 dpf wild-type larva. Hair cell stereocilia are labelled with Alexa-phalloidin, and are arranged in a stepped array. In the stereociliary bundle on the extreme left, four different stereociliary lengths are visible [compare with panel **(A′)**]. Scale bar = 5 μm.

the olfactory rod is not oligovillous, but appears to be a single structure (**Figures 1B′,C‴,D′**). This contrasts with the stepped array of multiple stereocilia present on the apical surface of mechanosensory hair cells (**Figure 1F**).

To characterise the timing of appearance and development of the olfactory rods during embryonic and larval stages, we stained fixed samples from 36 hpf, just after formation of the olfactory pits (Hansen and Zeiske, 1993), to 5 dpf. Occasional olfactory rods were present in olfactory pits at 36 hpf, but were only consistently present beyond 46 hpf (**Figures 2A,B**). Although the number of olfactory rods per pit varied at each stage, the average number increased over time. By 5 dpf, each pit contained 10.7 ± 2.9 (mean ± standard deviation, SD) olfactory rods (**Figure 2B**). After measuring the olfactory rods in 3D, we found an increase in projection length (from the base of the phalloidin-positive projection to the tip) from 36 hpf to 5 dpf, with the most significant increase occurring by 48 hpf, despite a relatively large range in length at each stage. At 5 dpf in fixed samples, the mean projection length was 10.4 ± 2.2 (SD) μm, with the largest measuring 17.5 μm (**Figure 2C**).

Olfactory Rod Cell Projections Can Develop in the Absence of Olfactory Cilia

As described above, olfactory rods differ from olfactory cilia in terms of size, shape, cytoskeletal composition, and distribution

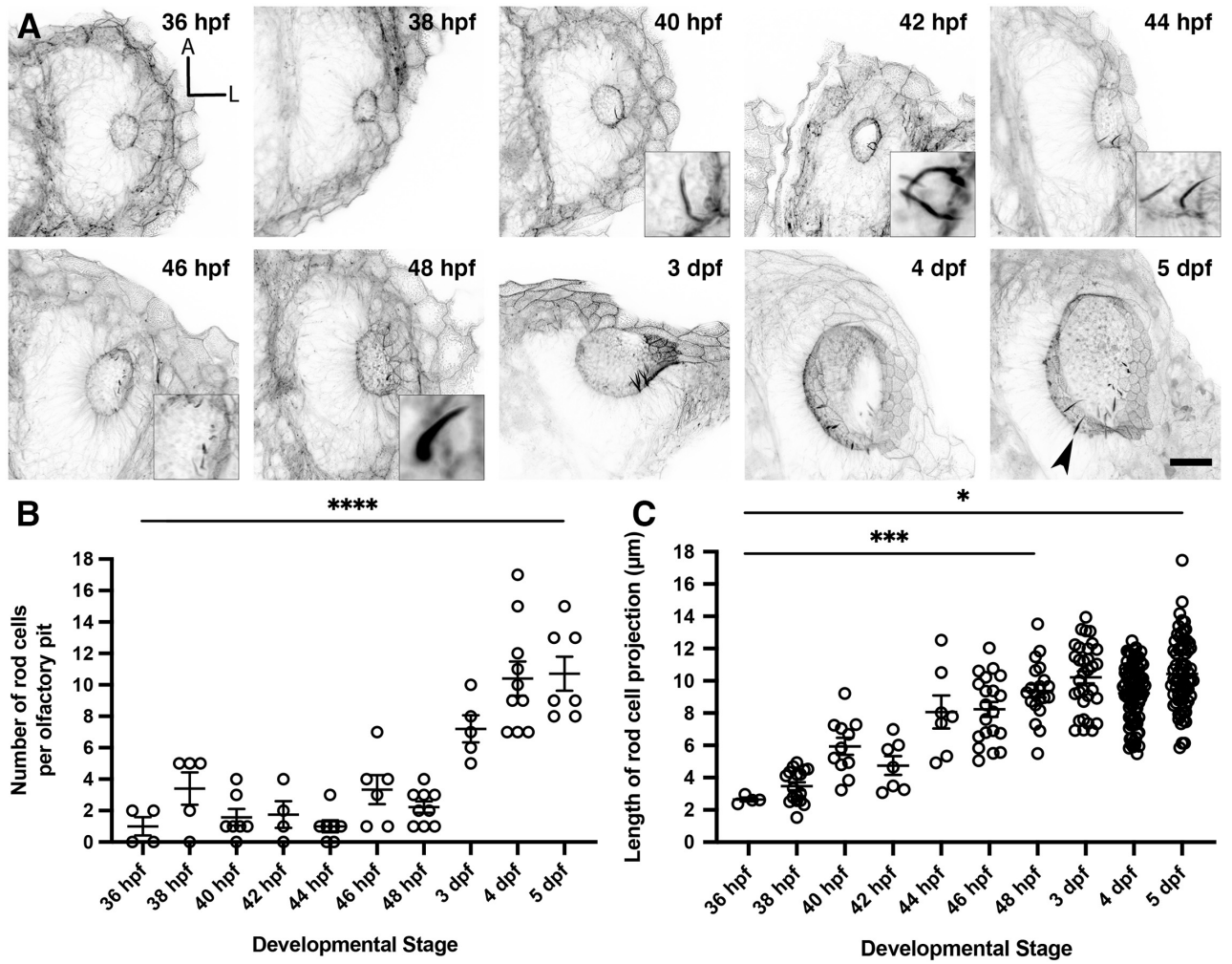

FIGURE 2 | Olfactory rod cells arise early during zebrafish olfactory pit development. **(A)** Maximum intensity projections of Airyscan confocal images showing the wild-type development of olfactory pit and olfactory rod cells at various embryonic and larval stages, using Alexa-phalloidin as a marker; anterior "A" to the top, lateral "L" to the right. Grayscale values from the original fluorescence image have been inverted. Arrowhead marks one example olfactory rod. Scale bar = 20 μm. Selected inserts show olfactory rods at higher magnification. **(B)** The change in number of olfactory rod cells per olfactory pit during embryonic development—36 hpf (*N* of olfactory pits = 4), 38 hpf (*N* = 5), 40 hpf (*N* = 7), 42 hpf (*N* = 4), 44 hpf (*N* = 7), 46 hpf (*N* = 6), 48 hpf (*N* = 9), 3 dpf (*N* = 5), 4 dpf (*N* = 10), and 5 dpf (*N* = 7). Bars indicate mean ± SEM for each stage. Linear regression analysis; ∗∗∗∗ indicates $P < 0.0001$. **(C)** The change in lengths of olfactory rod cell projections during embryonic development—36 hpf (*N* of olfactory pits = 2, *n* of olfactory rods = 4), 38 hpf (*N* = 4, *n* = 17), 40 hpf (*N* = 6, *n* = 11), 42 hpf (*N* = 3, *n* = 7), 44 hpf (*N* = 5, *n* = 7), 46 hpf (*N* = 6, *n* = 20), 48 hpf (*N* = 9, *n* = 20), 3 dpf (*N* = 5, *n* = 32), 4 dpf (*N* = 10, *n* = 82), and 5 dpf (*N* = 8, *n* = 71). Bars indicate mean ± S.E.M. for each stage. Linear regression analysis; ∗ indicates $P = 0.0251$, ∗∗∗ indicates $P = 0.0009$.

in the OE. We therefore hypothesised that olfactory rod cell projections would not be affected by mutations that disrupt the formation of cilia. To test this, we examined fish mutant for *ift88*, which codes for a component of the intraflagellar transport machinery necessary for the normal formation and maintenance of cilia (Tsujikawa and Malicki, 2004). A phalloidin stain revealed that olfactory rods were present in the OE of *ift88*$^{-/-}$ mutants at 5 dpf (**Figures 3A,B**).

The absence of cilia in *ift88*$^{-/-}$ mutants allowed us to examine morphology of the olfactory rods using scanning electron microscopy (SEM). In the phenotypically wild-type sibling OE, the olfactory rods were almost completely obscured by olfactory cilia, with only the occasional tip of a projection visible (**Figures 3C–E″**). However, SEM images of the olfactory pit of *ift88*$^{-/-}$ mutants at 4 dpf, which lack cilia, revealed the presence of rod-like projections with a similar size, number, smoothly tapering morphology, and spatial distribution to the actin-rich projections described above (**Figures 3F–I**). At their base, olfactory rods are wider in diameter (about 0.6 μm) than the olfactory cilia in wild-type larvae (0.2 μm in diameter, as is typical

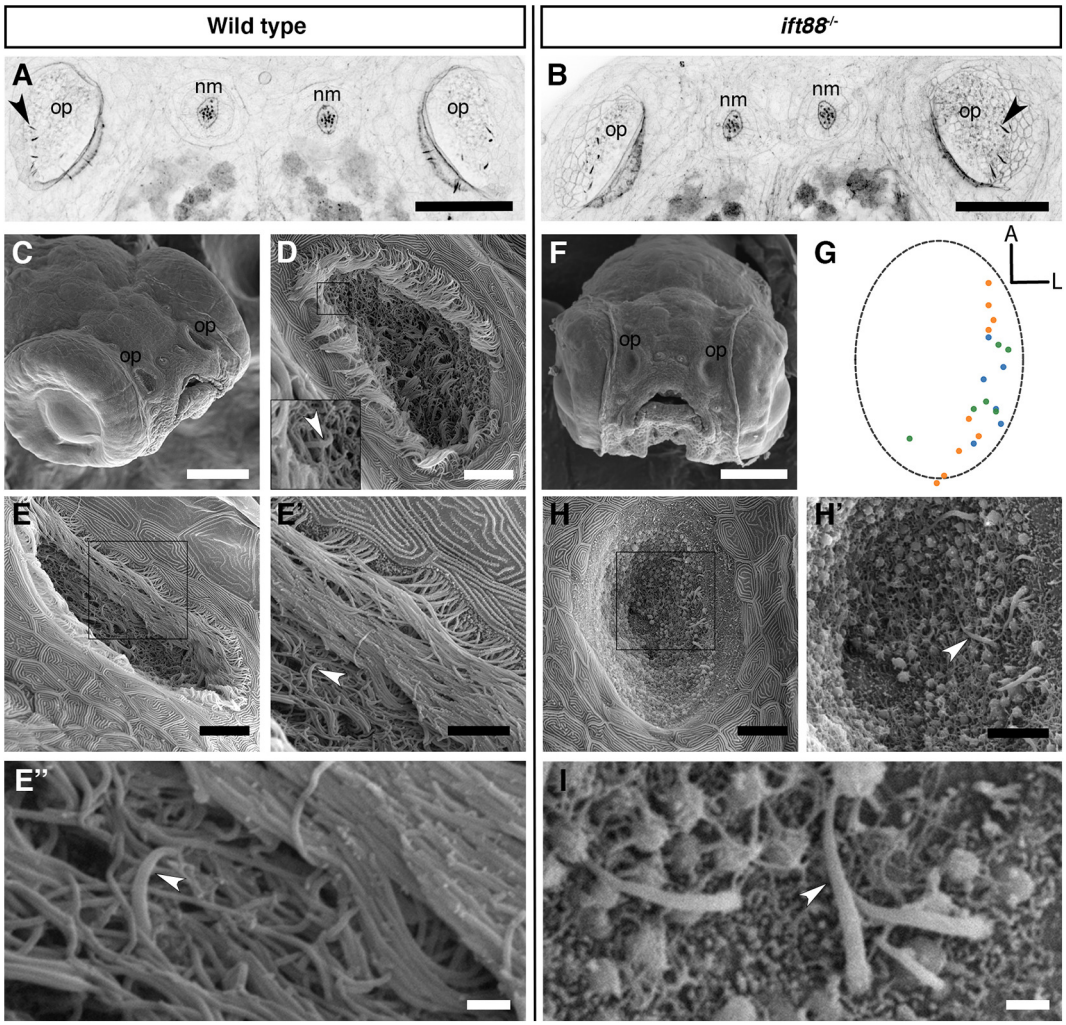

FIGURE 3 | Olfactory rod cells are present in the olfactory epithelia of *ift88*$^{-/-}$ zebrafish mutants, which lack cilia. **(A,B)** Maximum intensity projections of Airyscan confocal images of phalloidin stains of a 5 dpf wild-type **(A)** and *ift88*$^{-/-}$ mutant **(B)** larva; dorsal views, anterior to the top. Grayscale values from the original fluorescence image have been inverted. Abbreviations: nm, cranial neuromast; op, olfactory pit. Several olfactory rods (arrowheads mark examples) are visible in each olfactory pit. Scale bar = 50 μm. **(C)** SEM of the head of a 4 dpf wild-type larva. Scale bar = 100 μm. **(D,E)** SEM of 4 dpf larval wild-type olfactory pits [enlarged from panel **(C)**]. Scale bars = 10 μm. Insert in panel **(D)** shows enlarged view of boxed area in panel **(D)**. Arrowhead marks the tip of an olfactory rod cell apical projection surrounded by olfactory cilia. **(E′)** Enlarged view of boxed area in panel **(E)**. Arrowhead marks one olfactory rod. Scale bar = 5 μm. **(E″)** Enlargement of olfactory rod in panel **(E′)** (arrowhead). Scale bar = 1 μm. **(F)** Frontal view SEM of the head of a 4 dpf *ift88*$^{-/-}$ mutant larva. Scale bar = 100 μm. **(G)** A map of the positions of olfactory rod cell projection emergence through the OE in *ift88*$^{-/-}$ mutant larvae (*N* of olfactory pits = 3), based on SEM images at 4 dpf; anterior "A" to the top, lateral "L" to the right. One dot represents one olfactory rod. Different coloured dots represent olfactory rods from different larvae. (Compare with **Figure 1E**). **(H)** SEM of 4 dpf larval *ift88*$^{-/-}$ mutant olfactory pit [enlarged from panel **(F)**]. Scale bar = 10 μm. **(H′)** Enlarged view of boxed area in panel **(H)**. Arrowhead marks one example olfactory rod cell projection present despite the loss of cilia. Scale bar = 5 μm. **(I)** Enlarged SEM of olfactory rods (arrowhead marks example) in 4 dpf larval *ift88*$^{-/-}$ mutant olfactory pit (from a different individual). Scale bar = 1 μm.

for many cilia). We conclude that olfactory rods can develop in the absence of cilia.

Olfactory Rods Can Be Labelled in the Live Larva

To visualise olfactory rods in live larvae, we imaged the *Tg(actb2:Lifeact-RFP)* transgenic line at 4 and 6 dpf, and *Tg(actb2:Lifeact-GFP)* at 5 dpf (Behrndt et al., 2012). We found fluorescent apical projections in the olfactory pits of live larvae in all cases (*N* of fish = 4; **Figures 4A–C**, **Supplementary Movie 1**). These matched the size, shape, and posterolateral distribution of olfactory rod cells present in fixed samples (**Figures 4D,E**). Despite potential shrinkage due to fixation, there was no overall difference in the lengths of projections between live and fixed samples (**Figure 4E**). The zig-zag pattern exhibited by RFP-positive olfactory rods in raster-scanned images of live larvae suggested that olfactory rods were moving during image capture (**Figure 4B**). Fast-capture time series imaging of the *Tg(actb2:Lifeact-RFP)* transgenic line allowed us to observe that the projection oscillates (**Supplementary Movie 2**), possibly as a result of ciliary beating.

Neuronal Promoters Drive Reporter Expression in Olfactory Rod Cells

To test whether olfactory rod cells have features of neuronal cells, we imaged two transgenic lines that have broad neuronal expression of cytoplasmic fluorescent reporters—*Tg(Xla.tubb:jGCaMP7f)* (Chia et al., 2019) (*N* of olfactory pits = 4) and *Tg(elavl3:GCaMP6f)* (Dunn et al., 2016) (*N* = 5). Dendrites and dendritic knobs of OSNs were clearly labelled by both lines. In some examples, we observed faintly labelled projections extending from below the surface of the OE, with a similar length and morphology to olfactory rods (**Figures 5A–B′**). Imaging of double-transgenic

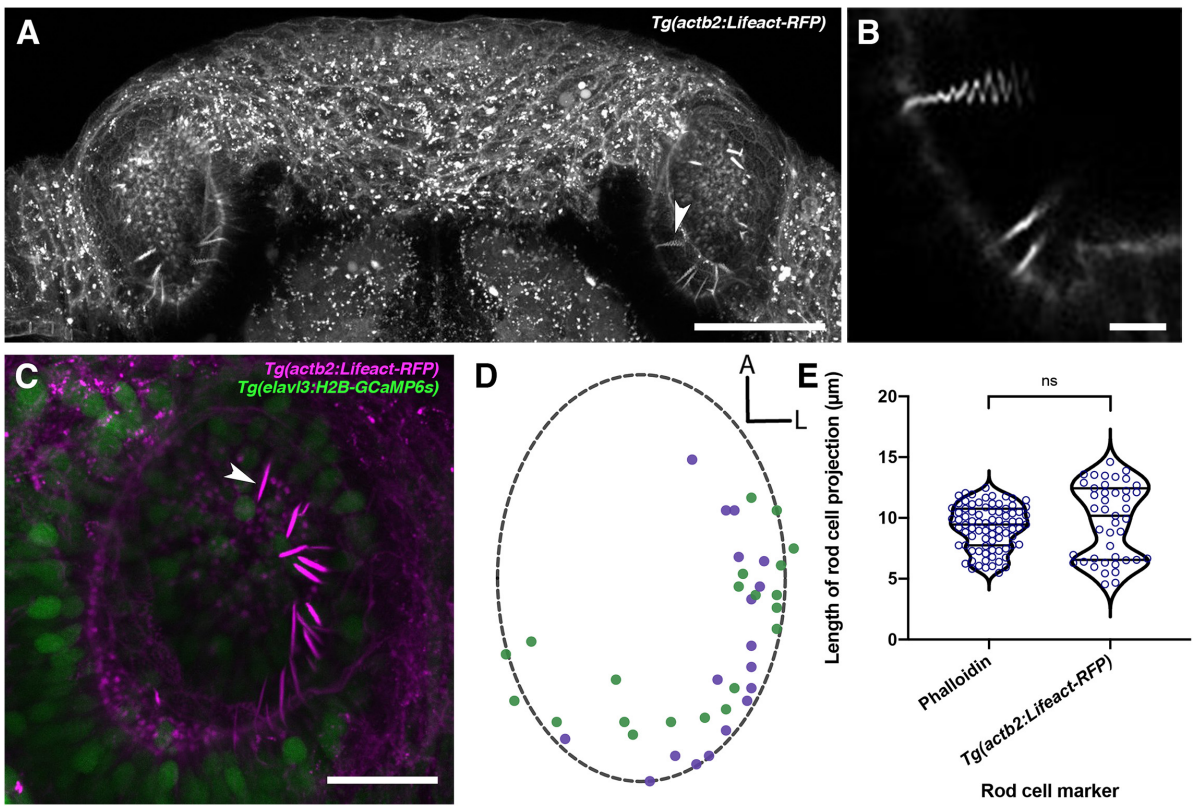

FIGURE 4 | Olfactory rods are labelled in the olfactory epithelia of live zebrafish larvae by the *Tg(actb2:Lifeact-RFP)* transgene. **(A)** Maximum intensity projection of dorsal view image of the olfactory pits of a live 6 dpf *Tg(actb2:Lifeact-RFP)* transgenic larva; anterior to the top. Arrowhead marks one example olfactory rod positive for the Lifeact-RFP transgene. Scale bar = 50 μm. **(B)** Enlargement of olfactory rods in panel **(A)** [arrowhead in panel **(A)**] oscillating during raster-scanned image capture. (Raster scanning was performed from top to bottom in the image, as it has been rotated 90° clockwise) (see **Supplementary Movie 2**). Scale bar = 5 μm. **(C)** Maximum intensity projection image of a live 4 dpf *Tg(actb2:Lifeact-RFP);Tg(elavl3:H2B-GCaMP6s)* double-transgenic larval olfactory pit; anterior to the top, lateral to the right. Arrowhead marks one example olfactory rod positive for the Lifeact-RFP transgene (magenta). Neuronal nuclei are labelled in green. Larvae were fully mounted in agarose, so olfactory rods were not moving. Scale bar = 20 μm (see **Supplementary Movie 1**). **(D)** A map of the positions of olfactory rod cell projection bases in olfactory pits of 4 dpf *Tg(actb2:Lifeact-RFP);Tg(elavl3:H2B-GCaMP6s)* double-transgenic larvae (*N* of olfactory pits = 2), based on 2D maximum intensity projections of confocal images; anterior "A" to the top, lateral "L" to the right. One dot represents one olfactory rod. Different coloured dots represent olfactory rods from different larvae, with purple corresponding to panel **(C)**. (Compare with **Figure 1E**). **(E)** A quantitative comparison of the lengths of olfactory rod cell projections in fixed larvae, using Alexa-phalloidin as a marker (*N* = 10, *n* of olfactory rods = 82) versus live larvae, using Lifeact-RFP as a marker (*N* = 2, *n* = 43). Violin plot; bars indicate the median and lower and upper quartiles for each group. Mann-Whitney *U* test; ns, not significant (*P* = 0.232).

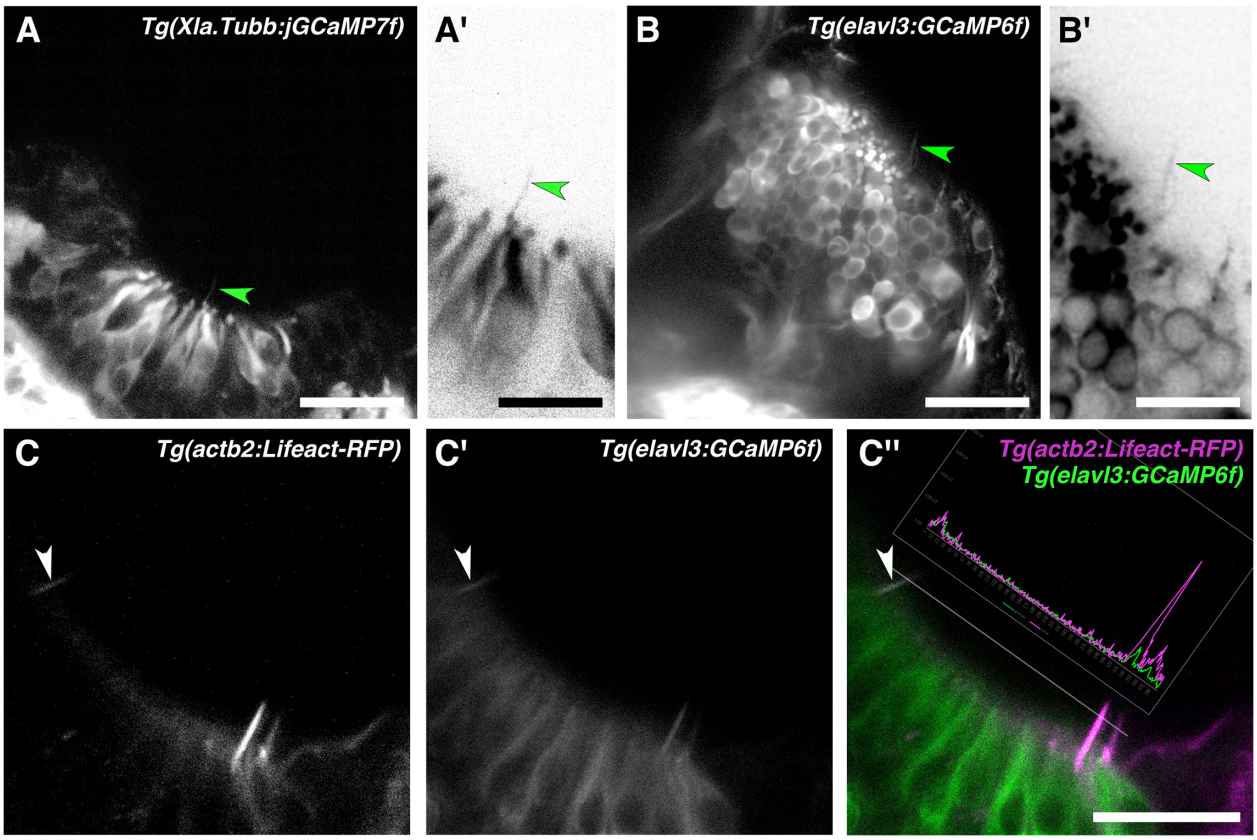

FIGURE 5 | Olfactory rod cells are labelled by the cytoplasmic neuronal markers *Tg(Xla.Tubb:jGCaMP7f)* and *Tg(elavl3:GCaMP6f)*. **(A)** Olfactory pit of a 4 dpf *Tg(Xla.Tubb:jGCaMP7f)* larva; anterior to the top, lateral to the right. Arrowhead marks one example olfactory rod, albeit faintly labelled. Scale bar = 20 μm. **(A′)** Enlargement of olfactory rod marked by arrowhead in panel **(A)** (grayscale values inverted). Scale bar = 10 μm. **(B)** Olfactory pit of a 5 dpf *Tg(elavl3:GCaMP6f)* larva; anterior to the top, lateral to the right. Arrowhead marks one example olfactory rod, albeit faintly labelled. Scale bar = 20 μm. **(B′)** Enlargement of olfactory rod marked by arrowhead in panel **(B)** (grayscale values inverted). Scale bar = 10 μm. **(C–C″)** Lifeact-RFP signal **(C)**, GCaMP6f signal **(C′)**, and merged signals **(C″)** in an olfactory pit of a 5 dpf *Tg(elavl3:GCaMP6f);Tg(actb2:Lifeact-RFP)* double-transgenic larva; anterior to the top, lateral to the right. The trace shows levels of red and green fluorescence along the dotted line, which passes through three olfactory rods positive for both Lifeact-RFP and GCaMP6f. The olfactory rod highlighted with the arrowhead shows similar levels of fluorescence in both the red and green channels. Scale bar = 20 μm.

Tg(elavl3:GCaMP6f);Tg(actb2:Lifeact-RFP) larvae at 5 dpf suggests that olfactory rod cells are GCaMP6f-positive (*N* of fish = 3; **Figures 5C–C″**). While some of the green fluorescence may be caused by bleed-through from RFP, this cannot account for all the signal, as we observed rods where the green fluorescence was detected even with dim red fluorescence (arrowhead, **Figures 5C–C″**; see trace of RFP and GCaMP6f levels); we also noted bright red pixels with no corresponding green signal. These observations suggest that olfactory rod cells may be a type of neuron.

Olfactory Rod Cells Are Not Hair-Cell-Like Cells

We initially observed the presence of olfactory rods when performing whole-mount phalloidin stains for the actin-rich stereociliary bundles of sensory hair cells in the inner ear and lateral line. Given the superficial similarity in appearance of olfactory rods to hair-cell stereocilia in low-magnification phalloidin stains (see, for example, **Figure 3A**), and a report of a rare cell type bearing stereocilia-like microvilli in the rat OE (Menco and Jackson, 1997), we were interested to test whether there is any similarity between olfactory rod cells and mechanosensory hair cells of the inner ear and lateral line. As shown in **Figures 1** and **3**, the zebrafish olfactory rod appears to be a single structure rather than a collection of microvilli or stereocilia. To test whether olfactory rod cells express sensory hair cell markers, we performed an Alexa-phalloidin co-stain on the *Tg(pou4f3:GFP)* transgenic line, a known marker for hair cells (Xiao et al., 2005). At 5 dpf, the stereociliary bundle of lateral line neuromast hair cells was clearly marked by both GFP and phalloidin, which acted as our positive control (**Figures 6A–A″**). However, the GFP did not co-localise with the phalloidin signal in the olfactory rods, or in the cell body beneath a phalloidin-positive olfactory rod (**Figures 6B–B″**).

Mechanosensory hair cells, including those of the zebrafish lateral line, are susceptible to oxidative damage by aminoglycoside antibiotics, which can preferentially enter hair cells via mechanotransduction channels, and cause cell death

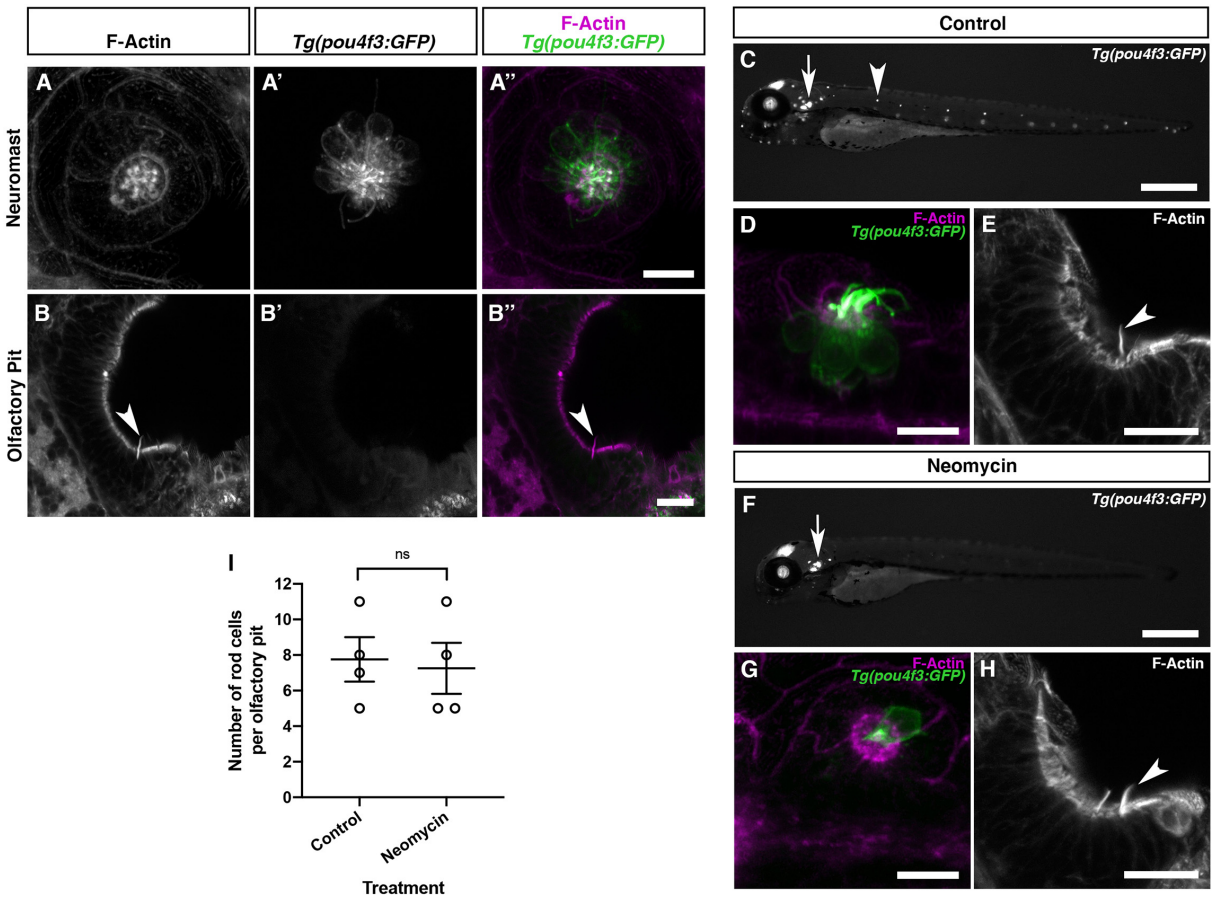

FIGURE 6 | Olfactory rod cells in the zebrafish olfactory epithelium are not hair-cell-like. **(A–A″)** Maximum intensity projection of Airyscan confocal image of Alexa-phalloidin signal **(A)**, *Tg(pou4f3:GFP)* signal **(A′)**, and merged signals **(A″)** in a cranial neuromast of a 5 dpf larva. Scale bar = 10 μm. **(B–B″)** Airyscan confocal image of Alexa-phalloidin signal **(B)**, *Tg(pou4f3:GFP)* signal **(B′)**, and merged signals **(B″)** in an olfactory pit of a 5 dpf larva; anterior to the top, lateral to the right. Arrowhead marks one olfactory rod. Scale bar = 20 μm. **(C,F)** Widefield imaging of 3 dpf *Tg(pou4f3:GFP)* larvae showing the damaging effects of 500 μM neomycin treatment for 60 min on lateral line neuromast hair cells. Fluorescence is lost or greatly reduced in both trunk (arrowhead) and cranial neuromasts, whereas fluorescence in hair cells of the inner ear maculae and cristae (arrow) is unaffected. Scale bars = 500 μm. **(D,G)** Maximum intensity projections of Airyscan confocal images showing the damaging effects of 500 μM neomycin treatment for 60 min on hair cells in a cranial neuromast of a 3 dpf larva, using *Tg(pou4f3:GFP)* (green) and Alexa-phalloidin (magenta) as markers. Scale bars = 10 μm. **(E,H)** Maximum intensity projections of Airyscan confocal images showing no effect of 500 μM neomycin treatment for 60 min on olfactory rods, using Alexa-phalloidin as a marker; anterior to the top, lateral to the right. Arrowheads mark olfactory rods. Scale bars = 20 μm. **(I)** The number of olfactory rod cell projections per olfactory pit of 3 dpf *Tg(pou4f3:GFP)* larvae after 500 μM neomycin treatment for 60 min (*N* of olfactory pits = 4), compared with an untreated group (*N* = 4). Bars indicate mean ± SEM. Welch's unpaired two-tailed *t*-test; ns, not significant (*P* = 0.8018).

following a calcium flux and release of reactive oxygen species by mitochondria (Esterberg et al., 2013, 2016; Pickett et al., 2018). To test whether olfactory rod cells are similarly sensitive, we investigated whether treatment with the aminoglycoside neomycin has the same damaging effect on olfactory rod cells as on lateral line hair cells. Following neomycin treatment at 500 μM for 60 min on 3 dpf *Tg(pou4f3:GFP)* larvae, lateral line hair cells were lost or severely damaged, as determined by a decrease in the number of GFP-positive cells (together with loss of their phalloidin-positive stereocilia) in both cranial and trunk neuromasts and a change in morphology of any remaining cells (**Figures 6C,D,F,G**). By contrast, olfactory rods appeared unaffected (**Figure 6E,H**), with no significant change in the number of olfactory rods present in each olfactory pit (**Figure 6I**). Taken together, the smooth appearance of the olfactory rods, lack of hair cell marker expression, and resistance to neomycin indicate that olfactory rod cells are not closely related to hair cells.

A Sub-population of Olfactory Rod Cells Expresses a Lifeact Transgene Driven by the *sox10* Promoter

Sox10 is a known marker of both neural crest and otic epithelium (Dutton et al., 2001). Robust transgene expression driven by the *sox10* promoter has been reported in the OE and other tissues in the zebrafish (Mongera et al., 2013; Saxena et al., 2013). We have generated a *Tg(sox10:Lifeact-mRFPruby)* transgenic line to visualise actin localisation and dynamics in the live embryo in *sox10*-expressing tissues. As reported for the

Tg(sox10:eGFP) transgene (Saxena et al., 2013), we observed OSNs expressing *Tg(sox10:Lifeact-mRFPruby)* in the OE at 4 and 5 dpf; based on morphology, most of these cells were microvillous OSNs. However, staining with Alexa-phalloidin on fixed samples revealed the co-expression of Lifeact-mRFPruby in a sub-population of phalloidin-positive olfactory rod cell projections (**Figures 7A–B″**). Not all olfactory rod cells expressed the transgene; an average of 64.4% of olfactory rod cells marked by phalloidin (*N* of olfactory pits = 5, *n* of olfactory rods = 59) also expressed Lifeact-mRFPruby (**Figure 7C**). As for the olfactory rods labelled with Lifeact-RFP, rods labelled with Lifeact-mRFPruby oscillated (**Supplementary Movie 3**).

The sparse expression of the *Tg(sox10:Lifeact-mRFPruby)* transgene allowed us to visualise the morphology of the cell body of olfactory rod cells and ask whether they have an axon. Lifeact-mRFPruby-expressing cell bodies were positioned apically in the OE and were rounded in shape (**Figures 7B–B″,E**). They were morphologically distinct from the well-described microvillous OSNs (**Figures 7D,E**) as well as ciliated and crypt OSNs. The axons of microvillous OSNs were visible in those cells labelled by the transgene (**Figure 7D**). However, with this marker, we were unable to observe an axon extending from the cell body of olfactory rod cells (*N* of olfactory pits = 5, *n* of cells = 9; **Figure 7E**).

To test whether the development of olfactory rod cells is dependent on *sox10* function, we stained $sox10^{-/-}$ homozygous mutants (Dutton et al., 2001) with Alexa-phalloidin. Olfactory rods were present in $sox10^{-/-}$ mutants at 5 dpf, but variable in number (*N* of olfactory pits = 8, *n* of olfactory rods = 53; **Figure 8**). Taken together, the data from *Tg(sox10:Lifeact-mRFPruby)* transgenic and $sox10^{-/-}$ mutant larvae indicate that *sox10* function is not essential for the formation of olfactory rod cells.

DISCUSSION

The zebrafish is a key model organism for the study of the olfactory system (reviewed in Kermen et al., 2013; Calvo-Ochoa and Byrd-Jacobs, 2019), and a complete inventory of the cell types present in the zebrafish OE will be an important resource and reference point for further study. Through the use of phalloidin staining, immunohistochemistry, transgenic zebrafish lines, SEM and high-resolution fluorescence confocal imaging, we have identified a rare cell type, the olfactory rod cell, in the zebrafish larval and juvenile OE. Olfactory rod cells, which have not previously been described in zebrafish to our knowledge, are morphologically distinct from the well-characterised OSNs and other known cell types in terms of their apical projections, cell shape, and distribution and positioning within the OE.

The Olfactory Rod: An Actin-Rich Apical Projection

The spectacular actin-rich projection of the olfactory rod cell adds to the rich repertoire of known F-actin-based cellular specialisations, which include microvilli, stereocilia, lamellipodia, filopodia, cytonemes and microridges (reviewed in Heath and Holifield, 1991; Theriot and Mitchison, 1991; Ramírez-Weber and Kornberg, 1999; Pinto et al., 2019; Inaba et al., 2020). Many sensory cell types, in both fish and mammals, bear actin-rich mechano- or chemosensory microvillous projections, including the stereocilia of sensory hair cells (Tilney et al., 1980; reviewed in Gillespie and Müller, 2009; Barr-Gillespie, 2015), and the microvilli of olfactory and vomeronasal microvillous neurons, SCCs of the skin and barbel (Kotrschal et al., 1997; Finger et al., 2003; Hansen and Finger, 2008), taste bud cells (Hansen et al., 2002; Zachar and Jonz, 2012), spinal cerebrospinal fluid-contacting neurons (CSF-cNs; Djenoune et al., 2014; Desban et al., 2019), Merkel cells, retinal Müller glia (Sekerková et al., 2004), and the brush and tuft cells of mammalian respiratory and intestinal epithelia, respectively (reviewed in Reid et al., 2005; Schneider et al., 2019). As a single structure with a smoothly tapering morphology, the zebrafish olfactory rod differs from these oligovillous structures. Adult zebrafish SCCs, found distributed over the entire body surface (Kotrschal et al., 1997), and mature light cells of the zebrafish taste bud (Hansen et al., 2002) each bear a single microvillus, but at 1–3 μm in length, these are much shorter than the olfactory rods we describe.

Olfactory rod cells are distinct from rodlet cells, which have been reported in many different epithelial tissues of marine and freshwater fish, including zebrafish, and contain several intracellular electron-dense rodlets within a thick cuticular-like wall (Bannister, 1966; reviewed in Morrison and Odense, 1978; Hansen and Zeiske, 1998; Dezfuli et al., 2007; DePasquale, 2020). Recently, phalloidin staining has demonstrated that the rodlets, which can be extruded from the cell, are not composed of F-actin (DePasquale, 2020). Thus, zebrafish olfactory rod cells, which are unique to the OE at the larval stages we have described, are not related to rodlet cells.

Olfactory Rod Cells in Other Teleost Species

Previous studies have provided descriptions of cell types similar to the olfactory rod cell in other teleost species, including the common minnow (Bannister, 1965), several eel species (Schulte, 1972; Yamamoto and Ueda, 1978), goldfish (Breipohl et al., 1973; Ichikawa and Ueda, 1977), rainbow trout (Rhein et al., 1981), common bleak (Hernádi, 1993), catfish (Datta and Bandopadhyay, 1997), and several cave fish and cave loach species (Waryani et al., 2013, 2015; Zhang et al., 2018).

Using transmission electron microscopy (TEM), Bannister (1965) reported sparsely populated rod-shaped protrusions, approximately 4 μm in length and shorter than surrounding sensory and non-sensory olfactory cilia, in the OE of adult (3.7 cm) common minnow (*Phoxinus phoxinus*). Here, the rod-like projection consisted of several bundles of fibres, consistent with the appearance of F-actin, extending from deep within the cell (Bannister, 1965). Similarly, using TEM and SEM respectively, Schulte (1972) and Yamamoto and Ueda (1978) reported the presence of olfactory rod cells in the OE of several adult eel species: European eel (*Anguilla anguilla*), Japanese eel (*A. japonica*), white-spotted conger (*Conger myriaster*), buffoon snake eel (*Microdonophis erabo*), and brutal moray

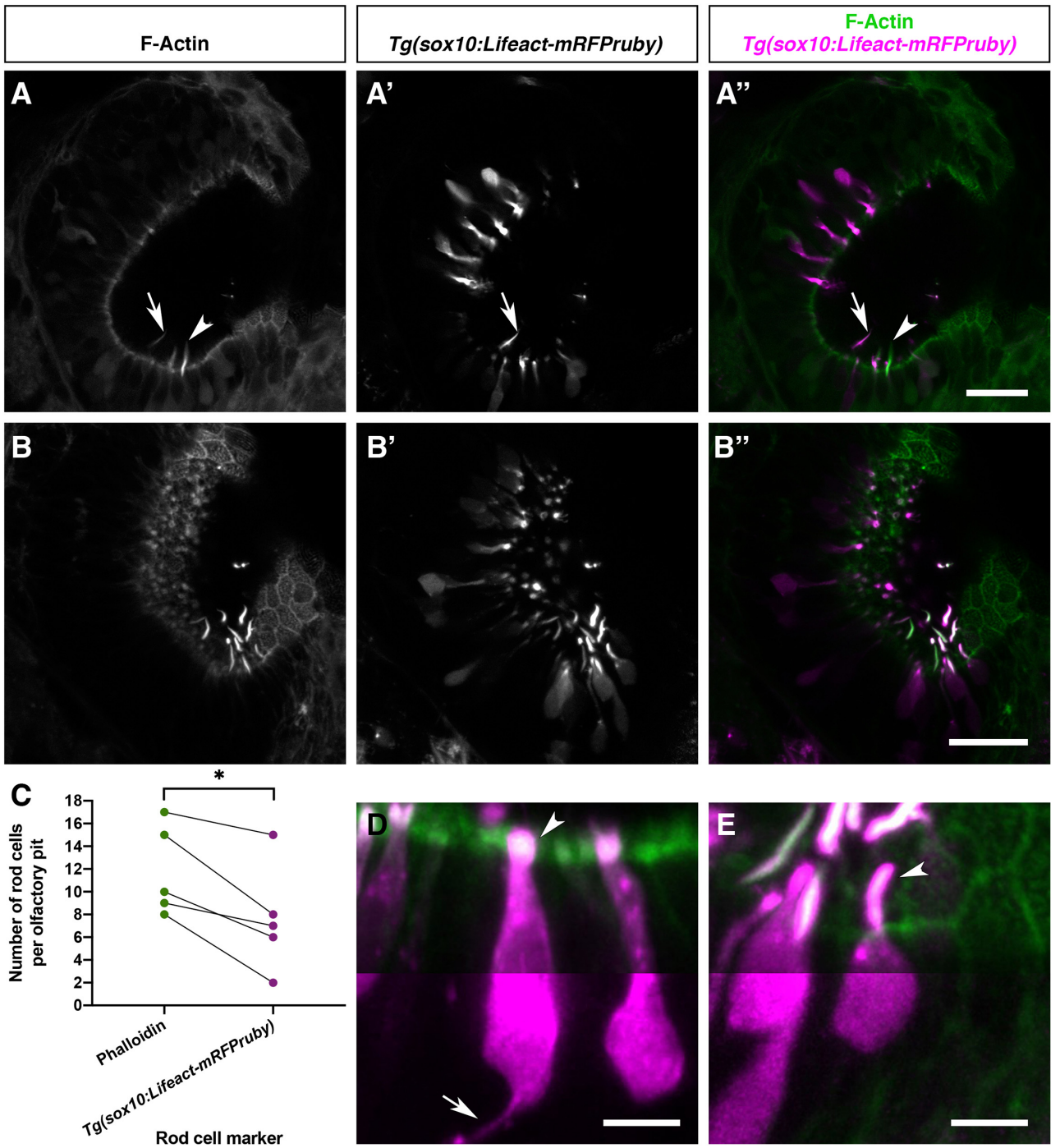

FIGURE 7 | Olfactory rod cells are apically located in the zebrafish olfactory epithelium, with a rounded cell body and no detectable axon. **(A–B″)** Airyscan confocal image of Alexa-phalloidin signal **(A,B)**, *Tg(sox10:Lifeact-mRFPruby)* signal **(A′,B′)**, and merged signals **(A″,B″)** in olfactory pits of 4–5 dpf larvae; anterior to the top, lateral to the right. Arrowhead marks one olfactory rod negative for Lifeact-mRFPruby. Arrow marks one olfactory rod positive for Lifeact-mRFPruby. Scale bars = 20 μm. **(C)** Number of olfactory rod cells positively marked by Alexa-phalloidin (*n* of olfactory rods = 59), compared with the number of those also marked by *Tg(sox10:Lifeact-mRFPruby)* (*n* = 38), in olfactory pits of 4–5 dpf larvae (*N* of olfactory pits = 5). Connecting lines indicate olfactory rods from the same olfactory pit. Paired two-tailed *t*-test; ∗ indicates $P = 0.0146$. **(D)** Enlargement of two microvillous OSNs, expressing Lifeact-mRFPruby, in the OE of a 4 dpf larva; Alexa-phalloidin signal (green), *Tg(sox10:Lifeact-mRFPruby)* signal (magenta). Arrowhead marks the microvillous apical projections. The gamma value for the magenta channel in the bottom half of the panel has been set to 0.5 to show the axon from one of the cells (arrow). Scale bar = 5 μm. **(E)** Enlargement of olfactory rod cells (of which both the apical actin projections and cell bodies are labelled by the *Tg(sox10:Lifeact-mRFPruby)* transgene) in the OE of a 4 dpf larva; Alexa-phalloidin signal (green), *Tg(sox10:Lifeact-mRFPruby)* signal (magenta). Arrowhead marks an olfactory rod cell apical projection, positive for both markers. The gamma value for the bottom half of the panel has been set to 0.5 as in panel **(D)**; no axon is visible. Scale bar = 5 μm. See also **Supplementary Movie 3**.

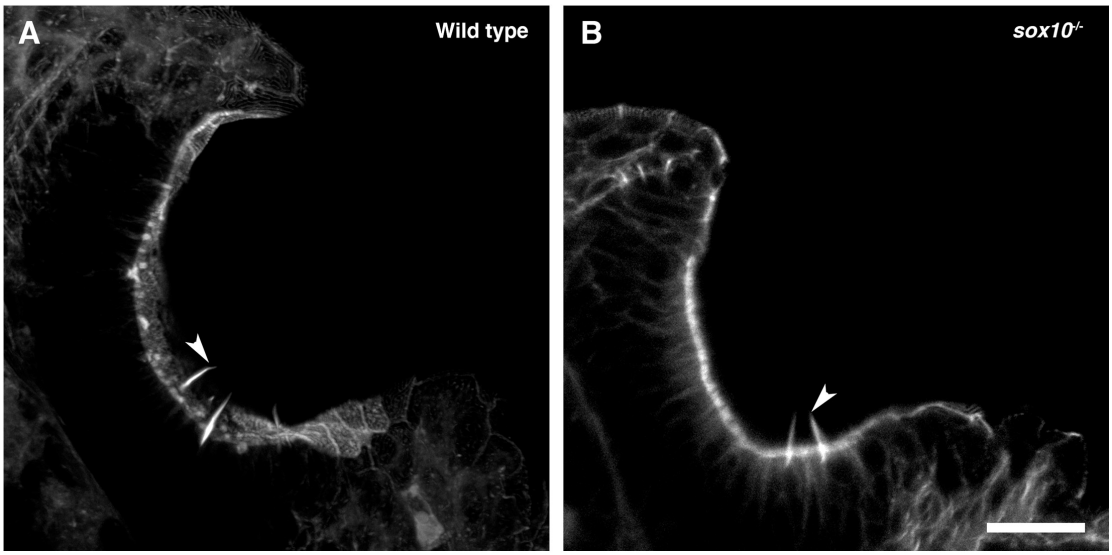

FIGURE 8 | Olfactory rod cells are present in the olfactory epithelia of *sox10*$^{-/-}$ zebrafish mutants. **(A)** Maximum intensity projection of Airyscan confocal image of phalloidin stain in a 5 dpf larval wild-type olfactory pit; anterior to the top, lateral to the right. Arrowhead marks one example olfactory rod. Scale bar = 20 μm. **(B)** Airyscan confocal image of phalloidin stain in a 5 dpf larval *sox10*$^{-/-}$ mutant olfactory pit; anterior to the top, lateral to the right. Arrowhead marks one example olfactory rod. Scale bar = 20 μm.

(*Gymnothorax kidako*). In European eels, the cells were described as a receptor with a single rod-shaped appendage, measuring 0.8 μm in diameter and extending 4 μm above the apical surface of the epithelium (Schulte, 1972). Olfactory rods in the other four species measured 1 μm in diameter and 10 μm in length. Olfactory rods were either found to exist solitarily or in a group; interestingly, it was noted that olfactory cilia were sparse in areas where olfactory rods occurred in a group (Yamamoto and Ueda, 1978).

More recent reports include comparisons of the surface structures of olfactory epithelia in different adult cave fish and loaches. SEMs in *Sinocyclocheilus jii* and *S. furcodorsalis* cave fish, and in *Oreonectes polystigmus* and *O. guananensis* cave loaches revealed that olfactory rods were clustered in different regions of olfactory rosette lamellae (Waryani et al., 2013, 2015). Another SEM study on the variations in olfactory systems of adult cave fish species of different habitats reported not just one, but three different cell types all classified as "rod cilia" in the olfactory epithelia of *S. anshuiensis* and *S. tianlinensis*. The first cell type had a long base with an oval apex, the second contained an oval base with a thin apex, while the third was rod-shaped and thin from base to tip, measuring 2.01–3.08 μm in length (Zhang et al., 2018). Despite the shorter length, this third type appeared morphologically consistent with zebrafish olfactory rod cells. Unlike other teleosts, olfactory rod cells were reported as the dominant cell type over ciliated and microvillous OSNs in the OE of *S. jii* (Waryani et al., 2013). This may be an example of the known compensatory enhancement of the olfactory system in blind morphs of cave fish (Bibliowicz et al., 2013; reviewed in Krishnan and Rohner, 2017).

Although there appear to be variations in the numbers and sizes of olfactory rod cells reported in these other teleost species, some of these cells may be homologous to the olfactory rod cells we describe in zebrafish larvae. However, all of these previous studies were limited to fixed adult samples by means of TEM and SEM, and none have tested or confirmed the cytoskeletal composition of the olfactory rod.

Olfactory Rod Cells Differ From Known Olfactory Sensory Neurons

We have detected weak expression of cytoplasmic fluorescent markers driven by neuronal promoters in olfactory rod cells. However, we were unable to detect an axon in nine individual olfactory rod cells imaged with a Lifeact-mRFPruby transgene at 4–5 dpf. Of note, Ichikawa and Ueda (1977) performed olfactory nerve bundle transection in adult goldfish to determine which cell types are OSNs. As expected, transection caused retrograde degeneration of both ciliated and microvillous OSNs. Olfactory rod cells, however, were still identifiable by SEM in the OE 10 days after nerve transection. The authors concluded that adult goldfish olfactory rod cells are not OSNs. This is similar to the observation that OB ablation did not lead to death of a subset of microvillous cells in the rat OE (Carr et al., 1991). It now appears that such microvillous cells are a class of sensory paraneuron, as they are cholinergic and express components of the taste transduction pathway (Genovese and Tizzano, 2018). Whether olfactory rod cells express similar genes remains to be determined.

Zebrafish Olfactory Rod Cells Are Not Artefacts

Since the first report of olfactory rod cells, several studies have proposed that they may represent senescent forms of OSNs or fixation artefacts (Muller and Marc, 1984; Moran et al., 1992;

reviewed in Hansen and Zielinski, 2005). A study in the goldfish (*Carassius auratus*) and channel catfish (*Ictalurus punctatus*), using TEM, SEM and filling with horseradish peroxidase, concluded that olfactory rods are most likely a result of fusion of olfactory cilia or microvilli—an indicator of ageing OSNs (Muller and Marc, 1984). A later study on the ultrastructure of olfactory mucosa in brown trout (*Salmo trutta*) also classified olfactory rods as products of the fusion of olfactory cilia during fixation (Moran et al., 1992). Indeed, TEM images in this study showed multiple ciliary axonemes surrounded by a single membrane (Moran et al., 1992). The presence of such fixation artefacts has led to frequent dismissal of olfactory rod cells in the literature, for example in juvenile and adult European eels (Sola et al., 1993). In the zebrafish, however, the olfactory rods we describe are clearly not a fixation artefact, as they are present in the live larva. Moreover, they are not formed by fusion of cilia, as the olfactory rods are F-actin-positive, do not stain with an anti-acetylated α-tubulin antibody, and are present in *ift88*$^{-/-}$ mutants which lack cilia.

Possible Functions of Olfactory Rod Cells

Actin-rich projections on sensory cells are known to have mechanosensory (reviewed in Gillespie and Müller, 2009), chemosensory (Höfer and Drenckhahn, 1999; Hansen et al., 2002; Zachar and Jonz, 2012), or multimodal functions (for example in CSF-cNs in zebrafish; Djenoune et al., 2014; Desban et al., 2019). A mechanosensory role for zebrafish olfactory rod cells, for example in detecting ciliary movement or ciliary-driven fluid flow, or a chemosensory role in detecting odorants, could aid olfactory perception in the larva. They may function similarly to microvillous cells that lack axons in the mammalian OE, and participate in volume release for local modulation of OSNs or non-sensory cells (Genovese and Tizzano, 2018), thereby acting as paraneurons (reviewed in Fujita, 1989). The activity of the *tubb* promoter in olfactory rod cells is consistent with this interpretation, as expression of neuronal tubulin has previously been detected in paraneurons (Iwanaga et al., 1982). Another possibility is that olfactory rod cells could correspond to brush or tuft cells in air-breathing mammals, which have important roles in immunity (Andres, 1975; reviewed in Reid et al., 2005; Howitt et al., 2016; reviewed in Schneider et al., 2019). These ideas remain to be tested.

Possible Origins of Olfactory Rod Cells

Our work does not address the developmental origin of olfactory rod cells, but it is of interest that they express a *sox10*-driven transgene, albeit in a mosaic fashion. *Sox10* mRNA is frequently described as a neural crest marker, but is also expressed strongly in otic epithelium (Dutton et al., 2001), a placodally derived tissue. The use of *sox10*-driven transgenic lines to identify neural crest derivatives remains controversial. Expression of a *sox10*:eGFP transgene together with photoconversion studies has led to the conclusion that a subpopulation of microvillous OSNs in the OE is derived from neural crest (Saxena et al., 2013), and use of an inducible *sox10*:*ER*^{T2}-*Cre* transgenic line has identified previously "contested" neural crest derivatives, including cells in the sensory barbels (Mongera et al., 2013). However, using lineage reconstruction through backtracking and photoconversion experiments, Aguillon et al. (2018) have argued that all olfactory neurons, including OSNs and gonadotropin-releasing hormone 3 (GnRH3) cells, are derived entirely from preplacodal progenitors. Given this controversy, we are unable to conclude whether olfactory rod cells are derived from the placode or neural crest.

The *Tg(sox10:Lifeact-mFRPruby)* line is expressed in a subset of both olfactory rod cells and of microvillous OSNs, with variation in the proportion of expressing cells between individuals. This could reflect true heterogeneity in the olfactory rod cell and microvillous OSN populations, or it could be a result of mosaic or leaky expression of the transgene. Mosaic expression is typical for many transgenes (Mosimann et al., 2013), while leaky expression, which can be explained through the lack of appropriate silencer elements (Jessen et al., 1999), is suspected for the *sox10* promoter fragment used in our transgenic construct (reviewed in Tang and Bronner, 2020). Nevertheless, the *Tg(sox10:Lifeact-mRFPruby)* line has proved a fortuitous tool for visualising olfactory rod cells in the live larva.

Concluding Remarks

A detailed understanding of the vertebrate olfactory system is important both from a cellular and developmental perspective and for its clinical relevance. Olfactory dysfunction can signify underlying cellular disorders and can also be implicated in neurodegenerative diseases (reviewed in Whitlock, 2015; Bergboer et al., 2018). OSNs project directly to the OB, and thus provide an entry route for pathogens to the brain (reviewed in Dando et al., 2014). Cells in the OE can themselves be damaged by viral infection, leading to a reduction, change, or loss of sense of smell (Brann et al., 2020; Gupta et al., 2020; Kraus et al., 2020). The identification of zebrafish olfactory rod cells, with their unique flexible actin-rich protrusion, offers new opportunities to explore the biology of these cells in a genetically tractable model organism, and thus to understand their contribution to the multimodal sensory functions of the vertebrate olfactory epithelium.

DATA AVAILABILITY STATEMENT

The raw data supporting the conclusions of the article will be made available at Figshare, doi: 10.6084/m9.figshare.13710100.

ETHICS STATEMENT

The animal study was reviewed and approved by ethics committees in Sheffield and Singapore. All zebrafish work in Sheffield was reviewed by the Project Applications and Amendments Committee of the Animal Welfare and Ethical Review Body (AWERB), and undertaken under licence from the UK Home Office, according to recommended

standard husbandry conditions (Aleström et al., 2019). All experiments in Singapore were performed under guidelines approved by the Institutional Animal Care and Use Committee of Biopolis (#181408).

AUTHOR CONTRIBUTIONS

KYC, TW, and SJ: designed the research, data analysis. KYC, SJ, TW, SB, NvH, MM, and CH: conducted the experiments. KYC and TW: writing (original draft). KYC, TW, and SJ, with additional contributions from SB, NvH, and CH: writing (review and editing). All authors contributed to the article and approved the submitted version.

FUNDING

KYC was funded by an A*STAR Research Attachment Programme Ph.D. studentship (ARAP-2019-01-0014). Research in Sheffield was supported by a BBSRC project grant (BB/S007008/1) to TW and SB. Imaging in Sheffield was carried out in the Sheffield Electron Microscopy Unit and Wolfson Light Microscopy Facility, with support from a BBSRC ALERT14 award (BB/M012522/1) to TW and SB for light-sheet microscopy. Work in the SJ lab was funded by a start-up grant from the Lee Kong Chian School of Medicine, Nanyang Technological University, Singapore.

ACKNOWLEDGMENTS

We thank Karen Camargo-Sosa and Robert Kelsh for providing fixed *sox10*$^{-/-}$ larvae. We thank Henry Roehl for making the p5E *-4725 sox10* promoter (originally from the Kelsh lab), *Lifeact-mRFPruby* construct (originally from the Wedlich-Söldner and Sixt labs), and Zeiss Axio Zoom.V16 microscope available to us, Ana Almeida Jones for help with imaging, Emily Glendenning for technical support, and members of the Whitfield lab for discussion. We are grateful to the Sheffield Aquarium Team for excellent fish care. We also thank Kathleen Cheow, Ruey-Kuang Cheng, Jason Lai, and Tim Saunders for assistance with fish in Singapore.

SUPPLEMENTARY MATERIAL

The Supplementary Material for this article can be found online at: https://www.frontiersin.org/articles/10.3389/fphys.2021.626080/full#supplementary-material

Supplementary Movie 1 | Olfactory rods are labelled in the olfactory epithelia of live zebrafish by the *Tg(actb2:Lifeact-RFP)* transgene. 3D rendering of a confocal image of a 4 dpf *Tg(actb2:Lifeact-RFP)*;*Tg(elavl3:H2B-GCaMPs)* double-transgenic larval olfactory pit; anterior to the top. Olfactory rods are labelled in magenta; neuronal nuclei are labelled in green.

Supplementary Movie 2 | Olfactory rods labelled with Lifeact-RFP in the olfactory epithelia of live zebrafish larvae oscillate. Fast-capture time series confocal imaging (5.98 frames per second, fps) of olfactory rods in a 6 dpf *Tg(actb2:Lifeact-RFP)* larva; anterior to the top, lateral to the left. Playback speed of the movie is 6 fps. Scale bar = 10 μm.

Supplementary Movie 3 | Olfactory rods labelled with Lifeact-mRFPruby in the olfactory epithelia of live zebrafish larvae oscillate. Fast-capture time series light-sheet imaging (50.04 fps) of a 5 dpf *Tg(sox10:Lifeact-mRFPruby)* larval olfactory pit; anterior to the top left, lateral to the top right. Beating olfactory cilia are visible in brightfield (grayscale), and oscillating olfactory rods are labelled by Lifeact-mRFPruby (magenta). Playback speed of the movie is 7 fps. Scale bar = 20 μm.

REFERENCES

Aguillon, R., Batut, J., Subramanian, A., Madelaine, R., Dufourcq, P., Schilling, T. F., et al. (2018). Cell-type heterogeneity in the early zebrafish olfactory epithelium is generated from progenitors within preplacodal ectoderm. *Elife* 7:e32041. doi: 10.7554/eLife.32041

Ahuja, G., Nia, S. B., Zapilko, V., Shiriagin, V., Kowatschew, D., Oka, Y., et al. (2014). Kappe neurons, a novel population of olfactory sensory neurons. *Sci. Rep.* 4:4037. doi: 10.1038/srep04037

Aleström, P., D'Angelo, L., Midtlyng, P. J., Schorderet, D. F., Schulte-Merker, S., Sohm, F., et al. (2019). Zebrafish: Housing and husbandry recommendations. *Lab. Anim.* 0, 1–12. doi: 10.1177/0023677219869037

Andres, K. H. (1975). Neue morphologische grundlagen zur physiologie des riechens und schmeckens. *Arch. Otorhinolaryngol.* 210, 1–41. doi: 10.1007/BF00453706

Axel, R. (1995). The molecular logic of smell. *Sci. Am.* 273, 154–159. doi: 10.1038/scientificamerican1095-154

Bannister, L. H. (1965). The fine structure of the olfactory surface of teleostean fishes. *Q. J. Microsc. Sci.* 106, 333–342.

Bannister, L. H. (1966). Is *Rhabdospora thelohani* (Laguesse) a sporozoan parasite or a tissue cell of lower vertebrates? *Parasitology* 56, 633–638. doi: 10.1017/S0031182000071651

Barr-Gillespie, P.-G. (2015). Assembly of hair bundles, an amazing problem for cell biology. *Mol. Biol. Cell* 26, 2727–2732. doi: 10.1091/mbc.E14-04-0940

Behrndt, M., Salbreux, G., Campinho, P., Hauschild, R., Oswald, F., Roensch, J., et al. (2012). Forces driving epithelial spreading in zebrafish gastrulation. *Science* 338, 257–260. doi: 10.1126/science.1224143

Bergboer, J. G. M., Wyatt, C., Austin-Tse, C., Yaksi, E., and Drummond, I. A. (2018). Assaying sensory ciliopathies using calcium biosensor expression in zebrafish ciliated olfactory neurons. *Cilia* 7:2. doi: 10.1186/s13630-018-0056-1

Bettini, S., Milani, L., Lazzari, M., Maurizii, M. G., and Franceschini, V. (2017). Crypt cell markers in the olfactory organ of *Poecilia reticulata*: analysis and comparison with the fish model *Danio rerio*. *Brain Struct. Funct.* 222, 3063–3074. doi: 10.1007/s00429-017-1386-2

Bibliowicz, J., Alié, A., Espinasa, L., Yoshizawa, M., Blin, M., Hinaux, H., et al. (2013). Differences in chemosensory response between eyed and eyeless *Astyanax mexicanus* of the Rio Subterráneo cave. *Evodevo* 4:25. doi: 10.1186/2041-9139-4-25

Biechl, D., Tietje, K., Gerlach, G., and Wullimann, M. F. (2016). Crypt cells are involved in kin recognition in larval zebrafish. *Sci. Rep.* 6:24590. doi: 10.1038/srep24590

Brann, D. H., Tsukahara, T., Weinreb, C., Lipovsek, M., Van den Berge, K., Gong, B., et al. (2020). Non-neuronal expression of SARS-CoV-2 entry genes in the olfactory system suggests mechanisms underlying COVID-19-associated anosmia. *Sci. Adv.* 6:eabc5801. doi: 10.1126/sciadv.abc5801

Breipohl, W., Bijvank, G. J., and Zippel, H. P. (1973). Rastermikroskopische untersuchungen der olfaktorischen rezeptoren im riechepithel des goldfisches (*Carassius auratus*). *Zeitschrift für Zellforsch. und Mikroskopische Anat.* 138, 439–454. doi: 10.1007/BF00307104

Brinkmann, A., and Schild, D. (2016). One special glomerulus in the olfactory bulb of *Xenopus laevis* tadpoles integrates a broad range of amino acids and mechanical stimuli. *J. Neurosci.* 36, 10978–10989. doi: 10.1523/JNEUROSCI.4631-15.2016

Byrd, C. A., and Brunjes, P. C. (1995). Organization of the olfactory system in the adult zebrafish: histological, immunohistochemical, and quantitative analysis. *J. Comp. Neurol.* 358, 247–259. doi: 10.1002/cne.903580207

Calvo-Ochoa, E., and Byrd-Jacobs, C. A. (2019). The olfactory system of zebrafish as a model for the study of neurotoxicity and injury: Implications for neuroplasticity and disease. *Int. J. Mol. Sci.* 20:1639. doi: 10.3390/ijms20071639

Carr, V. M., Farbman, A. I., Colletti, L. M., and Morgan, J. I. (1991). Identification of a new non-neuronal cell type in rat olfactory epithelium. *Neuroscience* 45, 433–449. doi: 10.1016/0306-4522(91)90239-K

Chia, J. S. M., Wall, E. S., Wee, C. L., Rowland, T. A. J., Cheng, R.-K., Cheow, K., et al. (2019). Bacteria evoke alarm behaviour in zebrafish. *Nat. Commun.* 10:3831. doi: 10.1038/s41467-019-11608-9

Dando, S. J., Mackay-Sim, A., Norton, R., Currie, B. J., St John, J. A., Ekberg, J. A. K., et al. (2014). Pathogens penetrating the central nervous system: Infection pathways and the cellular and molecular mechanisms of invasion. *Clin. Microbiol. Rev.* 27, 691–726. doi: 10.1128/CMR.00118-13.

Datta, N. C., and Bandopadhyay, S. K. (1997). Ultrastructure of cell types of the olfactory epithelium in a catfish, *Heteropneustes fossilis* (Bloch). *J. Biosci.* 22, 233–245. doi: 10.1007/BF02704736

Demirler, M. C., Sakizli, U., Bali, B., Kocagöz, Y., Eski, S. E., Ergönen, A., et al. (2019). Purinergic signalling selectively modulates maintenance but not repair neurogenesis in the zebrafish olfactory epithelium. *FEBS J.* 287, 2699–2722. doi: 10.1111/febs.15170

DePasquale, J. A. (2020). Tropomyosin and alpha-actinin in teleost rodlet cells. *Acta Zool.* 00, 1–10. doi: 10.1111/azo.12344

Desban, L., Prendergast, A., Roussel, J., Rosello, M., Geny, D., Wyart, C., et al. (2019). Regulation of the apical extension morphogenesis tunes the mechanosensory response of microvilliated neurons. *PLoS Biol.* 17:e3000235. doi: 10.1371/journal.pbio.3000235

Dezfuli, B. S., Capuano, S., Simoni, E., Previati, M., and Giari, L. (2007). Rodlet cells and the sensory systems in zebrafish (*Danio rerio*). *Anat. Rec.* 290, 367–374. doi: 10.1002/ar.20507

Djenoune, L., Khabou, H., Joubert, F., Quan, F. B., Figueiredo, S. N., Bodineau, L., et al. (2014). Investigation of spinal cerebrospinal fluid-contacting neurons expressing PKD2L1: evidence for a conserved system from fish to primates. *Front. Neuroanat.* 8:26. doi: 10.3389/fnana.2014.00026

Dummer, A., Poelma, C., DeRuiter, M. C., Goumans, M.-J. T. H., and Hierck, B. P. (2016). Measuring the primary cilium length: Improved method for unbiased high-throughput analysis. *Cilia* 5:7. doi: 10.1186/s13630-016-0028-2

Dunn, T. W., Mu, Y., Narayan, S., Randlett, O., Naumann, E. A., Yang, C.-T., et al. (2016). Brain-wide mapping of neural activity controlling zebrafish exploratory locomotion. *Elife* 5:e12741. doi: 10.7554/eLife.12741

Dutton, J. R., Antonellis, A., Carney, T. J., Rodrigues, F. S. L. M., Pavan, W. J., Ward, A., et al. (2008). An evolutionarily conserved intronic region controls the spatiotemporal expression of the transcription factor Sox10. *BMC Dev. Biol.* 8:105. doi: 10.1186/1471-213X-8-105

Dutton, K. A., Pauliny, A., Lopes, S. S., Elworthy, S., Carney, T. J., Rauch, J., et al. (2001). Zebrafish colourless encodes *sox10* and specifies non-ectomesenchymal neural crest fates. *Development* 128, 4113–4125.

Elsaesser, R., and Paysan, J. (2007). The sense of smell, its signalling pathways, and the dichotomy of cilia and microvilli in olfactory sensory cells. *BMC Neurosci.* 8:S1. doi: 10.1186/1471-2202-8-S3-S1

Esterberg, R., Hailey, D. W., Coffin, A. B., Raible, D. W., and Rubel, E. W. (2013). Disruption of intracellular calcium regulation is integral to aminoglycoside-induced hair cell death. *J. Neurosci.* 33, 7513–7525. doi: 10.1523/JNEUROSCI.4559-12.2013

Esterberg, R., Linbo, T., Pickett, S. B., Wu, P., Ou, H. C., Rubel, E. W., et al. (2016). Mitochondrial calcium uptake underlies ROS generation during aminoglycoside-induced hair cell death. *J. Clin. Invest.* 126, 3556–3566. doi: 10.1172/JCI84939

Finger, T. E., Böttger, B., Hansen, A., Anderson, K. T., Alimohammadi, H., and Silver, W. L. (2003). Solitary chemoreceptor cells in the nasal cavity serve as sentinels of respiration. *Proc. Natl. Acad. Sci. U. S. A.* 100, 8981–8986. doi: 10.1073/pnas.1531172100

Fujita, T. (1989). Present status of paraneuron concept. *Arch. Histol. Cytol.* 52, 1–8. doi: 10.1679/aohc.52.Suppl_1

Genovese, F., and Tizzano, M. (2018). Microvillous cells in the olfactory epithelium express elements of the solitary chemosensory cell transduction signaling cascade. *PLoS One* 13:e0202754. doi: 10.1371/journal.pone.0202754

Gillespie, P. G., and Müller, U. (2009). Mechanotransduction by hair cells: models, molecules, and mechanisms. *Cell* 139, 33–44. doi: 10.1016/j.cell.2009.09.010

Grosmaitre, X., Santarelli, L. C., Tan, J., Luo, M., and Ma, M. (2007). Dual functions of mammalian olfactory sensory neurons as odor detectors and mechanical sensors. *Nat. Neurosci.* 10, 348–354. doi: 10.1038/nn1856

Gupta, K., Mohanty, S. K., Mittal, A., Kalra, S., Kumar, S., Mishra, T., et al. (2020). The cellular basis of loss of smell in 2019-nCoV-infected individuals. *Brief. Bioinform.* 00, 1–9. doi: 10.1093/bib/bbaa168

Hansen, A. (2007). Olfactory and solitary chemosensory cells: two different chemosensory systems in the nasal cavity of the American alligator, *Alligator mississippiensis*. *BMC Neurosci.* 8:64. doi: 10.1186/1471-2202-8-64

Hansen, A., and Finger, T. E. (2008). Is TrpM5 a reliable marker for chemosensory cells? Multiple types of microvillous cells in the main olfactory epithelium of mice. *BMC Neurosci.* 9:115. doi: 10.1186/1471-2202-9-115

Hansen, A., and Zeiske, E. (1993). Development of the olfactory organ in the zebrafish, *Brachydanio rerio*. *J. Comp. Neurol.* 333, 289–300. doi: 10.1002/cne.903330213

Hansen, A., and Zeiske, E. (1998). The peripheral olfactory organ of the zebrafish, *Danio rerio*: and ultrastructural study. *Chem. Senses* 23, 39–48. doi: 10.1093/chemse/23.1.39

Hansen, A., and Zielinski, B. S. (2005). Diversity in the olfactory epithelium of bony fishes: Development, lamellar arrangement, sensory neuron cell types and transduction components. *J. Neurocytol.* 34, 183–208. doi: 10.1007/s11068-005-8353-1

Hansen, A., Reutter, K., and Zeiske, E. (2002). Taste bud development in the zebrafish, *Danio rerio*. *Dev. Dyn.* 223, 483–496. doi: 10.1002/dvdy.10074

Harris, J. A., Cheng, A. G., Cunningham, L. L., MacDonald, G., Raible, D. W., and Rubel, E. W. (2003). Neomycin-induced hair cell death and rapid regeneration in the lateral line of zebrafish (*Danio rerio*). *JARO* 4, 219–234. doi: 10.1007/s10162-002-3022-x

Heath, J., and Holifield, B. (1991). Actin alone in lamellipodia. *Nature* 352, 107–108. doi: 10.1038/352107a0

Hernádi, L. (1993). Fine structural characterization of the olfactory epithelium and its response to divalent cations Cd^{2+} in the fish *Alburnus alburnus* (Teleostei, Cyprinidae): a scanning and transmission electron microscopic study. *Neurobiology* 1, 11–31. doi: 10.2298/vetgl0302011f

Höfer, D., and Drenckhahn, D. (1999). Localisation of actin, villin, fimbrin, ezrin and ankyrin in rat taste receptor cells. *Histochem. Cell Biol.* 112, 79–86. doi: 10.1007/s004180050394

Howitt, M. R., Lavoie, S., Michaud, M., Blum, A. M., Tran, S. V., Weinstock, J. V., et al. (2016). Tuft cells, taste-chemosensory cells, orchestrate parasite type 2 immunity in the gut. *Science* 351, 1329–1333. doi: 10.1126/science.aaf1648

Ichikawa, M., and Ueda, K. (1977). Fine structure of the olfactory epithelium in the goldfish, *Carassius auratus*. *Cell Tissue Res.* 183, 445–455. doi: 10.1007/bf00225659

Inaba, Y., Chauhan, V., van Loon, A. P., Choudhury, L. S., and Sagasti, A. (2020). Keratins and plakin family cytolinker proteins control the length of epithelial microridge protrusions. *Elife* 9:e58149. doi: 10.7554/eLife.58149

Iwanaga, T., Fujita, T., and Ito, S. (1982). Immunohistochemical staining of enteroendocrine paraneurons with anti-brain tubulin antiserum. *Biomed. Res.* 3, 99–101. doi: 10.2220/biomedres.3.99

Iwata, R., Kiyonari, H., and Imai, T. (2017). Mechanosensory-based phase coding of odor identity in the olfactory bulb. *Neuron* 96, 1139–1152. doi: 10.1016/j.neuron.2017.11.008

Jessen, J. R., Willett, C. E., and Lin, S. (1999). Artificial chromosome transgenesis reveals long-distance negative regulation of *rag1* in zebrafish. *Nat. Genet.* 23, 15–16. doi: 10.1038/12609

Kawakami, K. (2007). *Tol2*: a versatile gene transfer vector in vertebrates. *Genome Biol.* 8:S7. doi: 10.1186/gb-2007-8-s1-s7

Kermen, F., Franco, L. M., Wyatt, C., and Yaksi, E. (2013). Neural circuits mediating olfactory-driven behavior in fish. *Front. Neural. Circuits* 7:62. doi: 10.3389/fncir.2013.00062

Kimmel, C. B., Ballard, W. W., Kimmel, S. R., Ullmann, B., and Schilling, T. F. (1995). Stages of embryonic development of the zebrafish. *Dev. Dyn.* 203, 253–310. doi: 10.1002/aja.1002030302

Kotrschal, K., Krautgartner, W.-D., and Hansen, A. (1997). Ontogeny of the solitary chemosensory cells in the zebrafish, *Danio Rerio*. *Chem. Senses* 22, 111–118. doi: 10.1093/chemse/22.2.111

Kraus, A., Casadei, E., Huertas, M., Ye, C., Bradfute, S., Boudinot, P., et al. (2020). A zebrafish model for COVID-19 recapitulates olfactory and cardiovascular pathophysiologies caused by SARS-CoV-2. *bioRxiv*. doi: 10.1101/2020.11.06.368191.

Krishnan, J., and Rohner, N. (2017). Cavefish and the basis for eye loss. *Philos. Trans. R. Soc. B Biol. Sci.* 372:20150487. doi: 10.1098/rstb.2015.0487

Kwan, K. M., Fujimoto, E., Grabher, C., Mangum, B. D., Hardy, M. E., Campbell, D. S., et al. (2007). The Tol2kit: A multisite gateway-based construction kit for *Tol2* transposon transgenesis constructs. *Dev. Dyn.* 236, 3088–3099. doi: 10.1002/dvdy.21343

Lin, W., Ezekwe, E. A. D. Jr., Zhao, Z., Liman, E. R., and Restrepo, D. (2008). TRPM5-expressing microvillous cells in the main olfactory epithelium. *BMC Neurosci.* 9:114. doi: 10.1186/1471-2202-9-114

Maier, E. C., Saxena, A., Alsina, B., Bronner, M. E., and Whitfield, T. T. (2014). Sensational placodes: Neurogenesis in the otic and olfactory systems. *Dev. Biol.* 389, 50–67. doi: 10.1016/j.ydbio.2014.01.023

Menco, B. P. M., and Jackson, J. E. (1997). Cells resembling hair cells in developing rat olfactory and nasal respiratory epithelia. *Tissue Cell* 29, 707–713. doi: 10.1016/S0040-8166(97)80046-8

Mongera, A., Singh, A. P., Levesque, M. P., Chen, Y. Y., Konstantinidis, P., and Nüsslein-Volhard, C. (2013). Genetic lineage labeling in zebrafish uncovers novel neural crest contributions to the head, including gill pillar cells. *Development* 140, 916–925. doi: 10.1242/dev.091066

Moran, D. T., Rowley, J. C. III., Aiken, G. R., and Jafek, B. W. (1992). Ultrastructural neurobiology of the olfactory mucosa of the brown trout, *Salmo trutta*. *Microsc. Res. Tech.* 23, 28–48. doi: 10.1002/jemt.1070230104

Morrison, C. M., and Odense, P. H. (1978). Distribution and morphology of the rodlet cell in fish. *J. Fish. Board Can.* 35, 101–116. doi: 10.1139/f78-014

Mosimann, C., Puller, A.-C., Lawson, K. L., Tschopp, P., Amsterdam, A., and Zon, L. I. (2013). Site-directed zebrafish transgenesis into single landing sites with the phiC31 integrase system. *Dev. Dyn.* 242, 949–963. doi: 10.1002/dvdy.23989

Muller, J. F., and Marc, R. E. (1984). Three distinct morphological classes of receptors in fish olfactory organs. *J. Comp. Neurol.* 222, 482–495. doi: 10.1002/cne.902220403

Nüsslein-Volhard, C., and Dahm, R. (2002). *Zebrafish: A Practical Approach*. Oxford: Oxford University Press.

Olivares, J., and Schmachtenberg, O. (2019). An update on anatomy and function of the teleost olfactory system. *PeerJ.* 7:e7808. doi: 10.7717/peerj.7808

Parisi, V., Guerrera, M. C., Abbate, F., Garcia-Suarez, O., Viña, E., Vega, J. A., et al. (2014). Immunohistochemical characterization of the crypt neurons in the olfactory epithelium of adult zebrafish. *Ann. Anat.* 196, 178–182. doi: 10.1016/j.aanat.2014.01.004

Pickett, S. B., Thomas, E. D., Sebe, J. Y., Linbo, T., Esterberg, R., Hailey, D. W., et al. (2018). Cumulative mitochondrial activity correlates with ototoxin susceptibility in zebrafish mechanosensory hair cells. *Elife* 7:e38062. doi: 10.7554/eLife.38062

Pinto, C. S., Khandekar, A., Bhavna, R., Kiesel, P., Pigino, G., and Sonawane, M. (2019). Microridges are apical epithelial projections formed of F-actin networks that organize the glycan layer. *Sci. Rep.* 9:12191. doi: 10.1038/s41598-019-48400-0

Ramírez-Weber, F.-A., and Kornberg, T. B. (1999). Cytonemes : cellular processes that project to the principal signaling center in *Drosophila* imaginal discs. *Cell* 97, 599–607. doi: 10.1016/S0092-8674(00)80771-0

Reid, L., Meyrick, B., Antony, V. B., Chang, L. Y., Crapo, J. D., and Reynolds, H. Y. (2005). The mysterious pulmonary brush cell: A cell in search of a function. *Am. J. Respir. Crit. Care Med.* 172, 136–139. doi: 10.1164/rccm.200502-203WS

Reiten, I., Uslu, F. E., Fore, S., Pelgrims, R., Ringers, C., Diaz Verdugo, C., et al. (2017). Motile-cilia-mediated flow improves sensitivity and temporal resolution of olfactory computations. *Curr. Biol.* 27, 166–174. doi: 10.1016/j.cub.2016.11.036

Rhein, L. D., Cagan, R. H., Orkand, P. M., and Dolack, M. K. (1981). Surface specializations of the olfactory epithelium of rainbow trout, *Salmo gairdneri*. *Tissue Cell* 13, 577–587. doi: 10.1016/0040-8166(81)90028-8

Riedl, J., Crevenna, A. H., Kessenbrock, K., Yu, J. H., Neukirchen, D., Bista, M., et al. (2008). Lifeact: a versatile marker to visualise F-actin. *Nat. Methods* 5, 605–607. doi: 10.1038/nmeth.1220.Lifeact

Rodrigues, F. S. L. M., Doughton, G., Yang, B., and Kelsh, R. N. (2012). A novel transgenic line using the Cre-lox system to allow permanent lineage-labeling of the zebrafish neural crest. *Genesis* 50, 750–757. doi: 10.1002/dvg.22033

Sato, Y., Miyasaka, N., and Yoshihara, Y. (2005). Mutually exclusive glomerular innervation by two distinct types of olfactory sensory neurons revealed in transgenic zebrafish. *J. Neurosci.* 25, 4889–4897. doi: 10.1523/JNEUROSCI.0679-05.2005

Saxena, A., Peng, B. N., and Bronner, M. E. (2013). Sox10-dependent neural crest origin of olfactory microvillous neurons in zebrafish. *Elife* 2:e00336. doi: 10.7554/eLife.00336

Schindelin, J., Arganda-Carreras, I., Frise, E., Kaynig, V., Longair, M., Pietzsch, T., et al. (2012). Fiji: An open-source platform for biological-image analysis. *Nat. Methods* 9, 676–682. doi: 10.1038/nmeth.2019

Schmid, B., Schindelin, J., Cardona, A., Longair, M., and Heisenberg, M. (2010). A high-level 3D visualization API for Java and ImageJ. *BMC Bioinform.* 11:274. doi: 10.1186/1471-2105-11-274

Schneider, C., O'Leary, C. E., and Locksley, R. M. (2019). Regulation of immune responses by tuft cells. *Nat. Rev. Immunol.* 19, 584–593. doi: 10.1038/s41577-019-0176-x

Schulte, E. (1972). Untersuchungen an der regio olfactoria des aals, *Anguilla anguilla* L. *Zeitschrift für Zellforsch. und Mikroskopische Anat.* 125, 210–228. doi: 10.1007/BF00306790

Sekerková, G., Zheng, L., Loomis, P. A., Changyaleket, B., Whitlon, D. S., Mugnaini, E., et al. (2004). Espins are multifunctional actin cytoskeletal regulatory proteins in the microvilli of chemosensory and mechanosensory cells. *J. Neurosci.* 24, 5445–5456. doi: 10.1523/JNEUROSCI.1279-04.2004

Sepahi, A., Kraus, A., Casadei, E., Johnston, C. A., Galindo-Villegas, J., Kelly, C., et al. (2019). Olfactory sensory neurons mediate ultrarapid antiviral immune responses in a TrkA-dependent manner. *Proc. Natl. Acad. Sci. U. S. A.* 116, 12428–12436. doi: 10.1073/pnas.1900083116

Sola, C., Giulianini, P. G., and Ferrero, E. A. (1993). Ultrastructural characterization of the olfactory organ in glass eels, *Anguilla anguilla* (Osteichthyes, Anguilliformes). *Ital. J. Zool.* 60, 253–261. doi: 10.1080/11250009309355820

Tang, W., and Bronner, M. E. (2020). Neural crest lineage analysis: from past to future trajectory. *Development* 147:dev193193. doi: 10.1242/dev.193193

Theriot, J. A., and Mitchison, T. J. (1991). Actin microfilament dynamics in locomoting cells. *Nature* 352, 126–131. doi: 10.1038/352126a0

Tilney, L. G., Derosier, D. J., and Mulroy, M. J. (1980). The organization of actin filaments in the stereocilia of cochlear hair cells. *J. Cell Biol.* 86, 244–259. doi: 10.1083/jcb.86.1.244

Tsujikawa, M., and Malicki, J. (2004). Intraflagellar transport genes are essential for differentiation and survival of vertebrate sensory neurons. *Neuron* 42, 703–716. doi: 10.1016/S0896-6273(04)00268-5

Wakisaka, N., Miyasaka, N., Koide, T., Masuda, M., Hiraki-Kajiyama, T., and Yoshihara, Y. (2017). An adenosine receptor for olfaction in fish. *Curr. Biol.* 27, 1437–1447. doi: 10.1016/j.cub.2017.04.014

Waryani, B., Zhao, Y., Zhang, C., Abbasi, A. R., Ferrando, S., Dai, R., et al. (2015). Surface architecture of the olfactory epithelium of two Chinese cave loaches (Cypriniformes: Nemacheilidae: *Oreonectes*). *Ital. J. Zool.* 82, 179–185.

Waryani, B., Zhao, Y., Zhang, C., Dai, R., and Abbasi, A. R. (2013). Anatomical studies of the olfactory epithelium of two cave fishes *Sinocyclocheilus jii* and *S. furcodorsalis* (Cypriniformes: Cyprinidae) from China. *Pak. J. Zool.* 45, 1091–1101. doi: 10.1080/11250003.2015.1018851

Whitlock, K. E. (2015). The loss of scents: Do defects in olfactory sensory neuron development underlie human disease? *Birth Defects Res. Part C Embryo Today Rev.* 105, 114–125. doi: 10.1002/bdrc.21094

Whitlock, K. E., and Westerfield, M. (2000). The olfactory placodes of the zebrafish form by convergence of cellular fields at the edge of the neural plate. *Development* 127, 3645–3653.

Xiao, T., Roeser, T., Staub, W., and Baier, H. (2005). A GFP-based genetic screen reveals mutations that disrupt the architecture of the zebrafish retinotectal projection. *Development* 132, 2955–2967. doi: 10.1242/dev.01861

Yamamoto, M., and Ueda, K. (1978). Comparative morphology of fish olfactory epithelium - IV. *Bull. Jap. Soc. Sci. Fish.* 44, 1207–1212. doi: 10.2331/suisan.44.1207

Zachar, P. C., and Jonz, M. G. (2012). Confocal imaging of Merkel-like basal cells in the taste buds of zebrafish. *Acta Histochem.* 114, 101–115. doi: 10.1016/j.acthis.2011.03.006

Zhang, X.-Y., Huang, Z.-Q., Ning, T., Xiang, X.-H., Li, C.-Q., Chen, S.-Y., et al. (2018). Microscopic and submicroscopic gradient variation of olfactory systems among six *Sinocyclocheilus* species living in different environments. *Zool. Soc. Japan* 35, 411–420. doi: 10.2108/zs170126

Conflict of Interest: The authors declare that the research was conducted in the absence of any commercial or financial relationships that could be construed as a potential conflict of interest.

frontiers in Physiology

PERSPECTIVE
published: 01 March 2021
doi: 10.3389/fphys.2021.634440

The Cranial Neural Crest in a Multiomics Era

Vanessa Chong-Morrison† *and Tatjana Sauka-Spengler**

Radcliffe Department of Medicine, Weatherall Institute of Molecular Medicine, University of Oxford, Oxford, United Kingdom

Neural crest ontogeny plays a prominent role in craniofacial development. In this Perspective article, we discuss recent advances to the understanding of mechanisms underlying the cranial neural crest gene regulatory network (cNC-GRN) stemming from *omics*-based studies. We briefly summarize how parallel considerations of transcriptome, interactome, and epigenome data significantly elaborated the roles of key players derived from pre-*omics* era studies. Furthermore, the growing cohort of cNC multiomics data revealed contribution of the non-coding genomic landscape. As technological improvements are constantly being developed, we reflect on key questions we are poised to address by taking advantage of the unique perspective a multiomics approach has to offer.

Keywords: neural crest, multiomics, gene regulatory network, non-coding, interactome, transcriptome, epigenome

OPEN ACCESS

Edited by:
Jean-Pierre Saint-Jeannet, New York University, United States

Reviewed by:
Anne H. Monsoro-Burq, Université Paris-Sud, France
Lukas Sommer, University of Zurich, Switzerland

****Correspondence:***
Tatjana Sauka-Spengler
tatjana.sauka-spengler@imm.ox.ac.uk

†Present address:
Vanessa Chong-Morrison, Division of Biosciences, Cell and Developmental Biology, Faculty of Life Sciences, University College London, London, United Kingdom

Specialty section:
This article was submitted to Developmental Physiology, a section of the journal Frontiers in Physiology

Received: *27 November 2020*
Accepted: *08 February 2021*
Published: *01 March 2021*

Citation:
Chong-Morrison V and Sauka-Spengler T (2021) The Cranial Neural Crest in a Multiomics Era. Front. Physiol. 12:634440. doi: 10.3389/fphys.2021.634440

1. INTRODUCTION

Gene regulatory networks (GRNs) coordinate the expression of genes encoding transcription factors (TFs), cell signaling pathway components and differentiation effectors in genetic cascades mediated by *cis*-regulatory elements (Levine and Davidson, 2005). GRNs present a unique perspective in the understanding of developmental pathways and mechanisms by focusing on the regulated activity of genes within a defined cellular context. The lengthy process of neural crest (NC) development, that starts at the end of gastrulation and proceeds into late organogenesis has been proposed to be orchestrated by a multi-module GRN (Sauka-Spengler and Bronner-Fraser, 2008; Simões-Costa and Bronner, 2015). Broadly-speaking, Wnt, Fgf, and Bmp signals at the neural plate border activate expression of genes from the *Msx*, *Pax*, and *Zic* families during NC induction (Ikeya et al., 1997; LaBonne and Bronner-Fraser, 1998; Monsoro-Burq et al., 2003, 2005; Lewis et al., 2004; Schumacher et al., 2011). Pax3 and Zic1 activate expression of *bona fide* NC factors, such as *Snai1* and *FoxD3*, thus driving the onset of NC specification defined by the expression of *Tfap2*, *Id*, *Myc*, *Myb*, *SoxE*, and *Ets* gene family members (Luo et al., 2003; Sato et al., 2005; Hong and Saint-Jeannet, 2007; Sauka-Spengler et al., 2007; Milet et al., 2013; Schock and LaBonne, 2020). The persisting expression of these TFs, as well as the downstream activation of cadherins, integrins, signaling receptors and metalloproteases, subsequently lead to epithelial-to-mesenchymal transition (EMT) and delamination of NC cells from the dorsal neural tube. Cranial NC (cNC) cells migrate via canonical, well-established pathways to their final destinations within the vertebrate embryo's head. Unlike the cNC that can give rise to ectomesenchymal derivatives (forming the cartilage, bones, and connective tissues of the craniofacial skeleton), non-cranial, more posterior NC (vagal, trunk, sacral) form mostly neuronal derivatives such as the sensory neurons and glia in the dorsal root ganglia, sympathetic ganglia and enteric nervous system. Although cranial and trunk NC express similar groups of early marker genes, some distinct TFs (e.g., *Sox8*, *Tfap2β*, *Ets1*) driving cranial vs. trunk NC identity have been described

(Simoes-Costa and Bronner, 2016). Recent work suggested that elaborate NC-GRN was progressively established during the evolution of vertebrates with trunk-like circuits being in place first (Martik et al., 2019). However, detailed analysis and understanding of the trunk NC-GRN remains to be done.

The dawn of the *-omics* era has contributed significantly to the elaboration and refinement of existing GRNs. Coupled with an increasing catalog of sequenced genomes, genome-wide approaches heralded an explosion of exploratory studies that not only recapitulated previous knowledge but also increased the rate of identification of novel developmental players. In the avian NC, RNA-seq identified multiple genes not known previously to be expressed in the migratory cNC such as *Lmo4*, *RxrG*, *Ltk*, and *Col9a3* (Simões-Costa et al., 2014). Furthermore, work to compare the transcriptomes of trunk and cNC populations coupled with subsequent functional assays led to identification of a cranial-specific module in the migratory cNC consisting of Brn3c, Lhx5, Dmbx1 in the neural plate border; Sox8, Tfap2β in premigratory NC; and Ets1 (activated by Tfap2β) (Simoes-Costa and Bronner, 2016). Overexpression of these factors in the trunk NC resulted in reprogramming of their identity, highlighted by the ectopic activity of a cNC-specific enhancer SOX10E2 (Betancur et al., 2010) and increased expression of chondrocyte-related genes *Runx2* and *Alx1*. Importantly, gene modules are not limited to the "gross" distinction between trunk vs. cNC, as key differences in the molecular signature between cNC cells from different axial-levels could also be detected using RNA-seq (Lumb et al., 2017). Altogether, these studies exemplify the amenability of the cNC-GRN to be interrogated via an *-omics*-type approach for the desired outcome of identifying gene modules specific to subpopulations within the cNC.

Such efforts to resolve spatiotemporal dynamics of the cNC-GRN were further strengthened by emerging single cell technologies. Single cell RNA-seq (scRNA-seq) of 406 cNC cells isolated from the avian embryo identified a fraction of invasive front cells (Trailblazers) with a distinct molecular signature that persisted through migration, therefore bringing to light subpopulations within one cell type with seemingly similar cell behavior (Morrison et al., 2017). Strikingly, scRNA-seq analysis of 1345 murine cNC cells detected a subtle but observable discrete cell state where cNC cells displayed a bias toward neuronal vs. mesenchymal fate during delamination from the neural tube (Soldatov et al., 2019). This finding refined and elaborated the long-held model of sequential (induction, specification, delamination, differentiation) developmental events underlying the cNC-GRN and demonstrated the fluid nature of cNC ontogeny at the transcriptional level. Pertinently, scRNA-seq addressed a constantly debated question within the field concerning hetero- or homogeneity of premigratory NC cells. Investigation of transcriptional heterogeneity of premigratory NC cells *in vivo* using scRNA-seq of FAC-sorted *foxd3*-positive cNC cells from 5 to 6 ss zebrafish embryos (Lukoseviciute et al., 2018) failed to identify multiple specific NC subpopulations but singled-out a small cluster of NC cells which expressed low levels of factors key to NC specification—*zic2b*, *tfap2a*, *sox10*, *twist1b*, *ets1*, *pax3a*, including *foxd3*. These cells expressed high levels of stem-cell state ("stemness") factors such as *snai1a*, *vent*, *vox*, and *cx43.4*, suggesting that they may represent non-specified cNC progenitors maintained in premigratory cNC. This finding echoes an observation made by machine learning-based image analysis that clustered cNC cells based on expression of a selected panel of genes (including pluripotency and NC markers) within similar-staged avian embryos (Lignell et al., 2017).

From a GRN perspective, scRNA-seq called into question the existence of one unifying NC-GRN or multiple NC-GRNs working in concert with each other to drive NC development. Previous iterations of the NC-GRN were largely based on candidate gene approach studies, thus representing a summation of parts averaged across the NC as a whole. ScRNA-seq dissected this "unified" NC-GRN model into their parts, by revealing subpopulations with distinct molecular signatures (even if they were pre-enriched for cNC) hinting at "multiple" NC-GRNs. In particular, comprehensive analysis of NC enhancer modules in the cranial region suggested that NC gene regulatory circuits controlling neuronal derivatives are established much earlier in the embryo and use non-exclusive *cis*-regulatory elements shared with neural programmes. In contrast, regulatory circuits underlying mesenchymal/canonical NC gene expression are laid down later when neural tissue is already defined. These later circuits use an intermediary cohort of enhancers active exclusively in the NC (Williams et al., 2019). Such dichotomy in regulatory element modules and NC circuits was also uncovered in the vagal NC giving rise to the enteric nervous system. The neuronal derivative programme was pleiotropic, whereas the GRN underlying neural/glial/mesenchymal derivatives was newly established and utilized by NC cells only (Ling and Sauka-Spengler, 2019).

Methodologically, "first-generation" scRNA-seq studies prior to Williams et al. (2019) utilized FAC-sorting followed by sequencing of full-length mRNA transcripts on a relatively small number of single cells, an approach that although robust, was also laborious and limited in statistical power for sensitive clustering of subpopulations of cells. Nonetheless, they played an important role in priming the NC field for droplet-based technologies allowing a significantly higher number of cells (by the thousands, not hundreds) to be profiled at any one time, therefore bypassing this limitation. The powerful use of the latter approach was also demonstrated in the proto-vertebrate *Ciona intestinalis*, where the resolution achieved enabled identification of an ancestral *Six*, *Msx*, and *Pax* regulatory module shared between cranial placodes and NC in vertebrates (Horie et al., 2018).

2. *CIS*-REGULATORY ELEMENTS UNIFY NC GENE MODULES

Positive *cis*-regulatory elements, also known as enhancers, serve as important "switches" within GRN modules by integrating inputs/binding of upstream factors in order to coordinate output/expression of downstream targets. SOX10E1 and SOX10E2 enhancers, situated 1 kb downstream of the coding region for NC master regulator *Sox10* (Kelsh, 2006; Sauka-Spengler and Bronner-Fraser, 2008; Schock and LaBonne, 2020) have been shown to control the expression of *Sox10* in the chicken

embryo (Betancur et al., 2010). Both enhancers demonstrated distinct spatiotemporal activity, where SOX10E2 alone was active in early delaminating cNC cells. Mutations at key binding motifs identified in SOX10E2, knockdown of upstream TFs and chromatin immunoprecipitation (ChIP) experiments confirmed Sox9, Ets1, and cMyb proteins as transcriptional inputs for endogenous *Sox10* gene expression. Similarly, two enhancers, NC1 and NC2, located 20 and 44 kb upstream of the NC specifier *FoxD3* have been shown to control *FoxD3* gene expression in the avian embryo (Simões-Costa et al., 2012). NC1 (but not NC2) was found to be active in the premigratory cNC, but its activity diminished during migration and no activity could be detected caudal to rhombomere 3. Knockdown of upstream factors such as *Pax7*, *Msx1*, *Ets1*, and *Zic1* confirmed their participation in the *FoxD3* module underlying gene regulation between trunk and cNC—Ets1 demonstrated cranial-specific control of NC1, Zic1 controlled vagal- and trunk-specific activity of NC2, while Pax7 and Msx1 inputs where shared between NC1 and NC2. Altogether, these case studies presented clear evidence for the role of enhancers in maintaining spatiotemporal expression of developmentally-regulated cNC genes. They spearheaded higher throughput genome-wide characterization of the global cNC landscape using approaches such as ChIP-seq (Barski et al., 2007) and ATAC-seq (Buenrostro et al., 2013) to profile large cohorts of NC enhancers both in the embryo and *in vitro*.

It has been shown that developmental enhancers display specific histone signatures, such as H3K27ac and H3K4me1, indicative of their active vs. poised chromatin states (Creyghton et al., 2010). Furthermore, several studies have demonstrated that chromatin remodelers and their associated histone marks are regulated during NC development (reviewed by Strobl-Mazzulla et al., 2012). Large-scale epigenomic mapping using p300, H3K27Ac, H3K4me1, and H3K4me3 enrichment profiles successfully facilitated the identification of enhancer elements in human cNC cell culture, uncovering the association of a key NC specifier, TFAP2A, with permissive chromatin landscape at putative NC enhancers (Rada-Iglesias et al., 2012). This coupling between epigenetic modulation of enhancers and function was further strengthened by studies in mouse embryonic stem cells (mESC) elucidating the mechanism by which another NC specifier, FOXD3, acted to decommission enhancers via recruitment of specific chromatin remodelers (Krishnakumar et al., 2016; Respuela et al., 2016). *In vivo*, epigenome profiling of subpopulations of mouse cNC cells exposed the differences in chromatin signature reflective of their positional identity (Minoux et al., 2017).

3. MULTIOMICS AND REBUILDING THE CNC-GRN

The cNC-GRN has benefited from the substantial body of *in vivo* data, occasionally complemented by *in vitro* studies, from numerous labs over the past few decades. Pre-*omics*, a glaring knowledge gap persisted as experimental limitations lacked detail on the extent of the inter-connectivity between gene modules. Taking full advantage of the multiomics revolution and the demonstration of its utility in proof-of-principle characterization of early human embryos (Li et al., 2018), a multiomics approach was employed in multiple model organisms to re-examine the cNC-GRN. These studies sought to parse substantial biological information obtained from multiple levels: the NC genome (regions of open chromatin), transcriptome (RNA transcripts, including nascent transcripts), epigenome (chromatin modifications, chromatin-looping), and interactome (protein-DNA or protein-protein interactions) into workable hypotheses to test novel mechanisms, gene modules and players (**Figure 1**). For instance, *omics* interrogation of chromatin accessibility and looping during cNC development, in combination with transcriptional dynamics analyzed at both population and single-cell level in chick revealed a rich tapestry of gene modules. This not only provided insight into subcircuits underlying cNC heterogeneity (with identification of some novel inputs) but also enabled reverse engineering of gene regulatory circuits for every gene expressed, thus facilitating reconstruction of the global NC-GRN with unrivaled resolution (Williams et al., 2019). Combined with gold standard molecular techniques in the embryo such as enhancer screens and knockout experiments (Hockman et al., 2019; Ling and Sauka-Spengler, 2019; Williams et al., 2019), the collective result yielded as powerful resources with the potential to not only recapitulate previous work but also significantly expand on them. Ultimately, these studies accelerate progress for the myriad of biological questions-of-interest within the NC research community with far-reaching implications in biology, evolution, health and disease. Here, we briefly highlight recent findings in cNC-GRN biology resulting from multiomics.

3.1. Molecular Mechanism of cNC Pioneer Factors

FOXD3 transcription factor is an important player in the NC-GRN (Lister et al., 2006; Montero-Balaguer et al., 2006; Stewart et al., 2006; Wang et al., 2011c) with evidence in embryonic stem cells documenting its possible cellular function as both a repressor and activator (Pohl and Knöchel, 2001; Yaklichkin et al., 2007; Krishnakumar et al., 2016; Respuela et al., 2016). A transgenic zebrafish line where the *foxd3* locus has been disrupted with a Citrine or mCherry fluorophore (Hochgreb-Hägele and Bronner, 2013) was used to characterize FoxD3 bimodal properties within its native context in a developing embryo. By performing genetic crosses between *foxd3*-mCherry and *foxd3*-Citrine heterozygote parents, *foxd3*-Citrine heterozygote and *foxd3*-mCherry/Citrine homozygote knockout NC cells were isolated by FACS for downstream multiomics analysis. Using a combination of RNA-seq, ATAC-seq and H3K27ac ChIP-seq, the NC transcriptome and epigenomic landscape were characterized across four embryonic stages key to cNC development within the context of the foxd3-DNA binding landscape (Lukoseviciute et al., 2018). Foxd3 was shown to prime NC gene expression in early pre-migratory cNC by binding to its target enhancers. Conversely, later in cNC development, it represses active enhancers associated with mesenchymal/neuronal genes in line with previous *in vitro* data (Krishnakumar et al., 2016; Respuela et al., 2016). In short, using multiomics to characterize the

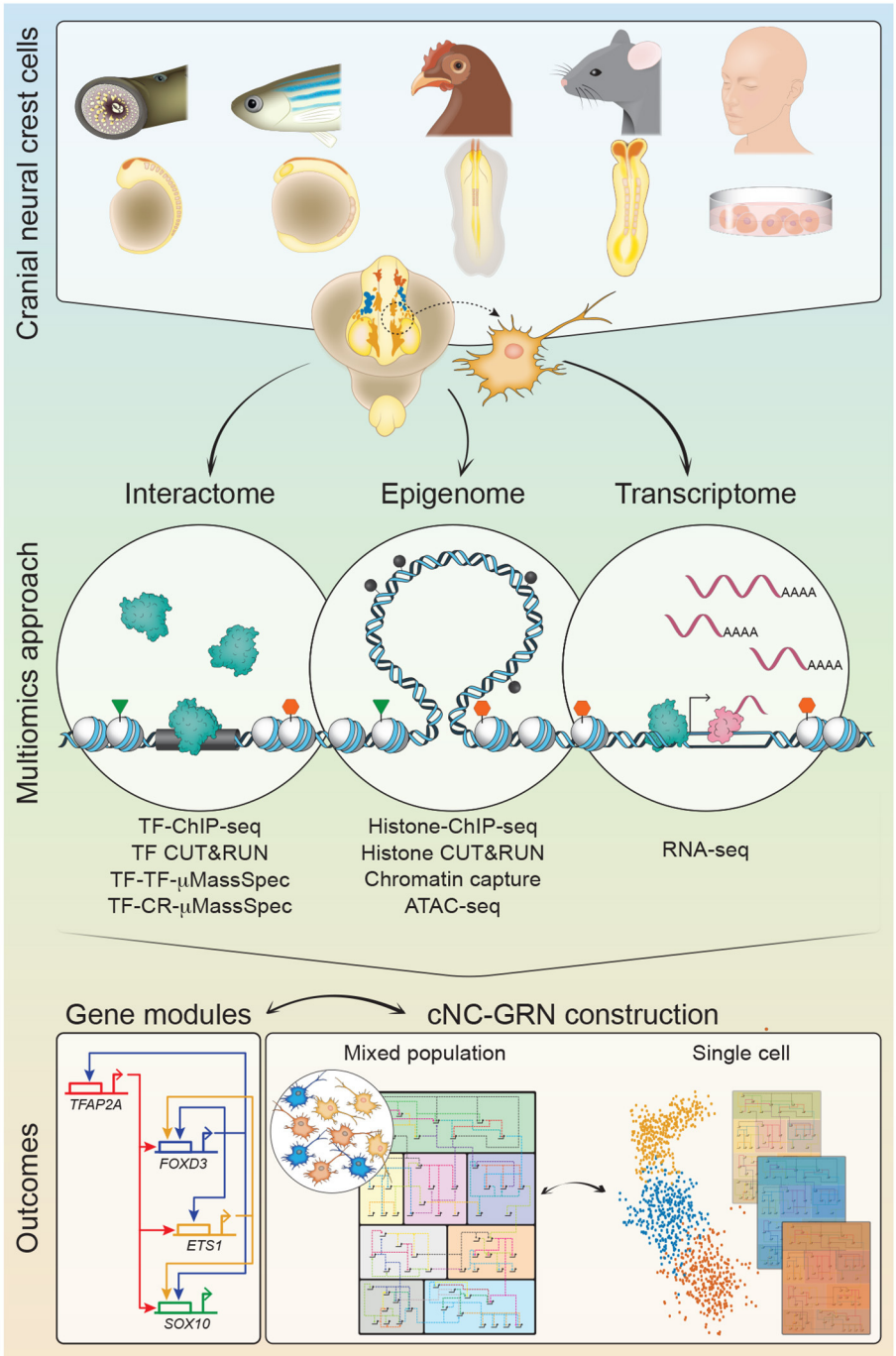

FIGURE 1 | A multiomics approach for construction of the cranial neural crest gene regulatory network (cNC-GRN). CNCCs from *in vivo* non-human embryo models and human pluripotent stem cell differentiation *in vitro* model were subjected to multiomics interrogation for global-level information. Interactome analyses resolve TF interactions to the genome (TF-ChIP-seq, TF CUT&RUN), other TFs (TF-TF-μMassSpec), or CRs (TF-CR-μMassSpec). Epigenome analyses reveal enhancers and promoters defined by regions of accessible chromatin (ATAC-seq) and/or specific histone modifications (Histone-ChIP-seq, Histone CUT&RUN). CUT&RUN is an alternative method to ChIP-seq that has its utility demonstrated in the chick embryo NC (Skene and Henikoff, 2017; Rothstein and Simoes-Costa, 2020). Direct epigenomic relationships between promoters and enhancers are obtained by profiling their physical proximity (Chromatin capture). Transcriptome analysis provides snapshot of expressed genes. Parsing of all the datasets results in substantial number of gene modules to elaborate on the cNC-GRN, especially if coupled with single cell technologies for subpopulation resolution. CNCC, cranial neural crest cell; TF, transcription factor; CR, chromatin remodeler; μMassSpec, micro mass spectrophotometry.

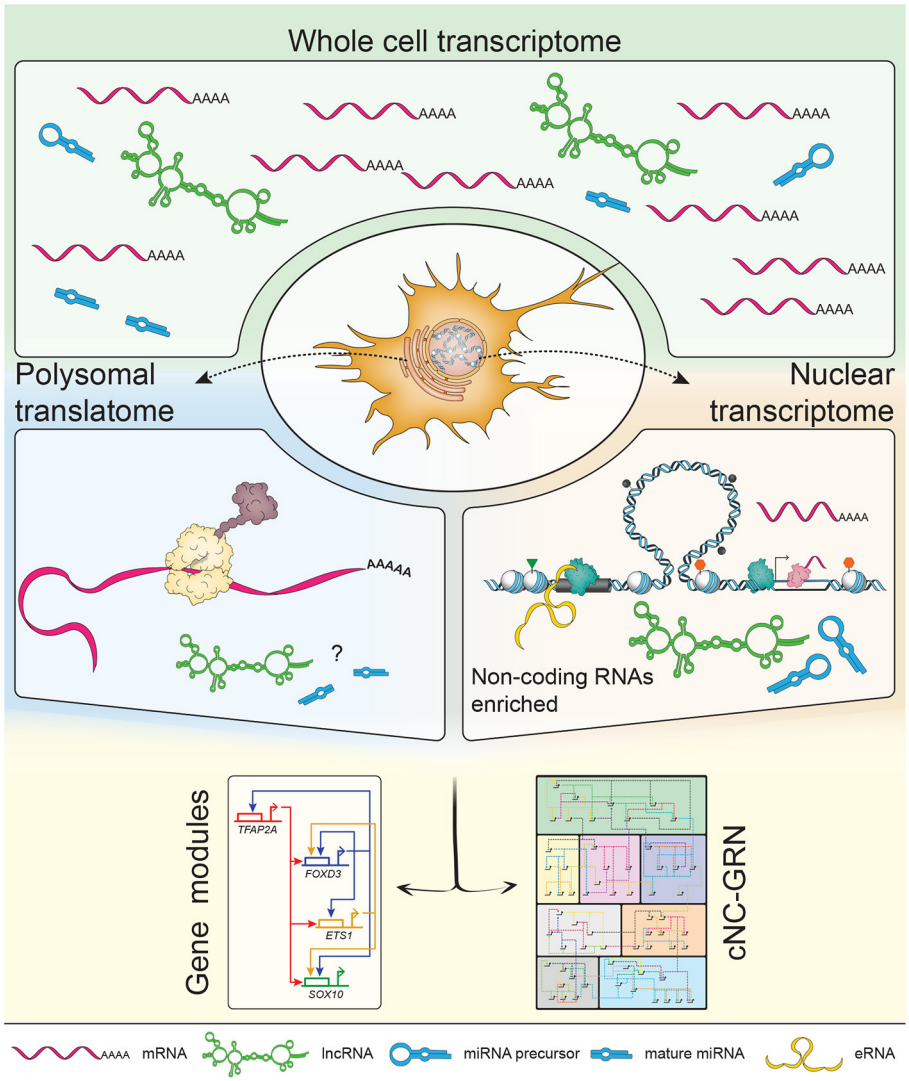

FIGURE 2 | Subcellular profiling increases resolution of the non-coding landscape. The transcriptome consists of a mixed population of protein-coding and non-coding RNAs, including but not limited to enhancer RNAs (eRNAs), long non-coding RNAs (lncRNAs) and microRNAs (miRNAs). Previous transcriptomic studies on populations of neural crest (NC) cells focused on polyadenylated mRNAs constituting mostly of protein-coding mRNAs. NC-specific subcellular profiling achieved by *in vivo* biotinylation of nuclei and ribosomes (i.e., polysomes) enables enrichment of RNA species subtypes already present in the whole cell transcriptome. The nuclear transcriptome provided higher definition of non-coding RNAs while the polysomal translatome minimized the "noise" of non-coding RNAs to inform on proteins being made (suggestive of dominant biological processes occurring at that stage). In depth exploration of non-coding RNAs' putative roles within the context of the cNC-GRN is currently underexplored but well-suited to the advantages provided by multiomics.

foxd3-GRN *in vivo* across cNC developmental stages revealed the transition between gene modules as *foxd3* shifted toward its canonical repressive activity after NC specification. This can be achieved by switching binding partners, a phenomenon that has been observed with another NC pioneer factor TFAP2A as it imposes its function in NC induction and specification modules by dimerising with TFAP2C or TFAP2B, respectively (Rothstein and Simoes-Costa, 2020).

3.2. Vertebrate Evolution

From an evolutionary perspective, NC enhancers are a distinct group of components within the cNC-GRN that are molded under evolutionary pressure leading to species divergence of craniofacial structures (Prescott et al., 2015). Due to their heavy contribution to the patterning of vertebrate craniofacial structures (reviewed in Santagati and Rijli, 2003), the cNC is of particular interest as a key contributor to the evolution of jawed vertebrates (Cerny et al., 2010). This is supported by candidate-based approach evidence in lamprey, a basal vertebrate, highlighting functional interactions between main components of the GRN underlying NC ontogeny (Sauka-Spengler et al., 2007; Nikitina et al., 2008). Genome-wide studies in the lamprey were initially inhibited due to programmed large-scale genome loss during embryonic development (Smith et al.,

2009), hampering acquisition of meaningful *omics* information despite the clear benefit for a more genome-wide approach as demonstrated in the basal chordate amphioxus (Yu et al., 2008). Publication of the lamprey germline genome (Smith et al., 2018) was a significant step forward in this regard and presented renewed opportunities to dissect the lamprey cNC-GRN using multiomics. By examining the transcriptional profiles of dorsal neural tube tissue containing the cNC, modules that were both previously known in other vertebrates and unique to the lamprey were identified (Hockman et al., 2019). Concurrently, another study highlighted the resemblance of lamprey cNC to amniote trunk NC (Martik et al., 2019). Nevertheless, by additionally analyzing ATAC-seq profiles in dorsal neural tube tissue, novel *cis*-regulatory elements for two lamprey NC-GRN players—*Tfap2B* and *SoxE1* were discovered. Strikingly, the lamprey SoxE1 enhancer was shown to be active in cNC-derived craniofacial features following integration into the zebrafish genome as well as in the amniote model, highlighting the potential for deep conservation of TF/enhancer interaction of NC-GRN enhancers (Hockman et al., 2019).

4. FUTURE DIRECTIONS

4.1. Non-coding RNAs Provide an Additional Facet to the cNC-GRN

RNAs derived from enhancers (enhancer RNAs or eRNAs) emerged following a study describing developmentally-regulated enhancers in mouse cortical neurons (Kim et al., 2010). Further studies demonstrated the sensitivity of eRNA induction as a hallmark of cellular response to biological stimuli (Wang et al., 2011a; Lam et al., 2013; Li et al., 2013), and suggested that eRNA transcription can be correlated to regulation of chromatin looping (Melo et al., 2013; Hsieh et al., 2014). While these *in vitro* studies painted an early picture of eRNA expression and their potential function in regulating enhancer-mediated gene expression, mechanistic details surrounding these observations remained elusive. Later studies attempted to address this conundrum by focusing on eRNA crosstalk with the chromatin landscape (Kaikkonen et al., 2013; Mousavi et al., 2013), eRNA potential function as molecular partners during gene regulation (Schaukowitch et al., 2014; Sigova et al., 2015), as well as attempted to distinguish between functionality of eRNA transcription or their RNA transcripts (Paralkar et al., 2016). Several recent studies have further shed light on eRNA transcription as a global indicator of activated gene expression programmes. Interrogation of the nuclear transcriptome of migrating cNC cells in zebrafish embryos detected bidirectional transcription at a global scale. This "feature" enabled clustering of putative enhancers that were also functionally associated with known NC genes (Trinh et al., 2017), in line with a previous report that suggested eRNA profiles were more indicative of enhancer activity compared to H3K27Ac ChIP-seq profiles (Zhu et al., 2013). A study by the FANTOM consortium further showed that genome-wide eRNA transcription appeared to be temporally regulated, often preceding transcription of associated protein-coding genes (Arner et al., 2015). In short, regardless of the biological function of eRNAs during development, their phenomenon in itself is able to highlight active regions of the non-coding genome. Therefore, characterization of eRNA transcriptomes has strong potential to inform on genome regulation mechanisms underlying the cNC-GRN.

Another class of under-explored non-coding RNA in development are long non-coding RNAs (lncRNAs). Landmark findings describing lncRNAs in the HOX locus, HOTAIR and HOTTIP, served as important case studies of modern lncRNA biology (Rinn et al., 2007; Tsai et al., 2010; Wang et al., 2011b). HOTAIR silenced gene expression at promoter regions of the HOXD locus by interacting with the chromatin remodeler Polycomb Repressive Complex 2 (PRC2) to facilitate H3K4 demethylation. Similar to the molecular mechanism of HOTAIR, HOTTIP from the HOXA locus was shown to recruit WDR5/MLL complexes and drive H3K4 trimethylation to activate gene transcription. Hence, coupling between lncRNA function and epigenetic regulation serves as a useful framework to address the roles of lncRNAs in GRNs underlying developmental programmes. It is also important to note that lncRNAs are not a completely novel discovery, as their presence at loci of imprinted genes were reported in the past. More recently, mechanisms of these "classical" lncRNAs were studied in detail. The "lncRNA-mediated chromatin regulation" model presented by HOTAIR and HOTTIP were echoed in studies involving *Airn*, *H19*, and *Xist* (Engreitz et al., 2013; Monnier et al., 2013; Santoro et al., 2013). Last but not least, RNA species from another class of non-coding RNA—microRNAs (miRNAs)—were also found to play roles in NC development with several candidates identified thus far (reviewed in Weiner, 2018). LncRNA and miRNA activities are not mutually exclusive and crosstalk between the two classes have been documented (Zheng et al., 2014; Tan et al., 2015). Altogether, the contribution of the non-coding genome serves as another exciting facet to development and evolution of the cNC-GRN—an uncharted territory ripe for exploration in the multiomics era.

4.2. Compartmentalizing NC Molecular Identity

Genome-wide profiling of polyadenylated transcripts from whole cell lysates provides a comprehensive snapshot of NC-GRN players being expressed at developmental stages-of-interest. Profiling polyadenylated transcripts alone, however, directly excludes non-polyadenylated RNAs enriched in the nucleus which form a large proportion of non-coding RNAs from intergenic regions (Carninci et al., 2005). This limitation can be addressed by subcellular profiling and rRNA-depletion during the construction of sequencing libraries. Isolating polysomes using recently-developed TRAP method (Heiman et al., 2014) and their associated mRNAs in the zebrafish migratory NC at 16–18 ss informed us of both known and novel NC markers forming the translatome at this developmental window (Chong, 2017). Enrichment of *elavl3* suggested that at least a subset of these cells (i.e., actively migrating cNC and premigratory trunk NC) were actively differentiating into their neuronal derivatives. On the other hand, by isolating nuclei transcriptomes at the

same developmental stage, we demonstrated that functional annotation of transcribed enhancers (eRNAs) and promoters reflected the molecular signature of migratory NC cells and derivatives (Trinh et al., 2017); however the corresponding genes were not being translated as yet. Thus, similar to chromatin accessibility profiles which pre-defined cellular identities of cranial and vagal NC prior to associated gene expression (Ling and Sauka-Spengler, 2019; Williams et al., 2019), eRNA profiles also preceded coding gene transcription, thus reflecting future steps in NC ontogeny. Taken together, the translatome data provides a clearer picture without the "noise" from cytoplasmic or nuclear transcripts and suggested that at a given time-point, specification and/or differentiation of neuronal derivatives seem to dominate over ectodermal, mesodermal, and neuroepithelial derivatives (depleted in the translatome). These findings also highlight the utility of technologies to genetically attain subcellular resolution using *in vivo* biotinylation (de Boer et al., 2003; Deal and Henikoff, 2010; Trinh et al., 2018) with sufficient clarity to elucidate the role of non-coding RNAs in the cNC-GRN (**Figure 2**).

The contrast between the two pictures painted from nuclei and polysomes of NC cells at the same developmental stage raised important questions relating to our interpretation of how development proceeds at the cellular level. Traditionally, cellular identity has perhaps been defined over-simplistically via the expression of all protein markers in a GRN. We are now in the position to expand this definition by not only taking into account what *protein(s)* and where *within the organism* these players are involved, but also what *non-coding element(s)* are responsible for gene activation and where *within a cell* these new players are exerting their functions. Integrating this information is a next complex task on the agenda and is non-trivial given that NC cells transition from being a stem cell-like population to many subpopulations committed to different, not necessarily binary fates. It is therefore crucial to perform and integrate multiplex genetic lineage tracing analyses into this picture, interpret multiomics data at single cell and with subcellular resolution, as well as develop new, non-biased functional genomics integration tools based on artificial intelligence and deep learning approaches.

5. DISCUSSION

Embryology has progressed in leaps and bounds leading to the modern incarnation of developmental biology as we know it today. From embryological techniques to advances in genome biology, our understanding of animal development has reached impressive heights. Here, at the forefront of modern developmental genetics and genomics, we propose using a combination of "traditional" and "modern" methods to deepen our understanding of genetic programmes underlying cNC development encoded within the genome.

The cNC is a multipotent population of cells key to vertebrate evolution. It is a versatile system for interrogation, as the genetic machinery underlying its biology reiterates throughout development and disease. This well-oiled system is also sensitive to fine-tuned regulation; disrupt a cog and development fails to proceed normally leading to neurocristopathies that account for roughly 1/3 of all birth defects. In order to discover ways to prevent or treat them, we first need to fully understand what the baseline scenarios are, at the level of genes within the context of a highly dynamic genome.

Tackling the non-coding genome has also uncovered non-coding RNA molecules that form part of the genetic regulation underlying cellular function. Previous work by many research groups has highlighted lncRNAs as molecular scaffolds that shuttle proteins to their target regions to regulate gene expression. eRNAs not only serve as "indicators" of when gene transcription onsets, but also have been proposed to facilitate chromosome-looping between enhancers and the promoters they regulate. Coupled with advances in gene editing including CRISPR/Cas, we are now in the position to design experiments with flexibility, efficiency and precision, from genome-wide screens of non-coding elements (Liu et al., 2016; Sanjana et al., 2016; Zhu et al., 2016) to *in vivo* decommissioning of NC enhancers for functional investigation (Williams et al., 2019).

In conclusion, we hope to not only propose fresh perspectives and potential avenues of investigation into the cNC-GRN but also challenge the reader to revisit how we study developmental biology as a whole. We are now ushering a new generation of scientists willing to embrace the exponential growth of molecular and computational tools at their disposal—the future is bright.

DATA AVAILABILITY STATEMENT

The original contributions presented in the study are included in the article/supplementary material, further inquiries can be directed to the corresponding author/s.

AUTHOR CONTRIBUTIONS

VC-M and TS-S contributed to the writing and editing of the manuscript. Both authors contributed to the article and approved the submitted version.

FUNDING

VC-M was funded by a Clarendon Fund doctorate scholarship. TS-S was funded by a Wellcome Trust Senior Research Fellowship (215615/Z/19/Z).

ACKNOWLEDGMENTS

In memory of José Luis Gómez-Skarmeta (1966–2020), a champion of multiomics, pioneering our efforts to understand genome regulation in development and evolution. We thank Véronique Juvin of SciArtWork for graphic design of the figures.

REFERENCES

Arner, E., Daub, C. O., Vitting-Seerup, K., and Andersson, R. (2015). Transcribed enhancers lead waves of coordinated transcription in transitioning mammalian cells. *Science* 347, 1010–1015. doi: 10.1126/science.1259418

Barski, A., Cuddapah, S., Cui, K., Roh, T. Y., Schones, D. E., Wang, Z., et al. (2007). High-resolution profiling of histone methylations in the human genome. *Cell* 129, 823–837. doi: 10.1016/j.cell.2007.05.009

Betancur, P., Bronner-Fraser, M., and Sauka-Spengler, T. (2010). Genomic code for Sox10 activation reveals a key regulatory enhancer for cranial neural crest. *Proc. Natl. Acad. Sci. U.S.A.* 107, 3570–3575. doi: 10.1073/pnas.0906596107

Buenrostro, J. D., Giresi, P. G., Zaba, L. C., Chang, H. Y., and Greenleaf, W. J. (2013). Transposition of native chromatin for fast and sensitive epigenomic profiling of open chromatin, DNA-binding proteins and nucleosome position. *Nat. Methods* 10, 1213–1218. doi: 10.1038/nmeth.2688

Carninci, P., Kasukawa, T., Katayama, S., Gough, J., Frith, M. C., Maeda, N., et al. (2005). The transcriptional landscape of the mammalian genome. *Science* 309, 1559–1563. doi: 10.1126/science.1112014

Cerny, R., Cattell, M., Sauka-Spengler, T., Bronner-Fraser, M., Yu, F., and Medeiros, D. M. (2010). Evidence for the prepattern/cooption model of vertebrate jaw evolution. *Proc. Natl. Acad. Sci. U.S.A.* 107, 17262–17267. doi: 10.1073/pnas.1009304107

Chong, V. (2017). *Biotagging, a genetically encoded toolkit in the zebrafish, reveals novel non-coding RNA players during neural crest and myocardium development* (Ph.D. thesis). University of Oxford, Oxford, United Kingdom.

Creyghton, M. P., Cheng, A. W., Welstead, G. G., Kooistra, T., Carey, B. W., Steine, E. J., et al. (2010). Histone H3K27ac separates active from poised enhancers and predicts developmental state. *Proc. Natl. Acad. Sci. U.S.A.* 107, 21931–21936. doi: 10.1073/pnas.1016071107

de Boer, E., Rodriguez, P., Bonte, E., Krijgsveld, J., Katsantoni, E., Heck, A., et al. (2003). Efficient biotinylation and single-step purification of tagged transcription factors in mammalian cells and transgenic mice. *Proc. Natl. Acad. Sci. U.S.A.* 100, 7480–7485. doi: 10.1073/pnas.1332608100

Deal, R. B., and Henikoff, S. (2010). A simple method for gene expression and chromatin profiling of individual cell types within a tissue. *Dev. Cell* 18, 1030–1040. doi: 10.1016/j.devcel.2010.05.013

Engreitz, J. M., Pandya-Jones, A., McDonel, P., Shishkin, A., Sirokman, K., Surka, C., et al. (2013). The Xist lncRNA exploits three-dimensional genome architecture to spread across the X chromosome. *Science* 341:1237973. doi: 10.1126/science.1237973

Heiman, M., Kulicke, R., Fenster, R. J., Greengard, P., and Heintz, N. (2014). Cell type-specific mRNA purification by translating ribosome affinity purification (TRAP). *Nat. Protoc.* 9, 1282–1291. doi: 10.1038/nprot.2014.085

Hochgreb-Hägele, T., and Bronner, M. E. (2013). A novel FoxD3 gene trap line reveals neural crest precursor movement and a role for FoxD3 in their specification. *Dev. Biol.* 374, 1–11. doi: 10.1016/j.ydbio.2012.11.035

Hockman, D., Chong-Morrison, V., Green, S. A., Gavriouchkina, D., Candido-Ferreira, I., Ling, I. T., et al. (2019). A genome-wide assessment of the ancestral neural crest gene regulatory network. *Nat. Commun.* 10:4689. doi: 10.1038/s41467-019-12687-4

Hong, C.-S., and Saint-Jeannet, J.-P. (2007). The activity of Pax3 and Zic1 regulates three distinct cell fates at the neural plate border. *Mol. Biol. Cell* 18, 2192–2202. doi: 10.1091/mbc.e06-11-1047

Horie, R., Hazbun, A., Chen, K., Cao, C., Levine, M., and Horie, T. (2018). Shared evolutionary origin of vertebrate neural crest and cranial placodes. *Nature* 560, 228–232. doi: 10.1038/s41586-018-0385-7

Hsieh, C.-L., Fei, T., Chen, Y., Li, T., Gao, Y., Wang, X., et al. (2014). Enhancer RNAs participate in androgen receptor-driven looping that selectively enhances gene activation. *Proc. Natl. Acad. Sci. U.S.A.* 111, 7319–7324. doi: 10.1073/pnas.1324151111

Ikeya, M., Lee, S. M. K., Johnson, J. E., McMahon, A. P., and Takada, S. (1997). Wnt signalling required for expansion of neural crest and CNS progenitors. *Nature* 389:6654. doi: 10.1038/40146

Kaikkonen, M. U., Spann, N. J., Heinz, S., Romanoski, C. E., Allison, K., a., et al. (2013). Remodeling of the enhancer landscape during macrophage activation is coupled to enhancer transcription. *Mol. Cell* 51, 310–325. doi: 10.1016/j.molcel.2013.07.010

Kelsh, R. N. (2006). Sorting out Sox10 functions in neural crest development. *Bioessays* 28, 788–798. doi: 10.1002/bies.20445

Kim, T.-K., Hemberg, M., Gray, J. M., Costa, A. M., Bear, D. M., Wu, J., et al. (2010). Widespread transcription at neuronal activity-regulated enhancers. *Nature* 465, 182–187. doi: 10.1038/nature09033

Krishnakumar, R., Chen, A. F., Pantovich, M. G., Danial, M., Parchem, R. J., Labosky, P. A., et al. (2016). FOXD3 regulates pluripotent stem cell potential by simultaneously initiating and repressing enhancer activity. *Cell Stem Cell* 18, 104–117. doi: 10.1016/j.stem.2015.10.003

LaBonne, C., and Bronner-Fraser, M. (1998). Neural crest induction in xenopus: evidence for a two-signal model. *Development* 125, 2403–2414.

Lam, M. T. Y., Cho, H., Lesch, H. P., Gosselin, D., Heinz, S., Tanaka-Oishi, Y., et al. (2013). Rev-Erbs repress macrophage gene expression by inhibiting enhancer-directed transcription. *Nature* 498, 511–515. doi: 10.1038/nature12209

Levine, M., and Davidson, E. H. (2005). Gene regulatory networks for development. *Proc. Natl. Acad. Sci. U.S.A.* 102, 4936–4942. doi: 10.1073/pnas.0408031102

Lewis, J. L., Bonner, J., Modrell, M., Ragland, J., Moon, R., Dorsky, R., et al. (2004). Reiterated Wnt signaling during zebrafish neural crest development. *Development* 131, 1299–1308. doi: 10.1242/dev.01007

Li, L., Guo, F., Gao, Y., Ren, Y., Yuan, P., Yan, L., et al. (2018). Single-cell multi-omics sequencing of human early embryos. *Nat. Cell Biol.* 20, 847–858. doi: 10.1038/s41556-018-0123-2

Li, W., Notani, D., Ma, Q., Tanasa, B., Nunez, E., Chen, A. Y., et al. (2013). Functional roles of enhancer RNAs for oestrogen-dependent transcriptional activation. *Nature* 498, 516–520. doi: 10.1038/nature12210

Lignell, A., Kerosuo, L., Streichan, S. J., Cai, L., and Bronner, M. E. (2017). Identification of a neural crest stem cell niche by Spatial Genomic Analysis. *Nat. Commun.* 8:1830. doi: 10.1038/s41467-017-01561-w

Ling, I. T., and Sauka-Spengler, T. (2019). Early chromatin shaping predetermines multipotent vagal neural crest into neural, neuronal and mesenchymal lineages. *Nat. Cell Biol.* 21, 1504–1517. doi: 10.1038/s41556-019-0428-9

Lister, J. A., Cooper, C., Nguyen, K., Modrell, M., Grant, K., and Raible, D. W. (2006). Zebrafish Foxd3 is required for development of a subset of neural crest derivatives. *Dev. Biol.* 290, 92–104. doi: 10.1016/j.ydbio.2005.11.014

Liu, S. J., Liu, S. J., Horlbeck, M. A., Cho, S. W., Birk, H. S., Malatesta, M., et al. (2016). CRISPRi-based genome-scale identification of functional long noncoding RNA loci in human cells. *Science* 355:aah7111. doi: 10.1126/science.aah7111

Lukoseviciute, M., Gavriouchkina, D., Williams, R. M., Hochgreb-Hagele, T., Senanayake, U., Chong-Morrison, V., et al. (2018). From pioneer to repressor: bimodal foxd3 activity dynamically remodels neural crest regulatory landscape *in vivo*. *Dev. Cell* 47, 608–628. doi: 10.1016/j.devcel.2018.11.009

Lumb, R., Buckberry, S., Secker, G., Lawrence, D., and Schwarz, Q. (2017). Transcriptome profiling reveals expression signatures of cranial neural crest cells arising from different axial levels. *BMC Dev. Biol.* 17:5. doi: 10.1186/s12861-017-0147-z

Luo, T., Lee, Y.-H., Saint-Jeannet, J.-P., and Sargent, T. D. (2003). Induction of neural crest in Xenopus by transcription factor AP2. *Proc. Natl. Acad. Sci. U.S.A.* 100, 532–537. doi: 10.1073/pnas.0237226100

Martik, M. L., Gandhi, S., Uy, B. R., Gillis, J. A., Green, S. A., Simoes-Costa, M., et al. (2019). Evolution of the new head by gradual acquisition of neural crest regulatory circuits. *Nature* 574, 675–678. doi: 10.1038/s41586-019-1691-4

Melo, C. A., Drost, J., Wijchers, P. J., van de Werken, H., de Wit, E., Vrielink, J., et al. (2013). ERNAs are required for p53-dependent enhancer activity and gene transcription. *Mol. Cell* 49, 524–535. doi: 10.1016/j.molcel.2012.11.021

Milet, C., Maczkowiak, F., Roche, D. D., and Monsoro-Burq, A. H. (2013). Pax3 and Zic1 drive induction and differentiation of multipotent, migratory, and functional neural crest in Xenopus embryos. *Proc. Natl. Acad. Sci. U.S.A.* 110, 5528–5533. doi: 10.1073/pnas.1219124110

Minoux, M., Holwerda, S., Vitobello, A., Kitazawa, T., Kohler, H., Stadler, M. B., et al. (2017). Gene bivalency at Polycomb domains regulates cranial neural crest positional identity. *Science* 355:6332. doi: 10.1126/science.aal2913

Monnier, P., Martinet, C., Pontis, J., Stancheva, I., Ait-Si-Ali, S., and Dandolo, L. (2013). H19 lncRNA controls gene expression of the Imprinted Gene Network by recruiting MBD1. *Proc. Natl. Acad. Sci. U.S.A.* 110, 20693–20698. doi: 10.1073/pnas.1310201110

Monsoro-Burq, A.-H., Fletcher, R., and Harland, R. (2003). Neural crest induction by paraxial mesoderm in Xenopus embryos requires FGF signals. *Development* 130, 3111–3124. doi: 10.1242/dev.00531

Monsoro-Burq, A.-H., Wang, E., and Harland, R. (2005). Msx1 and Pax3 cooperate to mediate FGF8 and WNT signals during Xenopus neural crest induction. *Dev. Cell* 8, 167–178. doi: 10.1016/j.devcel.2004.12.017

Montero-Balaguer, M., Lang, M. R., Sachdev, S. W., Knappmeyer, C., Stewart, R. A., De La Guardia, A., et al. (2006). The mother superior mutation ablates foxd3 activity in neural crest progenitor cells and depletes neural crest derivatives in zebrafish. *Dev. Dyn*. 235, 3199–3212. doi: 10.1002/dvdy.20959

Morrison, J. A., Mclennan, R., Wolfe, L. A., Gogol, M. M., Meier, S., McKinney, M. C., et al. (2017). Single-cell transcriptome analysis of avian neural crest migration reveals signatures of invasion and molecular transitions. *eLife* 6:e28415. doi: 10.7554/eLife.28415

Mousavi, K., Zare, H., Dell'Orso, S., Grontved, L., Gutierrez-Cruz, G., Derfoul, A., et al. (2013). ERNAs promote transcription by establishing chromatin accessibility at defined genomic loci. *Mol. Cell* 51, 606–617. doi: 10.1016/j.molcel.2013.07.022

Nikitina, N., Sauka-Spengler, T., and Bronner-Fraser, M. (2008). Dissecting early regulatory relationships in the lamprey neural crest gene network. *Proc. Natl. Acad. Sci. U.S.A*. 105, 20083–20088. doi: 10.1073/pnas.0806009105

Paralkar, V. R., Taborda, C. C., Huang, P., Yao, Y., Kossenkov, A. V., Prasad, R., et al. (2016). Unlinking an lncRNA from its associated cis element. *Mol. Cell* 62, 104–110. doi: 10.1016/j.molcel.2016.02.029

Pohl, B. S., and Knöchel, W. (2001). Overexpression of the transcriptional repressor FoxD3 prevents neural crest formation in Xenopus embryos. *Mech. Dev*. 103, 93–106. doi: 10.1016/S0925-4773(01)00334-3

Prescott, S. L., Srinivasan, R., Marchetto, M. C., Grishina, I., Narvaiza, I., Selleri, L., et al. (2015). Enhancer divergence and cis-regulatory evolution in the human and chimp neural crest. *Cell* 163, 68–84. doi: 10.1016/j.cell.2015.08.036

Rada-Iglesias, A., Bajpai, R., Prescott, S., Brugmann, S. A., Swigut, T., and Wysocka, J. (2012). Epigenomic annotation of enhancers predicts transcriptional regulators of human neural crest. *Cell Stem Cell* 11, 633–648. doi: 10.1016/j.stem.2012.07.006

Respuela, P., Nikolić, M., Tan, M., Frommolt, P., Zhao, Y., Wysocka, J., et al. (2016). Foxd3 promotes exit from naive pluripotency through enhancer decommissioning and inhibits germline specification. *Cell Stem Cell* 18, 118–133. doi: 10.1016/j.stem.2015.09.010

Rinn, J. L., Kertesz, M., Wang, J. K., Squazzo, S. L., Xu, X., Brugmann, S., et al. (2007). Functional demarcation of active and silent chromatin domains in human HOX loci by noncoding RNAs. *Cell* 129, 1311–1323. doi: 10.1016/j.cell.2007.05.022

Rothstein, M., and Simoes-Costa, M. (2020). Heterodimerization of TFAP2 pioneer factors drives epigenomic remodeling during neural crest specification. *Genome Res*. 30, 35–48. doi: 10.1101/gr.249680.119

Sanjana, N., Wright, J., Zheng, K., Shalem, O., Fontanillas, P., Joung, J., et al. (2016). High-resolution interrogation of functional elements in the noncoding genome. *Science* 353, 1545–1549. doi: 10.1126/science.aaf7613

Santagati, F., and Rijli, F. M. (2003). Cranial neural crest and the building of the vertebrate head. *Nat. Rev. Neurosci*. 4, 806–818. doi: 10.1038/nrn1221

Santoro, F., Mayer, D., Klement, R. M., Warczok, K. E., Stukalov, A., Barlow, D. P., et al. (2013). Imprinted Igf2r silencing depends on continuous Airn lncRNA expression and is not restricted to a developmental window. *Development* 140, 1184–1195. doi: 10.1242/dev.088849

Sato, T., Sasai, N., and Sasai, Y. (2005). Neural crest determination by co-activation of Pax3 and Zic1 genes in Xenopus ectoderm. *Development* 132, 2355–2363. doi: 10.1242/dev.01823

Sauka-Spengler, T., and Bronner-Fraser, M. (2008). A gene regulatory network orchestrates neural crest formation. *Nat. Rev. Mol. Cell Biol*. 9, 557–568. doi: 10.1038/nrm2428

Sauka-Spengler, T., Meulemans, D., Jones, M., and Bronner-Fraser, M. (2007). Ancient evolutionary origin of the neural crest gene regulatory network. *Dev. Cell* 13, 405–420. doi: 10.1016/j.devcel.2007.08.005

Schaukowitch, K., Joo, J.-Y., Liu, X., Watts, J. K., Martinez, C., and Kim, T.-K. (2014). Enhancer RNA facilitates NELF release from immediate early genes. *Mol. Cell* 56, 29–42. doi: 10.1016/j.molcel.2014.08.023

Schock, E. N., and LaBonne, C. (2020). Sorting sox: diverse roles for sox transcription factors during neural crest and craniofacial development. *Front. Physiol*. 11:1564. doi: 10.3389/fphys.2020.606889

Schumacher, J. A., Hashiguchi, M., Nguyen, V. H., and Mullins, M. C. (2011). An intermediate level of BMP signaling directly specifies cranial neural crest progenitor cells in zebrafish. *PLoS ONE* 6:e27403. doi: 10.1371/journal.pone.0027403

Sigova, A., Abraham, B., Ji, X., Molinie, B., Hannett, N., Guo, Y. E., et al. (2015). Transcription factor trapping by RNA in gene regulatory elements. *Science* 350, 978–982. doi: 10.1126/science.aad3346

Simões-Costa, M., and Bronner, M. E. (2015). Establishing neural crest identity: a gene regulatory recipe. *Development* 142, 242–257. doi: 10.1242/dev.105445

Simoes-Costa, M., and Bronner, M. E. (2016). Reprogramming of avian neural crest axial identity and cell fate. *Science* 352, 1570–1573. doi: 10.1126/science.aaf2729

Simões-Costa, M., Tan-Cabugao, J., Antoshechkin, I., Sauka-Spengler, T., and Bronner, M. E. (2014). Transcriptome analysis reveals novel players in the cranial neural crest gene regulatory network. *Genome Res*. 24, 281–290. doi: 10.1101/gr.161182.113

Simões-Costa, M. S., McKeown, S. J., Tan-Cabugao, J., Sauka-Spengler, T., and Bronner, M. E. (2012). Dynamic and differential regulation of stem cell factor FoxD3 in the neural crest is encrypted in the genome. *PLoS Genet*. 8:e1003142. doi: 10.1371/journal.pgen.1003142

Skene, P. J., and Henikoff, S. (2017). An efficient targeted nuclease strategy for high-resolution mapping of DNA binding sites. *eLife* 6:e21856. doi: 10.7554/eLife.21856

Smith, J. J., Antonacci, F., Eichler, E. E., and Amemiya, C. T. (2009). Programmed loss of millions of base pairs from a vertebrate genome. *Proc. Natl. Acad. Sci. U.S.A*. 106, 11212–11217. doi: 10.1073/pnas.0902358106

Smith, J. J., Timoshevskaya, N., Ye, C., Holt, C., Keinath, M. C., Parker, H. J., et al. (2018). The sea lamprey germline genome provides insights into programmed genome rearrangement and vertebrate evolution. *Nat. Genet*. 50, 270–277. doi: 10.1038/s41588-017-0036-1

Soldatov, R., Kaucka, M., Kastriti, M. E., Petersen, J., Chontorotzea, T., Englmaier, L., et al. (2019). Spatiotemporal structure of cell fate decisions in murine neural crest. *Science* 364:6444. doi: 10.1126/science.aas9536

Stewart, R. A., Arduini, B. L., Berghmans, S., George, R. E., Kanki, J. P., Henion, P. D., et al. (2006). Zebrafish foxd3 is selectively required for neural crest specification, migration and survival. *Dev. Biol*. 292, 174–188. doi: 10.1016/j.ydbio.2005.12.035

Strobl-Mazzulla, P. H., Marini, M., and Buzzi, A. (2012). Epigenetic landscape and miRNA involvement during neural crest development. *Dev. Dyn*. 241, 1849–1856. doi: 10.1002/dvdy.23868

Tan, J. Y., Sirey, T., Honti, F., Graham, B., Piovesan, A., Merkenschlager, M., et al. (2015). Extensive microRNA-mediated crosstalk between lncRNAs and mRNAs in mouse embryonic stem cells. *Genome Res*. 25, 655–666. doi: 10.1101/gr.181974.114

Trinh, L. A., Chong-Morrison, V., Gavriouchkina, D., Hochgreb-Hägele, T., Senanayake, U., Fraser, S. E., et al. (2017). Biotagging of specific cell populations in zebrafish reveals gene regulatory logic encoded in the nuclear transcriptome. *Cell Rep*. 19, 425–440. doi: 10.1016/j.celrep.2017.03.045

Trinh, L. A., Chong-Morrison, V., and Sauka-Spengler, T. (2018). Biotagging, an *in vivo* biotinylation approach for cell-type specific subcellular profiling in zebrafish. *Methods*. 150, 24–31. doi: 10.1016/j.ymeth.2018.07.011

Tsai, M.-C., Manor, O., Wan, Y., Mosammaparast, N., Wang, J. K., Shi, Y., et al. (2010). Long noncoding RNA as modular scaffold of histone modification complexes. *Science* 329, 689–693. doi: 10.1126/science.1192002

Wang, D., Garcia-Bassets, I., Benner, C., Li, W., Su, X., Zhou, Y., et al. (2011a). Reprogramming transcription by distinct classes of enhancers functionally defined by eRNA. *Nature* 474, 390–394. doi: 10.1038/nature10006

Wang, K. C., Yang, Y. W., Liu, B., Sanyal, A., Corces-Zimmerman, R., Chen, Y., et al. (2011b). A long noncoding RNA maintains active chromatin to coordinate homeotic gene expression. *Nature* 472, 120–124. doi: 10.1038/nature09819

Wang, W. D., Melville, D. B., Montero-Balaguer, M., Hatzopoulos, A. K., and Knapik, E. W. (2011c). Tfap2a and Foxd3 regulate early steps in the development of the neural crest progenitor population. *Dev. Biol*. 360, 173–185. doi: 10.1016/j.ydbio.2011.09.019

Weiner, A. M. (2018). MicroRNAs and the neural crest: from induction to differentiation. *Mech. Dev*. 154, 98–106. doi: 10.1016/j.mod.2018.05.009

Williams, R. M., Candido-Ferreira, I., Repapi, E., Gavriouchkina, D., Senanayake, U., Ling, I. T., et al. (2019). Reconstruction of the global neural crest gene regulatory network *in vivo*. *Dev. Cell* 51, 255–276. doi: 10.1016/j.devcel.2019.10.003

Yaklichkin, S., Steiner, A. B., Lu, Q., and Kessler, D. S. (2007). FoxD3 and Grg4 physically interact to repress transcription and induce mesoderm in Xenopus. *J. Biol. Chem*. 282, 2548–2557. doi: 10.1074/jbc.M607412200

Yu, J. K., Meulemans, D., McKeown, S. J., and Bronner-Fraser, M. (2008). Insights from the amphioxus genome on the origin of vertebrate neural crest. *Genome Res*. 18, 1127–1132. doi: 10.1101/gr.076208.108

Zheng, G. X. Y., Do, B. T., Webster, D. E., Khavari, P., a., and Chang, H. Y. (2014). Dicer-microRNA-Myc circuit promotes transcription of hundreds of long noncoding RNAs. *Nat. Struct. Mol. Biol*. 21, 585–590. doi: 10.1038/nsmb.2842

Zhu, S., Li, W., Liu, J., Chen, C.-H., Liao, Q., Xu, P., et al. (2016). Genome-scale deletion screening of human long non-coding RNAs using a paired-guide RNA CRISPR-Cas9 library. *Nat. Biotechnol*. 34, 1279–1286. doi: 10.1038/nbt.3715

Zhu, Y., Sun, L., Chen, Z., Whitaker, J. W., Wang, T., and Wang, W. (2013). Predicting enhancer transcription and activity from chromatin modifications. *Nucleic Acids Res*. 41, 10032–10043. doi: 10.1093/nar/gkt826

Conflict of Interest: The authors declare that the research was conducted in the absence of any commercial or financial relationships that could be construed as a potential conflict of interest.

Advantages of publishing in Frontiers

OPEN ACCESS
Articles are free to read for greatest visibility and readership

FAST PUBLICATION
Around 90 days from submission to decision

HIGH QUALITY PEER-REVIEW
Rigorous, collaborative, and constructive peer-review

TRANSPARENT PEER-REVIEW
Editors and reviewers acknowledged by name on published articles

Frontiers
Avenue du Tribunal-Fédéral 34
1005 Lausanne | Switzerland

Visit us: www.frontiersin.org
Contact us: frontiersin.org/about/contact

REPRODUCIBILITY OF RESEARCH
Support open data and methods to enhance research reproducibility

DIGITAL PUBLISHING
Articles designed for optimal readership across devices

FOLLOW US
@frontiersin

IMPACT METRICS
Advanced article metrics track visibility across digital media

EXTENSIVE PROMOTION
Marketing and promotion of impactful research

LOOP RESEARCH NETWORK
Our network increases your article's readership